

# UC San Diego

## UC San Diego Electronic Theses and Dissertations

### Title

Low Valent Cobalt Isocyanides: Exploration of Small Molecule Activations and Cobalt Phosphide Cluster Building Blocks

### Permalink

<https://escholarship.org/uc/item/0t98g1t0>

### Author

Chan, Chinglin

### Publication Date

2019

Peer reviewed|Thesis/dissertation

UNIVERSITY OF CALIFORNIA SAN DIEGO

**Low Valent Cobalt Isocyanides:  
Exploration of Small Molecule Activations and Cobalt Phosphide Cluster Building Blocks**

A dissertation submitted in partial satisfaction of the requirements for  
the degree Doctor of Philosophy

in

Chemistry

by

Chinglin Chan

Committee in charge:

Professor Joshua S. Figueroa, Chair  
Professor Guy Bertrand  
Professor Clifford P. Kubiak  
Professor Dionicio R. Siegel  
Professor Wei Xiong

2019

©

Chinglin Chan, 2019

All rights reserved.

This dissertation of Chinglin Chan is approved, and it is acceptable in quality and form for publication on microfilm and electronically:

---

---

---

---

---

---

Chair

University of California San Diego

2019

## DEDICATION

*To my grandparents and my family in Taiwan.*

Chignlin (Joanne) Chan

## TABLE OF CONTENTS

SIGNITURE PAGE .....	iii
DEDICATION .....	iv
TABLE OF CONTENTS .....	v
LIST OF FIGURES.....	ix
LIST OF TABLES .....	xxiv
LIST OF SCHEMES.....	xxvii
ACKNOWLEDGEMENTS .....	xxix
VITA .....	xxxiv
ABSTRACT OF THE DISSERTATION .....	xxxv
Chapter 1 Isocyano Analogues of Unsaturated Low-valent Cobalt Carbonyls .....	1
1.1 Introduction – Transition Metal Carbonyls.....	1
1.2 Isocyanides as Surrogates for Carbonyls .....	2
1.3 Unsaturated Low-Valent Cobalt Isocyanides.....	7
1.4 Synthesis of $\text{Co}(\text{CNAr}^{\text{Dipp}2})_3$ .....	10
1.5 Synthetic Procedures .....	14
1.6 Computational Studies on $\text{Co}(\text{CNXyl})_3$ .....	21
1.7 Crystallographic Structure Determinations.....	24
1.8 Concluding Remarks .....	27
1.9 Acknowledgement.....	28
1.10 References .....	28
Chapter 2 Associative Ligand Exchange and Substrate Activation Reactions by a Zero-Valent Cobalt Tetraisocyanide Complex .....	33

2.1	Introduction .....	33
2.2	L-type Ligand Substitution Chemistry of $\text{Co}(\text{CNAr}^{\text{Mes}_2})_4$ .....	35
2.3	Mechanistic Observations on $\text{Co}(\text{CNAr}^{\text{Mes}_2})_4$ Ligand Exchange Chemistry .....	39
2.4	Assessing the Radical-Type Behavior of $\text{Co}(\text{CNAr}^{\text{Mes}_2})_4$ .....	42
2.5	Concluding Remarks .....	46
2.6	Synthetic Procedures and Characterization Data. ....	47
2.7	Reaction Procedures and Selected NMR Spectra .....	54
2.8	Kinetic Measurements.....	60
2.9	Crystallography Structure Determination .....	65
2.10	Acknowledgement.....	76
2.11	References .....	77

Chapter 3 Conformational Dynamics in Zero-valent  $\text{CoL}_4$  Complexes Revealed by 2D IR Spectroscopy ..... 82

3.1	Introduction .....	82
3.2	Results and Discussion.....	84
3.3	Concluding Remarks .....	91
3.4	Synthetic Procedures .....	91
3.5	FTIR Experimental Set up, Data Collection, and Analysis .....	92
3.6	FTIR Experimental Set up, Data Collection, and Analysis .....	94
3.7	Obtaining Chemical Exchange Rate Constants from Time Dependent 2D IR Spectra .....	95
3.8	Computational Studies .....	97
3.9	Simulated IR Studies of Fixed Core Angle Geometries .....	118
3.10	Acknowledgement.....	121

3.11	References .....	121
Chapter 4 Controlled Stepwise Synthesis of a Nucleophilic Cobalt-phosphide Cluster		125
4.1	Introduction .....	125
4.2	Results and Discussions .....	126
4.3	Concluding Remarks .....	133
4.4	Synthetic Procedures and Characterization Data .....	133
4.5	Computational Studies .....	141
4.6	Calculation of Percent Buried Volume Parameter .....	149
4.7	Crystallographic Structure Determinations.....	150
4.8	Acknowledgement.....	159
4.9	References .....	160
Chapter 5 Dinitrogen Exchange and Intramolecular Oxygen-Atom-Transfer Behavior of a Persistent End-On Nitrous Oxide Complex of Cobalt .....		164
5.1	Introduction .....	164
5.2	Results and Discussions .....	166
5.3	Concluding Remarks .....	176
5.4	Synthetic Procedures and Characterization Data .....	176
5.5	Computational Studies .....	185
5.6	Spectroscopy Evidence of the O-atom Transfer Reaction .....	199
5.7	Catalytic O-atom Transfer from N <sub>2</sub> O to Isocyanide .....	209
5.8	Calculation of the N <sub>2</sub> /N <sub>2</sub> O Equilibrium Binding Constant .....	211
5.9	Crystallographic Structure Determinations.....	213
5.10	Acknowledgement.....	217



5.11	References .....	217
Chapter 6 Solid State Host-Guest Interaction of n-Hexane with a Coordinatively Unsaturated		
	Cobalt m-Terphenyl Isocyanide Complex .....	221
6.1	Organometallics Host-Guest Interaction with n-Hexane .....	221
6.2	Energy Decomposition Analysis on 1-hexane .....	224
6.3	NMR Study on the Weakly Coordinated Alkylamine Model.....	228
6.4	Concluding Remarks .....	232
6.5	Synthetic Procedures and Characterization Data .....	233
6.6	VT-NMR study of the vdW Interaction .....	236
6.7	Crystallography Structure Determination .....	239
6.8	Computational Details.....	242
6.9	Acknowledgement.....	243
6.10	References .....	243

## LIST OF FIGURES

Figure 1.1. Predicted geometries of late transition-metal unsaturated binary carbonyls Fe(CO) <sub>4</sub> (left), Co(CO) <sub>4</sub> (center), and Ni(CO) <sub>3</sub> (right) with corresponding geometries and electronic states denoted.....	2
Figure 1.2. Calculated frontier orbitals (BP86/TZ2P; iso = 0.04) used in metal bonding for carbonyl and the aryl isocyanide CNAr <sup>Mes2</sup> . <sup>27</sup> .....	3
Figure 1.3. Qualitative molecular orbital representations for transition metal isocyanide and transition metal carbonyl bonding. <sup>27</sup> .....	3
Figure 1.4. Prototypical <i>m</i> -terphenyl isocyanide ligands with varying electronic and steric profiles. (Left to right) CNAr <sup>Mes2</sup> , CNAr <sup>Dipp2</sup> , CNAr <sup>Tripp2</sup> , CNAr <sup>DArF2</sup> , <i>p</i> -F-CNAr <sup>DArF2</sup> .....	5
Figure 1.5. Selected thermostable isocyano analogues of unsaturated transition metal carbonyls. ....	5
Figure 1.6. Selected thermostable isocyano analogues of transition metal carbonyl clusters....	6
Figure 1.7 Abstract Image of Thesis: Low Valent Cobalt Isocyanides - Exploration of Small Molecule Activations and Cobalt Phosphide Cluster Building Blocks.....	7
Figure 1.8. Solid state structure of Na[Co(CNAr <sup>Dipp2</sup> ) <sub>3</sub> ] showing the agnostic interaction. ....	12
Figure 1.9. Molecular structures of A) (ACN)Co(CNAr <sup>Tripp2</sup> ) <sub>3</sub> B) (N <sub>2</sub> )Co(CNAr <sup>Dipp2</sup> ) <sub>3</sub> C) Co(CNAr <sup>Dipp2</sup> ) <sub>3</sub> .....	12
Figure 1.10. Molecular structures of A) I <sub>2</sub> Co(CNAr <sup>Tripp2</sup> ) <sub>2</sub> B) ICo(CNAr <sup>Tripp2</sup> ) <sub>3</sub> C) (18-c-6)K[Co(CNAr <sup>Tripp2</sup> ) <sub>3</sub> ] D) Na[(N <sub>2</sub> )Co(CNAr <sup>Dipp2</sup> ) <sub>3</sub> ]. .....	14
Figure 1.11. Selected molecular orbitals of Co(CNXyl) <sub>3</sub> that include cobalt d-orbital contributions. ....	24

Figure 2.1. Molecular Structures of $\text{Co(L)(CNAr}^{\text{Mes2}}\text{)}_3$ Complexes 1-7. ....	38
Figure 2.2. UV-Vis spectrum of 0.25mM $\text{Co(CNAr}^{\text{Mes2}}\text{)}_4$ in THF (red) and 0.25mM $\text{Co}(\eta^2\text{-C,C-PhCCH})(\text{CNAr}^{\text{Mes2}}\text{)}_3$ (4) in THF (blue).....	41
Figure 2.3. Plot of $\ln[\text{Co(CNAr}^{\text{Mes2}}\text{)}_4]$ vs time, showing the comparative observed rates of $\text{Co(CNAr}^{\text{Mes2}}\text{)}_4$ ligand exchange by PhCCH with the effect of 20 equiv $\text{CNAr}^{\text{Mes2}}$ present under pseudo-first-order conditions (10 and 20 equiv).....	42
Figure 2.4. Molecular Structures of Complexes 8-11. ....	45
Figure 2.5. $^1\text{H}$ NMR spectrum (400.1 MHz, $\text{C}_6\text{D}_6$ , $20^\circ\text{C}$ ) of $\text{Co(PPh}_3\text{)(CNAr}^{\text{Mes2}}\text{)}_3$ (1). *Small amount of free $\text{CNAr}^{\text{Mes2}}$ present in the sample. ....	55
Figure 2.6. $^1\text{H}$ NMR spectrum (400.1 MHz, $\text{C}_6\text{D}_6$ , $20^\circ\text{C}$ ) of $\text{Co(CN}^t\text{Bu)(CNAr}^{\text{Mes2}}\text{)}_3$ (2). *Small amount of free $\text{CNAr}^{\text{Mes2}}$ present in the sample. ....	56
Figure 2.7. $^1\text{H}$ NMR spectrum (300.1 MHz, $\text{C}_6\text{D}_6$ , $20^\circ\text{C}$ ) of $\text{Co}(\eta^2\text{-C,C-PhCCH})(\text{CNAr}^{\text{Mes2}}\text{)}_3$ (4). *Small amount of free $\text{CNAr}^{\text{Mes2}}$ present in the sample. ....	56
Figure 2.8. $^1\text{H}$ NMR spectrum (400.1 MHz, $\text{C}_6\text{D}_6$ , $20^\circ\text{C}$ ) of $\text{Co}(\eta^2\text{-C,C-MA})(\text{CNAr}^{\text{Mes2}}\text{)}_3$ (6). *Small amount of free $\text{CNAr}^{\text{Mes2}}$ present in the sample. ....	57
Figure 2.9. $^1\text{H}$ NMR spectrum (400.1 MHz, $\text{C}_6\text{D}_6$ , $20^\circ\text{C}$ ) of $\text{Co}(\eta^2\text{-C,O-PhC(O)H})(\text{CNAr}^{\text{Mes2}}\text{)}_3$ (7). *Small amount of free $\text{CNAr}^{\text{Mes2}}$ present in the sample. ....	57
Figure 2.10. $^1\text{H}$ NMR spectrum (500.1 MHz, $\text{C}_6\text{D}_6$ , $20^\circ\text{C}$ ) of $\text{Co}(\eta^3\text{-P}_3)(\text{CNAr}^{\text{Mes2}}\text{)}_3$ (9).....	58
Figure 2.11. $^{31}\text{P}\{^1\text{H}\}$ NMR spectrum (121.5 MHz, $\text{C}_6\text{D}_6$ , $20^\circ\text{C}$ ) of $\text{Co}(\eta^3\text{-P}_3)(\text{CNAr}^{\text{Mes2}}\text{)}_3$ (9). .....	58
Figure 2.12. $^1\text{H}$ NMR spectrum (300.1 MHz, $\text{C}_6\text{D}_6$ , $20^\circ\text{C}$ ) of $\text{Co}_2(\mu\text{-S}_2)_2(\mu\text{-S}_4)(\text{CNAr}^{\text{Mes2}}\text{)}_4$ (10). *Small amount of free $\text{CNAr}^{\text{Mes2}}$ present in the sample. ....	59

Figure 2.13. $^1\text{H}$ NMR spectrum (300.1 MHz, $\text{C}_6\text{D}_6$ , $20^\circ\text{C}$ ) of $\text{Co}(\text{SPh})_2(\text{CNAr}^{\text{Mes}2})_3$ (11). *Small amount of free $\text{CNAr}^{\text{Mes}2}$ present in the sample. ....	59
Figure 2.14. Kinetic UV-vis spectra of $\text{Co}(\text{CNAr}^{\text{Mes}2})_4$ with phenylacetylene (10 equiv) measured at $20^\circ\text{C}$ in THF at 120 seconds interval. ....	61
Figure 2.15. Kinetic UV-vis spectra of $\text{Co}(\text{CNAr}^{\text{Mes}2})_4$ with phenylacetylene (10 equiv) and $\text{CNAr}^{\text{Mes}2}$ (20 equiv) measured at $20^\circ\text{C}$ in THF at 120 seconds interval.....	62
Figure 2.16. Kinetic UV-vis spectra of $\text{Co}(\text{CNAr}^{\text{Mes}2})_4$ with phenylacetylene (20 equiv) measured at $20^\circ\text{C}$ in THF at 120 seconds interval. ....	63
Figure 2.17. Kinetic UV-vis spectra of $\text{Co}(\text{CNAr}^{\text{Mes}2})_4$ with phenylacetylene (20 equiv) and $\text{CNAr}^{\text{Mes}2}$ (20 equiv) measured at $20^\circ\text{C}$ in THF at 120 seconds interval.....	64
Figure 2.18. Plot of $\text{Co}(\text{CNAr}^{\text{Mes}2})_4$ absorbance vs time, showing the rate enhancement by adding more equivalents of phenylacetylene in the ligand substitution reaction of $\text{Co}(\text{CNAr}^{\text{Mes}2})_4$ and the reaction rate independence of the $\text{CNAr}^{\text{Mes}2}$ concentration. ....	64
Figure 2.19. Plot of $\ln[\text{Co}(\text{CNAr}^{\text{Mes}2})_4]$ vs time, showing the comparative observed rates of $\text{Co}(\text{CNAr}^{\text{Mes}2})_4$ ligand exchange by PhCCH with the effect of 20 equiv $\text{CNAr}^{\text{Mes}2}$ present under pseudo-first-order conditions (10 and 20 equiv).....	65
Figure 2.20. Molecular structure of $\text{Co}(\text{PPh}_3)(\text{CNAr}^{\text{Mes}2})_3$ (1). Hydrogen atoms omitted for clarity. Selected distances ( $\text{\AA}$ ) and angles ( $^\circ$ ): Co1-C1 = 1.823, Co1-C2 = 1.824, Co1-C3 = 1.825, Co1-P1 = 2.246(4), C1-Co1-C2 = 113.8, C2-Co1-C3 = 113.9, C3-Co1-C1 = 113.8, P1-Co1-C1 = 104.68, P1-Co1-C2 = 104.67. ....	67
Figure 2.21. Molecular structure of $\text{Co}(\text{CN}t\text{-Bu})(\text{CNAr}^{\text{Mes}2})_3 \cdot (\text{C}_6\text{H}_6) \cdot (\text{C}_5) (2 \cdot (\text{C}_6\text{H}_6) \cdot (\text{C}_5))$ , with benzene, pentane solvent molecules and hydrogen atoms omitted for clarity.	

Selected distances (Å) and angles (°): Co1-C1 = 1.852(3), Co1-C2 = 1.820(3),  
Co1-C3 = 1.824(3), C1-C4 = 1.844(4), C1-Co1-C2 = 105.3(1). ..... 67

Figure 2.22. Molecular structure of  $\text{Co}(\eta^2\text{-}C,C\text{-}^i\text{BuCHCH}_2)(\text{CNAr}^{\text{Mes}_2})_3 \cdot (\text{Et}_2\text{O})_2$  ( $3 \cdot (\text{Et}_2\text{O})_2$ ), with two ether solvent molecules and hydrogen atoms omitted for clarity. Selected distances (Å) and angles (°): Co1-C1 = 1.827(7), Co1-C2 = 1.842(7), Co1-C3 = 1.853(6), C1-C4 = 2.107(6), Co1-C5 = 2.063(6), C4-C5 = 1.395(8)..... 68

Figure 2.23. Molecular structure of  $\text{Co}(\eta^2\text{-}C,C\text{-PhCCH})(\text{CNAr}^{\text{Mes}_2})_3$  (4). Hydrogen atoms omitted for clarity. Selected distances (Å) and angles (°): Co1-C1 = 1.879(2), Co1-C2 = 1.842(3), Co1-C3 = 1.833(3), Co1-C4 = 1.939(3), Co1-C5 = 1.942(2), C4-C5 = 1.255(4), C1-Co1-C2 = 101.4(1), C2-Co1-C3 = 107.1(1). ..... 68

Figure 2.24. Molecular structure of  $\text{Co}(\eta^2\text{-}C,C\text{-PhCC-CCPh})(\text{CNAr}^{\text{Mes}_2})_3 \cdot (\text{PhCC-CCPh}) \cdot (\text{Et}_2\text{O})$  ( $5 \cdot (\text{PhCC-CCPh}) \cdot (\text{Et}_2\text{O})$ ), with PhCC-CCPh, ether solvent molecules and hydrogen atoms omitted for clarity. Selected distances (Å) and angles (°): Co1-C1 = 1.879(3), Co1-C2 = 1.846(4), Co1-C3 = 1.837(3)..... 69

Figure 2.25. Molecular structure of  $\text{Co}(\eta^2\text{-}C,C\text{-MA})(\text{CNAr}^{\text{Mes}_2})_3 \cdot (\text{C}_5)_2$  ( $6 \cdot (\text{C}_5)_2$ ), with pentane solvent molecules and hydrogen atoms omitted for clarity. Selected distances (Å) and angles (°): Co1-C1 = 1.861(4), Co1-C2 = 1.915(4), Co1-C3 = 1.850(4), C1-C4 = 2.030(4), Co1-C5 = 2.033(3), C4-C5 = 1.414(6). ..... 69

Figure 2.26. Molecular structure of  $\text{Co}(\eta^2\text{-}C,O\text{-BA})(\text{CNAr}^{\text{Mes}_2})_3$  (7). Hydrogen atoms omitted for clarity. Selected distances (Å) and angles (°): Co1-C1 = 1.861(4), Co1-C2 = 1.843(4), Co1-C3 = 1.873(3), Co1-O1 = 1.941(4), Co1-C4 = 2.038(5), O1-C4 = 1.261(8), C1-Co1-C2 = 100.7(2), C2-Co1-C3 = 105.6(2). ..... 70

Figure 2.27. Molecular structure of  $(\eta^2\text{-TEMPO})\text{Co}(\text{CNAr}^{\text{Mes}2})_2$  (8). Hydrogen atoms omitted for clarity. Selected distances (Å) and angles (°): Co1-C1 = 1.759(2), Co1-C2 = 1.751(2), Co1-O1 = 1.862(2), Co1-N1 = 1.920(2), C1-Co1-C2 = 95.5(1), O1-Co1-C1 = 109.76(9), O1-Co1-N1 = 33.43(7), N1-Co1-C2 = 111.45(9)..... 70

Figure 2.28. Molecular structure of  $(\eta^3\text{-P}_3)\text{Co}(\text{CNAr}^{\text{Mes}2})_3 \cdot (\text{FC}_6\text{H}_5) \cdot (\text{ACN})$  ( $9 \cdot (\text{FC}_6\text{H}_5) \cdot (\text{ACN})$ ), with fluorobenzene, acetonitrile solvent molecules and hydrogen atoms omitted for clarity. Selected distances (Å) and angles (°): Co1-C1 = 1.835(4), Co1-C2 = 1.839(4), Co1-C3 = 1.844(4), Co1-P1 = 2.317(1)..... 71

Figure 2.29. Molecular structure of  $[\text{Co}_2(\mu\text{-S}_2)_2(\mu\text{-S}_4)(\text{CNAr}^{\text{Mes}2})_4] \cdot (\text{THF})_2$  ( $10 \cdot (\text{THF})_2$ ), with two THF solvent molecule and hydrogen atoms omitted for clarity. Selected distances (Å) and angles (°): Co1-C1 = 1.843(2), Co1-C2 = 1.850(3), Co1-S1 = 2.2723(7), Co1-S2 = 2.2618(8), Co1-S3 = 2.2677(7), C1-Co1-C2 = 94.8(1)..... 71

Figure 2.30. Molecular structure of  $\text{Co}(\text{SPh})_2(\text{CNAr}^{\text{Mes}2})_3 \cdot (\text{C}_6\text{H}_6)$  ( $11 \cdot (\text{C}_6\text{H}_6)$ ), with a benzene solvent molecule and hydrogen atoms omitted for clarity. Selected distances (Å) and angles (°): Co1-C1 = 1.851(3), Co1-C2 = 1.937(3), Co1-C3 = 1.863(3), Co1-S1 = 1.221(1), Co1-S2 = 2.3037(8), C1-Co1-C2 = 103.7(1)..... 72

Figure 3.1. a) Molecular Structure of  $\text{Co}(\text{CNAr}^{\text{Mes}2})_4$  in  $D_{2d}$  and  $C_{3v}$  geometries. b) pulse sequence used in 2D IR experiment. c) 2D IR spectrum of  $\text{Co}(\text{CNAr}^{\text{Mes}2})_4$  at  $t_2 = 0$  fs, diagonal peaks are labeled as 1, 2, and 3. d) Normalized FTIR spectrum (black) of  $\text{Co}(\text{CNAr}^{\text{Mes}2})_4$ , and diagonal cut of 2D IR spectrum in c) (red). ..... 84

Figure 3.2. a) Molecular overlap of DFT calculated both  $C_{3v}$  (blue) and  $D_{2d}$  (red) geometries of  $\text{CoL}_4$  ( $L=\text{CO}$ ,  $\text{CNAr}^{\text{Mes}2}$ ). b) Simulated IR spectrum of both  $C_{3v}$  (blue) and  $D_{2d}$  (red)

Co(CNAr <sup>Mes2</sup> ) <sub>4</sub> using b3lyp/6-31g(d):lanl2dz. Wavenumbers are scaled with scaling factor of b3lyp/6-31g(d) = 0.9614.....	87
Figure 3.3. a) Dynamics traces of different cross peaks as functions of t <sub>2</sub> . b) Plot of ln(k) vs. 1/T. Rate of cross peak growth and rate of IVR (when mode splitting is 20 cm <sup>-1</sup> ) have different temperature dependent. ....	88
Figure 3.4. a) VT-FTIR spectrum of Co(CNAr <sup>Mes2</sup> ) <sub>4</sub> and b) van't hoff plot of lnKeq vs 1/T between C <sub>3v</sub> and D <sub>2d</sub> . ....	93
Figure 3.5. VT-FTIR spectrum of Co(CN <sup>t</sup> Bu)(CNAr <sup>Mes2</sup> ) <sub>3</sub> . ....	94
Figure 3.6. a) 2D IR spectrum at t <sub>2</sub> =0 fs b) 2D IR spectrum at t <sub>2</sub> =900 fs c) take cut along w <sub>3</sub> axis at red dash line in a) and fit with gaussian peak components for t <sub>2</sub> =0 fs d) take cut along w <sub>3</sub> axis at red dash line in b) and fit with gaussian peak components for t <sub>2</sub> =900 fs.....	97
Figure 3.7. Structural overlap images of optimized CoL <sub>4</sub> (L= CO, CNMe, CNXyl, CNAr <sup>Ar2</sup> , CNAr <sup>Mes2</sup> ) coordinates.....	98
Figure 3.8. DFT simulated IR spectrum of both Co(CNAr <sup>Mes2</sup> ) <sub>4</sub> C <sub>3v</sub> and D <sub>2d</sub> Isomers.....	100
Figure 3.9. Simulated IR spectrums of ( <sup>t</sup> BuNC)Co(CNAr <sup>Mes2</sup> ) <sub>3</sub> .....	115
Figure 3.10. Simulated IR spectrums of fixed core angles C <sub>3v</sub> Co(CNAr <sup>Mes2</sup> ) <sub>4</sub> geometries. .	119
Figure 3.11. Simulated IR spectrums of fixed core angles D <sub>2d</sub> Co(CNAr <sup>Mes2</sup> ) <sub>4</sub> geometries. .	119
Figure 3.12. Simulated IR spectrums of fixed core angles C <sub>3v</sub> Co(CNAr <sup>Mes2</sup> ) <sub>4</sub> geometries. .	120
Figure 3.13. Simulated IR spectrums of fixed core angles D <sub>2d</sub> Co(CNAr <sup>Mes2</sup> ) <sub>4</sub> geometries. .	120
Figure 4.1. (Left) Molecular structures of complexes 2-4 and 6. A) (PCl <sub>2</sub> )Co(CO) <sub>2</sub> (CNAr <sup>Mes2</sup> ) <sub>2</sub> (2), B) Co <sub>2</sub> (μ <sub>2</sub> -P-PCl)(μ <sub>2</sub> -C-CO)(CO) <sub>2</sub> (CNAr <sup>Mes2</sup> ) <sub>4</sub> (3), C) Co <sub>3</sub> (μ <sub>3</sub> -	

	P)(CO) <sub>6</sub> (CNAr <sup>Mes2</sup> ) <sub>3</sub> (4), and D) Co <sub>3</sub> (μ <sub>3</sub> -P)(μ <sub>2</sub> -C-CO) <sub>3</sub> (CO) <sub>3</sub> (CNAr <sup>Dipp2</sup> ) <sub>3</sub> (6).	
	(Right) E) Highest occupied molecular orbital (HOMO) of complex 4. ....	128
Figure 4.2.	Molecular structure of A) Co <sub>3</sub> (μ <sub>3</sub> -P)(CO) <sub>6</sub> (CNAr <sup>Dipp2</sup> ) <sub>3</sub> AuCl (7), B) [Co <sub>4</sub> (μ <sub>4</sub> -P)(CO) <sub>9</sub> (CNAr <sup>Dipp2</sup> ) <sub>4</sub> ]CoBr <sub>3</sub> (8), C) [Co <sub>3</sub> (μ <sub>3</sub> -P-PCH <sub>3</sub> )(CO) <sub>6</sub> (CNAr <sup>Dipp2</sup> ) <sub>3</sub> ]OTf (9), and D) Co <sub>3</sub> (μ <sub>3</sub> -P-PS)(CO) <sub>6</sub> (CNAr <sup>Dipp2</sup> ) <sub>3</sub> (10).....	132
Figure 4.3.	Geometry optimized structure of Co <sub>3</sub> (μ <sub>3</sub> -P)(CO) <sub>6</sub> (CNXyl) <sub>3</sub> (4m) with hydrogen atoms omitted for clarity. (B3LYP/6-31G(d):LANL2DZ) .....	145
Figure 4.4.	Highest occupied molecular orbital (HOMO) of Co <sub>3</sub> (μ <sub>3</sub> -P)(CO) <sub>6</sub> (CNXyl) <sub>3</sub> (4m) showing the phosphine lone-pair character. ....	145
Figure 4.5.	Geometry optimized structure of Co <sub>3</sub> (μ <sub>3</sub> -P)(μ <sub>2</sub> -C-CO) <sub>3</sub> (CO) <sub>3</sub> (CNXyl) <sub>3</sub> (6m) with hydrogen atoms omitted for clarity. (B3LYP/6-31G(d):LANL2DZ) .....	148
Figure 4.6.	Highest occupied molecular orbital -2 (HOMO-2) of Co <sub>3</sub> (μ <sub>3</sub> -P)(μ <sub>2</sub> -C-CO) <sub>3</sub> (CO) <sub>3</sub> (CNXyl) <sub>3</sub> (6m) showing the phosphine lone-pair character. ....	148
Figure 4.7.	Steric map of 6 viewing from the top through the AuCl (See Figure 4.13 for crystal structure image). ....	150
Figure 4.8.	Molecular structure of (PCl <sub>2</sub> )Co(CO) <sub>2</sub> (CNAr <sup>Mes2</sup> ) <sub>2</sub> (2), with benzene solvent molecule and hydrogen atoms omitted for clarity. Selected distances (Å) and angles (°): Co-P = 2.241(1), Co-C1 = 1.781(3), Co-C2 = 1.781(4), Co-C3 = 1.870(4), Co-C4 = 1.866(4), C4-N2 = 1.157(5), C3-N1 = 1.165(5). ....	151
Figure 4.9.	Molecular structure of Co <sub>2</sub> (μ <sub>2</sub> -P-PCl)(μ <sub>2</sub> -C-CO)(CO) <sub>2</sub> (CNAr <sup>Mes2</sup> ) <sub>4</sub> (3), with benzene solvent molecule and hydrogen atoms omitted for clarity. ....	152
Figure 4.10.	Molecular structure of Co <sub>3</sub> (μ <sub>3</sub> -P)(CO) <sub>6</sub> (CNAr <sup>Mes2</sup> ) <sub>3</sub> (4) with hydrogen atoms omitted for clarity. Selected distances (Å) and angles (°): Co-Co avg. = 2.517(3),	



Co-P avg. = 2.201(4),  $\text{Co}_{3\text{centroid}}\text{-P}$  = 1.653, Co-C3 avg. = 1.780(1), Co-C1 avg. = 1.800(1), Co-Co-Co avg. = 60.19(8),  $\Sigma$  Co-P-Co = 208.9(1)..... 152

Figure 4.11. Molecular structure of  $\text{NaCo}(\text{CO})_3(\text{CNAr}^{\text{Dipp}2})$  (5) with hydrogen atoms omitted for clarity. Selected distances (Å) and angles (°): Co-C1 = 1.766(5), Co-C2 = 1.751(4), Co-C3 = 1.762(4), Co-C4 = 1.819(4), C4-N = 1.178(5), C4-Co-C1 = 121.3(2), C4-Co-C2 = 105.4(2), C4-Co-C3 = 108.8(2). ..... 153

Figure 4.12. Molecular structure of  $\text{Co}_3(\mu_3\text{-P})(\mu_2\text{-C-CO})_3(\text{CO})_3(\text{CNAr}^{\text{Dipp}2})_3$  (6) with hydrogen atoms omitted for clarity. Selected distances (Å) and angles (°): Co-Co avg. = 2.529(3), Co-P avg. = 2.252(5),  $\text{Co}_{3\text{centroid}}\text{-P}$  = 1.715, Co-C3 eq. = 1.77(2), Co''-C3'' = 1.74(2), Co-C1 eq. = 1.84(2), Co''-C1'' = 1.81(2)..... 153

Figure 4.13. Molecular structure of  $\text{Co}_3(\mu_3\text{-P})(\text{CO})_6(\text{CNAr}^{\text{Dipp}2})_3\text{AuCl}$  (7) with hydrogen atoms omitted for clarity. Selected distances (Å) and angles (°): Co-Co' = 2.5514(7), Co'-Co'' = 2.5380(6), Co''-Co = 2.5973(7), Co-P = 2.1428(7), Co'-P = 2.1604(7), Co''-P = 2.1375(7),  $\text{Co}_{3\text{centroid}}\text{-P}$  = 1.559, P-Au = 2.2065(7). ..... 154

Figure 4.14. Molecular structure of  $[\text{Co}_4(\mu_4\text{-P})(\text{CO})_8(\text{CNAr}^{\text{Mes}2})_5]\text{CoBr}_3$  (8) with hydrogen atoms omitted for clarity. Selected distances (Å) and angles (°): Co1-P = 2.149(2), Co2-P = 2.152(2), Co3-P = 2.143(3), Co4-P = 2.220(3), Co1-Co2 = 2.567(1), Co2-Co3 = 2.552(2), Co3-Co1 = 2.583(2),  $\text{Co}_{3\text{centroid}}\text{-P}$  = 1.555. ..... 154

Figure 4.15. Molecular structure of  $[\text{Co}_3(\mu_3\text{-P-PCH}_3)(\text{CO})_6(\text{CNAr}^{\text{Dipp}2})_3]\text{OTf}$  (9) with triflate ion and hydrogen atoms omitted for clarity. Selected distances (Å) and angles (°): Co-Co' = 2.565(5), Co'-Co'' = 2.570(4), Co''-Co = 2.550(5), Co-P = 2.112(9), Co'-P = 2.104(7), Co''-P = 2.111(7),  $\text{Co}_{3\text{centroid}}\text{-P}$  = 1.504, P-C4 = 1.83(2). .... 155

Figure 4.16. Molecular structure of $\text{Co}_3(\mu_3\text{-P-PS})(\text{CO})_6(\text{CNAr}^{\text{Dipp}2})_3$ (10) with benzene solvent molecule and hydrogen atoms omitted for clarity. Selected distances (Å) and angles (°): Co-Co' = 2.571(1), Co'-Co'' = 2.571(1), Co''-Co = 2.555(2), Co-P = 2.151(1), Co'-P = 2.159(1), Co''-P = 2.149(2), $\text{Co}_{3\text{centroid}}\text{-P} = 1.563$ .....	155
Figure 4.17. Molecular structure of $[\text{Co}(\text{CO})_3(\text{CNAr}^{\text{Mes}2})_2]\text{CoBr}_3\cdot\text{Et}_2\text{O}$ (11) with ether solvent and $\text{CoBr}_3\cdot\text{Et}_2\text{O}$ molecules plus hydrogen atoms omitted for clarity. Selected distances (Å) and angles (°): Co-C1 = 1.910(4), Co-C2 = 1.839(6), Co-C3 = 1.812(6), Co-C4 = 1.859(5), Co-C5 = 1.837(5), C1-N1 = 1.146(6). .....	156
Figure 5.1. (Left) FTIR spectrum of 3 as prepared in $\text{C}_6\text{H}_6$ solution shown in red, and $3\text{-}^{15}\text{N}$ as prepared in $\text{C}_6\text{D}_6$ solution shown in blue. (Right) FTIR spectrum of 3 after 12 h in $\text{C}_6\text{D}_6$ solution shown in red, and $3\text{-}^{15}\text{N}$ after 12 h in $\text{C}_6\text{D}_6$ solution shown in blue. All spectrums had solvent background subtraction applied. ....	173
Figure 5.2. $^1\text{H}$ NMR spectrum (500 MHz, $\text{C}_6\text{D}_6$ , 20°C) of $(\kappa^1\text{-N-N}_2\text{O})\text{Co}(\text{SiMe}_3)(\text{CNAr}^{\text{Mes}2})_3$ (3). .....	180
Figure 5.3 $^1\text{H}$ NMR spectrum (800 MHz, $\text{C}_6\text{D}_6$ , 20°C) of $(\kappa^1\text{-N-N}_2\text{O})\text{Co}(\text{SiMe}_3)(\text{CNAr}^{\text{Mes}2})_3$ (3). .....	180
Figure 5.4. FTIR ( $\text{C}_6\text{H}_6$ , KBr windows, 25 °C) of $(\kappa^1\text{-N-N}_2\text{O})\text{Co}(\text{SiMe}_3)(\text{CNAr}^{\text{Mes}2})_3$ (3).....	181
Figure 5.5. ATR-IR spectrum ( $\text{Ar}_{(\text{g})}$ , 25°C) of $(\kappa^1\text{-N-N}_2\text{O})\text{Co}(\text{SiMe}_3)(\text{CNAr}^{\text{Mes}2})_3$ (3). .....	181
Figure 5.6. $^{13}\text{C}\{^1\text{H}\}$ NMR spectrum (125.8 MHz, $\text{C}_6\text{D}_6$ , 20°C) of $(\kappa^1\text{-N-N}_2\text{O})\text{Co}(\text{SiMe}_3)(\text{CNAr}^{\text{Mes}2})_3$ (3).....	182

Figure 5.7. Overlapped FTIR spectrum ( $C_6H_6$ , KBr windows, $25^\circ C$ ) of $(\kappa^1-N-N_2O)Co(SiMe_3)(CNAr^{Mes2})_3$ (3) in red and $(\kappa^1-N-^{15}N_2O)Co(SiMe_3)(CNAr^{Mes2})_3$ ( $3-^{15}N$ ) in blue showing the red-shift of $\nu_{NNO}$ upon $^{15}N$ -labeling .	183
Figure 5.8. $^{15}N\{^1H\}$ NMR spectrum (50.8 MHz, $d_8$ -toluene, $-25^\circ C$ ) of $(\kappa^1-N-^{15}N_2O)Co(SiMe_3)(CNAr^{Mes2})_3$ ( $3-^{15}N$ ).	183
Figure 5.9. $^{15}N\{^1H\}$ NMR spectrum (81.1 MHz, $C_6D_6$ , $20^\circ C$ ) of $(\kappa^1-N-^{15}N_2O)Co(SiMe_3)(CNAr^{Mes2})_3$ ( $3-^{15}N$ ).	184
Figure 5.10. $^{15}N\{^1H\}$ NMR spectrum (50.8 MHz, $d_8$ -toluene, $-60^\circ C$ ) of $(^{15}N_2)Co(SiMe_3)(CNAr^{Mes2})_3$ ( $4-^{15}N$ ). Singlet shown at 300 ppm attributed from free $^{15}N_{2(g)}$ .	185
Figure 5.11. Geometry optimized structure of $(N_2O)Co(SiMe_3)(CNAr^{Mes2})_3$ (3) with hydrogen atoms omitted for clarity. (B3LYP/6-31G(d):LANL2DZ)	195
Figure 5.12. Geometry optimized structure of $(N_2)Co(SiMe_3)(CNAr^{Mes2})_3$ (4) with hydrogen atoms omitted for clarity. (B3LYP/6-31G(d):LANL2DZ)	196
Figure 5.13. Calculated molecular orbitals (MOs) of $(N_2O)Co(SiMe_3)(CNAr^{Mes2})_3$ (3) and $(N_2)Co(SiMe_3)(CNAr^{Mes2})_3$ (4) showing MOs with cobalt d-orbital character. Atomic orbital contributions (AO%) to the molecular orbitals are listed. The AO% to these MOs reveal the similarity between $N_2O$ and $N_2$ binding.	197
Figure 5.14. Overlapped FTIR spectrum ( $C_6H_6$ , KBr windows, $25^\circ C$ ) of the first data point (pure compound 3) in red and the second data point (12 h) in blue showing the formation of 4 and $OCNAr^{Mes2}$ .	200

Figure 5.15. Overlapped FTIR spectrum ( $C_6H_6$ , KBr windows, 25 °C) of the first data point (pure compound 3- $^{15}N$ ) in blue and the second data point (12 h) in red showing the formation of 4- $^{15}N$ and $OCNAr^{Mes_2}$ .....	201
Figure 5.16. Overlapped $^1H$ NMR spectrum ( $C_6D_6$ , 25 °C) of the first data point (pure compound 3- $^{15}N$ ) in blue and the final data point (12 h) in red showing the formation of 4- $^{15}N$ and $OCNAr^{Mes_2}$ .....	202
Figure 5.17. Stacked $^1H$ NMR spectrum ( $C_6D_6$ , 25 °C) of the <i>O</i> -atom transfer reaction of 3.	203
Figure 5.18. Zoomed-in stacked $^1H$ NMR spectrum ( $C_6D_6$ , 25 °C) of the <i>O</i> -atom transfer reaction of 3 showing the growth of $OCNAr^{Mes_2}$ overtime. ....	203
Figure 5.19. Stacked $^1H$ NMR spectrum ( $C_6D_6$ , 25 °C) of the <i>O</i> -atom transfer reaction of 3 with 1 equiv. of $CNAr^{Mes_2}$ .....	204
Figure 5.20. Zoomed-in stacked $^1H$ NMR spectrum ( $C_6D_6$ , 25 °C) of the <i>O</i> -atom transfer reaction of 3 with 1 equiv. of $CNAr^{Mes_2}$ .....	204
Figure 5.21. Overlapped time-dependent $^1H$ NMR spectrum zoomed in at the $SiMe_3$ peak region. (Left) Decomposition of 3 itself in $C_6D_6$ at 25 °C over 12 hours. (Right) Decomposition of 3 with 1 equiv. of $CNAr^{Mes_2}$ added in $C_6D_6$ at 25 °C over 15 hours. ....	205
Figure 5.22. Time-dependent $^{15}N$ NMR spectrum taken in $C_6D_6$ with the initial 3- $^{15}N$ concentration at 30mM showing the disappearance of 3- $^{15}N$ signals overtime. No apparent signals were shown after 260 minutes. ....	205
Figure 5.23. Overlapped time-dependent $^{15}N$ NMR spectrum taken in $C_6D_6$ with the initial 3- $^{15}N$ concentration at 30mM. The peak shifting feature indicated an exchange between $N_\alpha$ (138 ppm) and $N_\beta$ (246 ppm). ....	206

Figure 5.24. Time-dependent $^{15}\text{N}$ NMR spectrum taken in $\text{C}_6\text{D}_6$ with the initial $3\text{-}^{15}\text{N}$ concentration at 45mM showing the disappearance of $3\text{-}^{15}\text{N}$ signals overtime. No apparent signals were shown after 300 minutes. Note that with higher initial concentration, the rate of disappearance is slower. ....	206
Figure 5.25. Time-dependent $^{15}\text{N}$ NMR spectrum taken in $\text{C}_6\text{D}_6$ with the initial $3\text{-}^{15}\text{N}$ concentration at 13mM showing the disappearance of $3\text{-}^{15}\text{N}$ signals overtime. No apparent signals were shown after 140 minutes. Note that with lower initial concentration, the rate of disappearance is faster. ....	207
Figure 5.26. Stacked $^1\text{H}$ NMR spectrum ( $\text{C}_6\text{D}_6$ , 25 °C) of the decomposition of 3 under the presence of $\text{PCy}_3$ .....	208
Figure 5.27. Stacked $^{31}\text{P}$ NMR spectrum ( $\text{C}_6\text{D}_6$ , 25 °C) of the decomposition of 3 under the presence of $\text{PCy}_3$ .....	208
Figure 5.28. Stacked $^1\text{H}$ NMR spectrum ( $\text{C}_6\text{D}_6$ , 25 °C) of the decomposition of 3 with excess $\text{N}_2\text{O}_{(\text{g})}$ . ....	209
Figure 5.29. Zoomed in stacked $^1\text{H}$ NMR spectrum ( $\text{C}_6\text{D}_6$ , 25 °C) of the decomposition of 3 with excess $\text{N}_2\text{O}_{(\text{g})}$ showing the formation of $\text{OCNAr}^{\text{Mes}_2}$ and $(\text{SiMe}_3)_2\text{O}$ . ....	210
Figure 5.30. Stacked $^1\text{H}$ NMR spectrum ( $\text{C}_6\text{D}_6$ , 25 °C) showing the catalytic <i>O</i> -atom transfer reaction to $\text{CNAr}^{\text{Tripp}_2}$ using 20 mol% of 3 with 1ATM $\text{N}_2\text{O}_{(\text{g})}$ .....	211
Figure 5.31. $^1\text{H}$ NMR spectrum zoomed in at the $\text{SiMe}_3$ peak region. Trace in black is the original spectra which was then deconvoluted into 3 (shown in blue) and 4 (shown in red) using the program Mnova. ....	212

Figure 5.32. Temperature-dependent  $^1\text{H}$  NMR spectrum zoomed in at the  $\text{SiMe}_3$  peak region.

The ratio of complexes 3/4 showed a steady decrease upon lowering the temperature, indicates that complex 4 is more thermodynamically favored. .... 213

Figure 5.33. Molecular structure of  $\text{Co}(\text{SiMe}_3)(\text{CNAr}^{\text{Mes}_2})_3$  (2), with toluene solvent molecule and hydrogen atoms omitted for clarity. Selected distances ( $\text{\AA}$ ) and angles ( $^\circ$ ): Co-C = 1.792(3), Co-Si = 2.249(3), C-N = 1.178(3), C-Co-C = 119.9(2), C-Co-Si = 88.0(1). ..... 215

Figure 5.34. Molecular structure of  $(\kappa^1\text{-N-N}_2\text{O})\text{Co}(\text{SiMe}_3)(\text{CNAr}^{\text{Mes}_2})_3$  (3), with benzene, pentane solvent molecules and hydrogen atoms omitted for clarity. Selected distances ( $\text{\AA}$ ) and angles ( $^\circ$ ): Co-C = 1.806(4), Co-Si = 2.295(1), C-N = 1.190(5), N-N = 1.110(5), N-O = 1.210(5), C-Co-C = 114.9(2), C-Co-Si = 84.6(1). ..... 215

Figure 5.35. Molecular structure of  $(\eta^2\text{-C,C-PhCCPh})\text{Co}(\text{SiMe}_3)(\text{CNAr}^{\text{Mes}_2})_2$  (5), with hydrogen atoms omitted for clarity. Selected distances ( $\text{\AA}$ ) and angles ( $^\circ$ ): Co-C1 = 1.869(2), Co-C1' = 1.884(2), C1-C1' = 1.292(3), Co-Si = 2.2506(6), C1-Co-Si = 106.69(6), C1'-Co-Si = 113.62(6). ..... 216

Figure 6.1. Molecular structures of *n*-hexane containing  $\text{Co}(\text{SiMe}_3)(\text{CNAr}^{\text{Mes}_2})_3$  (1) inclusion complexes. Left: Polymorph 1A-hexane  $(\mu^2\text{-}(\eta^2\text{-H,C,}-(n\text{-C}_6\text{H}_{14}))[\text{Co}(\text{SiMe}_3)(\text{CNAr}^{\text{Mes}_2})_3] \cdot (n\text{-C}_6\text{H}_{14}) \cdot 2(\text{C}_6\text{H}_6)$ . Right: Polymorph 1B-hexane  $(\mu^2\text{-}(\eta^2\text{-H,C,}-(n\text{-C}_6\text{H}_{14}))[\text{Co}(\text{SiMe}_3)(\text{CNAr}^{\text{Mes}_2})_3] \cdot 1(\text{C}_6\text{H}_6)$ . ..... 223

Figure 6.2 Molecular structure of  $(\mu^2\text{-}(\eta^2\text{-H,C,}-(n\text{-C}_6\text{H}_{14}))[\text{Co}(\text{SiMe}_3)(\text{CNAr}^{\text{Mes}_2})_3] \cdot 1(\text{C}_6\text{H}_6)$  1B-hexane. Asymmetric unit shown with close contacts (light blue) between the

encapsulated <i>n</i> -hexane in orange (carbon) and red (hydrogen) and the surrounding m-terphenyl framework. <sup>1</sup> .....	224
Figure 6.3. Energy decomposition analyses of 1-hexane using model with different fragmentation: 1m-1 (Co-TMS + hexane), 1m-2 (terphenyl cage + hexane) and 1m-3 (tephenyl-Co-TMS + hexane). .....	225
Figure 6.4. Energy decomposition analyses of 1-hexane using model with different fragmentation: 1m-1mono (monoCo-TMS + hexane), 1m-2mono (mono terphenyl cage + hexane) and 1m-3mono (mono tephenyl-Co-TMS + hexane). .....	226
Figure 6.5. Energy decomposition analyses of 1-hexane using model with different fragmentation: 1m-4 (mono terphenyl cage + mono terphenyl cage) and 1m-5 (mono tephenyl-Co-TMS + methane). .....	227
Figure 6.6. (Left) Crystal structure of a <i>n</i> -hexane containing Co(SiMe <sub>3</sub> )(CNAr <sup>Mes2</sup> ) <sub>3</sub> inclusion complex, 1A-hexane. (Right) Crystal structure of (μ <sup>2</sup> - <i>N</i> -(N <sub>2</sub> C <sub>6</sub> H <sub>18</sub> )[Co(SiMe <sub>3</sub> )(CNAr <sup>Mes2</sup> ) <sub>3</sub> ] <sub>2</sub> (2). .....	229
Figure 6.7. Molecular structure of (μ <sup>2</sup> - <i>N</i> -(N <sub>2</sub> C <sub>6</sub> H <sub>18</sub> )[Co(SiMe <sub>3</sub> )(CNAr <sup>Mes2</sup> ) <sub>3</sub> ] <sub>2</sub> (2). Asymmetric unit shown with close contacts (light green) between the encapsulated 1,6-diaminohexane in light blue (nitrogen), orange (carbon) and red (hydrogen) and the surrounding m-terphenyl framework. ....	229
Figure 6.8. Stacked VT-NMR spectra of (μ <sup>2</sup> - <i>N</i> -(N <sub>2</sub> C <sub>6</sub> H <sub>18</sub> )[Co(SiMe <sub>3</sub> )(CNAr <sup>Mes2</sup> ) <sub>3</sub> ] <sub>2</sub> (2) in <i>d</i> <sub>8</sub> -THF. ....	231
Figure 6.9. Overlapped VT-NMR spectra of (μ <sup>2</sup> - <i>N</i> -(N <sub>2</sub> C <sub>6</sub> H <sub>18</sub> )[Co(SiMe <sub>3</sub> )(CNAr <sup>Mes2</sup> ) <sub>3</sub> ] <sub>2</sub> (2) in <i>d</i> <sub>8</sub> -THF zoomed in at the alkyl region. ....	231

Figure 6.10. Molecular structure of $(\text{C}_6\text{H}_{13}\text{NH}_2)[\text{Co}(\text{SiMe}_3)(\text{CNAr}^{\text{Mes}_2})_3]_2$ (4). Showing the encapsulated 1-hexylamine sitting in the <i>m</i> -terphenyl pocket. ....	232
Figure 6.11. Stacked VT-NMR spectra of $(\mu^2\text{-}N\text{-}(\text{N}_2\text{C}_6\text{H}_{18}))[\text{Co}(\text{SiMe}_3)(\text{CNAr}^{\text{Mes}_2})_3]_2$ (2) in $d_8$ -THF.....	237
Figure 6.12. Stacked VT-NMR spectra of (2) in $d_8$ -THF zoomed in at the aromatic proton region. ....	237
Figure 6.13. Stacked VT-NMR spectra of (2) in $d_8$ -THF zoomed in at the mesityl proton region. ....	238
Figure 6.14. Stacked VT-NMR spectra of (2) in $d_8$ -THF zoomed in at the alkyl proton region. ....	238
Figure 6.15. Stacked VT-NMR spectra of (2) in $d_8$ -THF zoomed in at the trimethylsilyl proton region. ....	239
Figure 6.16. Molecular structure of $(\mu^2\text{-}N\text{-}(\text{N}_2\text{C}_6\text{H}_{18}))[\text{Co}(\text{SiMe}_3)(\text{CNAr}^{\text{Mes}_2})_3]_2$ (2) with two benzene solvent molecule and hydrogen atoms omitted. ....	240
Figure 6.17. Molecular structure of $(\text{C}_6\text{H}_{13}\text{NH}_2)\text{Co}(\text{SiMe}_3)(\text{CNAr}^{\text{Mes}_2})_3$ (3) $\cdot 2\text{Et}_2\text{O}$ with two ether solvent molecule and hydrogen atoms omitted. ....	241
Figure 6.18. Molecular structure of $(\text{C}_6\text{H}_{13}\text{NH}_2)[\text{Co}(\text{SiMe}_3)(\text{CNAr}^{\text{Mes}_2})_3]_2$ (4) with benzene solvent molecule and hydrogen atoms omitted. ....	241



## LIST OF TABLES

Table 1.1. Crystallographic Data Collection and Refinement Information.....	26
Table 1.2. Crystallographic Data Collection and Refinement Information.....	27
Table 2.1. Observed Rate Constants in the Ligand Substitution Reaction of $\text{Co}(\text{CNAr}^{\text{Mes}2})_4$ by PhCCH Under Pseudo-First-Order Conditions with Extra $\text{CNAr}^{\text{Mes}2}$ Added. ....	42
Table 2.2. Crystallographic Data Collection and Refinement Information.....	73
Table 2.3. Crystallographic Data Collection and Refinement Information.....	74
Table 2.4. Crystallographic Data Collection and Refinement Information.....	75
Table 2.5. Crystallographic Data Collection and Refinement Information.....	76
Table 3.1. Calculated core bond angles of $\text{Co}(\text{CNAr}^{\text{Mes}2})_4$ $\text{C}_{3v}$ and $\text{D}_{2d}$ Isomers.....	99
Table 3.2. Calculated Frequencies and Symmetries of CN Stretching Modes in Relevant $\text{Co}(\text{CNAr}^{\text{Mes}2})_4$ $\text{C}_{3v}$ and $\text{D}_{2d}$ Isomers. ....	100
Table 3.3. Calculated Energy Differences Between $\text{Co}(\text{L})_4$ ( $\text{L} = \text{CNAr}^{\text{Ar}2}, \text{CNAr}^{\text{Mes}2}$ ) $\text{C}_{3v}$ and $\text{D}_{2d}$ Isomers Using Different Functional with 6-31g(d):lanl2dz basis sets. *All $\text{C}_{3v}$ in lower energy.....	101
Table 3.4. Calculated Energy Differences Between $\text{CoL}_4$ ( $\text{L} = \text{CO}, \text{CNMe}, \text{CNXyl}, \text{CNAr}^{\text{Ar}2},$ $\text{CNAr}^{\text{Mes}2}$ ) $\text{C}_{3v}$ and $\text{D}_{2d}$ Isomers Using 6-31g(d):lanl2dz basis sets. *All $\text{C}_{3v}$ in lower energy .....	102
Table 3.5. Calculated Core bond angles of $(t\text{BuNC})\text{Co}(\text{CNAr}^{\text{Mes}2})_3$ .....	114
Table 3.6. Calculated Frequencies and Symmetries of CN Stretching Modes in $(t\text{BuNC})\text{Co}(\text{CNAr}^{\text{Mes}2})_3$ .....	114
Table 4.1. Selected bond lengths and angles from solid-state structures of complexes 4 and 6- 10.....	130

Table 4.2. Comparison of calculated and experimental structural parameters between 4m and 4. ....	146
Table 4.3. Comparison of calculated and experimental structural parameters between 6m and 6. ....	149
Table 4.4. Summary of %V <sub>bur</sub> . ....	149
Table 4.5. Crystallographic Data Collection and Refinement Information.....	157
Table 4.6. Crystallographic Data Collection and Refinement Information.....	158
Table 4.7. Crystallographic Data Collection and Refinement Information.....	159
Table 5.1. Experimental and Computational Parameters of Compound 3, 3- <sup>15</sup> N, 3m, 4, 4- <sup>15</sup> N and 4m. ....	169
Table 5.2. Comparison of calculated and experimental structural parameters for 3. ....	196
Table 5.3. Comparison of calculated and experimental structural parameters for 4. ....	197
Table 5.4. Energy decomposition analyses of (N <sub>2</sub> O)Co(SiMe <sub>3</sub> )(CNAr <sup>Ph2</sup> ) <sub>3</sub> (3m) and (N <sub>2</sub> )Co(SiMe <sub>3</sub> )(CNAr <sup>Ph2</sup> ) <sub>3</sub> (4m) showing N <sub>2</sub> O binds more weakly than N <sub>2</sub> with E <sub>orb</sub> significantly lower for N <sub>2</sub> O. Energies are shown in kcal/mol.....	199
Table 5.5. Natural orbitals for chemical valence (NOCV) orbitals of (N <sub>2</sub> O)Co(SiMe <sub>3</sub> )(CNAr <sup>Ph2</sup> ) <sub>3</sub> (3m). NOCV1 involves σ-donation from the N <sub>2</sub> O ligand to the metal; NOCV2 and NOCV3 are the two perpendicular π-backbondings from metal to N <sub>2</sub> O, in competition with the CNAr <sup>Ph2</sup> ligands.....	198
Table 5.6. NOCV analyses of (N <sub>2</sub> O)Co(SiMe <sub>3</sub> )(CNAr <sup>Ph2</sup> ) <sub>3</sub> (3m) and (N <sub>2</sub> )Co(SiMe <sub>3</sub> )(CNAr <sup>Ph2</sup> ) <sub>3</sub> (4m) showing N <sub>2</sub> O and N <sub>2</sub> are each better π-acceptors than σ-donors. N <sub>2</sub> O is a	

weaker donor and a weaker acceptor than is N <sub>2</sub> . *stabilization energies for orbital components contributing to overall E <sub>orb</sub> . .....	199
Table 5.7. Equilibrium constants and Gibbs free energies determination.....	213
Table 5.8. Crystallographic Data Collection and Refinement Information.....	216
Table 6.1. Energy decomposition analyses of 1m-1, 1m-2 and 1m-3.....	226
Table 6.2. Energy decomposition analyses of 1m-1mono, 1m-2mono and 1m-3mono.....	227
Table 6.3. Energy decomposition analyses of 1m-4 and 1m-5. ....	228
Table 6.4. Crystallographic Data Collection and Refinement Information.....	242

## LIST OF SCHEMES

Scheme 1.1. Synthesis of $D_{3d}$ -type $\text{Co}_2(\text{CO})_4(\text{CNAr}^{\text{Mes}2})_4$ and $C_{2v}$ -type $(\mu\text{-CO})_2[\text{Co}_2(\text{CO})_2(\text{CNAr}^{\text{Dipp}2})]_2$ .	8
Scheme 1.2. Synthesis of $[\text{Co}(\text{CNAr}^{\text{Mes}2})_4]_n$ ( $n = 0$ and $-1$ ).	9
Scheme 1.3. Synthesis of the coordinatively unsaturated $\text{Co}(\text{SiMe}_3)(\text{CNAr}^{\text{Mes}2})_3$ .	10
Scheme 1.4. Synthesis of $[\text{Co}(\text{CNR})_3]_n$ ( $\text{CNR} = \text{CNAr}^{\text{Dipp}2}$ or $\text{CNAr}^{\text{Tripp}2}$ , $n = 0, -1$ ) series....	12
Scheme 1.5. Synthesis of $\text{I}_2\text{Co}(\text{CNR})_2$ and $\text{ICo}(\text{CNR})_3$ .	13
Scheme 2.1. Synthesis of $\text{Co}(\text{L})(\text{CNAr}^{\text{Mes}2})_3$ Complexes 1-7.	36
Scheme 2.2. Potential Mechanisms for the Ligand Substitution Chemistry of $\text{Co}(\text{CNAr}^{\text{Mes}2})_4$ .	40
Scheme 2.3. Synthesis of Complexes 8-11.	44
Scheme 4.1. (top) Step-wise synthesis of cluster 4 through complex 2 and 3. (bottom) Synthesis of cluster 6.	127
Scheme 4.2. Reaction scheme of 4 and 6 showing the nucleophilicity of the bridging phosphide.	131
Scheme 5.1. Synthesis of 2 and Its Two Reaction Pathways to Form 3. Path A leads to an orange solution (3-solution) that shows reversible $\text{N}_2\text{O}$ binding, path B leads to an orange solid (3-solid) that is stable under vacuum. The molecular structure of 3 is also shown with thermal ellipsoid set at 30% probability.	167
Scheme 5.2. Reaction scheme of $\text{N}_2\text{O}$ and $\text{N}_2$ binding equilibrium on 2 under $18^\circ\text{C}$ in a $d_8$ -toluene solution.	169
Scheme 5.3. <i>O</i> -atom Transfer Reaction of 3 in $\text{C}_6\text{D}_6$ Solution to Generate 4 and $\text{OCNAr}^{\text{Mes}2}$ .	173

Scheme 5.4. (Left) Reaction condition of 4 catalyzed N <sub>2</sub> O oxidation of isocyanides to isocyanates. (Right) Published reaction condition of (N <sub>2</sub> )CoH(PPh <sub>3</sub> ) <sub>3</sub> catalyzed N <sub>2</sub> O oxidation of phosphines to phosphine oxides.....	174
Scheme 5.5. Proposed mechanism for the decomposition <i>O</i> -atom transfer of 3. ....	175
Scheme 5.6. Reaction scheme of N <sub>2</sub> O and N <sub>2</sub> binding equilibrium on 2 under 18°C in a <i>d</i> <sub>8</sub> -toluene solution. ....	212
Scheme 6.1. Synthesis of the coordinatively unsaturated Co(SiMe <sub>3</sub> )(CNAr <sup>Mes2</sup> ) <sub>3</sub> (1) and its coordination chemistry towards L-type ligands. ....	222

## ACKNOWLEDGEMENTS

I have always wondered what the end of PhD would be like, but I guess it is just another comma in life while we are on our way to our bigger dreams. I once read a quote somewhere that is obviously in mandarin, but I am going to use my poor translation skills to transcribe: “If you believe in what you do with your whole heart, just do it, and you will meet people along the way to support you.” Indeed, I will not be here without the help from many people who show up in my journey.

First of all, I want to thank my advisor Josh Figueroa. I still remember my first interaction with Josh back in Winter 2014 when I was 5 years younger and naïve. It was a skype interview to get into UCSD, where the conversation is no longer remembered but left with a picture in my head of a very enthusiastic and brilliant human being and his one-year old baby kid. There was really no hesitation for me to join the lab at the time, I was attracted to the Figueroa Chemistry and dedicated to it. (I doubt anyone would not if the first reaction they have ever done in the lab worked and got crystals. This has to be our future recruiting strategy.) I am really grateful to Josh who shows only support and trust throughout my whole PhD program even when I was young and still did not know what I was doing. His passion towards science really keeps students going and pushes us to our maximum abilities. Quote from Alex Carpenter, “he has gone above and beyond what any doctoral student could ask for.”

The second important people I need to thank is the Figueroa group. All the people that I have worked with had made my 5 years of research life more than just fun. To the “scary” first generation (a.k.a. ABCD): I will never forget the lab with Alex Carpenter, his fanaticism towards science and how that dragged the whole lab into it. I have to honestly say that he has set the lab standard, intense but driven by chemistry. Brandon, who I don't think I get to talk to

until my second year, every conversation with him since were all great advice and smart inputs on how we should be doing things. He definitely made grad school look easy. The most unforgettable thing with Chuck is how he saved a little first year when she was nearly freaking out in the glovebox when the fritted was clogged during her first time making  $\text{LiAr}^{\text{Mes}2}$ . I will not mention who that little first year is, but you do feel extra very super extremely safe whenever you are working with Chuck. Doug is the most efficient person I have ever seen; he always has a specific goal and am always working towards it. He helped me probably one of the most in the beginning when I was still sharing the glove box with him and Kyle.

To the second and the most important generation I am in: Kyle, you match everything I thought of a popular guy in those American high school movies before I came to the US, besides you are a little older. This is a compliment. I think I feel the most comfortable talking to you about my struggle in research/life and you are always a great listener. Your passion towards chemistry also inspires me a lot, same as Myles'. I could not be happier to learn that Myles was joining the lab with me even though it took him a minute to decide. But it has been great in past five years where we discussed about projects, future career plans and "dream molecules". To highlight, Ale is probably the best of all in my personal opinion. Maybe I did not talk to you in my first year either, but I think you will agree with me that we are now best friends and I sincerely wish to continue this relationship after I graduate. As I always say, Michael talks too much. But Mike is actually great to have in lab and very needed when meeting with new people. He has taught me so many random American cultures and is giving full energies to everyone all the time. To the newbies in the Figueroa group: Vincent, you have brought all the positives to the lab and gave me lots of valuable advice at the most needed time. Heaun, Ritchie and Adam, it is very brave of you to join the lab when there was a two-year gap, but we are all here

for a reason. I believe in you and look forward to seeing all the new molecules/materials that you will be making.

I also want to thank the X-ray Crystallography and the NMR facilities. Prof. Arnie Rheingold for letting me access to one of the best small-molecular crystallography facilities on the planet. Dr. Curtis Moore and Dr. Milan Gembicky, both of you have helped me and taught me everything I know about crystallography. I am also very grateful of Dr. Anthony Mrse for answering my NMR instrument trouble shoot texts at any time. Him and Dr. Xuemei Huang have helped me a lot through the hardest project in my PhD with all the  $^{15}\text{N}$  NMR measurements. I would like to thank my committee members Prof. Cliff Kubiak, Prof. Guy Bertrand, Prof. Wei Xiong, Prof. Adam Burgasser and Prof. Dionicio Siegel for the support through my PhD program with all the valuable discussions. Prof. Charles Perrin, Prof. Stanley Opella and Dr. Anna De Angelis are also thanked for the guidance of  $^{15}\text{N}$  NMR kinetic and solid-state NMR experiments. Prof. Cliff Kubiak and Dr. Taylor Porter for the access of UV-Vis instrumentation. My collaborators: Prof. Wei Xiong and Dr. Jiaxi Wang for figuring out the 2D-IR study on one of the most air sensitive compounds. Prof. Francesco Paesani and Colin Egan for the computation input on the most complicated system we have. And of course Aaron for making sure we work late every day!

Other than people that I work with, I would like to express my thanks to all my friends whether in the US or across the Pacific Ocean back in Taiwan. Dr. Pauline Olsen for being my first US friend. My ex-roommate Xu Ji and friend Shaun Li who helped me through a very tough time, Tianjiao Zhang and Dr. Yina Wei for the late-night chats after a whole day of work. Also, my material science PhD friends Haowen Ren, Shuai Zhang, Yu Gang, Shi Chen and Yuesong Shi. Not to mention my basketball buddies for keeping me in shape both physically



and mentally, Dr. Cheryl Cai, Zhong Zeng, Dr. Xin Li and Jeff Wang. Dr. Kevin Hung for being my best friend since collage and I am really grateful to have an old friend that lives “close”. Also, my best and only roomies from college Ling Ziting, Yuting Su, Vera Chen, Suende Wong and Rongjing Lin, even though we only meet once a year now, but I love you all.

Most importantly, Heidou Zhu (a.k.a. Blackbean, Bean Cat) and the person who stole my cat, Ben Zhou. I am still very grateful that you decided to ask me out to play basketball with you on the bus back in the recruitment weekend 2017. Grad school with you is the best grad school I can ever imagine. Thank you for being here with me. And thank you bean cat for just continue being the cutest. I also want to thank Ben’s parents for welcoming me and making me feel like home every time I visit. It is nice to have a US family to avoid being homesick too much.

Lastly, I want to thank my family for supporting me. I know me leaving the country is hard for my grandparents, but they have never talk me down. Every time I call them, they only ask if I have enough money and if I am eating well. My parents have also always been encouraging to what I want to do even that means seeing me only once a year. I am very grateful to have you as my grandparents and parents, and I feel extremely lucky. Thanks to my younger brother, my aunt and uncle-in-law for the support too.

I would not have been here without any of these helps. Many thanks again to these people and others who support me in the past years.

In Chapter 1, complexes discussed in section 1.4-1.6 are currently in preparation for publication by C. Chan, M. L. Neville, C. Mokhtarzadeh, A. L. Rheingold, J. S. Figueroa. The dissertation author is the primary author of this manuscript.

Chapter 2, in part, is a reprint of the material as it appears in C. Chan, A. E. Carpenter, M. Gembicky, C. E. Moore, A. L. Rheingold, J. S. Figueroa “Associative Ligand Exchange and Substrate Activation Reactions by a Zero-Valent Cobalt Tetraisocyanide Complex,” *Organometallics.*, **2019**, 38, 1436-1444. Copyright 2019, American Chemical Society. The dissertation author is the first author of this work.

Chapter 3 is currently in preparation as a manuscript by C. Chan, J. Wang, Y. Li, Xiang, B., W. Xiong, J. S. Figueroa. The dissertation author is the primary author of this manuscript. Prof. Clifford P. Kubiak and Tyler M. Porter are thanked for providing access to variable-temperature FTIR instrumentation and helpful discussions.

Chapter 4 is currently in preparation as a manuscript by C. Chan, M. L. Neville, M. Gembicky, A. L. Rheingold, J. S. Figueroa. The dissertation author is the primary author of this manuscript.

Chapter 5 is currently in preparation as a manuscript by C. Chan, A. E. Carpenter, R. P. Hughes, A. L. Rheingold, J. S. Figueroa. The dissertation author is the primary author of this manuscript. Prof. Stanley Opella, Prof. Charles L. Perrin, Dr. Anthony Mrse and Dr. XueMei Huang are thanked for assist of  $^{15}\text{N}$  NMR data collection and valuable discussions.

Chapter 6 is currently in preparation as a manuscript by C. Chan, A. E. Carpenter, C. K. Egan, M. Gembicky, C. E. Moore, A. L. Rheingold, F. Paesani, J. S. Figueroa. The dissertation author is the primary author of this manuscript.

## VITA

**2013 Bachelor of Science**, Chemistry, National Tsing Hua University, Taiwan

**2016 Master of Science**, Chemistry, University of California San Diego, USA

**2019 Doctor of Philosophy**, Chemistry, University of California San Diego, USA

## PUBLICATIONS

### Dissertation Related

**C. Chan**, A. E. Carpenter, M. Gembicky, C. E. Moore, A. L. Rheingold, J. S. Figueroa “Associative Ligand Exchange and Substrate Activation Reactions by a Zero-Valent Cobalt Tetraisocyanide Complex,” *Organometallics.*, **2019**, 38, 1436-1444.

**C. Chan**,<sup>+</sup> J. Wang,<sup>+</sup> Y. Li, B. Xiang, J. S. Figueroa, W. Xiong “Direct Observation of Conformational Dynamics in Zerovalent CoL<sub>4</sub> Complexes by 2D IR Spectroscopy,” *In Preparation*. <sup>+</sup>These authors contribute equally to this work.

**C. Chan**, A. E. Carpenter, R. P. Hughes, A. L. Rheingold, J. S. Figueroa “Dinitrogen Exchange and Intramolecular Oxygen-Atom-Transfer Behavior of a Persistent End-On Nitrous Oxide Complex of Cobalt,” *In Preparation*.

**C. Chan**, M. L. Neville, A. L. Rheingold, J. S. Figueroa “Controlled Step-wise Synthesis of a Nucleophilic Cobalt-phosphide Cluster,” *In Preparation*.

**C. Chan**, M. L. Neville, C. C. Mokhtarzadeh, A. L. Rheingold, J. S. Figueroa “Isolation of the First 15-electron CoL<sub>3</sub> Metalloradical,” *In Preparation*.

**C. Chan**, A. E. Carpenter, C. K. Egan, M. Gembicky, C. E. Moore, A. L. Rheingold, F. Paesani, J. S. Figueroa. “Solid State Host-Guest Interaction of *n*-Hexane with a Coordinatively Unsaturated Cobalt *m*-Terphenyl Isocyanide Complex,” *In Preparation*.

### Others

A. E. Carpenter, **C. Chan**, A. L. Rheingold, J. S. Figueroa “A Well-Defined Isocyno Analogue of HCo(CO)<sub>4</sub>. 2: Brønstead Acidity as a Function of Isocyanide Ligation,” *Organometallics.*, **2016**, 35, 2319-2326.

C. C. Mokhtarzadeh, **C. Chan**, C. E. Moore, A. L. Rheingold, J. S. Figueroa “Side-On Coordination of Nitrous Oxide to a Mononuclear Cobalt Center,” *J. Am. Chem. Soc.*, **2019**, 141, 15003-15007.

## ABSTRACT OF THE DISSERTATION

Low Valent Cobalt Isocyanides: Exploration of Small Molecule Activations and Cobalt Phosphide Cluster Building Blocks

by

Chinglin Chan

Doctor of Philosophy in Chemistry

University of California San Diego, 2019

Professor Joshua S. Figueroa, Chair

Sustained interest in the unsaturated mononuclear cobalt carbonyls arises from their presumed role as reactive intermediates in industrial hydroformylation and carbonylation processes, yet their observations have been limited to low temperature matrix isolations. Herein, we report a full library of isolobal analogues of unsaturated cobalt carbonyl complexes by using sterically encumbering *m*-terphenyl isocyanides. A detailed mechanistic study on both the

reactivity of  $\text{Co}(\text{CNAr}^{\text{Mes}2})_4$  along with the unique bond activation processes of  $(\text{SiMe}_3)\text{Co}(\text{CNAr}^{\text{Mes}2})_3$  with  $\text{N}_2\text{O}$  are presented. For the latter system, a demonstration of the catalytic capability of these cobalt complexes for the production of organoisonocyanates is presented, which provides an exciting opportunity to produce value-added products using  $\text{N}_2\text{O}$  as a terminal oxidant. Furthermore, a dispersion forced solid-state host-guest interaction with *n*-hexane is discussed with support of EDA (Energy Decomposition Analysis) calculation. A solution-phase persistence weakly coordinated 1,6-diaminohexane dimer complex,  $(\mu^2\text{-}N\text{-}(\text{N}_2\text{C}_6\text{H}_{18})[\text{Co}(\text{SiMe}_3)(\text{CNAr}^{\text{Mes}2})_3]_2$ , was made and the  $\text{CH}/\pi$  interactions was monitored by VT-NMR (Variable Temperature Nuclear Magnetic Resonance), providing new insight into the existence of  $\sigma$ -alkane adducts of  $\text{Co}(\text{SiMe}_3)(\text{CNAr}^{\text{Mes}2})_3$  forced by van der Waals ( $\text{CH}/\pi$ ) interactions in the solid-state. Solution phase 2D-IR (Ultrafast Two-Dimensional Infrared Spectroscopy) data and DFT (Density Functional Theory) calculations presented to provide the direct observation of rapid isomerization of  $\text{Co}(\text{CNAr}^{\text{Mes}2})_4$  between the  $\text{C}_{3v}$  and  $\text{D}_{2d}$  isomers. Furthermore, for the first time, a controlled, stepwise cobalt phosphide cluster synthesis using cobalt metallates as building blocks is achieved.

# Chapter 1 Isocyano Analogues of Unsaturated Low-valent Cobalt Carbonyls

## 1.1 Introduction – Transition Metal Carbonyls

For decades, unsaturated metal carbonyls (e.g.,  $\text{Fe}(\text{CO})_4$ ,  $\text{Co}(\text{CO})_4$  and  $\text{Ni}(\text{CO})_3$ ) have been known for their key presence in numerous catalytic cycles (e.g., hydroformylation and hydrosilylation) and their outstanding abilities toward small molecule activation (Figure 1.1).<sup>1-</sup>  
<sup>5</sup> However, due to their high thermal and kinetic instability, these reactive carbonyl species have not been isolated and their direct observation is limited only to experiments conducted in cryogenic inert-gas matrices.<sup>4,6,7</sup> For example, observation of these unsaturated transition metal carbonyls are primarily limited to cryogenic infrared matrix isolation studies, where generation via photo-dissociation of a carbonyl ligand (CO) in an “inert” matrix (e.g.  $\text{N}_2$ , Ar,  $\text{CH}_4$ ) provides a method for their observation.<sup>8-10</sup> As a result, there is limited structural information and few reactivity studies on these metal carbonyls. Even for well-studied metal carbonyls, a considerable number of uncertainties persist. For instance, it is unclear whether  $\text{Co}(\text{CO})_4$  adopts a  $\text{C}_{3v}$ ,  $\text{D}_{2d}$  or  $\text{C}_{2v}$  structure;<sup>11-15</sup> with DFT calculations suggest all geometries are within 2-3 kcal/mol of each other.<sup>16,17</sup> The dimeric form,  $\text{Co}_2(\text{CO})_8$ , continues to elude structural authentication in its  $\text{D}_{2d}$  geometry.<sup>18-20</sup> In the investigations proceeded this thesis, we have placed a particular emphasis on understanding the chemistry of mononuclear cobalt carbonyls

(e.g.,  $\text{Co}(\text{CO})_4$  and  $\text{XCo}(\text{CO})_3$  ( $\text{X} = \text{H}, \text{SiR}_3$ )) due to the presumed role as reactive intermediates in industrial hydroformylation and carbonylation processes using their isocyano analogues.<sup>2,3,14,21</sup>

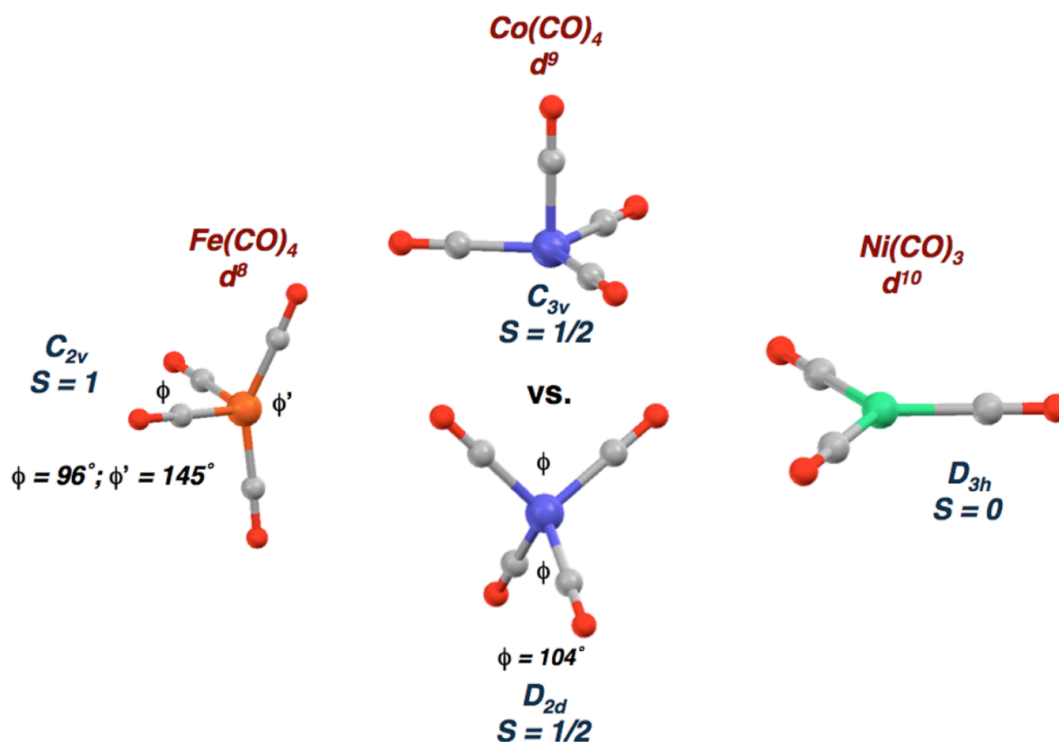


Figure 1.1. Predicted geometries of late transition-metal unsaturated binary carbonyls  $\text{Fe}(\text{CO})_4$  (left),  $\text{Co}(\text{CO})_4$  (center), and  $\text{Ni}(\text{CO})_3$  (right) with corresponding geometries and electronic states denoted.

## 1.2 Isocyanides as Surrogates for Carbonyls

Isocyanides ( $:\text{C}\equiv\text{N}-\text{R}$ ) are often viewed as surrogates for carbonyl ( $:\text{C}\equiv\text{O}$ ) due to their isolobal relationship. Shown in Figure 1.3, both ligand types possess a non-bonding lone-pair that is available for  $\sigma$ -donation, and low-lying  $\pi^*$  orbitals that are available for metal-to-ligand back donation. The isolobal relationship is illustrated in Figure 1.2 through the comparative DFT calculated molecular orbitals of carbon monoxide, CO and the aryl isocyanide,  $\text{CNAr}^{\text{Mes}2}$ .

As a result, isocyanides coordinate transition metals in a manner analogous to CO (Figure 1.3) and generally replicate the coordination geometry and electronic structure of metal carbonyls. Indeed, isocyano analogues to the binary transition-metal carbonyls have been synthesized. However, these transition-metal isocyanides are all coordinatively saturated despite the increased steric profile of isocyanides when compared to CO.<sup>22-26</sup>

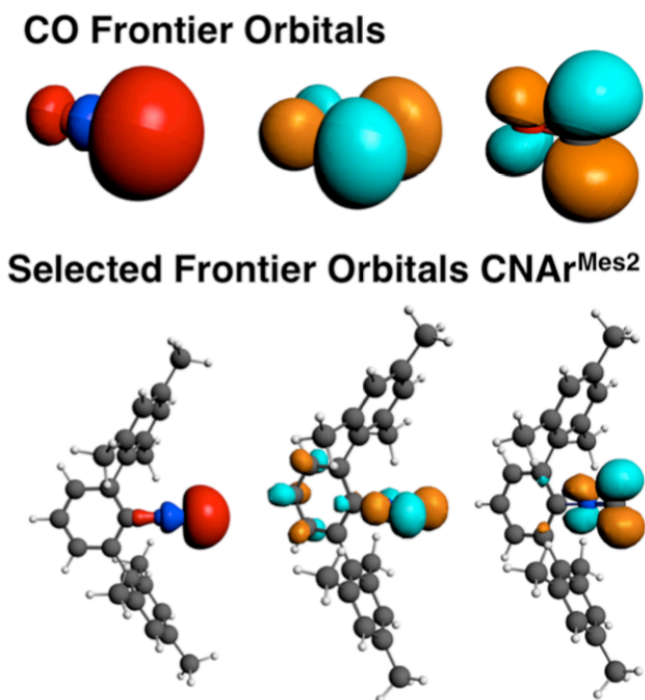


Figure 1.2. Calculated frontier orbitals (BP86/TZ2P; iso = 0.04) used in metal bonding for carbonyl and the aryl isocyanide CNAr<sup>Mes2</sup>.<sup>27</sup>

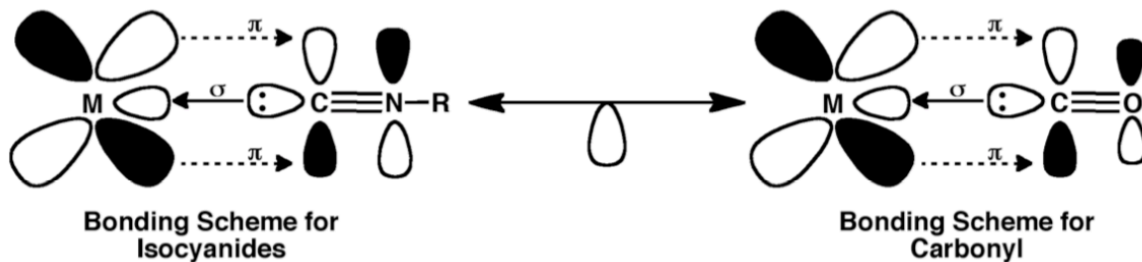


Figure 1.3. Qualitative molecular orbital representations for transition metal isocyanide and transition metal carbonyl bonding.<sup>27</sup>



Importantly, isocyanides also present the opportunity to modulate both the ligand electronic and steric profile through the N- bound organic backbone/substituent. To target unsaturated transition metal complexes that mimic the unsaturated carbonyls, our group has employed isocyanide ligands that feature the sterically encumbering *m*-terphenyl units. The *m*-terphenyl framework has shown a wide array of use as a ligand scaffold to transition metals for steric protection and stabilization. For example, purely  $\sigma$ -aryls,<sup>28,29</sup> amidos,<sup>30,31</sup> imidos,<sup>31,32</sup> thiolates,<sup>33</sup> and carboxylates<sup>34,35</sup> *m*-terphenyl complexes are well-known.

Since 2008, our group has created a library of sterically encumbered *m*-terphenyl isocyanide ligands shown in Figure 1.4.<sup>36-38</sup> Among them, we can effectively lower the  $\sigma$ -donor/ $\pi$ -acid ratio of an isocyano group by using distal polyfluorination in the CNp-FAr<sup>DArF2</sup> derivatives. However, the study of the electronic properties of these isocyanides demonstrate that the degree to which substituent variation can affect the electronic influence of an isocyano unit is substantially limited. Regardless, taking advantage of the steric properties provided by these *m*-terphenyl isocyanides, we have succeeded in isolating relatively stable isocyano mimics of a variety of reactive, unsaturated metal carbonyl complexes.<sup>37,39-42</sup> Shown in Figure 1.5 are some selected thermostable isocyano analogues to their earlier mentioned transition metal carbonyls.<sup>40,44-45</sup>

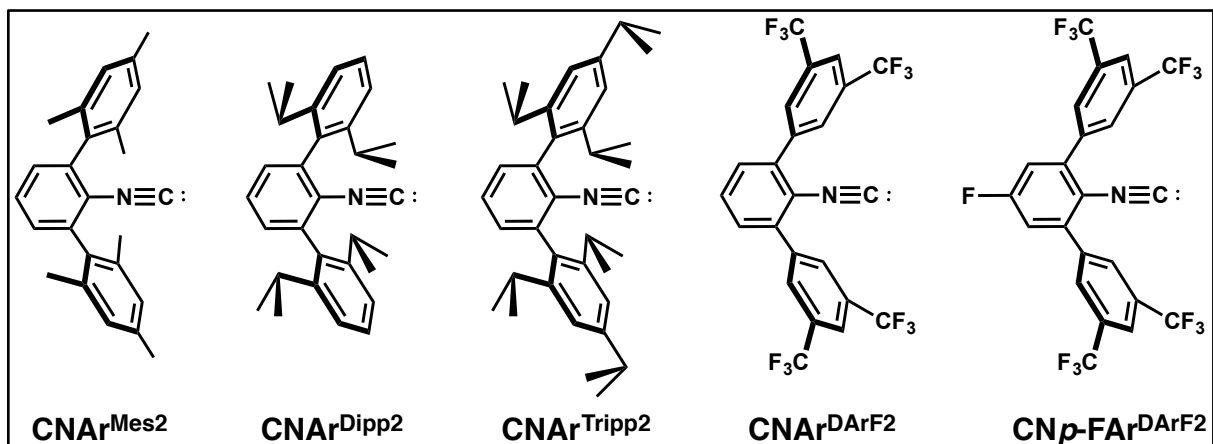


Figure 1.4. Prototypical *m*-terphenyl isocyanide ligands with varying electronic and steric profiles. (Left to right) CNAr<sup>Mes</sup>2, CNAr<sup>Dipp</sup>2, CNAr<sup>Tripp</sup>2, CNAr<sup>DARF</sup>2, *p*-F-CNAr<sup>DARF</sup>2.

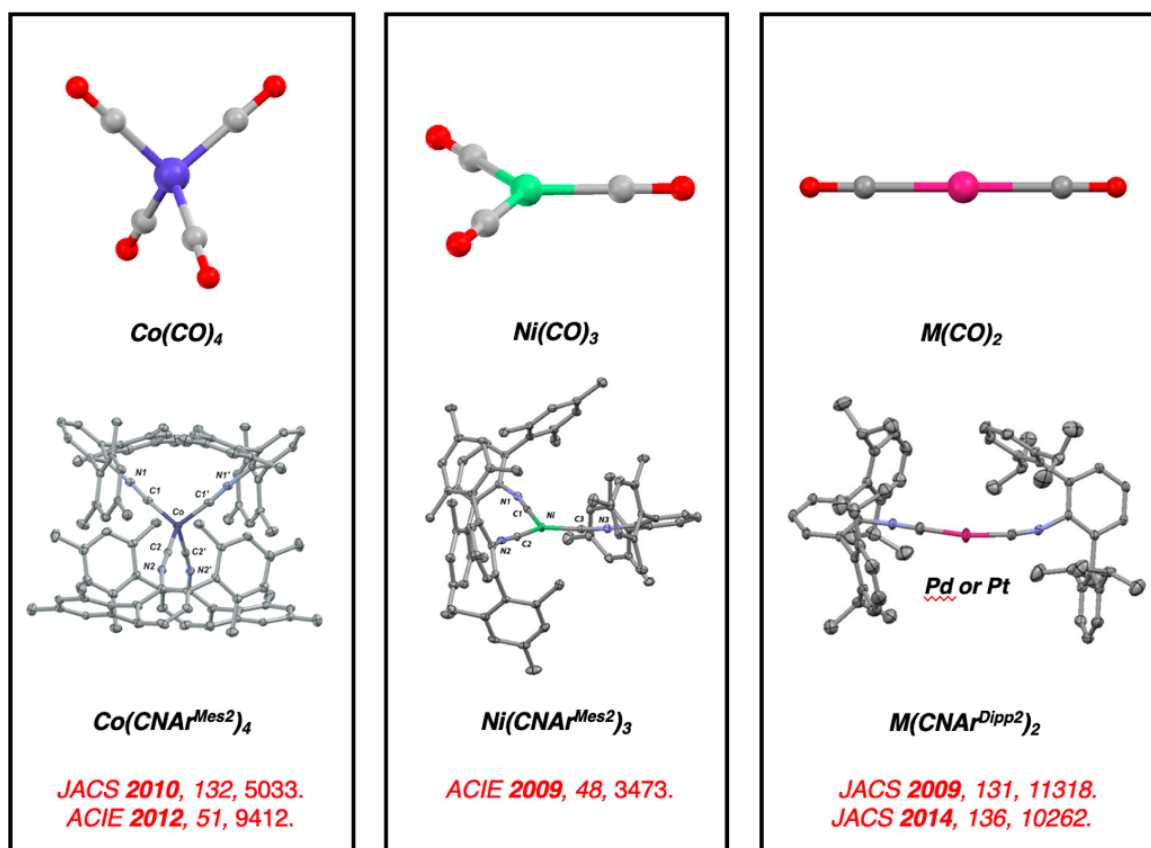


Figure 1.5. Selected thermostable isocyano analogues of unsaturated transition metal carbonyls.

More recently, we are able to extend our *m*-terphenyl isocyanides to low-valent transition metal cluster research. (Figure 1.6) By using the sterically encumbered CNAr<sup>Dipp</sup>2

ligand, a single layer of the normally stacked “chini clusters” is able to be isolated as a stable analogue.<sup>46</sup> Furthermore, we are able to enhance the nucleophilicity of an iron-nitride cluster by substituting carbonyl ligands with isocyanides.<sup>47</sup> As it is important to note, isocyanides are stronger  $\sigma$ -donors and weaker  $\pi$ -acceptors than CO that have been extensively employed as surrogates for carbon monoxide in the generation of neutral and anionic transition metal species.<sup>22-26,48-50</sup> Isocyano analogues to classical metal carbonyls (e.g.,  $\text{Fe}(\text{CN}t\text{-Bu})_5$ ) often exhibit greater nucleophilicity and diminished Brønsted acidity relative to their carbonyl congeners (e.g.,  $\text{Fe}(\text{CO})_5$ ).<sup>50</sup> Our study of equilibrium Brønsted acidities of a series of hydride complexes with the formulation  $\text{HCo}(\text{CO})_{4-n}(\text{CNR})_n$  ( $n = 0-4$ ) also showed that isocyanide complexes exhibit decreased Brønsted acidity relative to their carbonyl congeners.<sup>51</sup>

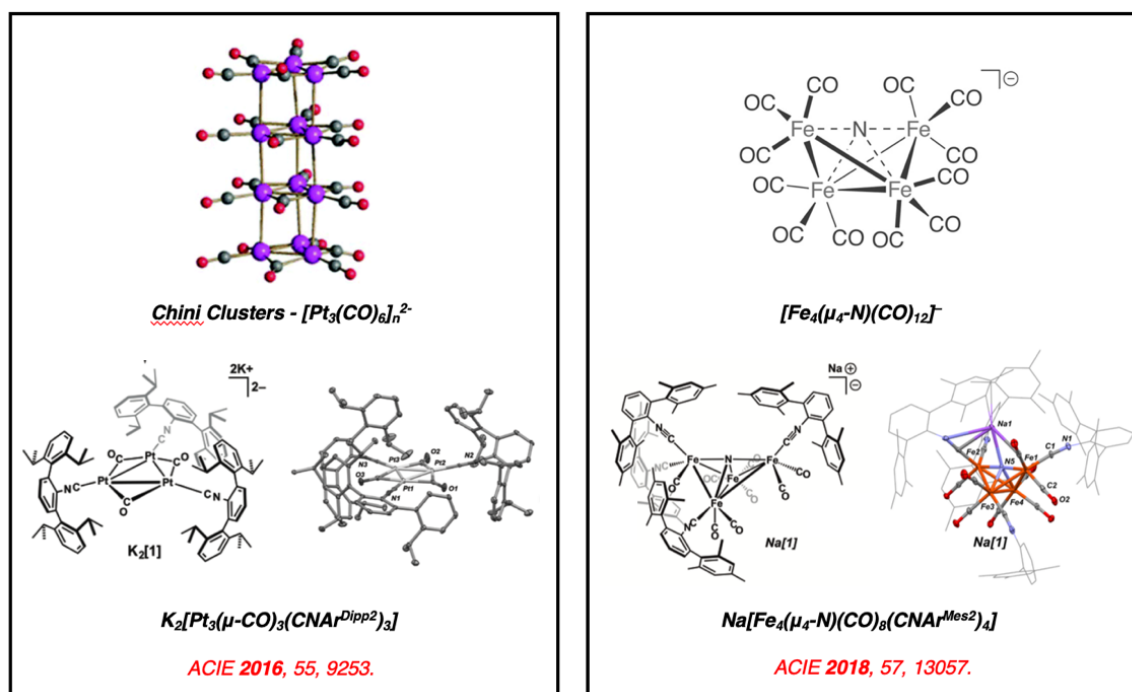
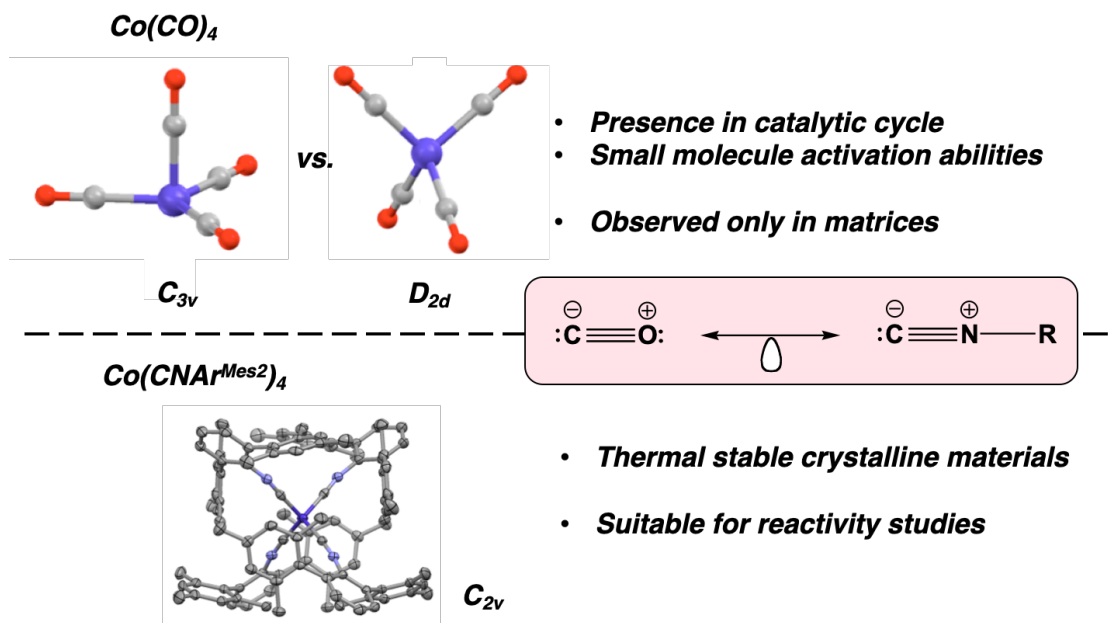


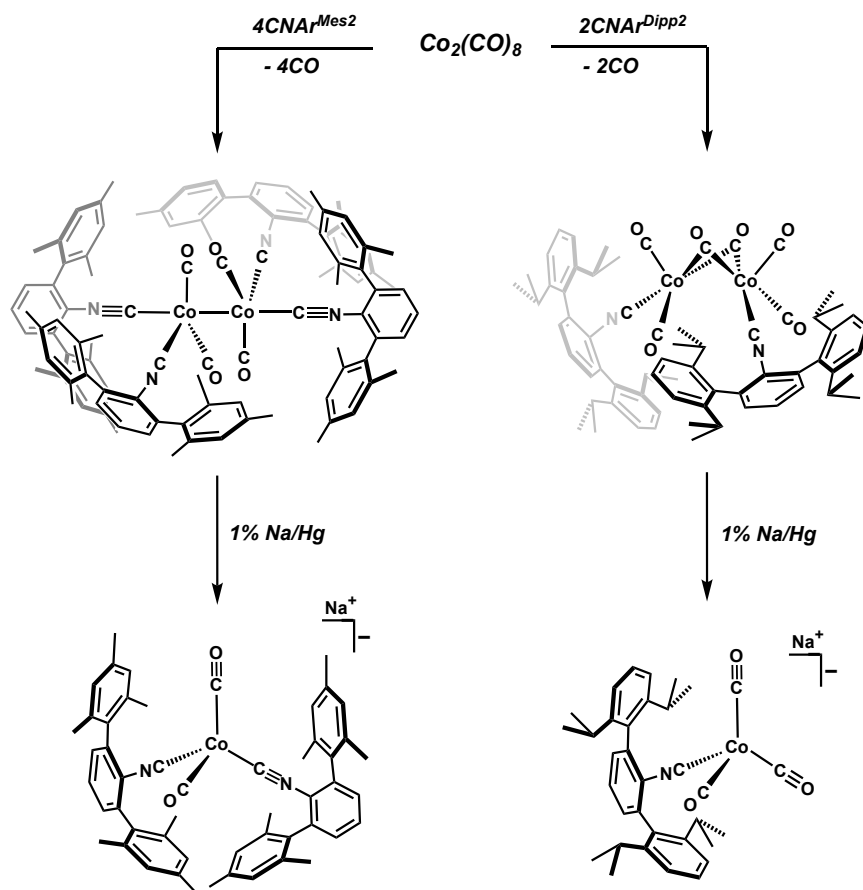
Figure 1.6. Selected thermostable isocyano analogues of transition metal carbonyl clusters.



**Figure 1.7 Abstract Image of Thesis: Low Valent Cobalt Isocyanides - Exploration of Small Molecule Activations and Cobalt Phosphide Cluster Building Blocks.**

### 1.3 Unsaturated Low-Valent Cobalt Isocyanides

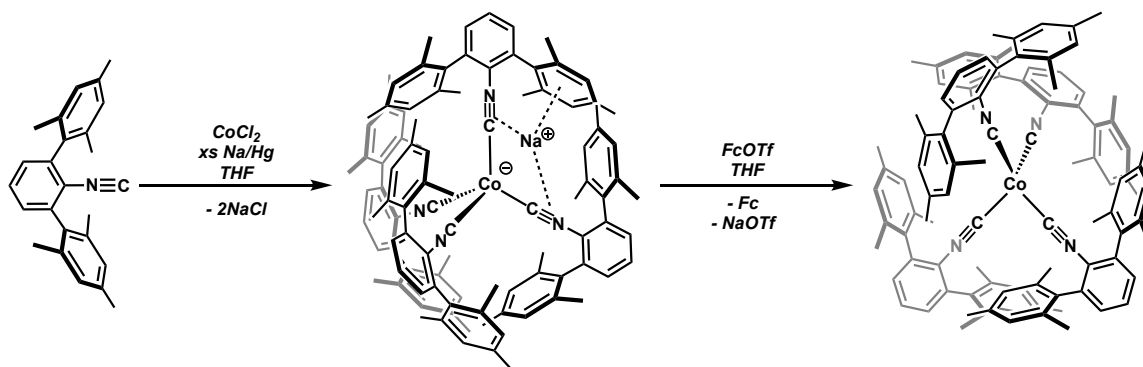
Given what we have learned about *m*-terphenyl isocyanides, we focus here on the cobalt isocyanides due to the presumed role of cobalt carbonyls as reactive intermediates in industrial hydroformylation and carbonylation processes as mentioned earlier. Synthetic entry to the stable  $\text{Co}_2(\text{CO})_{8-n}\text{L}_n$  ( $n = 2$  and  $4$ ,  $\text{L} = \text{CNAr}^{\text{Mes}2}$  and  $\text{CNAr}^{\text{Dipp}2}$ ) dimers are achieved by addition of  $\text{CNAr}^{\text{Mes}2}$  or  $\text{CNAr}^{\text{Dipp}2}$  to  $\text{Co}_2(\text{CO})_8$ .<sup>52</sup> (Scheme 1.1) Further reduction with sodium amalgam is able to generate a low-valent mixed isocyanide/carbonyl cobalt anion series,  $\text{Na}[\text{Co}(\text{CO})_{4-n}(\text{L})_n]$  ( $n = 2$  or  $3$ ,  $\text{L} = \text{CNAr}^{\text{Mes}2}$  and  $\text{CNAr}^{\text{Dipp}2}$ ),<sup>51</sup> which are discovered to be ideal cobalt phosphide cluster building blocks discussed in Chapter 4.



**Scheme 1.1.** Synthesis of  $D_{3d}$ -type  $\text{Co}_2(\text{CO})_4(\text{CNAr}^{\text{Mes}2})_4$  and  $C_{2v}$ -type  $(\mu\text{-CO})_2[\text{Co}_2(\text{CO})_2(\text{CNAr}^{\text{Dipp}2})_2]$ .

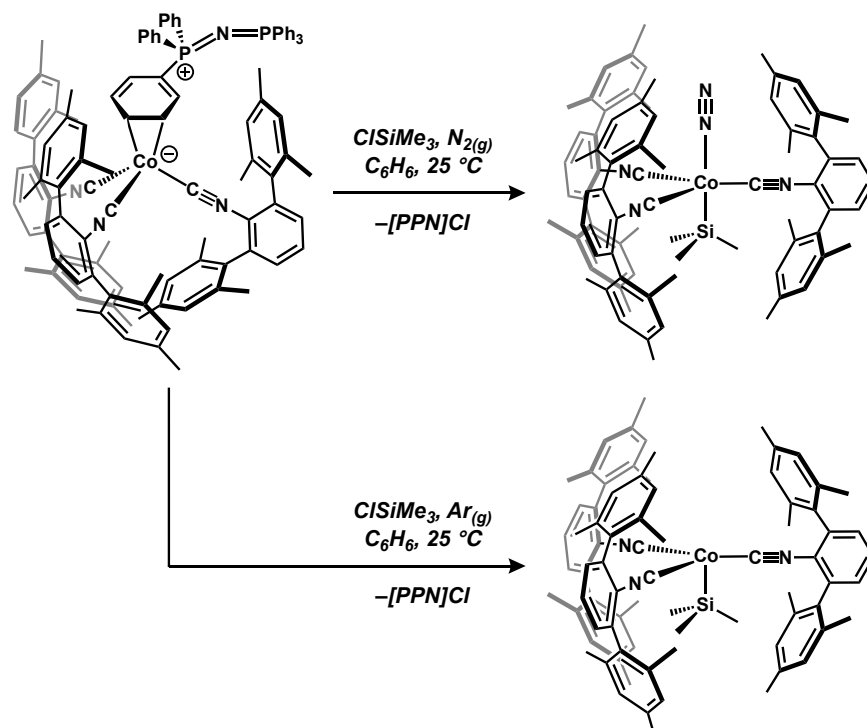
The homoleptic  $[\text{Co}(\text{CNAr}^{\text{Mes}2})_4]_n$  ( $n = +1, 0, -1$ ) system (Scheme 1.3) is achieved by the addition of sodium amalgam to a  $\text{CoCl}_2/\text{CNAr}^{\text{Mes}2}$  mixture in THF.<sup>43</sup> This protocol provides the dark red tetrakisocyanometallate salt  $\text{Na}[\text{Co}(\text{CNAr}^{\text{Mes}2})_4]$ , crystallographically characterized as a contact ion pair with interactions between the Na cation and isocyano CN units. Further treatment of  $\text{Na}[\text{Co}(\text{CNAr}^{\text{Mes}2})_4]$  with 1 equiv. of ferrocenium triflate ( $\text{FcOTf}$ ) affords the neutral, paramagnetic complex  $\text{Co}(\text{CNAr}^{\text{Mes}2})_4$  as determined by X-ray diffraction. In chapter 2 and 3, the zero-valent  $\text{Co}(\text{CNAr}^{\text{Mes}2})_4$  is shown to display a broad reactivity profile, including ligand exchange with L-type ligands (e.g. olefins, alkynes, aldehydes and phosphines), elemental phosphorus and sulfur activation and  $1e^-$  chemistry with certain substrates.<sup>53</sup> In

collaboration with Prof. Xiong's lab, solution phase 2D-IR (Ultrafast Two-Dimensional Infrared Spectroscopy) was utilized to observe the rapid isomerization of  $\text{Co}(\text{CNAr}^{\text{Mes}_2})_4$ . Combined with DFT calculations, this kinetically stable  $\text{Co}(\text{CO})_4$  analogue showed ultrafast conformation exchange dynamics between its  $\text{C}_{3v}$  and  $\text{D}_{2d}$  geometries on a 0.5 to 1 ps scale, with activation energies of 0.5 ( $\Delta\text{Ea}(\text{D}_{2d}\text{-C}_{3v})$ ) and 1.9 ( $\Delta\text{Ea}(\text{C}_{3v}\text{-D}_{2d})$ ) kcal/mol at room temperature.



**Scheme 1.2.** Synthesis of  $[\text{Co}(\text{CNAr}^{\text{Mes}_2})_4]_n$  ( $n = 0$  and  $-1$ ).

Previously we have shown that by treating  $(\eta^2\text{-PPN})\text{Co}(\text{CNAr}^{\text{Mes}_2})$  with excess chlorotrimethylsilane under a dinitrogen atmosphere, we are also able to access the  $\text{N}_2$  coordinated  $(\text{N}_2)\text{Co}(\text{SiMe}_3)(\text{CNAr}^{\text{Mes}_2})_3$ .<sup>54</sup> (Scheme 1.3) Interestingly, the coordinatively unsaturated  $16e^-$   $\text{Co}(\text{SiMe}_3)(\text{CNAr}^{\text{Mes}_2})_3$ , which is the isolobal analogue of  $\text{HCo}(\text{CO})_3$ , can be isolated with the same reaction condition but under an argon atmosphere with rigorous exclusion of Lewis bases, such as dinitrogen. Single-crystal X-ray diffraction studies showed a trigonal monopyramidal geometry in the solid-state with DFT calculations supporting a low-lying cobalt  $d_{z^2}$  LUMO suitable for small molecule binding.<sup>27,55</sup> Further reactivity of this molecule showing unique small molecule activation like nitrous oxide ( $\text{N}_2\text{O}$ ) and unusual van der Waals interaction with alkanes in the solid-state materials are discussed in Chapter 5 and 6.

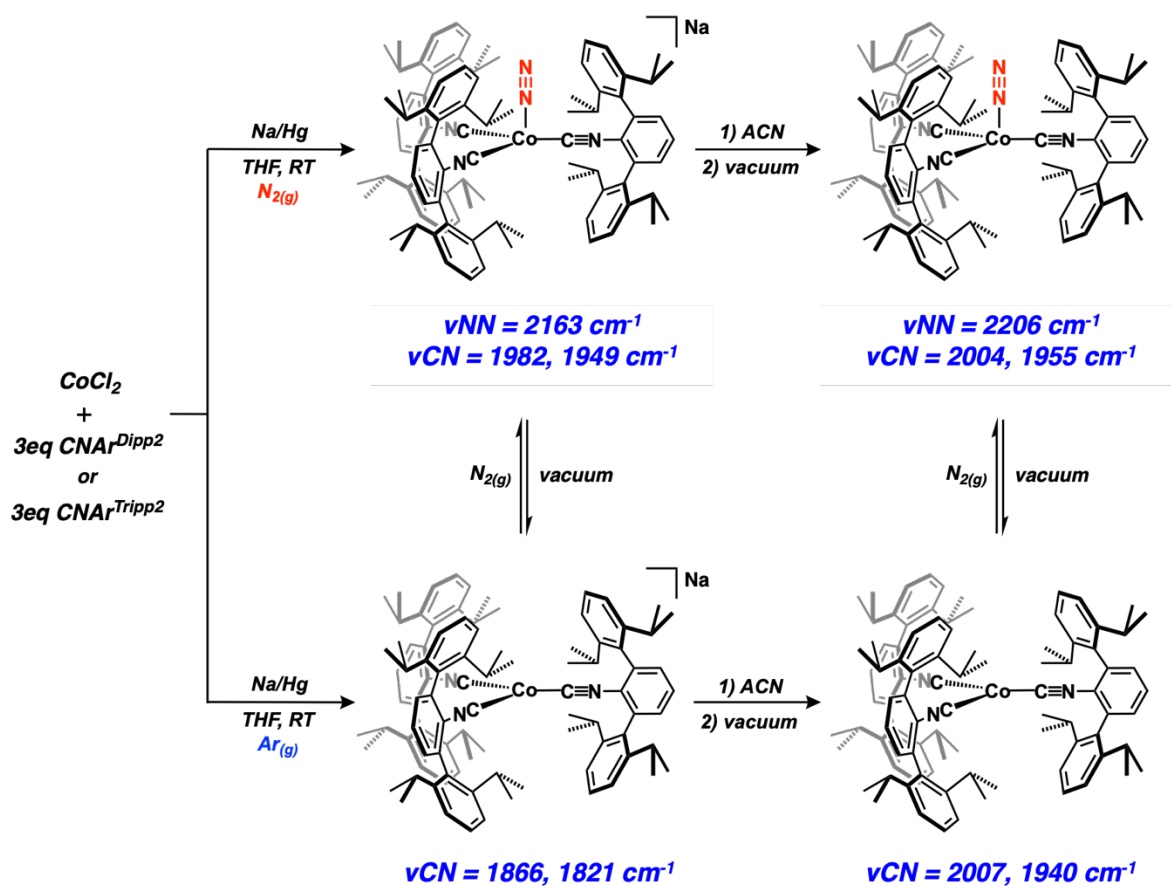


Scheme 1.3. Synthesis of the coordinatively unsaturated  $\text{Co}(\text{SiMe}_3)(\text{CNAr}^{\text{Mes}2})_3$ .

## 1.4 Synthesis of $\text{Co}(\text{CNAr}^{\text{Dipp}2})_3$

When moving from our smaller  $\text{CNAr}^{\text{Mes}2}$  ligand to a more protected  $\text{CNAr}^{\text{Dipp}2}$  or  $\text{CNAr}^{\text{Tripp}2}$  ligand, we surprisingly found that a coordinatively unsaturated  $[\text{Co}(\text{CNR})_3]_n$  ( $\text{CNR} = \text{CNAr}^{\text{Dipp}2}$  or  $\text{CNAr}^{\text{Tripp}2}$ ,  $n = 0, -1$ ) series can now be isolated. By using the same reaction condition of the  $[\text{Co}(\text{CNAr}^{\text{Mes}2})_4]_n$  generation, the 18-electron  $\text{Na}[(\text{N}_2)\text{Co}(\text{CNR})_3]$  and the 16-electron  $\text{Na}[\text{Co}(\text{CNR})_3]$  can be made within a nitrogen-filled glovebox and an argon-filled glovebox, respectively. (Scheme 1.4) Interestingly, when introducing a  $\text{N}_2(\text{g})$  atmosphere to the  $\text{Na}[\text{Co}(\text{CNAr}^{\text{Dipp}2})_3]$ , a slight color change from deep-red to wine-red was observed. The IR and  $^1\text{H}$  NMR spectrum of the new material match to the  $\text{Na}[(\text{N}_2)\text{Co}(\text{CNAr}^{\text{Dipp}2})_3]$  prepared in

the  $N_{2(g)}$  glovebox with an indicative  $\nu_{NN}$  stretch at  $2163\text{ cm}^{-1}$ . The wine-red color reversed back to deep-red under vacuum suggesting a reversible dinitrogen binding phenomenon. Solid state structure of  $Na[Co(CNAr^{Dipp2})_3]$  show interesting agnostic interaction of a Co-H distance at  $2.018\text{ \AA}$ . (Figure 1.7) Moreover, addition of acetonitrile (ACN) into a  $Na[Co(CNAr^{Dipp2})_3]$  pentane solution leads to a new clean purple product which was then crystallographic characterized as the oxidized  $(ACN)Co(CNAr^{Dipp2})_3$ . Further drying  $(ACN)Co(CNAr^{Dipp2})_3$  under vacuum leads to a deep-red material with x-ray crystallography revealed the 15-electron coordinatively unsaturated metalloradical  $Co(CNAr^{Dipp2})_3$ . (Figure 1.8C)



Scheme 1.4. Synthesis of  $[Co(CNR)_3]_n$  (CNR =  $CNAr^{Dipp2}$  or  $CNAr^{Tripp2}$ ,  $n = 0, -1$ ) series.



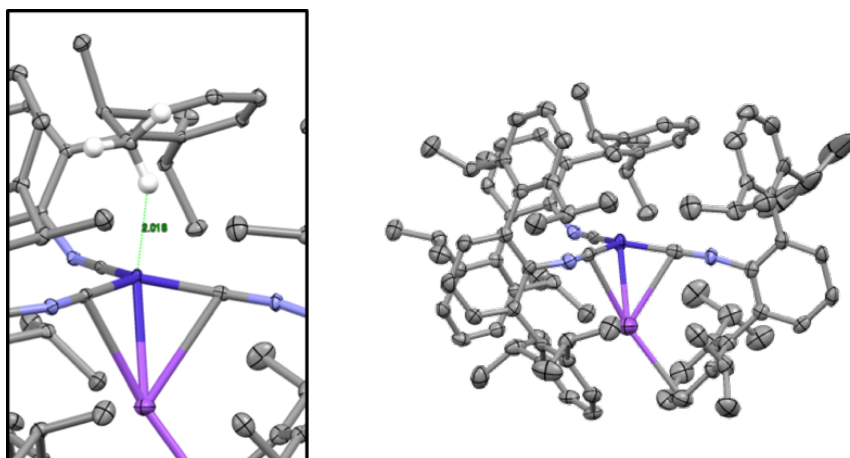


Figure 1.8. Solid state structure of  $\text{Na}[\text{Co}(\text{CNAr}^{\text{Dipp}2})_3]$  showing the agnostic interaction.

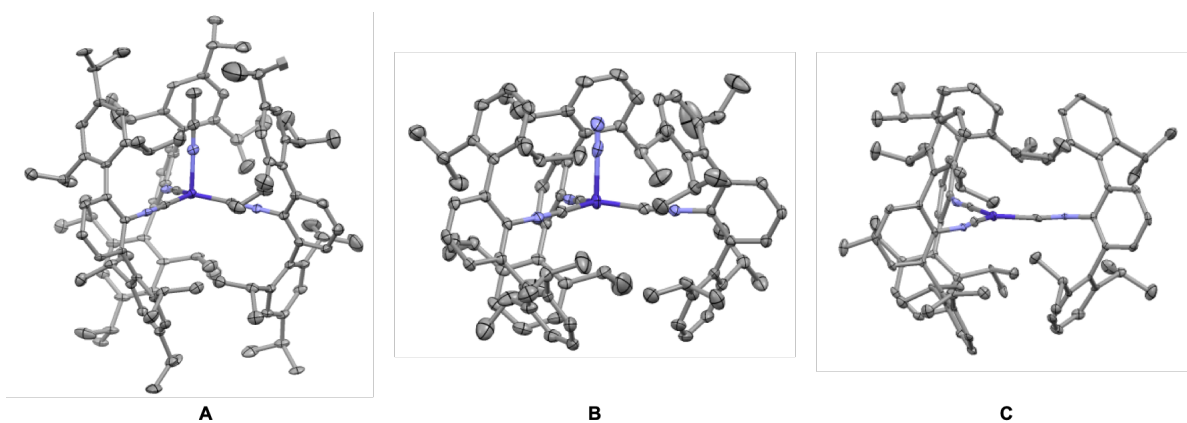
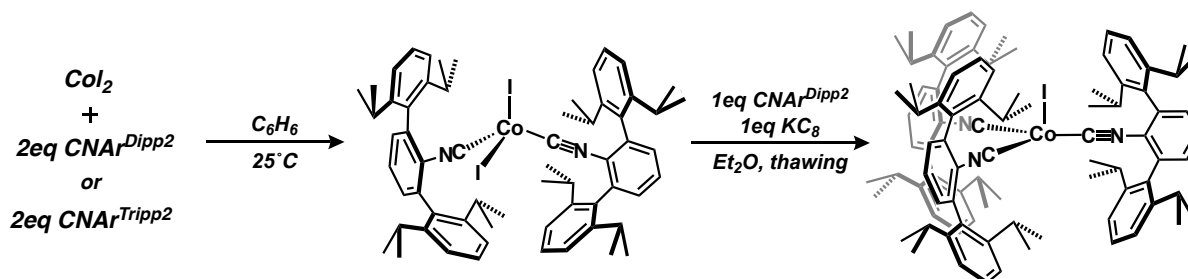


Figure 1.9. Molecular structures of A)  $(\text{ACN})\text{Co}(\text{CNAr}^{\text{Tripp}2})_3$  B)  $(\text{N}_2)\text{Co}(\text{CNAr}^{\text{Dipp}2})_3$  C)  $\text{Co}(\text{CNAr}^{\text{Dipp}2})_3$ .



**Scheme 1.5.** Synthesis of  $\text{I}_2\text{Co}(\text{CNR})_2$  and  $\text{ICo}(\text{CNR})_3$ .

This 15-electron  $\text{Co}(\text{CNAr}^{\text{Dipp}2})_3$  crystallize out in a triclinic P-1 space group and adopts a  $D_{3h}$  geometry in the solid state. Density functional theory (DFT) calculations on model  $\text{Co}(\text{CNXyl})_3$  showing the singly occupied molecular orbital (SOMO) on the cobalt  $d_{x^2-y^2}$  orbital. (Figure 1.10) To our best knowledge, this is the first example of a  $\text{CoL}_3$  (L = L-type ligand) formulism. Interestingly, similar to the  $\text{Na}[\text{Co}(\text{CNAr}^{\text{Dipp}2})_3]$  system,  $\text{Co}(\text{CNAr}^{\text{Dipp}2})_3$  also shows reversible  $\text{N}_2$  binding. The resulting  $(\text{N}_2)\text{Co}(\text{CNAr}^{\text{Dipp}2})_3$  has a less activated  $\nu_{\text{NN}}$  stretch at  $2206\text{ cm}^{-1}$  compared to  $\text{Na}[(\text{N}_2)\text{Co}(\text{CNAr}^{\text{Dipp}2})_3]$ . We are also able to isolate the Co(II) and Co(I) species with  $\text{CNAr}^{\text{Dipp}2}$  and  $\text{CNAr}^{\text{Tripp}2}$  using the reaction conditions shown in Scheme 1.5. Reactivity and detailed electronic structure studies of this new  $[\text{Co}(\text{CNR})_3]_n$  series are currently underway.

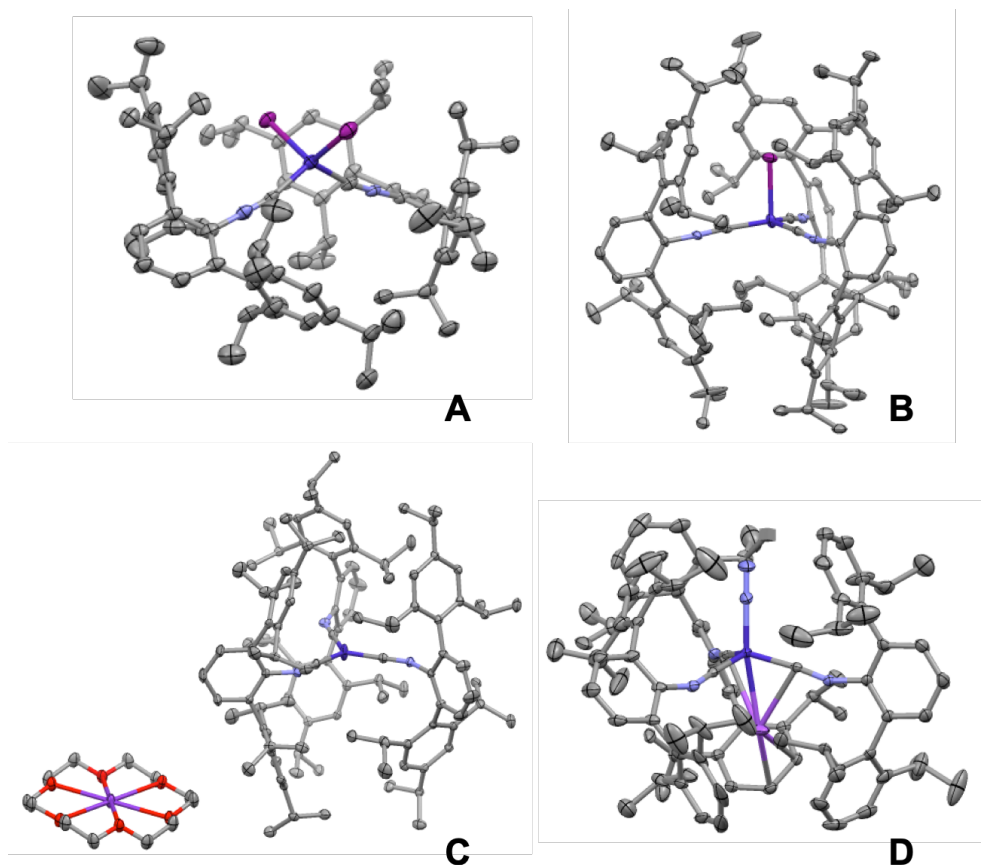


Figure 1.10. Molecular structures of A)  $\text{I}_2\text{Co}(\text{CNAr}^{\text{Tripp}2})_2$  B)  $\text{ICo}(\text{CNAr}^{\text{Tripp}2})_3$  C)  $(18\text{-c-}6)\text{K}[\text{Co}(\text{CNAr}^{\text{Tripp}2})_3]$  D)  $\text{Na}[(\text{N}_2)\text{Co}(\text{CNAr}^{\text{Dipp}2})_3]$ .

## 1.5 Synthetic Procedures

**General Considerations.** All manipulations were carried out under an atmosphere of dinitrogen using standard Schlenk and glovebox techniques. Unless otherwise stated, reagent grade starting materials were purchased from commercial sources and either used as received or purified by standard procedures.<sup>56</sup> Solvents were dried and deoxygenated according to standard procedures.<sup>57</sup> Benzene- $d_6$  and Toluene- $d_8$  were dried with Na/K and Benzophenone followed by distillation and stored on 4 Å molecular sieves for 3 days prior to use. Celite 405

(Fisher Scientific) was dried under vacuum (24 h) at a temperature above 250 °C and stored in the glovebox prior to use. The compounds  $\text{CNAr}^{\text{Dipp}2}$  and  $\text{CNAr}^{\text{Tripp}2}$  were prepared by previously reported methods.<sup>38,58</sup>

Solution  $^1\text{H}$  and  $^{13}\text{C}\{^1\text{H}\}$  spectra were recorded on Varian Mercury 300 and 400 spectrometers or a Varian X-Sens 500 spectrometer.  $^1\text{H}$  and  $^{13}\text{C}\{^1\text{H}\}$  chemical shifts are reported in ppm relative to  $\text{SiMe}_4$  ( $^1\text{H}$  and  $^{13}\text{C}$   $\delta = 0.0$  ppm) with reference to residual solvent resonances of 7.16 ppm ( $^1\text{H}$ ) and 128.06 ppm ( $^{13}\text{C}$ ) for  $\text{C}_6\text{D}_6$ . FTIR spectra were recorded on a Thermo-Nicolet iS10 FTIR spectrometer. For solution FTIR spectra, solvent peaks were digitally subtracted from all spectra by comparison with an authentic spectrum obtained immediately prior to that of the sample. The following abbreviations were used for the intensities and characteristics of important IR absorption bands: vs = very strong, s = strong, m = medium, w = weak, vw = very weak; b = broad, vb = very broad, sh = shoulder. Combustion analyses were performed by Midwest Microlab LLC of Indianapolis, IN (USA). Samples for combustion analysis were obtained from the first recrystallized batch of the reaction mixture. In a typical preparation, the crude, dry reaction mixture was dissolved in a minimum amount of solvent and stored at  $-35$  °C for several days to produce crystalline material. This material was then collected, thoroughly dried under vacuum and then packaged under vacuum for shipment. In most cases, this material was also used for single-crystal X-ray structure determination.

The following procedures are identical for both  $\text{CNAr}^{\text{Dipp}2}$  and  $\text{CNAr}^{\text{Tripp}2}$  versions of synthesis otherwise stated.

**Synthesis of  $\text{I}_2\text{Co}(\text{CNAr}^{\text{Tripp}2})$ :** To a benzene slurry solution of  $\text{CoI}_2$  (0.066 g, 0.211 mmol, 1 equivalent) (3 mL) was added a benzene solution of  $\text{CNAr}^{\text{Tripp}2}$  (0.214 g, 0.422 mmol, 2

equivalents) (3 mL). The resulting purple solution was then allowed to stir at room temperature for 12 hours where then all volatiles were removed under reduced pressure to yield a dark purple powder. To the resulting solid, acetonitrile (5 mL) was added and allowed to stir at room temperature for 1 hour where upon the precipitation of a purple solid was observed. The resulting solution was then decanted, and the precipitate was washed with MeCN (5 mL) to collect a pink-purple solid (0.266 g, 0.2 mmol, 95 % yield). X-ray diffraction crystals were grown from a saturated *n*-pentane/Et<sub>2</sub>O spiked with 5 drops of C<sub>6</sub>H<sub>6</sub> over 3 days at -40 °C. FTIR (C<sub>6</sub>D<sub>6</sub>, KBr windows, 25 °C):  $\nu_{\text{CN}} = 2163$  (s), 2143 (vs) cm<sup>-1</sup>, also 2961 (s), 2927 (m), 2868 (w), 1463 (m), 1383 (w), 1363 (w) cm<sup>-1</sup>. Anal. Calcd. for C<sub>74</sub>H<sub>98</sub>N<sub>2</sub>CoI<sub>2</sub>: C, 66.91; H, 7.44; N, 2.11. Found C, 66.42; H, 7.14; N, 2.04.

**Synthesis of ICo(CNAr<sup>Tripp2</sup>)<sub>3</sub>:** To a thawing Et<sub>2</sub>O (100 mL) suspension of I<sub>2</sub>Co(CNAr<sup>Tripp2</sup>)<sub>2</sub> (0.134 g, 0.1 mmol, 1 equivalent) and one equivalent of CNAr<sup>Tripp2</sup> (0.05 g, 0.1 mmol, 1 equivalent) was added KC<sub>8</sub> (0.013 g, 0.1 mmol, 1 equivalent). The resulting mixture was allowed to stir under -35 °C for 1 hour, where upon a color change to brown-yellow was observed. The resulting residue was then slurred in *n*-pentane (15 mL) allowed to stir for 5 min and then concentrated to dryness. Extraction of the resulting residue with benzene (10 mL), followed by filtration through Celite produced a deep-red solid. Following the purple solid was dissolved in C<sub>6</sub>H<sub>6</sub> (10 mL) frozen in the cold well and lyophilized to remove MeCN which resulted in a color change from purple to red to yield CoCl(CNAr<sup>Tripp2</sup>) as a fluffy solid, 0.100 g, 0.058 mmol, 58 % yield. X-ray diffraction quality crystals were grown from a saturated solution of *n*-pentane (1.5 mL) spiked with 5 drops of Et<sub>2</sub>O and 5 drops C<sub>6</sub>H<sub>6</sub> at -40 °C over 1 week. FTIR (C<sub>6</sub>D<sub>6</sub>, KBr windows, 25 °C):  $\nu_{\text{CN}} = 2101$  (m), 2040 (vs), 1982 (sh) cm<sup>-1</sup>, also 2961

(s), 2927 (m), 2868 (w), 1463 (m), 1383 (w), 1363 (w)  $\text{cm}^{-1}$ . Anal. Calcd. for  $\text{C}_{111}\text{H}_{147}\text{N}_3\text{CoI}$ : C, 78.00; H, 8.67; N, 2.46. Found C, 77.64; H, 8.65; N, 2.39.

**Synthesis of  $\text{Na}[(\text{N}_2)\text{Co}(\text{CNAr}^{\text{Dipp}2})_3]$ :** This reaction procedure is carried out under  $\text{N}_2(\text{g})$  atmosphere. To a THF (10 mL) suspension of  $\text{CoCl}_2$  (0.054 g, 0.42 mmol, 1 equivalent) was added  $\text{CNAr}^{\text{Dipp}2}$  (0.500 g, 1.26 mmol, 3 equivalents). The resulting mixture was allowed to stir for 10 minutes, after which 0.1 % NaHg (Na: 0.96 g, 4.2 mmol, 10 equivalents; Hg: 9.6 g) was added. The reaction mixture was shaken by hand for ca. 7 min, where upon a color change to deep purple was observed. The reaction mixture was allowed to stir for an additional 20 mins upon which time the solution was decanted from the sodium amalgam via filtration over Celite packed on a medium porosity glass sintered frit and evaporated to dryness. The resulting residue was then slurred in *n*-pentane (15 mL) allowed to stir for 5 min and then concentrated to dryness. This step was repeated two additional times to desolvate residual NaCl by-products where upon a color change from purple to red was observed. Extraction of the resulting residue with benzene (10 mL), followed by filtration through Celite produced a deep-red solid.  $\text{Na}[(\text{N}_2)\text{Co}(\text{CNAr}^{\text{Dipp}2})_3]$  is isolated as a fluffy red solid, 0.400 g, 0.29 mmol, 69 % yield. FTIR ( $\text{C}_6\text{D}_6$ , KBr windows, 25 °C):  $\nu_{\text{NN}} = 2159$  (m)  $\text{cm}^{-1}$ ,  $\nu_{\text{CN}} = 2018$  (w), 1946 (m), 1840 (vs)  $\text{cm}^{-1}$ , also 2961 (s), 2927 (m), 2868 (w), 1463 (m), 1383 (w), 1363 (w)  $\text{cm}^{-1}$ . Anal. Calcd. for  $\text{C}_{93}\text{H}_{111}\text{N}_3\text{CoNa}$ : C, 80.89; H, 8.10; N, 5.07. Found C, 80.46; H, 8.28; N, 5.06.

**Synthesis of  $\text{K}[\text{Co}(\text{N}_2)(\text{CNAr}^{\text{Tripp}2})_3]$  from  $\text{ICo}(\text{CNAr}^{\text{Tripp}2})_3$  and  $\text{KC}_8$ :** To a ether solution (15 mL) of  $\text{ICo}(\text{CNAr}^{\text{Tripp}2})_3$  (200 mg, 0.12 mmol, 1 equivalent) was added  $\text{KC}_8$  (0.031 g, 0.24 mmol, 2 equivalents) all at once. An immediate color change from red to purple was observed. Thereafter the reaction mixture was allowed to react for 10 minutes at room temperature. Following the reaction mixture was filtered over Celite packed on fiberglass (2 cm) to remove

C<sub>8</sub> where upon all volatiles were removed under reduced pressure. The resulting purple solid was then slurred in *n*-pentane (5 mL) allowed to stir for 5 minutes where upon all volatiles were removed under vacuum. This step was repeated two additional times to desolvate any residual KCl. Thereafter a color change from purple to red was observed upon removal of residual THF. The resulting red solid was then taken up in C<sub>6</sub>H<sub>6</sub> and filtered over Celite packed on fiberglass (2 cm) so as to remove any remaining KCl, after which the deep red solution was frozen in the cold-well and lyophilized to yield K[Co(N<sub>2</sub>)(CNAr<sup>Tripp2</sup>)<sub>3</sub>] as a dark brick red fluffy solid 180 mg, 0.11 mmol, 91 % yield. X-ray diffraction quality crystals were grown from a saturated *n*-pentane solution spiked with 5 drops of Et<sub>2</sub>O and 5 drops C<sub>6</sub>H<sub>6</sub> over 1 week at -40 °C. <sup>1</sup>H NMR (400.1 MHz, C<sub>6</sub>D<sub>6</sub>, 20 °C): δ = 7.19 (s, 12H, *m*-Tripp), 6.81 (b, 3H, *p*-Ph), 6.75 (d, 6H, *J* = 7 Hz, *m*-Ph), 2.98 (sept, *J* = 7 Hz, 18H, CH(CH<sub>3</sub>)<sub>2</sub>), 1.44 (d, *J* = 8 Hz, 36H, CH(CH<sub>3</sub>)<sub>2</sub>), 1.21 (d, *J* = 8 Hz, 72H, CH(CH<sub>3</sub>)<sub>2</sub>) ppm. FTIR (C<sub>6</sub>D<sub>6</sub>, KBr windows, 25 °C): ν<sub>NN</sub> = 2158 (m) cm<sup>-1</sup>, ν<sub>CN</sub> = 1943 (w), 1823 (vs), 1760 (sh) cm<sup>-1</sup>, also 2961 (s), 2927 (m), 2906 (w), 2868 (m), 1568 (m), 1405 (w), 1382 (w) cm<sup>-1</sup>.

**Synthesis of Na[Co(CNAr<sup>Dipp2</sup>)<sub>3</sub>]:** The synthesis procedure of Na[(N<sub>2</sub>)Co(CNAr<sup>Dipp2</sup>)<sub>3</sub>] is followed under Ar(g) atmosphere. Na[Co(CNAr<sup>Dipp2</sup>)<sub>3</sub>] is isolated as a fluffy deep-red solid, 0.300 g, 0.22 mmol, 52 % yield. <sup>1</sup>H NMR (499.9 MHz, C<sub>6</sub>D<sub>6</sub>, 20 °C): δ = 7.27 (t, 6H, *J* = 5 Hz, *p*-Dipp), 7.15 (d, 12H, *J* = 5 Hz, *m*-Dipp), 6.94 (d, 6H, *J* = 5 Hz, *m*-Ph), 6.86 (t, 3H, *J* = 5 Hz, *p*-Ph), 2.89 (sept, *J* = 5 Hz, 12H, CH(CH<sub>3</sub>)<sub>2</sub>), 1.15 (d, *J* = 5 Hz, 36H, CH(CH<sub>3</sub>)<sub>2</sub>), 1.02 (d, *J* = 5 Hz, 36H, CH(CH<sub>3</sub>)<sub>2</sub>) ppm. <sup>13</sup>C{<sup>1</sup>H} NMR (125.7 MHz, C<sub>6</sub>D<sub>6</sub>, 20 °C): δ = 205.6(CNR), 147.8, 138.6, 134.6, 132.6, 130.4, 128.6, 128.4, 127.9, 121.6, 31.2, 25.0, 23.9 ppm. (The CNR resonance extremely broadened, presumably due to coupling to <sup>59</sup>Co (*I* = 7/2, 100 %)). FTIR

(C<sub>6</sub>D<sub>6</sub>, KBr windows, 25 °C):  $\nu_{\text{CN}} = 2068$  (w), 2018 (m), 1934 (vs), 1815 (s) cm<sup>-1</sup>, also 2961 (s), 2927 (m), 2868 (w), 1463 (m), 1383 (w), 1363 (w) cm<sup>-1</sup>. Elemental analysis not performed due to sensitivity towards N<sub>2</sub>.

**Synthesis of K[Co(CNAr<sup>Tripp2</sup>)<sub>3</sub>] from ICo(CNAr<sup>Tripp2</sup>)<sub>3</sub> and KC<sub>8</sub>:** The synthesis procedure of K[(N<sub>2</sub>)Co(CNAr<sup>Tripp2</sup>)<sub>3</sub>] is followed under Ar(g) atmosphere. K[Co(CNAr<sup>Tripp2</sup>)<sub>3</sub>] is isolated as a fluffy deep-red solid, 0.180 g, 0.11 mmol, 92 % yield. <sup>1</sup>H NMR (400.1 MHz, C<sub>6</sub>D<sub>6</sub>, 20 °C):  $\delta = 7.18$  (s, 12H, *m*-Tripp), 6.84 (b, 3H, *p*-Ph), 6.76 (d, 6H, *J* = 7 Hz, *m*-Ph), 2.97 (sept, *J* = 7 Hz, 18H, CH(CH<sub>3</sub>)<sub>2</sub>), 1.42 (d, *J* = 8 Hz, 36H, CH(CH<sub>3</sub>)<sub>2</sub>), 1.22 (d, *J* = 8 Hz, 72H, CH(CH<sub>3</sub>)<sub>2</sub>) ppm. FTIR (C<sub>6</sub>D<sub>6</sub>, KBr windows, 25 °C):  $\nu_{\text{CN}} = 2001$  (w), 1940 (m), 1901 (m), 1665 (sh) cm<sup>-1</sup>, also 2961 (s), 2927 (m), 2906 (w), 2868 (m), 1604 (m), 1568 (w), 1554 (w) cm<sup>-1</sup>.

**Synthesis of (18-crown-6)K[Co(CNAr<sup>Tripp2</sup>)<sub>3</sub>]:** An 18-crown-6 ether solution is added to a concentrated pentane solution of K[Co(CNAr<sup>Tripp2</sup>)<sub>3</sub>] (80 mg, 0.05 mmol, 1 equivalent) and store under -35 °C for 1 week until single crystals of (18-crown-6)K[Co(CNAr<sup>Tripp2</sup>)<sub>3</sub>] have grown. The product is isolated as a crystalline material after washing with cold pentane, 0.04 g, 0.02 mmol, 42 % yield. <sup>1</sup>H NMR (400.1 MHz, C<sub>6</sub>D<sub>6</sub>, 20 °C):  $\delta = 7.17$  (s, 12H, *m*-Tripp), 6.85 (d, 6H, *J* = 7 Hz, *m*-Ph), 6.77 (t, 6H, *J* = 7 Hz, *p*-Ph), 3.47 (s, 36H, 12-crown-6), 3.02 (sept, *J* = 7 Hz, 12H, CH(CH<sub>3</sub>)<sub>2</sub>), 2.95 (sept, *J* = 7 Hz, 6H, CH(CH<sub>3</sub>)<sub>2</sub>), 1.42 (d, *J* = 8 Hz, 36H, CH(CH<sub>3</sub>)<sub>2</sub>), 1.24 (d, *J* = 8 Hz, 36H, CH(CH<sub>3</sub>)<sub>2</sub>), 1.10 (d, *J* = 8 Hz, 36H, CH(CH<sub>3</sub>)<sub>2</sub>) ppm. <sup>13</sup>C {<sup>1</sup>H} NMR (125.7 MHz, C<sub>6</sub>D<sub>6</sub>, 20 °C):  $\delta = 147.6, 136.9, 133.3, 132.6, 130.4, 128.6, 128.4, 127.9, 120.9, 71.1, 34.6, 30.2, 25.1, 24.6, 22.7$  ppm. (The CNR resonance cannot be detected, presumably due to coupling to <sup>59</sup>Co (*I* = 7/2, 100 %)) FTIR (C<sub>6</sub>D<sub>6</sub>, KBr windows, 25 °C):  $\nu_{\text{CN}} = 1937$  (m) cm<sup>-1</sup>, also 2961 (s), 2927 (m), 2906 (w), 2868 (m), 1604 (m), 1568 (w), 1554 (w) cm<sup>-1</sup>.



**Synthesis of (ACN)Co(CNAr<sup>Dipp2</sup>)<sub>3</sub>:** To a pentane solution of Na[Co(CNAr<sup>Dipp2</sup>)<sub>3</sub>] (0.300 g, 0.22 mmol, 1 equivalent) was added 10 mL of acetonitrile (ACN). An immediate color change to purple with solid precipitation observed. The purple solid was then collected by vacuum filtration and recrystallized with pentane with a drop of benzene under -35°C to yield single crystals suitable for X-ray diffraction. 0.100 g, 0.07 mmol, 33 % yield. FTIR (C<sub>6</sub>D<sub>6</sub>, KBr windows, 25 °C):  $\nu_{\text{CN}} = 2018$  (s), 1918 (vs)  $\text{cm}^{-1}$ , also 2961 (s), 2927 (m), 2868 (w), 1463 (m), 1383 (w), 1363 (w)  $\text{cm}^{-1}$ .

**Synthesis of (N<sub>2</sub>)Co(CNAr<sup>Dipp2</sup>)<sub>3</sub>:** This reaction procedure is carried out under N<sub>2(g)</sub> atmosphere. To a THF solution of Na[(N<sub>2</sub>)Co(CNAr<sup>Dipp2</sup>)<sub>3</sub>] (0.200 g, 0.14 mmol, 1 equivalent) was added 10 mL of acetonitrile (ACN). An immediate color change to dark-red with solid precipitation observed. The red solid was then collected by vacuum filtration. Further recrystallization with pentane with a drop of benzene under -35°C to yield single crystals suitable for X-ray diffraction. 0.110 g, 0.08 mmol, 57 % yield. FTIR (C<sub>6</sub>D<sub>6</sub>, KBr windows, 25 °C):  $\nu_{\text{NN}} = 2204$  (vw)  $\text{cm}^{-1}$ ,  $\nu_{\text{CN}} = 2070$  (sh), 2015 (m), 1940 (vs)  $\text{cm}^{-1}$ , also 2961 (s), 2927 (m), 2868 (w), 1463 (m), 1383 (w), 1363 (w)  $\text{cm}^{-1}$ .

**Synthesis of Co(CNAr<sup>Dipp2</sup>)<sub>3</sub>:** Co(CNAr<sup>Dipp2</sup>)<sub>3</sub> is isolated through applying active vacuum on (ACN)Co(CNAr<sup>Dipp2</sup>)<sub>3</sub> over 12 h. The product is obtained as a fluffy deep-red solid, 0.080 g, 0.06 mmol, 27 % yield. FTIR (C<sub>6</sub>D<sub>6</sub>, KBr windows, 25 °C):  $\nu_{\text{CN}} = 2070$  (sh), 2018 (m), 1930 (vs)  $\text{cm}^{-1}$ , also 2961 (s), 2927 (m), 2868 (w), 1463 (m), 1383 (w), 1363 (w)  $\text{cm}^{-1}$ . Anal. Calcd. for C<sub>93</sub>H<sub>111</sub>N<sub>3</sub>Co: C, 84.00; H, 8.41; N, 3.16. Found C, 83.41; H, 8.78; N, 2.89.

## 1.6 Computational Studies on Co(CNXyl)<sub>3</sub>

**Computational details.** Density Functional Theory (DFT) calculations were carried out on Co(CNXyl)<sub>3</sub> as a model for Co(CNAr<sup>Dipp2</sup>)<sub>3</sub>. The starting geometry was obtained from the crystal structure coordinates of Co(CNAr<sup>Dipp2</sup>)<sub>3</sub>. Calculations were all carried out with the Gaussian 09 software package.<sup>59</sup> Geometry optimizations, frequency and single point energy calculations were performed using the B3LYP functional,<sup>60,61</sup> with the 6-31g(d) basis set<sup>62</sup> for H, C, O and N atoms and the LANL2DZ basis set plus f-type polarization functions for cobalt atoms.<sup>63</sup> Viewing of optimized structures and rendering of molecular orbitals was performed using the program *Chemcraft*.<sup>64</sup>

### Input file for Co(CNXyl)<sub>3</sub>

```
%chk=CoL3-Xyl-b3lyp.chk
%nprocs=8
%mem=30GB
# opt freq gen nosymm geom=connectivity b3lyp pseudo=read SCF=QC
```

Title Card Required

```
0 2
C      -4.33110400  0.90272100  0.93530600
Co     -0.02124600  0.02709000  0.64595400
N      -2.99367600  0.60639200  0.83537000
N       0.98572300 -2.60221700 -0.48572600
N       1.96277000  2.09494600  1.64278900
C      -1.81670900  0.36950600  0.75742800
C       0.58609400 -1.55628200 -0.04455900
C      -4.95894900  0.89040600  2.21748900
C      -5.06780000  1.21794400 -0.24596700
C       1.24369900 -4.98477600 -0.14621200
C       1.17414600  1.27618100  1.24923300
C       3.15222900  4.17059500  1.29799100
C       1.40528900 -3.82166700 -0.95925300
C       2.90065600  3.00046800  2.07581100
C       1.69267500 -6.21761300 -0.65544000
C       1.99684600 -3.90473300 -2.25527400
C       3.60401600  2.75667800  3.29395600
C       4.55434200  3.70739300  3.71099500
C      -6.33180600  1.19263000  2.28549800
C       2.42345200 -5.16479700 -2.71313900
```

C	-7.07158300	1.50524500	1.13540600
C	4.11640500	5.08331500	1.76235600
C	2.27886900	-6.31709500	-1.92589400
C	-6.43607900	1.51776100	-0.11547000
C	4.81626900	4.86174800	2.95858200
H	1.56313900	-7.11254400	-0.03596000
H	5.10302100	3.51895500	4.64088900
H	-6.81539700	1.19165800	3.26908800
H	2.87559200	-5.22898100	-3.70956200
H	-8.13842200	1.74131100	1.21387900
H	4.31197600	5.98137800	1.16520000
H	2.61596900	-7.28870400	-2.30312900
H	-7.00409100	1.75753200	-1.02168100
H	5.56552700	5.58405800	3.30049600
C	0.59594354	-4.91749208	1.24931146
H	1.19814452	-4.31112978	1.89318936
H	-0.38168616	-4.49016043	1.16851644
H	0.52130859	-5.90443685	1.65584514
C	2.16881827	-2.66417153	-3.15139496
H	1.23714677	-2.14260550	-3.22108770
H	2.90861429	-2.01773677	-2.72745634
H	2.48018095	-2.97022416	-4.12827012
C	-4.39882939	1.23783264	-1.63293591
H	-3.78596921	2.11051515	-1.72084290
H	-3.79317676	0.36345992	-1.74937144
H	-5.15253819	1.25334158	-2.39226623
C	-4.17495267	0.56608921	3.50270041
H	-3.58191460	-0.31082147	3.34702925
H	-3.53693643	1.38912382	3.74856481
H	-4.86128255	0.39462837	4.30547840
C	3.34792480	1.49688636	4.14186066
H	2.31716835	1.46226158	4.42689095
H	3.58891703	0.62610451	3.56865763
H	3.95975561	1.52698359	5.01916176
C	2.39373800	4.43684847	-0.01555401
H	2.58202041	3.63968401	-0.70401500
H	1.34416545	4.49519151	0.18417968
H	2.72802489	5.36066417	-0.43948422

C H N O  
6-31g(d)  
\*\*\*\*

Co 0  
f 1 1.0  
2.78 1.0  
\*\*\*\*

Co 0  
lanl2dz  
\*\*\*\*

Co 0  
lanl2dz

### Output coordinates for Co(CNXyl)<sub>3</sub>

C	-4.32440400	0.91804200	0.94609600
Co	-0.01236100	0.02158100	0.66790300
N	-2.98143400	0.63810100	0.85390900
N	0.93711300	-2.63759000	-0.45324400
N	2.01538900	2.06814500	1.63214700
C	-1.82000000	0.39604100	0.77796200
C	0.56428900	-1.59657300	-0.01663000
C	-5.01492600	0.57577500	2.13056400
C	-4.97096600	1.53915700	-0.14618200
C	1.55408700	-4.92689300	-0.06889800
C	1.22239500	1.26723100	1.25400300
C	3.45006800	3.93378900	1.15125800
C	1.37140000	-3.84161200	-0.95538700
C	2.93185800	2.99442700	2.07106900
C	1.99653300	-6.13804300	-0.60498900
C	1.62102200	-3.95529300	-2.34165300
C	3.32571500	2.97749800	3.42807700
C	4.25775200	3.92900100	3.84755600
C	-6.37825300	0.87060400	2.19776100
C	2.06183900	-5.18909500	-2.82485700
C	-7.03941900	1.48306900	1.13279300
C	4.37884900	4.86337500	1.62383900
C	2.25029200	-6.27546100	-1.97000200
C	-6.33529800	1.81171300	-0.02594700
C	4.78400400	4.86694300	2.95887200
H	2.14278100	-6.98391300	0.06208400
H	4.57247200	3.93082900	4.88813600
H	-6.92573400	0.61406700	3.10129000
H	2.25940200	-5.29480600	-3.88865600
H	-8.10058300	1.70388700	1.20574900
H	4.78839500	5.59376800	0.93050200
H	2.59390100	-7.22670800	-2.36651100
H	-6.84928400	2.28932900	-0.85637400
H	5.50788500	5.59894000	3.30578200
C	1.27593500	-4.76623000	1.40380800
H	1.90343300	-3.98341300	1.84791900
H	0.23402000	-4.47458800	1.58576100
H	1.46658500	-5.70053600	1.93995700
C	1.41364600	-2.77433600	-3.25514100
H	0.37529300	-2.42119900	-3.22517100
H	2.04306700	-1.92480600	-2.96212100
H	1.65457700	-3.03579700	-4.28970700
C	-4.19933000	1.88970100	-1.39262100
H	-3.37406200	2.57859000	-1.17324000
H	-3.75179300	0.99919600	-1.85140000
H	-4.85057800	2.36339700	-2.13304600
C	-4.28993700	-0.08586900	3.27462900
H	-3.84913200	-1.04346500	2.97042200
H	-3.46488000	0.53749300	3.64123600
H	-4.97124800	-0.27466500	4.10942500
C	2.74947000	1.95970500	4.37899300

H	1.65721000	2.04213700	4.44147600
H	2.96914100	0.93552500	4.05249900
H	3.15900500	2.09151100	5.38480100
C	3.00521900	3.91944800	-0.28886000
H	3.23509500	2.96075000	-0.77035600
H	1.92091500	4.06256700	-0.37547900
H	3.49999900	4.71290000	-0.85664800

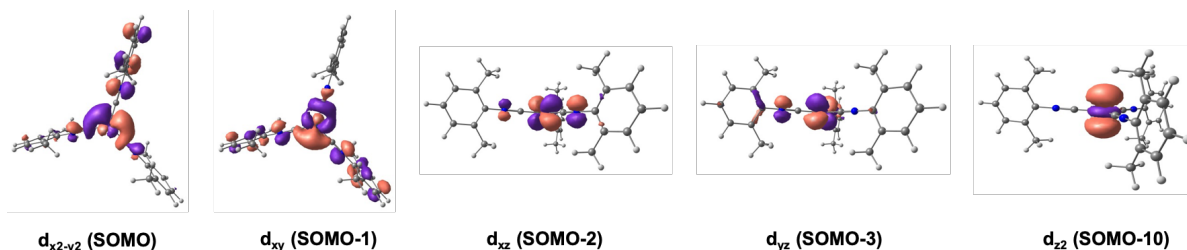


Figure 1.11. Selected molecular orbitals of  $\text{Co}(\text{CNXyl})_3$  that include cobalt d-orbital contributions.

## 1.7 Crystallographic Structure Determinations

**General.** Single crystal X-ray structure determinations were carried out at low temperature on a Bruker P4, Platform or Kappa Diffractometer equipped with a Mo or Cu radiation source and a Bruker APEX detector. All structures were solved by direct methods with SIR 2004<sup>65</sup> or SHELXS<sup>66</sup> and refined by full-matrix least-squares procedures utilizing SHELXL within Olex 2 small-molecule solution, refinement, and analysis software package.<sup>67</sup> Crystallographic data collection and refinement information are listed in Table 1.1 and 1.2.

**Information on crystallographic disorder.** All disordered components were successfully modeled and refined anisotropically unless otherwise stated.

$\text{Na}(\text{N}_2)\text{Co}(\text{CNAr}^{\text{Dipp}2})_3 \cdot 2\text{C}_6\text{H}_6$  contains severely disordered solvent molecules of co-crystallization that could not be successfully modeled. The PLATON routine SQUEEZE<sup>68</sup> was

used to account for these disordered components as a diffuse contribution to the overall scattering without specific atom positions.

The solid-state structure of  $\text{Na}(\text{N}_2)\text{Co}(\text{CNAr}^{\text{Dipp}2})_3 \cdot 2\text{C}_6\text{H}_6$  exhibits positional disorder over two positions of two  $\text{Ar}^{\text{Dipp}2}$  group at C52 and C83. These  $\text{Ar}^{\text{Dipp}2}$  group were split and linked via a free variable and refined anisotropically. Constrains of AFIX, SADI, EADP and RIGU are used through the refinement.

Complex  $(\text{ACN})\text{Co}(\text{CNAr}^{\text{Dipp}2})_3 \cdot \text{C}_6\text{H}_6$  contains compositional disorder of 16%  $\text{ICo}(\text{CNAr}^{\text{Dipp}2})_3$  and 84%  $(\text{ACN})\text{Co}(\text{CNAr}^{\text{Dipp}2})_3$  at the apical position refined anisotropically.

The solid-state structure of  $(\text{N}_2)\text{Co}(\text{CNAr}^{\text{Dipp}2})_3$  exhibits a merohedral twin. Addition to this, the  $\text{N}_2$ -Co fragment is positional disordered over two positions. The group was split and linked via a free variable and refined anisotropically.

**Table 1.1. Crystallographic Data Collection and Refinement Information.**

Name	$\text{Na}[(\text{N}_2)\text{Co}(\text{CNAr}^{\text{Dipp}2})_3] \cdot 2\text{C}_6\text{H}_6$	$\text{Na}[\text{Co}(\text{CNAr}^{\text{Dipp}2})_3] \cdot \text{C}_5$	$(\text{ACN})\text{Co}(\text{CNAr}^{\text{Dipp}2})_3 \cdot \text{C}_6\text{H}_6$
Formula	C99 H117 Co N5 Na	C104 H123 Co N3 Na	C100.49 H114.61 Co I0.16 N3.84
Crystal System	Monoclinic	Orthorhombic	Triclinic
Space Group	P 1 21/c 1	Pna2 / 1	P-1
a, Å	12.5833(5)	26.175(2)	12.8222(3)
b, Å	25.3208(10)	22.4836(18)	15.1166(4)
c, Å	28.7835(10)	16.1776(13)	22.5579(5)
$\alpha$ , deg	90	90	87.8670(10)
$\beta$ , deg	94.4430(10)	90	84.3880(10)
$\gamma$ , deg	90	90	83.8690(10)
V, Å <sup>3</sup>	9143.4(6)	9520.8(13)	4324.93(18)
Z	4	4	2
Radiation ( $\lambda$ , Å)	Mo-K $\alpha$ , 0.71073	Mo-K $\alpha$ , 0.71073	Mo-K $\alpha$ , 0.71073
$\rho$ (calcd.), g/cm <sup>3</sup>	1.060	1.044	1.118
$\mu$ , mm <sup>-1</sup>	0.238	0.229	0.303
Temp, K	100	100	100
$\theta$ max, deg	25.732	25.026	24.714
data/parameters	17440 / 1155	16819 / 1007	14732 / 982
$R_1$	0.0617	0.0731	0.0705
$wR_2$	0.1526	0.1988	0.1671
GOF	1.032	1.076	1.027

**Table 1.2. Crystallographic Data Collection and Refinement Information.**

Name	(N <sub>2</sub> )Co(CNAr <sup>Dipp2</sup> ) <sub>3</sub>	Co(CNAr <sup>Dipp2</sup> ) <sub>3</sub> ·C <sub>6</sub> H <sub>6</sub>
Formula	C93 H111 Co N5	C99 H117 Co N3
Crystal System	Monoclinic	Triclinic
Space Group	P 1 21/n 1	P-1
a, Å	12.1906(8)	14.4825(13)
b, Å	25.5269(16)	14.6228(13)
c, Å	26.0851(16)	23.461(2)
α, deg	90	101.862(2)
β, deg	90.022(2)	93.171(2)
γ, deg	90	119.460(3)
V, Å <sup>3</sup>	8117.4(9)	4161.7(7)
Z	4	2
Radiation (λ, Å)	Mo-K <sub>α</sub> , 0.71073	Mo-K <sub>α</sub> , 0.71073
ρ(calcd.), g/cm <sup>3</sup>	1.111	1.124
μ, mm <sup>-1</sup>	0.259	0.254
Temp, K	100	100
θ max, deg	25.401	25.378
data/parameters	14928 / 948	15254 / 952
R <sub>1</sub>	0.0404	0.0517
wR <sub>2</sub>	0.0925	0.1072
GOF	1.052	1.038

## 1.8 Concluding Remarks

The research projects listed in this thesis focus on the solution-phase dynamics and novel reactivity of low-valent cobalt isocyanides, with the aim of comparing and contrasting their behavior with the chemistry associated with their carbonyl analogues. Chapter 2 and 3 will be focusing on the reactivity and dynamics of the isolobal analogue of Co(CO)<sub>4</sub>, Co(CNAr<sup>Mes2</sup>)<sub>4</sub>. The usage of cobalt anions as cobalt phosphide cluster building blocks will be



discussed in Chapter 4. Research on unique small molecule activations using coordinatively unsaturated  $\text{Co}(\text{SiMe}_3)(\text{CNAr}^{\text{Mes}_2})_3$  will be covered in Chapter 5 and 6.

## 1.9 Acknowledgement

Complexes discussed in section 1.4-1.6 are currently in preparation for publication by C. Chan, M. L. Neville, C. Mokhtarzadeh, A. L. Rheingold, J. S. Figueroa. The dissertation author is the primary author of this manuscript.

## 1.10 References

- (1) Stolz, I. W.; Dobson, G. R.; Sheline, R. K. *J. Am. Chem. Soc.* **1962**, *84* (18), 3589–3590.
- (2) Nalesnik, T. E.; Orchin, M. *Organometallics* **1982**, *1* (1), 222–223.
- (3) Klingler, R. J.; Rathke, J. W. *J. Am. Chem. Soc.* **1994**, *116* (11), 4772–4785.
- (4) Wegman, R. W.; Brown, T. L. *J. Am. Chem. Soc.* **1980**, *102* (7), 2494–2495.
- (5) Paulik, F. E. *Catalysis Reviews* **1972**, *6* (1), 49–84.
- (6) Wawersik, H.; Keller, H. J. *Zeitschrift für Naturforschung B* **1965**, No. 20, 938–942.
- (7) Crichton, O.; Poliakoff, M.; Rest, A. J.; Turner, J. J. *J. Chem. Soc., Dalton Trans.* **1973**, *0* (12), 1321–1324.
- (8) Zhou, M.; Andrews, L.; Bauschlicher, C. W. *Chem. Rev.* **2001**, *101* (7), 1931–1962.
- (9) Weitz, E. *The Journal of Physical Chemistry* **2002**, *91* (15), 3945–3953.
- (10) Moskovits, M.; Ozin, G. A. *Cryochemistry*; Wiley, 1976.
- (11) Ozin, G. A.; Vander Voet, A. *Acc. Chem. Res.* **2002**, *6* (9), 313–318.
- (12) Elian, M.; Hoffmann, R. *Inorg. Chem.* **1975**, *14* (5), 1058–1076.

- (13) Sweany, R. L. *Inorg. Chem.* **1980**, *19*, 3512–3516.
- (14) Hanlan, L. A.; Huber, H.; Kuendig, E. P.; McGarvey, B. R.; Ozin. *J. Am. Chem. Soc.* **1975**, *97* (24), 7054–7068.
- (15) Crichton, O.; Poliakoff, M.; Rest, A. J.; Turner, J. J. *J. Chem. Soc., Dalton Trans.* **1973**, No. 12, 1321–1324.
- (16) Huo, C.-F.; Li, Y.-W.; Wu, G.-S.; Beller, M.; Jiao, H. *J. Phys. Chem. A* **2002**, *106* (50), 12161–12169.
- (17) Ryeng, H.; Gropen, O.; Swang, O. *J. Phys. Chem. A* **1997**, *101* (47), 8956–8958.
- (18) Bor, G.; Dietler, U. K.; Noack, K. *Journal of the Chemical Society, Chemical Communications* **1976**, No. 22, 914–916.
- (19) Sweany, R. L.; Brown, T. L. *Inorg. Chem.* **2002**, *16* (2), 415–421.
- (20) Aullón, G.; Alvarez, S. *European Journal of Inorganic Chemistry* **2001**, *2001* (12), 3031–3038.
- (21) Heck, R. F.; Breslow, D. S. *J. Am. Chem. Soc.* **1961**, *83* (19), 4023–4027.
- (22) Mann, K. R.; Cimolino, M.; Geoffroy, G. L.; Hammond, G. S.; Orio, A. A.; Albertin, G.; Gray, H. B. *Inorganica Chimica Acta* **1976**, *16*, 97–101.
- (23) Yamamoto, Y.; (null), H. Y. *Inorg. Chem.* **1978**, *17* (11), 3111.
- (24) Yamamoto, Y. *Coordination Chemistry Reviews* **1980**, *32* (3), 193–233.
- (25) Otsuka, S.; Yoshida, T.; Tatsuno, Y. *J. Am. Chem. Soc.* **2002**, *93* (24), 6462–6469.
- (26) Barker, G. K.; Galas, A. M. R.; Green, M.; Howard, J. A. K.; Stone, F. G. A.; Turney, T. W.; Welch, A. J.; Woodward, P. *Journal of the Chemical Society, Chemical Communications* **1977**, *0* (8), 256–258.
- (27) Carpenter, A. E. *Low-Valent Cobalt Isocyanides : Analogues to Classical Carbonyls.*; University of California San Diego, 2015.
- (28) Twamley, B.; Haubrich, S. T.; Power, P. P. *Advances in Organometallic Chemistry* **1999**, *44*, 1–65.
- (29) Clyburne, J. A. C.; McMullen, N. *Coordination Chemistry Reviews* **2000**, *210* (1), 73–99.
- (30) Gavenonis, J.; Tilley, T. D. *Organometallics* **2002**, *21* (25), 5549–5563.

- (31) Wright, R. J.; Steiner, J.; Beaini, S.; Power, P. P. *Inorganica Chimica Acta* **2006**, *359* (6), 1939–1946.
- (32) Gavenonis, J.; Tilley, T. D. *Organometallics* **2004**, *23* (1), 31–43.
- (33) Ito, M.; Matsumoto, T.; Tatsumi, K. *Inorg. Chem.* **2009**, *48* (5), 2215–2223.
- (34) Hagadorn, J. R.; Que, L.; Tolman, W. B.; Prisecaru, I.; Münck, E. *J. Am. Chem. Soc.* **1999**, *121* (41), 9760–9761.
- (35) Yoon, S.; Lippard, S. J. *J. Am. Chem. Soc.* **2005**, *127* (23), 8386–8397.
- (36) Fox, B. J.; Sun, Q. Y.; DiPasquale, A. G.; Fox, A. R.; Rheingold, A. L.; Figueroa, J. S. *Inorg. Chem.* **2008**, *47* (19), 9010–9020.
- (37) Ditri, T. B.; Fox, B. J.; Moore, C. E.; Rheingold, A. L.; Figueroa, J. S. *Inorg. Chem.* **2009**, *48* (17), 8362–8375.
- (38) Carpenter, A. E.; Mokhtarzadeh, C. C.; Ripatti, D. S.; Havrylyuk, I.; Kamezawa, R.; Moore, C. E.; Rheingold, A. L.; Figueroa, J. S. *Inorg. Chem.* **2015**, *54* (6), 2936–2944.
- (39) Fox, B. J.; Millard, M. D.; DiPasquale, A. G.; Rheingold, A. L.; Figueroa, J. S. *Angew. Chem. Int. Ed.* **2009**, *48* (19), 3473–3477.
- (40) Labios, L. A.; Millard, M. D.; Rheingold, A. L.; Figueroa, J. S. *J. Am. Chem. Soc.* **2009**, *131* (32), 11318–11319.
- (41) Mokhtarzadeh, C. C.; Margulieux, G. W.; Carpenter, A. E.; Weidemann, N.; Moore, C. E.; Rheingold, A. L.; Figueroa, J. S. *Inorg. Chem.* **2015**, *54* (11), 5579–5587.
- (42) Carpenter, A. E.; Rheingold, A. L.; Figueroa, J. S. *Organometallics* **2016**, *35* (14), 2309–2318.
- (43) Margulieux, G. W.; Weidemann, N.; Lacy, D. C.; Moore, C. E.; Rheingold, A. L.; Figueroa, J. S. *J. Am. Chem. Soc.* **2010**, *132* (14), 5033–5035.
- (44) Fox, B. J.; Millard, M. D.; DiPasquale, A. G.; Rheingold, A. L.; Figueroa, J. S. *Angew. Chem. Int. Ed.* **2009**, *48* (19), 3473–3477.
- (45) Barnett, B. R.; Moore, C. E.; Rheingold, A. L.; Figueroa, J. S. *J. Am. Chem. Soc.* **2014**, *136* (29), 10262–10265.
- (46) Barnett, B. R.; Rheingold, A. L.; Figueroa, J. S. *Angew. Chem. Int. Ed.* **2016**, *55* (32), 9253–9258.

- (47) Drance, M. J.; Mokhtarzadeh, C. C.; Melaimi, M.; Agnew, D. W.; Moore, C. E.; Rheingold, A. L.; Figueroa, J. S. *Angew. Chem. Int. Ed.* **2018**, *57* (40), 13057–13061.
- (48) Barybin, M. V.; Young, V. G.; Ellis, J. E. *J. Am. Chem. Soc.* **2000**, *122* (19), 4678–4691.
- (49) Leach, P. A.; Geib, S. J.; Corella, J. A., II; Warnock, G. F.; Cooper, N. J. *J. Am. Chem. Soc.* **2002**, *116* (19), 8566–8574.
- (50) Bassett, J.-M.; Berry, D. E.; Barker, G. K.; Green, M.; Howard, J. A. K.; Stone, F. G. A. *J. Chem. Soc., Dalton Trans.* **1979**, No. 6, 1003–1011.
- (51) Carpenter, A. E.; Chan, C.; Rheingold, A. L.; Figueroa, J. S. *Organometallics* **2016**, *35* (14), 2319–2326.
- (52) Carpenter, A. E.; Wen, I.; Moore, C. E.; Rheingold, A. L.; Figueroa, J. S. *Chem. Eur. J.* **2013**, *19* (32), 10452–10457.
- (53) Chan, C.; Carpenter, A. E.; Gembicky, M.; Moore, C. E.; Rheingold, A. L.; Figueroa, J. S. *Organometallics* **2018**, *38* (7), 1436–1444.
- (54) Carpenter, A. E.; Margulieux, G. W.; Millard, M. D.; Moore, C. E.; Weidemann, N.; Rheingold, A. L.; Figueroa, J. S. *Angew. Chem. Int. Ed.* **2012**, *51* (37), 9412–9416.
- (55) Millard, M. D. *Isolation of Four-Coordinate Iridium(I) Monohydrides and the X-ray Crystal Structure of a Cobalt Tris-Isocyanide Alkane sigma-Complex*; University of California San Diego, **2013**.
- (56) *Purification of Laboratory Chemicals*; Elsevier, 2003.
- (57) Pangborn, A. B.; Giardello, M. A.; Grubbs, R. H.; Rosen, R. K.; Timmers, F. J. *Organometallics* **1996**, *15* (5), 1518–1520.
- (58) Fox, B. J.; Sun, Q. Y.; DiPasquale, A. G.; Fox, A. R.; Rheingold, A. L.; Figueroa, J. S. *Inorg. Chem.* **2008**, *47* (19), 9010–9020.
- (59) Gaussian 09, Revision D.01, M. J. Frisch, G. W. Trucks, H. B. Schlegel, G. E. Scuseria, M. A. Robb, J. R. Cheeseman, G. Scalmani, V. Barone, B. Mennucci, G. A. Petersson, H. Nakatsuji, M. Caricato, X. Li, H. P. Hratchian, A. F. Izmaylov, J. Bloino, G. Zheng, J. L. Sonnenberg, M. Hada, M. Ehara, K. Toyota, R. Fukuda, J. Hasegawa, M. Ishida, T. Nakajima, Y. Honda, O. Kitao, H. Nakai, T. Vreven, J. A. Montgomery, Jr., J. E. Peralta, F. Ogliaro, M. Bearpark, J. J. Heyd, E. Brothers, K. N. Kudin, V. N. Staroverov, T. Keith, R. Kobayashi, J. Normand, K. Raghavachari, A. Rendell, J. C. Burant, S. S. Iyengar, J. Tomasi, M. Cossi, N. Rega, J. M. Millam,

- M. Klene, J. E. Knox, J. B. Cross, V. Bakken, C. Adamo, J. Jaramillo, R. Gomperts, R. E. Stratmann, O. Yazyev, A. J. Austin, R. Cammi, C. Pomelli, J. W. Ochterski, R. L. Martin, K. Morokuma, V. G. Zakrzewski, G. A. Voth, P. Salvador, J. J. Dannenberg, S. Dapprich, A. D. Daniels, O. Farkas, J. B. Foresman, J. V. Ortiz, J. Cioslowski, D. J. Fox, Gaussian, Inc., Wallingford CT, (2013).
- (60) Becke, A. D. *The Journal of Chemical Physics* **1993**, *98* (7), 5648–5652.
- (61) Stephens, P. J.; Devlin, F. J.; Chabalowski, C. F.; Frisch, M. J. *The Journal of Physical Chemistry* **1994**, *98* (45), 11623–11627.
- (62) Hariharan, P. C.; Pople, J. A. *Theoretica Chimica Acta* **1973**, *28* (3), 213–222.
- (63) Ehlers, A. W.; Böhme, M.; Dapprich, S.; Gobbi, A.; Höllwarth, A.; Jonas, V.; Köhler, K. F.; Stegmann, R.; Veldkamp, A.; Frenking, G. *Chemical Physics Letters* **1993**, *208* (1-2), 111–114.
- (64) Zhurko, G. A.; Zhurko, D. A. *Chemcraft ver. 1.5*; 2011.
- (65) Burla, M. C.; Caliandro, R.; Camalli, M.; Carrozzini, B.; Cascarano, G. L.; De Caro, L.; Giacovazzo, C.; Polidori, G.; Spagna, R. *Journal of Applied Crystallography* **2005**, *38* (2), 381–388.
- (66) Sheldrick, G. M. *Acta Crystallogr., A, Found. Crystallogr.* **2008**, *64* (Pt 1), 112–122.
- (67) Dolomanov, O. V.; Bourhis, L. J.; Gildea, R. J.; Howard, J. A. K.; Puschmann, H. *Journal of Applied Crystallography* **2009**, *42* (2), 339–341.
- (68) Spek, A. L. *Journal of Applied Crystallography* **2003**, *36* (1), 7–13.

# Chapter 2 Associative Ligand Exchange and Substrate Activation Reactions by a Zero-Valent Cobalt Tetraisocyanide Complex

## 2.1 Introduction

Within the past decade, there has been increasing attention on the synthesis, characterization and study of mononuclear zero-valent Co complexes.<sup>1-3</sup> In contrast to the far more common valence states of 1, 2 and 3, and to some extent the formal oxidation state of  $-1$ , the zero-valent state represents a significantly underexplored electronic environment for mononuclear Co coordination compounds. Accordingly, there have been several factors that have contributed to this recent interest. These include findings that mononuclear zero-valent Co centers are adept at dinitrogen binding<sup>4,5</sup> and activation<sup>6-8</sup>, as well as efforts aimed at the development of new chemical transformations that exploit either the Co  $0/+1$ ,  $0/+2$  or  $0/+4$  formal redox couples.<sup>9-12</sup> Additionally, fundamental questions in structure, bonding and reactivity have arisen due to the inherent metalloradical nature of mononuclear zero-valent Co centers.

The research projects listed in this thesis focus on the solution-phase dynamics and novel reactivity of low-valent cobalt isocyanides, with the aim of comparing and contrasting their behavior with the chemistry associated with their carbonyl analogues.

Prior to this renewed interest, the most well-considered mononuclear zero-valent Co species was the simple binary carbonyl,  $\text{Co}(\text{CO})_4$ . This 17-electron,  $S = 1/2$  metalloradical has been proposed as an intermediate in hydroformylation (oxo catalysis) initiated by photolytic or thermal activation of  $\text{Co}_2(\text{CO})_8$ .<sup>13-16</sup> Additionally,  $\text{Co}(\text{CO})_4$  has been postulated as an intermediate in radical-type hydrogenation of olefins by  $\text{HCo}(\text{CO})_4$  at high pressures,<sup>17-24</sup> but its direct observation has been limited to low temperature matrix isolation studies. Since the first detection of  $\text{Co}(\text{CO})_4$  by Keller and Wawersik using EPR spectroscopy in 1965,<sup>25</sup> and its unequivocal matrix isolation by Poliakoff and Turner in 1974,<sup>26</sup> a number of derivatives stemming from this zero-valent carbonyl have been generated via gas-phase reactions, including  $(\text{O}_2)\text{Co}(\text{CO})_3$ ,  $(\text{PR}_3)\text{Co}(\text{CO})_3$  and  $(\eta^2\text{-C,C-alkene})\text{Co}(\text{CO})_3$ .<sup>27-29</sup> However, none of these complexes are long-lived enough for detailed spectroscopic or structural investigations, and the instability of  $\text{Co}(\text{CO})_4$  has limited the exploration of its reactivity or mechanism of action with substrates in greater detail. While it is recognized that 17-electron transition-metal carbonyl radicals (e.g.,  $\text{V}(\text{CO})_6$  and  $\text{M}(\text{CO})_5$ ;  $\text{M} = \text{Mn, Re}$ ) undergo ligand substitution reactions<sup>28,30-32</sup> via a second-order associative mechanism,<sup>33-36</sup> no direct experimental studies have been carried out on  $\text{Co}(\text{CO})_4$  and its simple ligand substitution pathways. Indeed, both dissociative and associative substitution mechanisms have been proposed for the reaction of  $\text{Co}(\text{CO})_4$  with incoming ligands.<sup>37-45</sup> For the dissociative processes in particular, it is notable that the high energy,  $15e^-$  species  $\text{Co}(\text{CO})_3$  has been postulated as a viable intermediate, although rigorous experimental data has not been disclosed to support this claim.<sup>28,41</sup>

Nevertheless, following these reports, dissociative mechanisms have been proposed for certain other zero-valent  $S = \frac{1}{2}$   $\text{CoL}_4$  complexes,<sup>46,47</sup> yet detailed kinetic information supporting such proposals have also not appeared.

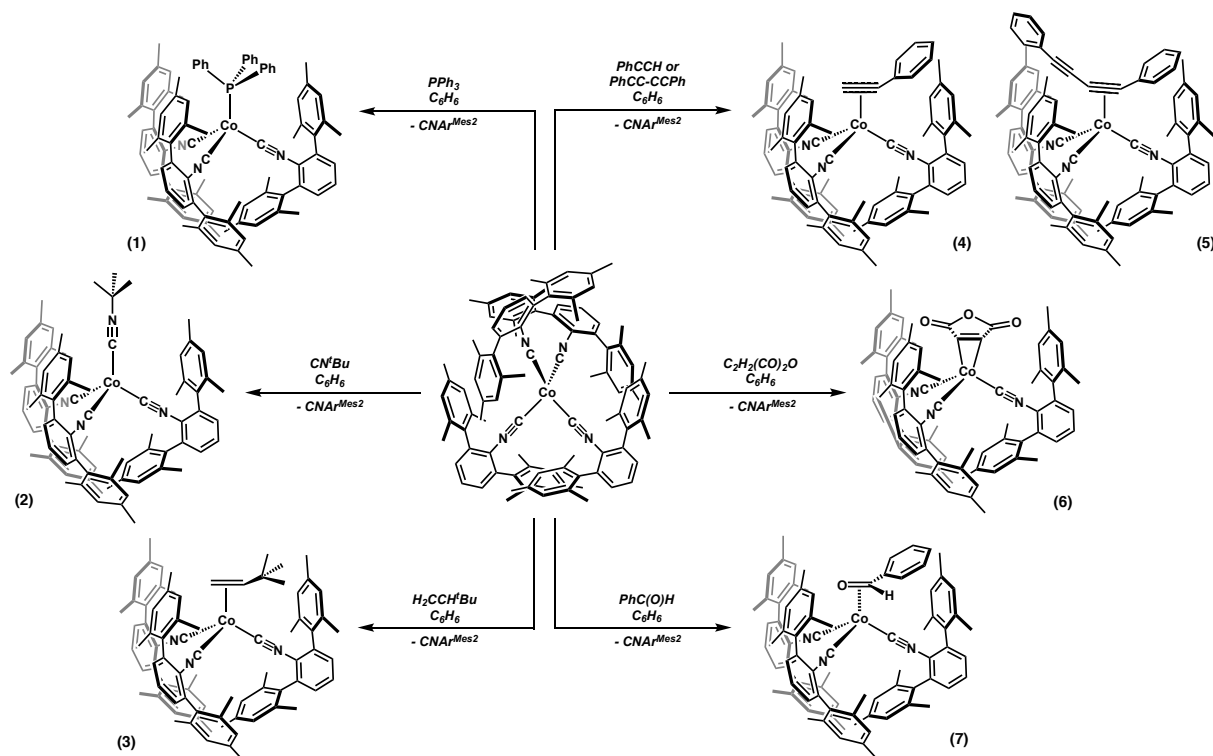
Given our interest in isolating and studying precise electronic-structure mimics of the binary unsaturated metal carbonyls (*i.e.*  $\text{M}(\text{CO})_n$ ;  $n \leq 5$ ) with encumbering *m*-terphenyl isocyanides,<sup>48-55</sup> we have previously reported that the tetrakisocyanide complex,  $\text{Co}(\text{CNAr}^{\text{Mes}_2})_4$  ( $\text{Ar}^{\text{Mes}_2} = 2,6\text{-}(2,4,6\text{-Me}_3\text{C}_6\text{H}_2)_2\text{C}_6\text{H}_3$ ), can be isolated as a crystalline solid and displays marked stability at room temperature in both solution and the solid state. Accordingly, herein we report a more detailed reactivity study on  $\text{Co}(\text{CNAr}^{\text{Mes}_2})_4$ , which includes an assessment of its ligand substitution kinetics. Most notably, despite the large steric profile of  $\text{Co}(\text{CNAr}^{\text{Mes}_2})_4$ , our data indicate that it reacts with incoming substrates via an associative ligand substitution mechanism which we believe may be general for this class of zero-valent complexes. In addition, the reactivity profiles of  $\text{Co}(\text{CNAr}^{\text{Mes}_2})_4$  indicates that it reacts in a multi-, rather than single-, electron fashion with reducible substrates.

## 2.2 L-type Ligand Substitution Chemistry of $\text{Co}(\text{CNAr}^{\text{Mes}_2})_4$

As with  $\text{Co}(\text{CO})_4$ ,  $\text{Co}(\text{CNAr}^{\text{Mes}_2})_4$  readily undergoes ligand substitution reactions. Treatment of  $\text{Co}(\text{CNAr}^{\text{Mes}_2})_4$  with one equivalent of triphenylphosphine ( $\text{PPh}_3$ ), followed by analysis by FTIR spectroscopy indicated the formation of free  $\text{CNAr}^{\text{Mes}_2}$  ligand and a new  $C_{3v}$ -symmetric product. The product was determined to be phosphine-substituted  $\text{Co}(\text{PPh}_3)(\text{CNAr}^{\text{Mes}_2})_3$  (**1**; Scheme 2.1) by X-ray diffraction. Additionally, Evans method magnetic moment determination in  $\text{C}_6\text{H}_6$  solution indicated a  $\mu_{\text{eff}}$  value of  $1.82(\pm 0.11) \mu_{\text{B}}$ , consistent with an  $S = \frac{1}{2}$  paramagnet. Ligand exchange with a less sterically hindered ligand,



*tert*-butyl isocyanide (CN*t*-Bu), also was achieved, and Co(CN*t*-Bu)(CNAr<sup>Mes2</sup>)<sub>3</sub> (**2**; Scheme 2.1) was isolated as a red crystalline material that gives rise to an effective magnetic moment of 1.76 (± 0.03) μ<sub>B</sub> when dissolved in C<sub>6</sub>D<sub>6</sub> solution. Like Co(CNAr<sup>Mes2</sup>)<sub>4</sub>, complex **2** is stable at room temperature in solution and does not readily dimerize to a diamagnetic species over a 24 h period.



**Scheme 2.1.** Synthesis of Co(L)(CNAr<sup>Mes2</sup>)<sub>3</sub> Complexes 1-7.

Certain olefins and acetylenes also add cleanly to Co(CNAr<sup>Mes2</sup>)<sub>4</sub> with displacement of a single isocyanide ligand. As shown in Scheme 1, treatment of Co(CNAr<sup>Mes2</sup>)<sub>4</sub> with *tert*-butyl ethylene or phenylacetylene produce the paramagnetic products Co(η<sup>2</sup>-C,C-*t*-BuCHCH<sub>2</sub>)(CNAr<sup>Mes2</sup>)<sub>3</sub> (**3**; Scheme 2.1) and Co(η<sup>2</sup>-C,C-PhCCH)(CNAr<sup>Mes2</sup>)<sub>3</sub> (**4**; Scheme 2.1), respectively, as determined by X-ray crystallography. Both the olefin and alkyne ligands in complexes **3** and **4** bind to the Co center in an η<sup>2</sup>-fashion, with the C4–C5 bond lengths of **3**

and **4** (1.391(8) Å and 1.255(4) Å, respectively) being only slightly elongated from that of the similar and structurally characterized free olefins (t-butyl(5-hydroxy-2,6,6-trimethyloct-7-en-4-yl)carbamate) and alkyne (4-ethynyl-1-methoxybenzene) C–C bonds (1.313(3)<sup>56</sup> and 1.198(2)<sup>57</sup> Å, respectively). Similarly, Co(CNAr<sup>Mes2</sup>)<sub>4</sub> reacts readily with diphenyldiacetylene to form the  $\eta^2$ -alkyne complex, Co( $\eta^2$ -C,C-PhCC-CCPh)(CNAr<sup>Mes2</sup>)<sub>3</sub> (**5**; Scheme 2.1) in which only one acetylenic unit is bound to a Co center (**5**; Figure 2.1). This binding arrangement allows for an internal comparison of acetylenic bond lengths, which again confirmed that the  $\eta^2$ -bound alkyne C-C bond is only slightly elongated relative to the unbound alkyne (1.275(4) Å vs. 1.205(4) Å, respectively).

Notably, heating both **3** and **4** at 40 °C in benzene solution for days showed no evidence of further bond activation processes. However, placement of complex **3** under an H<sub>2</sub> atmosphere at room temperature resulted in the formation of the known, *m*-terphenyl aldimine, H<sub>2</sub>C=NAr<sup>Mes2</sup>,<sup>54</sup> via 1,1-hydrogenation of the CNAr<sup>Mes2</sup> ligand. More interestingly, analysis of the reaction mixture showed only trace amounts of 2,2-dimethylbutane, thereby indicating that complex **3** is not a competent pre-catalyst for olefin hydrogenation.<sup>23</sup>

To determine whether Co(CNAr<sup>Mes2</sup>)<sub>4</sub> could engage in radical-type 1e<sup>-</sup> reaction with organic compounds, its reactivity with carbonyl-containing substrates were probed. Notably, Co(CNAr<sup>Mes2</sup>)<sub>4</sub> failed to react with benzophenone after 36 h in C<sub>6</sub>D<sub>6</sub>, which we attribute to both the size and topology of the substrate. Therefore, we next chose maleic anhydride (MA) and benzaldehyde (BA) due to their relatively small steric profile and their potential to form a stabilized ketyl-radical-type complex. However, rather than conclusively eliciting 1e<sup>-</sup> radical-type chemistry from Co(CNAr<sup>Mes2</sup>)<sub>4</sub>, both substrates displayed simple ligand substitution

chemistry, yielding the  $\eta^2$ -C,C bound maleic anhydride complex,  $\text{Co}(\eta^2\text{-C,C-MA})(\text{CNAr}^{\text{Mes}_2})_3$  (**6**; Scheme 2.1), and the  $\eta^2$ -C,O bound benzaldehyde complex  $(\eta^2\text{-C,O-PhC(O)H})(\text{CNAr}^{\text{Mes}_2})_3$  (**7**; Scheme 2.1) as determined by single-crystal X-ray diffraction. Both reactions were accompanied by the loss of one  $\text{CNAr}^{\text{Mes}_2}$  ligand. From the crystallographic data, the C–C bond length of  $\text{Co}(\eta^2\text{-C,C-MA})(\text{CNAr}^{\text{Mes}_2})_3$  (**6**) (1.414(8) Å) showed a *ca.* 0.1 Å elongation from free MA, indicating stronger  $\pi$ - back-bonding from the cobalt center relative to the olefin and alkyne complexes **3-5**. Contrastingly, the C–O bond length of  $\text{Co}(\eta^2\text{-C,O-PhC(O)H})(\text{CNAr}^{\text{Mes}_2})_3$  (**7**) (1.261(8) Å) displayed a more modest bond elongation as in complexes **3-5**.

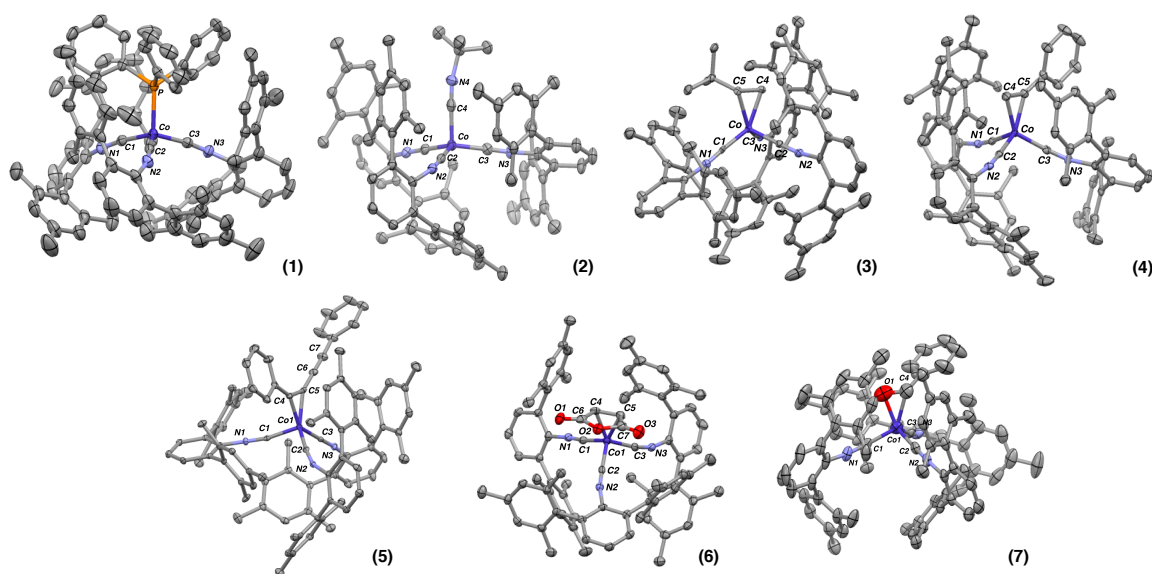


**Figure 2.1.** Molecular Structures of  $\text{Co}(\text{L})(\text{CNAr}^{\text{Mes}_2})_3$  Complexes 1-7.

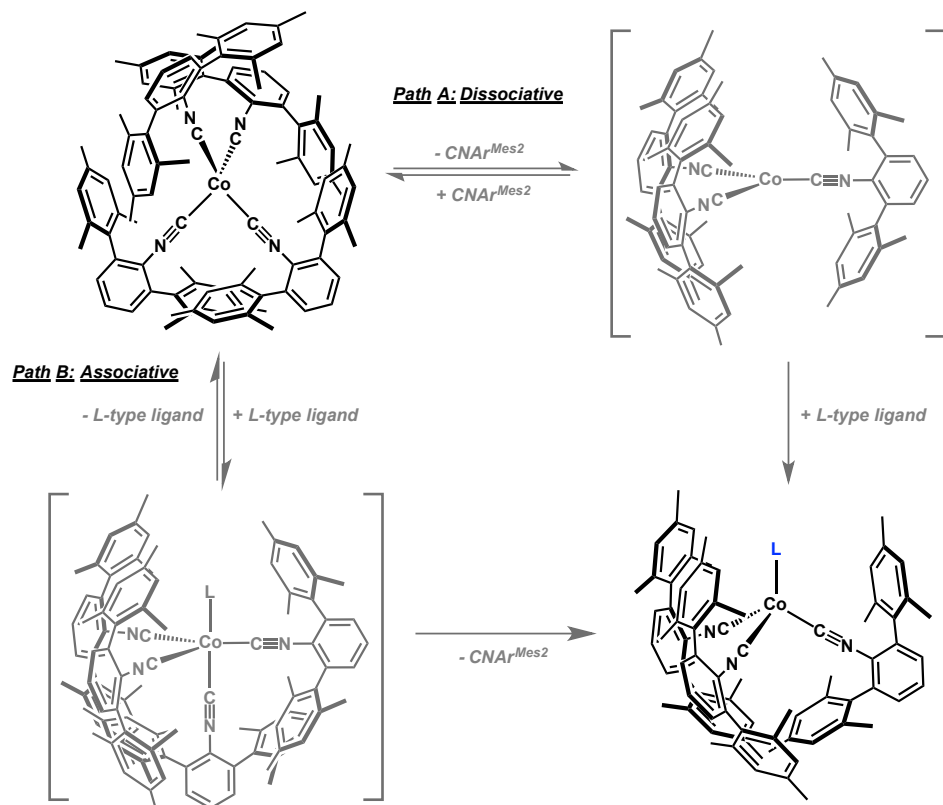
## 2.3 Mechanistic Observations on $\text{Co}(\text{CNAr}^{\text{Mes}_2})_4$ Ligand Exchange

### Chemistry

While the formation of  $\text{Co}(\text{L})(\text{CNAr}^{\text{Mes}_2})_3$  from  $\text{Co}(\text{CNAr}^{\text{Mes}_2})_4$  is reminiscent of the outcome of the ligand substitution chemistry for  $\text{Co}(\text{CO})_4$ , the mechanism by which these transformations occur has not been conclusively elucidated. Scheme 2.2 outlines both dissociative and associative ligand substitution pathways for  $\text{Co}(\text{CNAr}^{\text{Mes}_2})_4$ . Path **A** represents rate-determining  $\text{CNAr}^{\text{Mes}_2}$  dissociation to form the 15  $e^-$  species  $\text{Co}(\text{CNAr}^{\text{Mes}_2})_3$ . This mechanism is similar to that proposed for other zero-valent  $\text{CoL}_4$  complexes where a low-coordinate  $\text{CoL}_3$  species is invoked as the key intermediate. Alternatively, Path **B** depicts an associative mechanism featuring an idealized 19 $e^-$   $\text{Co}(\text{L})(\text{CNAr}^{\text{Mes}_2})_4$  intermediate, which proceeds to the final tris-isocyanide product after post-rate-determining  $\text{CNAr}^{\text{Mes}_2}$  dissociation. As a representative case for measuring ligand substitution kinetics in this system, phenylacetylene was selected as the incoming ligand due to the significantly differentiated optical properties between maroon-red  $\text{Co}(\text{CNAr}^{\text{Mes}_2})_4$  and the brown-yellow  $\eta^2\text{-C,C-PhCCH}$  complex **4**. UV-vis spectra of 0.25 mM THF solutions of  $\text{Co}(\text{CNAr}^{\text{Mes}_2})_4$  and **4** are shown in Figure 2.2, where the well-separated absorption of  $\text{Co}(\text{CNAr}^{\text{Mes}_2})_4$  at 485 nm serves as a convenient spectroscopic feature to measure reaction progression.

Under pseudo-first-order conditions (10 and 20 equiv of PhCCH) at 20 °C, the reaction between  $\text{Co}(\text{CNAr}^{\text{Mes}_2})_4$  and PhCCH proceeded with a rate constant of  $k_{obs} = 1.41(6) \times 10^{-3} \text{ s}^{-1}$  for 10 equiv of PhCCH and a rate constant of  $k_{obs} = 3.29(2) \times 10^{-3} \text{ s}^{-1}$  for 20 equiv of PhCCH (Figure 2.3 and Table 2.1). Plotting  $\ln[\text{Co}(\text{CNAr}^{\text{Mes}_2})_4]$  versus time revealed a linear relationship, in accordance with pseudo-first-order conditions. The roughly two-fold increase

in  $k_{obs}$  upon increasing the concentration of PhCCH is suggestive of an associative reaction mechanism with a concentration dependence on the incoming ligand.



**Scheme 2.2.** Potential Mechanisms for the Ligand Substitution Chemistry of  $\text{Co}(\text{CNAr}^{\text{Mes}2})_4$ .

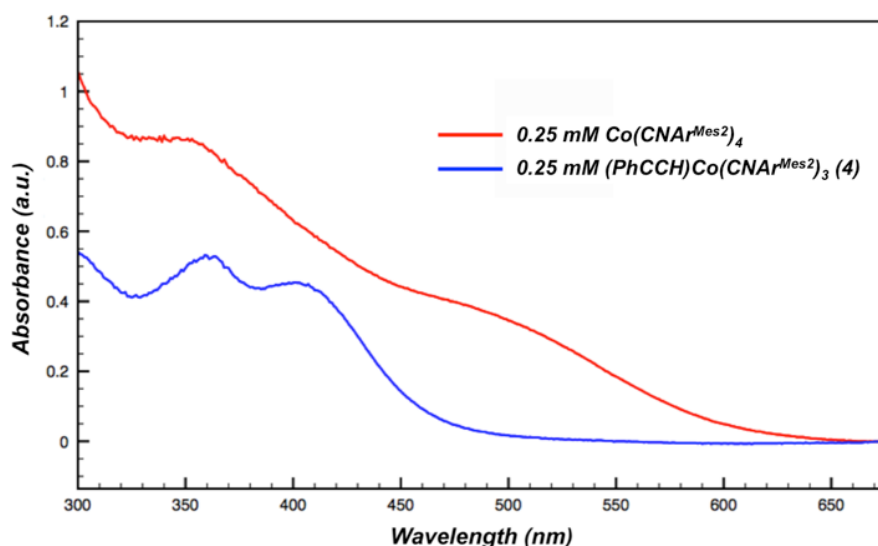


**Figure 2.2.** UV-Vis spectrum of 0.25mM  $\text{Co}(\text{CNAr}^{\text{Mes}2})_4$  in THF (red) and 0.25mM  $\text{Co}(\eta^2\text{-C,C-PhCCH})(\text{CNAr}^{\text{Mes}2})_3$  (**4**) in THF (blue).

To further support the associative mechanism and exclude a dissociative pathway, free  $\text{CNAr}^{\text{Mes}2}$  was added to the reaction mixture for the purpose of suppressing the potential formation of the three-coordinate,  $15e^-$  species  $\text{Co}(\text{CNAr}^{\text{Mes}2})_3$  (Scheme 2.2, Path A). As shown in Figure 2.3 and Table 2.1, addition of  $\text{CNAr}^{\text{Mes}2}$  (20 equiv) to reactions between  $\text{Co}(\text{CNAr}^{\text{Mes}2})_4$  and either 10 or 20 equiv of PhCCH showed a negligible effect on  $k_{\text{obs}}$  for the formation of complex **4**. Accordingly, the insensitivity of the rate constants with respect to  $[\text{CNAr}^{\text{Mes}2}]$  suggests strongly that  $\text{CNAr}^{\text{Mes}2}$  dissociation from  $\text{Co}(\text{CNAr}^{\text{Mes}2})_4$  is not the rate determining step in this ligand substitution process. In this respect,  $\text{Co}(\text{CNAr}^{\text{Mes}2})_4$  shares an operational similarity with the neutral, 17-electron metal carbonyl radicals  $\text{V}(\text{CO})_6$  and  $\text{M}(\text{CO})_5$  ( $\text{M} = \text{Mn}, \text{Re}$ ), for which detailed kinetic information has established associative ligand exchange mechanisms.<sup>42,43</sup> This finding is significant in that the encumbering steric environment provided by four  $\text{CNAr}^{\text{Mes}2}$  ligands could be expected to discourage direct attack of an incoming ligand. However, the fact that  $\text{Co}(\text{CNAr}^{\text{Mes}2})_4$  reacts with HCCPh by an apparent

associative process suggests that Co(0) complexes with smaller steric profiles may react similarly, and not via dissociative mechanisms as has been proposed.

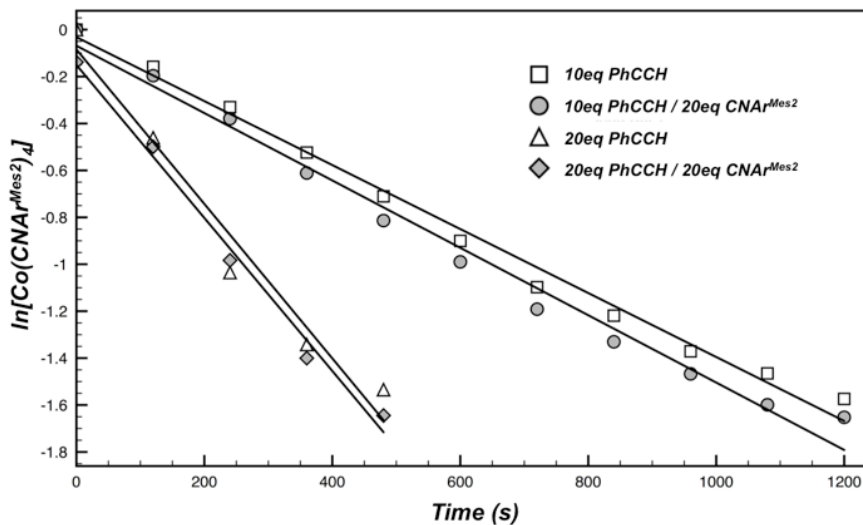


**Figure 2.3.** Plot of  $\ln[\text{Co}(\text{CNAr}^{\text{Mes}2})_4]$  vs time, showing the comparative observed rates of  $\text{Co}(\text{CNAr}^{\text{Mes}2})_4$  ligand exchange by PhCCH with the effect of 20 equiv  $\text{CNAr}^{\text{Mes}2}$  present under pseudo-first-order conditions (10 and 20 equiv).

**Table 2.1.** Observed Rate Constants in the Ligand Substitution Reaction of  $\text{Co}(\text{CNAr}^{\text{Mes}2})_4$  by PhCCH Under Pseudo-First-Order Conditions with Extra  $\text{CNAr}^{\text{Mes}2}$  Added.

Equiv PhCCH	Equiv $\text{CNAr}^{\text{Mes}2}$	$k_{\text{obs}}$ ( $\text{s}^{-1}$ )
10	0	$1.41(6) \times 10^{-3}$
10	20	$1.51(3) \times 10^{-3}$
20	0	$3.29(2) \times 10^{-3}$
20	20	$3.26(1) \times 10^{-3}$

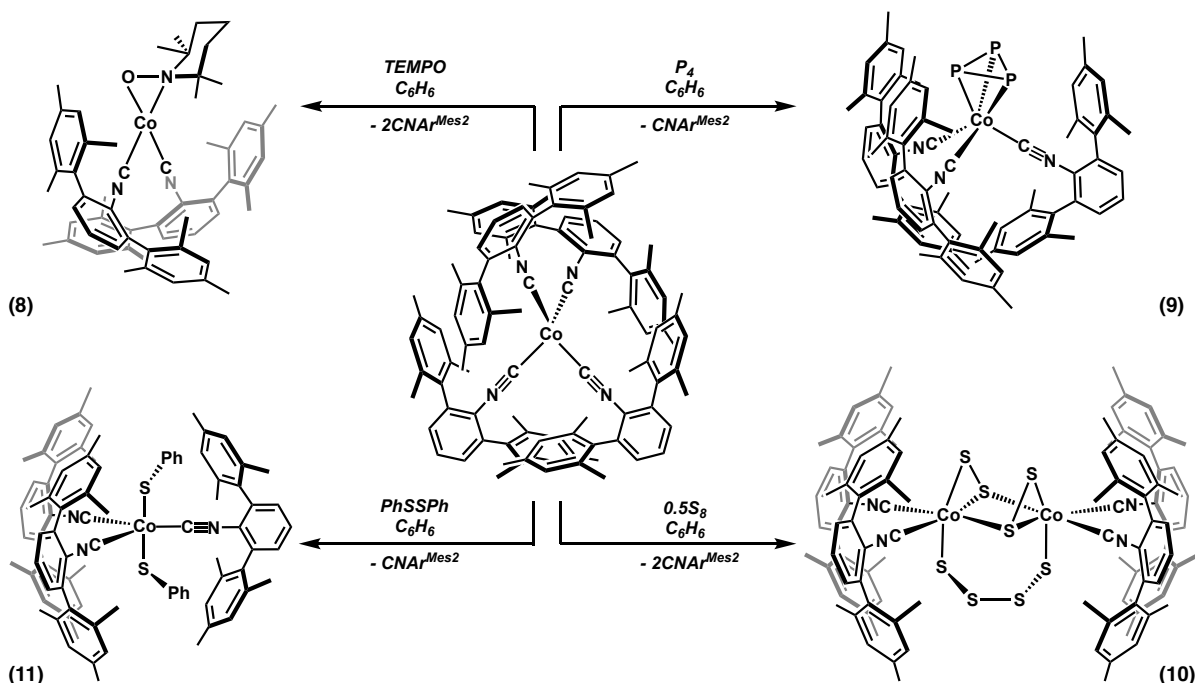
## 2.4 Assessing the Radical-Type Behavior of $\text{Co}(\text{CNAr}^{\text{Mes}2})_4$

Upon obtaining evidence that  $\text{Co}(\text{CNAr}^{\text{Mes}2})_4$  reacts with neutral L-type donor substrates by an associative mechanism, we next focused on exploring its ability to engage in  $1e^-$  radical type reactivity. As noted above, the carbonyl complex  $\text{Co}(\text{CO})_4$  has been proposed as an intermediate in radical-chain hydrogenation of olefins at high temperature and pressure.

However, it has not been conclusively established to engage in  $1e^-$  type reactivity, such as halogen- or hydrogen-atom abstraction reactions, under ambient conditions. Furthermore, this behavior of  $\text{Co}(\text{CO})_4$  contrasts with the chemistry of the  $17e^-$  radical  $\text{Mn}(\text{CO})_5$ , which is a potent halogen- and hydrogen-atom abstraction reagent. Similarly,  $\text{Co}(\text{CNAr}^{\text{Mes}_2})_4$  does not engage in straightforward  $1e^-$  chemistry despite being a more electron-rich analogue of  $\text{Co}(\text{CO})_4$ . For example,  $\text{Co}(\text{CNAr}^{\text{Mes}_2})_4$  does not react readily with  $\text{HSnBu}_3$  in  $\text{C}_6\text{D}_6$  solution. Analysis of this reaction by  $^1\text{H}$  NMR spectroscopy after 24 h showed predominantly unreacted  $\text{Co}(\text{CNAr}^{\text{Mes}_2})_4$  with only a trace of the known hydride complex  $\text{HCo}(\text{CNAr}^{\text{Mes}_2})_4$  (ca. 2%).<sup>54,55</sup> In addition, treatment of  $\text{Co}(\text{CNAr}^{\text{Mes}_2})_4$  with  $\text{HCCl}_3$  leads to a mixture of products, wherein the known monochloride complex  $\text{ClCo}(\text{CNAr}^{\text{Mes}_2})_3$  is formed in only ca. 20% yield. In contrast, the isolable  $S = 1/2$  metalloradical  $\text{Mn}(\text{CO})_3(\text{CNAr}^{\text{Dipp}_2})_2$  reacts upon mixing with both  $\text{HSnBu}_3$  and  $\text{HCCl}_3$  to cleanly produce products indicative of hydrogen- or chlorine-atom abstraction, respectively, as the major species.<sup>58</sup> To date, we have not identified a substrate class where  $\text{Co}(\text{CNAr}^{\text{Mes}_2})_4$  functions in its reaction chemistry as a simple metalloradical capable of  $X\cdot$  abstraction. In fact, even when treated with the stable radical TEMPO,  $\text{Co}(\text{CNAr}^{\text{Mes}_2})_4$  undergoes substantial electronic reorganization and loss of two ligands to form the diamagnetic, square planar complex,  $(\eta^2\text{-}O,N\text{-TEMPO})\text{Co}(\text{CNAr}^{\text{Mes}_2})_2$  (**8**; Scheme 2.3). Notably, the analogous carbonyl complex  $(\eta^2\text{-}O,N\text{-TEMPO})\text{Co}(\text{CO})_2$  has been isolated and structurally



characterized from the reaction of photogenerated  $\text{Co}(\text{CO})_4$  with TEMPO and shows structural features similar to those of **8**.<sup>59</sup>



**Scheme 2.3.** Synthesis of Complexes **8-11**.

As an additional probe for  $1e^-$  metalloradical behavior from  $\text{Co}(\text{CNAr}^{\text{Mes}2})_4$ , its reactivity toward elemental phosphorus was surveyed as this reagent can react via  $1e^-$  pathways with sterically constrained metal centers.<sup>58,60</sup> As shown in Scheme 2.3,  $\text{Co}(\text{CNAr}^{\text{Mes}2})_4$  readily reacts with  $\text{P}_4$  in benzene solution. However, rather than producing a product indicative of a  $1e^-$  reduction by  $\text{Co}(\text{CNAr}^{\text{Mes}2})_4$ , this reaction generates the diamagnetic *cyclo*- $\text{P}_3$  complex ( $\eta^3\text{-P}_3$ ) $\text{Co}(\text{CNAr}^{\text{Mes}2})_3$  (**9**) as the only cobalt-containing product. Complex **9** gives rise to a distinctive singlet at  $\delta = -278$  ppm in its  $^{31}\text{P}\{^1\text{H}\}$  NMR spectrum, which is consistent with other *cyclo*- $\text{P}_3$  transition metal complexes. Accordingly, this product outcome illustrates a preference of the Co center in  $\text{Co}(\text{CNAr}^{\text{Mes}2})_4$  to undergo multi-electron transformations, rather than execute a simple  $1e^-$  reduction reaction. In this respect it is also notable that  $\text{P}_4$  also reacts with

Co<sub>2</sub>(CO)<sub>8</sub> to produce (η<sup>3</sup>-P<sub>3</sub>)Co(CO)<sub>3</sub>, which was the first reported *cyclo*-P<sub>3</sub> transition metal complex.<sup>61,62</sup> However, this *cyclo*-P<sub>3</sub> complex is not stable at room temperature and readily decomposes to a complex mixture in which only the nonacobalt cluster, [P<sub>3</sub>Co<sub>9</sub>(CO)<sub>24</sub>], has been identified.<sup>63</sup> In contrast, complex **9**, on account of its encumbered steric profile, shows outstanding thermal stability at room temperature in solution and also retains its integrity for days when heated to 60 °C.

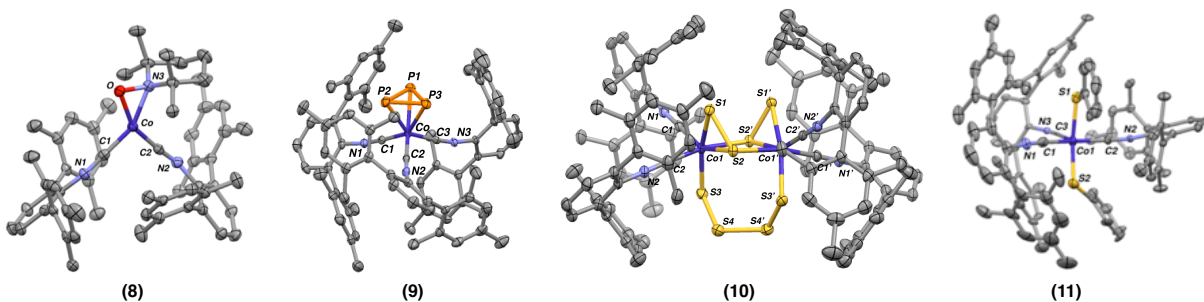


**Figure 2.4.** Molecular Structures of Complexes **8-11**.

Similar to its reaction with P<sub>4</sub>, zero-valent Co(CNAr<sup>Mes2</sup>)<sub>4</sub> reacts in a multi-electron fashion with both elemental sulfur (S<sub>8</sub>) and diphenyl disulfide (PhSSPh). Treatment of Co(CNAr<sup>Mes2</sup>)<sub>4</sub> with 0.5 equiv. of S<sub>8</sub> produces the dimeric diamagnetic complex [Co<sub>2</sub>(μ-S<sub>2</sub>)<sub>2</sub>(μ-S<sub>4</sub>)(CNAr<sup>Mes2</sup>)<sub>4</sub>] (**10**; Scheme 2.3) along with free CNAr<sup>Mes2</sup>. Crystallographic structure determination of complex **10** revealed that each Co center is bound by an η<sup>2</sup>-disulfide unit, which also forms a dative κ<sup>1</sup>-interaction to the neighboring cobalt atom. Both Co centers are also linked by a catenated S<sub>4</sub> unit to form a dinuclear molecular core resembling the head of a cat when viewed along a vector coincident with the Co<sub>2</sub> plane (**10**; Scheme 2.3). While unusual, this fragmentation mode of S<sub>8</sub> has been observed previously with molecular molybdenum and tungsten complexes.<sup>64,65</sup> Whereas Co<sub>2</sub>(CO)<sub>8</sub> has been shown to react with S<sub>8</sub> to form a variety of Co/S clusters,<sup>66,67</sup> dinuclear **10** is the only identifiable Co-containing species when

$\text{Co}(\text{CNAr}^{\text{Mes}2})_4$  is used as a precursor. Again, as with  $\text{P}_4$ ,  $\text{Co}(\text{CNAr}^{\text{Mes}2})_4$  reacts in a multi-electron manner that to produce a formally Co(III) product. Similarly, treatment of  $\text{Co}(\text{CNAr}^{\text{Mes}2})_4$  with 1.0 equiv. of PhSSPh produces the bis-thiolate complex  $\text{Co}(\text{SPh})_2(\text{CNAr}^{\text{Mes}2})_3$  (**11**) as the exclusive Co-containing product. Notably, when 0.5 equiv. of PhSSPh was employed in this reaction, an equimolar mixture of **11** and unreacted  $\text{Co}(\text{CNAr}^{\text{Mes}2})_4$  is obtained. While circumstantial, this reactivity toward PhSSPh seemingly indicates that substrate reductions by  $\text{Co}(\text{CNAr}^{\text{Mes}2})_4$  proceeds via an inner-sphere mechanism akin to a prototypical oxidative addition, rather than via discrete  $1e^-$  steps. In fact, to our knowledge there are no known instances to date where a zero-valent Co complex reacts with a substrate via a well-defined or conclusive  $1e^-$  pathway.

## 2.5 Concluding Remarks

The zero-valent state of cobalt is becoming the subject of increasing interest for the discovery of new chemical transformations. Using the tetrakisocyanide  $\text{Co}(\text{CNAr}^{\text{Mes}2})_4$ , which is an analogue of the simple binary carbonyl  $\text{Co}(\text{CO})_4$ , we have developed a convenient platform for assessing the fundamental reaction dynamics of a zero-valent Co center. We have found that  $\text{Co}(\text{CNAr}^{\text{Mes}2})_4$  readily undergoes ligand-substitution reactions with a host of neutral,  $2e^-$ -donors. Kinetic analysis of the reaction between  $\text{Co}(\text{CNAr}^{\text{Mes}2})_4$  and phenylacetylene, in both the presence and absence of free  $\text{CNAr}^{\text{Mes}2}$ , strongly indicate that an associative mechanism is operative for these ligand substitution reactions. This finding is consistent with the proposed mechanisms of other isolable  $17 e^-$ ,  $S = \frac{1}{2}$  transition metal carbonyls (e.g.  $\text{V}(\text{CO})_6$ ), but contrasts with proposals of  $\text{Co}(\text{CO})_4$  dissociative mechanisms. On account of the encumbering steric profile of  $\text{Co}(\text{CNAr}^{\text{Mes}2})_4$ , we believe it is reasonable to suggest that other

CoL<sub>4</sub> complexes react generally via an associative mechanism, especially those with strong 2e<sup>-</sup> donor ligands such as Co(PMe<sub>3</sub>)<sub>4</sub>. We have also surveyed the reaction chemistry of Co(CNAr<sup>Mes2</sup>)<sub>4</sub> with a range of substrates that can function as multi-electron oxidants. Despite its *S* = ½ ground state, d<sup>9</sup> Co(CNAr<sup>Mes2</sup>)<sub>4</sub> does not react with any substrate surveyed via discrete 1e<sup>-</sup> steps. Instead, Co(CNAr<sup>Mes2</sup>)<sub>4</sub> reacts in a manner that produces formal Co(I) to Co(III) products. The results reported here illustrate that molecular zero-valent Co species may have an inherent preference to react via associative ligand substitution pathways and inner-sphere multi-electron substrate reduction/activation events.

## 2.6 Synthetic Procedures and Characterization Data.

**General Considerations.** All manipulations were carried out under an atmosphere of dinitrogen using standard Schlenk and glovebox techniques. Unless otherwise stated, reagent grade starting materials were purchased from commercial sources and either used as received or purified by standard procedures.<sup>68</sup> Solvents were dried and deoxygenated according to standard procedures.<sup>69</sup> Benzene-*d*<sub>6</sub> and Toluene-*d*<sub>8</sub> were dried with Na/K and Benzophenone followed by distillation and stored on 4 Å molecular sieves for 3 days prior to use. Celite 405 (Fisher Scientific) was dried under vacuum (24 h) at a temperature above 250 °C and stored in the glovebox prior to use. The compounds CNAr<sup>Mes2</sup> and Co(CNAr<sup>Mes2</sup>)<sub>4</sub> were prepared by previously reported methods.<sup>51,70</sup>

Solution <sup>1</sup>H, <sup>13</sup>C {<sup>1</sup>H} and <sup>31</sup>P {<sup>1</sup>H} NMR spectra were recorded on Varian Mercury 300 and 400 spectrometers or a Varian X-Sens 500 spectrometer. <sup>1</sup>H and <sup>13</sup>C {<sup>1</sup>H} chemical shifts are reported in ppm relative to SiMe<sub>4</sub> (<sup>1</sup>H and <sup>13</sup>C δ = 0.0 ppm) with reference to residual solvent resonances of 7.16 ppm (<sup>1</sup>H) and 128.06 ppm (<sup>13</sup>C) for C<sub>6</sub>D<sub>6</sub>. <sup>31</sup>P {<sup>1</sup>H} NMR chemical shifts are

reported in ppm relative to an internal standard of 85% H<sub>3</sub>PO<sub>4</sub> (0 ppm) in a sealed capillary. FTIR spectra were recorded on a Thermo-Nicolet iS10 FTIR spectrometer. Samples were prepared as KBr pellets or as solutions injected into a ThermoFisher solution cell equipped with KBr windows. For solution FTIR spectra, solvent peaks were digitally subtracted from all spectra by comparison with an authentic spectrum obtained immediately prior to that of the sample. The following abbreviations were used for the intensities and characteristics of important IR absorption bands: vs = very strong, s = strong, m = medium, w = weak, vw = very weak; b = broad, vb = very broad, sh = shoulder. UV-vis spectra were collected on a Shimadzu UV-3600 UV/vis/NIR spectrometer. Combustion analyses were performed by Midwest Microlab LLC of Indianapolis, IN (USA). Samples for combustion analysis were obtained from the first recrystallized batch of the reaction mixture. In a typical preparation, the crude, dry reaction mixture was dissolved in a minimum amount of solvent and stored at -35 °C for several days to produce crystalline material. This material was then collected, thoroughly dried under vacuum and then packaged under vacuum for shipment. In most cases, this material was also used for single-crystal X-ray structure determination.

**Synthesis of Ligand Substitution Products 1-7.** Ligand substitution reactions were performed using 0.015-0.070 mmol of Co(CNAr<sup>Mes2</sup>)<sub>4</sub>. To a benzene solution of Co(CNAr<sup>Mes2</sup>)<sub>4</sub> (3 mL) was added 1.0 equiv of L-type ligand as a benzene solution (1 mL). Resulting mixture was allowed to stir at room temperature for 12 h. Thereafter, the reaction mixture was concentrated to a solid under reduced pressure and then extracted with Et<sub>2</sub>O. This Et<sub>2</sub>O solution was then filtered through Celite and evaporated to dryness. Single crystals of the corresponding Co(L)(CNAr<sup>Mes2</sup>)<sub>3</sub> **1-7** products were obtained from concentrated solutions stored at -35 °C for 1-3 days.

**Data for Co(PPh<sub>3</sub>)(CNAr<sup>Mes2</sup>)<sub>3</sub> (1):** Red crystals from THF layered with *n*-pentane. Yield: 0.015 g, 0.011 mmol, 80 %. <sup>1</sup>H NMR (400.1 MHz, C<sub>6</sub>D<sub>6</sub>, 20 °C): δ = 10.88 (bs, 12H, *m*-Mes), 8.97 (bs, 9H, *m*- and *p*-Ph), 6.72 (bs, 9H, *p*- and *m*-PPh<sub>3</sub>), 5.91 (bs, 6H, *o*-PPh<sub>3</sub>), 2.08 (bs, 36H, *o*-CH<sub>3</sub> Mes), 1.93 (bs, 18H, *p*-CH<sub>3</sub> Mes) ppm. μ<sub>eff</sub> (Evans Method, C<sub>6</sub>D<sub>6</sub> / (SiMe<sub>3</sub>)<sub>2</sub>O, 400.1 MHz, 20 °C, 3 independent runs) = 1.82(±0.11) μ<sub>B</sub>. FTIR (C<sub>6</sub>D<sub>6</sub>, KBr windows, 25 °C): ν<sub>CN</sub> = 1944 (vs) and 2050 (m) also 2912 (m), 2848 (m), 1582 (m), 1433 (m), 1411 (m), 1347 (m), 1035 (m), 853 (m), 750 (m) cm<sup>-1</sup>. Anal. Calcd. for C<sub>93</sub>H<sub>90</sub>N<sub>3</sub>PCo: C, 83.83; H, 6.77; N, 3.14. Found C, 83.58; H, 7.34; N, 3.37.

**Data for Co(CN<sup>t</sup>Bu)(CNAr<sup>Mes2</sup>)<sub>3</sub> (2):** Red crystals from *n*-pentane:benzene (4:1). Yield: 0.013 g, 0.011 mmol, 32 %. <sup>1</sup>H NMR (400.1 MHz, C<sub>6</sub>D<sub>6</sub>, 20 °C): δ = 9.48 (bs, 12H, *m*-Mes), 6.95 (bs, 9H, *m*- and *p*-Ph), 5.66 (bs, 9H, CN<sup>t</sup>Bu), 2.48 (bs, 36H, *o*-CH<sub>3</sub> Mes), 2.14 (bs, 18H, *p*-CH<sub>3</sub> Mes) ppm. μ<sub>eff</sub> (Evans Method, C<sub>6</sub>D<sub>6</sub>/(SiMe<sub>3</sub>)<sub>2</sub>O, 400.1 MHz, 20 °C, 3 independent runs) = 1.76(±0.03) μ<sub>B</sub>. FTIR (C<sub>6</sub>D<sub>6</sub>, KBr windows, 25 °C): ν<sub>CN</sub> = 2021 (s), 1997 (vs), 1927 (vs), 1826 (sh) cm<sup>-1</sup>, also 2955 (m), 2919 (m), 2852 (m), 1578 (m), 1413 (m), 1375 (m) cm<sup>-1</sup>. Anal. Calcd. for C<sub>80</sub>H<sub>84</sub>N<sub>4</sub>Co: C, 82.80; H, 7.30; N, 4.83. Found C, 82.54; H, 7.70; N, 4.35.

**Data for Co(η<sup>2</sup>-C,C-<sup>t</sup>BuCHCH<sub>2</sub>)(CNAr<sup>Mes2</sup>)<sub>3</sub> (3):** Orange crystals from Et<sub>2</sub>O. Yield: 0.004 g, 0.004 mmol, 10 %. FTIR (C<sub>6</sub>D<sub>6</sub>, KBr windows, 25 °C): ν<sub>CN</sub> = 1975 (vs), 2027 (vs), also 2963 (m), 2905 (m), 2865 (m), 1465 (m), 1417 (m), 1383 (m), 1361 (s), 1211 (m), 997 (m), 912 (m) cm<sup>-1</sup>. Anal. Calcd. for C<sub>81</sub>H<sub>87</sub>N<sub>3</sub>Co·(C<sub>4</sub>H<sub>10</sub>O)<sub>3</sub>: C, 80.72; H, 8.52; N, 3.04. Found C, 79.02; H, 7.45; N, 3.11.

**Data for Co(η<sup>2</sup>-C,C-PhCCH)(CNAr<sup>Mes2</sup>)<sub>3</sub> (4):** Brown-yellow crystals from Et<sub>2</sub>O. Yield: 0.036 g, 0.031 mmol, 44 %. <sup>1</sup>H NMR (400.1 MHz, C<sub>6</sub>D<sub>6</sub>, 20 °C): δ = 6.40 (bs), 4.73 (bs), 2.20 (bs)

ppm.  $\mu_{\text{eff}}$  (Evans Method,  $\text{C}_6\text{D}_6$  /  $(\text{SiMe}_3)_2\text{O}$ , 400.1 MHz, 20 °C, 3 independent runs) = 1.84( $\pm$ 0.02)  $\mu_{\text{B}}$ . FTIR ( $\text{C}_6\text{D}_6$ , KBr windows, 25 °C):  $\nu_{\text{CN}}$  = 2087 (m), 2025 (vs), 1997 (vs)  $\text{cm}^{-1}$ , 1966 (vs)  $\text{cm}^{-1}$ ,  $\nu_{\text{CC}}$  = 1759 (m) also 3036 (m), 2946 (m), 2919 (m), 1580 (m), 1479 (m), 1440 (m), 1417 (m), 1376 (m), 851 (m), 756 (m), 679 (m)  $\text{cm}^{-1}$ . Anal. Calcd. for  $\text{C}_{83}\text{H}_{81}\text{N}_3\text{Co}\cdot(\text{C}_4\text{H}_{10}\text{O})_3$ : C, 81.39; H, 7.98; N, 3.00. Found C, 79.57; H, 6.67; N, 3.59.

**Data for  $\text{Co}(\eta^2\text{-C,C-PhCC-CCPh})(\text{CNAr}^{\text{Mes}2})_3$  (5):** Green crystals from *n*-pentane. Yield: 0.025 g, 0.019 mmol, 76 %.  $^1\text{H}$  NMR (400.1 MHz,  $\text{C}_6\text{D}_6$ , 20 °C):  $\delta$  = 10.23 (bs), 6.32 (bs), 4.89 (bs), 2.01 (bs) ppm.  $\mu_{\text{eff}}$  (Evans Method,  $\text{C}_6\text{D}_6$  /  $(\text{SiMe}_3)_2\text{O}$ , 400.1 MHz, 20 °C, 3 independent runs) = 1.78( $\pm$ 0.02)  $\mu_{\text{B}}$ . FTIR ( $\text{C}_6\text{D}_6$ , KBr windows, 25 °C):  $\nu_{\text{CN}}$  = 2089 (m), 2021 (vs), 1990 (vs)  $\text{cm}^{-1}$ ,  $\nu_{\text{CC}}$  = 1814 (m) also 3086 (m), 3068 (m), 3031 (m), 2920 (m), 2847 (m), 1634 (m), 1590 (m), 1486 (m), 1479 (m), 1416 (m), 1377 (m), 1037 (m), 915 (m), 850 (m), 754 (m)  $\text{cm}^{-1}$ . Anal. Calcd. for  $\text{C}_{91}\text{H}_{85}\text{N}_3\text{Co}\cdot(\text{C}_4\text{H}_{10}\text{O})_4$ : C, 81.54; H, 7.99; N, 2.67. Found C, 78.30; H, 6.42; N, 2.70. Multiple attempts to acquire satisfactory elemental analysis were unsuccessful. We tentatively attribute this observation to the presence of Co-containing insoluble impurities.

**Data for  $\text{Co}(\eta^2\text{-C,C-MA})(\text{CNAr}^{\text{Mes}2})_3$  (6):** Green crystals from  $\text{Et}_2\text{O}$ . Yield: 0.070 g, 0.059 mmol, 85 %.  $^1\text{H}$  NMR (400.1 MHz,  $\text{C}_6\text{D}_6$ , 20 °C):  $\delta$  = 8.59 (bs, 3H, *p*-Ph), 6.96 (bs, 2H, *MA*), 6.85 (bs, 12H, *m*-Mes), 6.36 (bs, 6H, *m*-Ph), 2.20 (bs, 54H, *o*- and *p*- $\text{CH}_3$  Mes) ppm.  $\mu_{\text{eff}}$  (Evans Method,  $\text{C}_6\text{D}_6$  /  $(\text{SiMe}_3)_2\text{O}$ , 400.1 MHz, 20 °C, 3 independent runs) = 1.82( $\pm$ 0.08)  $\mu_{\text{B}}$ . FTIR ( $\text{C}_6\text{D}_6$ , KBr windows, 25 °C):  $\nu_{\text{CN}}$  = 2049 (vs), 1996 (s)  $\text{cm}^{-1}$ ,  $\nu_{\text{CO}}$  = 1795 (s), 1731 (s),  $\nu_{\text{CC}}$  = 1612 (s), also 3036 (m), 2919 (m), 2850 (m), 2733 (m), 1223 (m), 1038 (m)  $\text{cm}^{-1}$ . Anal. Calcd. for  $\text{C}_{79}\text{H}_{77}\text{O}_3\text{N}_3\text{Co}$ : C, 80.72; H, 6.60; N, 3.57. Found C, 80.65; H, 6.59; N, 3.25.

**Data for Co( $\eta^2$ -C,O-PhC(O)H)(CNAr<sup>Mes2</sup>)<sub>3</sub> (7):** Yellow crystals from Et<sub>2</sub>O. Yield: 0.035 g, 0.030 mmol, 59 %. <sup>1</sup>H NMR (400.1 MHz, C<sub>6</sub>D<sub>6</sub>, 20 °C):  $\delta$  = 10.42 (bs, 1H, Ph(O)H), 8.21 (bs, 3H, *m*- and *p*-Ph(O)H), 7.86 (bs, 2H, *o*-Ph(O)H), 6.78 (bs, 12H, *m*-Mes), 5.38 (bs, 9H, *m*- and *p*-Ph), 2.35 (bs, 18H, *p*-CH<sub>3</sub> Mes), 2.11 (bs, 36H, *o*-CH<sub>3</sub> Mes) ppm.  $\mu_{\text{eff}}$  (Evans Method, C<sub>6</sub>D<sub>6</sub>/(SiMe<sub>3</sub>)<sub>2</sub>O, 400.1 MHz, 20 °C, 3 independent runs) = 1.91( $\pm$ 0.07)  $\mu_{\text{B}}$ . FTIR (C<sub>6</sub>D<sub>6</sub>, KBr windows, 25 °C):  $\nu_{\text{CN}}$  = 2024 (vs), 1990 (vs) cm<sup>-1</sup>,  $\nu_{\text{CO}}$  = 1705 (s), also 2925 (m), 2849 (m), 2810 (m), 2729 (m), 2690 (m), 1595 (m), 1579 (m), 1199 (m), 1163 (m) cm<sup>-1</sup>. Anal. Calcd. for C<sub>82</sub>H<sub>81</sub>N<sub>3</sub>OC<sub>o</sub>·C<sub>7</sub>H<sub>6</sub>O: C, 82.89; H, 6.80; N, 3.26. Found C, 81.08; H, 6.69; N, 2.77.

**Synthesis of Co( $\eta^2$ -N,O-TEMPO)(CNAr<sup>Mes2</sup>)<sub>2</sub> (8)** A thawing THF solution of Co(CNAr<sup>Mes2</sup>)<sub>4</sub> (0.020 g, 0.014 mmol, 15 mL) was combined with solid TEMPO (0.002 g, 0.014 mmol, 1.0 equiv). The resulting reaction mixture was allowed to stir for 1.5 h while warming to room temperature. A color change from red to brown was observed. The material was then concentrated to a solid under reduced pressure. The solid residue was dissolved in 1 mL of Et<sub>2</sub>O and stored at -30 °C to afford brown crystals which were collected and dried *in vacuo*. Trace free CNAr<sup>Mes2</sup> was removed by washing crystals with MeCN (3 x 2 mL). Yield: 0.008 g, 0.009 mmol, 64 %. <sup>1</sup>H NMR (400.1 MHz, C<sub>6</sub>D<sub>6</sub>, 20 °C):  $\delta$  = 6.96 (d, 2H, *J* = 7 Hz, *o*-Ph), 6.94 (d, 2H, *J* = 7 Hz, *o*-Ph), 6.92 (t, 1H, *J* = 7 Hz, *p*-Ph), 6.91 (s, 4H, *m*-Mes), 6.90 (t, 1H, *J* = 7 Hz, *p*-Ph), 6.82 (s, 4H, *m*-Mes), 2.31 (s, 6H, *p*-Mes), 2.29 (s, 6H, *p*-Mes), 2.17 (s, 12H, *o*-Mes), 2.07 (s, 12H, *o*-Mes), 1.34–1.10 (m, 6H, TEMPO), 1.03 (s, 6H, TEMPO-CH<sub>3</sub>), 0.97 (s, 6H, TEMPO-CH<sub>3</sub>) ppm. <sup>13</sup>C{<sup>1</sup>H} NMR (125.8 MHz, C<sub>6</sub>D<sub>6</sub>, 20 °C):  $\delta$  = 183.9 (CNR), 179.4 (CNR), 138.2, 138.2, 136.8, 136.6, 136.4, 136.3, 136.2, 135.9, 131.6, 131.3, 129.7, 129.2, 128.8, 128.7, 125.8, 125.5, 63.65, 38.1, 33.1, 23.7, 21.5, 21.3, 20.7, 20.6, 17.6 ppm. FTIR (C<sub>6</sub>D<sub>6</sub>, KBr windows, 25



$^{\circ}\text{C}$ ):  $\nu_{\text{CN}} = 2060$  (s), 2021 (s), 1932 (vs)  $\text{cm}^{-1}$  also, 2973, 2942, 2926, 2862, 1613, 1582, 1446, 1418, 1374, 1240, 1171, 1119, 847, 758, 636  $\text{cm}^{-1}$ . Anal. Calcd. For  $\text{C}_{59}\text{H}_{68}\text{N}_3\text{CoO}\cdot(\text{C}_4\text{H}_{10}\text{O})_3$ : C, 76.38; H, 8.85; N, 3.76. Found: C, 75.43; H, 7.55; N, 4.31.

**Synthesis of  $\text{Co}(\eta^3\text{-P}_3)(\text{CNAr}^{\text{Mes}_2})_3$  (**9**):**  $\text{Co}(\text{CNAr}^{\text{Mes}_2})_4$  (0.200 g, 0.141 mmol) was dissolved in benzene (10 mL) and allowed to stir for 5 m. Elemental phosphorus ( $\text{P}_4$ ) (0.002 g, 0.169 mmol, 1.2 equiv) was added to this reaction mixture as a solid. The resulting solution was allowed to stir at room temperature for 12 h. The reaction mixture was then concentrated to a brown solid under reduced pressure. The material was suspended in acetonitrile (5 mL) and filtered. The precipitate was washed with acetonitrile (3 x 3 mL) to afford a brown powder. Single brown crystals of  $\text{Co}(\eta^3\text{-P}_3)(\text{CNAr}^{\text{Mes}_2})_3$  were obtained from a concentrated fluorobenzene solution with three drops of *n*-pentane stored at  $-35^{\circ}\text{C}$  for 12 hours. Yield: 0.089 g, 0.076 mmol, 54 %.  $^1\text{H}$  NMR (500.1 MHz,  $\text{C}_6\text{D}_6$ ,  $20^{\circ}\text{C}$ ): = 6.94 (s, 12H, *m*-Mes), 6.87 (bt, 3H, *p*-Ph), 6.81 (d,  $J = 5$  Hz, 6H, *m*-Ph), 2.30 (s, 18H, *p*- $\text{CH}_3$  Mes), 2.04 (s, 36H, *o*- $\text{CH}_3$  Mes) ppm.  $^{13}\text{C}\{^1\text{H}\}$  NMR (125.8 MHz,  $\text{C}_6\text{D}_6$ ,  $20^{\circ}\text{C}$ ):  $\delta = 175.55$  (*broad*, CNR), 138.80, 137.16, 135.97, 135.22, 129.94, 129.27, 128.35, 128.16, 127.97, 21.56, 20.67 ppm. (The CNR resonance extremely broadened, presumably due to coupling to  $^{59}\text{Co}$  ( $I = 7/2$ , 100 %)).  $^{31}\text{P}\{^1\text{H}\}$  NMR (121.5 MHz,  $\text{C}_6\text{D}_6$ ,  $20^{\circ}\text{C}$ ): =  $-279.55$  (s,  $\eta^3\text{-P}_3$ ) ppm. FTIR ( $\text{C}_6\text{D}_6$ , KBr windows,  $25^{\circ}\text{C}$ ):  $\nu_{\text{CN}} = 2056$  (vs), 2007 (m), 1969 (sh)  $\text{cm}^{-1}$ , also 2919 (m), 1415 (m), 1374 (m), 1035 (s), 852 (m), 755 (m), 652 (m)  $\text{cm}^{-1}$ . Anal. Calcd. for  $\text{C}_{75}\text{H}_{75}\text{N}_3\text{P}_3\text{Co}\cdot\text{P}_4$ : C, 69.61; H, 5.84; N, 3.25. Found C, 68.04; H, 5.90; N, 2.45. Repeated attempts to obtain a more satisfactory elemental analysis were unsuccessful. We believe this is due to a small amount  $\text{P}_4$  that accompanies the bulk crystallization of (**9**).

**Synthesis of  $\text{Co}_2(\mu\text{-S}_2)_2(\mu\text{-S}_4)(\text{CNAr}^{\text{Mes}_2})_4$  (10).**  $\text{Co}(\text{CNAr}^{\text{Mes}_2})_4$  (0.050 g, 0.035 mmol) was dissolved in benzene (5 mL) and allowed to stir for 5 min. To this solution, a toluene solution of elemental sulfur ( $\text{S}_8$ ) (0.005 g, 0.018 mmol, 2 mL, 0.5 equiv) was added. The resulting solution was allowed to stir at room temperature for 2 h. Thereafter, the reaction mixture was concentrated to a black solid under reduced pressure. Single crystals of  $\text{Co}_2(\mu\text{-S}_2)_2(\mu\text{-S}_4)(\text{CNAr}^{\text{Mes}_2})_4$  were obtained from a concentrated THF solution stored at  $-35\text{ }^\circ\text{C}$  for 1 d. Yield: 0.010 g, 0.006 mmol, 32 %.  $^1\text{H}$  NMR (300.1 MHz,  $\text{C}_6\text{D}_6$ ,  $20\text{ }^\circ\text{C}$ ): = 7.21 (s, 4H, *m*-Mes), 7.02 (s, 4H, *m*-Mes), 6.96 (s, 4H, *m*-Mes), 6.91 (s, 4H, *m*-Mes), 6.88 (t,  $J = 2\text{ Hz}$ , 4H, *p*-Ph), 6.85 (d,  $J = 2\text{ Hz}$ , 1H, *m*-Ph), 6.81 (d,  $J = 2\text{ Hz}$ , 4H, *m*-Ph), 2.45 (s, 12H, *p*- $\text{CH}_3$  Mes), 2.38 (s, 12H, *p*- $\text{CH}_3$  Mes), 2.17 (s, 12H, *o*- $\text{CH}_3$  Mes), 2.15 (s, 12H, *o*- $\text{CH}_3$  Mes), 2.10 (s, 12H, *o*- $\text{CH}_3$  Mes), 1.99 (s, 12H, *o*- $\text{CH}_3$  Mes) ppm.  $^{13}\text{C}\{^1\text{H}\}$  NMR (125.8 MHz,  $\text{C}_6\text{D}_6$ ,  $20\text{ }^\circ\text{C}$ ):  $\delta = 162.96$  (*broad*, CNR), 160.12 (*broad*, CNR), 140.02, 139.83, 137.89, 137.43, 136.13, 135.54, 135.50, 135.12, 133.92, 129.66, 129.64, 129.57, 129.07, 128.78, 128.59, 128.35, 128.16, 127.97, 127.76, 127.64, 30.26, 21.91, 21.78, 20.96, 20.78, 20.61, 20.40, 20.35 ppm. (The CNR resonance extremely broadened, presumably due to coupling to  $^{59}\text{Co}$  ( $I = 7/2$ , 100 %)). FTIR ( $\text{C}_6\text{D}_6$ , KBr windows,  $25\text{ }^\circ\text{C}$ ):  $\nu_{\text{CN}} = 2148$  (vs), also 3090 (s), 3035 (m), 2922 (w), 2851 (m), 1609 (m), 1381 (m), 1274 (m), 1252 (m), 1185 (m), 855 (m)  $\text{cm}^{-1}$ . Anal. Calcd. for  $\text{C}_{100}\text{H}_{100}\text{N}_4\text{S}_8\text{Co}_2 \cdot (\text{C}_4\text{H}_8\text{O})_3$ : C, 69.03; H, 6.41; N, 2.88. Found C, 67.68; H, 5.68; N, 2.90.

**Synthesis of  $\text{Co}(\text{SPh})_2(\text{CNAr}^{\text{Mes}_2})_3$  (11)**  $\text{Co}(\text{CNAr}^{\text{Mes}_2})_4$  (0.020 g, 0.014 mmol) was dissolved in benzene (3 mL) and allowed to stir for 5 m. To this reaction mixture, a benzene solution of phenyldisulfide (0.032 g, 0.014 mmol, 1.0 equiv) was added. The resulting solution was allowed to stir at room temperature for 12 h. Thereafter, the reaction mixture was concentrated

to a black solid under reduced pressure. Single crystals of  $\text{Co}(\text{SPh})_2(\text{CNAr}^{\text{Mes}2})_3$  were obtained from a concentrated ether solution stored at  $-35\text{ }^\circ\text{C}$  for 12 hours. Yield: 0.013 g, 0.01 mmol, 71 %.  $^1\text{H}$  NMR (400.1 MHz,  $\text{C}_6\text{D}_6$ ,  $20\text{ }^\circ\text{C}$ ):  $\delta = 8.81$  (bs), 6.41 (bs), 6.05 (bs), 2.24 (bs), 1.89 (bs) ppm.  $\mu_{\text{eff}}$  (Evans Method,  $\text{C}_6\text{D}_6$  /  $(\text{SiMe}_3)_2\text{O}$ , 400.1 MHz,  $20\text{ }^\circ\text{C}$ , 3 independent runs) =  $1.61(\pm 0.05)\ \mu_{\text{B}}$ . FTIR ( $\text{C}_6\text{D}_6$ , KBr windows,  $25\text{ }^\circ\text{C}$ ):  $\nu_{\text{CN}} = 2066$  (m)  $\text{cm}^{-1}$ , also 2973 (vs), 2931 (vs), 2859 (vs), 2803 (m), 2775 (m), 1446 (m), 1413 (w), 1382 (s), 1352 (m)  $\text{cm}^{-1}$ . Anal. Calcd. for  $\text{C}_{87}\text{H}_{85}\text{N}_3\text{S}_2\text{Co}\cdot(\text{C}_4\text{H}_{10}\text{O})_2$ : C, 79.02; H, 7.33; N, 2.91. Found C, 75.96; H, 6.09; N, 2.54. Repeated attempts to obtain a more satisfactory elemental analysis were unsuccessful. We believe this to a small amount unreacted  $(\text{SPh})_2$  that accompanies the bulk crystallization of (11).

## 2.7 Reaction Procedures and Selected NMR Spectra

**Reaction of  $\text{Co}(\eta^2\text{-C},\text{C-}^t\text{BuCHCH}_2)(\text{CNAr}^{\text{Mes}2})_3$  (3) with  $\text{H}_2$ .** In the glovebox, a 0.5 mL  $d_6$ -benzene solution of  $\text{Co}(\eta^2\text{-C},\text{C-}^t\text{BuCHCH}_2)(\text{CNAr}^{\text{Mes}2})_3$  (3) (0.017 mmol, 20 mg) was prepared in a J-young NMR tube. 1 ATM of  $\text{H}_2$  was added to the solution at room-temperature after two freeze-pump-thaw cycles. The reaction was then monitored by  $^1\text{H}$  NMR spectroscopy. After 2 days of reaction time, the reaction resulted in mostly the formation of the known, *m*-terphenyl aldimine,  $\text{H}_2\text{C}=\text{NAr}^{\text{Mes}2}$ .

**Reaction of  $\text{Co}(\text{CNAr}^{\text{Mes}2})_4$  with  $\text{HSnBu}_3$ .** In the glovebox, 1.0 equiv of  $\text{HSnBu}_3$  (0.004 mmol, 1.2 mg, 1.08  $\mu\text{L}$ ) was added to a 0.5 mL  $d_6$ -benzene solution of  $\text{Co}(\text{CNAr}^{\text{Mes}2})_4$  (0.004 mmol, 5 mg). The reaction was then transferred into an NMR tube and monitored by  $^1\text{H}$  NMR

spectroscopy. After 24 h of reaction time, the reaction showed mainly unreacted starting material.

**Reaction of  $\text{Co}(\text{CNAr}^{\text{Mes}_2})_4$  with  $\text{HCCl}_3$ .** In the glovebox, 1.0 equiv of  $\text{HCCl}_3$  (0.004 mmol, 0.5 mg, 0.32  $\mu\text{L}$ ) was added to a 0.5 mL  $d_6$ -benzene solution of  $\text{Co}(\text{CNAr}^{\text{Mes}_2})_4$  (0.004 mmol, 5 mg). The reaction was then transferred into an NMR tube, monitored by  $^1\text{H}$  NMR and IR spectroscopy. After 20 minutes of reaction time, the reaction led to a mixture of products where only  $\text{ClCo}(\text{CNAr}^{\text{Mes}_2})_3$  was identified in a ca. 20% yield.

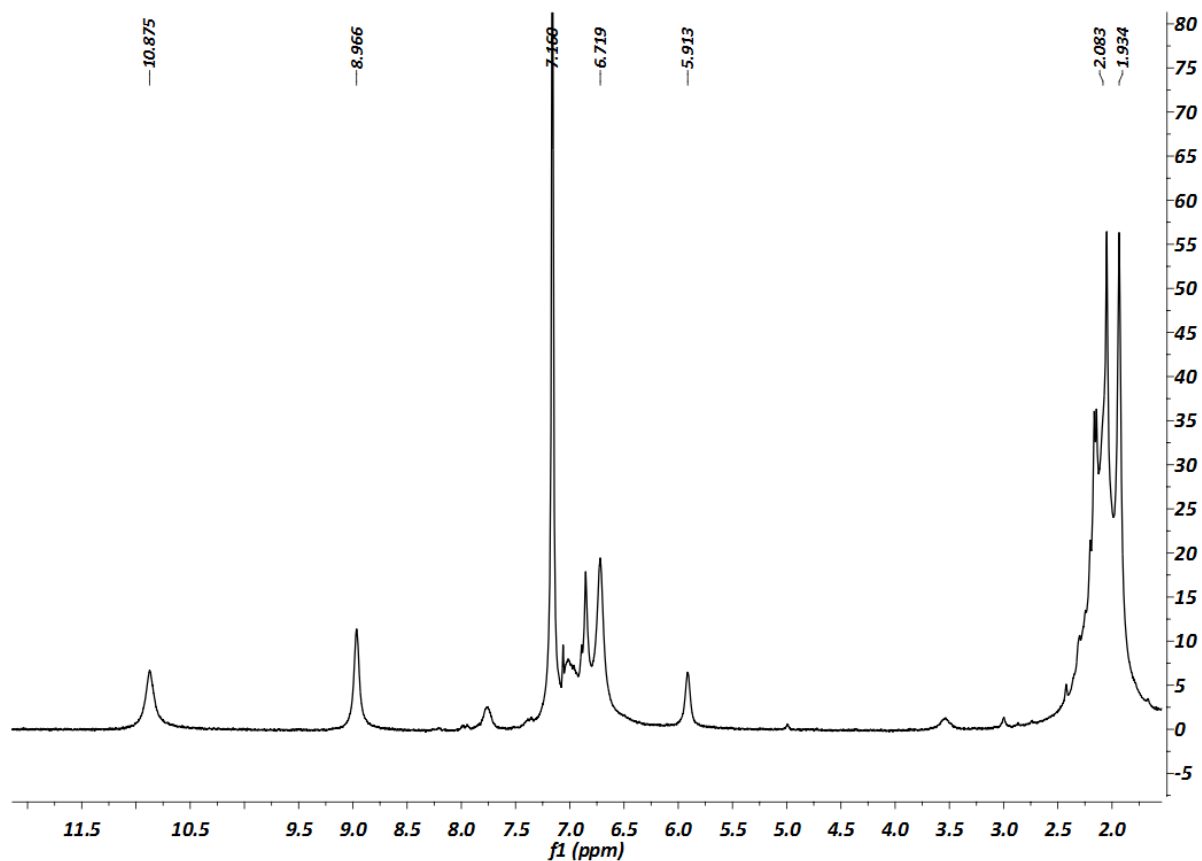


**Figure 2.5.**  $^1\text{H}$  NMR spectrum (400.1 MHz,  $\text{C}_6\text{D}_6$ , 20°C) of  $\text{Co}(\text{PPh}_3)(\text{CNAr}^{\text{Mes}_2})_3$  (**1**). \*Small amount of free  $\text{CNAr}^{\text{Mes}_2}$  present in the sample.

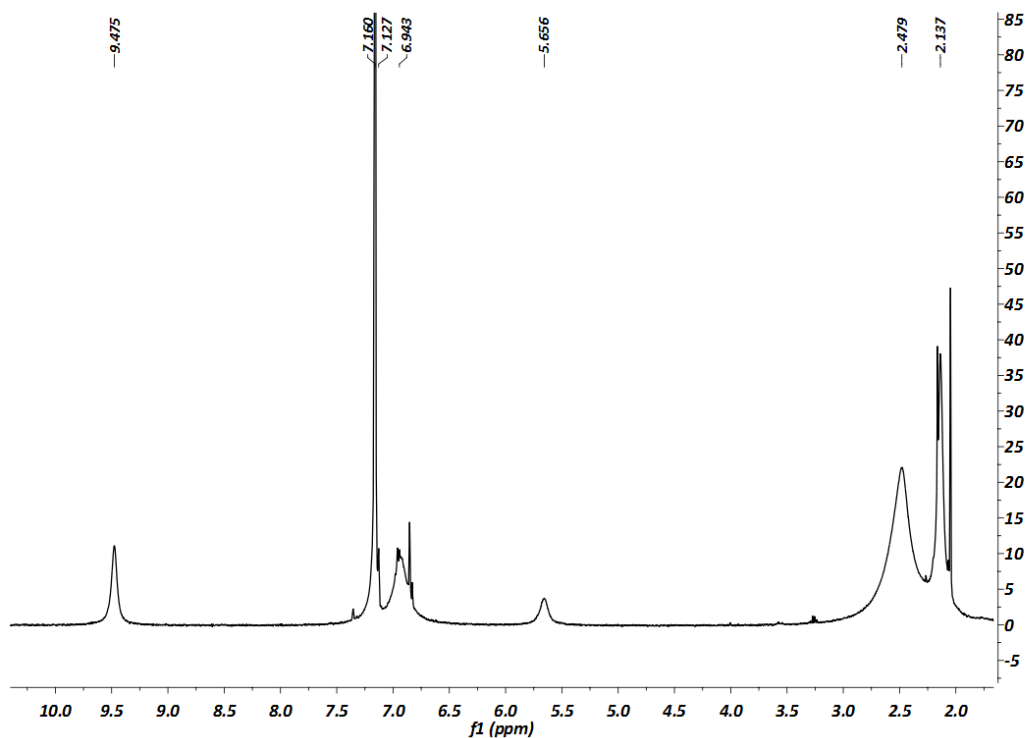


**Figure 2.6.**  $^1\text{H}$  NMR spectrum (400.1 MHz,  $\text{C}_6\text{D}_6$ ,  $20^\circ\text{C}$ ) of  $\text{Co}(\text{CN}^t\text{Bu})(\text{CNAr}^{\text{Mes}_2})_3$  (**2**). \*Small amount of free  $\text{CNAr}^{\text{Mes}_2}$  present in the sample.

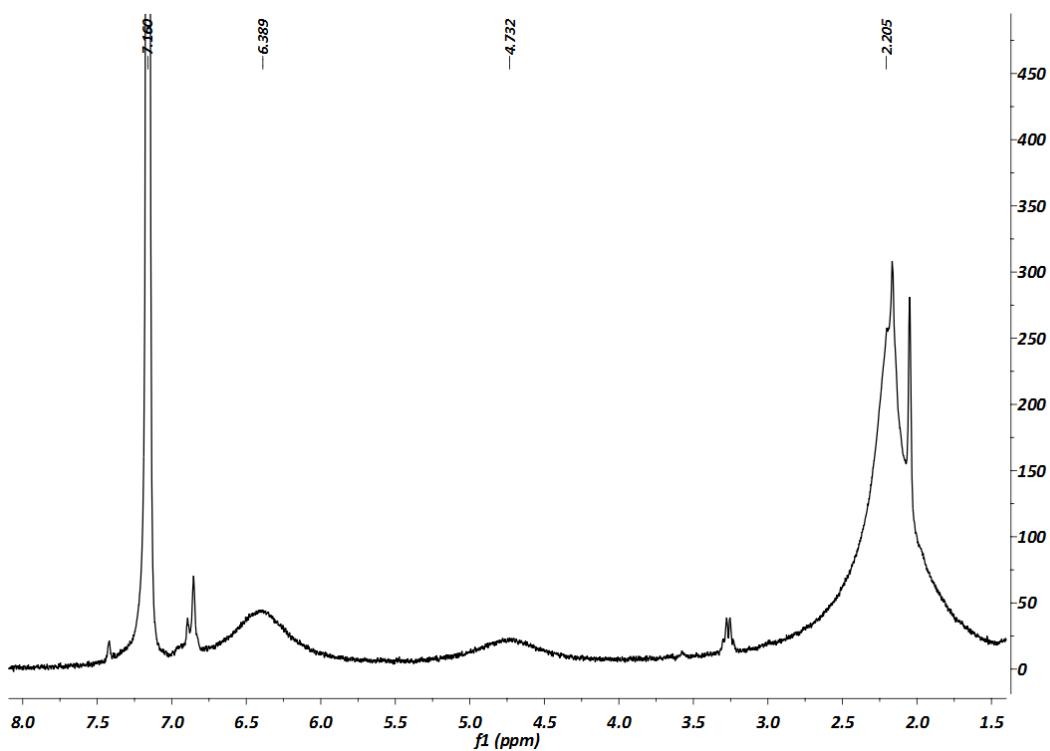


**Figure 2.7.**  $^1\text{H}$  NMR spectrum (300.1 MHz,  $\text{C}_6\text{D}_6$ ,  $20^\circ\text{C}$ ) of  $\text{Co}(\eta^2\text{-C,C-PhCCH})(\text{CNAr}^{\text{Mes}_2})_3$  (**4**). \*Small amount of free  $\text{CNAr}^{\text{Mes}_2}$  present in the sample.

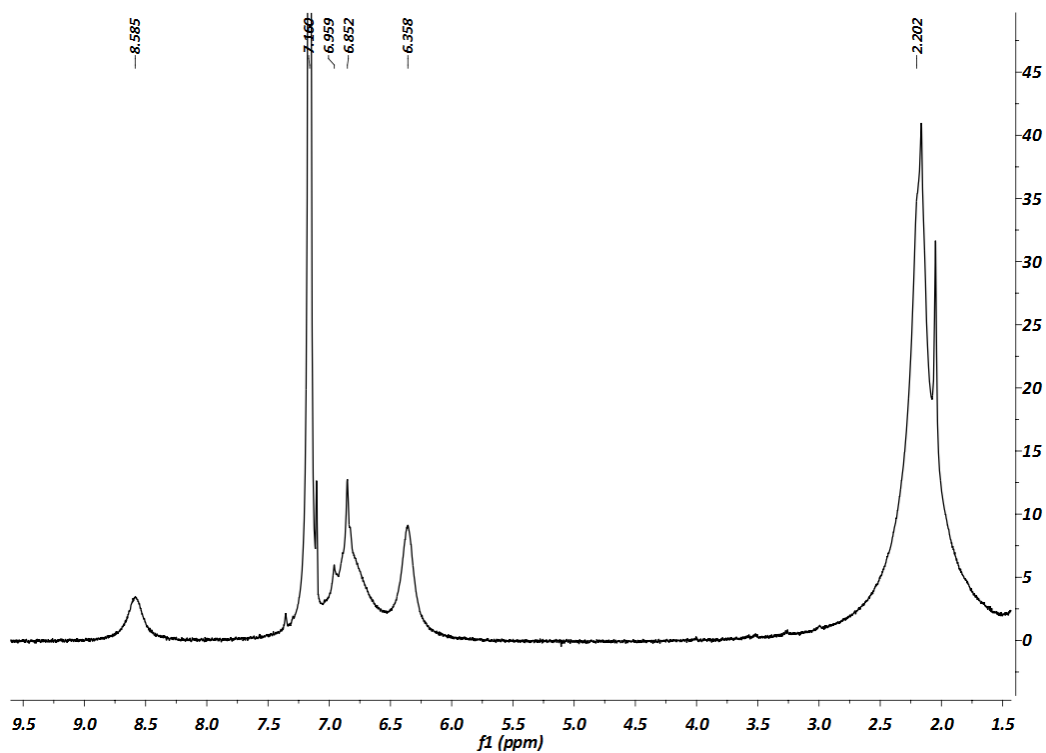


**Figure 2.8.** <sup>1</sup>H NMR spectrum (400.1 MHz, C<sub>6</sub>D<sub>6</sub>, 20 °C) of Co(η<sup>2</sup>-C,C-MA)(CNAr<sup>Mes2</sup>)<sub>3</sub> (**6**). \*Small amount of free CNAr<sup>Mes2</sup> present in the sample.

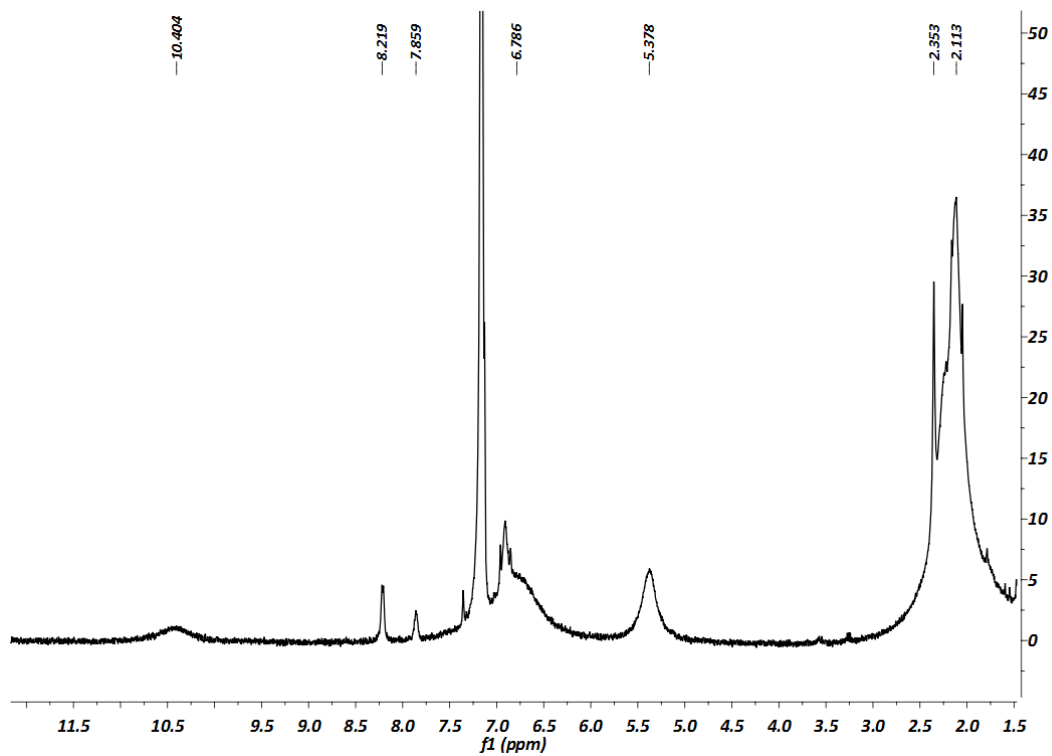


**Figure 2.9.** <sup>1</sup>H NMR spectrum (400.1 MHz, C<sub>6</sub>D<sub>6</sub>, 20 °C) of Co(η<sup>2</sup>-C,O-PhC(O)H)(CNAr<sup>Mes2</sup>)<sub>3</sub> (**7**). \*Small amount of free CNAr<sup>Mes2</sup> present in the sample.

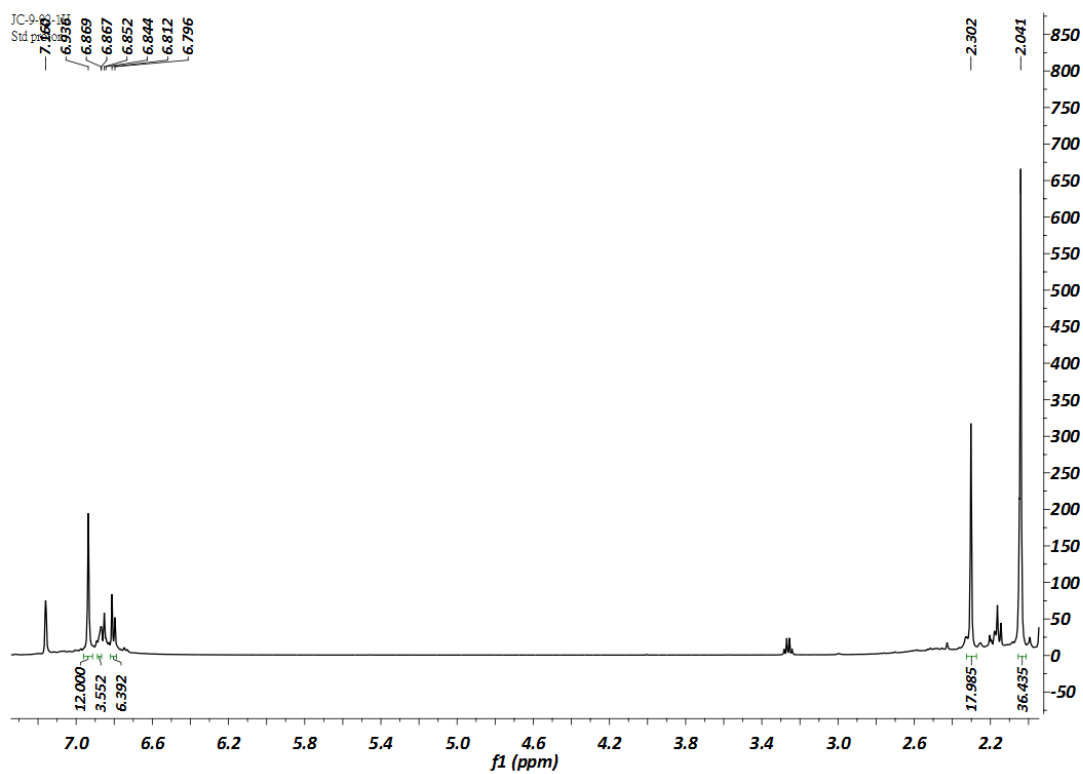


**Figure 2.10.**  $^1\text{H}$  NMR spectrum (500.1 MHz,  $\text{C}_6\text{D}_6$ ,  $20^\circ\text{C}$ ) of  $\text{Co}(\eta^3\text{-P}_3)(\text{CNAr}^{\text{Mes}_2})_3$  (9).

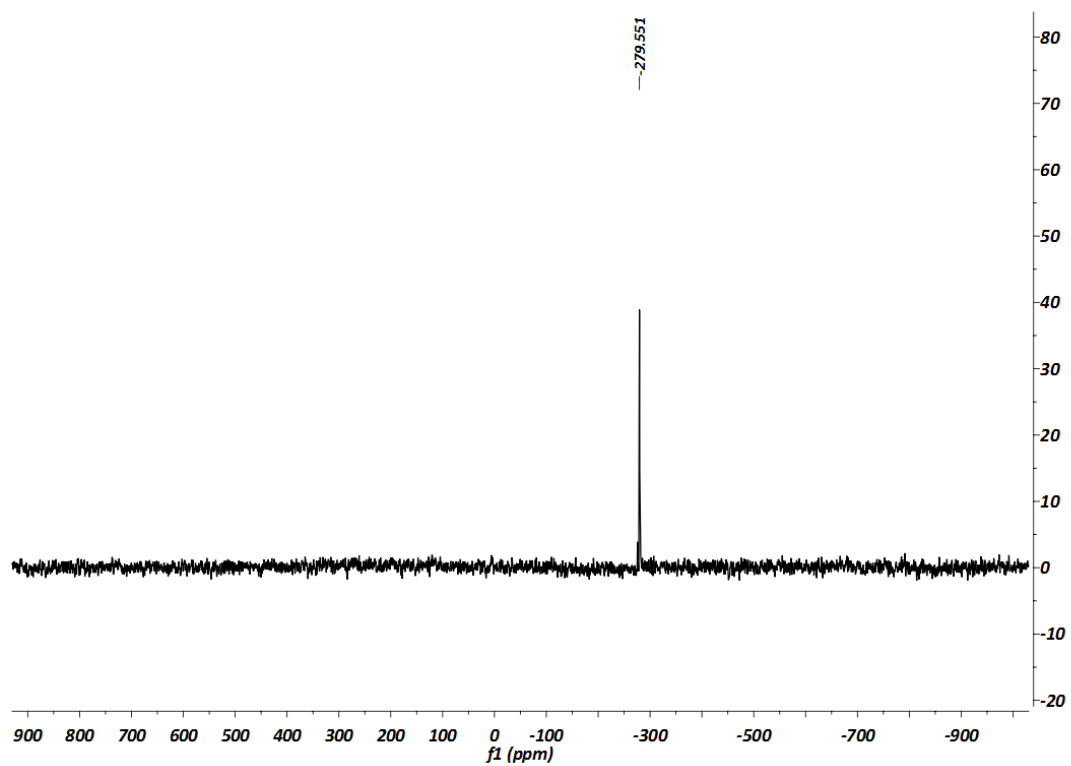


**Figure 2.11.**  $^{31}\text{P}\{^1\text{H}\}$  NMR spectrum (121.5 MHz,  $\text{C}_6\text{D}_6$ ,  $20^\circ\text{C}$ ) of  $\text{Co}(\eta^3\text{-P}_3)(\text{CNAr}^{\text{Mes}_2})_3$  (9).

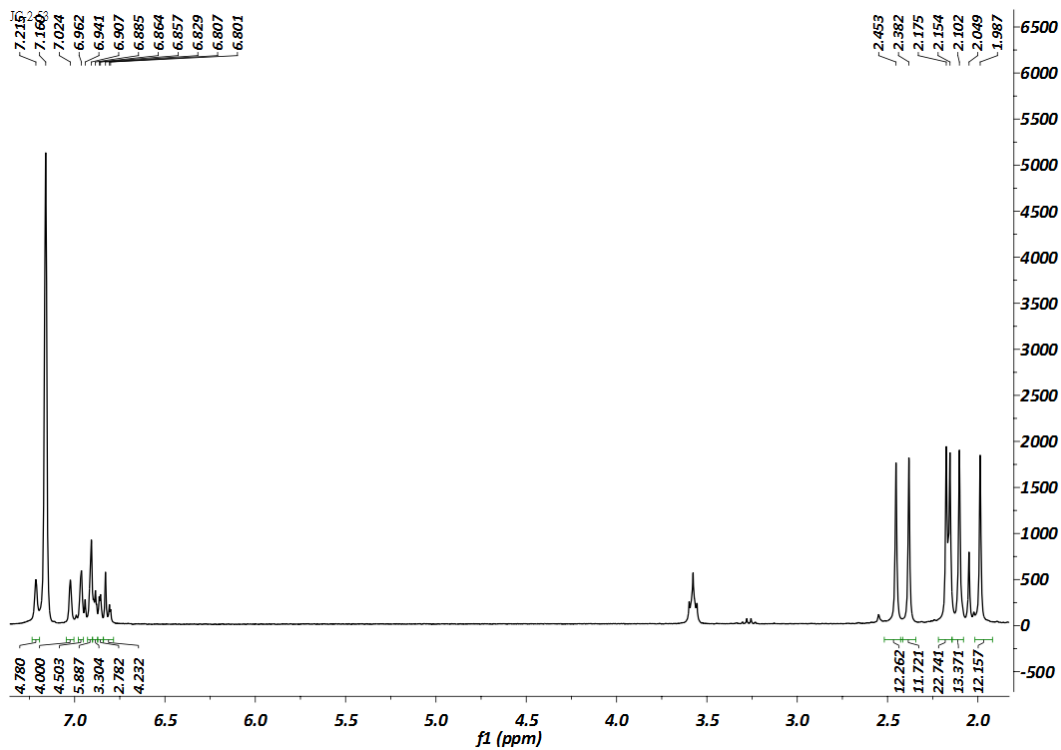


**Figure 2.12.**  $^1\text{H}$  NMR spectrum (300.1 MHz,  $\text{C}_6\text{D}_6$ ,  $20^\circ\text{C}$ ) of  $\text{Co}_2(\mu\text{-S}_2)_2(\mu\text{-S}_4)(\text{CNAr}^{\text{Mes}_2})_4$  (**10**). \*Small amount of free  $\text{CNAr}^{\text{Mes}_2}$  present in the sample.

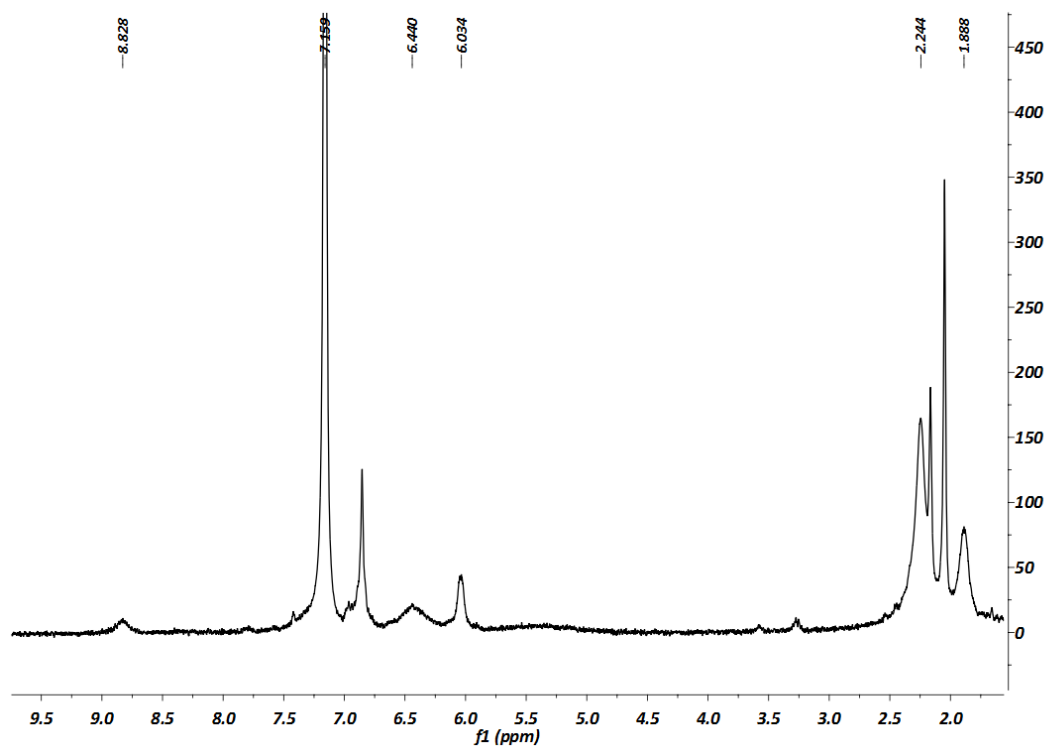


**Figure 2.13.**  $^1\text{H}$  NMR spectrum (300.1 MHz,  $\text{C}_6\text{D}_6$ ,  $20^\circ\text{C}$ ) of  $\text{Co}(\text{SPh})_2(\text{CNAr}^{\text{Mes}_2})_3$  (**11**). \*Small amount of free  $\text{CNAr}^{\text{Mes}_2}$  present in the sample.



## 2.8 Kinetic Measurements

**Kinetic Measurements.** Kinetic data for the reaction between  $\text{Co}(\text{CNAr}^{\text{Mes}2})_4$  and PhCCH were obtained via UV-vis spectroscopy using a Shimadzu UV-3600 UV/vis/NIR spectrometer. In an air-tight cuvette, 0.25 mM THF solutions of  $\text{Co}(\text{CNAr}^{\text{Mes}2})_4$  were treated with 2.5 mM (10 equiv) or 5 mM (20 equiv) THF solutions of PhCCH. In separate experiments, 0.25 mM THF solutions of  $\text{Co}(\text{CNAr}^{\text{Mes}2})_4$  containing 5 mM of free  $\text{CNAr}^{\text{Mes}2}$  (20 equiv) were treated with THF solutions containing 2.5 mM (10 equiv) or 5 mM (20 equiv) PhCCH. Reaction progress was measured by following the decay of the 485 nm absorption band of  $\text{Co}(\text{CNAr}^{\text{Mes}2})_4$ . UV-vis traces and kinetic analysis plots can be found in Figures 2.14-2.19.

**Kinetic analysis of the ligand substitution reaction of  $\text{Co}(\text{CNAr}^{\text{Mes}2})_4$  with 10 equiv of phenylacetylene.** In the glovebox, a solution of  $\text{Co}(\text{CNAr}^{\text{Mes}2})_4$  (0.25 mM) in THF (0.5 mL) was frozen in an air-tight quartz cuvette. To the frozen solution was added a thawed solution of phenylacetylene (2.5 mM, 10 equiv) in THF (0.5 mL). The entire solution was refrozen, and then the sealed cuvette was removed from the glovebox. The cuvette was brought out to the spectrometer and equilibrated at 20 °C for 5 minutes before the first data point was collected. The experiment was repeated three times, with the data from one trial shown below.

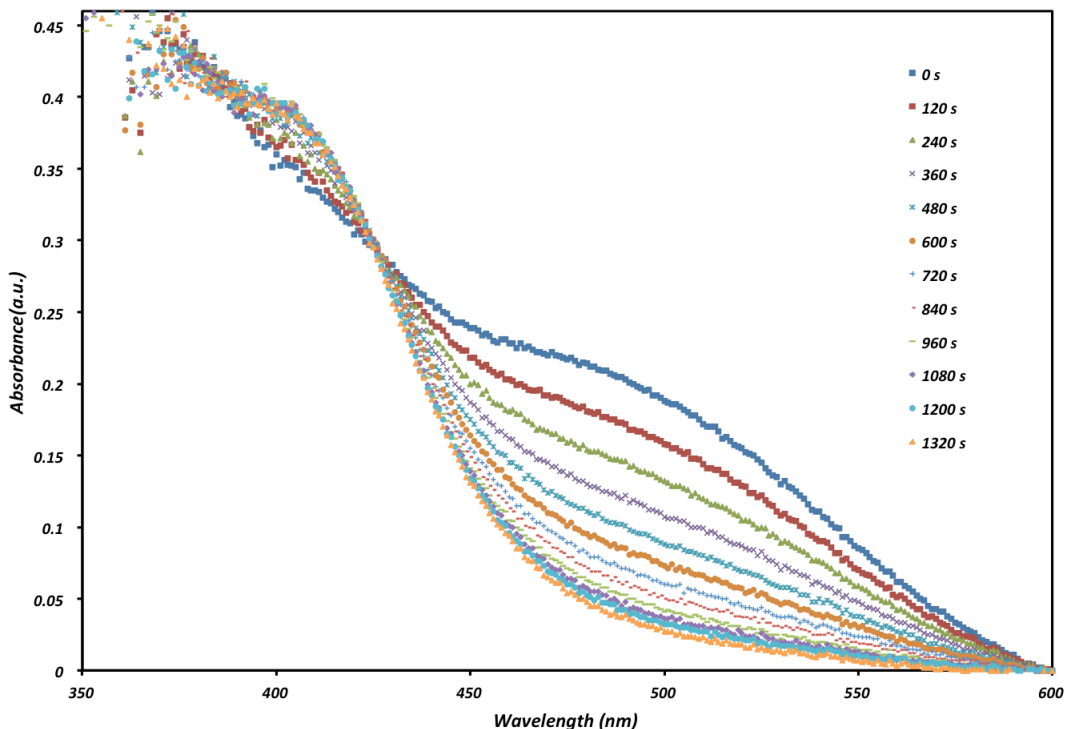


**Figure 2.14.** Kinetic UV-vis spectra of  $\text{Co}(\text{CNAr}^{\text{Mes}2})_4$  with phenylacetylene (10 equiv) measured at  $20^\circ\text{C}$  in THF at 120 seconds interval.

**Kinetic analysis of the ligand substitution reaction of  $\text{Co}(\text{CNAr}^{\text{Mes}2})_4$  with 10 equiv. of phenylacetylene and additional 20 equiv. of  $\text{CNAr}^{\text{Mes}2}$ .** In the glovebox, a solution of  $\text{Co}(\text{CNAr}^{\text{Mes}2})_4$  (0.25 mM) and  $\text{CNAr}^{\text{Mes}2}$  (5 mM, 20 equiv) in THF (0.5 mL) was frozen in an air tight quartz cuvette. To the frozen solution was added a thawed solution of phenylacetylene (2.5 mM, 10 equiv) in THF (0.5 mL). The entire solution was refrozen, and then the sealed cuvette was removed from the glovebox. The cuvette was brought out to the spectrometer and equilibrated at  $20^\circ\text{C}$  for 5 minutes before the first data point was collected. The experiment was repeated three times, with the data from one trial shown below.

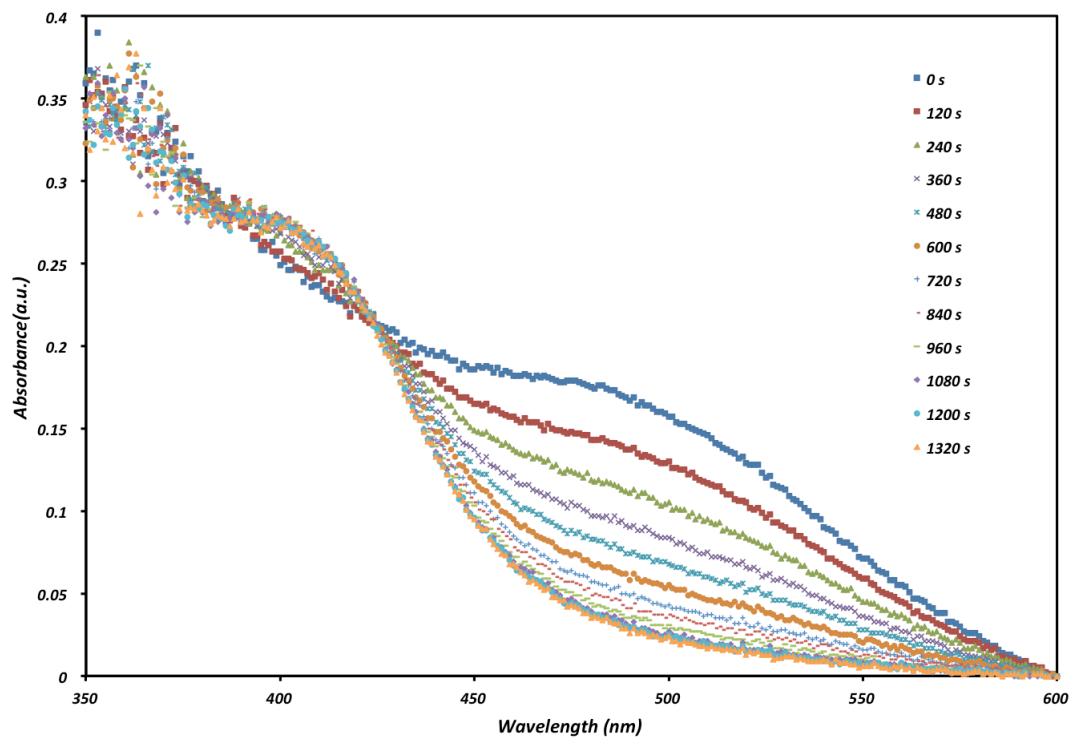


**Figure 2.15.** Kinetic UV-vis spectra of  $\text{Co}(\text{CNAr}^{\text{Mes}2})_4$  with phenylacetylene (10 equiv) and  $\text{CNAr}^{\text{Mes}2}$  (20 equiv) measured at 20 °C in THF at 120 seconds interval.

**Kinetic analysis of the ligand substitution reaction of  $\text{Co}(\text{CNAr}^{\text{Mes}2})_4$  with 20 equiv. phenylacetylene.** Using General Procedure 2.8, except the phenylacetylene solution concentration was doubled (5 mM, 20 equiv) in THF (0.5 mL). The experiment was repeated three times, with the data from one trial shown below.

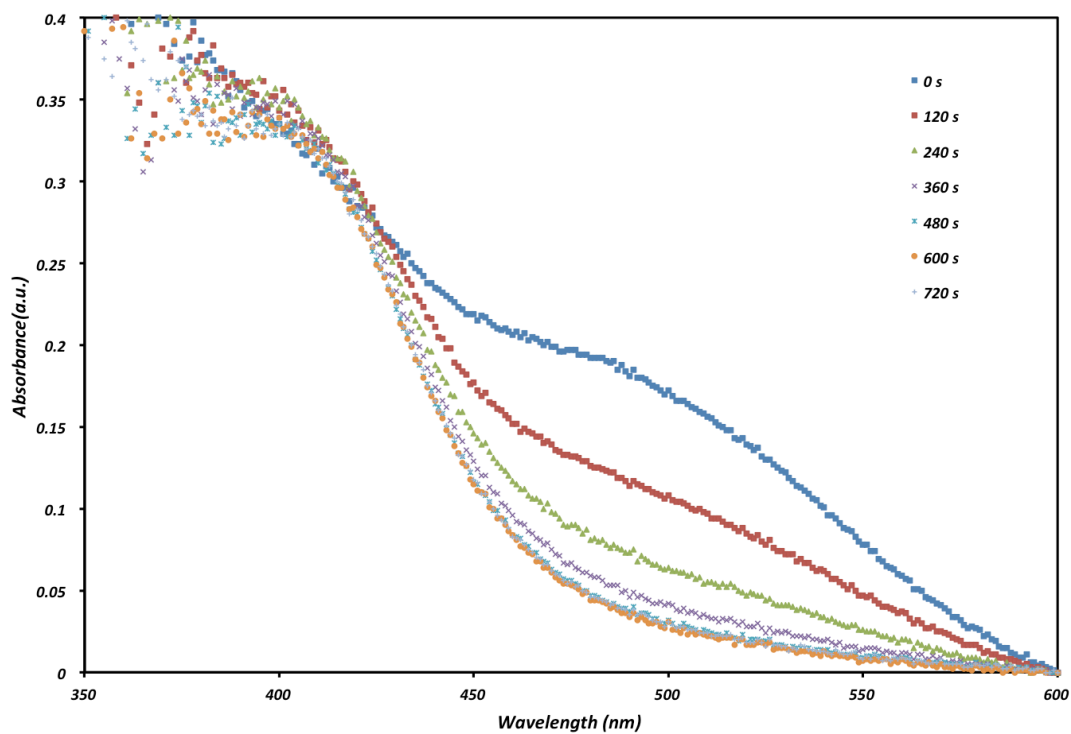


**Figure 2.16.** Kinetic UV-vis spectra of  $\text{Co}(\text{CNAr}^{\text{Mes}2})_4$  with phenylacetylene (20 equiv) measured at 20 °C in THF at 120 seconds interval.

**Kinetic analysis of the ligand substitution reaction of  $\text{Co}(\text{CNAr}^{\text{Mes}2})_4$  with 20 equiv. phenylacetylene and additional 20 equiv. of  $\text{CNAr}^{\text{Mes}2}$ .** Using General Procedure 2.8, except the phenylacetylene solution concentration was doubled (5 mM, 20 equiv) in THF (0.5 mL). The experiment was repeated three times, with the data from one trial shown below.

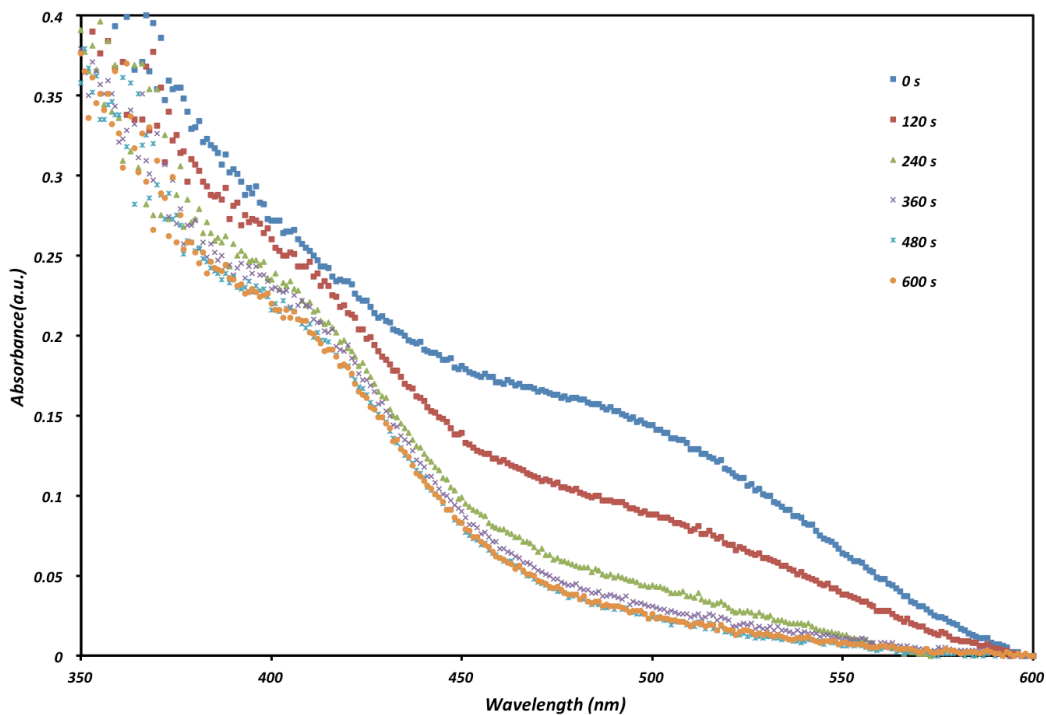


**Figure 2.17.** Kinetic UV-vis spectra of  $\text{Co}(\text{CNAr}^{\text{Mes}2})_4$  with phenylacetylene (20 equiv) and  $\text{CNAr}^{\text{Mes}2}$  (20 equiv) measured at  $20^\circ\text{C}$  in THF at 120 seconds interval.

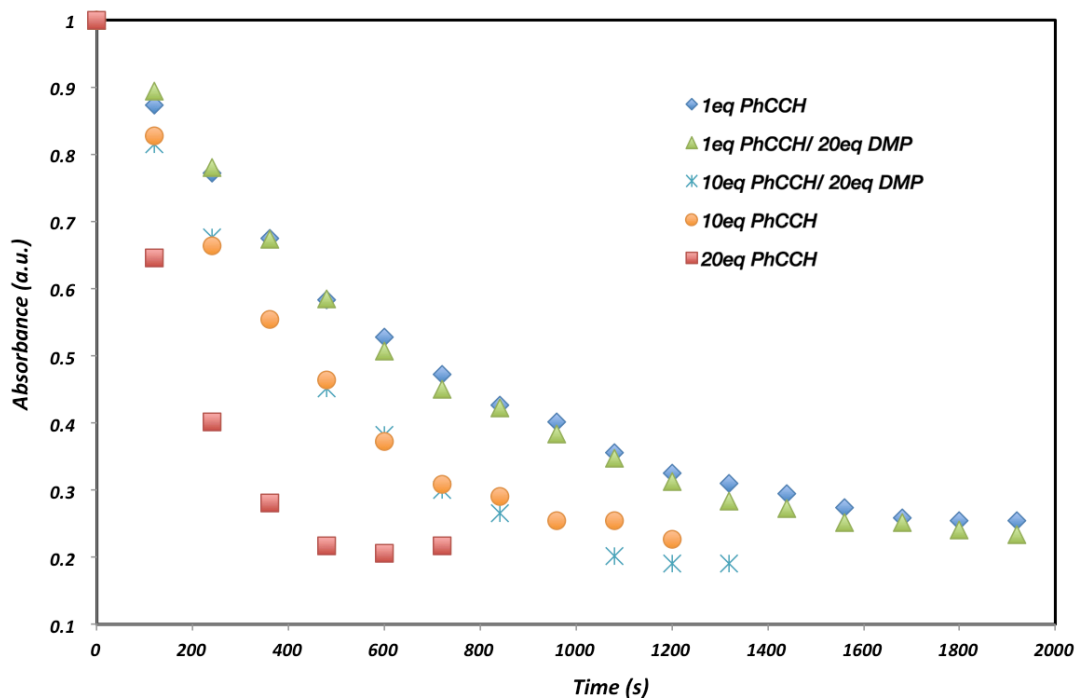


**Figure 2.18.** Plot of  $\text{Co}(\text{CNAr}^{\text{Mes}2})_4$  absorbance vs time, showing the rate enhancement by adding more equivalents of phenylacetylene in the ligand substitution reaction of  $\text{Co}(\text{CNAr}^{\text{Mes}2})_4$  and the reaction rate independence of the  $\text{CNAr}^{\text{Mes}2}$  concentration.

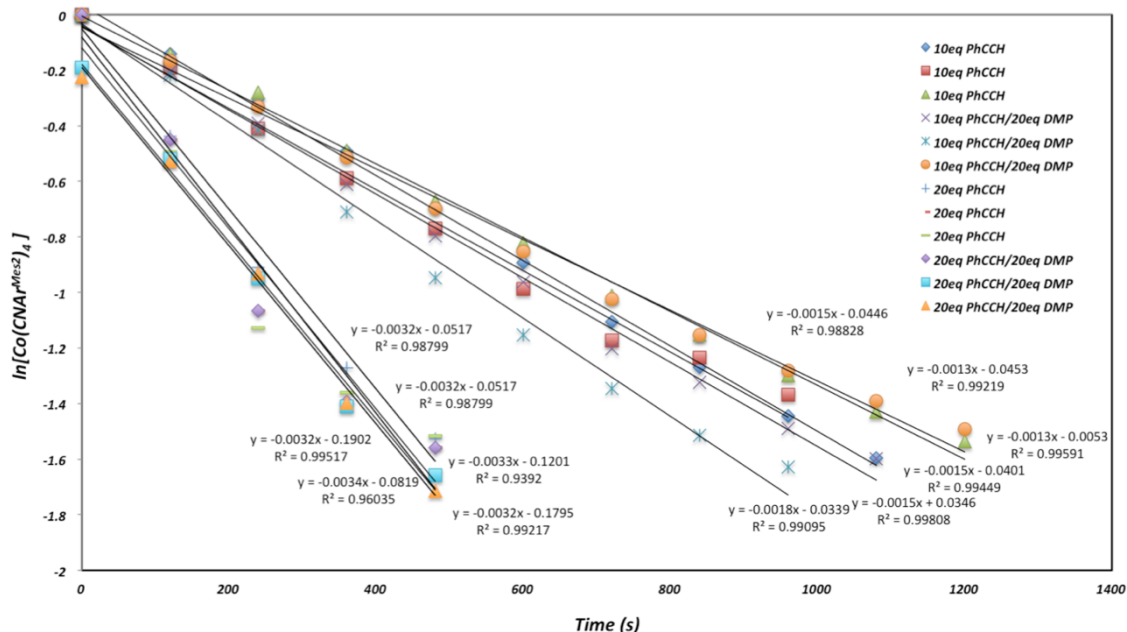


**Figure 2.19.** Plot of  $\ln[\text{Co}(\text{CNAr}^{\text{Mes}2})_4]$  vs time, showing the comparative observed rates of  $\text{Co}(\text{CNAr}^{\text{Mes}2})_4$  ligand exchange by PhCCH with the effect of 20 equiv  $\text{CNAr}^{\text{Mes}2}$  present under pseudo-first-order conditions (10 and 20 equiv).

## 2.9 Crystallography Structure Determination

**General.** Single crystal X-ray structure determinations were carried out at low temperature on a Bruker P4, Platform or Kappa Diffractometer equipped with a Mo or Cu radiation source and a Bruker APEX detector. All structures were solved by direct methods with SIR 2004<sup>71</sup> or SHELXS<sup>72</sup> and refined by full-matrix least-squares procedures utilizing SHELXL within Olex 2 small-molecule solution, refinement, and analysis software package.<sup>73</sup> Crystallographic data collection and refinement information are listed in Table 2.2-2.5.

**Information on crystallographic disorder.** All disordered components were successfully modeled and refined anisotropically unless otherwise stated.

The solid-state structure of  $\text{Co}(\eta^2\text{-}C, C\text{-}^i\text{BuCHCH}_2)(\text{CNAr}^{\text{Mes}2})_3 \cdot (\text{Et}_2\text{O})_2$  (**3**·( $\text{Et}_2\text{O}$ )<sub>2</sub>) contains two-site disorder of the co-crystallized ether molecule by a crystallographic inversion center.

Complex  $(\eta^3\text{-P}_3)\text{Co}(\text{CNAr}^{\text{Mes}_2})_3 \cdot (\text{FC}_6\text{H}_5) \cdot (\text{ACN})$  (**9**·(FC<sub>6</sub>H<sub>5</sub>)·(ACN)) contains one FC<sub>6</sub>H<sub>5</sub> molecule of solvation that has positional disorder of the fluorine atom over two position. Each fluorine atom is modeled at 75% and 25% occupancy for part 1 and part 2 respectively, and refined anisotropically. Complex  $\text{Co}(\text{SPh})_2(\text{CNAr}^{\text{Mes}_2})_3 \cdot (\text{C}_6\text{H}_6)$  (**11**·(C<sub>6</sub>H<sub>6</sub>)) exhibits positional disorder over two positions of one Ar<sup>Mes<sub>2</sub></sup> group at C01H. This Ar<sup>Mes<sub>2</sub></sup> group was split and linked via a free variable and refined anisotropically. The following molecules contained severely disordered solvent molecules of co-crystallization that could not be successfully modeled:  $\text{Co}(\text{PPh}_3)(\text{CNAr}^{\text{Mes}_2})_3$  (**1**),  $\text{Co}(\eta^2\text{-C,C-PhCCH})(\text{CNAr}^{\text{Mes}_2})_3$  (**4**),  $\text{Co}(\eta^2\text{-C,O-BA})(\text{CNAr}^{\text{Mes}_2})_3$  (**7**),  $(\eta^2\text{-TEMPO})\text{Co}(\text{CNAr}^{\text{Mes}_2})_2$  (**8**) and  $[\text{Co}_2(\mu\text{-S}_2)_2(\mu\text{-S}_4)(\text{CNAr}^{\text{Mes}_2})_4] \cdot 2(\text{THF})$  (**10**·2(THF)). The PLATON routine SQUEEZE<sup>74</sup> or the Olex2 implementation of BYPASS<sup>75</sup> was used to account for these disordered components as a diffuse contribution to the overall scattering without specific atom positions.

**CCDC Deposition.** All crystal structures reported herein have been deposited with the Cambridge Crystallographic Data Center (CCDC) and have been assigned the following CCDC deposition numbers: CCDC 1874204-1874214

CCDC 1874207 :  $\text{Co}(\text{PPh}_3)(\text{CNAr}^{\text{Mes}_2})_3$  (**1**)

CCDC 1874213 :  $\text{Co}(\text{CN}^t\text{Bu})(\text{CNAr}^{\text{Mes}_2})_3$  (**2**·(C<sub>6</sub>H<sub>6</sub>)·(*n*-C<sub>5</sub>H<sub>12</sub>))

CCDC 1874212 :  $\text{Co}(\eta^2\text{-C,C-}^t\text{BuCHCH}_2)(\text{CNAr}^{\text{Mes}_2})_3$  (**3**·(Et<sub>2</sub>O)<sub>2</sub>)

CCDC 1874205 :  $\text{Co}(\eta^2\text{-C,C-PhCCH})(\text{CNAr}^{\text{Mes}_2})_3$  (**4**)

CCDC 1874204 :  $\text{Co}(\eta^2\text{-C,C-PhCC-CCPh})(\text{CNAr}^{\text{Mes}_2})_3$  (**5**·(PhCCCCPh)·(Et<sub>2</sub>O))

CCDC 1874209 :  $\text{Co}(\eta^2\text{-C,C-MA})(\text{CNAr}^{\text{Mes}_2})_3$  (**6**·(*n*-C<sub>5</sub>H<sub>12</sub>)<sub>2</sub>)

CCDC 1874214 :  $\text{Co}(\eta^2\text{-C,O-PhC(O)H})(\text{CNAr}^{\text{Mes}_2})_3$  (**7**)

CCDC 1874208 :  $\text{Co}(\eta^2\text{-N,O-TEMPO})(\text{CNAr}^{\text{Mes}_2})_2$  (**8**)

CCDC 1874211 :  $\text{Co}(\eta^3\text{-P}_3)(\text{CNAr}^{\text{Mes}_2})_3$  (**9**·(FC<sub>6</sub>H<sub>5</sub>)·(ACN))

CCDC 1874206 :  $\text{Co}_2(\mu\text{-S}_2)_2(\mu\text{-S}_4)(\text{CNAr}^{\text{Mes}_2})_4$  (**10**·(THF)<sub>2</sub>)

CCDC 1874210 :  $\text{Co}(\text{SPh})_2(\text{CNAr}^{\text{Mes}_2})_3$  (**11**·(C<sub>6</sub>H<sub>6</sub>))

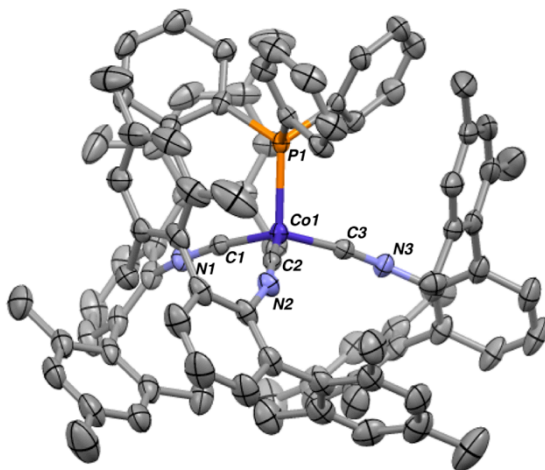


**Figure 2.20.** Molecular structure of  $\text{Co}(\text{PPh}_3)(\text{CNAr}^{\text{Mes}_2})_3$  (**1**). Hydrogen atoms omitted for clarity. Selected distances (Å) and angles (°): Co1-C1 = 1.823, Co1-C2 = 1.824, Co1-C3 = 1.825, Co1-P1 = 2.246(4), C1-Co1-C2 = 113.8, C2-Co1-C3 = 113.9, C3-Co1-C1 = 113.8, P1-Co1-C1 = 104.68, P1-Co1-C2 = 104.67, P1-Co1-C3 = 104.67.

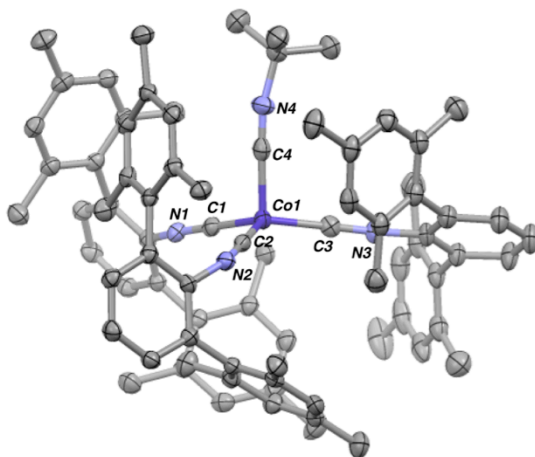


**Figure 2.21.** Molecular structure of  $\text{Co}(\text{CN}t\text{-Bu})(\text{CNAr}^{\text{Mes}_2})_3 \cdot (\text{C}_6\text{H}_6) \cdot (\text{C}_5)$  (**2**·(C<sub>6</sub>H<sub>6</sub>)·(C<sub>5</sub>)), with benzene, pentane solvent molecules and hydrogen atoms omitted for clarity. Selected distances (Å) and angles (°): Co1-C1 = 1.852(3), Co1-C2 = 1.820(3), Co1-C3 = 1.824(3), C1-C4 = 1.844(4), C1-Co1-C2 = 105.3(1), C2-Co1-C3 = 118.2(1), C3-Co1-C1 = 127.7(1), C1-Co1-C4 = 101.7(1), C2-Co1-C4 = 103.1(1), C3-Co1-C4 = 95.6(1).



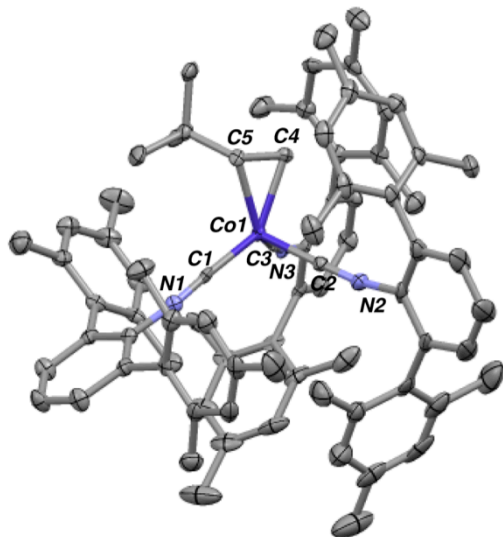


**Figure 2.22.** Molecular structure of  $\text{Co}(\eta^2\text{-C,C}^i\text{BuCHCH}_2)(\text{CNAr}^{\text{Mes}2})_3 \cdot (\text{Et}_2\text{O})_2$  (**3**· $(\text{Et}_2\text{O})_2$ ), with two ether solvent molecules and hydrogen atoms omitted for clarity. Selected distances (Å) and angles (°): Co1-C1 = 1.827(7), Co1-C2 = 1.842(7), Co1-C3 = 1.853(6), C1-C4 = 2.107(6), Co1-C5 = 2.063(6), C4-C5 = 1.395(8), C1-Co1-C2 = 107.8(3), C2-Co1-C3 = 96.6(3), C3-Co1-C1 = 112.0(3), C1-Co1-C5 = 96.6(3), C3-Co1-C4 = 96.3(3).

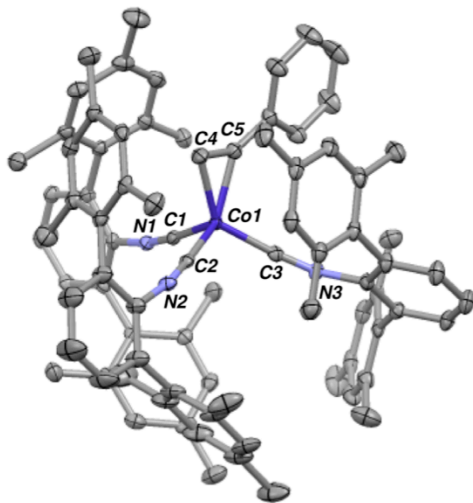


**Figure 2.23.** Molecular structure of  $\text{Co}(\eta^2\text{-C,C-PhCCH})(\text{CNAr}^{\text{Mes}2})_3$  (**4**). Hydrogen atoms omitted for clarity. Selected distances (Å) and angles (°): Co1-C1 = 1.879(2), Co1-C2 = 1.842(3), Co1-C3 = 1.833(3), Co1-C4 = 1.939(3), Co1-C5 = 1.942(2), C4-C5 = 1.255(4), C1-Co1-C2 = 101.4(1), C2-Co1-C3 = 107.1(1), C3-Co1-C1 = 102.0(1).

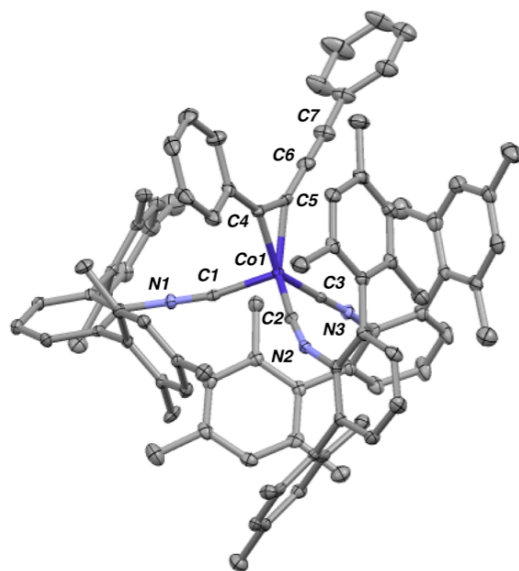


**Figure 2.24.** Molecular structure of  $\text{Co}(\eta^2\text{-C,C-PhCC-CCPh})(\text{CNAr}^{\text{Mes}2})_3 \cdot (\text{PhCC-CCPh}) \cdot (\text{Et}_2\text{O})$  (**5**·(PhCC-CCPh)·(Et<sub>2</sub>O)), with PhCC-CCPh, ether solvent molecules and hydrogen atoms omitted for clarity. Selected distances (Å) and angles (°): Co1-C1 = 1.879(3), Co1-C2 = 1.846(4), Co1-C3 = 1.837(3), Co1-C4 = 1.916(4), Co1-C5 = 1.955(3), C4-C5 = 1.275(4), C5-C6 = 1.397(4), C6-C7 = 1.203(5), C1-Co1-C2 = 99.4(1), C2-Co1-C3 = 100.2(1), C3-Co1-C1 = 105.3(1).

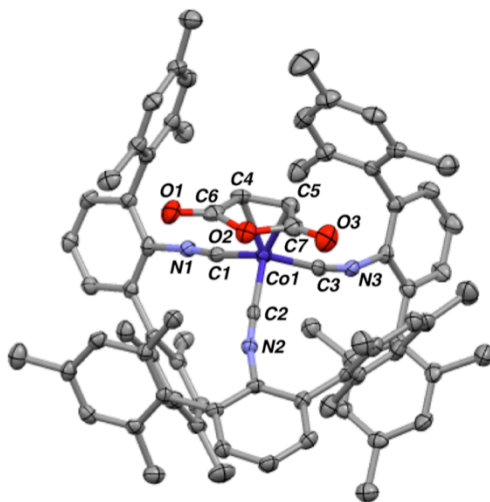


**Figure 2.25.** Molecular structure of  $\text{Co}(\eta^2\text{-C,C-MA})(\text{CNAr}^{\text{Mes}2})_3 \cdot (\text{C}_5\text{H}_5\text{O}_2)$  (**6**·(C<sub>5</sub>H<sub>5</sub>O<sub>2</sub>)), with pentane solvent molecules and hydrogen atoms omitted for clarity. Selected distances (Å) and angles (°): Co1-C1 = 1.861(4), Co1-C2 = 1.915(4), Co1-C3 = 1.850(4), C1-C4 = 2.030(4), Co1-C5 = 2.033(3), C4-C5 = 1.414(6), C1-Co1-C2 = 105.8(2), C2-Co1-C3 = 103.9(2), C3-Co1-C1 = 101.3(2), C1-Co1-C4 = 98.3(2), C3-Co1-C4 = 100.5(2).

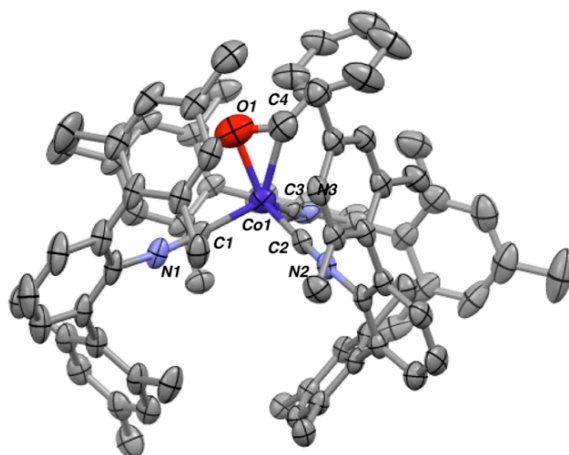


**Figure 2.26.** Molecular structure of  $\text{Co}(\eta^2\text{-C,O-BA})(\text{CNAr}^{\text{Mes}2})_3$  (**7**). Hydrogen atoms omitted for clarity. Selected distances ( $\text{\AA}$ ) and angles ( $^\circ$ ):  $\text{Co1-C1} = 1.861(4)$ ,  $\text{Co1-C2} = 1.843(4)$ ,  $\text{Co1-C3} = 1.873(3)$ ,  $\text{Co1-O1} = 1.941(4)$ ,  $\text{Co1-C4} = 2.038(5)$ ,  $\text{O1-C4} = 1.261(8)$ ,  $\text{C1-Co1-C2} = 100.7(2)$ ,  $\text{C2-Co1-C3} = 105.6(2)$ ,  $\text{C3-Co1-C1} = 108.9(2)$ ,  $\text{C1-Co1-O1} = 94.9(2)$ ,  $\text{C3-Co1-C4} = 106.4(2)$ .

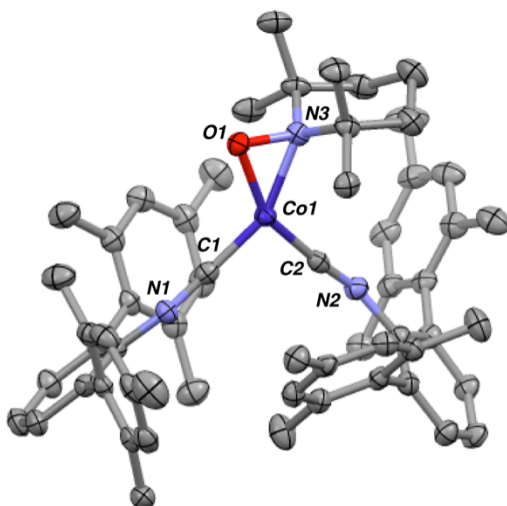


**Figure 2.27.** Molecular structure of  $(\eta^2\text{-TEMPO})\text{Co}(\text{CNAr}^{\text{Mes}2})_2$  (**8**). Hydrogen atoms omitted for clarity. Selected distances ( $\text{\AA}$ ) and angles ( $^\circ$ ):  $\text{Co1-C1} = 1.759(2)$ ,  $\text{Co1-C2} = 1.751(2)$ ,  $\text{Co1-O1} = 1.862(2)$ ,  $\text{Co1-N1} = 1.920(2)$ ,  $\text{C1-Co1-C2} = 95.5(1)$ ,  $\text{O1-Co1-C1} = 109.76(9)$ ,  $\text{O1-Co1-N1} = 33.43(7)$ ,  $\text{N1-Co1-C2} = 111.45(9)$ .

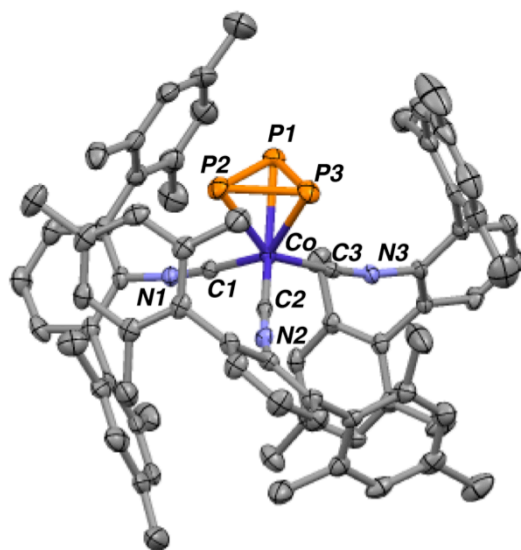


**Figure 2.28.** Molecular structure of  $(\eta^3\text{-P}_3)\text{Co}(\text{CNAr}^{\text{Mes}_2})_3 \cdot (\text{FC}_6\text{H}_5) \cdot (\text{ACN})$  (**9**·(FC<sub>6</sub>H<sub>5</sub>)·(ACN)), with fluorobenzene, acetonitrile solvent molecules and hydrogen atoms omitted for clarity. Selected distances (Å) and angles (°): Co1-C1 = 1.835(4), Co1-C2 = 1.839(4), Co1-C3 = 1.844(4), Co1-P1 = 2.317(1), Co1-P2 = 2.312(1), Co1-P3 = 2.313(1), C1-Co1-C2 = 107.1(2), C2-Co1-C3 = 107.6(2), C3-Co1-C1 = 102.8(2), P1-P2-P3 = 59.79(5), P2-P3-P1 = 59.86(5), P3-P2-P1 = 60.34(5).

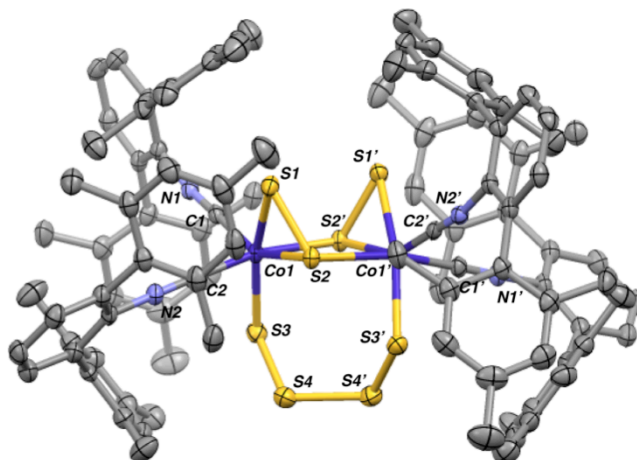


**Figure 2.29.** Molecular structure of  $[\text{Co}_2(\mu\text{-S}_2)_2(\mu\text{-S}_4)(\text{CNAr}^{\text{Mes}_2})_4] \cdot (\text{THF})_2$  (**10**·(THF)<sub>2</sub>), with two THF solvent molecule and hydrogen atoms omitted for clarity. Selected distances (Å) and angles (°): Co1-C1 = 1.843(2), Co1-C2 = 1.850(3), Co1-S1 = 2.2723(7), Co1-S2 = 2.2618(8), Co1-S3 = 2.2677(7), C1-Co1-C2 = 94.8(1), S2-Co1-S2' = 81.67(2)

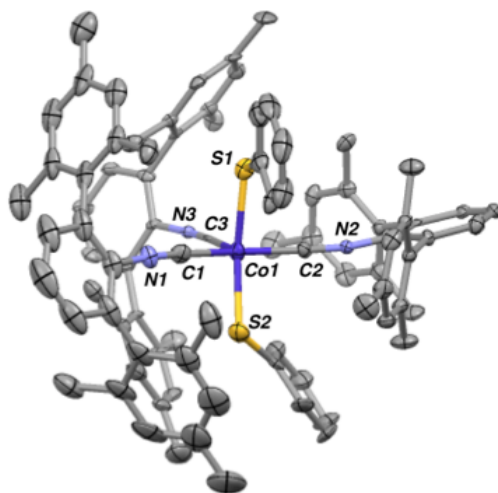


**Figure 2.30.** Molecular structure of  $\text{Co}(\text{SPh})_2(\text{CNAr}^{\text{Mes}2})_3 \cdot (\text{C}_6\text{H}_6)$  (**11**· $\text{C}_6\text{H}_6$ ), with a benzene solvent molecule and hydrogen atoms omitted for clarity. Selected distances (Å) and angles (°):  $\text{Co1-C1} = 1.851(3)$ ,  $\text{Co1-C2} = 1.937(3)$ ,  $\text{Co1-C3} = 1.863(3)$ ,  $\text{Co1-S1} = 1.221(1)$ ,  $\text{Co1-S2} = 2.3037(8)$ ,  $\text{C1-Co1-C2} = 103.7(1)$ ,  $\text{C2-Co1-C3} = 101.5(1)$ ,  $\text{C3-Co1-C1} = 154.3(1)$ .

**Table 2.2.** Crystallographic Data Collection and Refinement Information.

Name	Co(PPh <sub>3</sub> ) (CNAr <sup>Mes2</sup> ) <sub>3</sub> ( <b>1</b> )	Co(CN <sup>t</sup> -Bu) (CNAr <sup>Mes2</sup> ) <sub>3</sub> ( <b>2</b> ·(C <sub>6</sub> H <sub>6</sub> )·(C <sub>5</sub> ))	Co(η <sup>2</sup> -C, C- <sup>t</sup> BuCHCH <sub>2</sub> ) (CNAr <sup>Mes2</sup> ) <sub>3</sub> ( <b>3</b> ·(Et <sub>2</sub> O) <sub>2</sub> )
Formula	C93 H90 Co1 N3	C80 H84 Co N4	C81 H87 Co N3
	P1		
Crystal System	Trigonal	Triclinic	Triclinic
Space Group	R-3	P-1	P-1
a, Å	23.4252(13)	14.6928(3)	12.8207(13)
b, Å	23.4252(13)	20.6695(4)	23.916(2)
c, Å	28.205(2)	24.2931(5)	24.411(2)
α, deg	90	88.1930(10)	97.624(2)
β, deg	90	84.0160(10)	100.418(3)
γ, deg	120	86.4970(10)	100.524(3)
V, Å <sup>3</sup>	13403.6(18)	7321.4(3)	7130.6(12)
Z	6	4	4
Radiation (λ, Å)	Mo-K <sub>α</sub> , 0.71073	Cu-K <sub>α</sub> , 1.54184	Mo-K <sub>α</sub> , 0.71073
ρ(calcd.), g/cm <sup>3</sup>	0.996	1.121	1.134
μ, mm <sup>-1</sup>	0.251	2.177	0.287
Temp, K	100	100	100
θ max, deg	25.395	66.592	23.263
data/parameters	5480/301	25347/1674	20168/1664
R <sub>1</sub>	0.0473	0.0599	0.0723
wR <sub>2</sub>	0.1361	0.152	0.1374
GOF	0.981	1.078	0.967

**Table 2.3.** Crystallographic Data Collection and Refinement Information.

Name	Co( $\eta^2$ -C,C-PhCCH) (CNAr <sup>Mes2</sup> ) <sub>3</sub> ( <b>4</b> )	Co( $\eta^2$ -C,C-PhCC- CCPh) (CNAr <sup>Mes2</sup> ) <sub>3</sub> ( <b>5</b> ·(PhCC- CCPh)·(Et <sub>2</sub> O))	Co( $\eta^2$ -C,C-MA) (CNAr <sup>Mes2</sup> ) <sub>3</sub> ( <b>6</b> ·(C <sub>5</sub> ) <sub>2</sub> )
Formula	C83 H81 Co N3	C103 H100 Co N3 O	C89 H101 Co N3 O3
Crystal System	Triclinic	Triclinic	Monoclinic
Space Group	P-1	P-1	P 1 2 <sub>1</sub> /c 1
a, Å	14.0733(9)	12.177(3)	23.6310(11)
b, Å	14.1810(10)	14.5484(19)	13.9220(7)
c, Å	21.2214(16)	26.190(5)	23.1093(12)
$\alpha$ , deg	92.342(2)	82.754(16)	90
$\beta$ , deg	94.632(2)	81.31(2)	101.9010(10)
$\gamma$ , deg	116.769(2)	66.803(16)	90
V, Å <sup>3</sup>	3754.8(5)	4204.4(16)	7439.3(6)
Z	2	2	4
Radiation ( $\lambda$ , Å)	Mo-K $\alpha$ , 0.71073	Mo-K $\alpha$ , 0.71073	Mo-K $\alpha$ , 0.71073
$\rho$ (calcd.), g/cm <sup>3</sup>	1.043	1.149	1.178
$\mu$ (Mo-K $\alpha$ ), mm <sup>-1</sup>	0.270	0.254	0.282
Temp, K	100	100	100
$\theta$ max, deg	25.392	25.302	25.408
data/parameters	13759/806	15207/993	13689/887
$R_1$	0.0365	0.0602	0.0598
$wR_2$	0.0922	0.1166	0.1353
GOF	1.034	1.000	0.915

**Table 2.4.** Crystallographic Data Collection and Refinement Information.

Name	Co( $\eta^2$ -C,O-BA) (CNAr <sup>Mes2</sup> ) <sub>3</sub> ( <b>7</b> )	( $\eta^2$ -TEMPO) Co(CNAr <sup>Mes2</sup> ) <sub>2</sub> ( <b>8</b> )	( $\eta^3$ - P <sub>3</sub> )Co(CNAr <sup>Mes2</sup> ) <sub>3</sub> ( <b>9</b> ·(FC <sub>6</sub> H <sub>5</sub> )·(ACN))
Formula	C82 H81 Co N3 O	C59 H68 Co N3 O	C75 H75 Co N3 P3, C2 H3 N, C6 H4 F
Crystal System	Triclinic	Monoclinic	Orthorhombic
Space Group	P-1	P 1 2 <sub>1</sub> /n 1	Pna2 <sub>1</sub>
a, Å	13.9492(6)	10.6761(5)	23.8288(7)
b, Å	14.4446(7)	46.335(2)	22.7856(8)
c, Å	19.3692(7)	11.4074(5)	13.5658(4)
$\alpha$ , deg	83.465(2)	90	90
$\beta$ , deg	71.893(2)	110.821(2)	90
$\gamma$ , deg	84.0300(10)	90	90
V, Å <sup>3</sup>	3675.6(3)	5274.5(4)	7365.6(4)
Z	2	4	4
Radiation ( $\lambda$ , Å)	Mo-K $\alpha$ , 0.71073	Mo-K $\alpha$ , 0.71073	Mo-K $\alpha$ , 0.71073
$\rho$ (calcd.), g/cm <sup>3</sup>	1.069	1.126	1.178
$\mu$ (Mo-K $\alpha$ ), mm <sup>-1</sup>	0.277	0.366	0.346
Temp, K	100	100	100
$\theta$ max, deg	25.784	25.416	25.701
data/parameters	14067/802	9681/593	12730/851
$R_1$	0.0667	0.0482	0.0385
$wR_2$	0.1701	0.1478	0.0816
GOF	1.036	1.130	1.019



**Table 2.5.** Crystallographic Data Collection and Refinement Information.

Name	[Co <sub>2</sub> (μ-S <sub>2</sub> ) <sub>2</sub> (μ-S <sub>4</sub> ) (CNAr <sup>Mes</sup> ) <sub>4</sub> ] ( <b>10</b> ·(THF) <sub>2</sub> )	Co(SPh) <sub>2</sub> (CNAr <sup>Mes</sup> ) <sub>3</sub> ( <b>11</b> ·(C <sub>6</sub> H <sub>6</sub> ))
Formula	C100 H100 Co2 N4 S8, 2(C4 H8 O)	C87 H85 Co N3 S2, C6 H6
Crystal System	Monoclinic	Monoclinic
Space Group	P 1 2/n 1	P 1 2 <sub>1</sub> /c 1
a, Å	15.4614(8)	13.7500(4)
b, Å	12.5260(7)	19.0623(6)
c, Å	27.9988(15)	29.2336(9)
α, deg	90	90
β, deg	93.8010(10)	91.181(2)
γ, deg	90	90
V, Å <sup>3</sup>	5410.6(5)	7660.7(4)
Z	2	4
Radiation (λ, Å)	Mo-K <sub>α</sub> , 0.71073	Mo-K <sub>α</sub> , 0.71073
ρ(calcd.), g/cm <sup>3</sup>	1.152	1.191
μ (Mo-K <sub>α</sub> ), mm <sup>-1</sup>	0.508	0.327
Temp, K	100	100
θ max, deg	25.411	25.385
data/parameters	9967/571	14005/996
R <sub>1</sub>	0.0426	0.0530
wR <sub>2</sub>	0.1374	0.1349
GOF	1.166	1.030

## 2.10 Acknowledgement

Chapter 2 is adapted from C. Chan, A. E. Carpenter, M. Gembicky, C. E. Moore, A. L. Rheingold, J. S. Figueroa “Associative Ligand Exchange and Substrate Activation Reactions by a Zero-Valent Cobalt Tetrakisocyanide Complex,” *Organometallics.*, **2019**, 38, 1436-1444. Copyright 2019, American Chemical Society. Permission to include published material in this dissertation has been obtained from all coauthors. The dissertation author is the first author of this paper. Prof. Clifford P. Kubiak and Tyler M. Porter are thanked for providing access to UV-vis instrumentation and helpful discussions.

## 2.11 References

- (1) Rudd, P. A.; Liu, S.; Gagliardi, L.; Young, V. G.; Lu, C. C. *J. Am. Chem. Soc.* **2011**, *133* (51), 20724–20727.
- (2) Ung, G.; Rittle, J.; Soleilhavoup, M.; Bertrand, G.; Peters, J. C. *Angew. Chem. Int. Ed.* **2014**, *53* (32), 8427–8431.
- (3) Mondal, K. C.; Roy, S.; De, S.; Parameswaran, P.; Dittrich, B.; Ehret, F.; Kaim, W.; Roesky, H. W. *Chemistry* **2014**, *20* (37), 11646–11649.
- (4) Clouston, L. J.; Bernales, V.; Carlson, R. K.; Gagliardi, L.; Lu, C. C. *Inorg. Chem.* **2015**, *54* (19), 9263–9270.
- (5) Suess, D. L. M.; Tsay, C.; Peters, J. C. *J. Am. Chem. Soc.* **2012**, *134* (34), 14158–14164.
- (6) Del Castillo, T. J.; Thompson, N. B.; Suess, D. L. M.; Ung, G.; Peters, J. C. *Inorg. Chem.* **2015**, *54* (19), 9256–9262.
- (7) Siedschlag, R. B.; Bernales, V.; Vogiatzis, K. D.; Planas, N.; Clouston, L. J.; Bill, E.; Gagliardi, L.; Lu, C. C. *J. Am. Chem. Soc.* **2015**, *137* (14), 4638–4641.
- (8) Gao, Y.; Li, G.; Deng, L. *J. Am. Chem. Soc.* **2018**, *140* (6), 2239–2250.
- (9) Mo, Z.; Chen, D.; Leng, X.; Deng, L. *Organometallics* **2012**, *31* (20), 7040–7043.
- (10) Sun, J.; Gao, Y.; Deng, L. *Inorg. Chem.* **2017**, *56* (17), 10775–10784.
- (11) Zhang, L.; Liu, Y.; Deng, L. *J. Am. Chem. Soc.* **2014**, *136* (44), 15525–15528.
- (12) Du, J.; Wang, L.; Xie, M.; Deng, L. *Angew. Chem. Int. Ed.* **2015**, *54* (43), 12640–12644.
- (13) Nalesnik, T. E.; Orchin, M. *Organometallics* **1982**, *1* (1), 222–223.
- (14) Klingler, R. J.; Rathke, J. W. *J. Am. Chem. Soc.* **1994**, *116* (11), 4772–4785.
- (15) Wegman, R. W.; Brown, T. L. *J. Am. Chem. Soc.* **1980**, *102* (7), 2494–2495.
- (16) Paulik, F. E. *Catalysis Reviews* **1972**, *6* (1), 49–84.
- (17) Susuki, T.; Tsuji, J. *Tetrahedron Letters* **1968**, *9* (8), 913–915.
- (18) Seyferth, D.; Millar, M. D. *Journal of Organometallic Chemistry* **1972**, *38* (2), 373–383.
- (19) Rathke, J. W.; Feder, H. M. *J. Am. Chem. Soc.* **1978**, *100* (11), 3623–3625.

- (20) Roth, J. A.; Orchin, M. *Journal of Organometallic Chemistry* **1979**, *182* (2), 299–311.
- (21) Brunet, J. J.; Sidot, C.; Loubinoux, B.; Caubere, P. *The Journal of Organic Chemistry* **1979**, *44* (13), 2199–2202.
- (22) Heck, R. *Organotransition Metal Chemistry A Mechanistic Approach*; Elsevier, 2012.
- (23) Ungváry, F.; Markó, L. *Journal of Organometallic Chemistry* **1981**, *219* (3), 397–400.
- (24) Ungváry, F. *Acta Chim. (Budapest)* **1982**, *111* (2), 117–130.
- (25) Wawersik, H.; Keller, H. J. *Zeitschrift für Naturforschung B* **1965**, No. 20, 938–942.
- (26) Crichton, O.; Poliakoff, M.; Rest, A. J.; Turner, J. J. *J. Chem. Soc., Dalton Trans.* **1973**, No. 12, 1321–1324.
- (27) Fieldhouse, S. A.; Fullam, B. W.; Neilson, G. W.; Symons, M. C. R. *J. Chem. Soc., Dalton Trans.* **1974**, *0* (6), 567–569.
- (28) Pályi, G.; Ungváry, F.; Galamb, V.; Markó, L. *Coordination Chemistry Reviews* **1984**.
- (29) Reichel, C. L.; Wrighton, M. S. *J. Am. Chem. Soc.* **1979**, *101* (22), 6769–6772.
- (30) Basolo, F. *Polyhedron* **1990**, *9* (13), 1503–1535.
- (31) Shi, Q.; Richmond, T. G.; Trogler, W. C.; Basolo, F. *J. Am. Chem. Soc.* **1982**, *104* (14), 4032–4034.
- (32) McCullen, S. B.; Walker, H. W.; Brown, T. L. *J. Am. Chem. Soc.* **1982**, *104* (14), 4007–4008.
- (33) Shi, Q. Z.; Richmond, T. G.; Trogler, W. C.; Basolo, F. *J. Am. Chem. Soc.* **1984**, *106* (1), 71–76.
- (34) Fox, A.; Malito, J.; Poë, A. *Journal of the Chemical Society, Chemical Communications* **1981**, *0* (20), 1052–1053.
- (35) Herrinton, T. R.; Brown, T. L. *J. Am. Chem. Soc.* **1985**, *107* (20), 5700–5703.
- (36) Fawcett, J. P.; Jackson, R. A.; Poë, A. *Journal of the Chemical Society, Chemical Communications* **1975**, *0* (18), 733–734.
- (37) Hieber, W.; Freyer, W. *European Journal of Inorganic Chemistry* **1958**, *91* (6), 1230–1234.
- (38) Hieber, W.; Freyer, W. *European Journal of Inorganic Chemistry* **1960**, *93* (2), 462–467.

- (39) Bezems, G. J.; Rieger, P. H.; Visco, S. *Journal of the Chemical Society, Chemical Communications* **1981**, 0 (6), 265–266.
- (40) Absi-Halabi, M.; Brown, T. L. *J. Am. Chem. Soc.* **1976**, 99 (9), 2982–2988.
- (41) Brown, T. L. *Annals of the New York Academy of Sciences* **1980**, 333 (1), 80–89.
- (42) Therien, M. J.; Trogler, W. C. *J. Am. Chem. Soc.* **1988**, 110 (15), 4942–4953.
- (43) Tyler, D. R. *Acc. Chem. Res.* **1991**, 24 (11), 325–331.
- (44) Tyler, D. R.; Mao, F. *Coordination Chemistry Reviews* **1990**, 97, 119–140.
- (45) Depew, M. C. *Res Chem Intermed* **1991**, 16 (3), 279–279.
- (46) Fallon, B. J.; Corcé, V.; Amatore, M.; Aubert, C.; Chemla, F.; Ferreira, F.; Perez-Luna, A.; Petit, M. *New Journal of Chemistry* **2016**, 40 (12), 9912–9916.
- (47) Rajpurohit, J.; Kumar, P.; Shukla, P.; Shanmugam, M.; Shanmugam, M. *Organometallics* **2018**, 37 (14), 2297–2304.
- (48) Fox, B. J.; Millard, M. D.; DiPasquale, A. G.; Rheingold, A. L.; Figueroa, J. S. *Angew. Chem. Int. Ed.* **2009**, 48 (19), 3473–3477.
- (49) Labios, L. A.; Millard, M. D.; Rheingold, A. L.; Figueroa, J. S. *J. Am. Chem. Soc.* **2009**, 131 (32), 11318–11319.
- (50) Ditri, T. B.; Fox, B. J.; Moore, C. E.; Rheingold, A. L.; Figueroa, J. S. *Inorg. Chem.* **2009**, 48 (17), 8362–8375.
- (51) Margulieux, G. W.; Weidemann, N.; Lacy, D. C.; Moore, C. E.; Rheingold, A. L.; Figueroa, J. S. *J. Am. Chem. Soc.* **2010**, 132 (14), 5033–5035.
- (52) Emerich, B. M.; Moore, C. E.; Fox, B. J.; Rheingold, A. L.; Figueroa, J. S. *Organometallics* **2011**, 30 (9), 2598–2608.
- (53) Mokhtarzadeh, C. C.; Margulieux, G. W.; Carpenter, A. E.; Weidemann, N.; Moore, C. E.; Rheingold, A. L.; Figueroa, J. S. *Inorg. Chem.* **2015**, 54 (11), 5579–5587.
- (54) Carpenter, A. E.; Rheingold, A. L.; Figueroa, J. S. *Organometallics* **2016**, 35 (14), 2309–2318.
- (55) Carpenter, A. E.; Chan, C.; Rheingold, A. L.; Figueroa, J. S. *Organometallics* **2016**, 35 (14), 2319–2326.
- (56) Beveridge, R. E.; Batey, R. A. *Org. Lett.* **2014**, 16 (9), 2322–2325.

- (57) Dai, C.; Yuan, Z.; Collings, J. C.; Fasina, T. M.; Thomas, R. L.; Roscoe, K. P.; Stimson, L. M.; Yufit, D. S.; Batsanov, A. S.; Howard, J. A. K.; Marder, T. B. *CrystEngComm* **2004**, *6* (32), 184–188.
- (58) Agnew, D. W.; Moore, C. E.; Rheingold, A. L.; Figueroa, J. S. *Angew. Chem. Int. Ed.* **2015**, *54* (43), 12673–12677.
- (59) Jaitner, P.; Huber, W.; Gieren, A.; Betz, H. *Journal of Organometallic Chemistry* **1986**, *311* (3), 379–385.
- (60) Pelties, S.; Herrmann, D.; de Bruin, B.; Hartl, F.; Wolf, R. *Chemical Communications* **2014**, *50* (53), 7014–7016.
- (61) Vizi-Orosz, A. *Journal of Organometallic Chemistry* **1976**, *111* (1), 61–64.
- (62) Caporali, M.; Gonsalvi, L.; Rossin, A.; Peruzzini, M. *Chem. Rev.* **2010**, *110* (7), 4178–4235.
- (63) Vizi-Orosz, A.; Galamb, V.; Pályi, G.; Markó, L. *Journal of Organometallic Chemistry* **1981**, *216* (1), 105–111.
- (64) Shibahara, T.; Iwai, N.; Sasaki, M.; Sakane, G. *Chem. Lett.* **1997**, *26* (5), 445–446.
- (65) Shibahara, T.; Nishiura, K.; Tsuboi, M.; Akashi, H.; Sakane, G. *Chem. Lett.* **2001**, *30* (10), 1002–1003.
- (66) Markó, L.; Bor, G.; Almásy, G. *Chem. Ber.* **1961**, *94* (3), 847–850.
- (67) Markó, L.; Bor, G.; Klumpp, E.; Markó, B.; Almásy, G. *European Journal of Inorganic Chemistry* **1963**, *96* (4), 955–964.
- (68) *Purification of Laboratory Chemicals*; Elsevier, 2003.
- (69) Pangborn, A. B.; Giardello, M. A.; Grubbs, R. H.; Rosen, R. K.; Timmers, F. J. *Organometallics* **1996**, *15* (5), 1518–1520.
- (70) Fox, B. J.; Sun, Q. Y.; DiPasquale, A. G.; Fox, A. R.; Rheingold, A. L.; Figueroa, J. S. *Inorg. Chem.* **2008**, *47* (19), 9010–9020.
- (71) Burla, M. C.; Caliandro, R.; Camalli, M.; Carrozzini, B.; Cascarano, G. L.; De Caro, L.; Giacovazzo, C.; Polidori, G.; Spagna, R. *Journal of Applied Crystallography* **2005**, *38* (2), 381–388.
- (72) Sheldrick, G. M. *Acta Crystallogr., A, Found. Crystallogr.* **2008**, *64* (Pt 1), 112–122.
- (73) Dolomanov, O. V.; Bourhis, L. J.; Gildea, R. J.; Howard, J. A. K.; Puschmann, H. *Journal of Applied Crystallography* **2009**, *42* (2), 339–341.

- (74) Spek, A. L. *Journal of Applied Crystallography* **2003**, 36 (1), 7–13.
- (75) van der Sluis, P.; Spek, A. L. *Acta Crystallogr., A, Found. Crystallogr.* **1990**, 46 (3), 194–201.

# Chapter 3 Conformational Dynamics in Zero-valent $\text{CoL}_4$ Complexes Revealed by 2D IR Spectroscopy

## 3.1 Introduction

2D IR spectroscopy provides an avenue to visualize kinetic processes that involved reactive organometallic species which serve as important intermediates in catalytic reactions.<sup>1-</sup>  
<sup>4</sup> Probing structures and dynamics of these intermediate species is at the heart of understanding the mechanism of catalytic reactions. Since 2D IR spectroscopy is a time resolved technique that can follow chemical exchange occurring from hundreds of femtosecond to picosecond time scales,<sup>1-7</sup> the often time short lived and fast transforming catalytic intermediates can be monitored. Furthermore, because vibrational modes in organometallic compounds are mostly local, by selectively probing vibrational modes that are near the metal center, dynamics around metal center can be tracked, which is mostly relevant to catalytic intermediates of interests. These unique advantages make 2D IR uniquely useful to resolving conformations and following structural dynamics of organometallic compounds and other molecules.<sup>6,8-12</sup>

Since early 2000,<sup>13</sup> 2D IR has been widely used to study dynamics of organometallic molecules. However, there has been little progress in studying unstable species.  $\text{Co}(\text{CO})_4$ ,

known as an important intermediate of hydroformylation and hydrogenation catalysis, but also a great example of classic labile organometallic complex, became our choice of study.<sup>14-25</sup>

Known to be photogenerated from  $\text{Co}_2(\text{CO})_8$  through Co-Co bond homoleptic cleavage,  $\text{Co}(\text{CO})_4$  serves as a  $S = 1/2$  metalloradical observed only in low temperature matrices.<sup>26,27</sup> Its geometric/electronic structures have been long debated due to near-thermoneutral nature of its  $C_{3v}$  and  $D_{2d}$  ground states.<sup>28,29</sup> So far, these species have been well studied by static spectroscopic methods under cryogenic or gas phase conditions, which have concluded that the method of observation directly affects the geometric preference.<sup>30-34</sup> These studies, coupled with computational evidence, have indicated that there exists fast exchange between isomers. However, this exchange has never been observed under ambient conditions (or those related to catalysis) in a direct, time resolved manner.

The tetrakisocyanide complex,  $\text{Co}(\text{CNAr}^{\text{Mes}_2})_4$  ( $\text{Ar}^{\text{Mes}_2} = 2,6\text{-}(2,4,6\text{-Me}_3\text{C}_6\text{H}_2)_2\text{C}_6\text{H}_3$ ), serves as a crystallographically characterized, thermally stable isocyano analogue of the reactive binary carbonyl  $\text{Co}(\text{CO})_4$  (Figure 3.1a).<sup>35,36</sup> Through our recent studies, this compound mimics well the electronic structure of  $\text{Co}(\text{CO})_4$  due to the isolobal analogues between carbomonoxide (CO) and isocyanides (CNR).<sup>35,37-43</sup> A combination of static X-ray crystallography, EPR and FTIR experiments suggested that similar to  $\text{Co}(\text{CO})_4$ , more than one conformation of  $\text{Co}(\text{CNAr}^{\text{Mes}_2})_4$  could be present. For example, X-ray crystallographic collections showed slight geometry distortions from  $D_{2d}$  to  $C_{2v}$  upon increasing temperatures, again indicates the possible dynamic feature in  $\text{Co}(\text{CNAr}^{\text{Mes}_2})_4$ .

With the advent of both kinetically stabilized model complexes of  $\text{Co}(\text{CO})_4$  and ultrafast time-resolved 2D spectroscopic techniques, the question of dynamic conformational changes in such reactive species can now be directly interrogated.



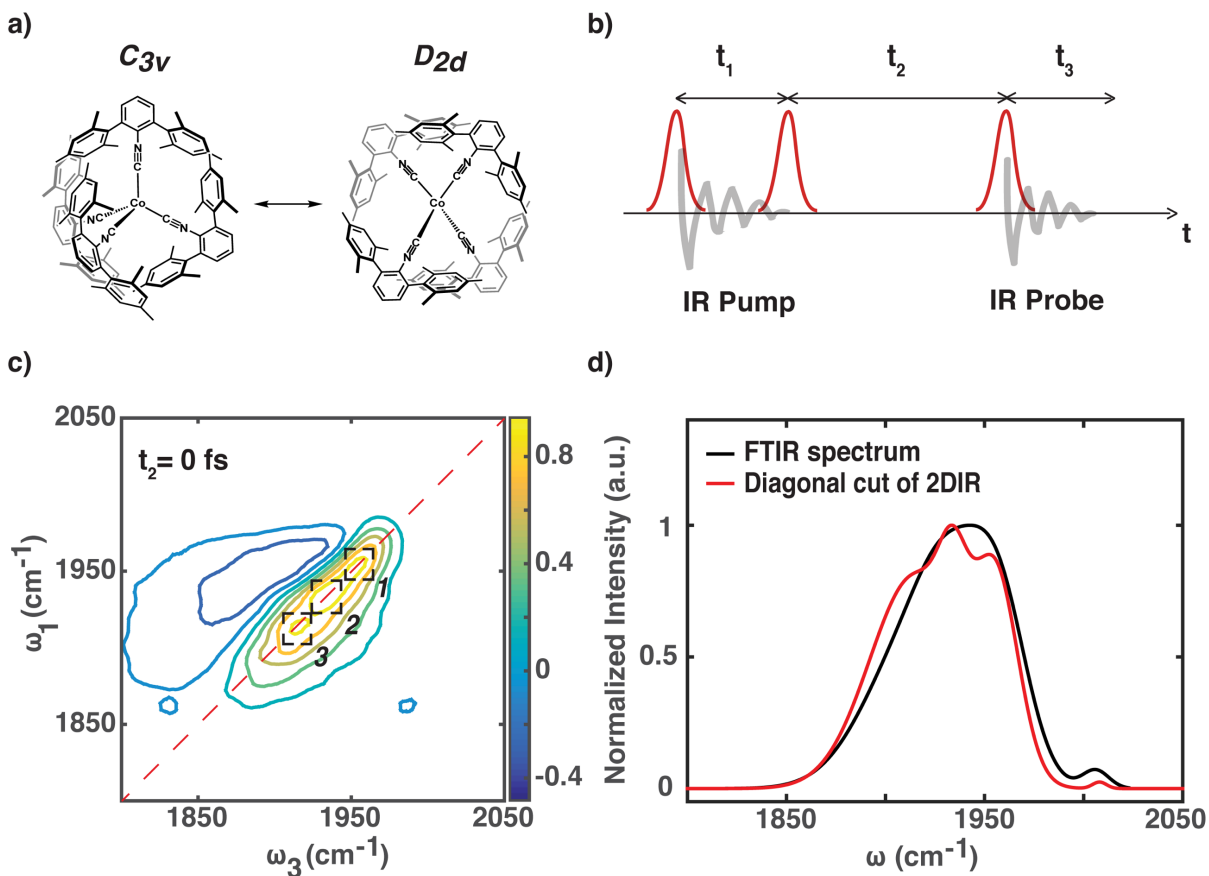


**Figure 3.1.** a) Molecular Structure of  $\text{Co}(\text{CNAr}^{\text{Mes}_2})_4$  in  $D_{2d}$  and  $C_{3v}$  geometries. b) pulse sequence used in 2D IR experiment. c) 2D IR spectrum of  $\text{Co}(\text{CNAr}^{\text{Mes}_2})_4$  at  $t_2 = 0$  fs, diagonal peaks are labeled as 1, 2, and 3. d) Normalized FTIR spectrum (black) of  $\text{Co}(\text{CNAr}^{\text{Mes}_2})_4$ , and diagonal cut of 2D IR spectrum in c) (red).

## 3.2 Results and Discussion

The FTIR spectrum of  $\text{Co}(\text{CNAr}^{\text{Mes}_2})_4$  shows a broad main peak with lower frequency shoulder at  $1940 \text{ cm}^{-1}$  plus a separate small peak at higher frequency ( $\sim 2005 \text{ cm}^{-1}$ ). (Figure 3.1d). These peaks correspond to the isocyanide CN vibrations. It is noticeable that the main peak has about  $80 \text{ cm}^{-1}$  full-width-at-half-max, which is 3-5 times broader than the linewidth of any typical carbonyl or isocyanide vibration peaks. One possible explanation is that this

broad feature contains multiple peaks. In agreement with the statement that both  $C_{3v}$  and  $D_{2d}$  isomers exist, as indicated from its EPR spectra at 100 K.

Indeed, 2D IR spectrum of  $\text{Co}(\text{CNAr}^{\text{Mes}2})_4$  shows a clear signature of multiple peaks (Figure 3.1c). This is because 2D IR is proportional to the vibrational transition dipole moment to the fourth order,  $\mu^4$ , comparing to the  $\mu^2$  dependence of linear IR spectroscopy.<sup>44</sup> The fourth order dependence in  $\mu$  makes 2D IR able to distinguish convoluted spectral peaks. The peaks along diagonal of 2D IR spectrum clearly displays at least three pairs of closely spaced peaks, labeled as peak 1 ( $\sim 1960 \text{ cm}^{-1}$ ), peak 2 ( $\sim 1938 \text{ cm}^{-1}$ ), and peak 3 ( $\sim 1915 \text{ cm}^{-1}$ ). For each pair, the positive peak that resides along diagonal line is the fundamental vibrational transition, whereas the negative peak that is redshifted relative to the positive one is the overtone transition. Interestingly, by taking cut along the diagonal line of a 2D spectrum we show high frequency peak at  $2005 \text{ cm}^{-1}$  is rather “hidden” than “missing” in the 2D contour due to its weak intensity – the diagonal cut of 2D spectrum is consistent with FTIR data (Figure 3.1d). These multiple peaks span across the linewidth of corresponding FTIR spectrum, which supports that multiple absorption peaks are responsible for the extremely broad peak in FTIR.

Temperature dependent FTIR spectroscopy confirms that these peaks are originated from different isomers, such as  $C_{3v}$  and  $D_{2d}$  geometries, rather than they could be different normal modes of the same isomers. The FTIR spectra of  $\text{Co}(\text{CNAr}^{\text{Mes}2})_4$  in  $d_8$ -toluene at different temperature shows that the intensity of peak 2 increases in relative to peak 1 and 3 as temperature decreases from 308 K to 268 K. At this temperature variation range, it is unlikely that the transition dipoles vary significantly. Thus, the different temperature dependence between peak 2, and peaks 1/3 must be due to that peak 2 belongs to a different conformer from

peak 1 and 3, and the two conformations have different free energy. To further identify the two conformations and examine our interpretation of temperature dependent FTIR results, we conducted DFT calculation on both  $C_{3v}$  and  $D_{2d}$  geometries and simulate corresponding IR spectra. After applying proper scale factor, the calculated peak positions agree with experimental measurements well. Peaks 1 and peak 3 correspond to the E and  $B_2$  modes of  $D_{2d}$  geometry respectively, whereas peak 2 is from the double-degenerated E modes of  $C_{3v}$  (Figure 3.2). The calculations also predict that for  $C_{3v}$  geometry at higher frequency there should be another peak with lower intensity, which matches well with the high frequency small peak shown in FTIR and diagonal cut spectrum of 2D IR (Figure 3.1d).

With two conformations identified, we further examined the dynamics between these conformations by measuring 2D IR spectral cross peak at a series  $t_2$  time delay. The cross peaks in 2D IR spectra are features that have different frequency positions onto  $\omega_1$  and  $\omega_3$  axes. Constrained by vibrational lifetime of isocyanide mode, we measured early stage cross peak dynamics (0 to 1500 fs, in a step of 150 fs). The normalized cross peak dynamics (Figure 3.3a) show that cross peaks between 1 and 2, 2 and 3 increase their intensity, whereas cross peak between 1 and 3 remain constant. This result agrees with the diagonal peak assignments: cross peak between 1 and 2, and 2 and 3 represents the dynamic conformational exchange between the  $C_{3v}$  and  $D_{2d}$  isomers.

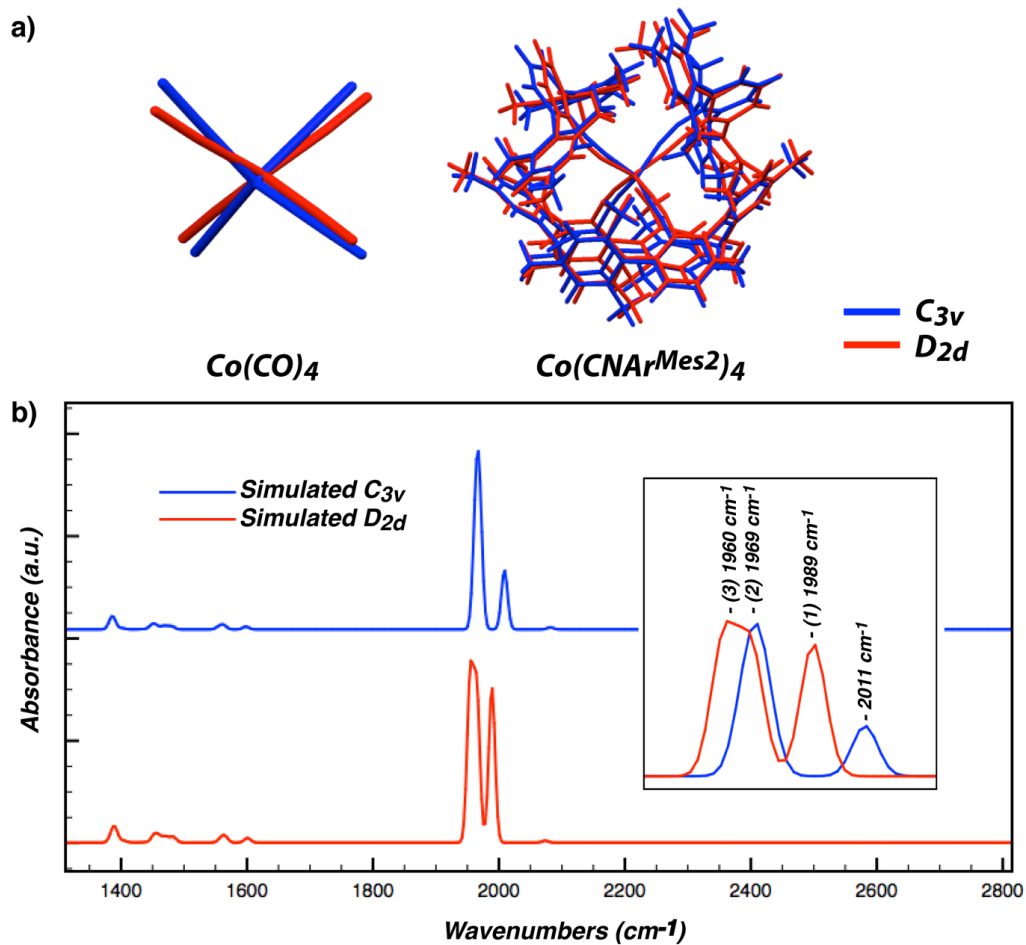


**Figure 3.2.** a) Molecular overlap of DFT calculated both  $\text{C}_{3v}$  (blue) and  $\text{D}_{2d}$  (red) geometries of  $\text{CoL}_4(\text{L}=\text{CO}, \text{CNAr}^{\text{Mes}2})$ . b) Simulated IR spectrum of both  $\text{C}_{3v}$  (blue) and  $\text{D}_{2d}$  (red)  $\text{Co}(\text{CNAr}^{\text{Mes}2})_4$  using b3lyp/6-31g(d):lanl2dz. Wavenumbers are scaled with scaling factor of b3lyp/6-31g(d) = 0.9614.

Despite the consistency between peak assignments and cross peak dynamics points to what we observed is conformation exchanges, we still examined the other possibility of cross peak dynamics – intramolecular vibrational redistribution (IVR), by measuring 2D IR cross peak dynamics at different temperature. IVR and conformational exchanges have different temperature dependence.<sup>45-48</sup> We found the rate of cross peak growth slows down steadily as temperature decreases (Figure 3.3b). This trend agrees better with the strong temperature dependence of conformation exchange, whereas IVR has weak temperature dependence — for

IVR to happen it requires energy from solvent bath as in phonon modes to match with the splitting between two vibrational modes. From the temperature dependence of cross peaks dynamics, we determined the exchange activation energy barrier of conformation exchanges to be  $\Delta E_{a(D2d-C3v)}=0.5 \pm 0.1$  kcal/mol, while  $\Delta E_{a(C3v-D2d)}=1.9 \pm 0.4$  kcal/mol.

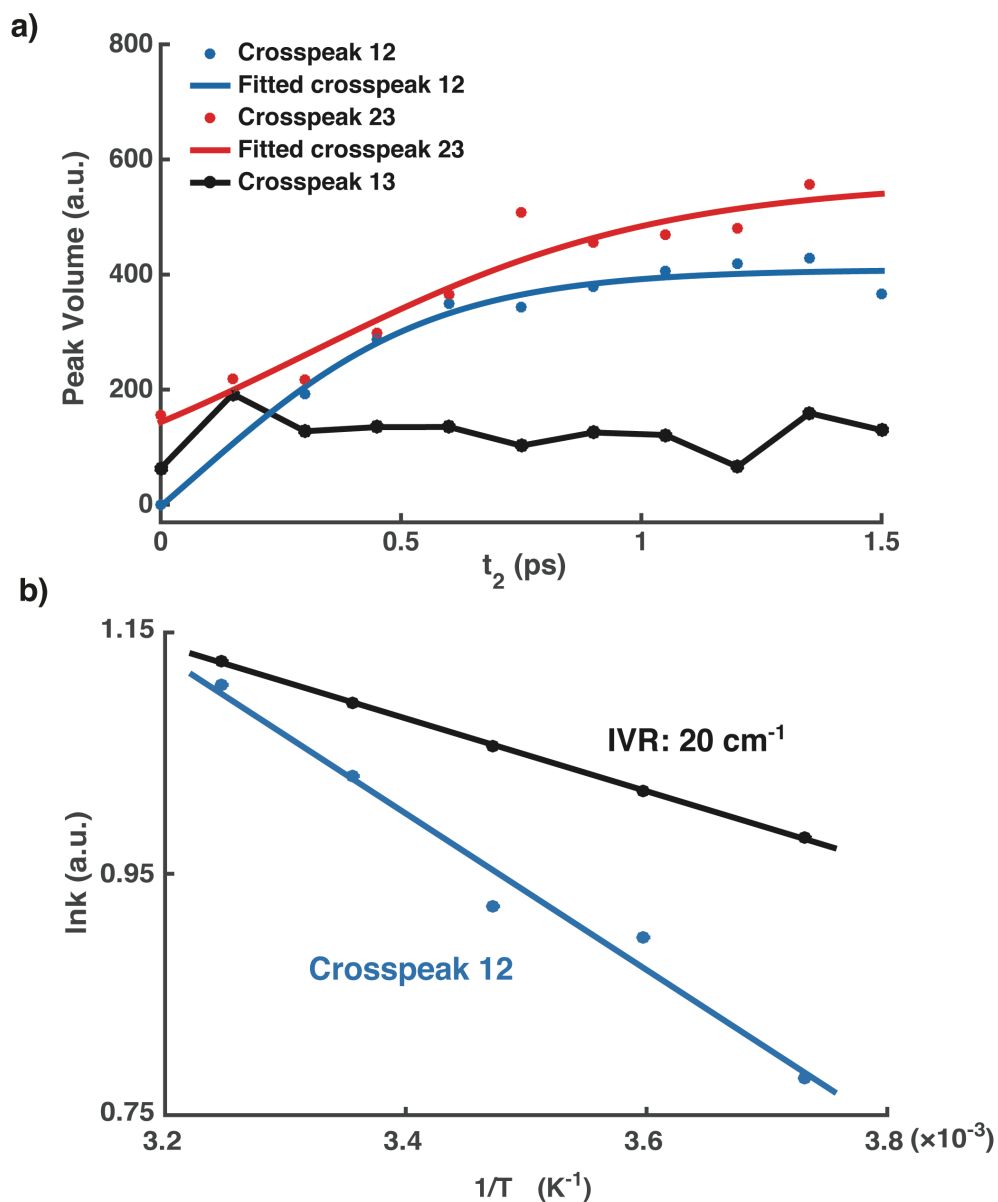


**Figure 3.3.** a) Dynamics traces of different cross peaks as functions of  $t_2$ . b) Plot of  $\ln(k)$  vs.  $1/T$ . Rate of cross peak growth and rate of IVR (when mode splitting is  $20\text{ cm}^{-1}$ ) have different temperature dependent.

We therefore conclude that the observed cross peak dynamics is originated from conformation exchange. However, the time scale of the dynamics is unexpectedly fast considering the bulky ligands (about 0.5 to 1 ps depending on temperature). For example, previous research on  $\text{Fe}(\text{CO})_5$  measured 2.5 kcal/mol activation energy barrier and less than 10 ps cross peak dynamics.<sup>2</sup>  $\text{Co}(\text{CNAr}^{\text{Mes}2})_4$ , on the other hand, are coordinated with bulky *m*-terphenyl ligands, which intuitively should slow down conformational exchanges comparing to Berry pseudorotation of  $\text{Fe}(\text{CO})_5$ . Therefore, an important scientific question to address is how ultrafast conformation exchanges could occur in  $\text{Co}(\text{CNAr}^{\text{Mes}2})_4$ ?

This surprising result could be understood by considering the nature of molecular vibrational transitions in 2D IR spectroscopy. Because the CN group directly attach to Co, its vibrational frequency probes the electronic structures of the Co metal core, whereas the fluctuation and structural rearrangement of the outer sphere *m*-terphenyl ligands– $\text{Ar}^{\text{Mes}2}$  should only have minor effect to the CN vibrational modes. Detailed DFT calculations agree that as long as the  $\text{Co}(\text{CNAr}^{\text{Mes}2})_4$  core symmetry remains the same, twisting outer sphere geometry does not affect the IR spectrum of CN stretches (Fig 3.10 – Fig 3.11). This preferential sensitivity of CN group makes 2D IR measures the isomerization of electronic structure near the Co core (C-Co-C), rather than the isomerization of the entire molecule. In other words, the slow motion of the bulky  $\text{Ar}^{\text{Mes}2}$  ligands at outer sphere does not matter: even if they are still in the original positions, as long as the core changed symmetry and its corresponding electronic structures changes, this Co core isomerization is measured by 2D IR.

From detailed DFT studies, it appears only a few degrees of core-ligands movements are enough to change the degree of Co  $d_{x^2-y^2}$   $\pi$ -backbonding to the isocyanide p orbitals, which is the essential of the core isomerization. The calculated  $C_{3v}$  and  $D_{2d}$  isomers of  $\text{CoL}_4$  (L= CO,

CNAr<sup>Mes2</sup>) are very similar in geometry even though they are different electronic structures (Figure 3.2a). Unlike the case of Fe(CO)<sub>5</sub>, whose CO swings 90 degree in isomerization, isomerization of CoL<sub>4</sub> only involves small angle changes. Therefore, the mechanical movements of ligands (and imaginary frequency of the transition states) should not be the limiting factor for isomerization, and instead, the electronic structure of Co core at different geometry and activation energy of Co isomerization should be the key factor, and the latter has been determined to be small ( $\Delta E_{a(D2d-C3v)}=0.5 \pm 0.1$  kcal/mol,  $\Delta E_{a(C3v-D2d)}=1.9 \pm 0.4$  kcal/mol).

A complete the energy schematic of conformation exchanges is further estimated from both experimental and theoretical results. From the VT-FTIR, we estimate  $\Delta H$  to be  $1.4 \pm 0.2$  kcal/mol. The experimental results suggest that these two isomers may be equi-energetic as has been traditionally proposed for Co(CO)<sub>4</sub>. DFT calculation on all CoL<sub>4</sub> (L=CO, CNMe, CNXyl, CNAr<sup>Ar2</sup>, CNAr<sup>Mes2</sup>) isomers results  $\Delta H$  in the range of 1-4.5 kcal/mol with C<sub>3v</sub> lower in energy at all cases. (Table 3.4.) The presence of increased steric encumbrance resulted in larger  $\Delta H$ . It is interesting to note that the experimental determined value of Co(CNAr<sup>Mes2</sup>)<sub>4</sub> is closer to the DFG computational  $\Delta H$  of CoL<sub>4</sub>. One possibility is steric hindrance of the bulky ligands creates local minimums, which lies higher in energy than the fully relaxed geometry and also experience smaller activation energy for isomerization - agree with the experimental measured  $\Delta E_a$ . This picture of equi-energetic states rationalizes the solid-state structure of Co(CNAr<sup>Mes2</sup>)<sub>4</sub>, which is likely to be an intermediate geometry between C<sub>3v</sub> and D<sub>2d</sub> and can be affected by low-energies on the order of crystal packing forces.

Finally, does the observed ultrafast conformation exchange of Co(CNAr<sup>Mes2</sup>)<sub>4</sub> also represents the isomerization of Co(CO)<sub>4</sub>? We argue because experimentally we showed that

the bulky outer sphere ligands matter little and it is the core electronic structure dictating the isomerization dynamics of metal core, the  $\text{Co}(\text{CNAr}^{\text{Mes}2})_4$  isomerization dynamics measured here should closely mimic the dynamics of catalytic intermediate  $\text{Co}(\text{CO})_4$ , due to their similarity in electronic structures. This is a significant implication, because many bulky ligands stabilized isoelectronic molecules similar to  $\text{Co}(\text{CNAr}^{\text{Mes}2})_4$  can be used to not only learn electronic structure of unstable unsaturated catalytic intermediates, but also their structural dynamics.

### 3.3 Concluding Remarks

Despite 2D IR has been used successfully for studying ultrafast conformation exchanges of organometallic compounds, this is the first time a kinetically stabled unsaturated compound being investigated. Surprisingly, ultrafast conformation exchange dynamics is observed, irrespective to the presence of bulky ligands at outer spheres. Combining this result with detailed DFT calculations, we show that 2D IR probes the electronic structure change accompanied with the isomerization at Co core, whereas the bulky ligands position matter little. This result confirms the long-time speculated dual-conformations and exchange dynamics exists for  $\text{Co}(\text{CNAr}^{\text{Mes}2})_4$  and likely, in  $\text{Co}(\text{CO})_4$ .

### 3.4 Synthetic Procedures

All manipulations were carried out under an atmosphere of dinitrogen using standard Schlenk and glovebox techniques.<sup>45</sup> Unless otherwise stated, reagent-grade starting materials were purchased from commercial sources and either used as received or purified by standard procedures. Solvents were dried and deoxygenated according to standard procedures.<sup>46</sup>



Benzene- $d_6$  and Toluene- $d_8$  were dried with Na/K and Benzophenone followed by distillation and stored on 4 Å molecular sieves for 3 days prior to use. The compounds  $\text{Co}(\text{CNAr}^{\text{Mes}_2})_4$  and  $\text{Co}(\text{CN}^t\text{Bu})(\text{CNAr}^{\text{Mes}_2})_3$  were prepared by previously reported methods.<sup>35</sup>

### 3.5 FTIR Experimental Set up, Data Collection, and Analysis

**FTIR of  $\text{Co}(\text{CNAr}^{\text{Mes}_2})_4$  and  $\text{Co}(\text{CN}^t\text{Bu})(\text{CNAr}^{\text{Mes}_2})_3$ .** All spectra were recorded on a Thermo-Nicolet iS10 FTIR spectrometer. Samples were prepared as solutions injected into a ThermoFisher solution cell equipped with KBr windows. For solution FTIR spectra, solvent peaks were digitally subtracted from all spectra by comparison with an authentic spectrum obtained immediately prior to that of the sample.

**VT-FTIR of  $\text{Co}(\text{CNAr}^{\text{Mes}_2})_4$  and  $\text{Co}(\text{CN}^t\text{Bu})(\text{CNAr}^{\text{Mes}_2})_3$ .** Variable temperature infrared spectra were collected on a Bruker Equinox 55 FTIR spectrometer using a SPECAC flow through optical cryostat (model, 21525) with a 1.12 mm path length (determined from infringing pattern),  $\text{CaF}_2$  windowed cell enclosed in a vacuum jacketed housing.

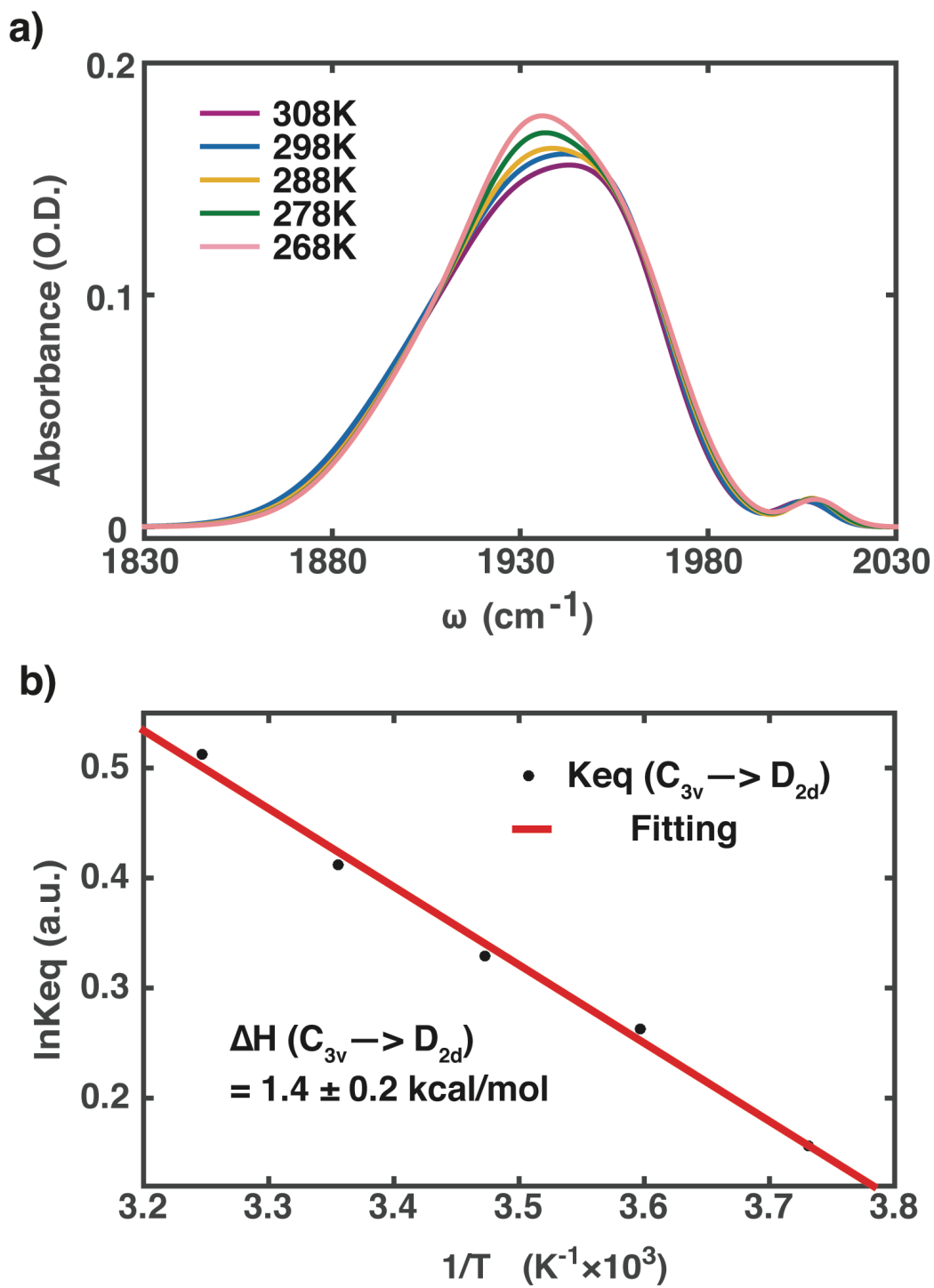


**Figure 3.4.** a) VT-FTIR spectrum of  $\text{Co}(\text{CNAr}^{\text{Mes}2})_4$  and b) van't hoff plot of  $\ln\text{Keq}$  vs  $1/T$  between  $C_{3v}$  and  $D_{2d}$ .

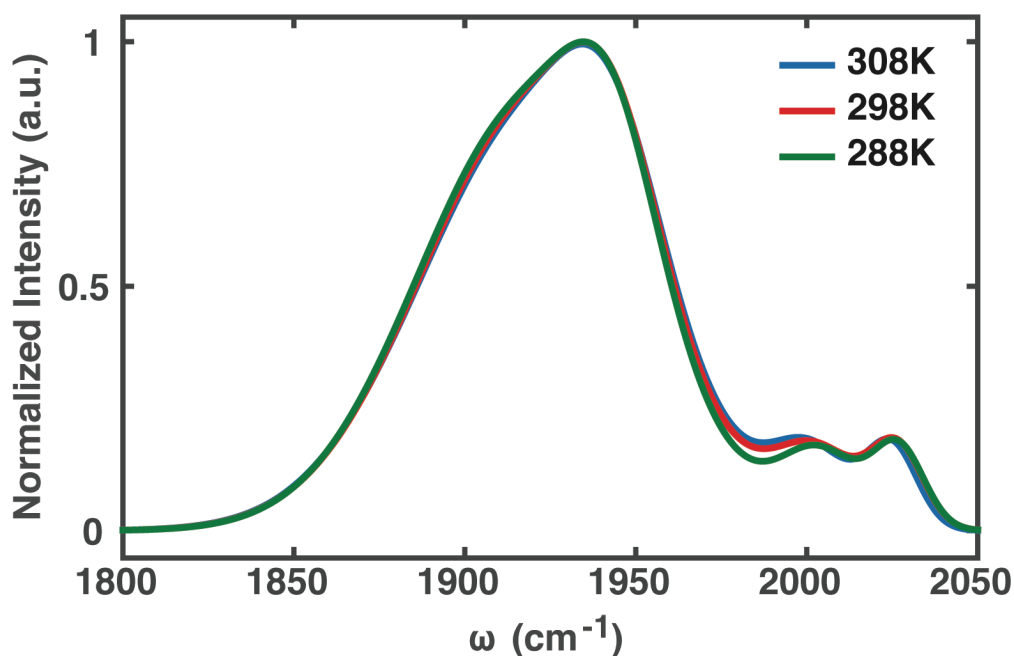


**Figure 3.5.** VT-FTIR spectrum of  $\text{Co}(\text{CN}^t\text{Bu})(\text{CNAr}^{\text{Mes}2})_3$ .

### 3.6 FTIR Experimental Set up, Data Collection, and Analysis

2D IR spectra were collected in pump-probe geometry.<sup>47,48</sup> The pulse sequence is described in Figure 1. In brief, three mid-IR pulses were sent to interact with the sample, where two vibrational coherences were created during  $t_1$  and  $t_3$  period. To generate the pulse sequence, 800nm laser pulses ( $\sim 35$  fs,  $\sim 6$  W, 1 kHz) were generated by ultrafast Ti:Sapphire regenerative amplifier (Astrella, Coherent). The 800nm was converted into mid-IR pulses by optical parametric amplifier (TOPAS, Coherent) followed by a different frequency generation process on a Type II AgGaS<sub>2</sub> crystal (Eksma). The mid-IR pulse (30  $\mu\text{J}$ ) was split into two beams by a beam-splitter. The majority (95%) was sent into a Ge-AOM based pulse shaper (QuickShape Kit, PhaseTech) to prepare the two pump pulse in the pulse sequences, whereas 5% mid-IR served as the probe. The pump pulse pairs (2  $\mu\text{J}$  at the sample), the probe ( $< 0.5$   $\mu\text{J}$ ) were all

focused and spatially overlapped on the sample by a  $f = 10$  cm parabolic mirror and collimated by another parabolic mirror in a symmetric geometry.

In the 2D IR experiments, two vibrational coherences were generated during  $t_1$  and  $t_3$  periods, respectively. The first coherence was measured by scanning  $t_1$  time from 0 to 2000 fs in steps of 20 fs using the pulse shaper, where a rotating frame at  $f_0 = 1583 \text{ cm}^{-1}$  was used to shift the oscillation period to 80 fs, so that the scanning step can meet with the Nyquist frequency requirement. In order to detect the 2D IR signal (the second vibrational coherence) by the CCD camera ( $256 \times 1,024$ , Andor), the collimated signal and the probe beam were then upconverted by a residue 800 nm beam on a 5%Mg: LiNbO<sub>3</sub> crystal.<sup>49,50</sup> Since the 800 nm served as a window function, the  $t_3$  time delay were covered by the upconversion process and the 800 nm pulse duration determined how long  $t_3$  was “scanned”.<sup>51,52</sup> The up-converted 2D IR signals were experimentally Fourier transformed by a spectrograph and detected by a CCD camera. To get full absorptive 2D IR spectra, the first vibrational coherence was numerical Fourier transformed along  $t_1$  axis. The pump and probe pulses had the same polarization in 2D IR measurements. For the time dependent 2D IR measurements,  $t_2$  was scanned by a computerized delay stage.

### **3.7 Obtaining Chemical Exchange Rate Constants from Time Dependent 2D IR Spectra**

The volume of each peak with respect to  $t_2$  was obtained from the  $t_2$ -dependent 2D IR spectra.<sup>7,53</sup> As shown in Figure 2.6, multiple Gaussian functions were used to fit the 2D IR spectral cut along the probe axis at the peak 2 frequency ( $\sim 1940 \text{ cm}^{-1}$ ) on the pump axis. All

2D IR spectra at different  $t_2$  times were fit following the same method. Each Gaussian function represents one species in the 2D IR spectrum. For example, at  $t_2 = 0$  fs, the single Gaussian was used to fit the positive peak of the spectral cut corresponding to the fundamental transition of diagonal peak 2. Similarly, at  $t_2 = 900$  fs, three Gaussians were needed to account for the cross peaks resulting from chemical exchange. Peak volumes for each species were obtained from the Gaussian fitting parameters, assuming a circular 2D Gaussian distribution for each peak component. In the generalized transition of a species A to B, the lower corner cross peak of the diagonal peak ratios in the 2D IR spectrum can be expressed as functions of  $t_2$ .<sup>44</sup>

$$\begin{aligned} \frac{S_{BA}}{S_{AA}} &= \frac{1 - e^{-(k_{AB}+k_{BA})\cdot t_2}}{1 + \frac{k_{AB}}{k_{BA}} \cdot e^{-(k_{AB}+k_{BA})\cdot t_2}} \\ &= \frac{1 - e^{-k_{sum}\cdot t_2}}{1 + K_{eq(A\leftrightarrow B)} \cdot e^{-k_{sum}\cdot t_2}} \end{aligned}$$

The sum of the rate constants of a transition ( $k_{for} + k_{rev}$ ) was directly obtained from fitting  $S_{cross\ peak}/S_{diagonal\ peak}$  with respect to  $t_2$ . Given the  $K_{eq}$  from VT-FTIR data in Figure S2.1.,  $k_{for}$  and  $k_{rev}$  can be calculated separately. Based on Eyring plot, the forward and reverse activation energy barrier between  $D_{2d}$  and  $C_{3v}$  can be obtained as 0.5 kcal/mol and 1.9 kcal/mol, respectively.

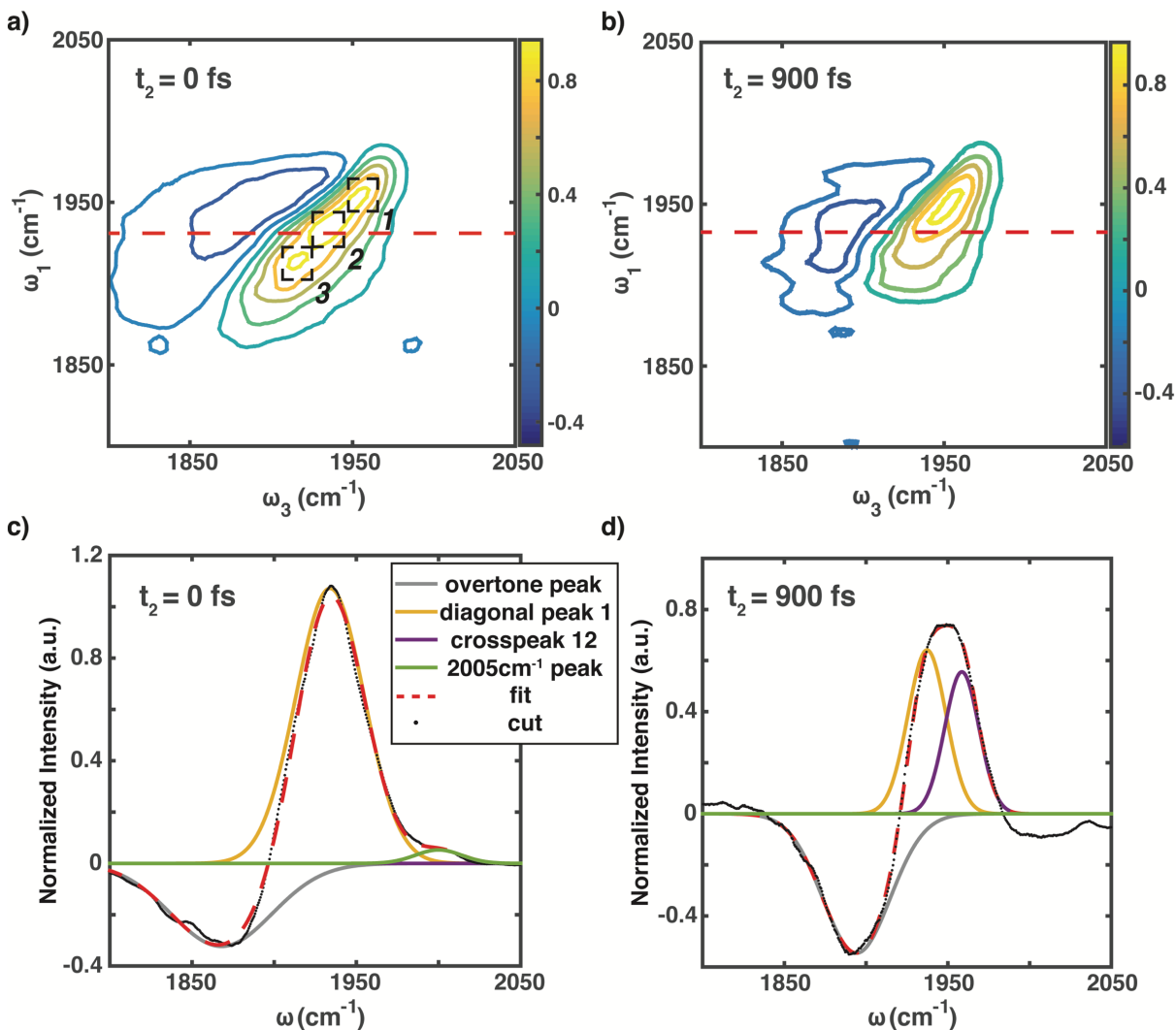
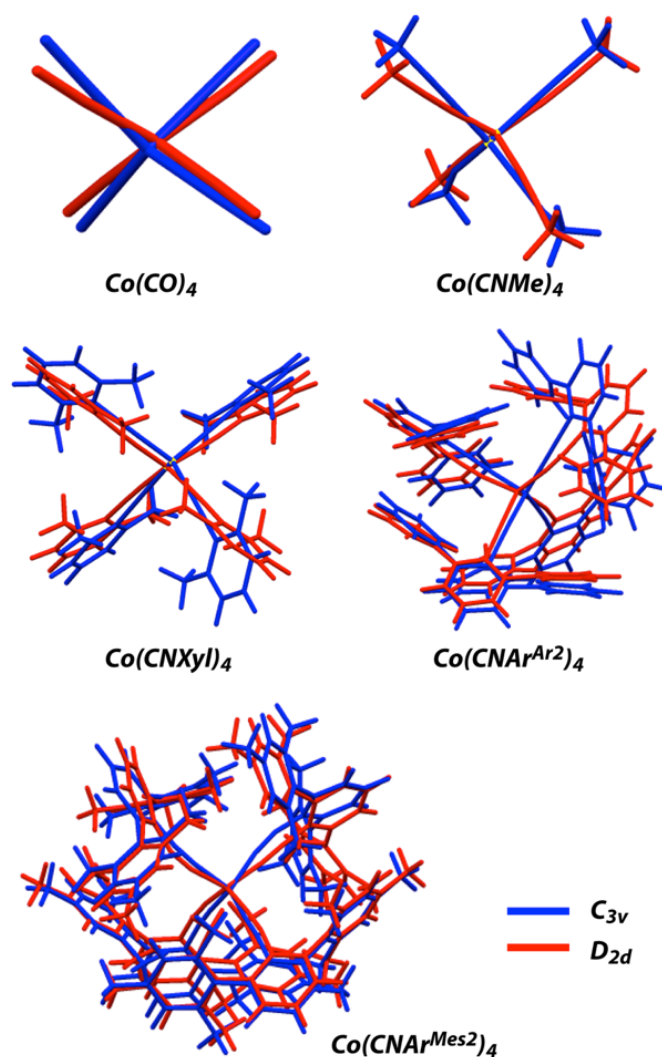


**Figure 3.6.** a) 2D IR spectrum at  $t_2=0$  fs b) 2D IR spectrum at  $t_2=900$  fs c) take cut along  $w_3$  axis at red dash line in a) and fit with gaussian peak components for  $t_2=0$  fs d) take cut along  $w_3$  axis at red dash line in b) and fit with gaussian peak components for  $t_2=900$  fs.

### 3.8 Computational Studies

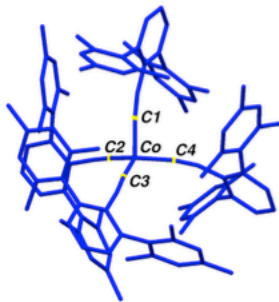
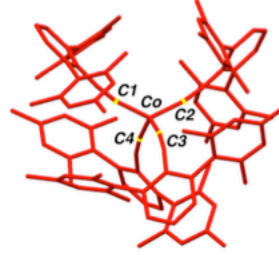
**Computational details.** Density Functional Theory (DFT) calculations were carried out on both  $C_{3v}$  and  $D_{2d}$  geometry of  $CoL_4$  ( $L = CO, CNMe, CNXyl, CNAr^{Ar2}$  and  $CNAr^{Mes2}$ ). All  $C_{3v}$  calculations were accomplished by freely refined the coordinates.  $D_{2d}$  calculations were achieved by starting from the coordinates of  $[Ni(CNAr^{Mes2})_4]OTf$  molecule which shows  $D_{2d}$

geometry in the crystal structure<sup>54</sup>, with constrains at the core angles. Also, calculation on  $\text{Co}(\text{CN}^t\text{Bu})(\text{CNAr}^{\text{Mes}2})_3$  was obtained by starting from the crystal structure coordinates. Calculations were all carried out with the Gaussian 09 software package.<sup>55</sup> Geometry optimizations, frequency and single point energy calculations were performed using the B3LYP functional, with the 6-31g(d) basis set for H, C, O and N atoms and the LANL2DZ basis set plus f-type polarization functions for cobalt atoms. Viewing of optimized structures and rendering of molecular orbitals was performed using the program *Chemcraft*.



**Figure 3.7.** Structural overlap images of optimized  $\text{CoL}_4$  ( $L = \text{CO}, \text{CNMe}, \text{CNXyl}, \text{CNAr}^{\text{Ar}2}, \text{CNAr}^{\text{Mes}2}$ ) coordinates.

**Table 3.1.** Calculated core bond angles of  $\text{Co}(\text{CNAr}^{\text{Mes}_2})_4$   $\text{C}_{3v}$  and  $\text{D}_{2d}$  Isomers.

Symmetry	Converged Coordinates*	Angle	Bond angle (°)
$\text{C}_{3v}$		<b>C1-Co-C2</b>	<b>101</b>
		<b>C1-Co-C3</b>	<b>107</b>
		<b>C1-Co-C4</b>	<b>95</b>
		<b>C2-Co-C3</b>	<b>118</b>
		<b>C3-Co-C4</b>	<b>116</b>
		<b>C4-Co-C1</b>	<b>114</b>
$\text{D}_{2d}$		<b>C1-Co-C2</b>	<b>130</b>
		<b>C4-Co-C3</b>	<b>125</b>
		<b>C1-Co-C4</b>	<b>104</b>
		<b>C2-Co-C3</b>	<b>103</b>
		<b>C1-Co-C3</b>	<b>97</b>
		<b>C2-Co-4</b>	<b>98</b>

\*H-atoms omitted for clarity.



**Table 3.2.** Calculated Frequencies and Symmetries of CN Stretching Modes in Relevant  $\text{Co}(\text{CNAr}^{\text{Mes}_2})_4$   $C_{3v}$  and  $D_{2d}$  Isomers.

Assigned Mode	Symmetry	Frequency* ( $\text{cm}^{-1}$ )
0	$C_{3v}$	a1
2		e
2		e
1	$D_{2d}$	b2
3		e
3		e

\* Scaled with scaling factor b3lyp/6-31g(d)=0.9614.

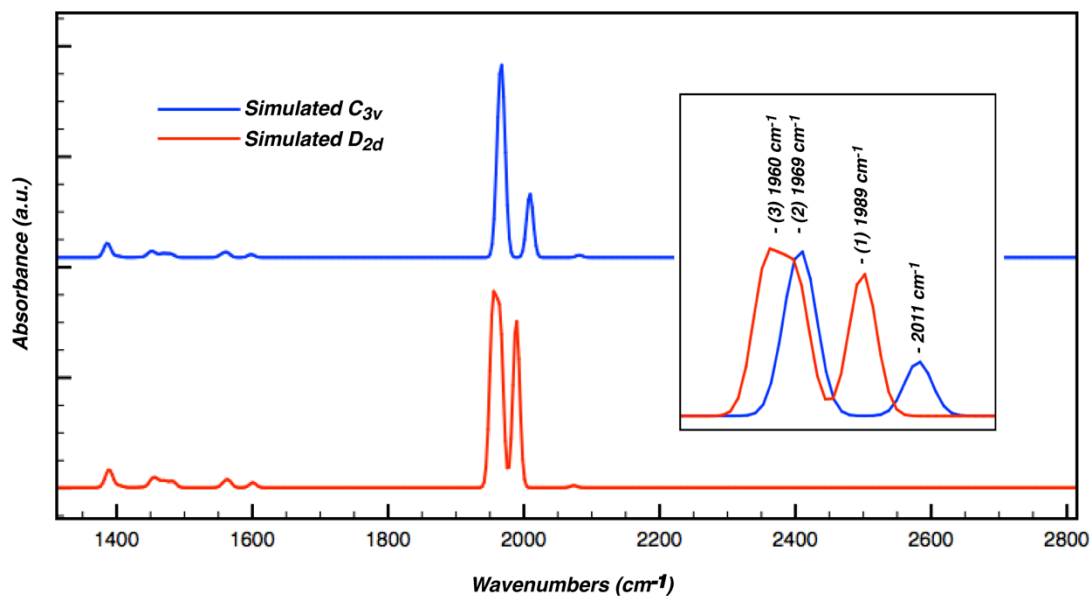


**Figure 3.8.** DFT simulated IR spectrum of both  $\text{Co}(\text{CNAr}^{\text{Mes}_2})_4$   $C_{3v}$  and  $D_{2d}$  Isomers.

**Table 3.3.** Calculated Energy Differences Between  $\text{Co(L)}_4$  ( $\text{L} = \text{CNAr}^{\text{Ar}2}, \text{CNAr}^{\text{Mes}2}$ )  $\text{C}_{3v}$  and  $\text{D}_{2d}$  Isomers Using Different Functional with 6-31g(d):lanl2dz basis sets. \*All  $\text{C}_{3v}$  in lower energy.

Functional	$\Delta E$ (kcal/mol)*	$\Delta E$ (kcal/mol)*
	$\text{Co}(\text{CNAr}^{\text{Ar}2})_4$	$\text{Co}(\text{CNAr}^{\text{Mes}2})_4$
<b>B3LYP</b>	<b>6.91</b>	<b>8.88</b>
<b>O3LYP</b>	<b>6.08</b>	-
<b>B3P86</b>	<b>6.71</b>	-
<b>WB97X</b>	<b>7.43</b>	<b>10.03</b>
<b>WB97XD</b>	<b>6.18</b>	<b>9.20</b>
<b>B3PW91</b>	-	<b>8.80</b>
<b>B3PW91-D3</b>	-	<b>6.92</b>
<b>BP86</b>	<b>3.09</b>	<b>4.48</b>
<b>BP86-D3</b>	-	<b>2.67</b>
<b>OLYP</b>	<b>4</b>	-

**Table 3.4.** Calculated Energy Differences Between CoL<sub>4</sub> (L= CO, CNMe, CNXyl, CNAr<sup>Ar2</sup>, CNAr<sup>Mes2</sup>) C<sub>3v</sub> and D<sub>2d</sub> Isomers Using 6-31g(d):lanl2dz basis sets. \*All C<sub>3v</sub> in lower energy

Ligand (L)	ΔE (kcal/mol)*	ΔE (kcal/mol)*	ΔE (kcal/mol)
	b3lyp	b3lyp/PCM(C <sub>6</sub> H <sub>6</sub> )	bp86
CO	3.53	-	1.29
CNMe	3.73	-	1.34
CNXyl	3.45	-	0.34
CNAr <sup>Ar2</sup>	6.91	7.07	2.80
CNAr <sup>Mes2</sup>	8.88	8.97	4.48

**Optimized Coordinates of CoL<sub>4</sub> (L= CO, CNMe, CNXyl, CNAr<sup>Ar2</sup>, CNAr<sup>Mes2</sup>) C<sub>3v</sub> and D<sub>2d</sub> Isomers.**

**Co(CO)<sub>4</sub> in C<sub>3v</sub> symmetry**

Co 0.21738600 -0.06340600 0.00000000  
 C 1.01933100 1.59513400 0.00000000  
 C -1.57028400 0.46813600 0.00000000  
 C 0.24051400 -1.02107200 1.57344600  
 C 0.24051400 -1.02107200 -1.57344600  
 O -2.66796000 0.79511200 0.00000000  
 O 0.24051400 -1.61569300 2.55481000  
 O 0.24051400 -1.61569300 -2.55481000  
 O 1.50569700 2.63442800 0.00000000

**Co(CNMe)<sub>4</sub> in C<sub>3v</sub> symmetry**

Co 0.01692500 0.06506900 -0.31620600  
 N -1.30292100 2.75853000 -0.83590200  
 C -0.78707200 1.71165100 -0.62728900  
 C 0.02674800 0.04827500 1.57584200  
 N 0.04613400 0.04388600 2.75666700  
 N -1.72238600 -2.36847900 -0.88588100  
 C -1.04944700 -1.42061800 -0.65893700  
 C 1.82415300 -0.08997500 -0.64943400  
 N 2.99514400 -0.16165300 -0.86598700  
 C 0.08479800 0.04717800 4.16824300  
 H 0.34598100 -0.94780200 4.54736300

**Co(CO)<sub>4</sub> in D<sub>2d</sub> symmetry**

Co -0.00023100 0.00015500 0.22649500  
 C 1.44537300 -1.10234000 0.52342900  
 C 0.23248900 1.80390200 0.52003800  
 C -1.67861400 -0.69930100 0.52205500  
 C 0.00069900 -0.00229800 -1.63830500  
 O 0.37787400 2.92961700 0.68824200  
 O -2.72621600 -1.13569300 0.69160100  
 O 0.00136200 -0.00417700 -2.78367500  
 O 2.34779900 -1.79024100 0.69400000

**Co(CNMe)<sub>4</sub> in D<sub>2d</sub> symmetry**

Co 0.02759200 -0.03582000 0.34158400  
 N -2.08956000 -1.74786600 1.69271000  
 C -1.23743200 -1.08986700 1.19906900  
 C 0.26500100 0.12720400 -1.49190400  
 N 0.40096200 0.16344500 -2.66794800  
 N -0.96454500 2.66187100 1.33335900  
 C -0.59864100 1.61714300 0.91244900  
 C 1.67405000 -0.81250400 0.71122700  
 N 2.75125300 -1.24675000 0.94279200  
 C 0.53624900 0.16910300 -4.07223100  
 H 0.80155500 1.17145700 -4.42998700

H 0.83218400 0.76321000 4.52964100  
H -0.89216800 0.32886900 4.57816400  
C -1.62274600 4.11445000 -1.07819800  
H -0.71631500 4.73285300 -1.10566700  
H -2.14348100 4.21640200 -2.03711200  
H -2.28214800 4.49644600 -0.29046500  
C -2.67706100 -3.37767900 -1.13964100  
H -2.62597200 -4.15362600 -0.36701300  
H -3.69319300 -2.96287300 -1.14974100  
H -2.48457800 -3.84886400 -2.11041400  
C 4.21509000 -0.85680500 -1.09066800  
H 4.95229700 -0.58109800 -0.32827800  
H 4.06659500 -1.94438900 -1.05942600  
H 4.62784900 -0.58694800 -2.06911300

**Co(CNXyl)<sub>4</sub> in C<sub>3v</sub> symmetry**

Co 0.02973700 -0.01716100 -0.25806800  
N -0.97262600 2.81614600 -0.74079800  
C -0.58556900 1.70754600 -0.56013900  
C 0.02017600 -0.02382200 1.62710600  
N -0.01169600 -0.00510900 2.81194900  
N -1.87680400 -2.31907100 -0.83506000  
C -1.13964500 -1.41623400 -0.60530900  
C 1.82309300 -0.33738500 -0.62574700  
N 2.95962600 -0.54352700 -0.90385500  
C 4.26747300 -0.76979600 -1.26760000  
C 4.66423200 -0.49597300 -2.59578900  
C 5.17150200 -1.27028200 -0.30488900  
C 5.99595500 -0.73658800 -2.94132800  
C 6.49246600 -1.49077200 -0.70131600  
C 6.90763200 -1.22871500 -2.00707600  
H 6.31901300 -0.53207200 -3.95904500  
H 7.20168000 -1.87593400 0.02711500  
H 7.93944600 -1.40786500 -2.29625400  
C -2.72061700 -3.37149600 -1.10589500  
C -3.15492100 -3.57575000 -2.43460500  
C -3.12493800 -4.21564600 -0.04791900  
C -4.00876500 -4.65270400 -2.68353400  
C -3.98131100 -5.27666900 -0.35045600  
C -4.42263900 -5.49946400 -1.65496300  
H -4.35246600 -4.82555000 -3.70035300

H 1.32111100 -0.52883500 -4.38814800  
H -0.40423400 -0.12930500 -4.55135900  
C -3.12432300 -2.53258700 2.24399200  
H -3.00480100 -2.61813600 3.33097900  
H -4.10301400 -2.08160100 2.03942400  
H -3.11276900 -3.54236600 1.81615100  
C -1.37224900 3.90498200 1.86146500  
H -0.83369300 4.72701900 1.37466400  
H -2.44712400 4.05601700 1.70362100  
H -1.17273000 3.95108700 2.93904300  
C 4.04758000 -1.72437400 1.22888500  
H 4.19968400 -2.71481200 0.78276400  
H 4.80825000 -1.04450600 0.82600200  
H 4.19758800 -1.80823000 2.31203300

**Co(CNXyl)<sub>4</sub> in D<sub>2d</sub> symmetry**

Co 11.15792900 14.05244000 6.27156300  
N 8.85699700 14.73960900 8.12003600  
N 13.53790900 13.40995300 8.04325000  
N 10.82876000 16.36911700 4.33695700  
N 11.18296700 11.55325700 4.55702900  
C 7.86729400 14.64889100 10.30735100  
C 10.94038400 15.44075000 5.07020300  
C 6.75586000 14.89889000 11.11551100  
H 6.80882900 14.65257900 12.17306000  
C 7.77464500 14.97629200 8.93614800  
C 11.02793100 17.31460800 2.13677700  
C 14.65646900 13.14836100 8.80111000  
C 6.60404500 15.53679500 8.37844700  
C 15.65457500 12.29626400 8.27842200  
C 12.58375700 13.64647400 7.37571000  
C 9.78939500 14.50380600 7.42129500  
C 5.59009700 15.45381200 10.58691700  
H 4.73602100 15.64021900 11.23212400  
C 14.77159100 13.74148500 10.07803200  
C 10.71523900 17.46088700 3.50648400  
C 5.52051700 15.76730500 9.22934900  
H 4.61092400 16.19715400 8.81736300  
C 11.20497700 12.55381100 5.19855800  
C 11.13601000 10.37559100 3.84638300  
C 11.32228200 9.15381600 4.53079400

H -4.30274500	-5.93655100	0.45153900	C 10.29077300	18.69396100	4.04967600
H -5.08770300	-6.33131200	-1.86958800	C 10.90198000	18.43647800	1.31431800
C -1.41289200	4.10659300	-0.92374900	H 11.13834900	18.34275100	0.25736300
C -1.51408300	4.61676500	-2.23707500	C 10.90190000	10.42475200	2.45429200
C -1.74869200	4.88186500	0.20864400	C 15.91517100	13.45914900	10.82861300
C -1.96137400	5.93061000	-2.39377800	H 16.02152600	13.90662400	11.81364200
C -2.19023500	6.18975900	-0.00350900	C 10.18114700	19.78544800	3.18490000
C -2.29774000	6.71609200	-1.29102900	H 9.85622400	20.74254800	3.58514500
H -2.04515000	6.33998400	-3.39746000	C 10.48177000	19.66352700	1.82812300
H -2.45226300	6.80092600	0.85660600	H 10.39006800	20.52459100	1.17187900
H -2.64319500	7.73605900	-1.43475000	C 16.77840200	12.04538100	9.06907300
C -0.09941900	0.03377600	4.18797800	H 17.55709500	11.39206500	8.68361100
C -1.37619600	0.06052600	4.78994500	C 11.04226300	7.99803700	2.40971800
C 1.08918800	0.04845000	4.94861000	H 11.00550000	7.06857500	1.84825700
C -1.43808800	0.10214400	6.18509700	C 11.27033100	7.97332200	3.78580100
C 0.97308700	0.08993400	6.34017400	H 11.41024800	7.02353400	4.29593900
C -0.27710400	0.11642300	6.95817800	C 16.91268900	12.61858700	10.33384600
H -2.41196900	0.12405500	6.66757200	H 17.79487400	12.41130300	10.93325300
H 1.87751700	0.10210500	6.94309400	C 10.86000800	9.21640100	1.75503600
H -0.34669600	0.14878500	8.04194900	H 10.68085000	9.23526100	0.68292900
C -2.62250100	0.04463600	3.94243900	C 9.97380400	18.81246600	5.51815300
H -2.64402500	0.88953200	3.24345900	H 9.16737100	18.12849900	5.81054800
H -2.68004500	-0.86483100	3.33151500	H 10.84086000	18.55275200	6.13774400
H -3.51913300	0.09326700	4.56721500	H 9.66539600	19.83151600	5.76965300
C 2.43292200	0.02133900	4.26641100	C 11.48391800	15.98356700	1.59652000
H 2.55027400	-0.87850000	3.65041400	H 12.39569400	15.63960400	2.10013300
H 2.55778000	0.87957000	3.59470500	H 10.72661900	15.20614600	1.75568500
H 3.24341200	0.04101300	5.00093900	H 11.68821800	16.04783300	0.52362000
C 4.70896000	-1.55321300	1.10136600	C 6.54083100	15.86582900	6.90918900
H 4.33300400	-0.64545700	1.58942000	H 7.30295200	16.60456100	6.63107500
H 3.88669000	-2.27928200	1.11309100	H 6.72735600	14.97904700	6.29133600
H 5.52747700	-1.95256000	1.70766900	H 5.56029700	16.27072500	6.64182300
C 3.67083800	0.03734000	-3.59607700	C 9.13217700	14.04726600	10.86385100
H 2.83771800	-0.66083000	-3.74555900	H 9.38662300	13.10956700	10.35470000
H 3.22985200	0.98276800	-3.25730800	H 9.98849600	14.71937600	10.72685100
H 4.14889700	0.21001900	-4.56489200	H 9.02751400	13.84010900	11.93299900
C -2.63760100	-3.96685900	1.35645200	C 13.68644700	14.64939800	10.59731700
H -1.54255700	-3.99624400	1.41227100	H 13.52689400	15.50429200	9.92891700
H -2.94220800	-2.97586300	1.71628600	H 12.72563800	14.12455100	10.66742100
H -3.03604800	-4.71711900	2.04586400	H 13.94056800	15.03227600	11.59012600

C -2.70142500 -2.65270200 -3.53659700  
 H -2.98824500 -1.61383000 -3.33217500  
 H -1.60944600 -2.66079800 -3.64286100  
 H -3.13948100 -2.94628400 -4.49514400  
 C -1.62831700 4.30090900 1.59421700  
 H -2.26211400 3.41295400 1.71193500  
 H -0.60092400 3.98171300 1.80807500  
 H -1.92346000 5.03369100 2.35104700  
 C -1.14659900 3.75868000 -3.42060300  
 H -0.10210600 3.42751800 -3.36689800  
 H -1.76108200 2.85089800 -3.46422900  
 H -1.28278100 4.30819000 -4.35679600

**Co(CNAr<sup>Ar2</sup>)<sub>4</sub> in C<sub>3v</sub> symmetry**

Co -0.01022300 0.06560800 -0.33919400  
 N -1.36618100 2.72033700 -0.95408500  
 C -0.83848400 1.68151900 -0.71808800  
 C -0.02716800 0.19342100 1.54291900  
 N -0.08494900 0.32357700 2.71833000  
 N -1.51839900 -2.54726400 -0.71337000  
 C -0.97146900 -1.50332400 -0.56237500  
 C 1.79876300 -0.13288300 -0.68672100  
 N 2.95600100 -0.29550800 -0.90658500  
 C 4.29314800 -0.56252200 -1.09216400  
 C 5.11804800 0.40206000 -1.72545000  
 C 4.82789400 -1.79861500 -0.64534100  
 C 6.47869200 0.10759700 -1.88862800  
 C 6.19951000 -2.02912200 -0.81288700  
 C 7.02167400 -1.08935900 -1.42960400  
 H 7.11624600 0.84866000 -2.36147000  
 H 6.61049200 -2.97640900 -0.47644700  
 H 8.08143800 -1.29156800 -1.55697500  
 C -2.11040800 -3.77136700 -0.89675300  
 C -2.30337900 -4.26468900 -2.21629800  
 C -2.56431100 -4.50692800 0.23191000  
 C -2.98823200 -5.47706900 -2.37561500  
 C -3.24254100 -5.71210800 0.00535600  
 C -3.46427500 -6.19414200 -1.28168500  
 H -3.11976700 -5.86910800 -3.37968000  
 H -3.57436200 -6.28733300 0.86452800  
 H -3.98135900 -7.13780300 -1.43026600

C 15.49786200 11.68754100 6.90880700  
 H 14.59827100 11.06222400 6.84884800  
 H 15.39160500 12.45949900 6.13696000  
 H 16.36248300 11.06655800 6.65651900  
 C 10.70464200 11.74869200 1.76157400  
 H 9.84571100 12.29141500 2.17547300  
 H 11.57759000 12.40048200 1.88911800  
 H 10.53640900 11.60695900 0.68984900  
 C 11.56507800 9.14132500 6.01804300  
 H 12.47922200 9.68906100 6.27953700  
 H 10.74599400 9.62682800 6.56237800  
 H 11.66418400 8.11667800 6.38840700

**Co(CNAr<sup>Ar2</sup>)<sub>4</sub> in D<sub>2d</sub> symmetry**

Co 11.12936500 14.05376800 6.13058600  
 N 9.06634800 14.37751800 8.31534800  
 N 13.69252000 13.15272300 7.46879700  
 N 10.71689300 16.71279900 4.72384300  
 N 10.86235100 11.80479400 4.11423700  
 C 8.18749300 14.23221800 10.55707000  
 C 10.81024800 15.62712400 5.19701600  
 C 7.07203800 14.31317800 11.40226700  
 H 7.21929200 14.17923300 12.46969000  
 C 7.98229900 14.38065800 9.15972800  
 C 11.38815200 18.35594800 3.08302500  
 C 14.87144200 12.98771800 8.15690800  
 C 6.67873600 14.57303800 8.62632800  
 C 15.60058500 11.77623500 8.03304300  
 C 12.65889400 13.46134000 6.96802000  
 C 9.92543400 14.32848800 7.49605500  
 C 5.79217500 14.52427400 10.89728100  
 H 4.94072300 14.56927600 11.57051100  
 C 15.31481200 14.02324400 9.02251200  
 C 10.67161600 18.00766400 4.25966800  
 C 5.60367300 14.64396400 9.52309600  
 H 4.60238200 14.76893900 9.12194200  
 C 11.00026100 12.74408500 4.83239800  
 C 10.74036600 10.55252600 3.55183000  
 C 10.50815100 9.43598700 4.39797300  
 C 9.88379700 18.97019500 4.94704000  
 C 11.24767200 19.65907200 2.58486200

C -1.95445100	3.92906000	-1.23287600	H 11.81025800	19.93882300	1.69948900
C -2.83288600	4.03916200	-2.34432100	C 10.90388300	10.38382500	2.15271200
C -1.71816700	5.03717300	-0.37515600	C 16.45672100	13.79705900	9.79983700
C -3.46560400	5.26862100	-2.56838400	H 16.80141400	14.59029300	10.45681200
C -2.38494800	6.23959200	-0.64807300	C 9.78119300	20.25527200	4.39647900
C -3.25071100	6.36091100	-1.73140700	H 9.19528500	20.99977700	4.92676500
H -4.12301600	5.36266500	-3.42764100	C 10.44220700	20.59855300	3.22095200
H -2.19237300	7.09579500	-0.00846000	H 10.35790900	21.60518100	2.82121800
H -3.74353400	7.30788300	-1.93231300	C 16.74344700	11.61168400	8.82951900
C -0.25038900	0.44089400	4.08050600	H 17.32010200	10.69764600	8.72546600
C -1.54919000	0.66505300	4.60535500	C 10.70943400	7.97188800	2.46377400
C 0.86911900	0.27625100	4.93536700	H 10.69455200	6.97189600	2.03949100
C -1.70414300	0.67982400	5.99791300	C 10.51318200	8.15638400	3.83057900
C 0.65309300	0.30349000	6.32033200	H 10.33321500	7.30310400	4.47804000
C -0.61951800	0.49424100	6.85157100	C 17.16403400	12.59976900	9.71483400
H -2.69384300	0.86288900	6.40569000	H 18.05670500	12.44928600	10.31532600
H 1.50799000	0.19578300	6.98127900	C 10.88588900	9.07838800	1.63879100
H -0.76197000	0.52193800	7.92827600	H 10.98882500	8.94281700	0.56649900
C 4.60316500	1.70640200	-2.22599900	C 15.21285700	10.68464100	7.09915100
C 4.90147100	2.10934600	-3.53855700	C 15.27273600	9.34602300	7.52480300
C 3.88019500	2.58639800	-1.40462100	C 14.85491200	10.94179900	5.76445900
C 4.48961800	3.35288500	-4.01793100	C 14.99648100	8.29899900	6.64556500
H 5.44872900	1.43298800	-4.18977500	H 15.52720300	9.12746200	8.55836600
C 3.47953200	3.83489700	-1.88049500	C 14.57521100	9.89549300	4.88625200
H 3.64216700	2.29597500	-0.38627300	H 14.80977200	11.96476800	5.40661700
C 3.77966900	4.22221000	-3.18841900	C 14.64889100	8.56978500	5.32039100
H 4.72344700	3.64084400	-5.03952500	H 15.05137100	7.27198800	6.99781400
H 2.93842400	4.51158000	-1.22492700	H 14.30280100	10.11781100	3.85831600
H 3.46245000	5.19406000	-3.55674300	H 14.43337500	7.75688700	4.63212600
C 3.99063500	-2.86469200	-0.02940700	C 14.62119600	15.33735400	9.12018100
C 4.35998900	-3.42108600	1.20550700	C 14.22074700	15.83487600	10.36999600
C 2.87061300	-3.38943300	-0.69322900	C 14.41452500	16.13494200	7.98322600
C 3.62916500	-4.47013200	1.76346900	C 13.62346600	17.09092300	10.48096000
H 5.21388000	-3.01203500	1.73785000	H 14.35790000	15.22089200	11.25529900
C 2.14596000	-4.44497200	-0.14064700	C 13.82741200	17.39474700	8.09521600
H 2.57753900	-2.97803600	-1.65403500	H 14.72673500	15.77078100	7.00923200
C 2.52156400	-4.98865500	1.09049600	C 13.42732400	17.87684500	9.34416600
H 3.92500900	-4.88089300	2.72520100	H 13.30811600	17.45211500	11.45618300
H 1.28854800	-4.84667900	-0.67417100	H 13.68749900	18.00341800	7.20568900
H 1.95281600	-5.80806500	1.52138700	H 12.96616500	18.85719300	9.42878900

C	2.25225100	0.07281700	4.42524300	C	9.52753500	13.99464600	11.16011700
C	3.05991000	-0.93731400	4.97436400	C	10.40119000	13.01204900	10.66395700
C	2.80762600	0.91301600	3.44539400	C	9.91404400	14.71380800	12.30461500
C	4.38194500	-1.10246300	4.56100100	C	11.61469300	12.75253400	11.29979000
H	2.64089700	-1.60422700	5.72315800	H	10.12641300	12.43485200	9.78778700
C	4.12972000	0.74868100	3.03447200	C	11.12839800	14.45427600	12.93960700
H	2.20522100	1.70803700	3.01810700	H	9.25894200	15.48968500	12.69192800
C	4.92298000	-0.25781000	3.59032300	C	11.98223100	13.46859800	12.44126000
H	4.98774300	-1.89214800	4.99802900	H	12.27154400	11.98424300	10.90124100
H	4.54548800	1.41328200	2.28159100	H	11.40609400	15.02328400	13.82329400
H	5.95385100	-0.38051000	3.26893400	H	12.92583300	13.25862400	12.93835800
C	-2.74356000	0.87356900	3.74250500	C	6.40396800	14.70029900	7.16897800
C	-3.91138900	0.12862300	3.97450700	C	5.54534400	15.71228600	6.70722100
C	-2.75710700	1.84618700	2.73000300	C	6.92819900	13.79478700	6.23211700
C	-5.05949600	0.34570800	3.21309300	C	5.22091100	15.81680700	5.35510600
H	-3.90620600	-0.64352600	4.73832100	H	5.15069400	16.43640800	7.41379900
C	-3.90699000	2.06525700	1.97224200	C	6.60298200	13.89879300	4.88035600
H	-1.87117900	2.44375200	2.54275400	H	7.59240900	13.00324600	6.56029800
C	-5.06130900	1.31615800	2.20966700	C	5.74772000	14.90854000	4.43527900
H	-5.94982400	-0.24925600	3.39959300	H	4.56153200	16.61332000	5.02005400
H	-3.89791900	2.82332800	1.19420700	H	7.02141600	13.18664500	4.17401800
H	-5.95427900	1.48492000	1.61365900	H	5.49729500	14.98910500	3.38083200
C	-3.12985900	2.89348200	-3.24549100	C	9.18749300	18.69525600	6.23331900
C	-4.46507900	2.58097900	-3.55208000	C	7.86338500	19.12839300	6.41810100
C	-2.11179800	2.12278700	-3.83016800	C	9.85102200	18.09726300	7.31768500
C	-4.77455700	1.52313400	-4.40679800	C	7.22472800	18.97538000	7.64835100
H	-5.26445700	3.15879600	-3.09577400	H	7.32916900	19.57696800	5.58491100
C	-2.42127900	1.06397400	-4.68234300	C	9.21256900	17.94634000	8.54818900
H	-1.07269400	2.35434600	-3.61981300	H	10.87631000	17.76054600	7.20874200
C	-3.75281400	0.75836600	-4.97156500	C	7.89827100	18.38557800	8.71981400
H	-5.81461000	1.29084900	-4.62108700	H	6.19954500	19.31673400	7.76828100
H	-1.62179100	0.46828800	-5.11286800	H	9.74842100	17.48366500	9.37212900
H	-3.98872100	-0.07666800	-5.62523900	H	7.40184000	18.26412100	9.67878800
C	-0.80879900	4.96872600	0.80089800	C	12.29717800	17.41842600	2.37013700
C	-1.22371700	5.49644800	2.03657700	C	12.27983100	17.36047700	0.96559000
C	0.48834500	4.43665900	0.70736000	C	13.24798100	16.64316300	3.05511200
C	-0.37164200	5.49627800	3.14129800	C	13.18380100	16.55971000	0.26907500
H	-2.23047900	5.89362900	2.13337600	H	11.54175700	17.94105900	0.41867300
C	1.34223600	4.44427800	1.81027100	C	14.14894700	15.83956700	2.35767900
H	0.83254300	4.02196500	-0.23349500	H	13.29388800	16.67876000	4.13805900



C 0.91754500 4.97223100 3.03201500  
 H -0.71865600 5.90087400 4.08834900  
 H 2.34699100 4.04123800 1.71166800  
 H 1.58408900 4.97260600 3.89012200  
 C -2.34630600 -4.06126700 1.63500400  
 C -3.40329600 -4.12127100 2.55941500  
 C -1.08303500 -3.65023300 2.09287500  
 C -3.20425200 -3.78778100 3.89897400  
 H -4.39148100 -4.41868700 2.21892400  
 C -0.88482400 -3.31740800 3.43236700  
 H -0.24526200 -3.60530300 1.40567600  
 C -1.94268100 -3.38522800 4.34157300  
 H -4.03749300 -3.83999100 4.59537000  
 H 0.10211600 -3.00635800 3.76330500  
 H -1.78497100 -3.12111600 5.38386000  
 C -1.80966100 -3.56076100 -3.43138200  
 C -2.64772300 -3.43093800 -4.55253000  
 C -0.49169000 -3.08358000 -3.53027000  
 C -2.18289400 -2.85620600 -5.73533600  
 H -3.67629100 -3.77500800 -4.48867800  
 C -0.02640700 -2.50760700 -4.71203600  
 H 0.17785400 -3.17578300 -2.68182900  
 C -0.86775400 -2.39427800 -5.82141000  
 H -2.84895000 -2.77094500 -6.59028900  
 H 0.99987600 -2.15427900 -4.76774500  
 H -0.50081800 -1.95296700 -6.74440500

**Co(CNAr<sup>Mes2</sup>)<sub>4</sub> in C<sub>3v</sub> symmetry**

Co -0.07460500 -0.06505900 0.00825300  
 N -1.33290500 2.69069300 -0.54354700  
 C -0.93527300 1.60729400 -0.24350800  
 C -0.18137300 -0.05738400 1.95777800  
 N -0.36912400 0.03261200 3.12650200  
 N -1.69881200 -2.58114400 -0.68275300  
 C -1.14482000 -1.56873300 -0.38638700  
 C 1.72844900 -0.13150900 -0.44908300  
 N 2.82988400 -0.15761900 -0.90967200  
 C 4.06914300 -0.36882600 -1.48073100  
 C 4.52916200 0.48855900 -2.51533400  
 C 4.87866800 -1.44682200 -1.03231100  
 C 5.77527700 0.22451400 -3.09862300

C 14.12250200 15.79445500 0.96285800  
 H 13.15117800 16.53093100 -0.81692800  
 H 14.87759200 15.25115200 2.90882400  
 H 14.82364400 15.16499100 0.42198100  
 C 11.08417200 11.52052400 1.21119300  
 C 12.03675300 11.43147300 0.18134500  
 C 10.26899400 12.66370100 1.26683800  
 C 12.16230300 12.44328900 -0.76960500  
 H 12.69110100 10.56512000 0.13472200  
 C 10.39533600 13.67538500 0.31651800  
 H 9.52184500 12.75364200 2.04826900  
 C 11.33795400 13.56759400 -0.70778600  
 H 12.90701700 12.35326000 -1.55634700  
 H 9.75380400 14.55006300 0.37693400  
 H 11.43242300 14.35733500 -1.44764000  
 C 10.24047600 9.56871900 5.85798600  
 C 11.05240000 8.90384100 6.78947100  
 C 9.12642300 10.28300600 6.32588300  
 C 10.75958200 8.95328100 8.15294000  
 H 11.92877700 8.36495500 6.44240200  
 C 8.82771100 10.32372800 7.68752500  
 H 8.48157900 10.79206300 5.61534000  
 C 9.64360700 9.65864500 8.60658200  
 H 11.40561700 8.43901700 8.85967900  
 H 7.95212800 10.86837800 8.03102400  
 H 9.40906100 9.68995400 9.66731000

**Co(CNAr<sup>Mes2</sup>)<sub>4</sub> in D<sub>2d</sub> symmetry**

Co 11.18333700 14.04224000 6.22217000  
 N 9.27551600 14.32818200 8.59852000  
 N 13.95247100 13.15652800 7.20176000  
 N 10.67763400 16.75905400 4.89284800  
 N 10.65293400 11.75909400 4.22130800  
 C 8.21970400 13.69445100 10.69488600  
 C 10.76131400 15.65336000 5.32440100  
 C 7.07878100 13.20634000 11.34826100  
 H 7.15535700 12.97116300 12.40628200  
 C 8.13178800 13.99863400 9.31263000  
 C 11.66279700 18.21063700 3.23587000  
 C 15.27231800 13.05389800 7.60338700  
 C 6.87416100 13.94484500 8.65044900

C	6.12324300	-1.64934400	-1.64125100	C	16.08555600	11.99340000	7.12787700
C	6.57427400	-0.83267600	-2.67379000	C	12.83213100	13.42285400	6.89275900
H	6.11323300	0.87458200	-3.90100600	C	10.11862100	14.31898500	7.75154900
H	6.74134000	-2.46807800	-1.28362300	C	5.86782900	13.04383400	10.68315000
H	7.54027000	-1.01334900	-3.13699000	H	4.99967200	12.65219600	11.20597500
C	-2.11533900	-3.84007700	-1.06945300	C	15.81144800	14.02595300	8.48834800
C	-2.23494300	-4.15143700	-2.45072500	C	10.79889500	18.02284500	4.34539500
C	-2.40368500	-4.82830500	-0.09125000	C	5.77258800	13.43950200	9.35213900
C	-2.65000700	-5.43836300	-2.81703400	H	4.82150900	13.37530800	8.83055300
C	-2.81556600	-6.09719400	-0.52186700	C	10.89392700	12.70771700	4.90406700
C	-2.94598300	-6.41222300	-1.86957800	C	10.53612000	10.52041000	3.61052800
H	-2.72162100	-5.66926500	-3.87625000	C	10.23396800	9.36506300	4.38797000
H	-3.01522500	-6.85095800	0.23444200	C	10.09599100	19.12299000	4.89897200
H	-3.25632900	-7.40676300	-2.17726200	C	11.75414100	19.48193900	2.65823700
C	-1.47028100	3.94021400	-1.12940600	H	12.41833200	19.61355800	1.80852600
C	-2.31716400	4.07541200	-2.26006500	C	10.72099200	10.39902000	2.20656300
C	-0.76022900	5.06413200	-0.63002500	C	17.14894700	13.90418000	8.88482500
C	-2.29964700	5.28032100	-2.97275100	H	17.54742800	14.64257100	9.57469300
C	-0.78071600	6.24492000	-1.38664500	C	10.23550300	20.37631100	4.28398800
C	-1.50959600	6.35262200	-2.56735900	H	9.71134700	21.22049400	4.72240800
H	-2.93329400	5.36739200	-3.85117100	C	11.03935500	20.56329000	3.16518700
H	-0.21057700	7.09385000	-1.01986500	H	11.13023600	21.54619100	2.71119600
H	-1.49567200	7.27567900	-3.14032000	C	17.41967600	11.92920200	7.55237100
C	-0.79383900	0.28743200	4.42299900	H	18.03841300	11.12080300	7.17314700
C	-2.15668200	0.61648100	4.65655200	C	10.59872400	7.96864600	2.41845500
C	0.12434100	0.23329700	5.49934900	H	10.64545400	6.98369600	1.96225300
C	-2.55559800	0.92853300	5.96135600	C	10.31143300	8.10894900	3.77219300
C	-0.33576100	0.54961800	6.78622500	H	10.11029300	7.23149500	4.38029800
C	-1.65874500	0.90501700	7.02513300	C	17.95687800	12.86859000	8.42616500
H	-3.59525200	1.19588000	6.12833200	H	18.99290100	12.79525200	8.74497200
H	0.37694000	0.51721700	7.60560600	C	10.75657400	9.11330700	1.64604800
H	-1.98776500	1.15777400	8.02929800	H	10.88987700	9.02701500	0.57187700
C	3.77729400	1.67765200	-3.03129700	C	15.63767200	10.92841200	6.17518800
C	2.72367200	1.51743900	-3.95479800	C	15.46707100	9.60783200	6.64165000
C	4.22740100	2.97381200	-2.70062600	C	15.55724100	11.20115200	4.79303300
C	2.13957600	2.65232200	-4.52638700	C	15.21640000	8.58523000	5.71962600
C	3.61328200	4.08160400	-3.29551600	C	15.31834400	10.14586300	3.90730600
C	2.56584900	3.94532000	-4.20983000	C	15.13991000	8.83052200	4.34692600
H	1.33816400	2.51912800	-5.25014300	H	15.08178700	7.56951700	6.08696800
H	3.96501000	5.07814400	-3.03469000	H	15.29238500	10.35654900	2.84071100

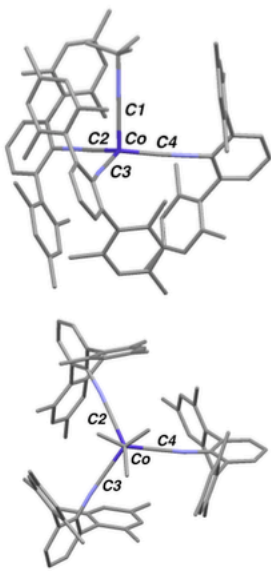
C	4.49470500	-2.37352300	0.07664700	C	15.03497900	15.17424900	9.04807300
C	4.53942400	-1.92790000	1.41521100	C	14.08754400	14.95203500	10.06917000
C	4.20991000	-3.72574500	-0.20550900	C	15.34885600	16.49100300	8.65159600
C	4.30437400	-2.84349500	2.44398900	C	13.48107100	16.05090000	10.68313900
C	3.98790400	-4.61017400	0.85663100	C	14.71611100	17.56269400	9.29254100
C	4.03816800	-4.19220200	2.18758600	C	13.79107900	17.36507800	10.31956800
H	4.32584600	-2.49166800	3.47188600	H	12.75104800	15.87202300	11.46801800
H	3.76970100	-5.65289900	0.63354200	H	14.96250700	18.57718400	8.98446600
C	1.57568300	-0.13518300	5.40201700	C	9.41513700	13.94347100	11.56679000
C	1.98951400	-1.42156400	5.81064800	C	10.16170500	12.86557500	12.08390300
C	2.53895500	0.85250400	5.11756100	C	9.65246800	15.25133100	12.04615200
C	3.35529500	-1.68355700	5.95833500	C	11.11125800	13.10701800	13.08420100
C	3.89602000	0.54812200	5.27845700	C	10.60822100	15.44707900	13.04851400
C	4.32719100	-0.70845500	5.71065000	C	11.34557100	14.38831800	13.58864400
H	3.66636900	-2.67086300	6.29565100	H	11.67604600	12.26661600	13.48378200
H	4.63306300	1.32415900	5.08054200	H	10.76825800	16.45435200	13.42946400
C	-3.20439600	0.63270000	3.58813000	C	6.61345800	14.47695700	7.27258800
C	-4.14146200	-0.41774300	3.52486800	C	5.96972200	15.72821000	7.15239900
C	-3.32534400	1.73810000	2.72233400	C	6.86088200	13.70432000	6.12284700
C	-5.15707300	-0.36478300	2.56379800	C	5.61577600	16.19315100	5.88199200
C	-4.35681300	1.75153800	1.77987300	C	6.48843800	14.20690800	4.87150300
C	-5.28091300	0.70676700	1.67827300	C	5.87181300	15.45128000	4.72608500
H	-5.87405200	-1.18204900	2.51332100	H	5.11605700	17.15566300	5.79680800
H	-4.44248900	2.60361200	1.10934400	H	6.67308300	13.59814100	3.98900100
C	-3.31734300	3.04210600	-2.68160700	C	9.27076300	19.09394600	6.14838400
C	-4.66643100	3.23961200	-2.31279300	C	7.89077500	19.38534400	6.07836800
C	-2.96934200	1.97100300	-3.52651900	C	9.90254700	18.99266400	7.40746400
C	-5.64109800	2.36616100	-2.80587700	C	7.18016900	19.60970400	7.26189600
C	-3.97637900	1.11970500	-3.99483900	C	9.14940300	19.22031500	8.56456300
C	-5.31892300	1.30245900	-3.65217200	C	7.79142700	19.54608500	8.51660900
H	-6.68138000	2.53184100	-2.53143300	H	6.12215100	19.85737300	7.19829700
H	-3.69827500	0.29905400	-4.65057200	H	9.65017700	19.17055100	9.52971500
C	-0.06848100	5.13780800	0.70007300	C	12.54713600	17.14485900	2.66971700
C	-0.68332100	5.90643500	1.71975900	C	12.17814700	16.48281100	1.48288900
C	1.21631800	4.60272900	0.91017600	C	13.82003500	16.92825800	3.23504100
C	0.00147600	6.12617400	2.91694700	C	13.10053900	15.63410000	0.86514000
C	1.87224600	4.86561900	2.12126500	C	14.71262200	16.06950300	2.58445500
C	1.28990900	5.62777300	3.13425300	C	14.37701800	15.42153000	1.39358200
H	-0.47755200	6.72069700	3.69302800	H	12.81465700	15.12997000	-0.05367800
H	2.87801500	4.47459400	2.26136000	H	15.70306300	15.92158800	3.01081000

C	-2.25457500	-4.66585900	1.39062700	C	10.77356000	11.52845300	1.22096000
C	-3.40737100	-4.70653800	2.20716200	C	11.91220500	11.69280500	0.40111100
C	-0.97480900	-4.69712100	1.98224600	C	9.60385500	12.27007200	0.94001000
C	-3.25738100	-4.82669000	3.59084500	C	11.84781700	12.55194900	-0.69982800
C	-0.87347900	-4.80449200	3.37529000	C	9.58614600	13.12203700	-0.17009100
C	-1.99914600	-4.88779200	4.19755800	C	10.68600300	13.25949000	-1.01990000
H	-4.14919800	-4.88094400	4.21226500	H	12.72813700	12.65908700	-1.33154500
H	0.11725500	-4.85717000	3.82215400	C	9.69877500	9.36332600	5.79186700
C	-1.91219200	-3.22444500	-3.58300800	C	10.53076200	9.47954400	6.92098300
C	-2.96035600	-2.73318000	-4.39189200	C	8.32515000	9.06331000	5.96344000
C	-0.57209800	-3.01255800	-3.96744800	C	9.98031300	9.29654500	8.19682100
C	-2.64900900	-2.05655700	-5.57569100	C	7.81915300	8.89385200	7.25439500
C	-0.30702600	-2.33210600	-5.16206200	C	8.62925700	9.00239900	8.38828100
C	-1.32756200	-1.84909800	-5.98412100	H	10.63854600	9.36453000	9.06065700
H	-3.46215300	-1.70007900	-6.20596200	H	6.76267400	8.66107800	7.37640500
H	0.72812200	-2.20188200	-5.46906100	C	16.36549700	16.77550400	7.56611300
C	0.98250600	-2.50702900	6.11813800	H	16.23336800	16.11720800	6.70135000
H	1.48741200	-3.45200900	6.34388600	H	16.28035000	17.81084300	7.22119100
H	0.35406200	-2.24989800	6.97929100	H	17.39444600	16.63063800	7.91900000
H	0.30678400	-2.67826200	5.27264100	C	13.74750900	13.55309800	10.52916300
C	2.12815000	2.23785200	4.68081500	H	13.15100700	13.57908300	11.44301300
H	2.99785100	2.89788300	4.61218600	H	13.16255500	13.01680700	9.77300300
H	1.64298200	2.22592800	3.69828000	H	14.65075300	12.96204200	10.72164000
H	1.41531200	2.68801600	5.38141700	C	13.16332300	18.53332300	11.04546800
C	5.79713800	-1.01521900	5.88503900	H	13.32316000	19.47419700	10.50843100
H	6.20661800	-1.52774200	5.00384500	H	12.08318000	18.39404700	11.17252100
H	6.38216600	-0.10104000	6.03097400	H	13.59071500	18.65332300	12.05021500
H	5.97009700	-1.66947200	6.74701800	C	15.75400400	12.59947000	4.25338600
C	-4.08925900	-1.58237400	4.48690200	H	14.88693500	13.23731900	4.46352600
H	-4.29383600	-1.26743800	5.51773000	H	16.62990000	13.08558900	4.69766500
H	-4.83237900	-2.33715400	4.21597200	H	15.89119800	12.57980000	3.16816600
H	-3.10860700	-2.06818300	4.48784500	C	15.56005000	9.27079000	8.11500600
C	-2.38685100	2.91547400	2.83254300	H	15.17523200	8.26385500	8.30587200
H	-1.36337300	2.65485500	2.54476000	H	16.59454600	9.30327700	8.47882100
H	-2.71058000	3.72807200	2.17838300	H	14.98966200	9.97601000	8.72923100
H	-2.34616400	3.30303600	3.85743700	C	14.85219300	7.71596700	3.36753500
C	-6.39561500	0.75323700	0.65945000	H	13.78825200	7.69167300	3.09670700
H	-7.11419500	1.55143200	0.89003100	H	15.41975900	7.84254500	2.43843300
H	-6.00847900	0.94958200	-0.34679000	H	15.10644200	6.73734100	3.78871100
H	-6.94984800	-0.19090600	0.63252000	C	8.35152400	12.12790200	1.77451200

C	4.86769800	-0.49064100	1.75254100	H	8.04730400	11.07878800	1.87020400
H	4.06513800	0.18790300	1.44189100	H	8.49895700	12.51771700	2.78779100
H	4.99799900	-0.36544900	2.82996000	H	7.52146800	12.67917500	1.32158700
H	5.78551700	-0.16010900	1.25170500	C	13.19792700	10.94219800	0.67183800
C	4.14741300	-4.24779900	-1.62553100	H	13.17286700	9.91995300	0.27319300
H	3.66760000	-5.23129500	-1.65330100	H	14.04582200	11.45151000	0.20200200
H	3.58275000	-3.57612600	-2.27999000	H	13.39574700	10.86001000	1.74408500
H	5.14526300	-4.35562600	-2.06927600	C	12.00437800	9.75986500	6.78273200
C	3.83135300	-5.16754900	3.32411600	H	12.19216500	10.82508200	6.61306400
H	3.14852600	-4.76179600	4.08011500	H	12.54054500	9.47374400	7.69269200
H	3.41785000	-6.11731700	2.96873500	H	12.44749300	9.21610800	5.94395700
H	4.77745700	-5.39238100	3.83474000	C	7.38414300	8.89877500	4.78760500
C	2.23897400	0.14532400	-4.35921900	H	6.34278900	8.93370400	5.12311200
H	1.55038900	0.21246200	-5.20628800	H	7.52402300	9.68273000	4.03614800
H	3.07105000	-0.50879600	-4.64532600	H	7.53412500	7.94174300	4.27285900
H	1.70403100	-0.34995500	-3.54077200	C	8.04682400	8.81318400	9.76972800
C	5.36256900	3.19206000	-1.72260900	H	7.54549300	9.72591900	10.11766000
H	5.42811500	4.24668700	-1.43654300	H	7.30106600	8.00982600	9.78146500
H	5.23041600	2.59936800	-0.81067200	H	8.82253000	8.56576500	10.50182800
H	6.33210400	2.90296000	-2.14658800	C	9.93908400	11.45236000	11.59567100
C	1.89954300	5.15663600	-4.82034800	H	10.73774300	10.79070100	11.94679300
H	1.01729200	5.45876200	-4.24033000	H	8.98754900	11.04204400	11.95517900
H	2.57994000	6.01470000	-4.85118700	H	9.91115600	11.40279500	10.50219000
H	1.56200600	4.95520800	-5.84330700	C	8.86850800	16.43517800	11.52590500
C	-1.53894900	1.75864000	-3.96445200	H	7.78754600	16.27375700	11.61298700
H	-1.15016800	2.63502100	-4.49766500	H	9.12018500	17.34201500	12.08541100
H	-0.87482200	1.58654300	-3.11076000	H	9.08058700	16.62534900	10.46698100
H	-1.45902000	0.88962600	-4.62357500	C	12.38641100	14.63098900	14.65701200
C	-5.09011600	4.38895300	-1.42270800	H	13.34176200	14.94658600	14.21595000
H	-5.00261100	5.35587100	-1.93335200	H	12.07422600	15.42074300	15.34962400
H	-6.13242300	4.27089700	-1.11013000	H	12.58042600	13.72501200	15.24086000
H	-4.47218000	4.45643700	-0.52033300	C	7.47675400	12.33426900	6.22714600
C	-6.39518800	0.37531000	-4.16860700	H	7.40567500	11.80644400	5.27286400
H	-6.16153000	0.01106800	-5.17523800	H	8.53743500	12.38971100	6.49238700
H	-6.50895100	-0.50536800	-3.52310700	H	6.98229200	11.72293500	6.98899400
H	-7.36834200	0.87679900	-4.20926700	C	5.62302900	16.55561400	8.37024100
C	1.91505700	3.77972900	-0.14190600	H	5.23398200	17.53347400	8.07493800
H	2.99700600	3.78362500	0.02089800	H	4.86529100	16.06467500	8.99287800
H	1.58311400	2.73488300	-0.11614600	H	6.49871600	16.72159700	9.00654700
H	1.72555900	4.15427900	-1.15158400	C	5.49829500	15.97954100	3.36004500

C	-2.05400200	6.52792200	1.54311600	H	6.33637600	16.51769300	2.89650700
H	-2.46026100	6.84142700	2.51001400	H	5.22033300	15.16778400	2.67836100
H	-2.02088300	7.41336100	0.89639500	H	4.65596400	16.67794300	3.41584700
H	-2.76691200	5.83482900	1.08464200	C	14.24433800	17.62746000	4.50620100
C	2.02005700	5.92021500	4.42500400	H	13.67215900	17.26978900	5.37089600
H	1.59917900	5.35056900	5.26343700	H	15.30306400	17.44591000	4.71289100
H	3.08141000	5.66153500	4.35165000	H	14.09214100	18.71136600	4.44495100
H	1.95021400	6.98189100	4.69047400	C	10.81597700	16.70365600	0.86322500
C	0.57828600	-3.53917200	-3.14046800	H	10.70042400	17.72798500	0.48698000
H	1.51921400	-3.46117000	-3.69381600	H	10.65333100	16.01495800	0.03080500
H	0.69221400	-2.97348000	-2.20783100	H	10.01408900	16.54149500	1.59259800
H	0.43263300	-4.58992500	-2.86594000	C	15.36152100	14.50961300	0.69856100
C	-4.41043000	-2.94262100	-4.01247000	H	15.17142900	13.45649700	0.94361100
H	-4.69804200	-3.99970000	-4.04930600	H	15.29576800	14.60416100	-0.39155200
H	-4.61003200	-2.59718400	-2.99154700	H	16.39218200	14.73294400	0.99465600
H	-5.07104000	-2.39468800	-4.69061500	C	11.37817800	18.69388100	7.53593400
C	-1.01669700	-1.11722400	-7.26982000	H	11.97664900	19.29677100	6.84392000
H	-1.74755900	-1.35193700	-8.05196500	H	11.72663500	18.89725000	8.55166400
H	-1.03747200	-0.02826600	-7.12666500	H	11.59470100	17.64091900	7.32274900
H	-0.02200300	-1.37713300	-7.64723100	C	7.16556100	19.47785400	4.75237900
C	0.28419200	-4.66449700	1.14846000	H	6.08225200	19.49941200	4.90734900
H	1.15901900	-4.91538300	1.75308000	H	7.43537400	20.38032400	4.19098400
H	0.23363700	-5.37050700	0.31164700	H	7.39802900	18.62269900	4.10875300
H	0.46001600	-3.66844300	0.72617200	C	7.01071900	19.81252900	9.78297900
C	-4.79987900	-4.63393900	1.61605200	H	6.67174800	18.87863800	10.25049100
H	-4.89435900	-3.79390500	0.91871900	H	7.62042000	20.34181500	10.52404400
H	-5.06428000	-5.53968500	1.05758100	H	6.11998000	20.41825300	9.58412200
H	-5.54645500	-4.50325900	2.40622000	C	10.61375100	14.11599400	-2.26367900
C	-1.87062700	-5.02728200	5.69722300	H	11.54925700	14.66042900	-2.43660900
H	-0.89127000	-5.42769300	5.97959900	H	10.43002400	13.50225000	-3.15592100
H	-1.98559800	-4.05888800	6.20235800	H	9.80315200	14.84960100	-2.20115400
H	-2.63896400	-5.69503000	6.10366900	H	8.67383000	13.67328200	-0.38944600

**Table 3.5.** Calculated Core bond angles of  $(^t\text{BuNC})\text{Co}(\text{CNAr}^{\text{Mes}_2})_3$ .

Converged Coordinates*	Angle	Bond angle (°)
	<b>C1-Co-C2</b>	<b>98</b>
	<b>C1-Co-C3</b>	<b>98</b>
	<b>C1-Co-C4</b>	<b>98</b>
	<b>C2-Co-C3</b>	<b>118</b>
	<b>C3-Co-C4</b>	<b>118</b>
	<b>C4-Co-C1</b>	<b>118</b>

\*H-atoms omitted for clarity.

**Table 3.6.** Calculated Frequencies and Symmetries of CN Stretching Modes in  $(^t\text{BuNC})\text{Co}(\text{CNAr}^{\text{Mes}_2})_3$ .

Assigned Mode	Symmetry	Frequency* (cm <sup>-1</sup> )
<b>0</b>	<b>a1</b>	<b>2138</b>
<b>1</b>	<b>a1</b>	<b>2068</b>
<b>2</b>	<b>e</b>	<b>1991</b>
<b>2</b>	<b>e</b>	<b>1990</b>

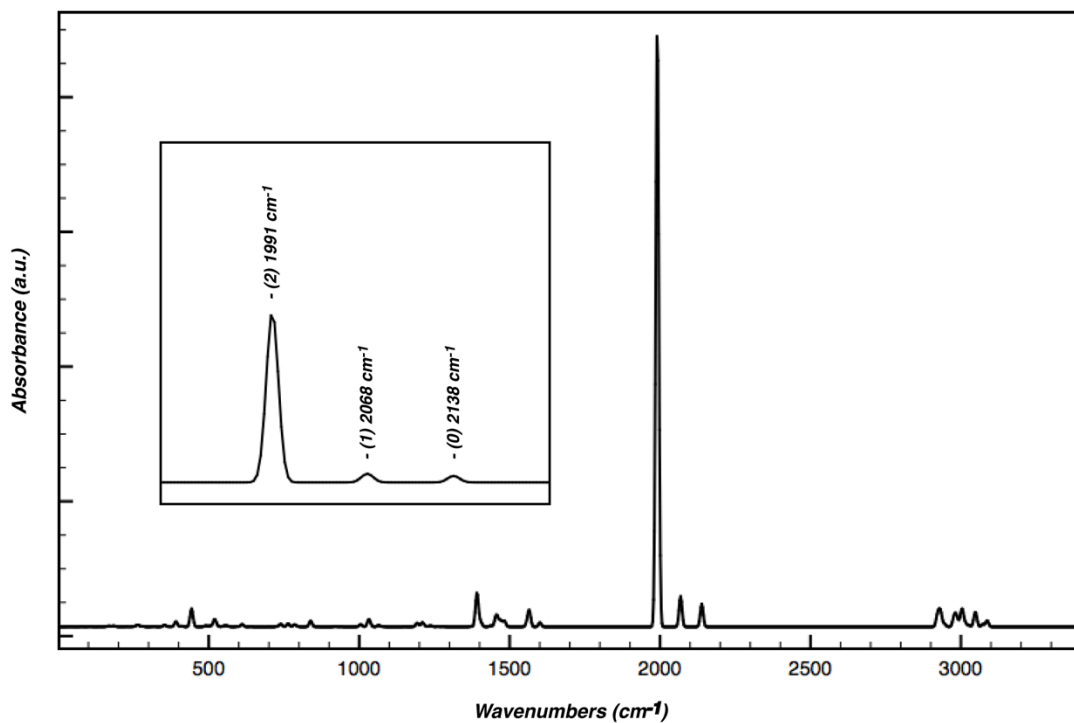


**Figure 3.9.** Simulated IR spectrums of  $(t\text{BuNC})\text{Co}(\text{CNAr}^{\text{Mes}2})_3$ .

**Optimized Coordinates of  $(t\text{BuNC})\text{Co}(\text{CNAr}^{\text{Mes}2})_3$ .**

Co	0.05181000	-0.09972600	-0.50919000
N	-1.24961800	2.65664300	-0.55138600
C	-0.73403800	1.58292400	-0.56617900
C	0.16246800	-0.27916800	1.40175000
N	0.23134500	-0.38817600	2.57083600
N	-1.70030400	-2.54041500	-1.02286000
C	-1.02424300	-1.57477000	-0.85043600
C	1.86471200	-0.23318500	-0.88920700
N	3.03732500	-0.30864700	-1.08619600
C	4.39044600	-0.27095500	-1.32456700
C	4.87739200	0.37344800	-2.49090300
C	5.28383400	-0.87881100	-0.40682800
C	6.26017400	0.41467600	-2.70126600
C	6.65751000	-0.80774000	-0.66847100
C	7.15224300	-0.16474100	-1.80098200
H	6.63124600	0.91731400	-3.59043600
H	7.34058300	-1.27841500	0.03364600
H	8.22230000	-0.12089400	-1.98344100
C	-2.35972600	-3.72617600	-1.24314200
C	-2.23263700	-4.37367400	-2.49879700
C	-3.15876100	-4.28850000	-0.21578300
C	-2.89101500	-5.59378600	-2.68879200
C	-3.79589300	-5.51086600	-0.46218900
C	-3.66489200	-6.16908500	-1.68289300
H	-2.78323900	-6.09336700	-3.64785000



H	-4.41229500	-5.93829800	0.32415800
H	-4.16747700	-7.11736800	-1.85149600
C	-1.94799700	3.84049900	-0.55314200
C	-2.78216100	4.15593900	-1.65600100
C	-1.82610400	4.73260400	0.54210500
C	-3.49796000	5.35779600	-1.62811700
C	-2.56536800	5.92146500	0.51637700
C	-3.40002600	6.23902000	-0.55290000
H	-4.14348500	5.59289600	-2.47013900
H	-2.46701400	6.60782900	1.35321900
H	-3.96441600	7.16730600	-0.55096100
C	3.97371600	0.99810000	-3.50774500
C	3.73206400	0.32788900	-4.72553200
C	3.43157600	2.28142600	-3.29139700
C	2.96101100	0.95848200	-5.70693100
C	2.66326000	2.87349300	-4.29913500
C	2.41422400	2.22982000	-5.51403400
H	2.78981600	0.44389800	-6.65061800
H	2.25456600	3.86809700	-4.13016000
C	4.83393400	-1.61465100	0.81805800
C	4.98386400	-1.02204700	2.08893500
C	4.36474400	-2.94151100	0.71266500
C	4.69168000	-1.77683100	3.23119100
C	4.07838200	-3.65748100	1.87944200
C	4.24997900	-3.10074200	3.15029100
H	4.82540400	-1.31990500	4.21019800
H	3.72708800	-4.68390300	1.79140000
C	-2.91840800	3.26015900	-2.84753900
C	-3.78238000	2.14688100	-2.80898300
C	-2.23554700	3.58102000	-4.03951900
C	-3.95691500	1.38160800	-3.96673300
C	-2.44119700	2.78988400	-5.17409200
C	-3.29579200	1.68450400	-5.15979100
H	-4.63251100	0.52884000	-3.93430400
H	-1.92369300	3.04936600	-6.09590800
C	-0.92916600	4.47929900	1.71474000
C	-1.48432900	4.11093400	2.95826200
C	0.45858400	4.71202800	1.60715100
C	-0.64670100	4.00888300	4.07523400
C	1.25968400	4.59415100	2.74772200
C	0.72654400	4.25945100	3.99571500
H	-1.08306400	3.73862600	5.03527100
H	2.32752000	4.78557500	2.65940700
C	-3.37812600	-3.63166100	1.11232300
C	-4.28831500	-2.56038100	1.23038300
C	-2.76006700	-4.15760300	2.26716100
C	-4.58059300	-2.05138900	2.50070700
C	-3.08506600	-3.62171300	3.51825000
C	-4.00384500	-2.57652700	3.65986100
H	-5.29224200	-1.23222700	2.58489600
H	-2.61606700	-4.04176100	4.40650800
C	-1.43712400	-3.80067900	-3.62989100
C	-2.11084300	-3.19669600	-4.71267600
C	-0.03397400	-3.93425400	-3.66051700
C	-1.36909400	-2.74913900	-5.81033100
C	0.66843900	-3.47050900	-4.77790800
C	0.02157800	-2.87521500	-5.86362800
H	-1.89438800	-2.29709200	-6.64971900
H	1.75059600	-3.58428700	-4.80071200
C	0.31036300	-0.51382800	4.00113000

C	-0.99127800	0.04702500	4.60417000
H	-0.96228100	-0.04368800	5.69604200
H	-1.10952300	1.10303400	4.34303300
H	-1.85637200	-0.50692400	4.22787400
C	0.47142900	-2.00697900	4.34305900
H	0.54649900	-2.13172900	5.42933500
H	-0.39100100	-2.57589200	3.98276000
H	1.37693800	-2.40951400	3.87953900
C	1.52946400	0.29284000	4.48597300
H	2.44902300	-0.10205700	4.04372700
H	1.42789300	1.34487700	4.20383800
H	1.60729300	0.22615000	5.57713500
C	-2.96394300	3.82717700	3.10608800
H	-3.18647400	3.43763900	4.10460900
H	-3.57154700	4.72769500	2.95672400
H	-3.30715200	3.09078400	2.37047500
C	1.08731800	5.10386900	0.28929600
H	2.13928700	5.37371300	0.42537500
H	1.04521900	4.27923700	-0.43179800
H	0.57265300	5.95826800	-0.16538400
C	1.60153700	4.21482100	5.22805300
H	1.69335500	5.20981300	5.68457400
H	1.18987000	3.54518700	5.99080400
H	2.61540200	3.87460300	4.99007300
C	-4.52729400	1.77743300	-1.54594700
H	-3.84124900	1.40284100	-0.77651300
H	-5.05509200	2.63793100	-1.11882700
H	-5.26321600	0.99206900	-1.74459600
C	-3.47777900	0.82923100	-6.39179900
H	-3.34058700	1.41196400	-7.30952200
H	-2.74684400	0.01008600	-6.41134700
H	-4.47558100	0.37752700	-6.42339700
C	-1.28896300	4.75980500	-4.11101900
H	-0.50060900	4.68519100	-3.35252100
H	-0.80758700	4.81082700	-5.09247200
H	-1.80260600	5.71299300	-3.93906200
C	4.29167600	-1.05374900	-4.98763200
H	3.91802400	-1.44969100	-5.93711000
H	5.38720200	-1.05307400	-5.03379200
H	4.01089500	-1.75674800	-4.19458600
C	3.67591000	3.02586400	-1.99841500
H	3.34259500	4.06528800	-2.07889300
H	3.12856200	2.56476000	-1.16723800
H	4.73752700	3.02893900	-1.72611000
C	1.55896900	2.87620700	-6.57857100
H	0.49866300	2.63244900	-6.43037300
H	1.64875200	3.96807300	-6.55801100
H	1.83643500	2.53258300	-7.58125700
C	5.45425200	0.40884500	2.23877200
H	5.41028800	0.72396700	3.28615300
H	6.48634000	0.54083300	1.89294800
H	4.83510500	1.09723800	1.65200200
C	4.18698200	-3.60305600	-0.63507100
H	3.37926900	-3.13021800	-1.20585400
H	5.09675000	-3.53137100	-1.24232300
H	3.93746000	-4.66248300	-0.51929200
C	4.00651400	-3.92058900	4.39719100
H	4.88559400	-4.52939300	4.64889700
H	3.79430400	-3.28350600	5.26241400
H	3.16419300	-4.60953500	4.26893700

C	-1.75583800	-5.28677800	2.17716200
H	-0.96653100	-5.06497000	1.44986000
H	-1.28222700	-5.46225500	3.14836900
H	-2.22160400	-6.22719600	1.85911900
C	-4.96461700	-1.96718500	0.01508500
H	-5.42779500	-2.74154700	-0.60713200
H	-5.74363600	-1.25763600	0.31132600
H	-4.24713100	-1.42988800	-0.61635400
C	-4.39446200	-2.06239700	5.02703400
H	-3.55551700	-2.10636200	5.73028500
H	-4.74408500	-1.02543000	4.98158500
H	-5.20868800	-2.66124300	5.45750600
C	0.71817900	-4.57617800	-2.51664700
H	1.75768300	-4.77317100	-2.79726800
H	0.73053100	-3.92300400	-1.63542900
H	0.26233700	-5.52517400	-2.21227800
C	-3.61493500	-3.02671500	-4.70828600
H	-4.13909800	-3.98960900	-4.73166000
H	-3.95618800	-2.50484600	-3.80656300
H	-3.94156100	-2.44755700	-5.57748500
C	0.80173100	-2.35999300	-7.05045800
H	1.10935000	-1.31756600	-6.89488900
H	1.71165900	-2.94700000	-7.21818900
H	0.20460500	-2.39140200	-7.96859100

### 3.9 Simulated IR Studies of Fixed Core Angle Geometries

Frequency calculations were carried out on both  $C_{3v}$  and  $D_{2d}$  geometry of  $\text{Co}(\text{CNAr}^{\text{Mes}2})_4$ , with two additional geometries for each isomer achieved from twisting the molecule without changing the core angles (C-Co-C). By fixing the core geometry at either  $C_{3v}$  or  $D_{2d}$ , we observed that the outer sphere of the molecule does not affect the isocyanide stretching frequencies ( $\nu_{\text{CN}}$ ) shown in Figure 3.10 and Fig 3.11 In other words, only the core angles decide the CN vibrations of the molecule.

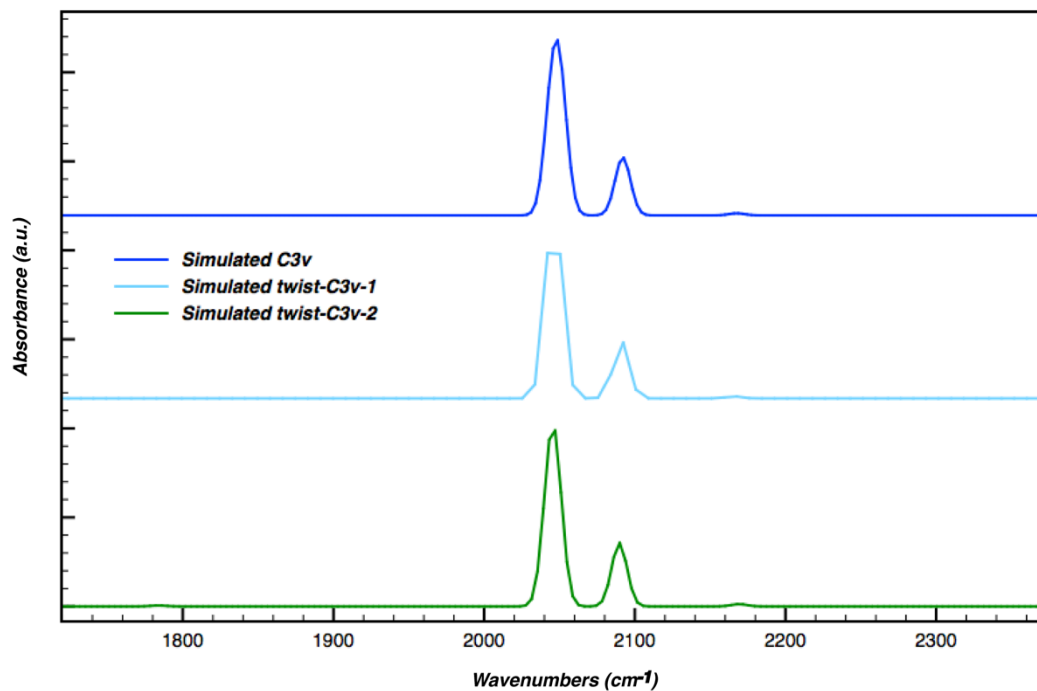


**Figure 3.10.** Simulated IR spectra of fixed core angles  $C_{3v}$   $\text{Co}(\text{CNAr}^{\text{Mes}2})_4$  geometries.

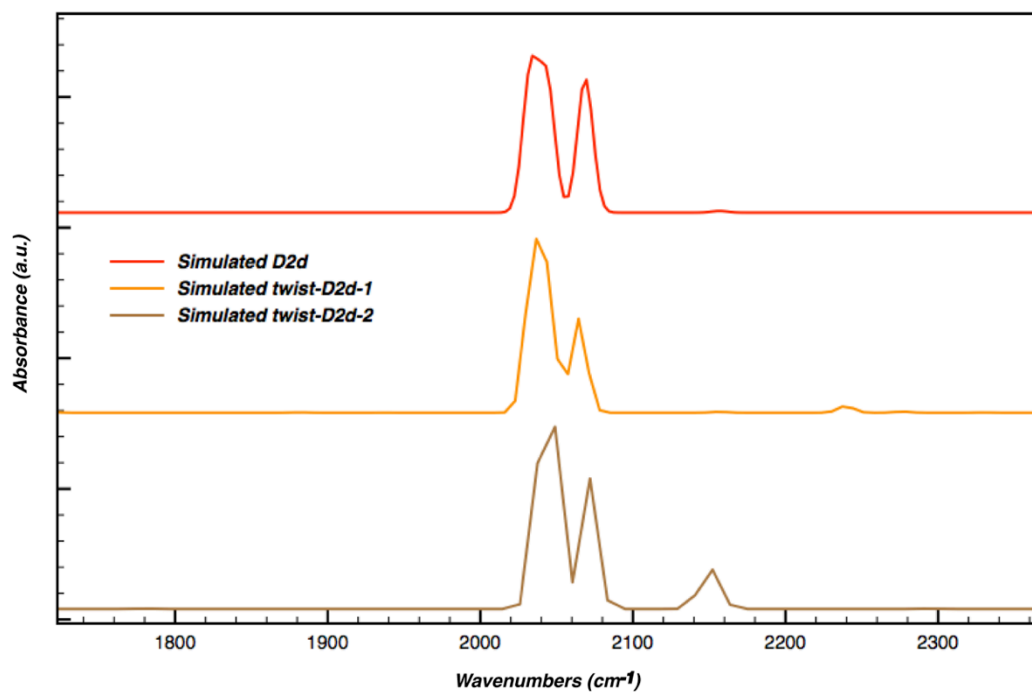


**Figure 3.11.** Simulated IR spectra of fixed core angles  $D_{2d}$   $\text{Co}(\text{CNAr}^{\text{Mes}2})_4$  geometries.

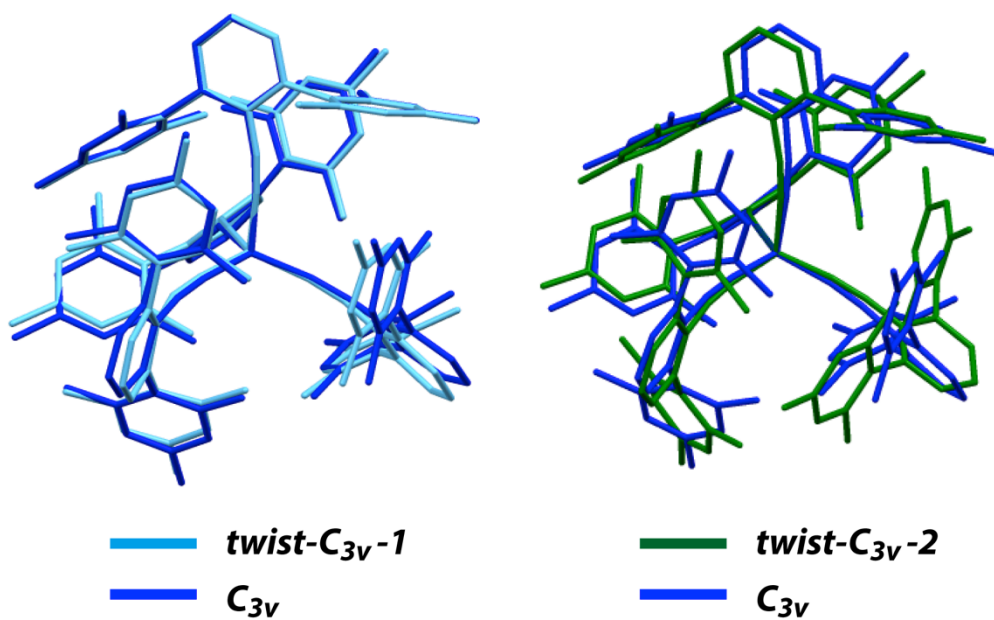


**Figure 3.12.** Simulated IR spectrums of fixed core angles  $C_{3v}$   $\text{Co}(\text{CNAr}^{\text{Mes}2})_4$  geometries.

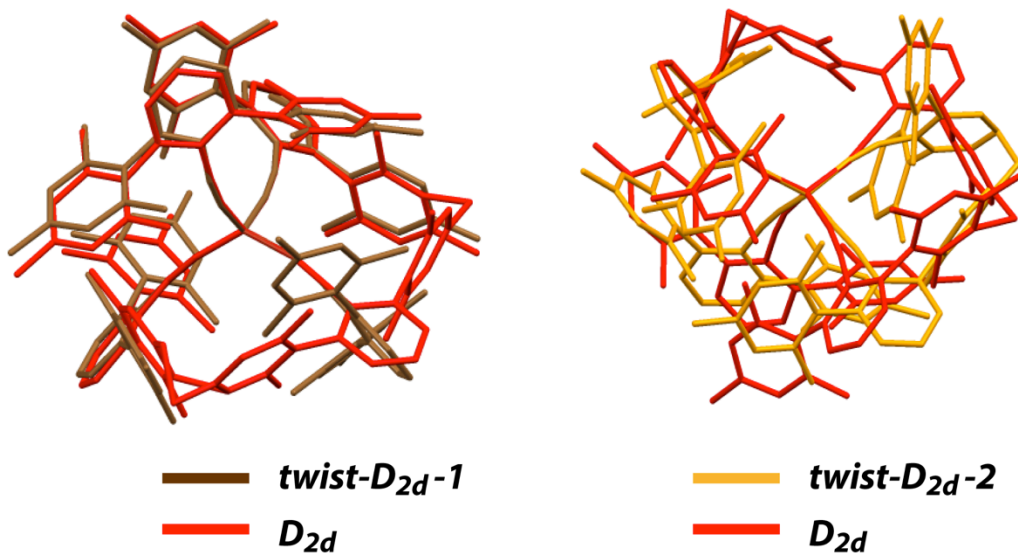


**Figure 3.13.** Simulated IR spectrums of fixed core angles  $D_{2d}$   $\text{Co}(\text{CNAr}^{\text{Mes}2})_4$  geometries.

### 3.10 Acknowledgement

Chapter 3 is currently in preparation as a manuscript by C. Chan, J. Wang, Y. Li, Xiang, B., W. Xiong, J. S. Figueroa. The dissertation author is the primary author of this manuscript. Prof. Clifford P. Kubiak and Tyler M. Porter are thanked for providing access to variable-temperature FTIR instrumentation and helpful discussions.

### 3.11 References

- (1) Porter, T. M.; Wang, J.; Li, Y.; Xiang, B.; Salsman, C.; Miller, J. S.; Xiong, W.; Kubiak, C. P. *Chem. Sci.* **2019**, *10*, 113–117.
- (2) Cahoon, J. F.; Sawyer, K. R.; Schlegel, J. P.; Harris, C. B. *Science* **2008**, *319* (5871), 1820.
- (3) Nilsen, I. A.; Osborne, D. G.; White, A. M.; Anna, J. M.; Kubarych, K. J. *The Journal of Chemical Physics* **2014**, *141* (13), 134313.
- (4) Anna, J. M.; Ross, M. R.; Kubarych, K. J. *J. Phys. Chem. A* **2009**, *113* (24), 6544–6547.
- (5) Zheng, J.; Kwak, K.; Asbury, J.; Chen, X.; Piletic, I. R.; Fayer, M. D. *Science* **2005**, *309* (5739), 1338–1343.
- (6) Kim, Y. S.; Hochstrasser, R. M. *Proceedings of the National Academy of Sciences of the United States of America* **2005**, *102* (32), 11185.
- (7) Kwak, K.; Zheng, J.; Cang, H.; Fayer, M. D. *J. Phys. Chem. B* **2006**, *110* (40), 19998–20013.
- (8) Roberts, S. T.; Ramasesha, K.; Tokmakoff, A. *Acc. Chem. Res.* **2009**, *42* (9), 1239–1249.
- (9) Anna, J. M.; Kubarych, K. J. *The Journal of Chemical Physics* **2010**, *133* (17), 174506.
- (10) Asplund, M. C.; Zanni, M. T.; Hochstrasser, R. M. *Proceedings of the National Academy of Sciences* **2000**, *97* (15), 8219.
- (11) Zheng, J.; Kwak, K.; Fayer, M. D. *Acc. Chem. Res.* **2007**, *40* (1), 75–83.

- (12) Hamm, P.; Lim, M.; Hochstrasser, R. M. *J. Phys. Chem. B* **1998**, *102* (31), 6123–6138.
- (13) Thompson, D. E.; Merchant, K. A.; Fayer, M. D. *The Journal of Chemical Physics* **2001**, *115* (1), 317–330.
- (14) Heck, R. *Organotransition Metal Chemistry A Mechanistic Approach*; Elsevier, 2012.
- (15) Klingler, R. J.; Rathke, J. W. *J. Am. Chem. Soc.* **1994**, *116* (11), 4772–4785.
- (16) Nalesnik, T. E.; Orchin, M. *Organometallics* **1982**, *1* (1), 222–223.
- (17) Ungváry, F. *Acta Chim. (Budapest)* **1982**, *111* (2), 117–130.
- (18) Ungváry, F.; Markó, L. *Journal of Organometallic Chemistry* **1981**, *219* (3), 397–400.
- (19) Brunet, J. J.; Sidot, C.; Loubinoux, B.; Caubere, P. *The Journal of Organic Chemistry* **1979**, *44* (13), 2199–2202.
- (20) Wegman, R. W.; Brown, T. L. *J. Am. Chem. Soc.* **1980**, *102* (7), 2494–2495.
- (21) Roth, J. A.; Orchin, M. *Journal of Organometallic Chemistry* **1979**, *182* (2), 299–311.
- (22) Rathke, J. W.; Feder, H. M. *J. Am. Chem. Soc.* **1978**, *100* (11), 3623–3625.
- (23) Paulik, F. E. *Catalysis Reviews* **1972**, *6* (1), 49–84.
- (24) Seyferth, D.; Millar, M. D. *Journal of Organometallic Chemistry* **1972**, *38* (2), 373–383.
- (25) Susuki, T.; Tsuji, J. *Tetrahedron Letters* **1968**, *9* (8), 913–915.
- (26) Crichton, O.; Poliakoff, M.; Rest, A. J.; Turner, J. J. *J. Chem. Soc., Dalton Trans.* **1973**, *0* (12), 1321–1324.
- (27) Wawersik, H.; Keller, H. J. *Zeitschrift für Naturforschung B* **1965**, No. 20, 938–942.
- (28) Huo, C.-F.; Li, Y.-W.; Wu, G.-S.; Beller, M.; Jiao, H. *J. Phys. Chem. A* **2002**, *106* (50), 12161–12169.
- (29) Ryeng, H.; Gropen, O.; Swang, O. *J. Phys. Chem. A* **1997**, *101* (47), 8956–8958.
- (30) Ozin, G. A.; Vander Voet, A. *Acc. Chem. Res.* **2002**, *6* (9), 313–318.
- (31) Elian, M.; Hoffmann, R. *Inorg. Chem.* **1975**, *14* (5), 1058–1076.
- (32) Sweany, R. L. *Inorg. Chem.* **1980**, *19*, 3512–3516.

- (33) Hanlan, L. A.; Huber, H.; Kuendig, E. P.; McGarvey, B. R.; Ozin. *J. Am. Chem. Soc.* **1975**, *97* (24), 7054–7068.
- (34) Crichton, O.; Poliakoff, M.; Rest, A. J.; Turner, J. J. *J. Chem. Soc., Dalton Trans.* **1973**, No. 12, 1321–1324.
- (35) Margulieux, G. W.; Weidemann, N.; Lacy, D. C.; Moore, C. E.; Rheingold, A. L.; Figueroa, J. S. *J. Am. Chem. Soc.* **2010**, *132* (14), 5033–5035.
- (36) Chan, C.; Carpenter, A. E.; Gembicky, M.; Moore, C. E.; Rheingold, A. L.; Figueroa, J. S. *Organometallics* **2018**, *38* (7), 1436–1444.
- (37) Fox, B. J.; Millard, M. D.; DiPasquale, A. G.; Rheingold, A. L.; Figueroa, J. S. *Angew. Chem. Int. Ed.* **2009**, *48* (19), 3473–3477.
- (38) Labios, L. A.; Millard, M. D.; Rheingold, A. L.; Figueroa, J. S. *J. Am. Chem. Soc.* **2009**, *131* (32), 11318–11319.
- (39) Ditri, T. B.; Fox, B. J.; Moore, C. E.; Rheingold, A. L.; Figueroa, J. S. *Inorg. Chem.* **2009**, *48* (17), 8362–8375.
- (40) Emerich, B. M.; Moore, C. E.; Fox, B. J.; Rheingold, A. L.; Figueroa, J. S. *Organometallics* **2011**, *30* (9), 2598–2608.
- (41) Mokhtarzadeh, C. C.; Margulieux, G. W.; Carpenter, A. E.; Weidemann, N.; Moore, C. E.; Rheingold, A. L.; Figueroa, J. S. *Inorg. Chem.* **2015**, *54* (11), 5579–5587.
- (42) Carpenter, A. E.; Rheingold, A. L.; Figueroa, J. S. *Organometallics* **2016**, *35* (14), 2309–2318.
- (43) Carpenter, A. E.; Chan, C.; Rheingold, A. L.; Figueroa, J. S. *Organometallics* **2016**, *35* (14), 2319–2326.
- (44) Hamm, P.; Zanni, M. *Concepts and methods of 2D infrared spectroscopy*; Cambridge University Press, 2011.
- (45) *Purification of Laboratory Chemicals*; Elsevier, 2003.
- (46) Pangborn, A. B.; Giardello, M. A.; Grubbs, R. H.; Rosen, R. K.; Timmers, F. J. *Organometallics* **1996**, *15* (5), 1518–1520.
- (47) Shim, S.-H.; Strasfeld, D. B.; Ling, Y. L.; Zanni, M. T. *Proceedings of the National Academy of Sciences* **9AD**, *104* (36), 14197.
- (48) Shim, S.-H.; Zanni, M. T. *Physical Chemistry Chemical Physics* **2009**, *11* (5), 748–761.



- (49) Nee, M. J.; McCanne, R.; Kubarych, K. J.; Joffre, M. *Opt. Lett.* **2007**, *32* (6), 713—715.
- (50) Rock, W.; Li, Y.-L.; Pagano, P.; Cheatum, C. M. *J. Phys. Chem. A* **2013**, *117* (29), 6073–6083.
- (51) HOMMEL, E. L.; ALLEN, H. C. *Analytical Sciences* **2001**, *17* (1), 137—139.
- (52) Laaser, J. E.; Xiong, W.; Zanni, M. T. *J. Phys. Chem. B* **2011**, *115* (11), 2536–2546.
- (53) Zheng, J.; Kwak, K.; Asbury, J.; Chen, X.; Piletic, I. R.; Fayer, M. D. *Science* **2005**, *309* (5739), 1338—1343.
- (54) Agnew, D. W.; DiMucci, I. M.; Arroyave, A.; Gembicky, M.; Moore, C. E.; MacMillan, S. N.; Rheingold, A. L.; Lancaster, K. M.; Figueroa, J. S. *J. Am. Chem. Soc.* **2017**, *139* (48), 17257–17260.
- (55) Gaussian 09, Revision D.01, M. J. Frisch, G. W. Trucks, H. B. Schlegel, G. E. Scuseria, M. A. Robb, J. R. Cheeseman, G. Scalmani, V. Barone, B. Mennucci, G. A. Petersson, H. Nakatsuji, M. Caricato, X. Li, H. P. Hratchian, A. F. Izmaylov, J. Bloino, G. Zheng, J. L. Sonnenberg, M. Hada, M. Ehara, K. Toyota, R. Fukuda, J. Hasegawa, M. Ishida, T. Nakajima, Y. Honda, O. Kitao, H. Nakai, T. Vreven, J. A. Montgomery, Jr., J. E. Peralta, F. Ogliaro, M. Bearpark, J. J. Heyd, E. Brothers, K. N. Kudin, V. N. Staroverov, T. Keith, R. Kobayashi, J. Normand, K. Raghavachari, A. Rendell, J. C. Burant, S. S. Iyengar, J. Tomasi, M. Cossi, N. Rega, J. M. Millam, M. Klene, J. E. Knox, J. B. Cross, V. Bakken, C. Adamo, J. Jaramillo, R. Gomperts, R. E. Stratmann, O. Yazyev, A. J. Austin, R. Cammi, C. Pomelli, J. W. Ochterski, R. L. Martin, K. Morokuma, V. G. Zakrzewski, G. A. Voth, P. Salvador, J. J. Dannenberg, S. Dapprich, A. D. Daniels, O. Farkas, J. B. Foresman, J. V. Ortiz, J. Cioslowski, D. J. Fox, Gaussian, Inc., Wallingford CT, (2013).

# Chapter 4 Controlled Stepwise Synthesis of a Nucleophilic Cobalt-phosphide Cluster

## 4.1 Introduction

Electrochemical water splitting represents as a sustainable approach for hydrogen generation through clean-energy technologies.<sup>1-3</sup> Cobalt phosphides nanomaterials ( $\text{Co}_x\text{P}_x$ ), known as one of the most active electrocatalyst toward hydrogen evolution reaction (HER) and oxygen evolution reaction (OER),<sup>4-8</sup> have received increasing interest due to HER and OER being two key reactions of electrochemical water splitting.<sup>1,3,9</sup> While the identification of systems able to substitute the currently best materials based on Pt (for HER) and  $\text{RuO}_2/\text{IrO}_2$  (for OER) are main areas of study,<sup>1,9</sup> the use of homogeneous molecular cobalt phosphide clusters to provide complementary reactivity insight is rare. This is due to several limits in design and synthesis of multi- nuclear assemblies, such as ligand lability and lack of coordination directionality as cluster synthesis is largely a self-assembly process.

With regards to the fundamental understanding of single phosphorous site reactivity in cobalt phosphide nanomaterials, one of the most intriguing complexes is the all-carbonyl  $\mu_3$ -bridging phosphide cluster  $\text{Co}_3(\mu_3\text{-P})(\text{CO})_9$ . Although reportedly synthesized through reaction of white phosphorous ( $\text{P}_4$ ) and  $\text{Co}_2(\text{CO})_8$ ,  $\text{Co}_3(\mu_3\text{-P})(\text{CO})_9$  has only been observed through in situ IR spectroscopy with a 10 minutes life time at room-temperature.<sup>10</sup> As we mentioned

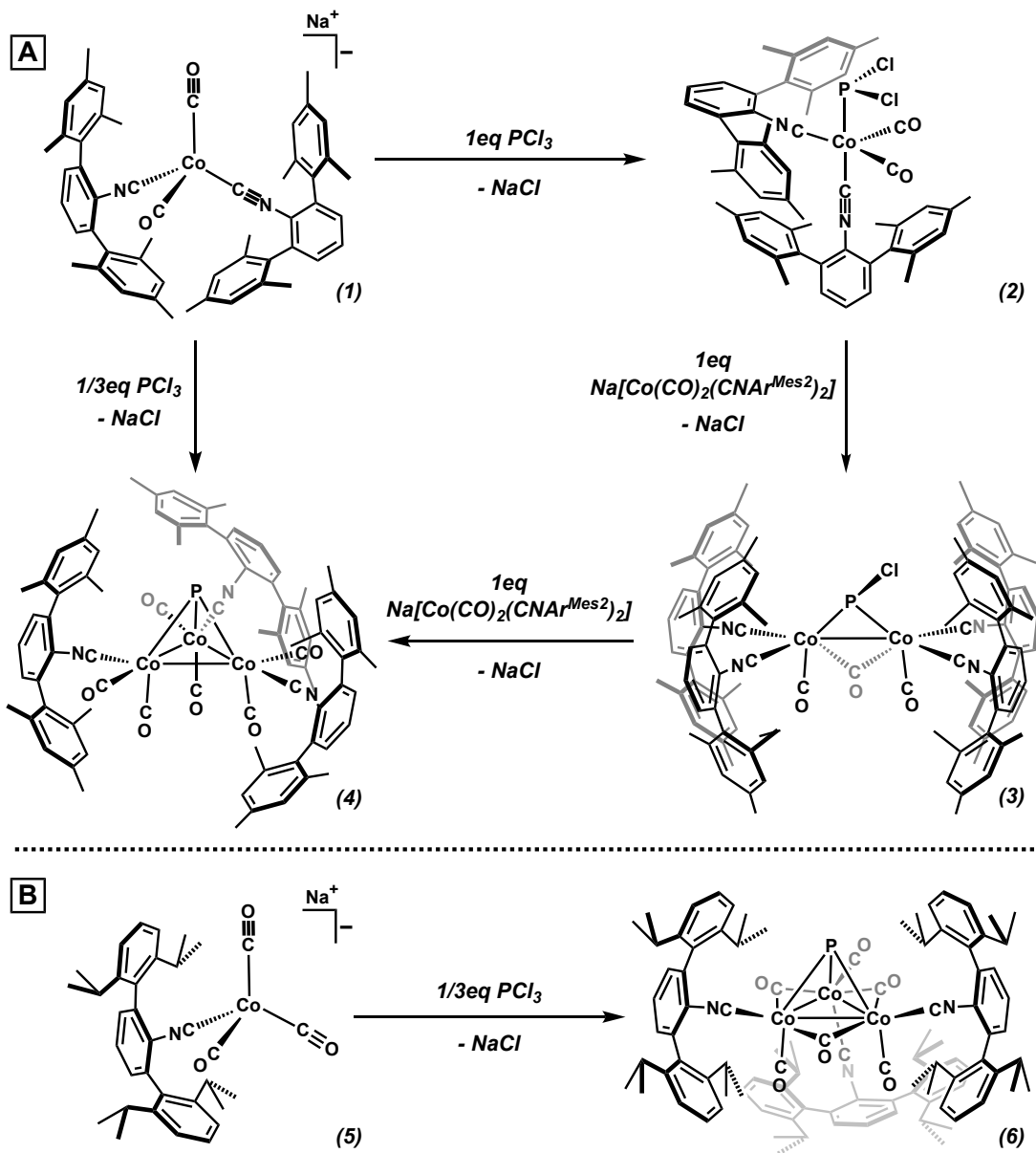
earlier, a commonly seen self-assemble cyclotrimerization to generate larger nucleus cluster  $[\text{PCo}(\text{CO})_8]_3$  was readily recognized as its thermodynamic product. Interestingly,  $[\text{PCo}(\text{CO})_8]_3$  was demonstrated to be trapped with  $\text{Fe}_2(\text{CO})_9$  to generate  $\text{Fe}(\text{CO})_4\text{PCo}_3(\text{CO})_9$ .<sup>11,12</sup> The only structurally characterized  $\mu_3\text{-P-Co}_3$  motif,  $\{\text{Cp}^{\text{R}}\text{Co}\}_3(\mu_3\text{-P})_2$  ( $\text{Cp}^{\text{R}} = \text{C}_5\text{H}_3\text{tBu}_{2-1,3}$ ), was obtained from reaction of  $[\{\text{Cp}^*\text{Fe}\}\{\text{Cp}^{\text{R}}\text{TaP}_5\}]$  and  $[\text{Cp}^{\text{R}}\text{Co}(\text{CO})_2]$  by Scherer and coworkers.<sup>13</sup> Until now, an ideal system that provide directionality which allows transition metal ions to interact cooperatively with main group building blocks remain undiscovered.

Given our success in isolating isocyno analogues to classical carbonyl metalates using sterically encumbering *m*-terphenyl isocyanides,<sup>14-21</sup> herein we report the preparation of a controlled step-wise isolation of thermal and air stable tricobalt  $\mu_3$ - bridging phosphide clusters featuring its nucleophilicity on the interstitial bridging phosphide.

## 4.2 Results and Discussions

To prepare a  $\mu_3$ - bridging phosphide complex, we chose to start with salt metathesis reactions of previously achieved cobalt anions with the widely used phosphorous feedstock, phosphorous trichloride ( $\text{PCl}_3$ ). The formally Co(-I) species,  $\text{Na}[\text{Co}(\text{CO})_2(\text{CNAr}^{\text{Mes}2})_2]$  (**1**) ( $\text{Ar}^{\text{Mes}2} = 2,6\text{-}(2,4,6\text{-Me}_3\text{C}_6\text{H}_2)_2\text{C}_6\text{H}_3$ ) was not only suitable for this approach but also ideal for a step-wise isolation of intermediates with the steric profile provided by the two *m*-terphenyl isocyanide ligands. Indeed, by quick addition of  $\text{PCl}_3$  to a THF solution of **1**, an immediate color change from orange to light yellow was observed. The reaction was completed in 5 minutes and  $(\text{PCl}_2)\text{Co}(\text{CO})_2(\text{CNAr}^{\text{Mes}2})_2$  (**2**) was isolated as a pale yellow crystalline material indicating an one equivalent salt-elimination of NaCl. (Scheme 4.1) X-ray crystallography

revealed a trigonal bipyramidal geometry with both CO and isocyanide ligands present in a *cis* position to its own kind. (Figure 4.1A) Complex **2** turned out to only be the kinetically stable product where ligand redistribution was noticed to generate  $(\text{PCl}_2)\text{Co}(\text{CO})_n(\text{CNAr}^{\text{Mes}2})_{4-n}$  ( $n < 4$ ) which lead to further decomposition upon sitting at room-temperature.



**Scheme 4.1.** (top) Step-wise synthesis of cluster **4** through complex **2** and **3**. (bottom) Synthesis of cluster **6**.

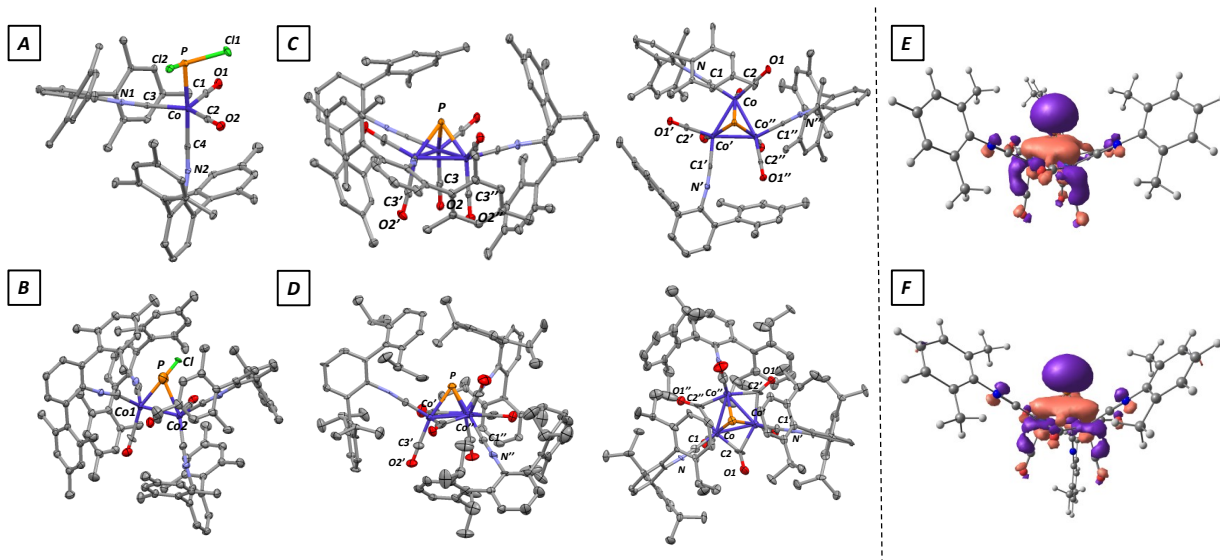


**Figure 4.1.** (Left) Molecular structures of complexes **2-4** and **6**. A)  $(\text{PCl}_2\text{Co}(\text{CO})_2(\text{CNAr}^{\text{Mes}2})_2)$  (**2**), B)  $\text{Co}_2(\mu_2\text{-P-PCl})(\mu_2\text{-C-CO})(\text{CO})_2(\text{CNAr}^{\text{Mes}2})_4$  (**3**), C)  $\text{Co}_3(\mu_3\text{-P})(\text{CO})_6(\text{CNAr}^{\text{Mes}2})_3$  (**4**), and D)  $\text{Co}_3(\mu_3\text{-P})(\mu_2\text{-C-CO})_3(\text{CO})_3(\text{CNAr}^{\text{Dipp}2})_3$  (**6**). (Right) E) Highest occupied molecular orbital (HOMO) of complex **4**. F) Highest occupied molecular orbital-2 (HOMO-2) of complex **6**.

Interestingly, by adding another equivalent of the Co(-I) anion **1** to complex **2**, we were able to proceed another equivalent of NaCl salt-elimination to generate a chloro-phosphinidene-bridged cobalt dimer,  $\text{Co}_2(\mu_2\text{-P-PCl})(\mu_2\text{-C-CO})(\text{CO})_2(\text{CNAr}^{\text{Mes}2})_4$  (**3**). This compound can also be synthesized by adding 0.7 equivalent of  $\text{PCl}_3$  to the cobalt anion **1**, and hence in isolated yield of 99%. Unfortunately, the structural comparison with the only other phosphinidene-bridged cobalt complex  $[(\text{IME}_4)_2\text{Co}(\mu\text{-PMes})]_2$  ( $\text{IME}_4 = 1,3,4,5\text{-tetramethylimidazolin-2-ylidene}$ )<sup>22</sup> remained difficult due to a four-fold positional disorder of bridging PCl and CO in complex **3**. However,  $^{31}\text{P}$  NMR spectra was able to show a downfield shift from  $\delta = 406$  ppm (complex **2**) to  $\delta = 524$  ppm during the **3** formation which is also in similar region to  $\delta = 449$  ppm for  $[(\text{IME}_4)_2\text{Co}(\mu\text{-PMes})]_2$ .

To further aim for the  $\mu_3$ - bridging phosphide complex, one more equivalent of cobalt anion **1** was added to **3**. After 1 hour of reaction time, the reaction mixture was taken up in

pentane and stored in the freezer (-35°C) to observe a color change from brown to green over 3 days. Green single crystals suitable for X-ray diffraction reported the phosphide bridged cobalt trimer  $\text{Co}_3(\mu_3\text{-P})(\text{CO})_6(\text{CNAr}^{\text{Mes}2})_3$  (**4**) with the support of a highly down fielded phosphorous signal at  $\delta = 751$  ppm. The nearly  $\text{C}_3$ -symmetric complex exhibits a highly pyramidalized phosphide ligand ( $\Sigma(\text{Co-P-Co}) = 208.9(1)^\circ$ ,  $\text{NH}_3$  is  $319.8^\circ$ ) that resides 1.653 Å above the mean tricobalt plane. Each cobalt center has a distorted octahedral geometry that was bound to two other cobalt metals, one carbonyl and one isocyanide ligand forming an equatorial plane with the apical CO ligand *trans*- to the bridging phosphide. (Figure 4.1C) However, due to the rigid geometry created by the tricobalt plane, the formation from **3** to **4** required a ligand redistribution process causing a relatively low yield (18%).

We turned to explore an alternative cobalt phosphide building block that has the preferred isocyanide to CO ligand ratio (3:1) to start with. In contrast to the 3 day reaction time of complex **4**,  $\text{Co}_3(\mu_3\text{-P})(\mu_2\text{-C-CO})_3(\text{CO})_3(\text{CNAr}^{\text{Dipp}2})_3$  (**6**) was generated in an hour through the addition of 1/3 equivalent of  $\text{PCl}_3$  to  $\text{NaCo}(\text{CO})_3(\text{CNAr}^{\text{Dipp}2})$  (**5**) with a 95% yield. (Scheme 1) From the crystallography data, cluster **6** also exhibits a highly pyramidalized phosphide ligand ( $\Sigma(\text{Co-P-Co}) = 204.9(1)^\circ$ ) that resides 1.715 Å above the mean tricobalt plane. The average Co-Co distance is 2.529(3) Å similar to 2.517(3) Å in cluster **4**. Interestingly, cluster **6** now displays bridging carbonyl ligands across all three cobalt nucleus with two isocyanide ligands pointing upward and one downward relative to the tricobalt plane. (Figure 4.1D) This bridging carbonyl feature is reflected on the more shielded  $^{31}\text{P}$  NMR signal at  $\delta = 503$  ppm compared to **4** presumably due to the more electron-rich cobalt centers from the lack of pi-back bonding. It is worth mention that both cluster **4** and **6** displayed outstanding thermal and air

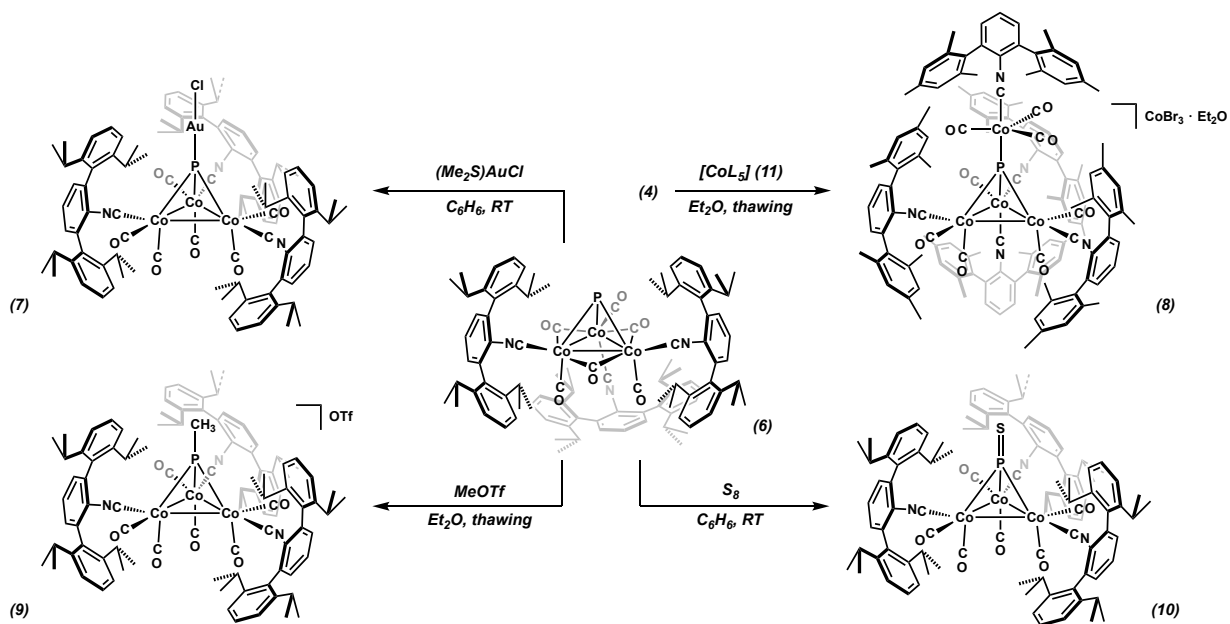
stability that showed no decomposition after a week heating at 40 °C in air, largely improved from the 15 minutes life time of the all-carbonyl cluster  $\text{Co}_3(\mu_3\text{-P})(\text{CO})_9$ .

**Table 4.1.** Selected bond lengths and angles from solid-state structures of complexes **4** and **6-10**.

Complex	Mean d(Co-Co) [Å]	d(P- $\text{Co}_3$ centroid) [Å]	$\Sigma(\text{Co-P-Co})$ [°]
<b>4</b>	2.517(3)	1.653	208.9(1)
<b>6</b>	2.529(3)	1.715	204.9(1)
<b>7</b>	2.5622(6)	1.559	219.23(2)
<b>8</b>	2.567(2)	1.555	220.18(8)
<b>9</b>	2.561(5)	1.504	225.3(2)
<b>10</b>	2.566(1)	1.563	219.40(5)

Density functional theory (DFT) computations on model  $\text{Co}_3(\mu_3\text{-P})(\text{CO})_6(\text{CNXyl})_3$  (Xyl = 2,6-( $\text{CH}_3$ )<sub>2</sub>C<sub>6</sub>H<sub>3</sub>) (**4m**) and  $\text{Co}_3(\mu_3\text{-P})(\mu_2\text{-C-CO})_3(\text{CO})_3(\text{CNXyl})_3$  (**6m**) showed a 7.6 kcal/mol energy difference in favor of the bridging carbonyl structure **6m**. Additionally, both **4m** and **6m** appeared a phosphine lone-pair character on its HOMO and HOMO-2 respectively, potentially suitable for 2-electron coordination. (Figure 4.1, E and F) Indeed, treatment of cluster **6** with  $(\text{Me}_2\text{S})\text{AuCl}$  resulted in a ligand substituted product  $\text{Co}_3(\mu_3\text{-P})(\text{CO})_6(\text{CNAr}^{\text{Dipp}2})_3\text{AuCl}$  (**7**). (Scheme 4.2) To quantitatively established the steric properties of **6**, the percent buried volume parameter (%Vbur) was determined here using the program SambVca. The %Vbur for **6** (60.6) is to our best knowledge the largest phosphine ligand compared to previously reported  $\text{PAu}_3$  (40.3) and  $\text{P}(\text{tBu})_3$  (40.0) in analogues gold complexes.

Note that upon coordination, the bridging carbonyl ligands in **6** transformed to non-bridging fashion similar to the cluster geometry in **4**.



**Scheme 4.2.** Reaction scheme of **4** and **6** showing the nucleophilicity of the bridging phosphide.

The unique feature of **4** and **6** relative to  $\text{Co}_3(\mu_3\text{-P})(\text{CO})_9$  not only is that with the steric protection provided by the *m*-terphenyl isocyanides, the thermal stability allows us for the structural study of cobalt-phosphorous interaction in clusters but also its increased electron-rich character allows for nucleophilic reactivity of the interstitial phosphide towards a variety of electrophilic substrates.<sup>12,23</sup> Similar isocyanide to carbonyl ligand substitution has shown an increased nucleophilicity in our previously published  $\text{Na}[\text{Fe}_4(\mu_4\text{-N})(\text{CO})_8(\text{CNAr}^{\text{Mes}2})_4]$  cluster.<sup>24</sup> For example, treatment of **6** with  $[\text{Co}(\text{CO})_3(\text{CNAr}^{\text{Mes}2})_2]\text{Co}_3\text{Br}_6$  (**11**) produces the  $\mu_4$ -bridging phosphide adduct  $[\text{Co}_4(\mu_4\text{-P})(\text{CO})_9(\text{CNAr}^{\text{Dipp}2})_4]\text{CoBr}_3$  (**8**), in which an  $[\text{Co}(\text{CO})_3(\text{CNAr}^{\text{Mes}2})]$  fragment has been incorporated into the core proximal to the interstitial phosphide. The  $\text{P-Co}_{3\text{centroid}}$  distance contracted from 1.715 Å to 1.555 Å after coordinating with the phosphide. The  $\text{P-Co}_{\text{axial}}$  distance being longer at 2.220(3) Å. In this case, the  $\text{Co}_3(\mu_3\text{-P})$  fragment can be



viewed as a multimetallic ligand to the  $[\text{Co}(\text{CO})_3(\text{CNAr}^{\text{Mes}2})]$  fragment with the single unpaired electron still mainly located on the new cobalt center based on DFT calculations.

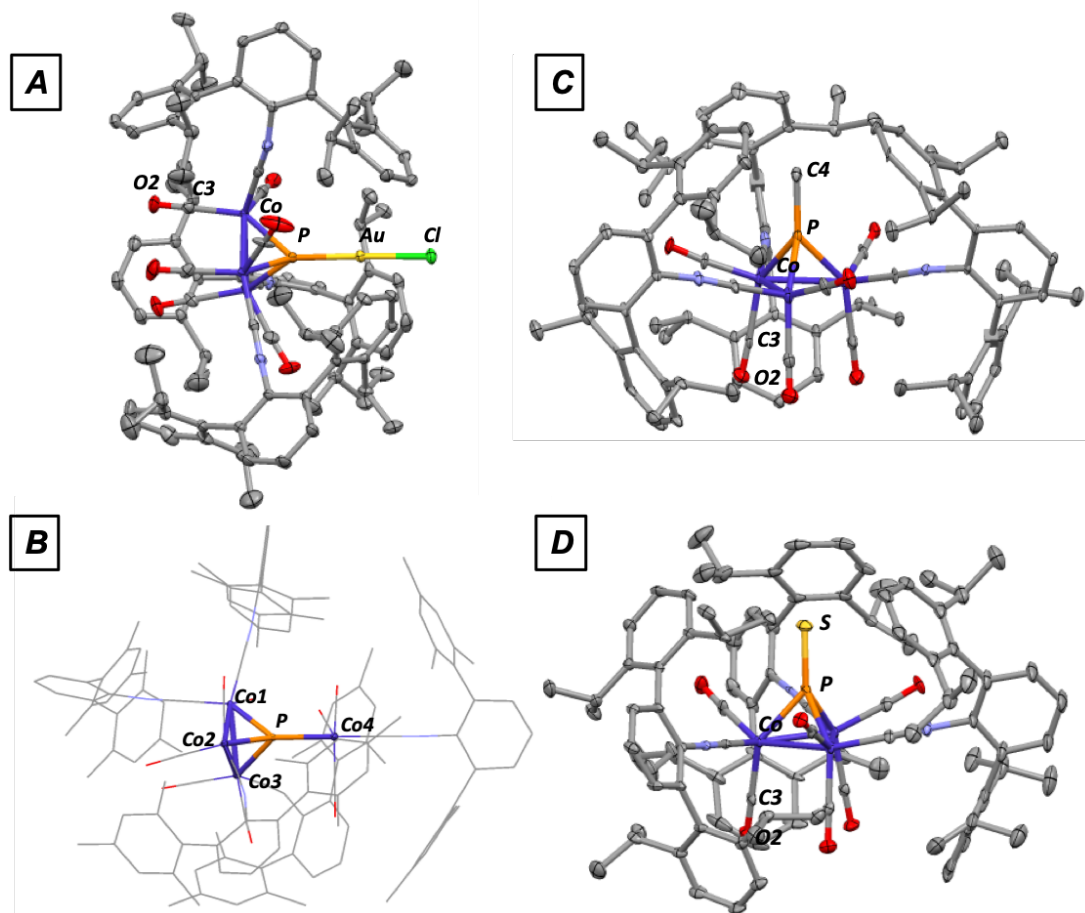


**Figure 4.2.** Molecular structure of A)  $\text{Co}_3(\mu_3\text{-P})(\text{CO})_6(\text{CNAr}^{\text{Dipp}2})_3\text{AuCl}$  (**7**), B)  $[\text{Co}_4(\mu_4\text{-P})(\text{CO})_9(\text{CNAr}^{\text{Dipp}2})_4]\text{CoBr}_3$  (**8**), C)  $[\text{Co}_3(\mu_3\text{-P-CH}_3)(\text{CO})_6(\text{CNAr}^{\text{Dipp}2})_3]\text{OTf}$  (**9**), and D)  $\text{Co}_3(\mu_3\text{-P-PS})(\text{CO})_6(\text{CNAr}^{\text{Dipp}2})_3$  (**10**).

The nucleophilicity of the phosphide in complex **6** can also be demonstrated by its rapid reaction with methyl triflate ( $\text{MeOTf}$ ,  $\text{OTf} = \text{CF}_3\text{SO}_3^-$ ) to afford a methylated phosphorous salt,  $[\text{Co}_3(\mu_3\text{-P-CH}_3)(\text{CO})_6(\text{CNAr}^{\text{Dipp}2})_3]\text{OTf}$  (**9**). Additionally, an oxidized cluster  $\text{Co}_3(\mu_3\text{-P-PS})(\text{CO})_6(\text{CNAr}^{\text{Dipp}2})_3$  (**10**) was isolated from complex **6** with 1 equivalent of elemental sulfur ( $\text{S}_8$ ). Previous examples of  $\text{ECo}_3(\text{CO})_9$  ( $\text{E} = \text{PR}$ ,  $\text{R} = \text{alkyl}$ ,  $\text{S}$ ) has been observed by generation from pre-installed  $\text{PRX}_2$  ( $\text{X} = \text{Cl}$ ,  $\text{Br}$ ) reagent with  $\text{Co}_2(\text{CO})_8$  or  $\text{K}[\text{Co}(\text{CO})_4]$ .<sup>12,25-28</sup> Even the

only other two examples of transition metal coordinated  $\text{ECo}_3(\text{CO})_9$  ( $\text{E} = \text{PM}$ ,  $\text{M} = \text{Mn}$ ,  $\text{W}$ ) were also made through salt metathesis of  $\text{Co}_2(\text{CO})_8$  with  $\text{CpMn}(\text{CO})_2\text{PX}_3^{29}$  and  $\text{K}[\text{Co}(\text{CO})_4]$  with  $\{\text{W}(\text{CO})_5\}_2\text{PCl}$ .<sup>30</sup> Again, this is the first time where we demonstrated the isolation of coordinatively unsaturated  $\text{Co}_3(\mu_3\text{-P})$  fragment which further reacts toward electrophilic substrates. Through the structural analysis of cluster **9** and **10**, both complexes showed a *ca.* 0.2 Å reduced  $\text{P-Co}_{3\text{centroid}}$  distance as 1.504 Å and 1.563 Å respectively compared to cluster **4**, suggesting a stronger orbital overlap between Co and P upon coordination.

### 4.3 Concluding Remarks

In summary, the kinetic stabilization afforded by encumbering *m*-terphenyl isocyanide ligand framework with their isolobal relationship to CO, allows for the isolation of the thermally and air stable tricobalt  $\mu_3$ - bridging phosphide. Remarkably, we were able to controllably isolate both intermediates toward the phosphide generation. The observed nucleophilic reactivity demonstrates the potential of  $\text{Co}_3(\mu_3\text{-P})$  fragment as a metal-based phosphine ligand. Work is currently underway to understand the redox potential of these complexes and canvass the scope of reactivity towards small- molecule substrates such as  $\text{H}_2$  and  $\text{O}_2$ , probing to better understand the outstanding catalytic ability of cobalt phosphide nanomaterials toward HER and OER.

### 4.4 Synthetic Procedures and Characterization Data

**General Considerations.** All manipulations were carried out under an atmosphere of Argon<sub>(g)</sub> using standard Schlenk and glovebox techniques. Unless otherwise stated, reagent-grade starting materials were purchased from commercial sources and either used as received or purified by standard procedures.<sup>31</sup> Solvents were dried and deoxygenated according to standard

procedures.<sup>32</sup> Benzene, benzene-*d*<sub>6</sub> and toluene-*d*<sub>8</sub> (Cambridge Isotope Laboratories) were dried with Na/K and Benzophenone followed by distillation; thereafter, 7 freeze-pump-thaw cycles were executed and the solvents were stored on 4 Å molecular sieves for 3 days prior to use. Celite 405 (Fisher Scientific) was dried under vacuum (24 h) at a temperature above 250 °C prior to use. The compounds Co(CO)<sub>4</sub>(CNAr<sup>Dipp2</sup>)<sub>4</sub>, Na[Co(CO)<sub>2</sub>(CNAr<sup>Mes2</sup>)<sub>2</sub>] and Co(CO)<sub>2</sub>(CNAr<sup>Dipp2</sup>)<sub>6</sub> were prepared by previously reported methods.<sup>21,33</sup>

Solution <sup>1</sup>H, <sup>13</sup>C{<sup>1</sup>H}, <sup>31</sup>P and <sup>15</sup>N NMR spectra were recorded on a Bruker Avance 300, a Bruker Avance 800, a Joel ECA 500, or a Varian X-Sens 500 spectrometer. <sup>1</sup>H and <sup>13</sup>C{<sup>1</sup>H} chemical shifts are reported in ppm relative to SiMe<sub>4</sub> (<sup>1</sup>H and <sup>13</sup>C δ = 0.0 ppm) with reference to residual solvent resonances of 7.16 ppm (<sup>1</sup>H) and 128.06 ppm (<sup>13</sup>C) for C<sub>6</sub>D<sub>6</sub>. <sup>31</sup>P{<sup>1</sup>H} NMR chemical shifts are reported in ppm relative to an internal standard of 85% H<sub>3</sub>PO<sub>4</sub> (0 ppm) in a sealed capillary. FTIR spectra were recorded on a Thermo-Nicolet iS10 FTIR spectrometer. For solution FTIR spectra, solvent peaks were digitally subtracted from all spectra by comparison with an authentic spectrum obtained immediately prior to that of the sample. The following abbreviations were used for the intensities and characteristics of important IR absorption bands: vs = very strong, s = strong, m = medium, w = weak, vw = very weak; b = broad, vb = very broad, sh = shoulder.

**Synthesis of (PCl<sub>2</sub>)Co(CO)<sub>2</sub>(CNAr<sup>Mes2</sup>)<sub>2</sub> (2).** A THF solution of PCl<sub>3</sub> (8.23 mg, 0.06 mmol, 1 equiv., 1 mL) was added to a THF solution of Na[Co(CO)<sub>2</sub>(CNAr<sup>Mes2</sup>)<sub>2</sub>] (50 mg, 0.06 mmol, 1 equiv., 1 mL) all at once. An immediate color change from orange to light brown was observed. After 5 minutes, the solution was pumped down as a light yellow solid. Benzene was added and filtered through celite. Thereafter, the product was recrystallized in pentane:benzene (8:2) mixture. Single crystals suitable for X-ray determination were collected after 1 day. Yield: 30

mg, 0.033 mmol, 56%.  $^1\text{H}$  NMR (499.9 MHz,  $\text{C}_6\text{D}_6$ , 20 °C):  $\delta$  = 6.88 (m, 10H, *p*-Ph and *m*-Mes), 6.81 (d, 4H,  $J$  = 5 Hz, *m*-Ph), 2.27 (s, 12H, *p*-Mes), 2.03 (s, 24H, *o*-Mes) ppm.  $^{13}\text{C}\{^1\text{H}\}$  NMR (125.7 MHz,  $\text{C}_6\text{D}_6$ , 20 °C):  $\delta$  = 199.2 (*broad*, CNR), 169.46 (*broad*, CO), 139.6, 138.02, 135.9, 135.7, 134.4, 129.5, 129.0, 128.9, 21.3 (*p*-Mes), 20.5 (*o*-Mes) ppm. (The CNR and CO resonance extremely broadened, presumably due to coupling to  $^{59}\text{Co}$  ( $I$  = 7/2, 100 %)).  $^{31}\text{P}\{^1\text{H}\}$  NMR (121.47 MHz,  $\text{C}_6\text{D}_6$ , 20 °C):  $\delta$  = 406 (s,  $\text{PCl}_2$ ) ppm. FTIR ( $\text{C}_6\text{H}_6$ , KBr windows, 25 °C):  $\nu_{\text{CN}}$  and  $\nu_{\text{CO}}$  = 2143 (m), 2084 (vs), 2054 (sh), 2020 (s), 1985 (s)  $\text{cm}^{-1}$  also, 2955 (m), 2920 (vw), 2867 (w)  $\text{cm}^{-1}$ .

**Synthesis of  $\text{Co}_2(\mu_2\text{-P-PCl})(\mu_2\text{-C-CO})(\text{CO})_2(\text{CNAr}^{\text{Mes}2})_4$  (3).** A THF solution of  $\text{PCl}_3$  (23.55 mg, 0.17 mmol, 0.7 equiv., 1 mL) was added dropwise to a THF solution of  $\text{Na}[\text{Co}(\text{CO})_2(\text{CNAr}^{\text{Mes}2})_2]$  (200 mg, 0.24 mmol, 1 equiv., 5 mL) at room-temperature. An immediate color change from orange to dark brown was observed. After 1-hour reaction time, the solution was pumped down as a brown solid. Benzene was added and filtered through celite. The solid was then dissolved in pentane:benzene (8:2) for recrystallization under -35 °C. Single crystals suitable for X-ray determination were collected after 1 day. Yield: 200 mg, 0.12 mmol, 99%.  $^1\text{H}$  NMR (499.9 MHz,  $\text{C}_6\text{D}_6$ , 20 °C):  $\delta$  = 7.00 (b, 4H, *m*-Ph), 6.95 (s, 16H, *m*-Mes), 6.91 (d, 8H,  $J$  = 5 Hz, *m*-Ph), 2.40 (s, 12H, *p*-Mes), 2.39 (s, 24H, *o*-Mes), 2.14 (s, 12H, *p*-Mes), 2.08 (s, 24H, *o*-Mes) ppm.  $^{13}\text{C}\{^1\text{H}\}$  NMR (125.7 MHz,  $\text{C}_6\text{D}_6$ , 20 °C):  $\delta$  = 217.4 (CNR), 139.1 (CO), 137.2 (CO), 135.6 (CO), 138.6, 137.1, 135.7, 134.9, 129.8, 129.5, 128.4, 128.3, 127.5, 127.3, 126.9, 21.7 (*p*-Mes), 21.6 (*p*-Mes), 20.7 (*o*-Mes), 20.6 (*o*-Mes) ppm. (One CO resonance could not be detected with the CNR and CO resonance extremely broadened, presumably due to coupling to  $^{59}\text{Co}$  ( $I$  = 7/2, 100 %)).  $^{31}\text{P}\{^1\text{H}\}$  NMR (121.47 MHz,  $\text{C}_6\text{D}_6$ , 20 °C):  $\delta$  = 524 (s,  $\mu_2\text{-P-PCl}$ ) ppm.

FTIR (C<sub>6</sub>H<sub>6</sub>, KBr windows, 25 °C):  $\nu_{\text{CN}}$  and  $\nu_{\text{CO}}$  = 2129 (w), 2093 (vs), 2062 (vs), 2007 (sh), 1990 (s), 1815 (s) cm<sup>-1</sup> also, 2961 (m), 2925 (vw), 2867 (w) cm<sup>-1</sup>.

**Synthesis of Co<sub>3</sub>( $\mu_3$ -P)(CO)<sub>6</sub>(CNAr<sup>Mes2</sup>)<sub>3</sub> (4).** A THF solution of PCl<sub>3</sub> (6.7 mg, 0.06 mmol, 0.4 equiv., 1 mL) was added dropwise to a THF solution of Na[Co(CO)<sub>2</sub>(CNAr<sup>Mes2</sup>)<sub>2</sub>] (100 mg, 0.12 mmol, 1 equiv., 1 mL) at room-temperature. An immediate color change from bright orange to yellow was observed. After 1-hour reaction time, the solution was pumped down as a brown solid. Benzene was added and filtered through celite. Thereafter, the product was recrystallized in pentane:benzene (8:2) mixture. The reaction mixture turned green in the freezer and green crystals were collected after 3 days under -35 °C. Yield: 10 mg, 0.007 mmol, 18%. <sup>1</sup>H NMR (499.9 MHz, C<sub>6</sub>D<sub>6</sub>, 20 °C):  $\delta$  = 6.99 (s, 12H, *m*-Mes), 6.89 (d, 6H, *J* = 5 Hz, *m*-Ph), 6.84 (t, 3H, *J* = 5 Hz, *m*-Ph), 2.34 (s, 18H, *p*-Mes), 2.09 (s, 36H, *o*-Mes) ppm. <sup>13</sup>C{<sup>1</sup>H} NMR (125.7 MHz, C<sub>6</sub>D<sub>6</sub>, 20 °C):  $\delta$  = 205.7 (CNR), 164.2 (CO), 139.2, 137.7, 135.7, 135.6, 134.4, 129.1, 129.0, 125.4, 20.6 (*p*-Mes), 20.4 (*o*-Mes) ppm. (One CO resonance could not be detected with the CNR and CO resonance extremely broadened, presumably due to coupling to <sup>59</sup>Co (*I* = 7/2, 100 %)). <sup>31</sup>P{<sup>1</sup>H} NMR (121.47 MHz, C<sub>6</sub>D<sub>6</sub>, 20 °C):  $\delta$  = 751 (s,  $\mu_3$ -P) ppm. FTIR (C<sub>6</sub>H<sub>6</sub>, KBr windows, 25 °C):  $\nu_{\text{CN}}$  and  $\nu_{\text{CO}}$  = 2087 (vs), 2068 (vs), 1995 (s), 1957 (m), 1812 (w) cm<sup>-1</sup> also, 2956 (m), 2914 (vw), 2867 (w) cm<sup>-1</sup>.

**Synthesis of NaCo(CO)<sub>3</sub>(CNAr<sup>Dipp2</sup>) (5).** Sodium amalgam (Na(Hg); 0.045 g, 2.5 mmol, 10 equiv, 0.1 wt%) was added to a stirring benzene solution of Co<sub>2</sub>(CO)<sub>4</sub>(CNAr<sup>Dipp2</sup>)<sub>2</sub> (0.280 g, 0.247 mmol, 10 mL). The resulting mixture was stirred for 2 h then filtered through Celite. A color change from dark brown to pale yellow was observed. The yellow filtrate was concentrated to a solid under vacuum. The solid residue was stirred in n-pentane (10 mL) for

20 min then reconcentrated to a solid. This step was repeated two additional times. Thereafter, the yellow product was suspended in n-pentane (2 mL), filtered, then washed with n-pentane (3 x 1 mL). The light-yellow precipitate was collected and dried in vacuo. Yield: 0.280 g, 0.474 mmol, 96 %. Single crystals of  $\text{NaCo}(\text{CO})_3(\text{CNAr}^{\text{Dipp}2})$  (**1**) were obtained by layering n-pentane on top of a concentrated THF solution followed by storage at  $-35\text{ }^\circ\text{C}$ .  $^1\text{H}$  NMR (499.9 MHz,  $\text{C}_6\text{D}_6$ ,  $20\text{ }^\circ\text{C}$ ):  $\delta = 7.37$  (t, 2H,  $J = 7$  Hz, *p*-Dipp), 7.30 (d, 4H,  $J = 7$  Hz, *m*-Dipp), 6.91 (m, 3H, *p*-Ph and *m*-Ph), 2.77 (sept,  $J = 13.5$  Hz, 4H,  $\text{CH}(\text{CH}_3)_2$ ), 1.42 (d,  $J = 13.5$  Hz, 12H,  $\text{CH}(\text{CH}_3)_2$ ), 1.13 (d,  $J = 13.5$  Hz, 12H,  $\text{CH}(\text{CH}_3)_2$ ) ppm.  $^{13}\text{C}\{^1\text{H}\}$  NMR (125.7 MHz,  $\text{C}_6\text{D}_6$ ,  $20\text{ }^\circ\text{C}$ ):  $\delta = 147.3$ , 137.6, 136.06, 130.8, 129.3, 129.2, 128.6, 126.1, 123.4, 31.4, 24.8, 24.1 ppm. (The CNR and CO resonance cannot be detected, presumably due to coupling to  $^{59}\text{Co}$  ( $I = 7/2$ , 100 %)). FTIR ( $\text{C}_6\text{H}_6$ , KBr windows,  $25\text{ }^\circ\text{C}$ ):  $\nu_{\text{CN}}$  and  $\nu_{\text{CO}} = 2060$  (s), 1943 (vs), 1898 (s), 1818 (s)  $\text{cm}^{-1}$  also, 2959 (m), 2925 (vw), 2864 (w)  $\text{cm}^{-1}$ .

**Synthesis of  $\text{Co}_3(\mu_3\text{-P})(\mu_2\text{-C-CO})_3(\text{CO})_3(\text{CNAr}^{\text{Dipp}2})_3$  (**6**).** A benzene solution of  $\text{PCl}_3$  (4.9  $\mu\text{L}$ , 0.057 mmol, 0.33 equiv., 1 mL) was added dropwise to a benzene slurry of  $\text{Na}[\text{Co}(\text{CO})_3(\text{CNAr}^{\text{Dipp}2})]$  (100 mg, 0.17 mmol, 1 equiv., 1 mL) at room-temperature. An immediate color change from light yellow to dark brown was observed. After 1-hour reaction time, the solution was filtered through celite and collected as a brown solid after drying under vacuum. The solid was then washed with pentane twice (10mL \* 2), dissolved in ether or DME for recrystallization under  $-35\text{ }^\circ\text{C}$ . Single crystals suitable for X-ray determination was collected after 1 day. Yield: 80 mg, 0.048 mmol, 95 %.  $^1\text{H}$  NMR (499.9 MHz,  $\text{C}_6\text{D}_6$ ,  $20\text{ }^\circ\text{C}$ ):  $\delta = 7.46$  (t, 2H,  $J = 5$  Hz, *p*-Dipp), 7.30 (d, 4H,  $J = 5$  Hz, *m*-Dipp), 7.02 (d, 2H,  $J = 5$  Hz, *m*-Ph), 6.94 (t, 1H,  $J = 5$  Hz, *p*-Ph), 2.74 (sept,  $J = 10$  Hz, 4H,  $\text{CH}(\text{CH}_3)_2$ ), 1.38 (d,  $J = 10$  Hz, 12H,  $\text{CH}(\text{CH}_3)_2$ ), 1.17 (d,  $J = 10$

Hz, 12H, CH(CH<sub>3</sub>)<sub>2</sub>) ppm. <sup>13</sup>C{<sup>1</sup>H} NMR (125.7 MHz, C<sub>6</sub>D<sub>6</sub>, 20 °C): δ = 215.2 (CNR), 166.1 (CO), 146.3, 139.5, 134.7, 129.8, 129.6, 129.3, 127.9, 127.8, 127.6, 123.5, 31.5, 25.0, 24.2 ppm. (One CO resonance could not be detected with the CNR and CO resonance extremely broadened, presumably due to coupling to <sup>59</sup>Co (*I* = 7/2, 100 %)). <sup>31</sup>P{<sup>1</sup>H} NMR (121.47 MHz, C<sub>6</sub>D<sub>6</sub>, 20 °C): δ = 503 (s, μ<sub>3</sub>-P) ppm. FTIR (C<sub>6</sub>H<sub>6</sub>, KBr windows, 25 °C): νCN and νCO = 2104 (vs), 2020 (s), 1993 (s), 1854 (s) cm<sup>-1</sup> also, 2961 (m), 2925 (vw), 2867 (w) cm<sup>-1</sup>.

**Synthesis of Co<sub>3</sub>(μ<sub>3</sub>-P)(CO)<sub>6</sub>(CNAr<sup>Dipp2</sup>)<sub>3</sub>AuCl (7).** A THF solution of (Me<sub>2</sub>S)AuCl (5.36 mg, 0.018 mmol, 1 equiv., 1 mL) was added dropwise to a benzene solution of Co<sub>3</sub>(μ<sub>3</sub>-P)(μ<sub>2</sub>-C-CO)<sub>3</sub>(CO)<sub>3</sub>(CNAr<sup>Dipp2</sup>)<sub>3</sub> (**6**) (30 mg, 0.018 mmol, 1 equiv., 1 mL) at room-temperature. An immediate color change from brown to dark purple was observed immediately. The reaction was concentrated to a green solid under vacuum. The solid residue was stirred in n-pentane (10 mL) for 20 min then reconcentrated to a solid. Dark green single crystals suitable for X-ray diffraction was collected after recrystallization in ether under room-temperature over 2 days. Yield: 30 mg, 0.016 mmol, 88 %. <sup>1</sup>H NMR (499.9 MHz, C<sub>6</sub>D<sub>6</sub>, 20 °C): δ = 7.70 (t, 2H, *J* = 10 Hz, *p*-Dipp), 7.52 (d, 4H, *J* = 10 Hz, *m*-Dipp), 7.09 (d, 2H, *J* = 5 Hz, *m*-Ph), 6.93 (t, 1H, *J* = 5 Hz, *p*-Ph), 2.56 (sept, *J* = 10 Hz, 4H, CH(CH<sub>3</sub>)<sub>2</sub>), 1.46 (d, *J* = 10 Hz, 12H, CH(CH<sub>3</sub>)<sub>2</sub>), 1.07 (d, *J* = 10 Hz, 12H, CH(CH<sub>3</sub>)<sub>2</sub>) ppm. <sup>13</sup>C{<sup>1</sup>H} NMR (125.7 MHz, C<sub>6</sub>D<sub>6</sub>, 20 °C): δ = 203.5 (CNR), 157.0 (CO), 154.3 (CO), 146.1, 139.4, 133.9, 130.6, 130.3, 128.4, 128.1, 127.9, 124.2, 31.3, 25.9, 24.1 ppm. (The CNR and CO resonance extremely broadened, presumably due to coupling to <sup>59</sup>Co (*I* = 7/2, 100 %)). <sup>31</sup>P{<sup>1</sup>H} NMR (121.47 MHz, C<sub>6</sub>D<sub>6</sub>, 20 °C): δ = 499 (s, μ<sub>4</sub>-P) ppm. FTIR (C<sub>6</sub>H<sub>6</sub>, KBr windows, 25 °C): νCN and νCO = 2130 (vs), 2112 (sh), 2048 (s), 2018 (s), 2007 (s) cm<sup>-1</sup> also, 2967 (m), 2925 (vw), 2867 (w) cm<sup>-1</sup>.

**Synthesis of  $[\text{Co}_4(\mu_4\text{-P})(\text{CO})_8(\text{CNAr}^{\text{Mes}2})_5]\text{CoBr}_3$  (8).** A THF solution of  $[\text{Co}(\text{CO})_3(\text{CNAr}^{\text{Mes}2})_2]\text{CoBr}_3\cdot\text{Et}_2\text{O}$  (**11**) (8 mg, 0.006 mmol, 1 equiv., 1 mL) was added dropwise to a benzene solution of  $\text{Co}_3(\mu_3\text{-P})(\text{CO})_6(\text{CNAr}^{\text{Mes}2})_3$  (**4**) (10 mg, 0.006 mmol, 1 equiv., 1 mL) at room-temperature. The reaction turned green after 10 minutes and was continued to stir for 12 hours before concentrated to a green solid under vacuum. Benzene was added and filtered through celite. Thereafter, the product was recrystallized in ether at room-temperature. Dark green single crystals suitable for X-ray diffraction was collected after 2 days. Yield: 10 mg, 0.004mmol, 66 %. FTIR ( $\text{C}_6\text{H}_6$ , KBr windows, 25 °C):  $\nu_{\text{CN}}$  and  $\nu_{\text{CO}} = 2107$  (vs), 2112 (sh), 2045 (s), 2018 (vs), 1990 (m), 1968 (sh)  $\text{cm}^{-1}$  also, 2967 (m), 2925 (vw), 2867 (w)  $\text{cm}^{-1}$ .

**Synthesis of  $[\text{Co}_3(\mu_3\text{-P-PCH}_3)(\text{CO})_6(\text{CNAr}^{\text{Dipp}2})_3]\text{OTf}$  (9).** Methyltriflate (2.99 mg, 0.018 mmol, 4.9  $\mu\text{L}$ , 1 equiv.) was added to a thawing ether solution of  $\text{Co}_3(\mu_3\text{-P})(\mu_2\text{-C-CO})_3(\text{CO})_3(\text{CNAr}^{\text{Dipp}2})_3$  (**6**) (30 mg, 0.018 mmol, 1 equiv., 1 mL). The solution turned black after 10 minutes at room-temperature. The reaction mixture was then pumped down as a purple solid and washed with pentane. Purple single crystal suitable for X-ray diffraction was collected after recrystallization in ether:benzene (9:1) under -35 °C over 2 days. Yield: 20 mg, 0.011 mmol, 62 %.  $^1\text{H}$  NMR (300.0 MHz,  $\text{C}_6\text{D}_6$ , 20 °C):  $\delta = 7.93$  (t, 2H,  $J = 8$  Hz, *p*-Dipp), 7.55 (d, 4H,  $J = 8$  Hz, *m*-Dipp), 6.96 (d, 2H,  $J = 6$  Hz, *m*-Ph), 6.94 (t, 1H,  $J = 6$  Hz, *p*-Ph), 2.75 (d,  $J = 15$  Hz, 3H,  $\text{CH}_3$ ), 2.47 (sept,  $J = 9$  Hz, 4H,  $\text{CH}(\text{CH}_3)_2$ ), 1.30 (d,  $J = 9$  Hz, 12H,  $\text{CH}(\text{CH}_3)_2$ ), 1.05 (d,  $J = 9$  Hz, 12H,  $\text{CH}(\text{CH}_3)_2$ ) ppm.  $^{13}\text{C}\{^1\text{H}\}$  NMR (125.7 MHz,  $\text{C}_6\text{D}_6$ , 20 °C):  $\delta = 151.9, 146.1, 139.7, 133.3, 131.3, 130.5, 128.6, 128.2, 127.9, 124.3, 31.4, 25.6, 23.8$  ppm. (The CNR and CO resonance could not be detected, presumably due to coupling to  $^{59}\text{Co}$  ( $I = 7/2$ , 100 %)).  $^{31}\text{P}\{^1\text{H}\}$



NMR (121.47 MHz, C<sub>6</sub>D<sub>6</sub>, 20 °C):  $\delta$  = 453 (s,  $\mu_4$ -P) ppm. FTIR (C<sub>6</sub>H<sub>6</sub>, KBr windows, 25 °C):  $\nu_{\text{CN}}$  and  $\nu_{\text{CO}}$  = 2148(vs), 2070 (s), 2043 (s) cm<sup>-1</sup> also, 2970 (m), 2923 (vw), 2867 (w), 1271 (m), 1154 (m), 1032 (m) cm<sup>-1</sup>.

**Synthesis of Co<sub>3</sub>( $\mu_3$ -P-PS)(CO)<sub>6</sub>(CNAr<sup>Dipp2</sup>)<sub>3</sub> (10).** Elemental sulfur (3 mg, 0.012 mmol, 1 equiv.) was added to a benzene solution of Co<sub>3</sub>( $\mu_3$ -P)( $\mu_2$ -C-CO)<sub>3</sub>(CO)<sub>3</sub>(CNAr<sup>Dipp2</sup>)<sub>3</sub> (**6**) (20 mg, 0.012 mmol, 1 equiv., 1 mL) as a solid at room-temperature. The reaction turned dark after 20 minutes and continued to stir for 2 hours. The solution was filtered through celite and pumped down as a purple solid. Single crystals suitable for X-ray diffraction was collected after recrystallization in ether:benzene (9:1) under -35 °C over 2 days. Yield: 10 mg, 0.006 mmol, 50 %. <sup>1</sup>H NMR (499.9 MHz, C<sub>6</sub>D<sub>6</sub>, 20 °C):  $\delta$  = 7.47 (t, 2H,  $J$ =10 Hz,  $p$ -Dipp), 7.34 (d, 4H,  $J$  = 10 Hz,  $m$ -Dipp), 7.05 (d, 2H,  $J$  = 5 Hz,  $m$ -Ph), 6.92 (t, 1H,  $J$  = 5 Hz,  $p$ -Ph), 2.67 (sept,  $J$  = 10 Hz, 4H, CH(CH<sub>3</sub>)<sub>2</sub>), 1.44 (d,  $J$  = 10 Hz, 12H, CH(CH<sub>3</sub>)<sub>2</sub>), 1.11 (d,  $J$  = 10 Hz, 12H, CH(CH<sub>3</sub>)<sub>2</sub>) ppm. <sup>13</sup>C{<sup>1</sup>H} NMR (125.7 MHz, C<sub>6</sub>D<sub>6</sub>, 20 °C):  $\delta$  = 203.8 (CNR), 162.2 (CO), 154.4 (CO), 146.7, 139.3, 134.6, 130.5, 129.7, 128.3, 128.2, 127.9, 123.6, 31.3, 25.7, 23.9 ppm. (The CNR and CO resonance extremely broadened, presumably due to coupling to <sup>59</sup>Co ( $I$  = 7/2, 100 %)). <sup>31</sup>P{<sup>1</sup>H} NMR (121.47 MHz, C<sub>6</sub>D<sub>6</sub>, 20 °C):  $\delta$  = 465 (s,  $\mu_4$ -P) ppm. FTIR (C<sub>6</sub>H<sub>6</sub>, KBr windows, 25 °C):  $\nu_{\text{CN}}$  and  $\nu_{\text{CO}}$  = 2115 (vs), 2095 (sh), 2034 (s), 2009 (s) cm<sup>-1</sup> also, 2956 (m), 2923 (vw), 2875 (w), 1729 (w), 1687 (w), 1243 (w) cm<sup>-1</sup>.

**Synthesis of [Co(CO)<sub>3</sub>(CNAr<sup>Mes2</sup>)<sub>2</sub>]CoBr<sub>3</sub>·Et<sub>2</sub>O (11).** BBr<sub>3</sub> (6.27 mg, 2.38  $\mu$ L, 0.025 mmol, 1 equiv.) was added to a benzene solution of Co<sub>2</sub>( $\mu_2$ -P-PCl)( $\mu_2$ -C-CO)(CO)<sub>2</sub>(CNAr<sup>Mes2</sup>)<sub>4</sub> (**3**) (40 mg, 0.025 mmol, 1 equiv., 1 mL) at room-temperature. The reaction turned green after 2 hours and was concentrated to a green solid under vacuum. Ether was added and filtered.

Thereafter, the product was recrystallized in ether at room-temperature. Dark brown-green single crystals suitable for X-ray diffraction was collected after 2 days. Yield: 10 mg, 0.012mmol, 24 %. FTIR (C<sub>6</sub>H<sub>6</sub>, KBr windows, 25 °C): ν<sub>CN</sub> and ν<sub>CO</sub> = 2168(m), 2137 (sh), 2107 (vs), 2037 (s), 2009 (m), 1968 (m) cm<sup>-1</sup> also, 2970 (m), 2923 (vw), 2867 (w), cm<sup>-1</sup>.

## 4.5 Computational Studies

**Computational details.** Density Functional Theory (DFT) calculations were carried out on compound Co<sub>3</sub>(μ<sub>3</sub>-P)(CO)<sub>6</sub>(CNXyl)<sub>3</sub> (**4m**) and Co<sub>3</sub>(μ<sub>3</sub>-P)(μ<sub>2</sub>-C-CO)<sub>3</sub>(CO)<sub>3</sub>(CNXyl)<sub>3</sub> (**6m**) with the Gaussian 09 software package.<sup>34</sup> Geometry optimizations, frequency and single point energy calculations were performed using the B3LYP<sup>35,36</sup> functional, with the 6-31g(d)<sup>37</sup> basis set for H, C, O and N atoms and the LANL2DZ basis set plus f-type polarization functions for cobalt atoms.<sup>38</sup> Viewing of optimized structures and rendering of molecular orbitals was performed using the program *Chemcraft*.<sup>39</sup>

### Input for Geometry Optimization of Co<sub>3</sub>(μ<sub>3</sub>-P)(CO)<sub>6</sub>(CNXyl)<sub>3</sub> (**4m**).

The input for the optimization of **4m** is listed below. The input for **6m** is identical except for the input coordinates.

```
%chk=4m.chk
%nprocs=8
%mem=30GB
# opt freq gen nosymm b3lyp pseudo=read

CSD ENTRY

0 1
Co 1.94300000 9.43000000 5.17600000
Co 1.37200000 10.62700000 3.03800000
Co 1.06500000 11.78500000 5.25700000
P 3.01300000 11.17400000 4.40300000
```

C	3.75900000	5.96400000	3.17700000
C	2.84700000	5.10300000	2.61000000
C	3.37700000	3.91200000	2.10200000
H	2.80300000	3.30300000	1.65300000
C	4.72200000	3.60000000	2.23700000
H	5.05500000	2.76600000	1.92600000
C	5.56700000	4.51200000	2.83200000
H	6.49200000	4.30200000	2.88600000
C	5.12600000	5.74500000	3.36200000
O	-1.29600000	9.44400000	2.64500000
O	3.17400000	9.28900000	1.18800000
N	1.45700000	12.09900000	8.20100000
O	-0.65800000	8.18300000	5.77200000
O	1.36900000	14.57800000	4.49900000
O	3.68900000	9.44000000	7.52800000
C	1.33300000	12.39400000	9.53900000
O	-1.84100000	11.30800000	5.37100000
N	1.16600000	13.24400000	1.62600000
C	2.42800000	15.00800000	0.66000000
C	0.38600000	8.68600000	5.54500000
C	2.43600000	16.25500000	0.03200000
H	3.26000000	16.64300000	-0.23700000
C	1.24200000	16.93100000	-0.19800000
H	1.25800000	17.78600000	-0.61100000
C	0.05200000	16.38100000	0.15800000
H	-0.75100000	16.85100000	-0.03200000
C	1.14100000	11.39300000	10.46900000
C	1.17500000	14.49800000	1.02500000
C	1.23500000	14.04900000	11.27700000
H	1.27500000	14.95100000	11.57000000
C	-0.01700000	15.15100000	0.79200000
C	-0.24500000	9.90600000	2.82500000
C	2.97800000	9.40300000	6.63900000
C	1.02400000	13.05700000	12.20500000
H	0.91600000	13.27400000	13.12400000
C	1.39400000	13.77300000	9.92900000
C	2.43600000	9.79400000	1.91300000
C	-0.70200000	11.44800000	5.29900000
C	0.96800000	11.75500000	11.79100000
H	0.80700000	11.07500000	12.43400000
C	1.34700000	11.94200000	7.02700000
C	1.22900000	13.49600000	4.81300000
C	1.22800000	12.20400000	2.15900000
N	3.20700000	7.18500000	3.73100000
C	2.71200000	8.06600000	4.30700000
C	1.07676410	9.91965288	10.02546644
H	0.30398006	9.80042279	9.29506312
H	2.01627226	9.63378917	9.60060603
H	0.86540857	9.30105787	10.87256092
C	1.57869787	14.86784793	8.86185675
H	2.46562730	14.66947998	8.29713881
H	0.73266195	14.87378214	8.20680866
H	1.66613335	15.82098741	9.34016646
C	3.67402723	14.14831372	0.94276428

H	3.79075695	14.02610926	1.99933432
H	3.55717053	13.18897297	0.48351507
H	4.53990006	14.63254470	0.54190945
C	-1.30113015	14.44036487	1.25848417
H	-1.33702786	13.45678241	0.83874986
H	-1.30353080	14.37275781	2.32634349
H	-2.15505172	14.99780165	0.93447463
C	6.06444335	6.77843595	4.01233393
H	6.02438649	7.69393437	3.45992278
H	5.75463744	6.95658313	5.02088928
H	7.06634119	6.40282667	4.00804494
C	1.35047150	5.43521904	2.46291851
H	0.93353877	5.63740232	3.42738158
H	1.23594897	6.29569809	1.83733046
H	0.84213142	4.60338409	2.02185052

C H N P O 0

6-31g(d)

\*\*\*\*

Co 0

f 1 1.0

2.78 1.0

\*\*\*\*

Co 0

lanl2dz

\*\*\*\*

Co 0

lanl2dz

### Optimized coordinates for $\text{Co}_3(\mu_3\text{-P})(\text{CO})_6(\text{CNXyl})_3$ (4m).

Co	0.78266661	9.12956947	4.87717214
Co	0.40460096	10.87961780	3.09921578
Co	0.06915599	11.46063590	5.53143348
P	2.04107787	10.95466164	4.61663641
C	3.71123035	6.22759330	3.35265202
C	3.47168224	4.86130362	3.60684505
C	4.41571368	3.94362201	3.13950838
H	4.25480538	2.88450950	3.32193940
C	5.55005867	4.36848639	2.44807985
H	6.27223824	3.63872293	2.09276742
C	5.75997534	5.72663834	2.21027278
H	6.64412945	6.05349377	1.66963531
C	4.84761177	6.68688041	2.65525741
O	-2.49412269	10.67734017	2.54779938
O	1.59397471	9.04589586	1.17898141
N	1.09842013	11.94164024	8.32017059
O	-1.77606868	7.75220137	4.32817491
O	-0.11473248	14.25520121	4.74305105
O	1.22692729	8.57711181	7.69925883
C	1.58572481	12.17643914	9.59352108
O	-2.73710336	10.67330572	6.03348685

N	1.11370315	13.41530553	1.63698338
C	2.37975823	15.45149015	1.46837951
C	-0.79146582	8.31134826	4.54114655
C	2.68560365	16.59407374	0.72457265
H	3.41200232	17.29912416	1.11970006
C	2.07422080	16.83806070	-0.50505123
H	2.32642687	17.73314205	-1.06680265
C	1.13894731	15.93807556	-1.01555472
H	0.66365662	16.13245020	-1.97325214
C	0.95757502	11.54258556	10.68538816
C	1.43256581	14.55881332	0.92580277
C	3.16283683	13.26234637	11.03884146
H	4.01341356	13.92327367	11.18243794
C	0.79658064	14.77987029	-0.31333195
C	-1.36865326	10.74164790	2.78547366
C	1.04362681	8.83200316	6.58667208
C	2.56123243	12.65015851	12.13831552
H	2.94452892	12.83566112	13.13782228
C	2.69009895	13.04054876	9.74303799
C	1.12428673	9.74900949	1.96730588
C	-1.64466311	10.96772115	5.81642850
C	1.47047655	11.79942184	11.95935757
H	1.00585321	11.32306542	12.81845884
C	0.70599417	11.72854421	7.23175343
C	-0.04180775	13.13566906	5.02180768
C	0.83782331	12.44328476	2.23971331
N	2.79166126	7.15545089	3.80971609
C	2.00956312	7.94492275	4.19590295
C	-0.21631641	10.62180264	10.47182635
H	-1.05269922	11.14384145	9.99024923
H	0.05128694	9.78085781	9.82154932
H	-0.57160811	10.21953893	11.42467724
C	3.32598841	13.69409923	8.54275191
H	3.66127978	12.95041300	7.80977448
H	2.61792035	14.35176526	8.02298402
H	4.18979781	14.29494867	8.84090847
C	3.02278871	15.17741317	2.80365457
H	2.27332773	15.13877772	3.60284985
H	3.54245886	14.21163161	2.81079589
H	3.74804986	15.95774117	3.05126235
C	-0.21335696	13.79745665	-0.84915728
H	0.22685557	12.80195306	-0.98604775
H	-1.05971182	13.67762784	-0.16170601
H	-0.60465310	14.13093261	-1.81435713
C	5.05445184	8.15742113	2.39794345
H	4.24546493	8.56920564	1.78322627
H	5.06649585	8.73242031	3.33175739
H	6.00104596	8.32973484	1.87796915
C	2.23981540	4.41899760	4.35464274
H	2.20283037	4.85337025	5.36133861
H	1.32343461	4.73310813	3.83995458
H	2.21680941	3.33021397	4.45420730

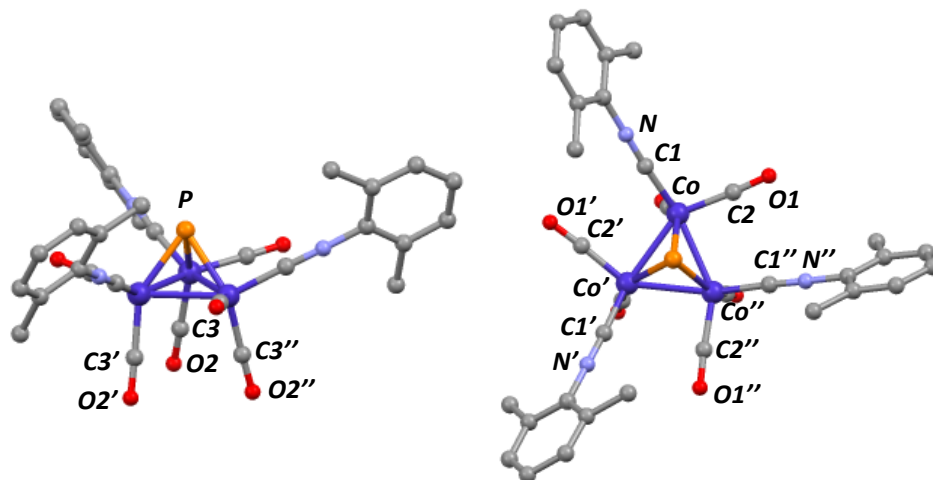


**Figure 4.3.** Geometry optimized structure of  $\text{Co}_3(\mu_3\text{-P})(\text{CO})_6(\text{CNXyl})_3$  (4m) with hydrogen atoms omitted for clarity. (B3LYP/6-31G(d):LANL2DZ)

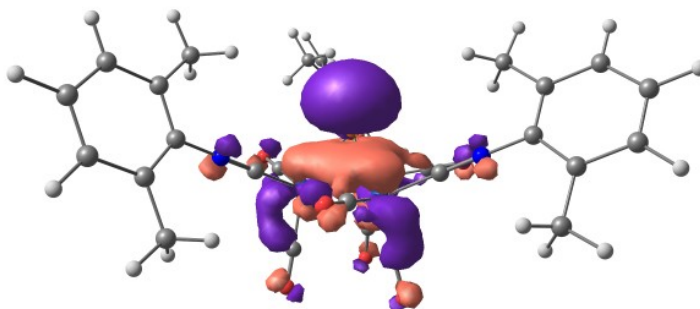


**Figure 4.4.** Highest occupied molecular orbital (HOMO) of  $\text{Co}_3(\mu_3\text{-P})(\text{CO})_6(\text{CNXyl})_3$  (4m) showing the phosphine lone-pair character.

**Table 4.2.** Comparison of calculated and experimental structural parameters between **4m** and **4**.

Parameter	Calculated	Experimental
d(Co-Co) avg.	2.523 Å	2.517(3) Å
d(Co-P) avg.	2.232 Å	2.201(4) Å
d(Co <sub>3</sub> centroid-P)	1.691 Å	1.653 Å
d(Co-C3) avg	1.800 Å	1.780(1) Å
d(Co-C1) avg	1.835 Å	1.800(1) Å
∠ Co-Co-Co avg.	60°	60.19(8)°
Σ Co-P-Co	206.45°	208.9(1)°

**Optimized coordinates for Co<sub>3</sub>(μ<sub>3</sub>-P)(μ<sub>2</sub>-C-CO)<sub>3</sub>(CO)<sub>3</sub>(CNXyl)<sub>3</sub> (6m).**

Co	9.62066099	15.56002509	27.93289451
Co	11.92382035	16.54873452	27.53231469
Co	10.76218442	15.30101971	25.68360275
P	11.48875151	14.30466108	27.61071765
N	7.48920441	17.71636534	27.79114888
N	11.46492610	12.96722162	23.94809405
C	15.87671878	15.47526291	30.76075354
N	14.55743005	16.29371003	28.92870883
C	6.50449704	18.68842822	27.73288875
C	16.90772498	16.78722936	28.93069521
C	15.79052105	16.18527421	29.54557933
C	5.33516439	18.50380109	28.49919043
C	18.14193931	16.65906851	29.57296832
H	19.01988628	17.11197443	29.12011103
C	11.44827448	10.60541175	23.51024083
C	17.13446314	15.37942409	31.36163151
H	17.22898859	14.83815800	32.29918897
C	11.82313253	11.91058245	23.13079789
C	4.35554409	19.49695984	28.42568125
H	3.44401533	19.38095614	29.00564935
C	18.25784553	15.96361043	30.77650652
H	19.22696588	15.87624766	31.25975134
C	12.54739589	9.79889662	21.49769488
H	12.83228206	8.96932862	20.85657510
C	12.90511251	11.10120204	21.14871343
H	13.46770730	11.28484480	20.23726500
C	12.55110934	12.18599545	21.95486518
C	6.71418866	19.81577103	26.91238407
C	11.82606306	9.55739499	22.66684739
H	11.55002775	8.54118443	22.93520741
C	5.70198180	20.77861761	26.87680013
H	5.83587889	21.65807744	26.25296905

C	4.53447796	20.62422856	27.62388839
H	3.76048307	21.38539309	27.58093756
C	8.31945229	16.88634368	27.84102289
O	10.73787455	17.12482047	30.16838100
C	13.51556911	16.37632079	28.38758694
C	11.18754869	13.87047263	24.64969741
O	13.46571691	16.28064417	25.03750654
O	8.48822125	13.72218044	29.87989510
C	10.75600305	16.65716490	29.09826590
O	11.72864645	19.43781846	27.01468885
O	8.04060980	14.18573807	25.85581153
C	11.80822079	18.30629287	27.21507066
C	8.95094395	14.44243021	29.10711962
C	12.53176256	16.13150175	25.72639922
C	8.98767806	14.73221206	26.26658838
O	9.67315733	17.24672407	23.76519536
C	10.10314930	16.48329625	24.51303664
C	10.67065475	10.36524614	24.77894763
H	11.21206838	10.73633539	25.65764195
H	9.70444155	10.88435902	24.76151626
H	10.48030864	9.29774994	24.92095573
C	12.92407664	13.60094789	21.59269330
H	12.03239720	14.22070801	21.43464626
H	13.50508293	14.08250157	22.38845714
H	13.51796713	13.62254705	20.67459978
C	16.76161761	17.53968030	27.63262627
H	16.32650135	16.91075658	26.84665571
H	16.09798144	18.40619154	27.74604695
H	17.73269998	17.90119975	27.28282074
C	14.65141723	14.84894152	31.37578901
H	13.88283252	15.60061013	31.59386586
H	14.19344474	14.11646036	30.69993557
H	14.90362622	14.33956836	32.31008843
C	7.97988973	19.96797744	26.10840979
H	8.86888089	19.97911471	26.75025147
H	8.11093089	19.14105448	25.40003323
H	7.96468488	20.90077818	25.53797434
C	5.16087306	17.27868209	29.35987891
H	5.20334975	16.35928684	28.76302058
H	5.95239091	17.20295741	30.11559488
H	4.19827408	17.30298361	29.87799117



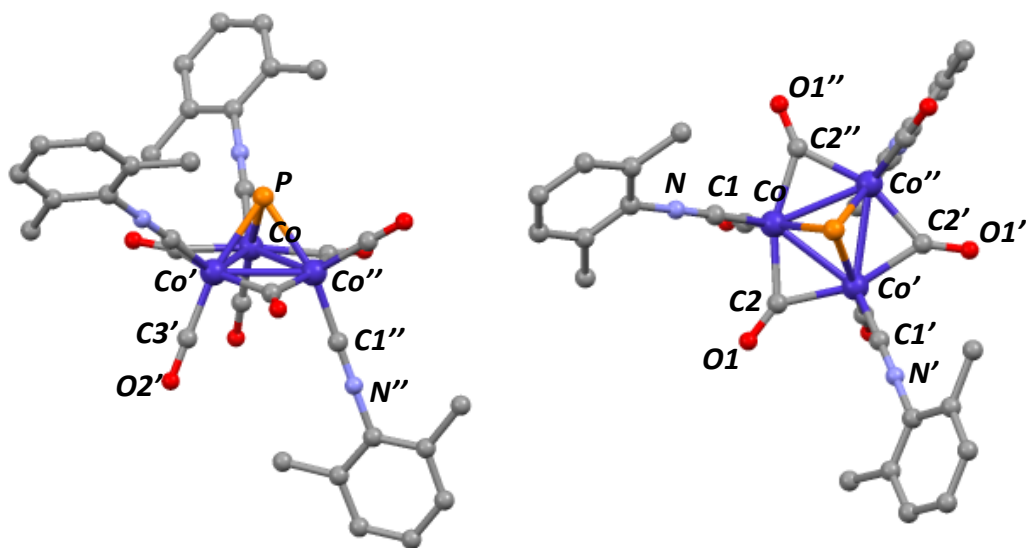


**Figure 4.5.** Geometry optimized structure of  $\text{Co}_3(\mu_3\text{-P})(\mu_2\text{-C-CO})_3(\text{CO})_3(\text{CNXyl})_3$  (**6m**) with hydrogen atoms omitted for clarity. (B3LYP/6-31G(d):LANL2DZ)

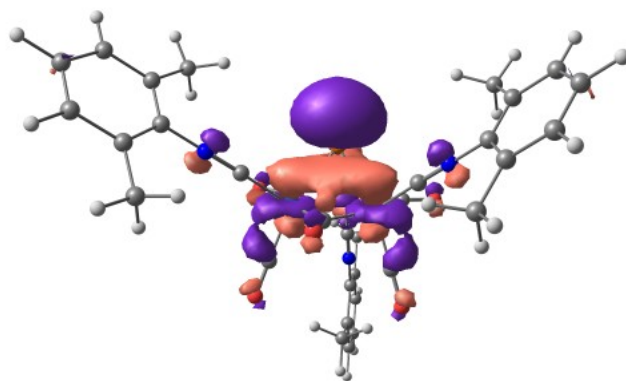


**Figure 4.6.** Highest occupied molecular orbital -2 (HOMO-2) of  $\text{Co}_3(\mu_3\text{-P})(\mu_2\text{-C-CO})_3(\text{CO})_3(\text{CNXyl})_3$  (**6m**) showing the phosphine lone-pair character.

**Table 4.3.** Comparison of calculated and experimental structural parameters between **6m** and **6**.

Parameter	Calculated	Experimental
d(Co-Co) avg.	2.529 Å	2.529(3) Å
d(Co-P) avg.	2.282 Å	2.252(5) Å
d(Co <sub>3</sub> centroid-P)	1.755 Å	1.715 Å
d(Co-C3) eq.	1.754 Å	1.77(2) Å
d(Co''-C3'') ax.	1.789 Å	1.74(2) Å
d(Co-C1) eq.	1.815 Å	1.84(2) Å
d(Co''-C1'') ax.	1.860 Å	1.81(2) Å
∠ Co-Co-Co avg.	60°	60.00(9)°
Σ Co-P-Co	206.45°	204.9(1)°

#### 4.6 Calculation of Percent Buried Volume Parameter

**General.** The percent buried volume parameter (%V<sub>bur</sub>) was determined here for Co<sub>3</sub>(μ<sub>3</sub>-P)(μ<sub>2</sub>-C-CO)<sub>3</sub>(CO)<sub>3</sub>(CNAr<sup>Dipp</sup>)<sub>3</sub> (**6**) and reported previously for complexes of PAd<sub>3</sub> and P(*t*-Bu)<sub>3</sub> using X-ray crystallographic data for (PAd<sub>3</sub>)Au(Cl)<sup>40</sup> and (P*t*-Bu<sub>3</sub>)Au(Cl)<sup>41</sup>. Percent buried volume calculation was performed using the SambVca software.<sup>42,43</sup> The following conditions were used for each calculation: sphere radius = 3.5 Å, d(M-P) = 2.28 Å, H atoms were included, and scaled Bondi radii were used.

**Table 4.4.** Summary of %V<sub>bur</sub>.

Parameter	P <i>t</i> -Bu <sub>3</sub>	PAd <sub>3</sub>	<b>6</b>
%V <sub>bur</sub>	40.0	40.3	60.6

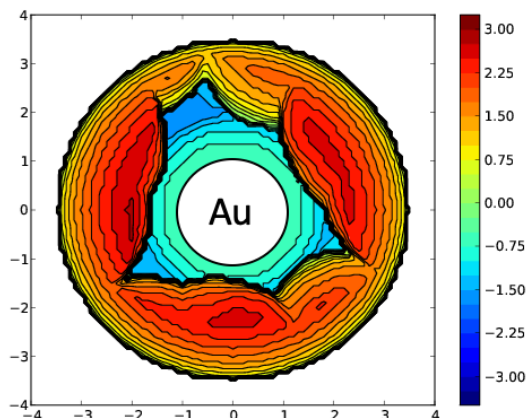


**Figure 4.7.** Steric map of **6** viewing from the top through the AuCl (See Figure 4.13 for crystal structure image).

## 4.7 Crystallographic Structure Determinations

**General.** Single crystal X-ray structure determinations were carried out at low temperature on a Bruker P4, Platform or Kappa Diffractometer equipped with a Mo or Cu radiation source and a Bruker APEX detector. All structures were solved by direct methods with SIR 2004<sup>44</sup> or SHELXS<sup>45</sup> and refined by full-matrix least-squares procedures utilizing SHELXL within Olex 2 small-molecule solution, refinement, and analysis software package.<sup>46</sup> Crystallographic data collection and refinement information are listed in Table 4.5 – 4.7.

**Information on crystallographic disorder.** All disordered components were successfully modeled and refined anisotropically unless otherwise stated.

The solid-state structure of  $\text{Co}_3(\mu_3\text{-P})(\mu_2\text{-C-CO})_3(\text{CO})_3(\text{CNAr}^{\text{Dipp}2})_3$  (**6**) exhibits positional disorder over two positions of  $\text{PCo}(\text{CO})$  group at Co3. The group was split and linked via a free variable and refined anisotropically. The structure also contains severely disordered solvent molecules of co-crystallization that could not be successfully modeled. The PLATON routine

SQUEEZE<sup>4</sup> was used to account for these disordered components as a diffuse contribution to the overall scattering without specific atom positions.

$\text{Co}_3(\mu_3\text{-P})(\text{CO})_6(\text{CNAr}^{\text{Dipp}2})_3\text{AuCl}$  (7) exhibits a positional disorder. The core of  $\text{Co}_3$  is rotated  $60^\circ$  degrees. The group was split and linked via a free variable and refined anisotropically.

$\text{Co}_3(\mu_3\text{-P-PS})(\text{CO})_6(\text{CNAr}^{\text{Dipp}2})_3$  (10)  $\cdot 2\text{C}_6\text{H}_6$  contains severely disordered solvent molecules of co-crystallization that could not be successfully modeled. The PLATON routine SQUEEZE<sup>4</sup> was used to account for these disordered components as a diffuse contribution to the overall scattering without specific atom positions.

$[\text{Co}(\text{CO})_3(\text{CNAr}^{\text{Mes}2})_2]\text{CoBr}_3\cdot\text{Et}_2\text{O}$  (11) contains severely disordered solvent molecules of co-crystallization that could not be successfully modeled. The PLATON routine SQUEEZE<sup>4</sup> was used to account for these disordered components as a diffuse contribution to the overall scattering without specific atom positions.

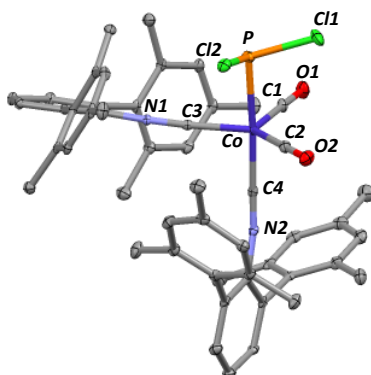


**Figure 4.8.** Molecular structure of  $(\text{PCl}_2)\text{Co}(\text{CO})_2(\text{CNAr}^{\text{Mes}2})_2$  (2), with benzene solvent molecule and hydrogen atoms omitted for clarity. Selected distances ( $\text{\AA}$ ) and angles ( $^\circ$ ):  $\text{Co-P} = 2.241(1)$ ,  $\text{Co-C1} = 1.781(3)$ ,  $\text{Co-C2} = 1.781(4)$ ,  $\text{Co-C3} = 1.870(4)$ ,  $\text{Co-C4} = 1.866(4)$ ,  $\text{C4-N2} = 1.157(5)$ ,  $\text{C3-N1} = 1.165(5)$ ,  $\text{P-Co-C1} = 88.9(1)$ ,  $\text{P-Co-C3} = 83.6(1)$ ,  $\text{P-Co-C2} = 88.9(1)$ ,  $\text{C3-Co-C4} = 93.4(2)$ ,  $\text{C2-Co-C4} = 90.6(2)$ ,  $\text{C1-Co-C4} = 95.7(2)$ .

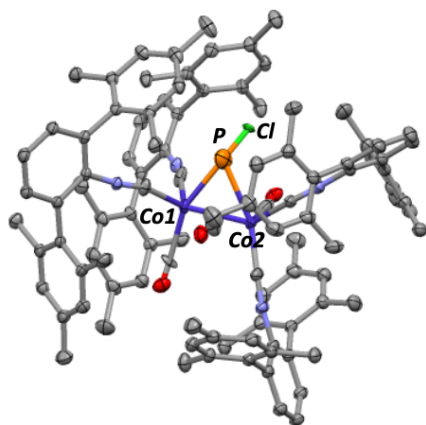


**Figure 4.9.** Molecular structure of  $\text{Co}_2(\mu_2\text{-P-PCl})(\mu_2\text{-C-CO})(\text{CO})_2(\text{CNAr}^{\text{Mes}_2})_4$  (**3**), with benzene solvent molecule and hydrogen atoms omitted for clarity.

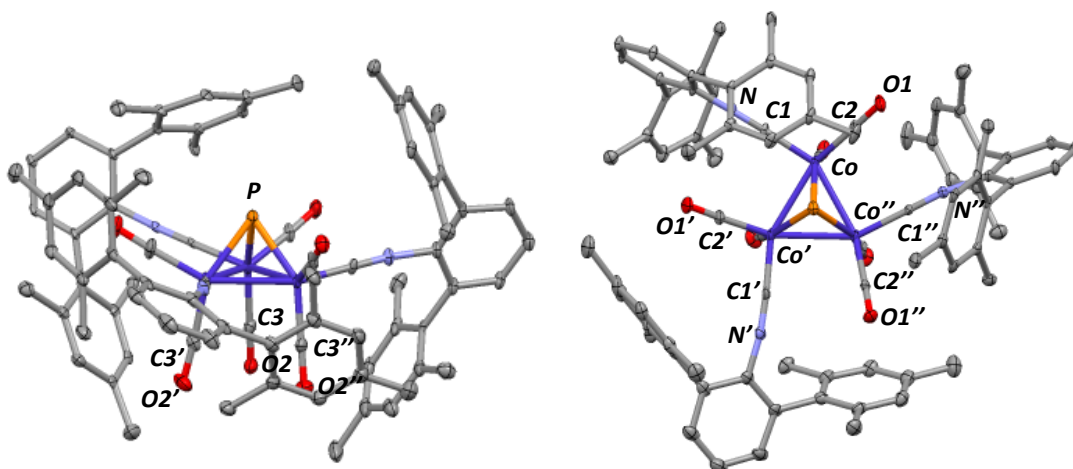


**Figure 4.10.** Molecular structure of  $\text{Co}_3(\mu_3\text{-P})(\text{CO})_6(\text{CNAr}^{\text{Mes}_2})_3$  (**4**) with hydrogen atoms omitted for clarity. Selected distances (Å) and angles (°): Co-Co avg. = 2.517(3), Co-P avg. = 2.201(4),  $\text{Co}_{3\text{centroid}}\text{-P}$  = 1.653, Co-C3 avg. = 1.780(1), Co-C1 avg. = 1.800(1), Co-Co-Co avg. = 60.19(8),  $\Sigma$  Co-P-Co = 208.9(1).

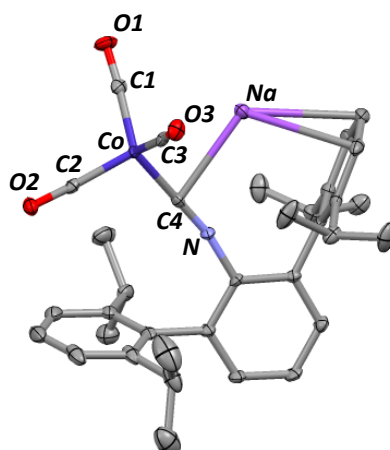


**Figure 4.11.** Molecular structure of  $\text{NaCo}(\text{CO})_3(\text{CNAr}^{\text{Dipp}2})$  (**5**) with hydrogen atoms omitted for clarity. Selected distances ( $\text{\AA}$ ) and angles ( $^\circ$ ):  $\text{Co-C1} = 1.766(5)$ ,  $\text{Co-C2} = 1.751(4)$ ,  $\text{Co-C3} = 1.762(4)$ ,  $\text{Co-C4} = 1.819(4)$ ,  $\text{C4-N} = 1.178(5)$ ,  $\text{C4-Co-C1} = 121.3(2)$ ,  $\text{C4-Co-C2} = 105.4(2)$ ,  $\text{C4-Co-C3} = 108.8(2)$ .

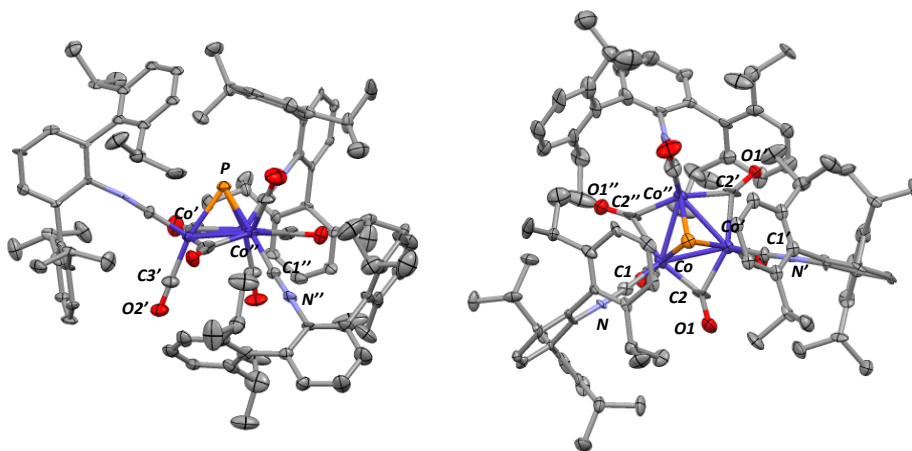


**Figure 4.12.** Molecular structure of  $\text{Co}_3(\mu_3\text{-P})(\mu_2\text{-C-CO})_3(\text{CO})_3(\text{CNAr}^{\text{Dipp}2})_3$  (**6**) with hydrogen atoms omitted for clarity. Selected distances ( $\text{\AA}$ ) and angles ( $^\circ$ ):  $\text{Co-Co avg.} = 2.529(3)$ ,  $\text{Co-P avg.} = 2.252(5)$ ,  $\text{Co}_{3\text{centroid}}\text{-P} = 1.715$ ,  $\text{Co-C3 eq.} = 1.77(2)$ ,  $\text{Co}''\text{-C3}'' = 1.74(2)$ ,  $\text{Co-C1 eq.} = 1.84(2)$ ,  $\text{Co}''\text{-C1}'' = 1.81(2)$ ,  $\text{Co-Co-Co avg.} = 60.00(9)$ ,  $\Sigma \text{Co-P-Co} = 204.9(1)$ .

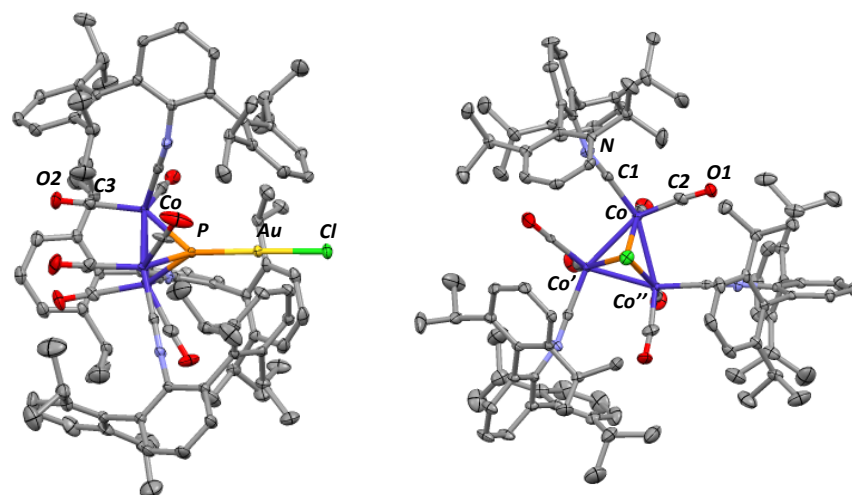


**Figure 4.13.** Molecular structure of  $\text{Co}_3(\mu_3\text{-P})(\text{CO})_6(\text{CNAr}^{\text{Dipp}2})_3\text{AuCl}$  (**7**) with hydrogen atoms omitted for clarity. Selected distances (Å) and angles ( $^\circ$ ):  $\text{Co-Co}' = 2.5514(7)$ ,  $\text{Co}'\text{-Co}'' = 2.5380(6)$ ,  $\text{Co}''\text{-Co} = 2.5973(7)$ ,  $\text{Co-P} = 2.1428(7)$ ,  $\text{Co}'\text{-P} = 2.1604(7)$ ,  $\text{Co}''\text{-P} = 2.1375(7)$ ,  $\text{Co}_{3\text{centroid}}\text{-P} = 1.559$ ,  $\text{P-Au} = 2.2065(7)$ ,  $\text{Co-C1 avg.} = 1.853$ ,  $\text{Co-C3 avg.} = 1.820$ ,  $\text{Co-Co-Co avg.} = 60.00(2)$ ,  $\Sigma \text{Co-P-Co} = 219.23(2)$ .

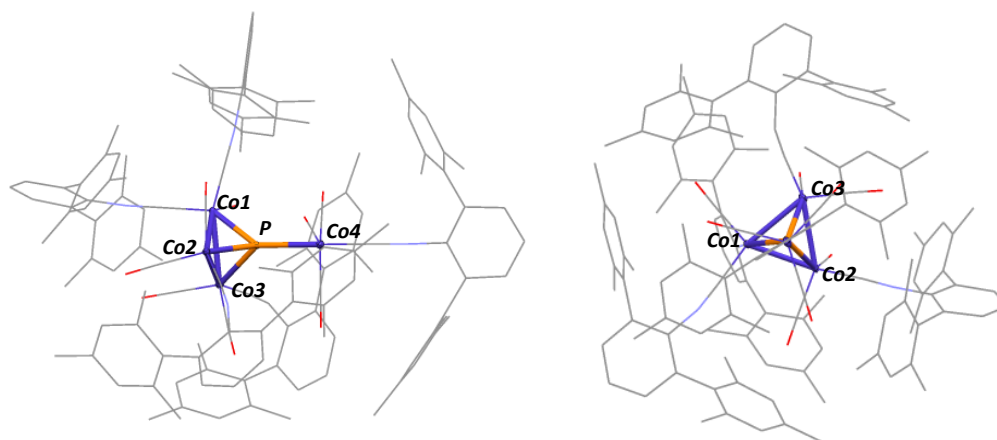


**Figure 4.14.** Molecular structure of  $[\text{Co}_4(\mu_4\text{-P})(\text{CO})_8(\text{CNAr}^{\text{Mes}2})_5]\text{CoBr}_3$  (**8**) with hydrogen atoms omitted for clarity. Selected distances (Å) and angles ( $^\circ$ ):  $\text{Co1-P} = 2.149(2)$ ,  $\text{Co2-P} = 2.152(2)$ ,  $\text{Co3-P} = 2.143(3)$ ,  $\text{Co4-P} = 2.220(3)$ ,  $\text{Co1-Co2} = 2.567(1)$ ,  $\text{Co2-Co3} = 2.552(2)$ ,  $\text{Co3-Co1} = 2.583(2)$ ,  $\text{Co}_{3\text{centroid}}\text{-P} = 1.555$ ,  $\text{Co-Co-Co avg.} = 60.00(5)$ ,  $\Sigma \text{Co-P-Co} = 220.18(8)$ .

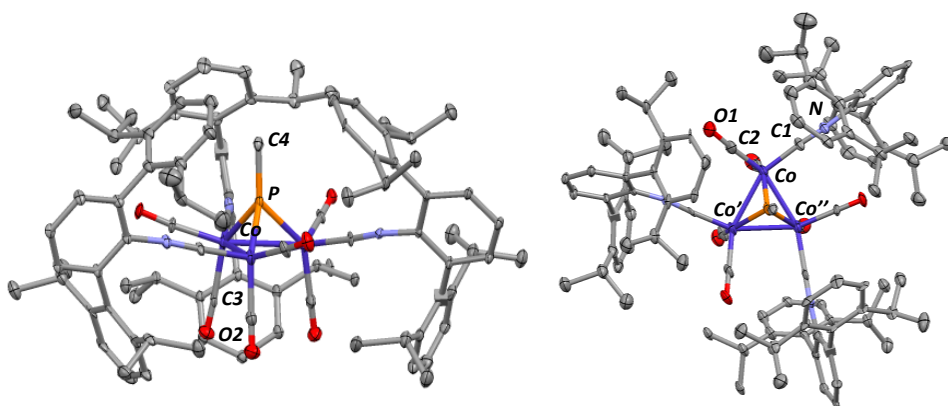


**Figure 4.15.** Molecular structure of  $[\text{Co}_3(\mu_3\text{-P-PCl}_3)(\text{CO})_6(\text{CNAr}^{\text{Dipp}2})_3]\text{OTf}$  (**9**) with triflate ion and hydrogen atoms omitted for clarity. Selected distances (Å) and angles ( $^\circ$ ): Co-Co' = 2.565(5), Co'-Co'' = 2.570(4), Co''-Co = 2.550(5), Co-P = 2.112(9), Co'-P = 2.104(7), Co''-P = 2.111(7),  $\text{Co}_{3\text{centroid}}\text{-P}$  = 1.504, P-C4 = 1.83(2), Co-C1 avg. = 1.88, Co-C3 avg. = 1.85, Co-Co-Co avg. = 60.0(1),  $\Sigma$  Co-P-Co = 225.3(2).

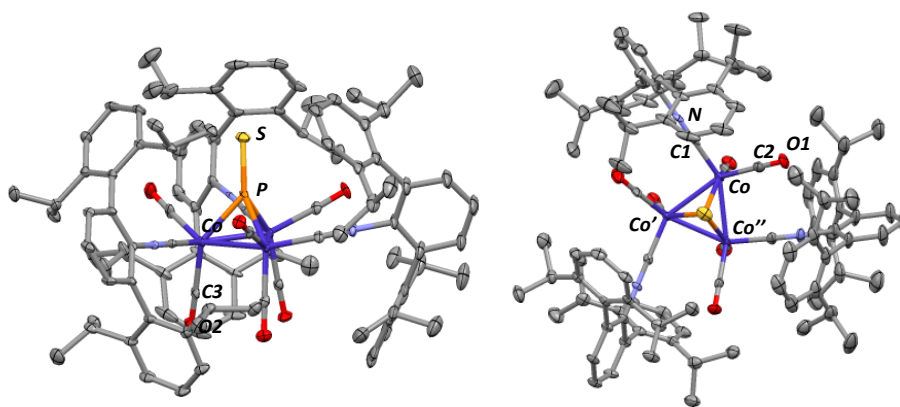


**Figure 4.16.** Molecular structure of  $\text{Co}_3(\mu_3\text{-P-PS})(\text{CO})_6(\text{CNAr}^{\text{Dipp}2})_3$  (**10**) with benzene solvent molecule and hydrogen atoms omitted for clarity. Selected distances (Å) and angles ( $^\circ$ ): Co-Co' = 2.571(1), Co'-Co'' = 2.571(1), Co''-Co = 2.555(2), Co-P = 2.151(1), Co'-P = 2.159(1), Co''-P = 2.149(2),  $\text{Co}_{3\text{centroid}}\text{-P}$  = 1.563, P-S = 1.927(2), Co-C1 avg. = 1.822, Co-C3 avg. = 1.820, Co-Co-Co = 60.21(3),  $\Sigma$  Co-P-Co = 219.40(5).



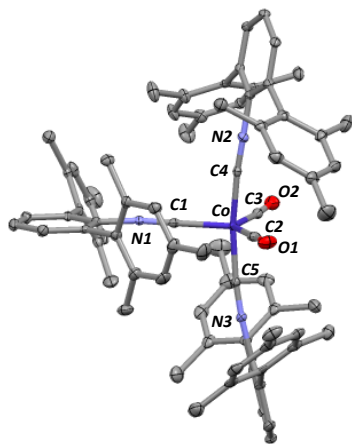


**Figure 4.17.** Molecular structure of  $[\text{Co}(\text{CO})_3(\text{CNAr}^{\text{Mes}2})_2]\text{CoBr}_3 \cdot \text{Et}_2\text{O}$  (**11**) with ether solvent and  $\text{CoBr}_3 \cdot \text{Et}_2\text{O}$  molecules plus hydrogen atoms omitted for clarity. Selected distances ( $\text{\AA}$ ) and angles ( $^\circ$ ):  $\text{Co}-\text{C}1 = 1.910(4)$ ,  $\text{Co}-\text{C}2 = 1.839(6)$ ,  $\text{Co}-\text{C}3 = 1.812(6)$ ,  $\text{Co}-\text{C}4 = 1.859(5)$ ,  $\text{Co}-\text{C}5 = 1.837(5)$ ,  $\text{C}1-\text{N}1 = 1.146(6)$ ,  $\text{C}2-\text{O}1 = 1.122(7)$ ,  $\text{C}3-\text{O}2 = 1.132(7)$ ,  $\text{C}4-\text{N}2 = 1.150(6)$ ,  $\text{C}5-\text{N}3 = 1.157(6)$ ,  $\text{C}4-\text{Co}-\text{C}1 = 95.2(2)$ ,  $\text{C}4-\text{Co}-\text{C}2 = 93.5(2)$ ,  $\text{C}4-\text{Co}-\text{C}3 = 86.3(2)$ ,  $\text{C}1-\text{Co}-\text{C}2 = 109.0(2)$ ,  $\text{C}2-\text{Co}-\text{C}3 = 131.9(3)$ ,  $\text{C}3-\text{Co}-\text{C}1 = 119.0(2)$ .

**Table 4.5. Crystallographic Data Collection and Refinement Information.**

Name	(PCl <sub>2</sub> )Co(CO) <sub>2</sub> (CNAr <sup>Mes2</sup> ) <sub>2</sub> (2) · C <sub>6</sub> H <sub>6</sub>	NaCo(CO) <sub>3</sub> (CNAr <sup>Dipp2</sup> ) <sub>3</sub> (5) · THF	Co <sub>3</sub> (μ <sub>3</sub> -P)(μ <sub>2</sub> -C-CO) <sub>3</sub> (CO) <sub>3</sub> (CNAr <sup>Dipp2</sup> ) <sub>3</sub> (6)
Formula	C58 H56 Cl2 Co N2 O2 P	C38 H44 Co N Na O4	C99 H111 Co3 N3 O6 P
Crystal System	Monoclinic	Orthorhombic	Monoclinic
Space Group	P 1 21/n 1	Fdd2	P 1 21/c 1
a, Å	12.6688(8)	32.1555(9)	26.286(3)
b, Å	21.2181(13)	33.2900(9)	15.861(2)
c, Å	19.5383(12)	13.4886(4)	26.043(3)
α, deg	90	90	90
β, deg	105.905(2)	90	92.263(2)
γ, deg	90	90	90
V, Å <sup>3</sup>	9143.4(6)	14439.0(7)	10849(2)
Z	4	16	4
Radiation (λ, Å)	Mo-K <sub>α</sub> , 0.71073	Mo-K <sub>α</sub> , 0.71073	Mo-K <sub>α</sub> , 0.71073
ρ(calcd.), g/cm <sup>3</sup>	1.281	1.216	1.008
μ, mm <sup>-1</sup>	0.521	0.525	0.513
Temp, K	100	100	100
θ max, deg	24.745	25.703	25.108
data/parameters	8600 / 607	6805 / 414	19268 / 1065
R <sub>I</sub>	0.0483	0.0379	0.0482
wR <sub>2</sub>	0.1170	0.0831	0.1265
GOF	1.011	1.024	1.043

**Table 4.6. Crystallographic Data Collection and Refinement Information.**

Name	$\text{Co}_3(\mu_3\text{-P})(\text{CO})_6$ ( $\text{CNAr}^{\text{Dipp}^2}$ ) <sub>3</sub> AuCl (7)	$[\text{Co}_3(\mu_3\text{-P-CH}_3)(\text{CO})_6$ ( $\text{CNAr}^{\text{Dipp}^2}$ ) <sub>3</sub> OTf (9)·2C <sub>6</sub> H <sub>6</sub>	$\text{Co}_3(\mu_3\text{-P-PS})(\text{CO})_6(\text{CNAr}^{\text{Dipp}^2})_3$ (10)·2C <sub>6</sub> H <sub>6</sub>
Formula	C99 H112 Au Cl Co3 N3 O6 P	C113 H126 Co3 F3 N3 O9 P S	C111 H123 Co3 N3 O6 P S
Crystal System	Monoclinic	Monoclinic	Monoclinic
Space Group	P 1 21/c 1	P 1 21/c 1	P 1 21/c 1
a, Å	27.1598(14)	22.724(2)	64.119(2)
b, Å	14.9117(8)	14.9117(8)	12.0561(5)
c, Å	22.9706(12)	38.240(4)	30.6029(10)
α, deg	90	90	90
β, deg	93.7640(10)	91.3500(10)	107.827(2)
γ, deg	90	90	90
V, Å <sup>3</sup>	9283.0(8)	10350.4(18)	22521.0(15)
Z	4	4	8
Radiation (λ, Å)	Mo-K <sub>α</sub> , 0.71073	Mo-K <sub>α</sub> , 0.71073	Mo-K <sub>α</sub> , 0.71073
ρ(calcd.), g/cm <sup>3</sup>	1.344	1.262	1.082
μ, mm <sup>-1</sup>	2.200	0.574	0.518
Temp, K	100	100	100
θ max, deg	25.740	25.911	24.707
data/parameters	17688 / 1202	19957 / 1223	19173 / 1126
R <sub>1</sub>	0.0271	0.0508	0.0767
wR <sub>2</sub>	0.0617	0.1231	0.1771
GOF	1.071	1.154	1.027

**Table 4.7. Crystallographic Data Collection and Refinement Information.**

Name	[Co(CO) <sub>3</sub> (CNAr <sup>Mes2</sup> ) <sub>2</sub> ]CoBr r <sub>3</sub> ·Et <sub>2</sub> O (11)	[Co <sub>4</sub> (μ <sub>4</sub> -P)(CO) <sub>8</sub> (CNAr <sup>Mes2</sup> ) <sub>5</sub> ]CoBr <sub>3</sub> (8)
Formula	C88 H96 Br3 Co2 N3 O4	C135.25 H126 Br3 Co5 N4 O8 P
Crystal System	Monoclinic	Triclinic
Space Group	P 1 21/c 1	P-1
a, Å	35.619(8)	15.091(3)
b, Å	14.841(5)	15.315(3)
c, Å	31.636(7)	29.751(6)
α, deg	90	90.070(2)
β, deg	101.874(7)	101.252(2)
γ, deg	90	114.831(2)
V, Å <sup>3</sup>	16366(8)	6094(2)
Z	8	2
Radiation (λ, Å)	Mo-K <sub>α</sub> , 0.71073	Mo-K <sub>α</sub> , 0.71073
ρ(calcd.), g/cm <sup>3</sup>	1.313	1.363
μ, mm <sup>-1</sup>	1.920	1.721
Temp, K	100	100
θ max, deg	25.389	23.413
data/parameters	14917 / 849	17667 / 1435
R <sub>1</sub>	0.0600	0.0821
wR <sub>2</sub>	0.1433	0.2099
GOF	1.023	1.049

## 4.8 Acknowledgement

Chapter 4 is currently in preparation as a manuscript by C. Chan, M. L. Neville, M. Gembicky, A. L. Rheingold, J. S. Figueroa. The dissertation author is the primary author of this manuscript.

## 4.9 References

- (1) Carmo, M.; Fritz, D. L.; Mergel, J.; Stolten, D. *International Journal of Hydrogen Energy* **2013**, *38* (12), 4901–4934.
- (2) Sapountzi, F. M.; Gracia, J. M.; Weststrate, C. J. K.-J.; Fredriksson, H. O. A.; Niemantsverdriet, J. W. H. *Progress in Energy and Combustion Science* **2017**, *58*, 1–35.
- (3) Wang, Y.; Kong, B.; Zhao, D.; Wang, H.; Selomulya, C. *Nano Today* **2017**, *15*, 26–55.
- (4) Chang, J.; Xiao, Y.; Xiao, M.; Ge, J.; Liu, C.; Xing, W. *ACS Catal.* **2015**, *5* (11), 6874–6878.
- (5) Zhu, Y.-P.; Liu, Y.-P.; Ren, T.-Z.; Yuan, Z.-Y. *Adv. Funct. Mater.* **2015**, *25* (47), 7337–7347.
- (6) Jin, Z.; Li, P.; Xiao, D. *Green Chem.* **2016**, *18* (6), 1459–1464.
- (7) Pan, Y.; Lin, Y.; Chen, Y.; Liu, Y.; Liu, C. *Journal of Materials Chemistry A* **2016**, *4* (13), 4745–4754.
- (8) Ha, D.-H.; Han, B.; Risch, M.; Giordano, L.; Yao, Koffi P.C.; Karayaylali, P.; Shao-Horn, Y. *Nano Energy* **2016**, *29*, 37–45.
- (9) Zhao, H.; Yuan, Z.-Y. *Catalysis Science & Technology* **2017**, *7* (2), 330–347.
- (10) Vizi-Orosz, A. *Journal of Organometallic Chemistry* **1976**, *111* (1), 61–64.
- (11) Vizi-Orosz, A. *Journal of Organometallic Chemistry* **1976**, *111* (1), 61–64.
- (12) Vizi-Orosz, A.; Pályi, G.; Markó, L. *Journal of Organometallic Chemistry* **1973**, *60* (1), C25–C26.
- (13) Scherer, O. J.; Weigel, S.; Wolmershäuser, G. *Chem. Eur. J.* **1998**, *4* (10), 1910–1916.
- (14) Fox, B. J.; Millard, M. D.; DiPasquale, A. G.; Rheingold, A. L.; Figueroa, J. S. *Angew. Chem. Int. Ed.* **2009**, *48* (19), 3473–3477.
- (15) Labios, L. A.; Millard, M. D.; Rheingold, A. L.; Figueroa, J. S. *J. Am. Chem. Soc.* **2009**, *131* (32), 11318–11319.
- (16) Ditri, T. B.; Fox, B. J.; Moore, C. E.; Rheingold, A. L.; Figueroa, J. S. *Inorg. Chem.* **2009**, *48* (17), 8362–8375.

- (17) Margulieux, G. W.; Weidemann, N.; Lacy, D. C.; Moore, C. E.; Rheingold, A. L.; Figueroa, J. S. *J. Am. Chem. Soc.* **2010**, *132* (14), 5033–5035.
- (18) Emerich, B. M.; Moore, C. E.; Fox, B. J.; Rheingold, A. L.; Figueroa, J. S. *Organometallics* **2011**, *30* (9), 2598–2608.
- (19) Mokhtarzadeh, C. C.; Margulieux, G. W.; Carpenter, A. E.; Weidemann, N.; Moore, C. E.; Rheingold, A. L.; Figueroa, J. S. *Inorg. Chem.* **2015**, *54* (11), 5579–5587.
- (20) Carpenter, A. E.; Rheingold, A. L.; Figueroa, J. S. *Organometallics* **2016**, *35* (14), 2309–2318.
- (21) Carpenter, A. E.; Chan, C.; Rheingold, A. L.; Figueroa, J. S. *Organometallics* **2016**, *35* (14), 2319–2326.
- (22) Pal, K.; Hemming, O. B.; Day, B. M.; Pugh, T.; Evans, D. J.; Layfield, R. A. *Angew. Chem. Int. Ed.* **2016**, *55* (5), 1690–1693.
- (23) Vizi-Orosz, A.; Galamb, V.; Pályi, G.; Markó, L. *Journal of Organometallic Chemistry* **1981**, *216* (1), 105–111.
- (24) Drance, M. J.; Mokhtarzadeh, C. C.; Melaimi, M.; Agnew, D. W.; Moore, C. E.; Rheingold, A. L.; Figueroa, J. S. *Angew. Chem. Int. Ed.* **2018**, *57* (40), 13057–13061.
- (25) Beurich, H.; Madach, T.; Richter, F.; Vahrenkamp, H. *Angew. Chem. Int. Ed. Engl.* **1979**, *18* (9), 690–691.
- (26) Arif, A. M.; Cowley, A. H.; Pakulski, M.; Hursthouse, M. B.; Karauloz, A. *Organometallics* **1985**, *4* (12), 2227–2228.
- (27) King, R. B.; Fu, W. K.; Holt, E. M. *Inorg. Chem.* **1986**, *25* (14), 2390–2394.
- (28) Sánchez-Nieves, J.; Sterenberg, B. T.; Udachin, K. A.; Carty, A. J. *Journal of Cluster Science* **2004**, *15* (2), 151–162.
- (29) Lang, H.; Huttner, G.; Sigwarth, B.; Jibril, I.; Zsolnai, L.; Orama, O. *Journal of Organometallic Chemistry* **1986**, *304* (1-2), 137–155.
- (30) Scheer, M.; Vogel, U.; Becker, U.; Balazs, G.; Scheer, P.; Hönle, W.; Becker, M.; Jansen, M. *European Journal of Inorganic Chemistry* **2004**, *2005* (1), 135–141.
- (31) *Purification of Laboratory Chemicals*; Elsevier, 2003.
- (32) Pangborn, A. B.; Giardello, M. A.; Grubbs, R. H.; Rosen, R. K.; Timmers, F. J. *Organometallics* **1996**, *15* (5), 1518–1520.

- (33) Carpenter, A. E.; Wen, I.; Moore, C. E.; Rheingold, A. L.; Figueroa, J. S. *Chem. Eur. J.* **2013**, *19* (32), 10452–10457.
- (34) Gaussian 09, Revision D.01, M. J. Frisch, G. W. Trucks, H. B. Schlegel, G. E. Scuseria, M. A. Robb, J. R. Cheeseman, G. Scalmani, V. Barone, B. Mennucci, G. A. Petersson, H. Nakatsuji, M. Caricato, X. Li, H. P. Hratchian, A. F. Izmaylov, J. Bloino, G. Zheng, J. L. Sonnenberg, M. Hada, M. Ehara, K. Toyota, R. Fukuda, J. Hasegawa, M. Ishida, T. Nakajima, Y. Honda, O. Kitao, H. Nakai, T. Vreven, J. A. Montgomery, Jr., J. E. Peralta, F. Ogliaro, M. Bearpark, J. J. Heyd, E. Brothers, K. N. Kudin, V. N. Staroverov, T. Keith, R. Kobayashi, J. Normand, K. Raghavachari, A. Rendell, J. C. Burant, S. S. Iyengar, J. Tomasi, M. Cossi, N. Rega, J. M. Millam, M. Klene, J. E. Knox, J. B. Cross, V. Bakken, C. Adamo, J. Jaramillo, R. Gomperts, R. E. Stratmann, O. Yazyev, A. J. Austin, R. Cammi, C. Pomelli, J. W. Ochterski, R. L. Martin, K. Morokuma, V. G. Zakrzewski, G. A. Voth, P. Salvador, J. J. Dannenberg, S. Dapprich, A. D. Daniels, O. Farkas, J. B. Foresman, J. V. Ortiz, J. Cioslowski, D. J. Fox, Gaussian, Inc., Wallingford CT, (2013).
- (35) Becke, A. D. *The Journal of Chemical Physics* **1993**, *98* (7), 5648–5652.
- (36) Stephens, P. J.; Devlin, F. J.; Chabalowski, C. F.; Frisch, M. J. *The Journal of Physical Chemistry* **1994**, *98* (45), 11623–11627.
- (37) Hariharan, P. C.; Pople, J. A. *Theoretica Chimica Acta* **1973**, *28* (3), 213–222.
- (38) Ehlers, A. W.; Böhme, M.; Dapprich, S.; Gobbi, A.; Höllwarth, A.; Jonas, V.; Köhler, K. F.; Stegmann, R.; Veldkamp, A.; Frenking, G. *Chemical Physics Letters* **1993**, *208* (1-2), 111–114.
- (39) Zhurko, G. A.; Zhurko, D. A. *Chemcraft ver. 1.5*; 2011.
- (40) Chen, L.; Ren, P.; Carrow, B. P. *J. Am. Chem. Soc.* **2016**, *138* (20), 6392–6395.
- (41) Sängler, I.; Lerner, H. W.; Sinke, T.; Bolte, M.; IUCr. *Acta Crystallogr Sect E Struct Rep Online* **2012**, *68* (5), m708–m708.
- (42) Clavier, H.; Nolan, S. P. *Chemical Communications* **2010**, *46* (6), 841–861.
- (43) Poater, A.; Cosenza, B.; Correa, A.; Giudice, S.; Ragone, F.; Scarano, V.; Cavallo, L. *European Journal of Inorganic Chemistry* **2009**, *2009* (13), 1759–1766.
- (44) Burla, M. C.; Caliandro, R.; Camalli, M.; Carrozzini, B.; Cascarano, G. L.; De Caro, L.; Giacovazzo, C.; Polidori, G.; Spagna, R. *Journal of Applied Crystallography* **2005**, *38* (2), 381–388.
- (45) Sheldrick, G. M. *Acta Crystallogr., A, Found. Crystallogr.* **2008**, *64* (Pt 1), 112–122.

- (46) Dolomanov, O. V.; Bourhis, L. J.; Gildea, R. J.; Howard, J. A. K.; Puschmann, H. *Journal of Applied Crystallography* **2009**, *42* (2), 339–341.
- (47) Spek, A. L. *Journal of Applied Crystallography* **2003**, *36* (1), 7–13.
- (48) van der Sluis, P.; Spek, A. L. *Acta Crystallogr., A, Found. Crystallogr.* **1990**, *46* (3), 194–201.



# Chapter 5 Dinitrogen Exchange and Intramolecular Oxygen-Atom-Transfer Behavior of a Persistent End-On Nitrous Oxide Complex of Cobalt

## 5.1 Introduction

Nitrous oxide, made famous as the laughing gas, is the third most abundant greenhouse gas on earth that holds ~300 times more warming potential than carbon dioxide (CO<sub>2</sub>) and remains the leading ozone-depleting substance in the stratosphere.<sup>1,2</sup> The major anthropogenic N<sub>2</sub>O emission sources are fertilized agricultural soils, biomass burning, fossil fuel combustion and nitric/adipic acid synthesis, whereas nature emissions mostly come from bacterial nitrification which recently caught attention by underestimated emission from permafrost thawing.<sup>3</sup> Nitrous oxide reductase (N<sub>2</sub>OR),<sup>4,5</sup> the natural enzyme that catalyzed N<sub>2</sub>O to N<sub>2</sub> and H<sub>2</sub>O in the last step of the microbial denitrification process,<sup>6</sup> lately revealed a N<sub>2</sub>O side-on manner on the face of a Cu-S cluster active site by single crystal X-ray structure,<sup>7</sup> a synthetic model of N<sub>2</sub>OR had also shown the ability to reduce N<sub>2</sub>O.<sup>8</sup> Synthetic chemists have shown transition metal induced N<sub>2</sub>O activations include oxo transfers involving N<sub>2</sub> release<sup>9,10</sup>, insertion of the oxygen atom into M-R (R = alkyl, hydride) bonds (with N<sub>2</sub> evolution)<sup>11-14</sup>, N-N bond scission,<sup>15</sup> and insertion to metal-olefin bonds<sup>16,17</sup> to yield N<sub>2</sub>O-containing

metallocycles.<sup>18,19</sup> Furthermore, N<sub>2</sub>O as a mild oxidant is in special interest due to the release of an environmentally benign N<sub>2</sub> byproduct. Both heterogenous<sup>20-22</sup> and homogeneous<sup>23</sup> metal-catalyzed reduction of N<sub>2</sub>O had been carried out on organic substrates.

Despite the use of nitrous oxide as an oxidant under thermodynamic conditions, the kinetic activation of N<sub>2</sub>O remains difficult due to its low dipole (0.161 D) and poor  $\sigma$ -donor/ $\pi$ -acceptor abilities, the binding and subsequent functionalization of N<sub>2</sub>O by transition metal remains a significant challenge in organometallic chemistry. To our best knowledge, there has only been four other published transition metal nitrous oxide adducts to date. The first two are reported by Armor and Taube<sup>24</sup> as [Ru(NH<sub>3</sub>)<sub>5</sub>(N<sub>2</sub>O)]<sup>+</sup> followed by *cis*-RuCl<sub>2</sub>( $\eta^1$ -NNO)(P-N)(PPh<sub>3</sub>) (P-N = 1-Ph<sub>2</sub>P-2-Me<sub>2</sub>NC<sub>6</sub>H<sub>4</sub>) from James and co-workers<sup>25</sup>, both complex proposed a  $k^1$ -N-bound N<sub>2</sub>O fragment,<sup>26</sup> however the thermal instability precluded their isolations in the solid state. Until recently, X-ray crystallographic data revealed two authentic  $k^1$ -N-bound transition metal-N<sub>2</sub>O complexes, (tpa<sup>Mes</sup>)V( $\eta^1$ -N<sub>2</sub>O) (tpa<sup>Mes</sup> = Tri-mesityl-tris(pyrrylmethyl)amine) by Chang<sup>27</sup> and Cu( $\eta^1$ -N<sub>2</sub>O)(An) (An = Al(OC(CF<sub>3</sub>)<sub>3</sub>)<sub>4</sub>) by Malinowski<sup>28</sup>. However, only *cis*-RuCl<sub>2</sub>( $\eta^1$ -NNO)(P-N)(PPh<sub>3</sub>) revealed an N<sub>2</sub>O-based oxidation reactivity overtime, while reversible N<sub>2</sub>O binding was observed commonly for these compounds. A stable transition metal N<sub>2</sub>O complex with N<sub>2</sub>O based reactivity became our goal of research.

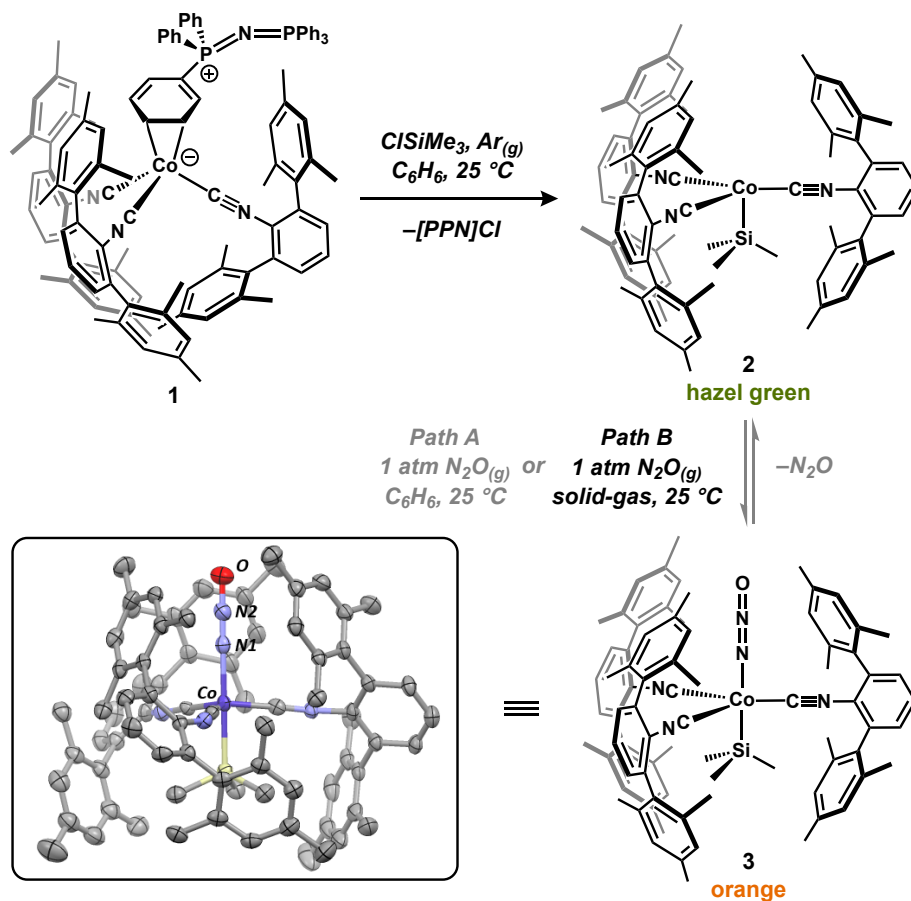
Herein, we reported the synthesis of a first thermally stable cobalt-N<sub>2</sub>O complex characterized by X-ray crystallography revealed a  $k^1$ -N-bound character. An intramolecular O-atom transfer reaction was observed to generate isocyanates upon the complex decomposes, further reaction condition of a N<sub>2</sub>O catalytic oxidation of isocyanides to isocyanates was demonstrated.

## 5.2 Results and Discussions

We were inspired by our previously reported synthesis<sup>29</sup> of a trimethylsilyl-dinitrogen cobalt(I) complex,  $(\text{N}_2)\text{Co}(\text{SiMe}_3)(\text{CNAr}^{\text{Mes}_2})_3$  ( $\text{Ar}^{\text{Mes}_2} = 2,6\text{-}(2,4,6\text{-Me}_3\text{C}_6\text{H}_2)_2\text{C}_6\text{H}_3$ ), resulted from the reaction of  $(\eta^2\text{-PPN})\text{Co}(\text{CNAr}^{\text{Mes}_2})_3$  (**1**) with trimethylsilyl chloride ( $\text{ClSiMe}_3$ ) under dinitrogen atmosphere. We proposed that the coordinatively unsaturated  $\text{Co}(\text{SiMe}_3)(\text{CNAr}^{\text{Mes}_2})_3$  species was generated first after the electrophilic silylation process, which then further binds dinitrogen in an end-on fashion. The same reaction process was carried out under argon atmosphere with *rigorous exclusion* of dinitrogen in non-coordinating solvents to successfully isolate a quantitative yield of the  $16e^-$   $\text{Co}(\text{SiMe}_3)(\text{CNAr}^{\text{Mes}_2})_3$  (**2**). (Scheme 5.1) Single-crystal X-ray diffraction studies of **2** show a trigonal monopyramidal geometry in the solid-state, and DFT calculations support a low-lying cobalt  $d_{z^2}$  LUMO capable of small molecule binding.

Interestingly, upon treating **2** with 1 atm of  $\text{N}_2\text{O}$  gas in benzene solution, an immediate color change from hazel green to orange was observed.  $^1\text{H}$  NMR spectroscopy also showed a significant shift of the  $\text{SiMe}_3$  protons from a  $-0.64$  ppm broad singlet to a sharp  $-0.72$  ppm singlet. However, the resulting orange solution reversed color back to hazel green when applying vacuum. The reappearance of the broad  $-0.64$  ppm resonance in the  $^1\text{H}$  NMR spectrum indicated to us a reverse  $\text{N}_2\text{O}$  binding phenomenon in solution. (Scheme 5.1, path A) Therefore, we believe there exists a binding equilibrium between free and cobalt bounded  $\text{N}_2\text{O}$  in solution phase that strongly favors the later. Inspired by the extreme Lewis acidity of the  $\text{Co}(\text{SiMe}_3)(\text{CNAr}^{\text{Mes}_2})_3$  (**2**) cobalt center, we developed a solvent-free solid-gas addition method to pursue the solid state isolation of an  $\text{N}_2\text{O}$ -adduct. By avoiding the  $\text{N}_2\text{O}$  dissociation dynamics

in solution, we were able to generate a vacuum stable orange power directly from the hazel green **2** powder after exposure to N<sub>2</sub>O atmosphere. (Scheme 5.1, path B) Orange single crystals were obtained successfully through pentane/benzene recrystallization at -35°C overnight, crystallographic data revealed the first end-on cobalt-N<sub>2</sub>O complex, (N<sub>2</sub>O)Co(SiMe<sub>3</sub>)(CNAr<sup>Mes2</sup>)<sub>3</sub> (**3**) (Scheme 5.1).



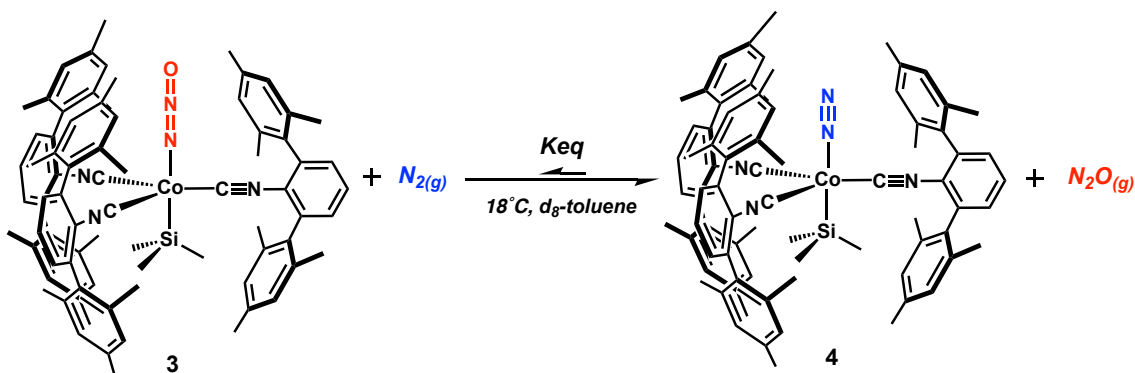
**Scheme 5.1.** Synthesis of **2** and Its Two Reaction Pathways to Form **3**. Path A leads to an orange solution (**3-solution**) that shows reversible N<sub>2</sub>O binding, path B leads to an orange solid (**3-solid**) that is stable under vacuum. The molecular structure of **3** is also shown with thermal ellipsoid set at 30% probability and hydrogen atoms omitted for clarity.

From the solid-state structure, N<sub>2</sub>O is linearly bound to the cobalt center sitting in the *m*-terphenyl pocket created by the isocyanide (CNAr<sup>Mes2</sup>) ligands, with a Co-N-N angle of 177.6(4)°. In previously reported transition metal-N<sub>2</sub>O complexes, N<sub>2</sub>O tends to bind *N*-end-on

to the metal; we turned to DFT calculation for verify this motif in our compound. Distinguishing between *N*-bound and *O*-bound N<sub>2</sub>O is relatively straightforward. The *N*-bound N<sub>2</sub>O complex converged smoothly to a geometry well aligned with the experimental crystal structure while the *O*-bound N<sub>2</sub>O converged with a significantly bent Co-N-N angle (119°); therefore, an *N*-bound linear N<sub>2</sub>O complex (k<sup>1</sup>-*N*-N<sub>2</sub>O)Co(SiMe<sub>3</sub>)(CNAr<sup>Mes2</sup>)<sub>3</sub> (**3**) was confirmed.

In the molecular structure of complex **3**, the N-N bond length of 1.111(5) Å is slightly shortened compared to the free N<sub>2</sub>O N-N distance of 1.128 Å, and the N-O bond length of 1.209(6) Å is slightly elongated compared to the free N<sub>2</sub>O N-O distance of 1.184 Å,<sup>30</sup> similar to Chang's (tpa<sup>Mes</sup>)V(N<sub>2</sub>O) complex (1.119(2) Å and 1.187(2) Å, respectively).<sup>27</sup> The FTIR spectrum of **3** shows two isocyanide vibration bands (νCN) at 1936 and 2023 cm<sup>-1</sup>, consistent with the solid state C<sub>3v</sub> geometry plus a Co(I) metal center. An additional higher energy vibration at 2262 cm<sup>-1</sup> was assigned as the NNO stretch after comparison with the solid-state ATR-IR spectrum and the DFT calculated νNNO value. (Figure 5.1 Left - red) To further support this assignment, an <sup>15</sup>N incorporation experiment was conducted. We synthesized the isotopic doubly-<sup>15</sup>N-labeled <sup>15</sup>N<sub>2</sub>O complex, (k<sup>1</sup>-*N*-<sup>15</sup>N<sub>2</sub>O)Co(SiMe<sub>3</sub>)(CNAr<sup>Mes2</sup>)<sub>3</sub> (**3**-<sup>15</sup>N), in a manner similar to the unlabeled species **3**. The FTIR spectrum of **3**-<sup>15</sup>N displays the same νCN vibrations as **3** but with a new vibration at 2189 cm<sup>-1</sup>. (Figure 5.1 Left - blue) Comparison of

the two sets of data allows us to conclude that the NNO stretch in **3** is red-shifted from 2262 to 2189  $\text{cm}^{-1}$  upon  $^{15}\text{N}$ -labeling.



**Scheme 5.2.** Reaction scheme of  $\text{N}_2\text{O}$  and  $\text{N}_2$  binding equilibrium on **2** under  $18^\circ\text{C}$  in a  $d_8$ -toluene solution.

Moreover, we surprisingly found that when treating **3** with 1 ATM of  $\text{N}_2$  in benzene solution, the  $\text{SiMe}_3$  protons shifted immediately from  $-0.728$  ppm to  $-0.741$  ppm according to the  $^1\text{H}$  NMR spectrum. Solution phase FTIR further showed the disappearance of  $\nu\text{NNO}$  at  $2262\text{ cm}^{-1}$  and emerged a new stretch at  $2224\text{ cm}^{-1}$  consistent with the  $\nu\text{NN}$  frequency of previously published  $\text{N}_2$  substituted product,  $(\text{N}_2)\text{Co}(\text{SiMe}_3)(\text{CNAr}^{\text{Mes}2})_3$  (**4**). Interestingly, if we take complex **4** with 1 ATM of  $\text{N}_2\text{O}$  in solution, both complexes **3** and **4** appeared at the  $^1\text{H}$  NMR spectrum indicating an equilibrium between  $\text{N}_2$  and  $\text{N}_2\text{O}$  binding. Through  $^1\text{H}$  NMR studies, we were able to obtain the equilibrium constant ( $K_{\text{eq}}$ ) of  $\text{N}_2\text{O}$  and  $\text{N}_2$  binding on **2** for the first time, which equals to 0.22 at  $18^\circ\text{C}$  in  $d_8$ -toluene. (Scheme 2) The experimental Gibbs free energy was calculated to be  $3.33\text{ kcal/mol}$  similar to the DFT calculated  $\Delta G = 3.95\text{ kcal/mol}$ . DFT computations showed a  $2\text{ kcal/mol}$  difference in the bond dissociation energy between  $\text{N}_2\text{O}$  and  $\text{N}_2$  ( $8\text{ kcal/mol}$  and  $10\text{ kcal/mol}$ , respectively) on complex **2**, with the HOMO/LUMO gap of **4** ( $3.12\text{ kcal/mol}$ ) being  $0.9\text{ kcal/mol}$  larger than complex **3** ( $3.21\text{ kcal/mol}$ ). This

demonstrated the stronger binding ability of N<sub>2</sub> than N<sub>2</sub>O, which helps explain the vastly greater number of known N<sub>2</sub> than N<sub>2</sub>O transition metal complexes in the literature.

**Table 5.1.** Experimental and Computational Parameters of Compound **3**, **3-<sup>15</sup>N**, **3m**, **4**, **4-<sup>15</sup>N** and **4m**.

Parameters\Compound	(N <sub>2</sub> O)Co(SiMe <sub>3</sub> ) (CNAr <sup>Mes</sup> <sub>2</sub> ) <sub>3</sub> <b>3</b>	(N <sub>2</sub> )Co(SiM <sub>3</sub> ) (CNAr <sup>Mes</sup> <sub>2</sub> ) <sub>3</sub> <b>4</b>
Experimental		
Co-Si	2.295(1) Å	2.286(2) Å
Co-N	1.969(4) Å	1.933(5) Å
vCN	1936 cm <sup>-1</sup> 2023 cm <sup>-1</sup>	1948 cm <sup>-1</sup> 2021 cm <sup>-1</sup>
vNNO	2262 cm <sup>-1</sup> 2189 cm <sup>-1</sup> ( <b>3-<sup>15</sup>N</b> )	-
vNN	-	2224 cm <sup>-1</sup> 2153 cm <sup>-1</sup> ( <b>4-<sup>15</sup>N</b> )
<sup>15</sup> N{ <sup>1</sup> H} NMR	132 ppm (N <sub>α</sub> ) 241 ppm (N <sub>β</sub> ) <sup>1</sup> J <sub>NN</sub> = 1.8 Hz	291 ppm (N <sub>α</sub> ) 332 ppm (N <sub>β</sub> ) <sup>1</sup> J <sub>NN</sub> = 1.7 Hz
Computational (kcal/mol)		
BDE	8	10
HOMO/LUMO gap	3.12	3.21
NOCV1 (σ)	-12.4	-15.1
NOCV2 (π)	-9.2	total -10.5
NOCV3 (π)	-6.7	total -22.1
		total -15.9

To our best knowledge, this is the first example where the σ-donor/π-acid properties of N<sub>2</sub> and N<sub>2</sub>O can be compared structurally. (Table 5.1) Based on the single crystal x-ray crystallography data, the Co-Si distance for **4** (2.286(2) Å) is only ca. 0.01 Å shorter than **3**

(2.295(1) Å), with a ca. 0.04 Å decrease in the Co-N distance for **4** (1.933(5) Å) compared to **3** (1.969(4) Å). This indicated a stronger  $\pi$ -back bonding of N<sub>2</sub> and similar  $\sigma$ -donor abilities between N<sub>2</sub> and N<sub>2</sub>O. The result is further supported by FTIR spectroscopy where the degree of  $\pi$ -back bonding was reflected on the blue shift of  $\nu$ CN stretch in **4** (1948 cm<sup>-1</sup>) compared to **3** (1936 cm<sup>-1</sup>). Energy decomposition analysis (EDA) was introduced to calculate the  $\sigma$ -donor and  $\pi$ -acid properties of N<sub>2</sub> and N<sub>2</sub>O with the model of (N<sub>2</sub>)Co(SiMe<sub>3</sub>)(CNAr<sup>Ph2</sup>)<sub>3</sub> (**4m**, Ar<sup>Ph2</sup>=2,6-(C<sub>6</sub>H<sub>5</sub>)<sub>2</sub>C<sub>6</sub>H<sub>3</sub>) and (N<sub>2</sub>O)Co(SiMe<sub>3</sub>)(CNAr<sup>Ph2</sup>)<sub>3</sub> (**3m**). (Table 5.4 - 5.6) By using the ADF program at b3lyp-d3/tz2p level, N<sub>2</sub>O was shown to bind 2.1kcal/mol weaker than N<sub>2</sub>. From the natural orbitals for chemical valence (NOCV), both N<sub>2</sub> and N<sub>2</sub>O are each better  $\pi$ -acceptors than  $\sigma$ -donors. Furthermore, NOCV revealed both a larger  $\sigma$ - and total- $\pi$ -stabilization energy for N<sub>2</sub> than N<sub>2</sub>O, suggesting N<sub>2</sub> being both stronger  $\sigma$ -donor and  $\pi$ -acceptor compared to N<sub>2</sub>O.

Although complex **3** displayed outstanding stability throughout the previously described characterization processes, we found that leaving **3** in benzene solution at room temperature for prolonged periods of time resulted in an *O*-atom transfer reaction. From FTIR spectroscopy studies, the  $\nu$ NNO stretch of complex **3** at 2262 cm<sup>-1</sup> had disappeared after 12 hours at room temperature with new vibrations grown in at 2224 and 2242 cm<sup>-1</sup>. (Figure 5.1 Right - red) These vibrations line up perfectly with the published **4**  $\nu$ NN stretch at 2224 cm<sup>-1</sup> and isocyanate OCNAr<sup>Mes2</sup>  $\nu$ OCN stretch<sup>31</sup> at 2242 cm<sup>-1</sup>. Another <sup>15</sup>N incorporation experiment helped support this result by using the **3**-<sup>15</sup>N molecule as the starting material. As the **3**-<sup>15</sup>N- $\nu$ NNO stretch faded, new vibrations appeared differently at 2153 cm<sup>-1</sup> and similar at 2242 cm<sup>-1</sup> after 12 hours compared to the unlabeled experiments. (Figure 5.1 Right - blue) We assigned the 2153 cm<sup>-1</sup> peak as the <sup>15</sup>N- $\nu$ NN stretch from (<sup>15</sup>N<sub>2</sub>)Co(SiMe<sub>3</sub>)(CNAr<sup>Mes2</sup>)<sub>3</sub> (**4**-<sup>15</sup>N) and the same isocyanate



OCNAr<sup>Mes2</sup> vOCN stretch at 2242 cm<sup>-1</sup>. It was concluded that an *O*-atom transfer reaction had occurred with the N<sub>2</sub>O-oxygen transferred to one of the isocyanide ligands (CNAr<sup>Mes2</sup>), generating OCNAr<sup>Mes2</sup> with **4** isolated as the major bi-product in 74% yield. (Scheme 5.3)

A well-resolved <sup>15</sup>N{<sup>1</sup>H} NMR spectrum of the <sup>15</sup>N isotopomer **3**-<sup>15</sup>N showed two singlets at chemical shifts of N<sub>β</sub> = 247 ppm and N<sub>α</sub> = 138 ppm, <sup>1</sup>J<sub>NN</sub> = 1.8 Hz. Comparing the <sup>15</sup>N NMR parameters for **3**-<sup>15</sup>N to free N<sub>2</sub>O (218 and 135 ppm, <sup>1</sup>J<sub>NN</sub> = 8.1 Hz),<sup>32</sup> slight upfield δ<sub>N</sub> shifts were observed upon coordination similar to phenomenon seen in the previously published N<sub>2</sub>O complex *cis*-RuCl<sub>2</sub>(η<sup>1-15</sup>N<sup>14</sup>NO)(P-N)(PPh<sub>3</sub>) (N<sub>terminal</sub> = 125.8 ppm).<sup>25</sup> After 12 hours of reaction time, δ N<sub>β</sub> and δ N<sub>α</sub> of **3**-<sup>15</sup>N had disappeared with the growth of new peaks at N<sub>β</sub> = 332 ppm and N<sub>α</sub> = 291 ppm, <sup>1</sup>J<sub>NN</sub> = 1.7 Hz establishing two chemically inequivalent nitrogen atoms from compound **4**-<sup>15</sup>N. However, due to the highly dynamic properties of **4** at room temperature, the <sup>15</sup>N peaks were only revealed at -60°C despite applying prolonged T<sub>1</sub> relaxation time applied. An <sup>15</sup>N spectrum was also taken on an authentic sample of **4**-<sup>15</sup>N generated from **2** with 1 atm of <sup>15</sup>N<sub>2</sub> that showed identical δ N chemical shifts under -60°C.

A control experiment of a stirred CNAr<sup>Mes2</sup> benzene solution under 1 atm of N<sub>2</sub>O tested negative, with no OCNAr<sup>Mes2</sup> vOCN stretch visible in the FTIR spectrum even after 12 hours. Furthermore, to exclude an intermolecular mechanism, tricyclohexylphosphine (PCy<sub>3</sub>) was added to the **3**-benzene solution. PCy<sub>3</sub> was tested to be oxidized immediately upon N<sub>2</sub>O exposure to generate tricyclohexylphosphine oxide (O=PCy<sub>3</sub>). After 2 hours reaction time of a **3**-benzene solution and one equivalent of PCy<sub>3</sub>, the <sup>31</sup>P NMR spectrum showed no evidence of O=PCy<sub>3</sub> formation but with the vOCN stretch appeared in the FTIR spectra. From this result,

we confirmed that **3** in solution does not undergo an  $\text{N}_2\text{O}$  dissociation process and that an intramolecular *O*-atom transfer reaction had taken place to generate **5**.

**Scheme 5.3.** *O*-atom Transfer Reaction of **3** in  $\text{C}_6\text{D}_6$  Solution to Generate **4** and  $\text{OCNAr}^{\text{Mes}_2}$ .

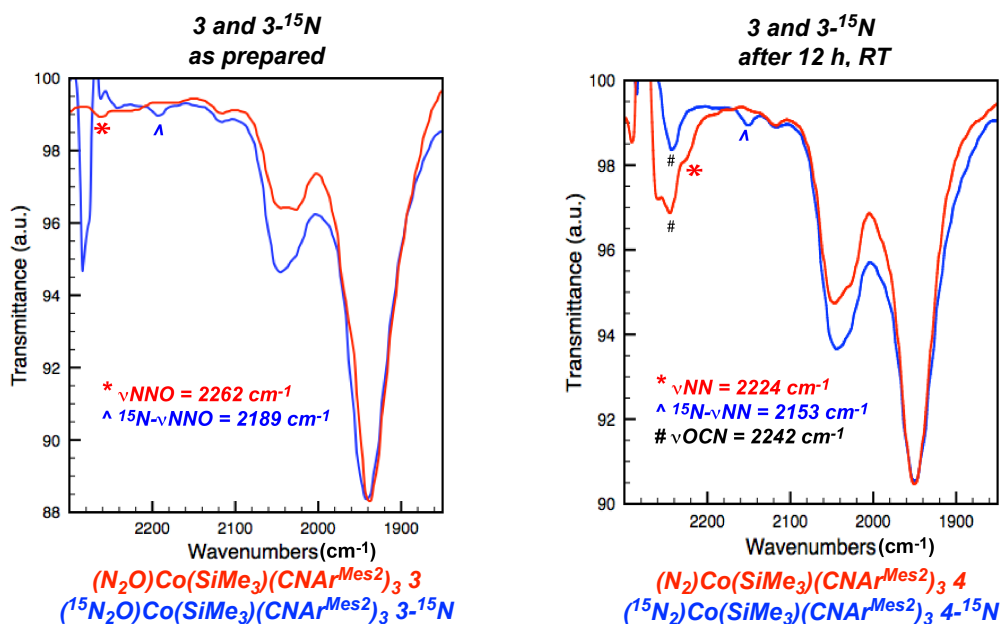
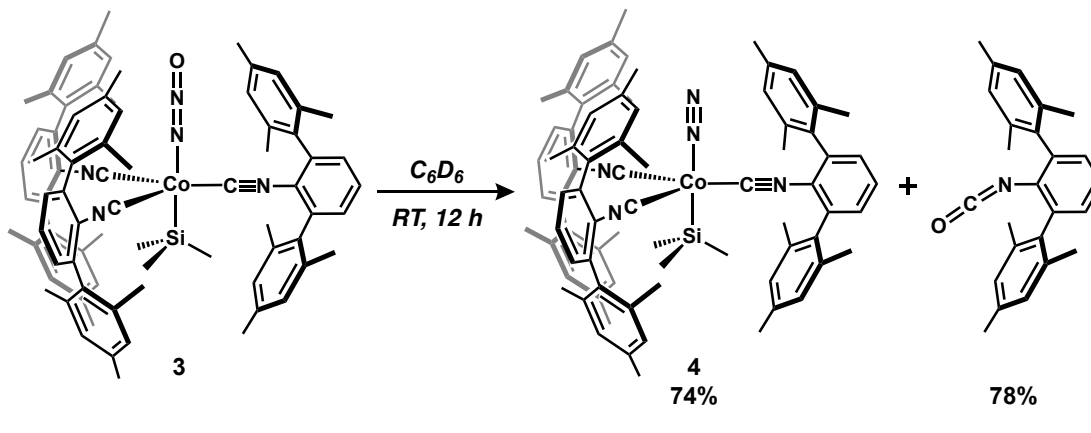
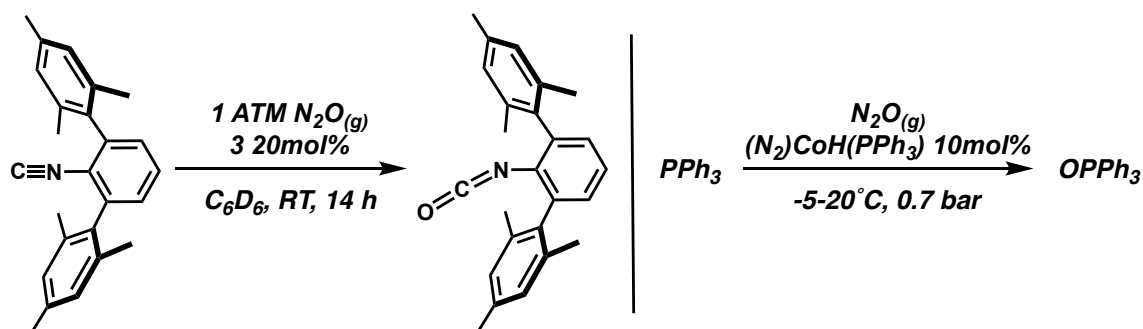


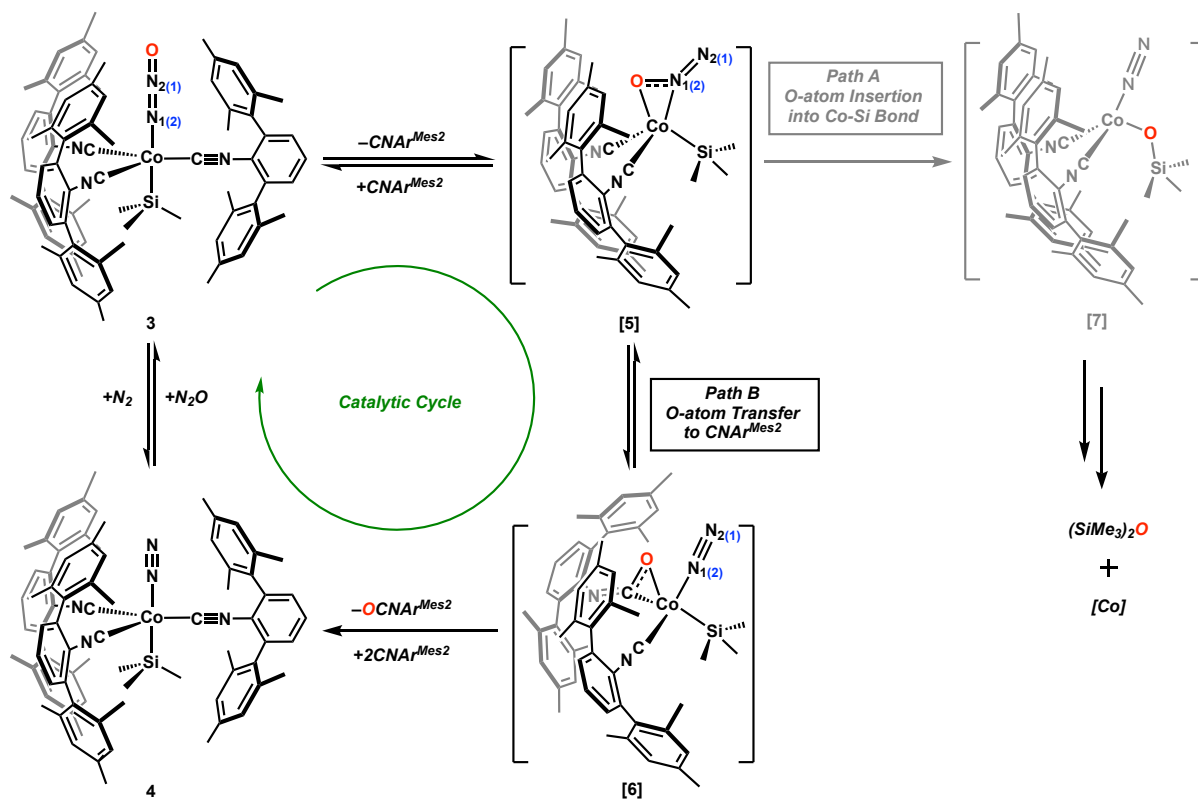
**Figure 5.1.** (Left) FTIR spectrum of **3** as prepared in  $\text{C}_6\text{H}_6$  solution shown in red, and **3-<sup>15</sup>N** as prepared in  $\text{C}_6\text{D}_6$  solution shown in blue. (Right) FTIR spectrum of **3** after 12 h in  $\text{C}_6\text{D}_6$  solution shown in red, and **3-<sup>15</sup>N** after 12 h in  $\text{C}_6\text{D}_6$  solution shown in blue. All spectra had solvent background subtraction applied.

Furthermore, by adding an extra equivalent of  $\text{CNAr}^{\text{Mes}_2}$  with **3** in a benzene solution for 12 hours at room-temperature resulted in an *O*-atom transfer reaction to  $\text{OCNAr}^{\text{Mes}_2}$  with quantitative yield of **4** monitored by  $^{13}\text{C}\{^1\text{H}\}$  NMR spectroscopy. We excitingly turned this

reaction into a catalytic generation of isocyanates from isocyanides. By using 20 mol% catalyst loading of **3** with 1 atm of N<sub>2</sub>O atmosphere, OCNAr<sup>Mes<sub>2</sub></sup> was afforded quantitatively from CNAr<sup>Mes<sub>2</sub></sup> after 14 hours at room temperature in C<sub>6</sub>H<sub>6</sub>. (Scheme 5.4 Left) Generation of a more sterically hindered OCNAr<sup>Tripp<sup>2</sup></sup> (Ar<sup>Tripp<sup>2</sup></sup> = 2,6-(2,4,6-(*i*-Pr)<sub>3</sub>C<sub>6</sub>H<sub>2</sub>)<sub>2</sub>C<sub>6</sub>H<sub>3</sub>; *i*-Pr = iso-propyl) can also be achieved by using the same catalytic condition with CNAr<sup>Tripp<sup>2</sup></sup>. (Table 5.30) It is important to mention that an isoelectronic system that catalytically oxidizes PPh<sub>3</sub> to O=PPh<sub>3</sub> with N<sub>2</sub>O has been proposed.<sup>33,34</sup> (Scheme 5.4 Right) By using (N<sub>2</sub>)CoH(PPh<sub>3</sub>)<sub>3</sub> as the initial catalyst, N<sub>2</sub>O coordination was suggested to generate the isoelectronic (N<sub>2</sub>O)CoH(PPh<sub>3</sub>)<sub>3</sub> to **3**, which further O-atom transferred to form O=PPh<sub>3</sub> and regenerated (N<sub>2</sub>)CoH(PPh<sub>3</sub>)<sub>3</sub>. Although (N<sub>2</sub>O)CoH(PPh<sub>3</sub>)<sub>3</sub> was never spectroscopically observed, we believe our system undergoes the similar mechanistic pathway. However, we were able to not only isolate and fully characterize the key intermediate **3**, but also capable of further study the reaction mechanism by spectroscopy with the advantage of the steric profile provided by our *m*-terphenyl isocyanide ligands.



**Scheme 5.4.** (Left) Reaction condition of **4** catalyzed N<sub>2</sub>O oxidation of isocyanides to isocyanates. (Right) Published reaction condition of (N<sub>2</sub>)CoH(PPh<sub>3</sub>)<sub>3</sub> catalyzed N<sub>2</sub>O oxidation of phosphines to phosphine oxides.



**Scheme 5.5.** Proposed mechanism for the decomposition *O*-atom transfer of **3**.

Proposed in Scheme 5.5 is an intramolecular mechanism to demonstrate the reaction pathways of the decomposition *O*-atom transfer of **3**. We anticipate that the first step should involve a reversible ligand dissociation process forcing  $k^1$ -*N*- $N_2O$  to bind in  $\eta^2$ -*O,N*- $N_2O$ , forming the  $16e^-$  ( $\eta^2$ -*O,N*- $N_2O$ )Co(SiMe<sub>3</sub>)(CNAr<sup>Mes2</sup>)<sub>2</sub> **[5]**. At this intermediate **[5]**, two plausible pathways are listed. Path A shows an *O*-atom insertion into the Co-Si bond to form a cobalt-silyloxide complex **[7]** that further decomposes through a bi-molecular process to generate trace amount of unidentified cobalt species plus 12% yield of (SiMe<sub>3</sub>)<sub>2</sub>O detected experimentally by both <sup>1</sup>H and <sup>13</sup>C NMR spectroscopy after 12 hours. Path B includes the *O*-atom transfer directly into CNAr<sup>Mes2</sup> generating the ( $\eta^2$ -*O,N*-OCNAr<sup>Mes2</sup>)Co(SiMe<sub>3</sub>)(CNAr<sup>Mes2</sup>)<sub>2</sub> **[6]**. Complex **[6]** can simply pick up two equivalents of free

CNAr<sup>Mes2</sup> in solution accompanied with the loss of OCNAr<sup>Mes2</sup>, affording the final dinitrogen complex **4**. Complex **4** is showed earlier to exchange with N<sub>2</sub>O to regenerate the catalyst **3**. The decomposition of **3** was readily monitored by <sup>1</sup>H and <sup>15</sup>N NMR spectroscopy as a function of time in C<sub>6</sub>D<sub>6</sub>. However, the kinetic informations are limited due to the geometric similarities between complexes **3** and **4** due to their identical ligand environments. (Figure 5.16 - 5.25)

### 5.3 Concluding Remarks

In summary, we have presented the synthesis of the first k<sup>1</sup>-N<sub>2</sub>O-cobalt complex, (k<sup>1</sup>-N-N<sub>2</sub>O)Co(SiMe<sub>3</sub>)(CNAr<sup>Mes2</sup>)<sub>3</sub> **3** supported by X-ray crystal structure along with DFT calculations for a k<sup>1</sup>-N-bound N<sub>2</sub>O adduct. Reduction of the N<sub>2</sub>O fragment was observed to generate OCNAr<sup>Mes2</sup> and (N<sub>2</sub>)Co(SiMe<sub>3</sub>)(CNAr<sup>Mes2</sup>)<sub>3</sub> **4** supported by a series of detailed spectroscopy studies that further pointed to the mechanistic model proposed. Taking advantage of the N<sub>2</sub>O reactivity of this molecule, catalytic oxidation of isocyanides to isocyanates can be carried out using **4** as catalyst with N<sub>2</sub>O as oxidant, highlighting an exciting potential application. Discovery of related species of activated N<sub>2</sub>O and a broader catalytic substrate scope are currently underway.

### 5.4 Synthetic Procedures and Characterization Data

**General Considerations.** All manipulations were carried out under an atmosphere of Argon(g) using standard Schlenk and glovebox techniques. Unless otherwise stated, reagent-grade starting materials were purchased from commercial sources and either used as received or purified by standard procedures.<sup>35</sup> Solvents were dried and deoxygenated according to standard procedures.<sup>36</sup> Benzene, benzene-*d*<sub>6</sub> and toluene-*d*<sub>8</sub> (Cambridge Isotope Laboratories) were dried

with Na/K and Benzophenone followed by distillation; thereafter, 7 freeze-pump-thaw cycles were executed and the solvents were stored on 4 Å molecular sieves for 3 days prior to use. Celite 405 (Fisher Scientific) was dried under vacuum (24 h) at a temperature above 250 °C prior to use. ClSiMe<sub>3</sub> (Sigma-Aldrich) was treated with 7 freeze-pump-thaw cycles and dried over CaH<sub>2</sub> for 3 days prior to use. <sup>15</sup>N<sub>2</sub>O (99.2%) was purchased from Sigma-Aldrich and used as received. The compounds CNAr<sup>Mes2</sup>, CNAr<sup>Tripp2</sup>, (η<sup>2</sup>-PPN)Co(CNAr<sup>Mes2</sup>)<sub>3</sub> (**1**) and (N<sub>2</sub>)Co(SiMe<sub>3</sub>)(CNAr<sup>Mes2</sup>)<sub>3</sub> (**4**) were prepared by previously reported methods.<sup>37,29,38</sup>

Solution <sup>1</sup>H, <sup>13</sup>C{<sup>1</sup>H}, <sup>31</sup>P and <sup>15</sup>N NMR spectra were recorded on a Bruker Avance 300, a Bruker Avance 800, a Joel ECA 500, or a Varian X-Sens 500 spectrometer. <sup>1</sup>H and <sup>13</sup>C{<sup>1</sup>H} chemical shifts are reported in ppm relative to SiMe<sub>4</sub> (<sup>1</sup>H and <sup>13</sup>C δ = 0.0 ppm) with reference to residual solvent resonances of 7.16 ppm (<sup>1</sup>H) and 128.06 ppm (<sup>13</sup>C) for C<sub>6</sub>D<sub>6</sub>. <sup>15</sup>N{<sup>1</sup>H} chemical shifts were externally referenced to (<sup>15</sup>NH<sub>4</sub>)<sub>2</sub>SO<sub>4</sub> in H<sub>2</sub>O and calibrated to <sup>15</sup>NH<sub>3</sub> (0 ppm). <sup>31</sup>P{<sup>1</sup>H} NMR chemical shifts are reported in ppm relative to an internal standard of 85% H<sub>3</sub>PO<sub>4</sub> (0 ppm) in a sealed capillary. FTIR spectra were recorded on a Thermo-Nicolet iS10 FTIR spectrometer. For solution FTIR spectra, solvent peaks were digitally subtracted from all spectra by comparison with an authentic spectrum obtained immediately prior to that of the sample. Solid-state IR spectra were collected at 2 cm<sup>-1</sup> resolution using a Bruker Platinum Alpha ATR-IR equipped with a diamond crystal. Air-free analyses were collected using this instrument inside an argon-filled glovebox. The following abbreviations were used for the intensities and characteristics of important IR absorption bands: vs = very strong, s = strong, m = medium, w = weak, vw = very weak; b = broad, vb = very broad, sh = shoulder.

Combustion analyses were performed by Midwest Microlab LLC of Indianapolis, IN (USA). Samples for combustion analysis were obtained from the first recrystallized batch of

the reaction mixture. In a typical preparation, the crude, dry reaction mixture was dissolved in a minimum amount of solvent and stored at  $-35\text{ }^{\circ}\text{C}$  for several days to produce crystalline material. This material was then collected, thoroughly dried under vacuum and then packaged under vacuum for shipment. In most cases, this material was also used for single-crystal X-ray structure determination.

**Synthesis of  $\text{Co}(\text{SiMe}_3)(\text{CNAr}^{\text{Mes}_2})_3$  (**2**).** Under rigorous exclusion of  $\text{N}_2$  and adventitious Lewis bases,  $\eta^2\text{-PPNCo}(\text{CNAr}^{\text{Mes}_2})_3$  (0.040 g, 0.025 mmol) was suspended in  $\text{C}_6\text{H}_6$  (1 mL) and treated with excess  $\text{ClSiMe}_3$  (0.086 g, 0.796 mmol, 0.1 mL, 32 equiv). The resulting reaction mixture was stirred for 2 min at which time it turned from dark black to hazel green in color. The reaction mixture was then filtered, and the resulting filtrate concentrated to a solid under reduced pressure. The resulting residue was extracted with pentane (2 mL), filtered and re-concentrated to a solid. This was repeated an additional time to afford  $\text{Co}(\text{SiMe}_3)(\text{CNAr}^{\text{Mes}_2})_3$  as an oily residue. Yield: 0.022 g, 0.02 mmol 80.0 %.  $^1\text{H}$  NMR (499.9 MHz,  $\text{C}_6\text{D}_6$ ,  $20\text{ }^{\circ}\text{C}$ ):  $\delta = 6.95$  (t, 3H,  $J=7$  Hz, *p*-Ph), 6.89 (d, 6H,  $J=7$  Hz, *m*-Ph), 6.76 (s, 12H, *m*-Mes), 2.21 (s, 18H, *p*-Mes), 2.14 (s, 36H, *o*-Mes),  $-0.67$  (br s, 9H,  $\text{SiMe}_3$ ) ppm.  $^{13}\text{C}\{^1\text{H}\}$  NMR (125.7 MHz,  $\text{C}_6\text{D}_6$ ,  $20\text{ }^{\circ}\text{C}$ ):  $\delta = 185.3$  (CNR), 136.9, 136.6, 136.4, 136.3, 132.0, 129.0, 127.7, 125.4, 21.4 (*p*-Mes), 21.0 (*o*-Mes), 5.5 ( $\text{SiMe}_3$ ) ppm. FTIR ( $\text{C}_6\text{H}_6$ , KBr windows,  $25\text{ }^{\circ}\text{C}$ ):  $\nu_{\text{CN}} = 2028$  (s), 1948 (vs), 1919 (sh), 1872 (sh)  $\text{cm}^{-1}$  also, 2953 (w), 2919 (m), 2855 (w), 1614 (w), 1575 (m), 1488 (w), 1462 (m), 1411 (m), 1377 (w), 1270 (vw), 1228 (vw) 1203 (vw), 1070 (vw), 1032 (w)  $\text{cm}^{-1}$ . Elemental Analysis was not performed due to the extreme sensitivity of  $\text{Co}(\text{SiMe}_3)(\text{CNAr}^{\text{Mes}_2})_3$  to  $\text{N}_2$  and other Lewis bases (e.g.,  $\text{H}_2\text{O}$ ,  $\text{CO}_2$ ).

**Synthesis of  $(\kappa^1\text{-N-N}_2\text{O})\text{Co}(\text{SiMe}_3)(\text{CNAr}^{\text{Mes}_2})_3$  (**3**).**  $\text{Co}(\text{SiMe}_3)(\text{CNAr}^{\text{Mes}_2})_3$  (**1**) (0.020 g, 0.012 mmol) was transferred to a J-young NMR tube in a pentane solution. After the sample

was connected to the Schlenk line, pentane was evacuated to generate a green solid coated along the side of J-young tube. The solid was then placed under an atmosphere of  $\text{N}_2\text{O}_{(\text{g})}$ , an instant color change from hazel green to bright orange was observed. The orange solid was brought back to the glove box and dissolved in pentane; the reaction mixture was stored directly into the fridge ( $-35\text{ }^\circ\text{C}$ ) for 12 hours. Bright orange single crystals were collected suitable for X-ray diffraction. Yield: 0.015 g, 0.004 mmol, 10 %.  $^1\text{H}$  NMR (499.9 MHz,  $\text{C}_6\text{D}_6$ ,  $20\text{ }^\circ\text{C}$ ):  $\delta$  = 6.96 (t, 3H,  $J=7$  Hz, *p*-Ph), 6.87 (m, 18H, *m*-Ph and *m*-Mes), 2.27 (s, 18H, *p*- $\text{CH}_3$  Mes), 2.17 (s, 36H, *o*- $\text{CH}_3$  Mes), -0.74 (s, 9H,  $\text{SiMe}_3$ ) ppm.  $^{13}\text{C}\{^1\text{H}\}$  NMR (125.7 MHz,  $\text{C}_6\text{D}_6$ ,  $20\text{ }^\circ\text{C}$ ):  $\delta$  = 181.9 (*broad*, CNR), 137.8, 136.9, 136.3, 136.2, 136.1, 135.2, 129.6, 128.6, 128.5, 127.6, 34.5, 30.3, 22.8, 21.4, 21.3, 21.1, 14.3 ppm. (The CNR resonance extremely broadened, presumably due to coupling to  $^{59}\text{Co}$  ( $I = 7/2$ , 100 %)). FTIR ( $\text{C}_6\text{H}_6$ , KBr windows,  $25\text{ }^\circ\text{C}$ ):  $\nu_{\text{NNO}} = 2262$  (vw),  $\nu_{\text{CN}} = 2021$  (s), 1942 (vs)  $\text{cm}^{-1}$ , also 2955 (m), 2916 (m), 2870 (m), 2853 (m), 1521 (m), 849 (m)  $\text{cm}^{-1}$ . ATR-IR ( $\text{Ar}_{(\text{g})}$ ,  $25\text{ }^\circ\text{C}$ ):  $\nu_{\text{NNO}} = 2257$  (vw),  $\nu_{\text{CN}} = 2016$  (s), 1929 (vs)  $\text{cm}^{-1}$ , also 2953 (m), 2917 (m), 2856 (m), 2728 (w), 1608 (m), 1575 (m), 1486(m), 1451 (m), 1400 (s), 1376 (m)  $\text{cm}^{-1}$ . Anal. Calcd. for  $\text{C}_{75}\text{H}_{75}\text{N}_5\text{OCo}$ : C, 80.33; H, 6.74; N, 6.25. Found C, 79.86; H, 6.55; N, 6.20.



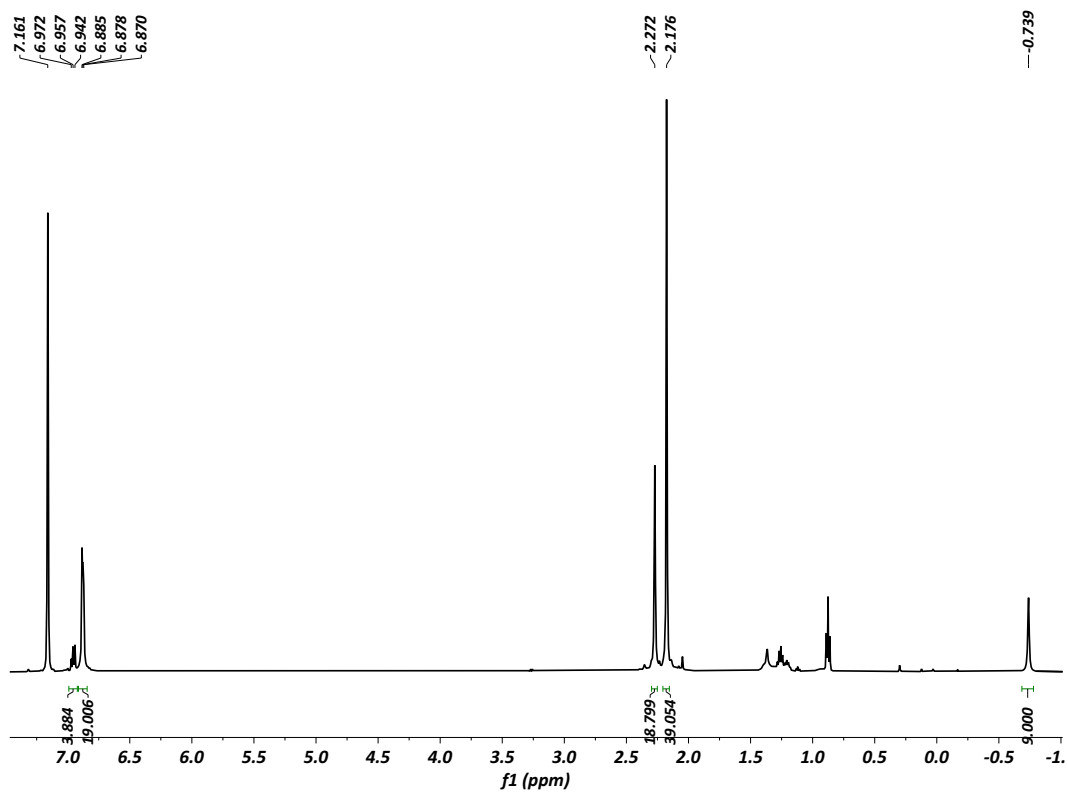


Figure 5.2.  $^1\text{H}$  NMR spectrum (500 MHz,  $\text{C}_6\text{D}_6$ ,  $20^\circ\text{C}$ ) of  $(\kappa^1\text{-N-N}_2\text{O})\text{Co}(\text{SiMe}_3)(\text{CNAr}^{\text{Mes}_2})_3$  (**3**).

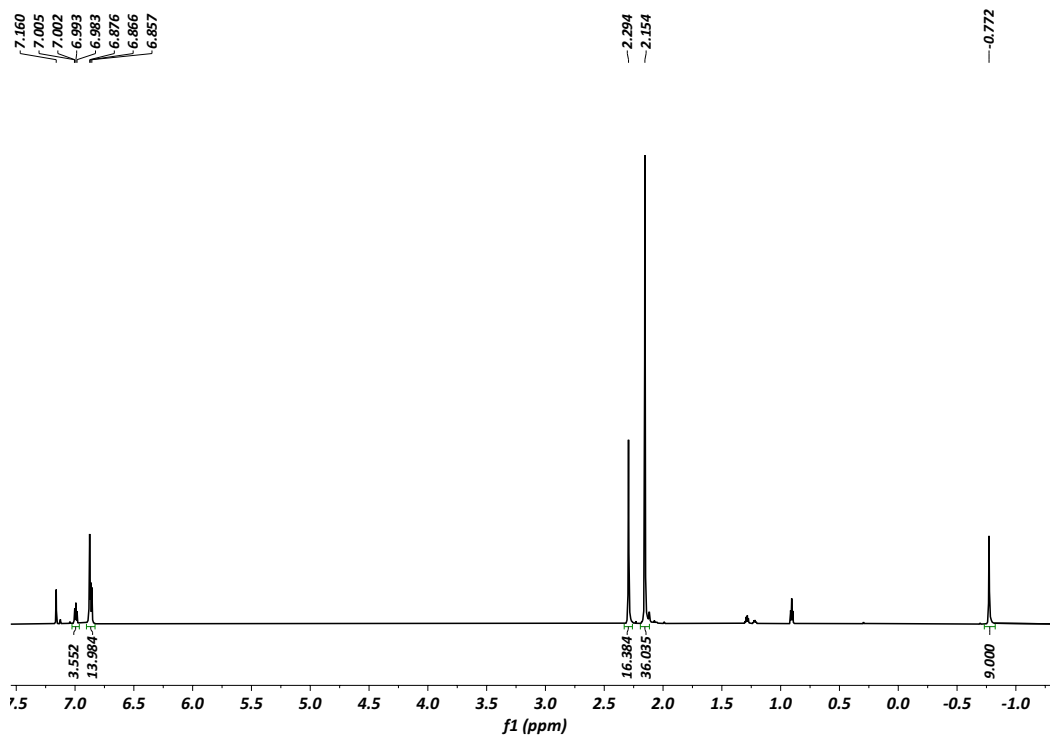


Figure 5.3  $^1\text{H}$  NMR spectrum (800 MHz,  $\text{C}_6\text{D}_6$ ,  $20^\circ\text{C}$ ) of  $(\kappa^1\text{-N-N}_2\text{O})\text{Co}(\text{SiMe}_3)(\text{CNAr}^{\text{Mes}_2})_3$  (**3**).

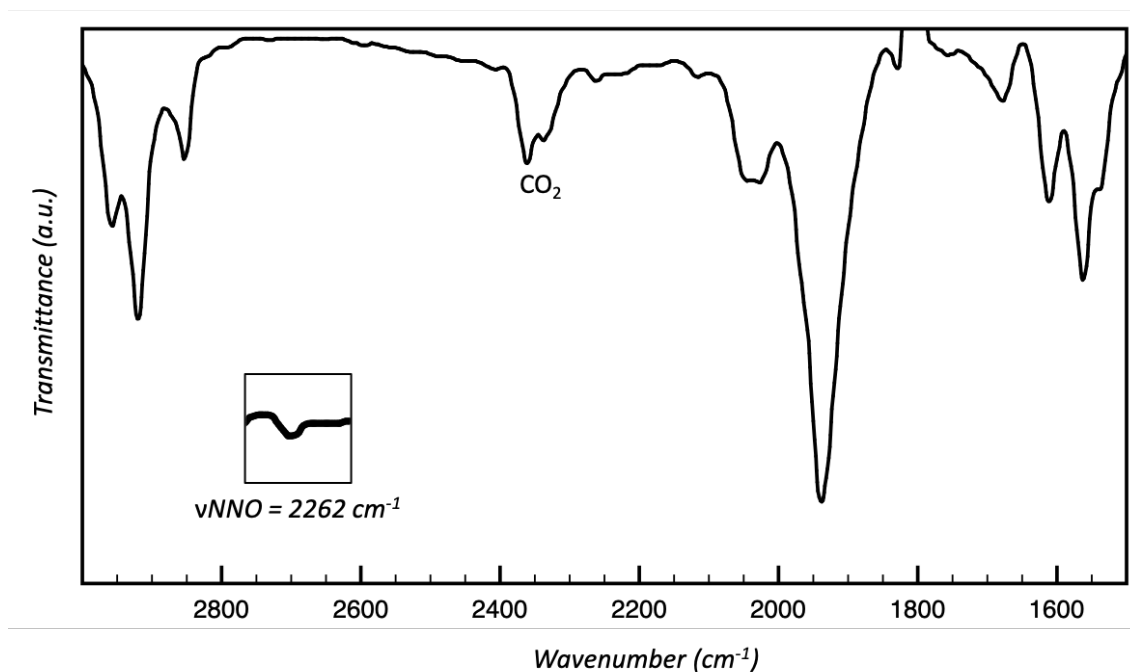


Figure 5.4. FTIR ( $\text{C}_6\text{H}_6$ , KBr windows,  $25^\circ\text{C}$ ) of  $(\kappa^1\text{-N-N}_2\text{O})\text{Co}(\text{SiMe}_3)(\text{CNAr}^{\text{Mes}2})_3$  (3).

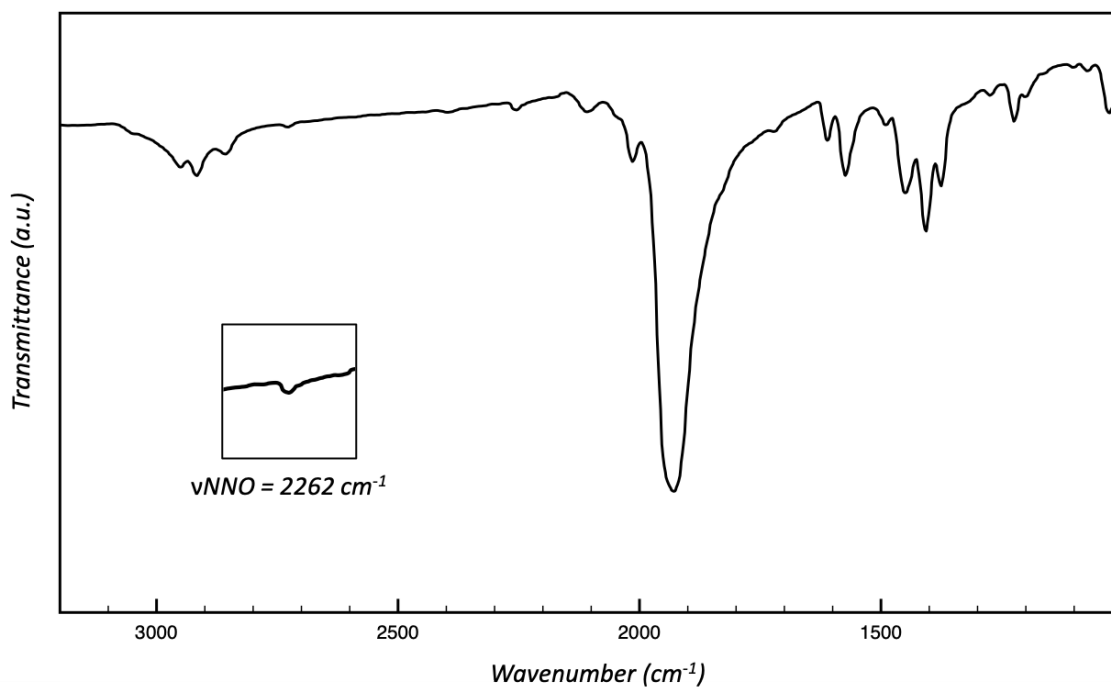


Figure 5.5. ATR-IR spectrum ( $\text{Ar}_{(\text{g})}$ ,  $25^\circ\text{C}$ ) of  $(\kappa^1\text{-N-N}_2\text{O})\text{Co}(\text{SiMe}_3)(\text{CNAr}^{\text{Mes}2})_3$  (3).

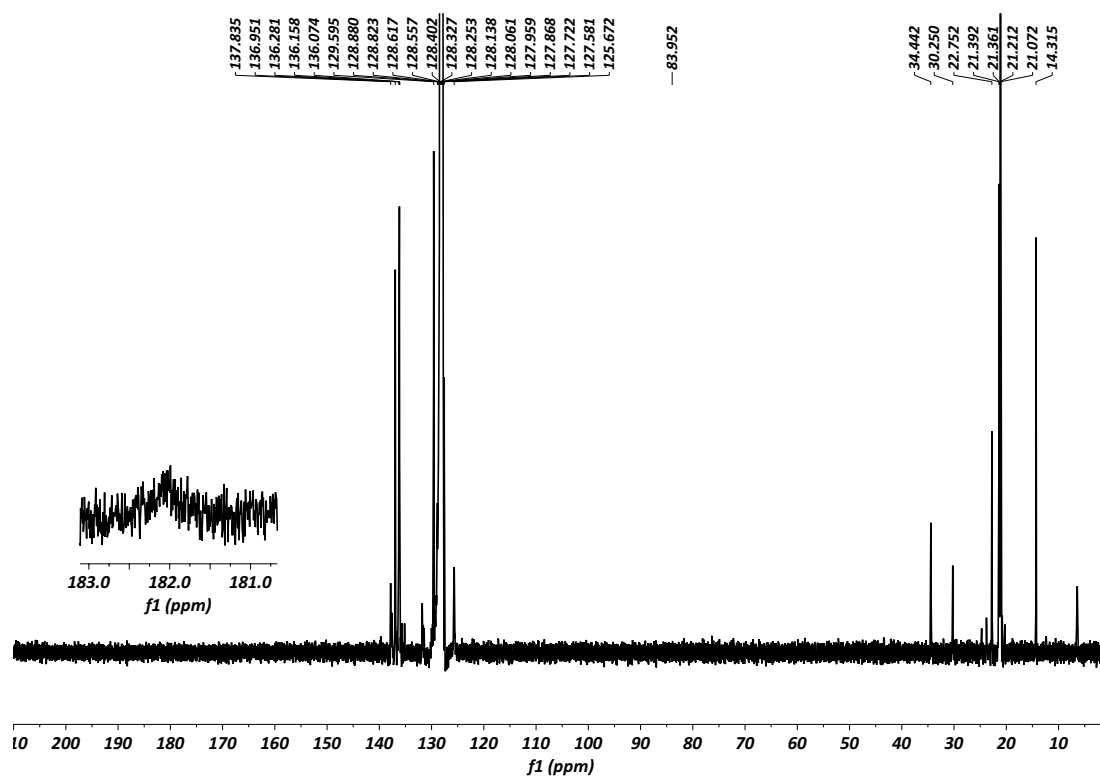


Figure 5.6.  $^{13}\text{C}\{^1\text{H}\}$  NMR spectrum (125.8 MHz,  $\text{C}_6\text{D}_6$ ,  $20^\circ\text{C}$ ) of  $(\kappa^1\text{-N-N}_2\text{O})\text{Co}(\text{SiMe}_3)(\text{CNAr}^{\text{Mes}2})_3$  (3).

**Synthesis of  $(\kappa^1\text{-N-}^{15}\text{N}_2\text{O})\text{Co}(\text{SiMe}_3)(\text{CNAr}^{\text{Mes}2})_3$  ( $3\text{-}^{15}\text{N}$ ):** Synthetic procedure of  $(\kappa^1\text{-N-N}_2\text{O})\text{Co}(\text{SiMe}_3)(\text{CNAr}^{\text{Mes}2})_3$  (3) was followed with  $^{15}\text{N}_2\text{O}_{(\text{g})}$  to isolate  $(\kappa^1\text{-N-}^{15}\text{N}_2\text{O})\text{Co}(\text{SiMe}_3)(\text{CNAr}^{\text{Mes}2})_3$ .  $^{15}\text{N}\{^1\text{H}\}$  NMR (50.7 MHz,  $d_8$ -toluene,  $-25^\circ\text{C}$ ): 133 ( $\text{N}_\alpha$ , d,  $J=1.8$  Hz, 1N), 241 ( $\text{N}_\beta$ , d,  $J=1.8$  Hz, 1N) ppm. FTIR ( $\text{C}_6\text{D}_6$ , KBr windows;  $25^\circ\text{C}$ ):  $\nu_{\text{NNO}} = 2189$  (w),  $\nu_{\text{CN}} = 2044$  (s), 1941 (vs)  $\text{cm}^{-1}$ , also 2958 (m), 2918 (s), 2874 (sh), 2850 (m), 1672 (m), 1561 (m), 1539 (sh)  $\text{cm}^{-1}$ .

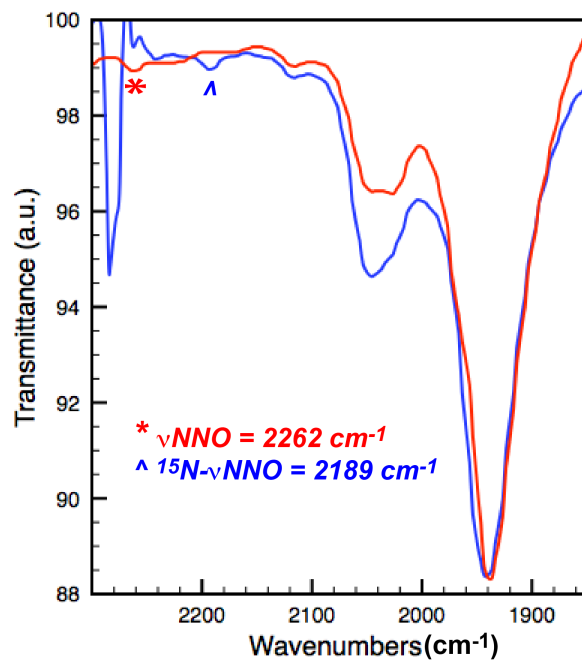


Figure 5.7. Overlapped FTIR spectrum (C<sub>6</sub>H<sub>6</sub>, KBr windows, 25 °C) of (κ<sup>1</sup>-N-N<sub>2</sub>O)Co(SiMe<sub>3</sub>)(CNAr<sup>Mes2</sup>)<sub>3</sub> (3) in red and (κ<sup>1</sup>-N-<sup>15</sup>N<sub>2</sub>O)Co(SiMe<sub>3</sub>)(CNAr<sup>Mes2</sup>)<sub>3</sub> (3-<sup>15</sup>N) in blue showing the red-shift of ν<sub>NNO</sub> upon <sup>15</sup>N-labeling .

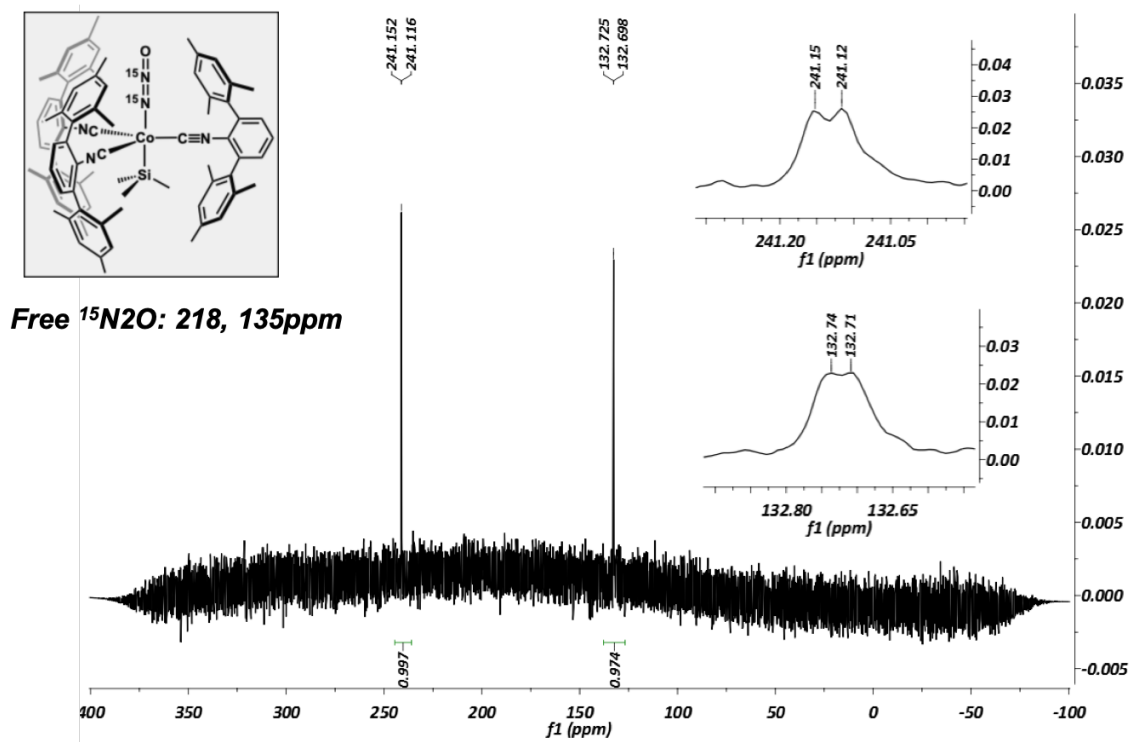
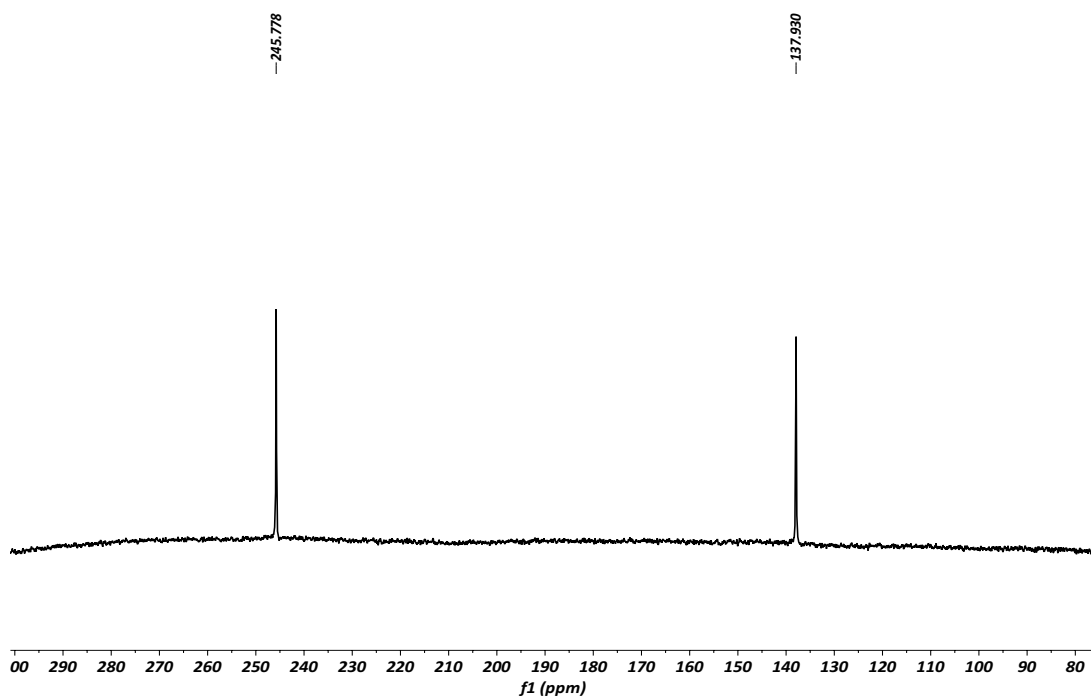


Figure 5.8. <sup>15</sup>N{<sup>1</sup>H} NMR spectrum (50.8 MHz, *d*<sub>8</sub>-toluene, -25 °C) of (κ<sup>1</sup>-N-<sup>15</sup>N<sub>2</sub>O)Co(SiMe<sub>3</sub>)(CNAr<sup>Mes2</sup>)<sub>3</sub> (3-<sup>15</sup>N).



**Figure 5.9.**  $^{15}\text{N}\{^1\text{H}\}$  NMR spectrum (81.1 MHz,  $\text{C}_6\text{D}_6$ ,  $20^\circ\text{C}$ ) of  $(\kappa^1\text{-N-}^{15}\text{N}_2\text{O})\text{Co}(\text{SiMe}_3)(\text{CNAr}^{\text{Mes}_2})_3$  ( $3\text{-}^{15}\text{N}$ ).

**Synthesis of  $(^{15}\text{N}_2)\text{Co}(\text{SiMe}_3)(\text{CNAr}^{\text{Mes}_2})_3$  ( $4\text{-}^{15}\text{N}$ ):** Synthetic procedure of  $(\kappa^1\text{-N-N}_2\text{O})\text{Co}(\text{SiMe}_3)(\text{CNAr}^{\text{Mes}_2})_3$  (3) was followed with  $^{15}\text{N}_{2(\text{g})}$  to isolate  $(^{15}\text{N}_2)\text{Co}(\text{SiMe}_3)(\text{CNAr}^{\text{Mes}_2})_3$ .  $^{15}\text{N}\{^1\text{H}\}$  NMR (50.7 MHz,  $d_8\text{-toluene}$ ,  $-60^\circ\text{C}$ ): 332 ( $\text{N}_\alpha$ , d,  $J=1.7$  Hz, 1N), 291 ( $\text{N}_\beta$ , d,  $J=1.7$  Hz, 1N) ppm. Note that there was no  $^{15}\text{N}$  signal detected at room-temperature even with prolonged T1 relaxation time applied. FTIR ( $\text{C}_6\text{D}_6$ , KBr windows;  $25^\circ\text{C}$ ):  $\nu_{\text{NN}} = 2154$  (vw),  $\nu_{\text{CN}} = 2043$  (s), 1957 (s)  $\text{cm}^{-1}$ , also 3050 (w), 2956 (m), 2917 (s), 2853 (m), 1612 (m), 1579 (m), 1560 (m), 1465 (m), 1440 (m), 1415 (m)  $\text{cm}^{-1}$ . ATR-IR ( $\text{N}_{2(\text{g})}$ ,  $25^\circ\text{C}$ ):  $\nu_{\text{NN}} = 2153$  (vw),  $\nu_{\text{CN}} = 2037$  (s), 1938 (vs)  $\text{cm}^{-1}$ , also 2950 (m), 2910 (m), 2854 (m), 2728 (w), 1610 (m), 1575 (m), 1489(m), 1444 (m), 1414 (s), 1374 (m)  $\text{cm}^{-1}$ . Note that  $^{15}\text{N}_{2(\text{g})}$  exchanged with  $\text{N}_{2(\text{g})}$  in the solid state within 15 minutes exposure.

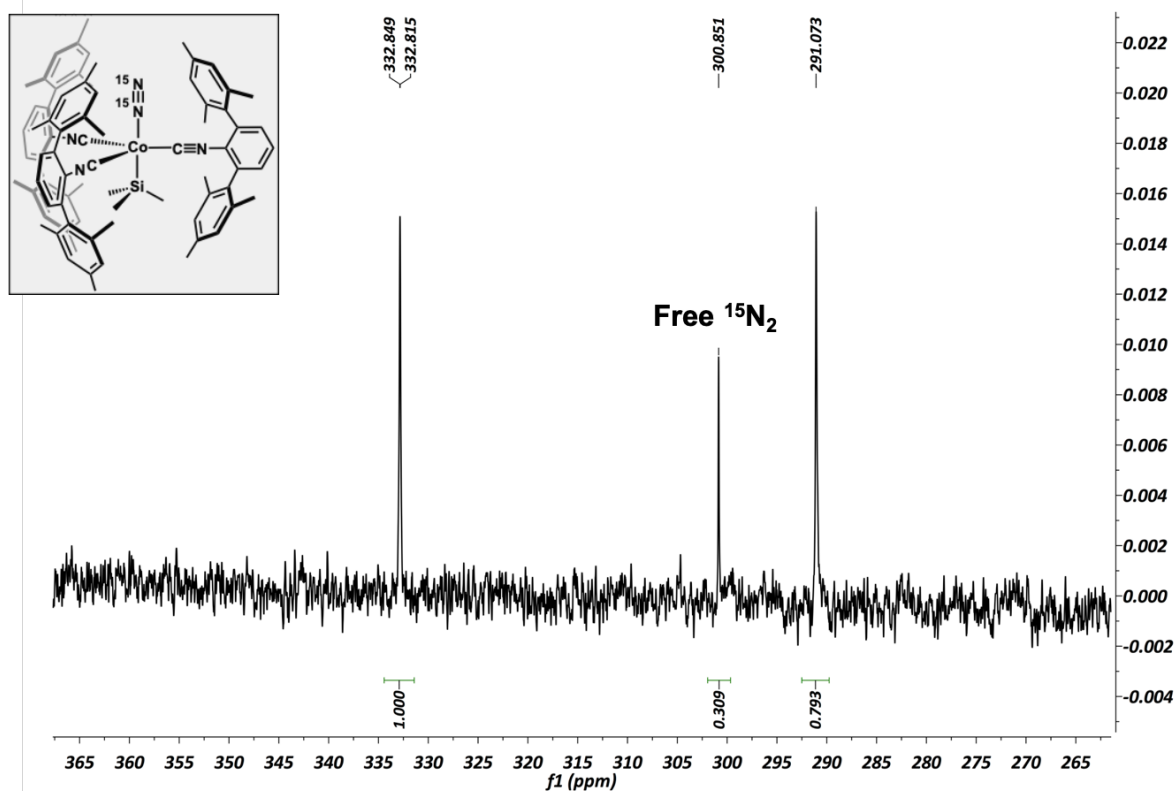


Figure 5.10.  $^{15}\text{N}\{^1\text{H}\}$  NMR spectrum (50.8 MHz,  $d_8$ -toluene,  $-60^\circ\text{C}$ ) of  $(^{15}\text{N}_2)\text{Co}(\text{SiMe}_3)(\text{CNAr}^{\text{Mes}_2})_3$  ( $4\text{-}^{15}\text{N}$ ). Singlet shown at 300 ppm attributed from free  $^{15}\text{N}_2(\text{g})$ .

## 5.5 Computational Studies

**Computational details.** Density Functional Theory (DFT) calculations were carried out on compound  $(\text{N}_2\text{O})\text{Co}(\text{SiMe}_3)(\text{CNAr}^{\text{Mes}_2})_3$  (**3**) and  $(\text{N}_2)\text{Co}(\text{SiMe}_3)(\text{CNAr}^{\text{Mes}_2})_3$  (**4**) with the Gaussian 09 software package.<sup>39</sup> Geometry optimizations, frequency and single point energy calculations were performed using the B3LYP<sup>40,41</sup> functional, with the 6-31g(d)<sup>42</sup> basis set for H, C, O and N atoms and the LANL2DZ basis set plus f-type polarization functions for cobalt atoms.<sup>43</sup> Viewing of optimized structures and rendering of molecular orbitals was performed using the program *Chemcraft*.<sup>44</sup> Wiberg bond indices and atom-atom overlap-weighted natural

atomic orbital (NAO) bond orders were determined using NBO 3.1<sup>45</sup> with the B3LYP functional and 6-31G(d) basis set using the ORCA computational suite 4.0.0.<sup>46</sup>

Separately, the DFT optimized geometries of (N<sub>2</sub>O)Co(SiMe<sub>3</sub>)(CNAr<sup>Ph2</sup>)<sub>3</sub> (**3m**) and (N<sub>2</sub>)Co(SiMe<sub>3</sub>)(CNAr<sup>Ph2</sup>)<sub>3</sub> (**4m**) (Ar<sup>Ph2</sup>= 2,6-(C<sub>6</sub>H<sub>5</sub>)<sub>2</sub>C<sub>6</sub>H<sub>3</sub>) were analyzed using the ADF program<sup>47-49</sup> at the B3LYP-D3/TZ2P level, using a closed shell NOCV analysis, with an energy threshold set at 0.5 kcal/mol.

### Input for Geometry Optimization of (N<sub>2</sub>O)Co(SiMe<sub>3</sub>)(CNAr<sup>Mes2</sup>)<sub>3</sub> (**3**)

The input for the optimization of **3** is listed below. The inputs for **4** is identical except for the input coordinates.

```
%chk=N-N2Ouncap-full.chk
%nprocs=16
%mem=30GB
# opt freq b3lyp/gen nosymm geom=connectivity pseudo=read
```

CSD ENTRY jfig979

```
0 1
Si      16.89253900  16.89396200  16.89591000
N       17.31587000  16.28548100  13.23377000
C       18.41411000  15.05204100  11.46373200
C       17.69626000  13.78634100  11.78048000
C       18.20360800  16.26058500  12.17935900
C       17.06673200  12.00957200  13.31635200
H       17.08918100  11.58874000  14.31796800
C       19.32906800  15.06147000  10.40242900
H       19.50075400  14.13615500  9.86037100
C       18.88901400  17.44757500  11.81869400
C       20.03381200  16.21249500  10.05989900
H       20.74766000  16.19210400  9.24136800
C       16.36631000  11.89603200  11.00991000
H       15.83734500  11.38984700  10.20679900
C       19.81227900  17.39157100  10.76654300
H       20.33666300  18.30109400  10.48871400
C       16.62001800  16.57673900  18.75651100
H       15.57019300  16.70783200  19.03865800
H       17.21495300  17.28818700  19.34586800
H       16.92836800  15.56577700  19.04562500
C       16.62782900  16.04500600  14.17614700
C       18.75349100  16.62221600  16.58007400
H       19.03588000  15.57251700  16.71165400
H       19.34214900  17.21754400  17.29177100
H       19.04321800  16.93038300  15.56923600
C       16.57618400  18.75489400  16.62467100
H       16.70878300  19.03788100  15.57526000
H       17.28701200  19.34352400  17.22106800
```

H	15.56490700	19.04407900	16.93191200
N	13.23045400	17.31586300	16.28432600
C	11.46240900	18.41605400	15.04982600
C	11.77982100	17.69851200	13.78411500
C	12.17678100	18.20447700	16.25891000
C	13.31699600	17.06857200	12.00862000
H	14.31904300	17.09045400	11.58878800
C	10.40180100	19.33182100	15.05869200
H	9.86070700	19.50432900	14.13296500
C	11.81555300	18.88957100	17.44589800
C	10.05875600	20.03628100	16.20974000
H	9.24077700	20.75075100	16.18894400
C	11.01013800	16.36992600	11.89249800
H	10.20713600	15.84177400	11.38529200
C	10.76415400	19.81366200	17.38936100
H	10.48588600	20.33783100	18.29887300
C	14.17341500	16.62830700	16.04478300
C	13.56852000	19.53437600	20.74727300
H	13.96351700	20.38343900	21.29878600
C	13.12854000	17.16803300	20.57040700
H	13.16852900	16.16677400	20.99095700
C	12.49239800	18.65065800	18.75049000
N	16.28202300	13.23139500	17.31615500
C	15.04732100	11.46102700	18.41233700
C	13.78217100	11.77883500	17.69399900
C	16.25626400	12.17633400	18.20309600
C	12.00650600	13.31595300	17.06439200
H	11.58616100	14.31776500	17.08722000
C	15.05581000	10.39900800	19.32648600
H	14.13018300	9.85718900	19.49724200
C	17.44272400	11.81468800	18.88889700
C	16.20630200	10.05546700	20.03159300
H	16.18519200	9.23637900	20.74478300
C	11.89228000	11.01002100	16.36242500
H	11.38603700	10.20748500	15.83264200
C	17.38578800	10.76182200	19.81128500
H	18.29489700	10.48321200	20.33597100
C	16.04259500	14.17452400	16.62880800
C	20.74237900	13.56848300	19.54015900
H	21.29268700	13.96249200	20.39046200
C	20.56852100	13.13195500	17.17295800
H	20.99022000	13.17366300	16.17225400
C	18.74719500	12.49264100	18.65248600
C	19.53686200	20.74694500	13.57430700
H	20.38651000	21.29760000	13.96926200
C	18.65128300	18.75166600	12.49692100
C	17.17013100	20.57184600	13.13574300
H	16.16913700	20.99294200	13.17676800
C	11.34136000	12.29297100	16.38530200
C	13.09931400	10.75587900	17.01373600
C	13.21661900	13.06370700	17.71207400
C	19.30678200	12.57054400	17.36684500
C	19.48386900	12.99823800	19.73565700
C	21.29028300	13.63448000	18.25848800
C	17.36524400	19.31046600	12.57395500
C	19.73359500	19.48879500	13.00369500
C	18.25480600	21.29405000	13.63947700
C	17.01707100	13.10356900	10.75675500
C	17.71385700	13.22018900	13.06509200
C	16.38869400	11.34451700	12.29261400



C	13.06501300	17.71537600	13.21926000
C	12.29340400	16.39158400	11.34226600
C	10.75626800	17.02036900	13.10006000
C	12.56807200	17.36424400	19.30861000
C	13.63230700	18.25196600	21.29370500
C	12.99923600	19.73220500	19.48869100
Co	15.54702600	15.54831700	15.54879000
N	14.40967600	14.41101200	14.41002100
N	13.75652700	13.75795600	13.75597800
O	13.06431700	13.06586700	13.06284700
C	16.97579228	13.71536768	9.34409848
H	17.92444818	13.57876137	8.86839825
H	16.21493848	13.23154389	8.76797693
H	16.75930952	14.76087854	9.41439960
C	18.45562558	13.93731832	14.20837889
H	18.00462113	13.67875840	15.14360173
H	19.48221373	13.63564989	14.21197434
H	18.39542631	14.99581170	14.06392192
C	15.66837111	10.01331989	12.57660202
H	14.62192414	10.12580766	12.38374130
H	16.06776479	9.24937216	11.94274986
H	15.81494052	9.73985758	13.60063120
C	16.16387172	18.53119542	12.00734931
H	15.79304445	17.85725032	12.75111347
H	15.39124795	19.21809006	11.73143579
H	16.47260343	17.97680486	11.14581821
C	21.14953492	18.88648949	12.94090793
H	21.53836772	18.99197674	11.94965545
H	21.78648997	19.40006867	13.63041841
H	21.10754905	17.84893821	13.19902520
C	18.03538669	22.68375238	14.26572174
H	18.34950718	22.66771490	15.28844904
H	18.60701382	23.41137688	13.72840897
H	16.99718543	22.93773737	14.21542512
C	14.20814652	18.45593403	13.93788337
H	15.09720465	17.86174330	13.90029310
H	14.38521465	19.39375274	13.45410351
H	13.93627502	18.62684941	14.95855659
C	9.34297309	16.97990786	13.71043725
H	8.86896800	17.92968514	13.57574394
H	8.76604924	16.22121085	13.22418861
H	9.41193781	16.76071496	14.75547234
C	12.57817695	15.67161328	10.01104606
H	13.56036652	15.92581658	9.67106911
H	12.51396297	14.61355330	10.15694203
H	11.85806295	15.97523081	9.28018887
C	12.00149714	16.16368645	18.52806243
H	12.74894961	15.78670131	17.86165641
H	11.71538221	15.39468534	19.21484882
H	11.14650056	16.47551947	17.96535378
C	12.93795105	21.14852951	18.88713548
H	11.95092439	21.54416140	19.00610512
H	13.63876772	21.78074656	19.39117675
H	13.18157998	21.10474976	17.84616080
C	14.25709048	18.03132921	22.68387226
H	15.27904023	18.34807046	22.66995568
H	13.71727571	18.60012416	23.41186424
H	14.20905810	16.99249343	22.93569189
C	18.88069362	12.93450011	21.15118409
H	19.00918078	11.94979914	21.54962486

H	19.37647303	13.64213779	21.78233517
H	17.83733779	13.16727801	21.10510738
C	18.52795906	12.00534203	16.16452160
H	17.69006275	12.63652836	15.95372884
H	19.17010656	11.96760249	15.30946470
H	18.18257785	11.01919009	16.39499110
C	22.68038050	14.26031989	18.04042065
H	22.64680520	15.29995416	18.29128569
H	23.39587309	13.76593015	18.66375776
H	22.96430978	14.14991195	17.01470419
C	13.93383860	14.20620727	18.45496644
H	13.90325194	15.09400919	17.85850000
H	13.44417642	14.38700886	19.38901233
H	14.95241518	13.93141853	18.63355229
C	13.71047302	9.34296280	16.97187346
H	13.56337842	8.86259946	17.91660318
H	13.23438624	8.77106498	16.20299489
H	14.75829071	9.41352288	16.76693602
C	10.01073806	12.57807309	15.66435676
H	9.67222159	13.56139144	15.91613369
H	10.15676548	12.51110219	14.60648583
H	9.27870444	11.85981594	15.96953448

Si C N H O 0

6-31g(d)

\*\*\*\*

Co 0

f 1 1.0

2.78 1.0

\*\*\*\*

Co 0

lan12dz

\*\*\*\*

Co 0

lan12dz

## S2.2. Optimized coordinates for $(\text{N}_2\text{O})\text{Co}(\text{SiMe}_3)(\text{CNAr}^{\text{Mes}_2})_3$ (3)

Si	0.000114066	0.000128293	2.324242175
N	-1.486221305	2.620743929	0.204357898
C	-1.552234582	4.707715207	-1.007548856
C	-0.679251862	4.185380516	-2.105414850
C	-1.941414895	3.921084374	0.106222831
C	1.513399457	3.794054591	-3.051889635
H	2.596601624	3.819236452	-2.948641332
C	-2.015209010	6.025934970	-1.089204831
H	-1.710025415	6.627436082	-1.941234398
C	-2.793944723	4.453503050	1.104619427
C	-2.843374563	6.567862157	-0.108722964
H	-3.191364328	7.593814795	-0.190018407
C	-0.441039019	3.354441586	-4.367344833
H	-0.897319177	3.026811996	-5.299327259
C	-3.225919117	5.779204085	0.973436418
H	-3.882303423	6.184290924	1.738788432

C	1.025530784	-1.433450380	3.045153634
H	0.656694846	-2.405130192	2.703607741
H	0.972358971	-1.422369396	4.142508037
H	2.079680041	-1.350078726	2.761089385
C	-0.910928376	1.578033383	0.149855959
C	0.728799072	1.604986292	3.045095222
H	1.754118497	1.772479345	2.702299865
H	0.747270543	1.552728409	4.142387482
H	0.128394261	2.475879697	2.762368645
C	-1.753965999	-0.171282641	3.045412441
H	-2.411713108	0.632999448	2.702865722
H	-1.717741093	-0.129324324	4.142709336
H	-2.208088044	-1.126628463	2.762648052
N	-1.526475317	-2.597540536	0.204086488
C	-3.300221355	-3.698071091	-1.008858301
C	-3.283997674	-2.680844781	-2.106698805
C	-2.424907485	-3.641953777	0.105317722
C	-4.041567759	-0.586550008	-3.053635534
H	-4.605114081	0.338885365	-2.950658983
C	-4.210262039	-4.758173191	-1.091057134
H	-4.883458697	-4.794518267	-1.943339472
C	-2.460074783	-4.646684837	1.103489922
C	-4.265880515	-5.746527471	-0.110782510
H	-4.980316887	-6.560886944	-0.192551164
C	-2.683241040	-2.059338654	-4.368658318
H	-2.171193771	-2.290820629	-5.300510825
C	-3.392055889	-5.683674780	0.971747282
H	-3.414949913	-6.454820690	1.736936234
C	-0.911134907	-1.577948156	0.149798621
C	-1.155186049	-4.386892466	4.657397066
H	-1.521048950	-4.079392613	5.635199657
C	0.586845209	-5.274517549	3.273341824
H	1.593416816	-5.672984537	3.159964720
C	-1.537734496	-4.666067750	2.282766744
N	3.012744323	-0.023133018	0.204882943
C	4.853153676	-1.010244844	-1.006402510
C	3.964685431	-1.504107109	-2.105027145
C	4.366391097	-0.279801921	0.107255792
C	2.529189135	-3.206146827	-3.053238053
H	2.008817807	-4.156586114	-2.950765070
C	6.226143109	-1.269237446	-1.087374903
H	6.594573900	-1.834374040	-1.939299528
C	5.253544158	0.191885669	1.106014334
C	7.109315220	-0.823691563	-0.106365076
H	8.171718536	-1.035964063	-0.187131978
C	3.127668559	-1.293520212	-4.367452943
H	3.073061522	-0.734129403	-5.299244963
C	6.617511593	-0.097730900	0.975531549
H	7.296384763	0.267824409	1.741168780
C	1.822097647	0.000000000	0.150024325
C	4.375297319	1.195442383	4.658794717
H	4.291849497	0.725822094	5.637063805
C	4.272830299	3.146449852	3.272721237
H	4.114423480	4.217248432	3.158211311
C	4.808774550	1.001360794	2.284436071
C	-3.221822581	3.192729093	4.658190694
H	-2.772941444	3.355839994	5.636152821
C	-3.271868316	3.663987280	2.283617925
C	-4.860596506	2.127297813	3.273480308
H	-5.708587433	1.454399085	3.159736347

C	2.441329247	-2.508020533	-4.259484434
C	3.886398478	-0.778153286	-3.313458328
C	3.277474801	-2.726000529	-1.970935166
C	4.594695231	2.388934820	2.142649753
C	4.707775180	0.400210444	3.556389447
C	4.150137022	2.568760559	4.539841445
C	-4.366282751	2.784390283	2.142831001
C	-2.700180110	3.877925725	3.555179769
C	-4.298340420	2.310672361	4.540216955
C	-1.267690436	3.753769334	-3.314096552
C	0.722434580	4.202062598	-1.970331257
C	0.953843749	3.368113901	-4.258357121
C	-3.999410468	-1.475309469	-1.971901704
C	-3.392749717	-0.858301719	-4.260007840
C	-2.615768851	-2.974714365	-3.315216442
C	-0.229001374	-5.174754474	2.142438977
C	0.146738762	-4.878862255	4.539883033
C	-2.009019616	-4.277472324	3.554114480
Co	0.000000000	0.000000000	0.000000000
N	0.000000000	0.000000000	-1.962926913
N	0.000132456	0.000211017	-3.094414500
O	0.000369170	0.000479058	-4.297393828
C	-2.771010592	3.721930513	-3.486061886
H	-3.212631715	4.723298121	-3.418297077
H	-3.041006374	3.300955151	-4.459250377
H	-3.251261242	3.113199724	-2.710609605
C	1.379575000	4.657997284	-0.687404080
H	2.460130314	4.766160473	-0.821303866
H	0.980929319	5.620014687	-0.346157786
H	1.216927022	3.934614785	0.121134777
C	1.819376473	2.913756582	-5.410308492
H	1.793319290	1.821025399	-5.507290207
H	1.472066308	3.331677138	-6.362625898
H	2.863083264	3.214073942	-5.270387724
C	-5.021195042	2.560811926	0.798080084
H	-4.338918414	2.063182553	0.098618542
H	-5.911075606	1.931768714	0.899823343
H	-5.324839507	3.506168315	0.333245829
C	-1.552427739	4.844930871	3.751546692
H	-1.869627387	5.885541529	3.609048855
H	-1.141095418	4.758166198	4.762041969
H	-0.738952864	4.663047222	3.041197532
C	-4.819617495	1.551297325	5.737801337
H	-4.339358827	0.566740996	5.817293867
H	-4.621187838	2.087629035	6.671996945
H	-5.899575164	1.380253121	5.666916081
C	-4.722935821	-1.133966500	-0.689091313
H	-4.015179619	-0.911860195	0.119119213
H	-5.357789173	-0.252983027	-0.823507012
H	-5.355883525	-1.960580402	-0.347114120
C	-1.836277275	-4.260596539	-3.486938643
H	-2.482510704	-5.143851222	-3.419060163
H	-1.336672296	-4.283989192	-4.460108684
H	-1.068973333	-4.371881848	-2.711455870
C	-3.432153130	0.118197738	-5.412165842
H	-4.214131253	0.871890144	-5.272363145
H	-2.472831884	0.642045868	-5.509323968
H	-3.620454148	-0.391754577	-6.364365219
C	0.292100758	-5.630806291	0.797929002
H	0.381705070	-4.791553947	0.097934657

H	1.281893058	-6.086718799	0.899860884
H	-0.374679160	-6.366864421	0.333580517
C	-3.420164842	-3.766293929	3.749958378
H	-4.163105243	-4.560894983	3.607009717
H	-3.550905374	-3.366758984	4.760451351
H	-3.668653153	-2.970628098	3.039606112
C	1.064528649	-4.950996148	5.737820535
H	1.676218537	-4.042348475	5.818564575
H	0.500474538	-5.048745173	6.671654606
H	1.753394352	-5.800077263	5.666402935
C	4.970762673	-1.077233941	3.753827811
H	6.030439913	-1.323413745	3.611484698
H	4.689842062	-1.389207153	4.764559708
H	4.406207668	-1.691052370	3.043947106
C	4.729074404	3.066909061	0.797454983
H	3.957084040	2.724558547	0.098026456
H	4.629528922	4.152195129	0.898375797
H	5.699671639	2.856578107	0.333039921
C	3.753308051	3.400812556	5.736838422
H	2.660528467	3.476519576	5.816970806
H	4.119449485	2.961975972	6.671247022
H	4.144436391	4.421790294	5.664690435
C	3.342359081	-3.523589721	-0.688262930
H	2.796356494	-3.021298997	0.119849344
H	2.895869944	-4.513391312	-0.823039492
H	4.374439880	-3.659528014	-0.345949817
C	4.611294554	0.539371346	-3.484366437
H	5.699182291	0.420642617	-3.415407134
H	4.382996322	0.983994305	-4.457714492
H	4.323719969	1.259632568	-2.709086606
C	1.615597421	-3.029502164	-5.412226412
H	1.353938755	-4.083707501	-5.273360888
H	0.682234443	-2.460637808	-5.509044861
H	2.151533775	-2.936728650	-6.364252915

### S2.3. Optimized coordinates for (N<sub>2</sub>)Co(SiMe<sub>3</sub>)(CNAr<sup>Mes</sup><sub>2</sub>)<sub>3</sub> (4)

Si	0.000000000	0.000000000	-2.335555673
N	3.012704569	0.022567201	-0.196644536
C	4.844057576	0.964762165	1.063766245
C	3.950464605	1.413811284	2.177581417
C	4.366269649	0.271401871	-0.077160188
C	2.473753370	3.056111653	3.168076279
H	1.925646016	3.992985593	3.086975933
C	6.216176531	1.224664426	1.158885740
H	6.579179154	1.763730723	2.029786699
C	5.259807512	-0.172083618	-1.082708717
C	7.105463572	0.812463373	0.168955502
H	8.166672038	1.025926170	0.261640115
C	3.136317921	1.137403152	4.440808152
H	3.107664058	0.560432702	5.363341380
C	6.622417754	0.115877159	-0.936038324
H	7.306977053	-0.227452637	-1.706851713
C	-1.755197045	0.163854772	-3.055597610
H	-2.406070308	-0.648508921	-2.718947751
H	-1.719215967	0.130486022	-4.153197606

H	-2.217019470	1.113349045	-2.765540892
C	1.822553515	0.000000000	-0.156599452
C	1.019402882	1.438322164	-3.055317208
H	0.640564070	2.408075656	-2.719217056
H	0.973314529	1.423506853	-4.152941157
H	2.072421230	1.364171319	-2.764417782
C	0.735355805	-1.602027501	-3.055661660
H	1.763393288	-1.761416448	-2.717104891
H	0.748557744	-1.553006046	-4.153176220
H	0.142041507	-2.476122609	-2.767730802
N	-1.486627409	-2.620506936	-0.195581182
C	-1.587503076	-4.676319255	1.066795044
C	-0.750635389	-4.126698384	2.179588778
C	-1.948747164	-3.916720407	-0.074810415
C	1.411050956	-3.669886301	3.168175579
H	2.496415989	-3.664627851	3.086364005
C	-2.049664239	-5.994040653	1.163437578
H	-1.764566793	-6.577292857	2.034854215
C	-2.780039286	-4.469273001	-1.079731134
C	-2.852054382	-6.558421962	0.174325201
H	-3.198720405	-7.583764045	0.268221957
C	-0.580664805	-3.281588763	4.441969495
H	-1.065087565	-2.967086396	5.364573692
C	-3.213168343	-5.792736845	-0.931524943
H	-3.853112576	-6.214241068	-1.701887552
C	-0.911193763	-1.578451091	-0.156099069
C	-3.152769793	-3.268385371	-4.660636762
H	-2.688508005	-3.447490319	-5.628603787
C	-4.813083044	-2.181358414	-3.319099978
H	-5.662643961	-1.506847073	-3.229647074
C	-3.238894938	-3.700179508	-2.279634915
N	-1.526306140	2.597663710	-0.195817970
C	-3.256540957	3.712696849	1.066459362
C	-3.197910953	2.714187415	2.180155074
C	-2.418331492	3.645578384	-0.075316373
C	-3.881679910	0.614360084	3.171160969
H	-4.419223543	-0.328653616	3.090486755
C	-4.167390782	4.771206867	1.162567318
H	-4.814906418	4.816065599	2.034085760
C	-2.481973139	4.641208191	-1.080754020
C	-4.255882828	5.747580312	0.172843111
H	-4.971113269	6.559997322	0.266359269
C	-2.550337206	2.147331412	4.443081164
H	-2.035779039	2.410956385	5.365312175
C	-3.412290442	5.677463276	-0.933052284
H	-3.457958104	6.441982569	-1.703816467
C	-0.911495116	1.578351910	-0.156264267
C	-1.255078959	4.363549201	-4.661474701
H	-1.641988732	4.050485894	-5.629398572
C	0.515582008	5.259791353	-3.320017350
H	1.524139144	5.659203093	-3.230590123
C	-1.586390978	4.654288283	-2.280569608
C	4.404882655	-1.100337371	-4.662049329
H	4.327420878	-0.610075745	-5.630670641
C	4.822769317	-0.955606245	-2.281410532
C	4.294485233	-3.079860773	-3.317705563
H	4.135291580	-4.152750455	-3.226699689
C	-3.221058396	0.923567195	4.362548973
C	-2.523771209	3.047933329	3.374171715
C	-3.880581339	1.485468188	2.075924498

C	-0.274944233	5.164044183	-2.170818881
C	-2.084308300	4.258239098	-3.539273336
C	0.048240018	4.858456143	-4.574871292
C	4.607553554	-2.345954438	-2.169628363
C	4.728987162	-0.328136684	-3.541004087
C	4.180813591	-2.476188879	-4.573423963
C	3.902863567	0.663697092	3.372010062
C	3.227518566	2.619193438	2.072923011
C	2.411549718	2.329944673	4.359806688
C	0.654688222	-4.104552856	2.073921492
C	0.814451037	-3.251435554	4.359970118
C	-1.375264802	-3.708820203	3.374070159
C	-4.335312612	-2.818334607	-2.169876466
C	-4.232173266	-2.386104462	-4.574005002
C	-2.647382109	-3.934146241	-3.538398482
Co	0.000000000	0.000000000	0.000000000
N	0.000244266	0.000197205	1.899240859
N	0.000469079	0.000325590	3.012724973
C	-1.777525458	4.356967541	3.516324830
H	-2.446865847	5.222531225	3.445314525
H	-1.265038142	4.408012332	4.481820545
H	-1.024078290	4.476720254	2.728601124
C	-4.613322548	1.102566956	0.810185633
H	-5.230990841	0.213899924	0.972212797
H	-5.264805652	1.909872379	0.457006212
H	-3.910775753	0.873887660	-0.000688084
C	-3.206038406	-0.044275291	5.522315759
H	-4.089226545	-0.692400722	5.516438856
H	-2.321071753	-0.692699343	5.477191283
H	-3.177245540	0.480672923	6.483755902
C	0.276987736	5.623556845	-0.839768705
H	0.387987146	4.785042606	-0.141936709
H	1.262029978	6.083766531	-0.965940303
H	-0.381457705	6.356585663	-0.359084853
C	-3.498051353	3.742343806	-3.701536366
H	-4.240115439	4.535415022	-3.546073394
H	-3.649583449	3.337663167	-4.707037389
H	-3.728416069	2.949281803	-2.982113692
C	0.938502622	4.927300912	-5.793596765
H	1.536520724	4.011639126	-5.895179361
H	0.353906849	5.038589495	-6.713240508
H	1.639454997	5.767199846	-5.732733558
C	3.261881568	3.444546086	0.806729852
H	2.712487649	2.949952655	-0.003779376
H	2.800995800	4.423809140	0.968339598
H	4.286682797	3.605082390	0.453261253
C	4.663630474	-0.636887853	3.514593594
H	5.747806346	-0.490026952	3.442223934
H	4.452654230	-1.105339803	4.480759623
H	4.389773990	-1.350027612	2.727834150
C	1.565870683	2.801148552	5.519457975
H	1.445187420	3.889956122	5.512621274
H	0.562223325	2.358002223	5.475086814
H	2.006695160	2.515018517	6.481007510
C	4.729248847	-3.051909508	-0.837598960
H	3.947791355	-2.727431155	-0.140154172
H	4.634716285	-4.135209319	-0.962283604
H	5.693449744	-2.848029544	-0.357287524
C	4.989777491	1.153787707	-3.705451623
H	6.047601688	1.399800244	-3.549726368

H	4.715793738	1.485878063	-4.711637179
H	4.417899246	1.751146264	-2.987315292
C	3.794334566	-3.283095897	-5.790851479
H	2.702247628	-3.344071680	-5.890892236
H	4.181469361	-2.833087927	-6.711442969
H	4.172059487	-4.309760520	-5.729473062
C	-2.881906141	-3.715921062	3.517677182
H	-3.297652416	-4.728095906	3.447619507
H	-3.181132705	-3.296834897	4.483210803
H	-3.362611457	-3.123376128	2.730052505
C	1.351084234	-4.548693287	0.807663445
H	1.197562766	-3.826150844	-0.003369571
H	2.429620490	-4.639940961	0.968672271
H	0.976652225	-5.516418347	0.455241942
C	1.646628428	-2.754328855	5.518571799
H	2.649144320	-3.195968656	5.512077400
H	1.766568211	-1.663851154	5.472462050
H	1.178329922	-2.990726645	6.480641004
C	-5.008787615	-2.569237573	-0.838765808
H	-4.337496385	-2.054364754	-0.141140661
H	-5.899269690	-1.945426379	-0.964914741
H	-5.315202940	-3.505607679	-0.357870501
C	-1.494570000	-4.901541826	-3.700623166
H	-1.810876599	-5.940306130	-3.543533307
H	-1.069246390	-4.831952100	-4.706614501
H	-0.691734082	-4.704151236	-2.982213823
C	-4.736355378	-1.649049585	-5.792670769
H	-4.243358704	-0.672670500	-5.892749420
H	-4.538748065	-2.209927730	-6.712578894
H	-5.814489474	-1.463197611	-5.732890542

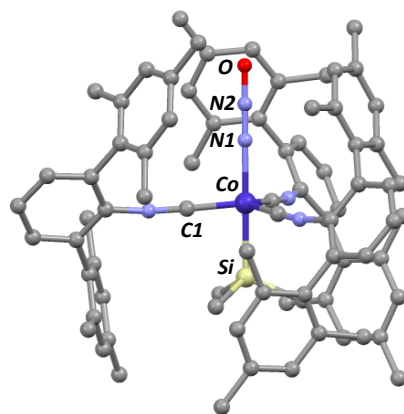


**Figure 5.11.** Geometry optimized structure of  $(\text{N}_2\text{O})\text{Co}(\text{SiMe}_3)(\text{CNAr}^{\text{Mes}_2})_3$  (3) with hydrogen atoms omitted for clarity. (B3LYP/6-31G(d):LANL2DZ)



**Table 5.2. Comparison of calculated and experimental structural parameters for 3.**

Parameter	Calculated	Experimental
d(Co-Si)	2.324 Å	2.295(1) Å
d(Co-N1)	1.963 Å	1.964(4) Å
d(N1-N2)	1.131 Å	1.111(5) Å
d(N2-O)	1.203 Å	1.209(6) Å
d(Co-C1)	1.828 Å	1.814(4) Å

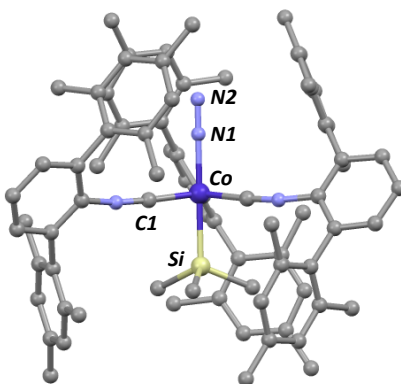
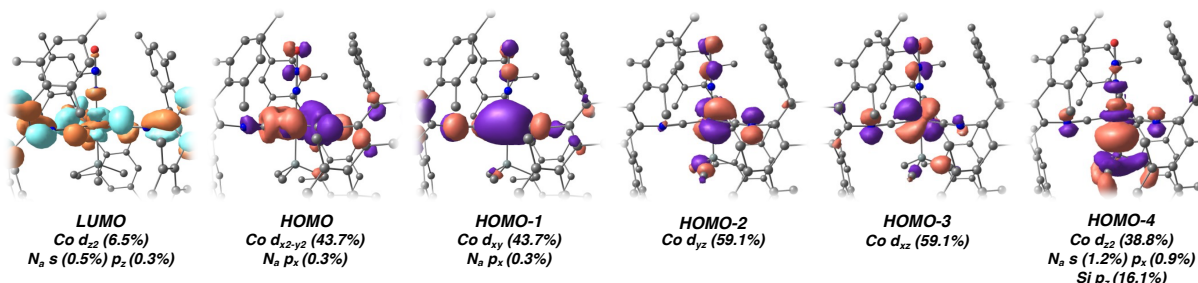


**Figure 5.12. Geometry optimized structure of  $(N_2)Co(SiMe_3)(CNAr^{Mes_2})_3$  (4) with hydrogen atoms omitted for clarity. (B3LYP/6-31G(d):LANL2DZ)**

Table 5.3. Comparison of calculated and experimental structural parameters for 4.

Parameter	Calculated	Experimental
d(Co-Si)	2.336 Å	2.286(2) Å
d(Co-N1)	1.899 Å	1.933(5) Å
d(N1-N2)	1.113 Å	1.046 Å
d(Co-C1)	1.829 Å	1.806(3) Å

$(N_2O)Co(SiMe_3)(CNAr^{Mes2})_3$



$(N_2)Co(SiMe_3)(CNAr^{Mes2})_3$

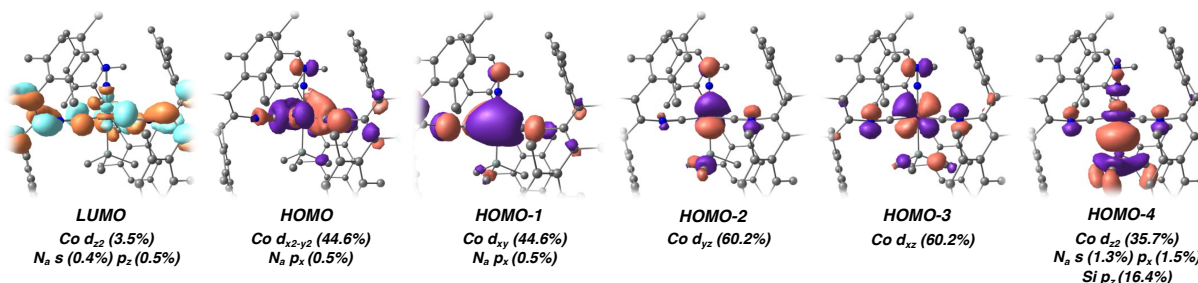
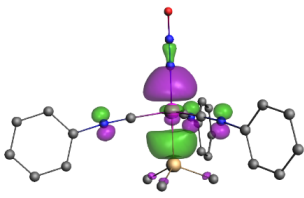
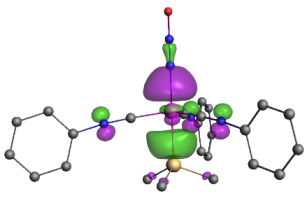
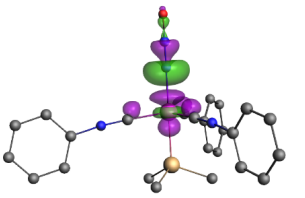
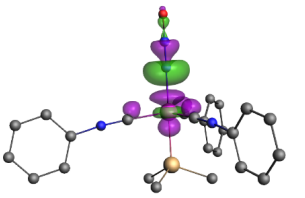
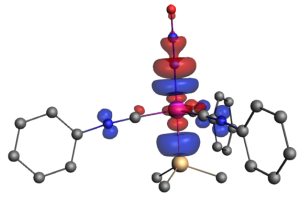
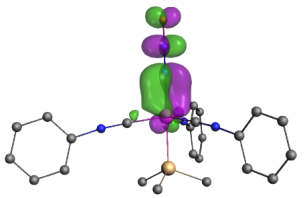
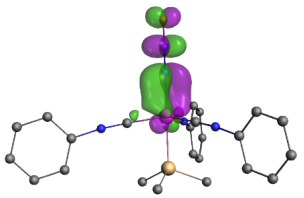
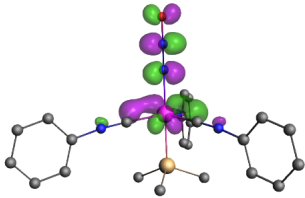
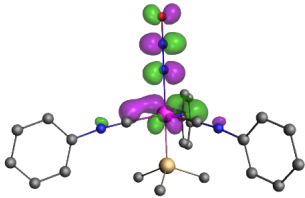
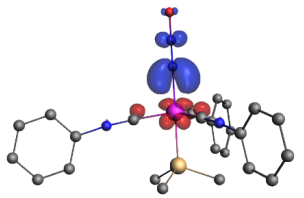
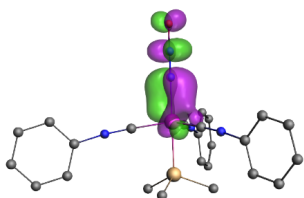
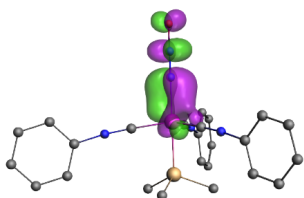
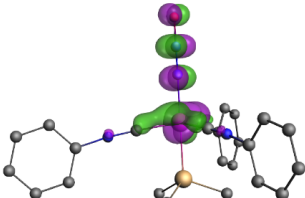
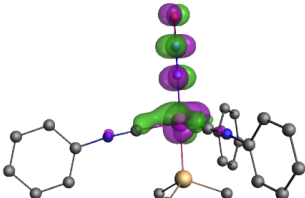
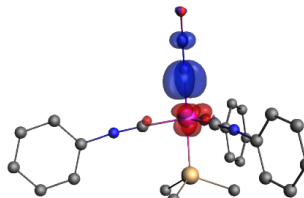
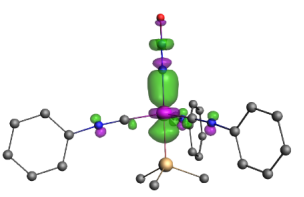
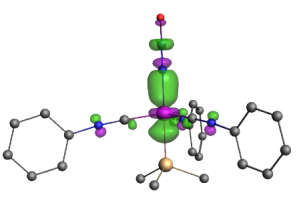
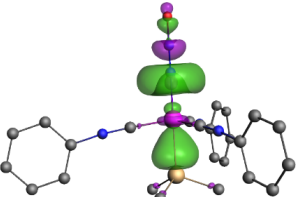
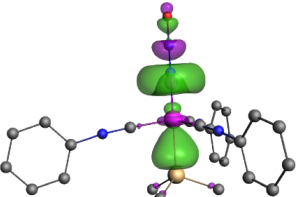
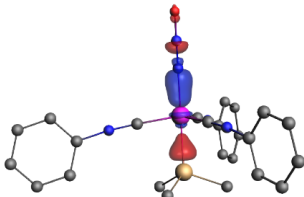


Figure 5.13. Calculated molecular orbitals (MOs) of  $(N_2O)Co(SiMe_3)(CNAr^{Mes2})_3$  (3) and  $(N_2)Co(SiMe_3)(CNAr^{Mes2})_3$  (4) showing MOs with cobalt d-orbital character. Atomic orbital contributions (AO%) to the molecular orbitals are listed. The AO% to these MOs reveal the similarity between  $N_2O$  and  $N_2$  binding upon coordination to  $Co(SiMe_3)(CNAr^{Mes2})_3$  (2).

**Table 5.4. Natural orbitals for chemical valence (NOCV) orbitals of  $(\text{N}_2\text{O})\text{Co}(\text{SiMe}_3)(\text{CNAr}^{\text{Ph}_2})_3$  (3m). NOCV1 involves  $\sigma$ -donation from the  $\text{N}_2\text{O}$  ligand to the metal; NOCV2 and NOCV3 are the two perpendicular  $\pi$ -backbondings from metal to  $\text{N}_2\text{O}$ , in competition with the  $\text{CNAr}^{\text{Ph}_2}$  ligands; and NOCV4 involves (the often overlooked, though significant) backdonation from the metal to the  $\pi^*$ -antibonding orbital of  $\text{N}_2\text{O}$ . The NOCV orbitals are in identical order for  $(\text{N}_2)\text{Co}(\text{SiMe}_3)(\text{CNAr}^{\text{Ph}_2})_3$  (4m).**

	NOCV Combination	Bonding	NOCV Combination	Antibonding	$\Delta\rho$ electron “flow” from red→blue regions
1					
2					
3					
4					

**Table 5.5.** NOCV analyses of  $(\text{N}_2\text{O})\text{Co}(\text{SiMe}_3)(\text{CNAr}^{\text{Ph}_2})_3$  (**3m**) and  $(\text{N}_2)\text{Co}(\text{SiMe}_3)(\text{CNAr}^{\text{Ph}_2})_3$  (**4m**) showing  $\text{N}_2\text{O}$  and  $\text{N}_2$  are each better  $\pi$ -acceptors than  $\sigma$ -donors.  $\text{N}_2\text{O}$  is a weaker donor and a weaker acceptor than is  $\text{N}_2$ . \*stabilization energies for orbital components contributing to overall  $E_{\text{orb}}$ .

	NOCV Eigenvalue			
	Stabilization energy (kcal/mol)*			
	NOCV1	NOCV2	NOCV3	NOCV4
<b>3m</b>	0.379	0.384	0.374	0.132
	-15.1	-10.5	-11.6	-4.3
	<b>Total <math>\pi</math> -22.1</b>			
<b>4m</b>	0.344	0.334	0.296	0.129
	-12.4	-9.2	-6.7	-3.8
	<b>Total <math>\pi</math> -15.9</b>			

**Table 5.6.** Energy decomposition analyses of  $(\text{N}_2\text{O})\text{Co}(\text{SiMe}_3)(\text{CNAr}^{\text{Ph}_2})_3$  (**3m**) and  $(\text{N}_2)\text{Co}(\text{SiMe}_3)(\text{CNAr}^{\text{Ph}_2})_3$  (**4m**) showing  $\text{N}_2\text{O}$  binds more weakly than  $\text{N}_2$  with  $E_{\text{orb}}$  significantly lower for  $\text{N}_2\text{O}$ . Energies are shown in kcal/mol.

	$E_{\text{Pauli}}$	$E_{\text{estat}}$	$E_{\text{steric}}$	$E_{\text{orb}}$	$E_{\text{disp}}$	$E_{\text{tot}}$
<b>3m</b>	75.1	-49.5	25.6	-42.9	-5.3	<b>-22.6</b>
<b>4m</b>	70.8	-45.8	25.0	-34.3	-11.5	<b>-20.7</b>

## 5.6 Spectroscopy Evidence of the O-atom Transfer Reaction

**General Procedure:** The experiments were performed using crystalline materials of **3** or **3-<sup>15</sup>N** dissolved in  $\text{C}_6\text{H}_6$ ,  $\text{C}_6\text{D}_6$  or  $d_8$ -toluene to ensure the purity and reliability of the results.

**FTIR Spectroscopy study of the *O*-atom transfer reaction.** In the glovebox, a solution of **3** (in C<sub>6</sub>H<sub>6</sub>) or **3-<sup>15</sup>N** (in C<sub>6</sub>D<sub>6</sub>) was transferred into an airtight IR cell. The cell was then brought out to the spectrometer to collect the first data point. The second data point was collected on the same sample after being sat at room-temperature for 12 hours to observe the *O*-atom transfer reaction.

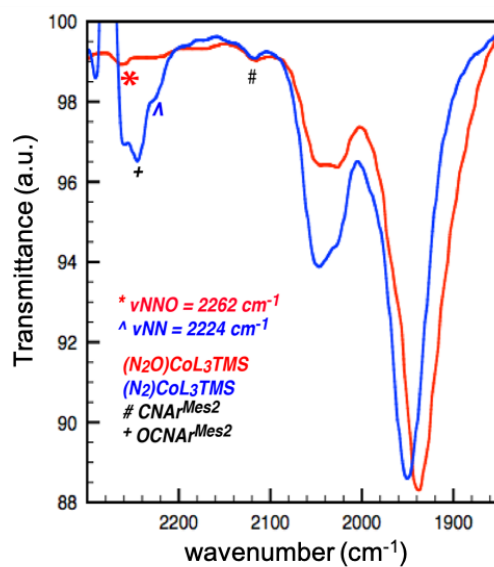


**Figure 5.14. Overlapped FTIR spectrum (C<sub>6</sub>H<sub>6</sub>, KBr windows, 25 °C) of the first data point (pure compound **3**) in red and the second data point (12 h) in blue showing the formation of **4** and OCNAr<sup>Mes2</sup>.**

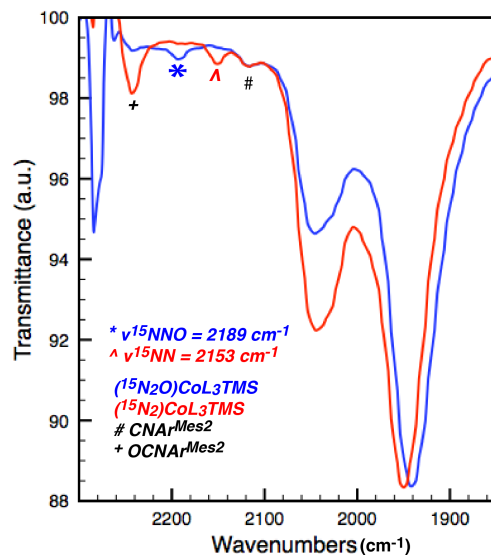


Figure 5.15. Overlapped FTIR spectrum (C<sub>6</sub>H<sub>6</sub>, KBr windows, 25 °C) of the first data point (pure compound 3-<sup>15</sup>N) in blue and the second data point (12 h) in red showing the formation of 4-<sup>15</sup>N and OCNAr<sup>Mes2</sup>.

**NMR Spectroscopy study of the *O*-atom transfer reaction.** In the glovebox, a solution of **3** (in C<sub>6</sub>D<sub>6</sub>) or 3-<sup>15</sup>N (in C<sub>6</sub>D<sub>6</sub>) was transferred into a J-young NMR tube. 1,3,5-*tert*-butylbenzene was added as internal standard shown at 1.35 ppm. The tube was then brought out to the spectrometer, with spectrum taken every 20 minutes under 25 °C until the concentration of **4** reached constant (around 12 hours).

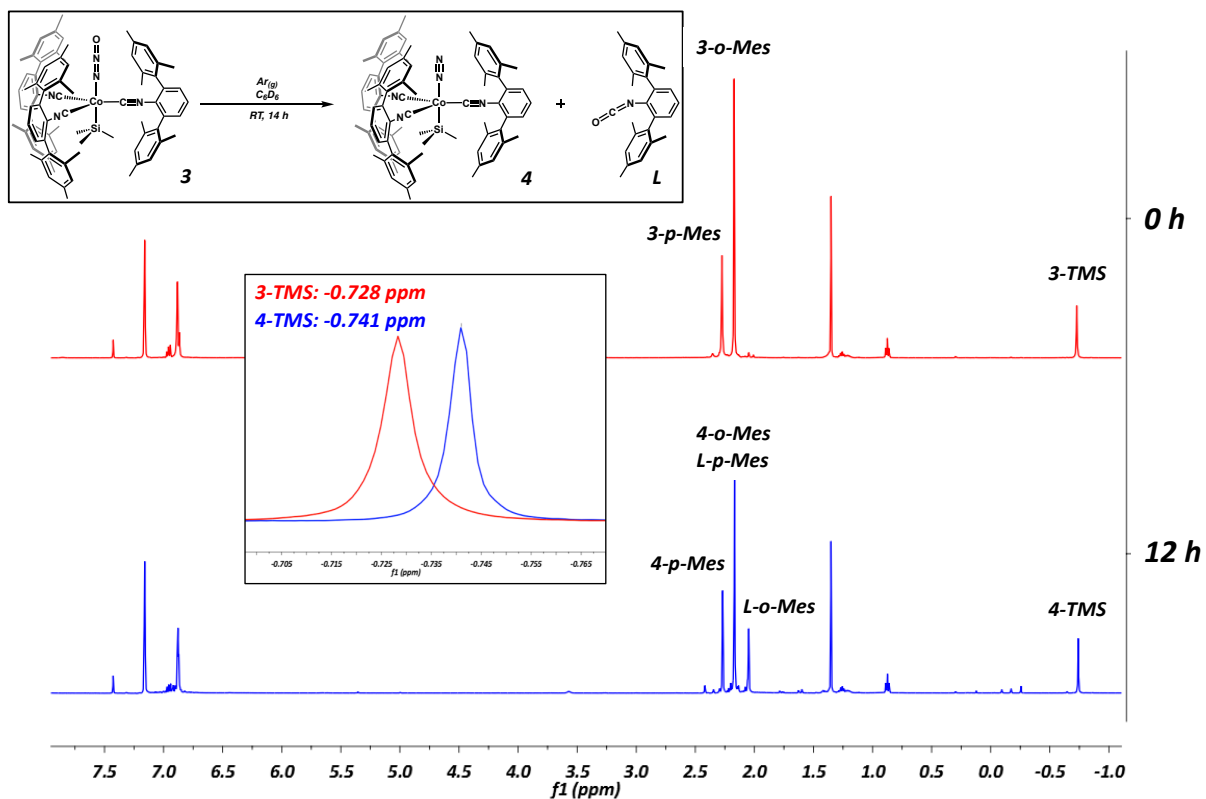


Figure 5.16. Overlapped  $^1\text{H}$  NMR spectrum ( $\text{C}_6\text{D}_6$ ,  $25^\circ\text{C}$ ) of the first data point (pure compound  $3\text{-}^{15}\text{N}$ ) in blue and the final data point (12 h) in red showing the formation of  $4\text{-}^{15}\text{N}$  and  $\text{OCNAr}^{\text{Mes}_2}$ .

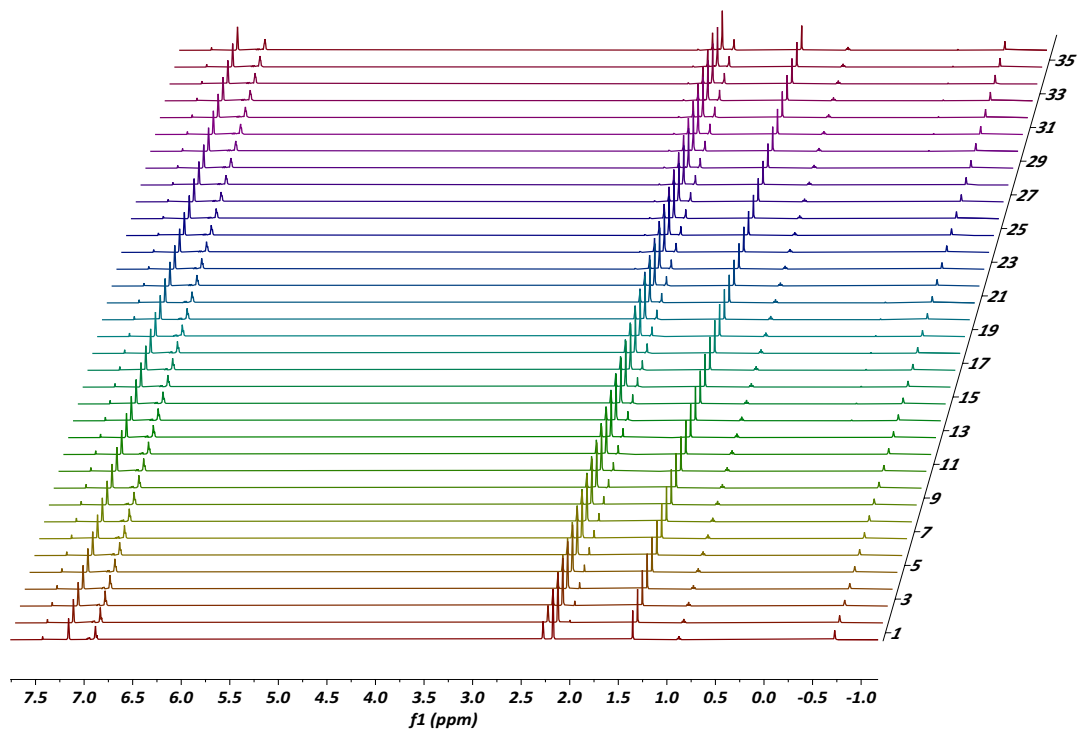


Figure 5.17. Stacked  $^1\text{H}$  NMR spectrum ( $\text{C}_6\text{D}_6$ ,  $25^\circ\text{C}$ ) of the  $O$ -atom transfer reaction of 3.

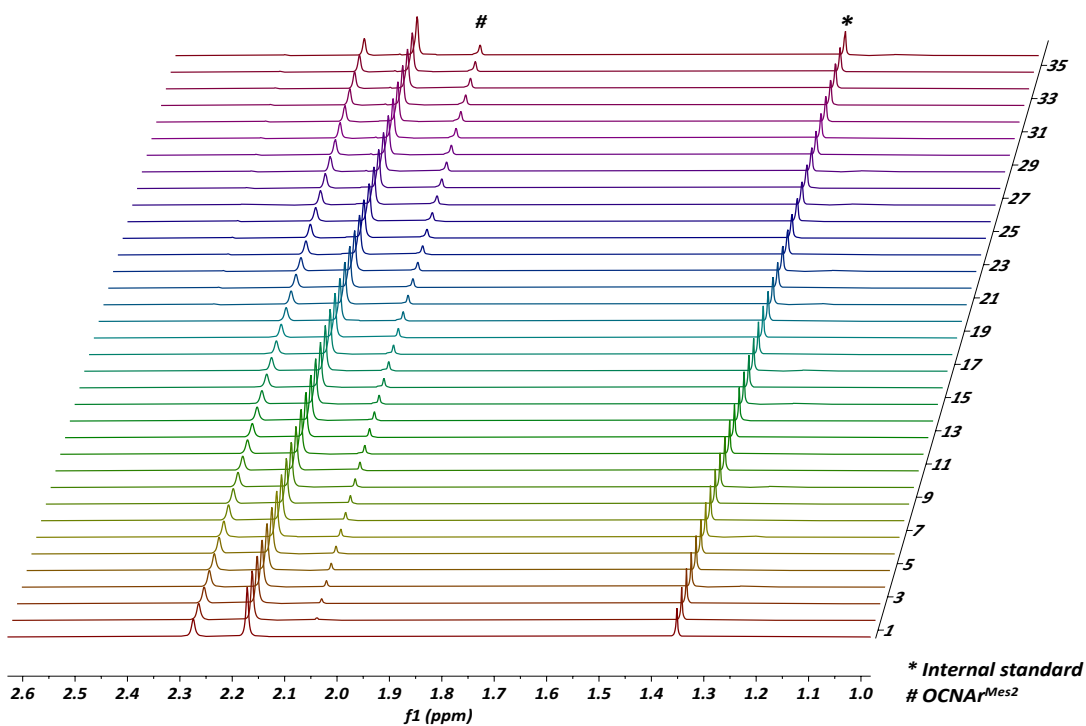


Figure 5.18. Zoomed-in stacked  $^1\text{H}$  NMR spectrum ( $\text{C}_6\text{D}_6$ ,  $25^\circ\text{C}$ ) of the  $O$ -atom transfer reaction of 3 showing the growth of  $\text{OCNAr}^{\text{Mes}_2}$  overtime.



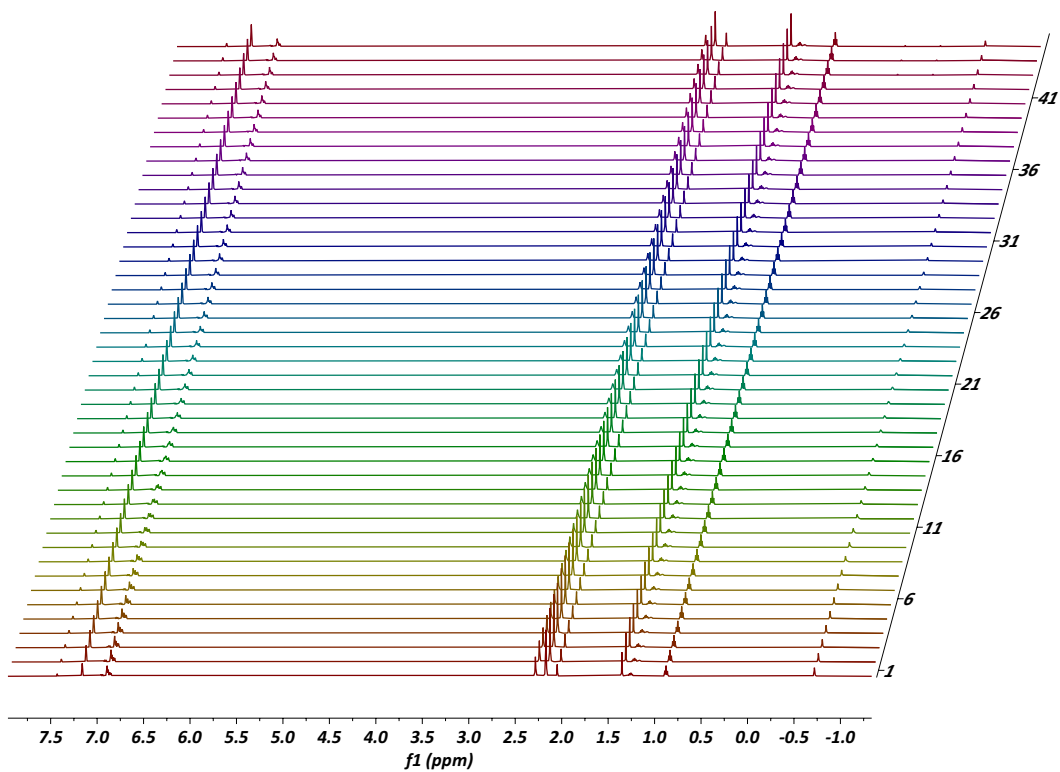


Figure 5.19. Stacked  $^1\text{H}$  NMR spectrum ( $\text{C}_6\text{D}_6$ ,  $25^\circ\text{C}$ ) of the *O*-atom transfer reaction of 3 with 1 equiv. of  $\text{CNAr}^{\text{Mes}_2}$ .

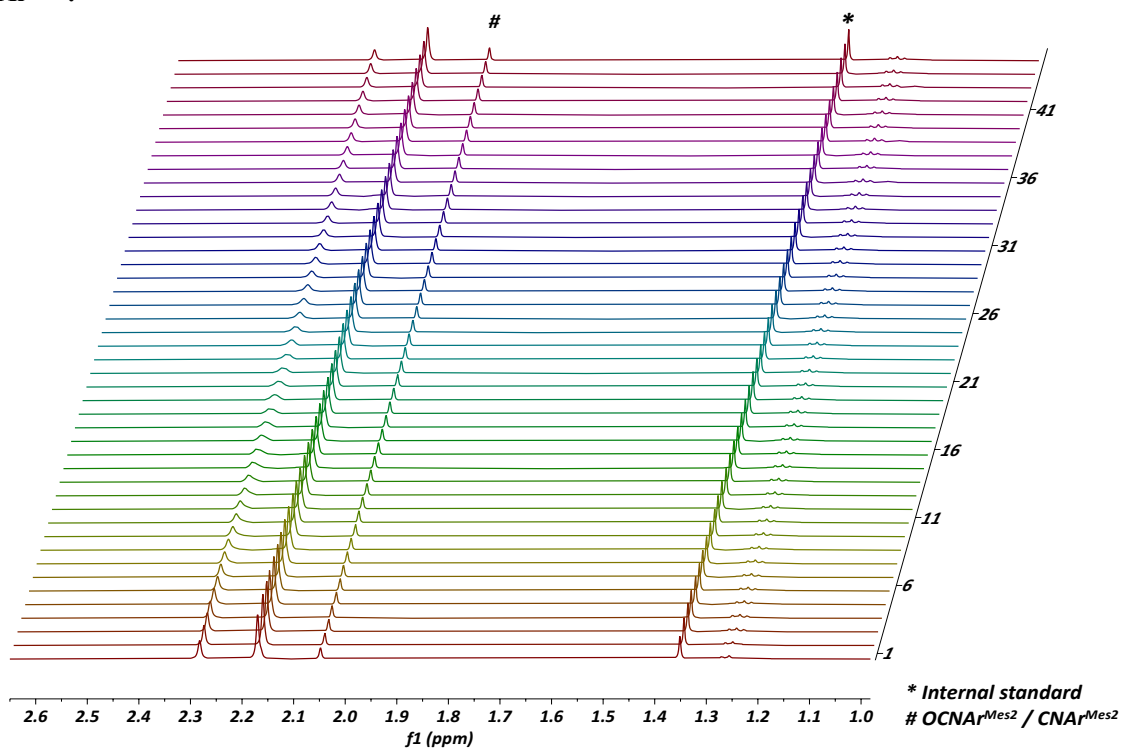


Figure 5.20. Zoomed-in stacked  $^1\text{H}$  NMR spectrum ( $\text{C}_6\text{D}_6$ ,  $25^\circ\text{C}$ ) of the *O*-atom transfer reaction of 3 with 1 equiv. of  $\text{CNAr}^{\text{Mes}_2}$ .

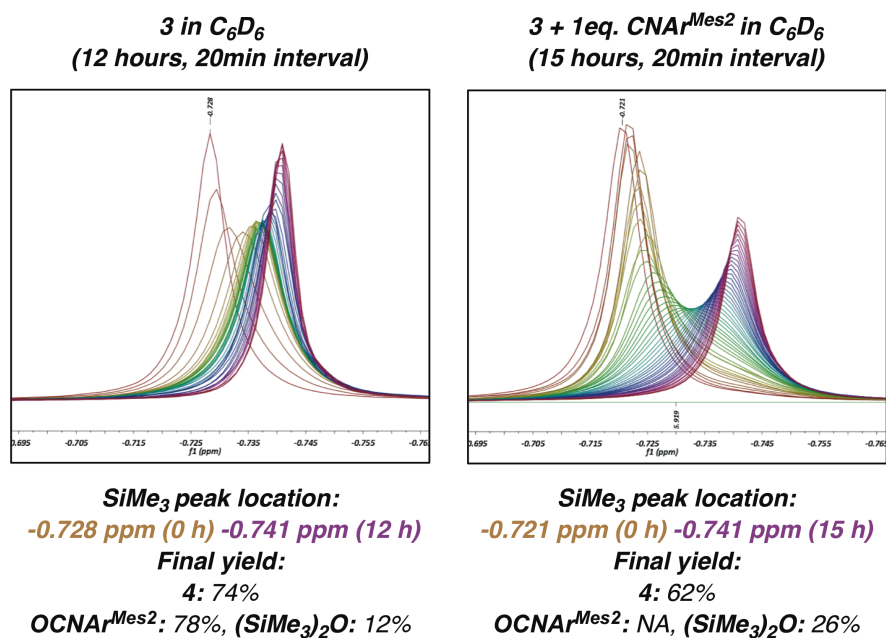


Figure 5.21. Overlapped time-dependent <sup>1</sup>H NMR spectrum zoomed in at the SiMe<sub>3</sub> peak region. (Left) Decomposition of 3 itself in C<sub>6</sub>D<sub>6</sub> at 25 °C over 12 hours. (Right) Decomposition of 3 with 1 equiv. of CNAr<sup>Mes2</sup> added in C<sub>6</sub>D<sub>6</sub> at 25 °C over 15 hours.

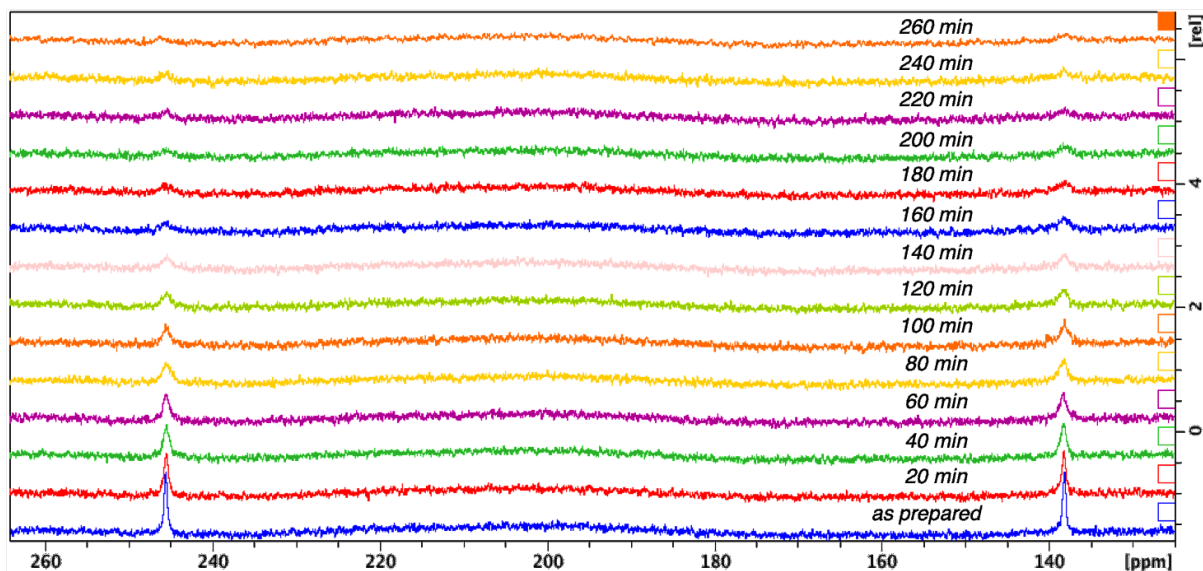


Figure 5.22. Time-dependent <sup>15</sup>N NMR spectrum taken in C<sub>6</sub>D<sub>6</sub> with the initial 3-<sup>15</sup>N concentration at 30mM showing the disappearance of 3-<sup>15</sup>N signals overtime. No apparent signals were shown after 260 minutes.

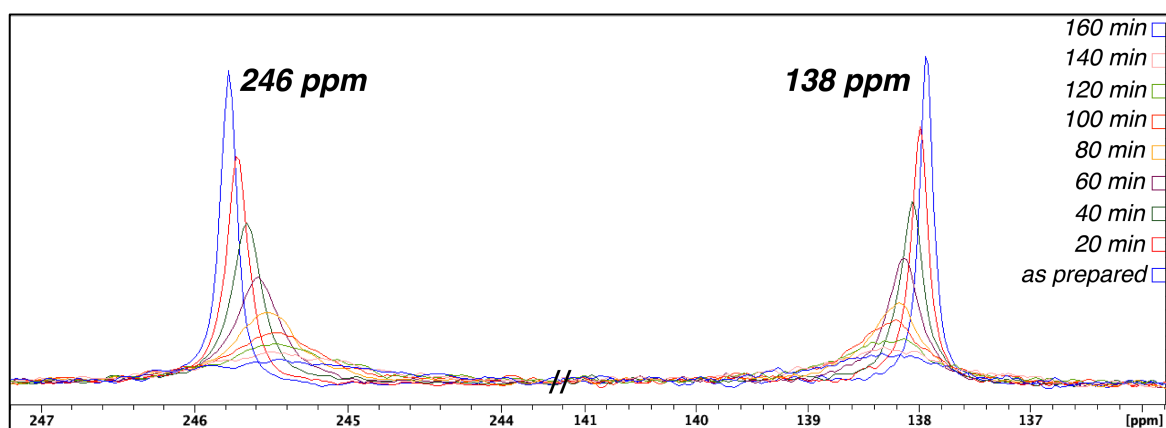


Figure 5.23. Overlapped time-dependent  $^{15}\text{N}$  NMR spectrum taken in  $\text{C}_6\text{D}_6$  with the initial  $3\text{-}^{15}\text{N}$  concentration at 30mM. The peak shifting feature indicated an exchange between  $\text{N}_\alpha$  (138 ppm) and  $\text{N}_\beta$  (246 ppm).

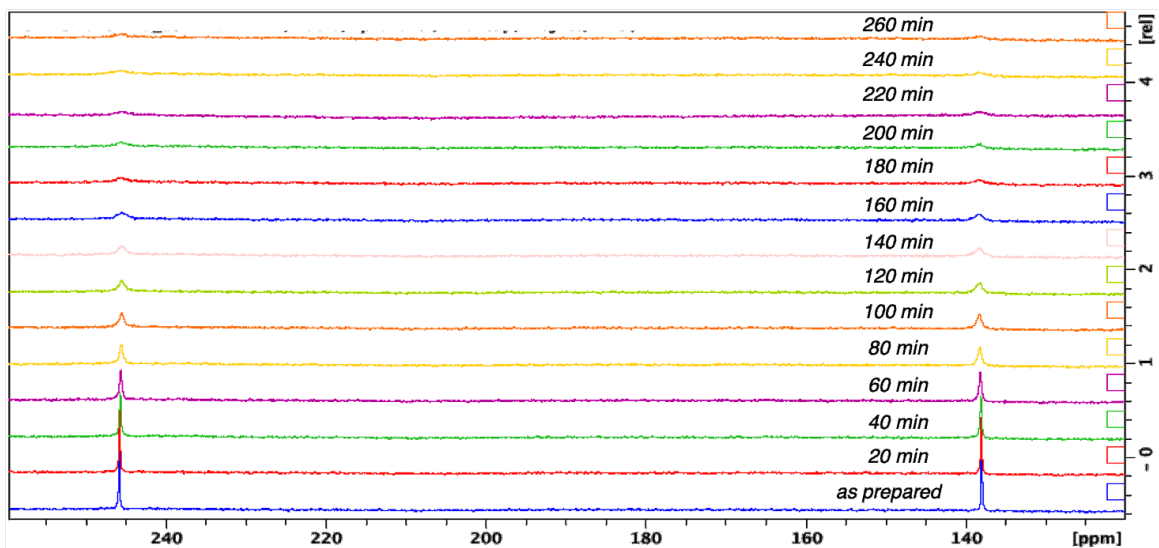
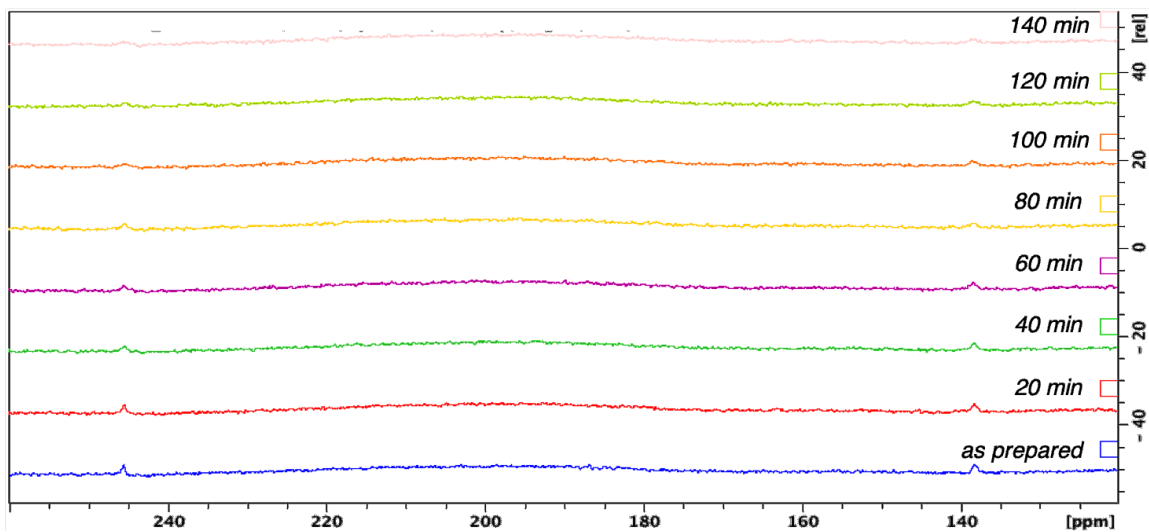


Figure 5.24. Time-dependent  $^{15}\text{N}$  NMR spectrum taken in  $\text{C}_6\text{D}_6$  with the initial  $3\text{-}^{15}\text{N}$  concentration at 45mM showing the disappearance of  $3\text{-}^{15}\text{N}$  signals overtime. No apparent signals were shown after 300 minutes. Note that with higher initial concentration, the rate of disappearance is slower.



**Figure 5.25.** Time-dependent <sup>15</sup>N NMR spectrum taken in C<sub>6</sub>D<sub>6</sub> with the initial 3-<sup>15</sup>N concentration at 13mM showing the disappearance of 3-<sup>15</sup>N signals overtime. No apparent signals were shown after 140 minutes. Note that with lower initial concentration, the rate of disappearance is faster.

**NMR Spectroscopy study of the *O*-atom transfer reaction under the presence of PCy<sub>3</sub>.** In the glovebox, a solution of **3** (in C<sub>6</sub>D<sub>6</sub>) and PCy<sub>3</sub> was transferred into a J-young NMR tube. The tube was then brought out to the spectrometer, with spectrum taken until the concentration of **4** reached constant. PCy<sub>3</sub> was tested to react with N<sub>2</sub>O<sub>(g)</sub> to generate OPCy<sub>3</sub> instantly. During this experiment, we do not see the generation of OPCy<sub>3</sub> even after 2 hours.

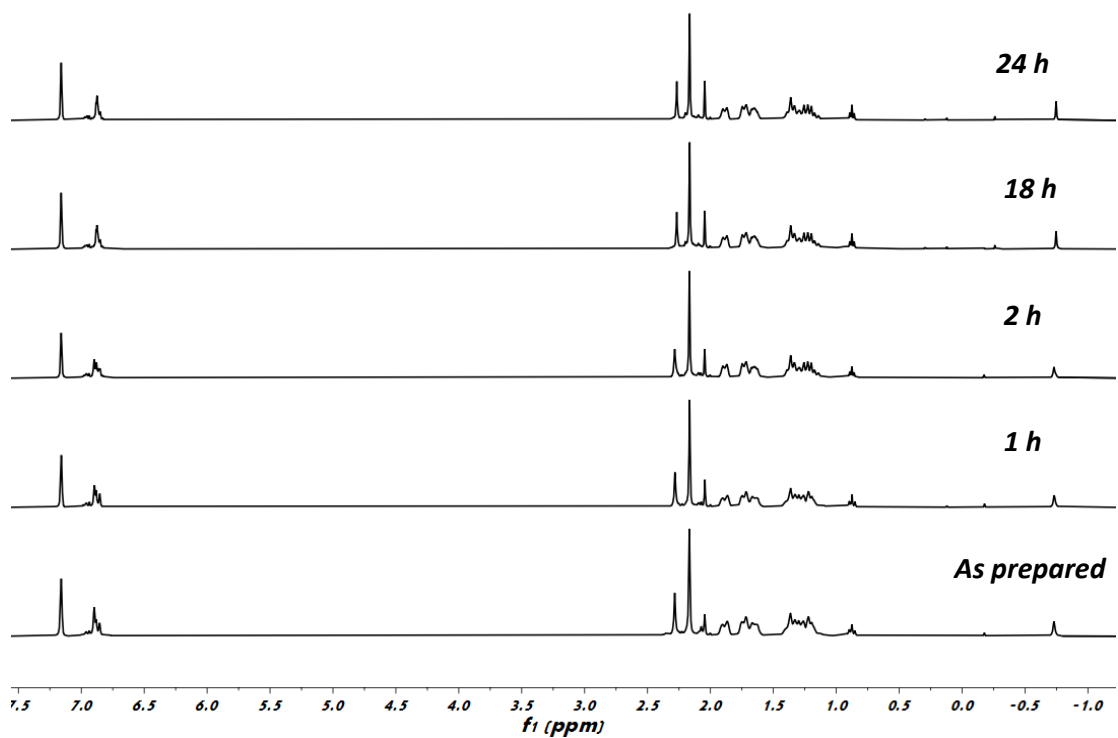


Figure 5.26. Stacked  $^1\text{H}$  NMR spectrum (C<sub>6</sub>D<sub>6</sub>, 25 °C) of the decomposition of 3 under the presence of PCy<sub>3</sub>.

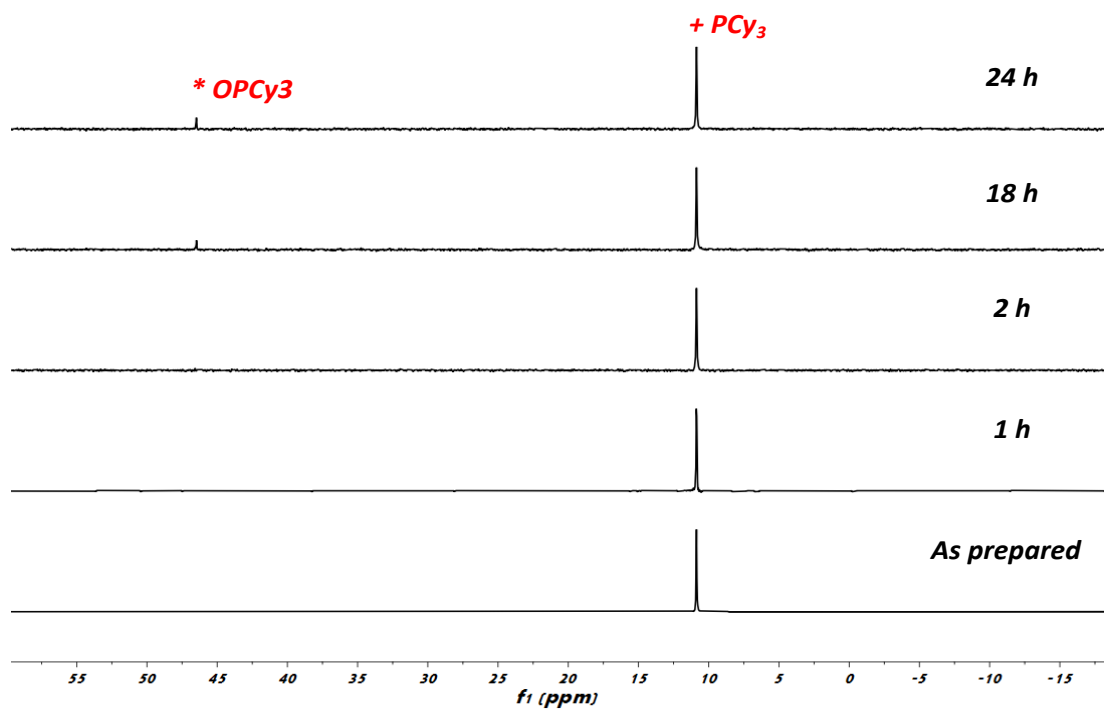
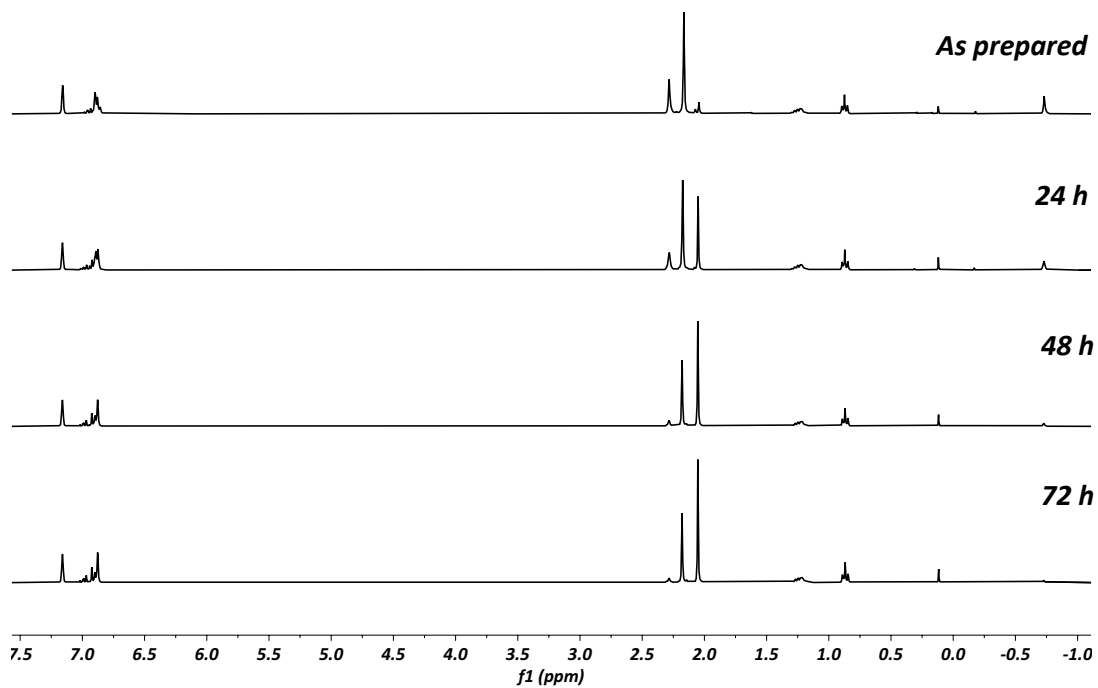


Figure 5.27. Stacked  $^{31}\text{P}$  NMR spectrum (C<sub>6</sub>D<sub>6</sub>, 25 °C) of the decomposition of 3 under the presence of PCy<sub>3</sub>.

## 5.7 Catalytic O-atom Transfer from N<sub>2</sub>O to Isocyanide

**The decomposition of 3 with excess N<sub>2</sub>O<sub>(g)</sub> to generate OCNAr<sup>Mes</sup><sub>2</sub> and (SiMe<sub>3</sub>)<sub>2</sub>O:** In the glovebox, a solution of 2 (in C<sub>6</sub>D<sub>6</sub>) was transferred into a J-young NMR tube. The tube was then brought out to the Schlenk line for N<sub>2</sub>O<sub>(g)</sub> addition after one freeze-pump-thaw cycle. The reaction was then monitored every 24 hours under 25 °C until the full conversion to isocyanate.



**Figure 5.28.** Stacked <sup>1</sup>H NMR spectrum (C<sub>6</sub>D<sub>6</sub>, 25 °C) of the decomposition of 3 with excess N<sub>2</sub>O<sub>(g)</sub>.

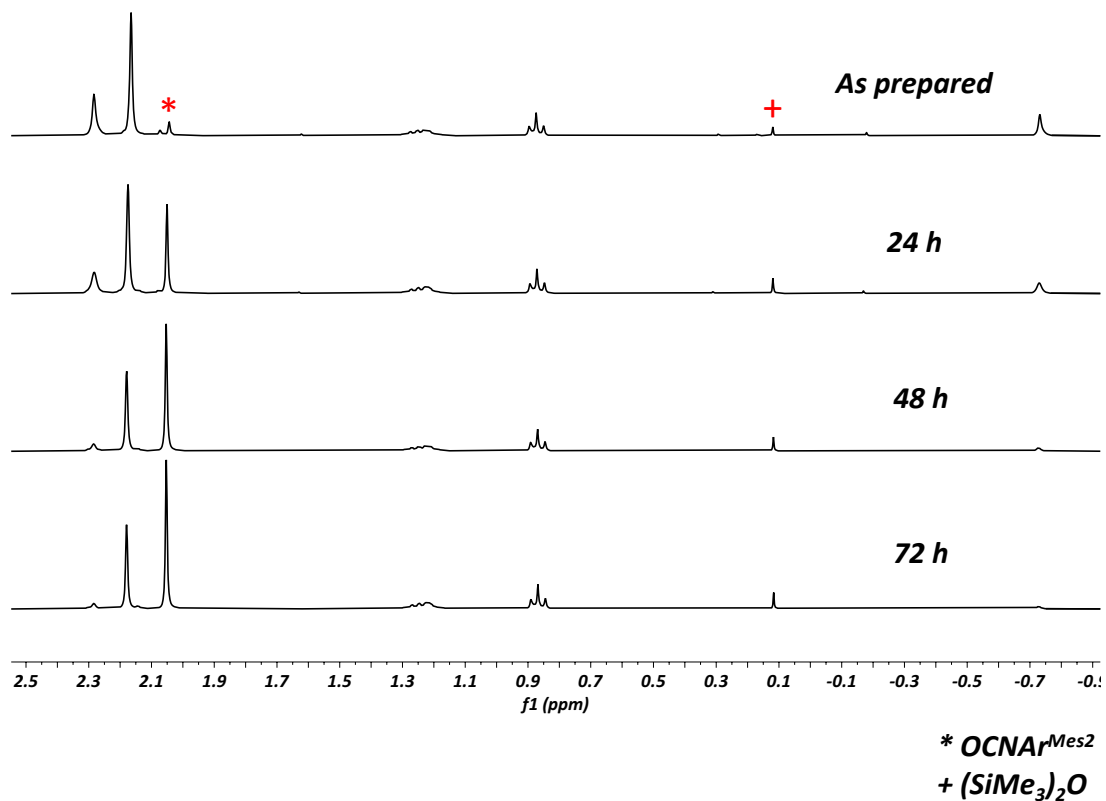


**Figure 5.29.** Zoomed in stacked  $^1\text{H}$  NMR spectrum ( $\text{C}_6\text{D}_6$ ,  $25^\circ\text{C}$ ) of the decomposition of **3** with excess  $\text{N}_2\text{O}_{(\text{g})}$  showing the formation of  $\text{OCNAr}^{\text{Mes}2}$  and  $(\text{SiMe}_3)_2\text{O}$ .

**Catalytic O-atom transfer reaction to additionally added  $\text{CNAr}^{\text{Tripp}2}$ :** In the glovebox, a solution of **2** (in  $\text{C}_6\text{D}_6$ ) and 5 equiv. of  $\text{CNAr}^{\text{Tripp}2}$  was transferred into a J-young NMR tube. The tube was then brought out to the Schlenk line for  $\text{N}_2\text{O}_{(\text{g})}$  addition after one freeze-pump-thaw cycle. The reaction was then monitored every 24 hours under  $25^\circ\text{C}$  until the full conversion to isocyanate.

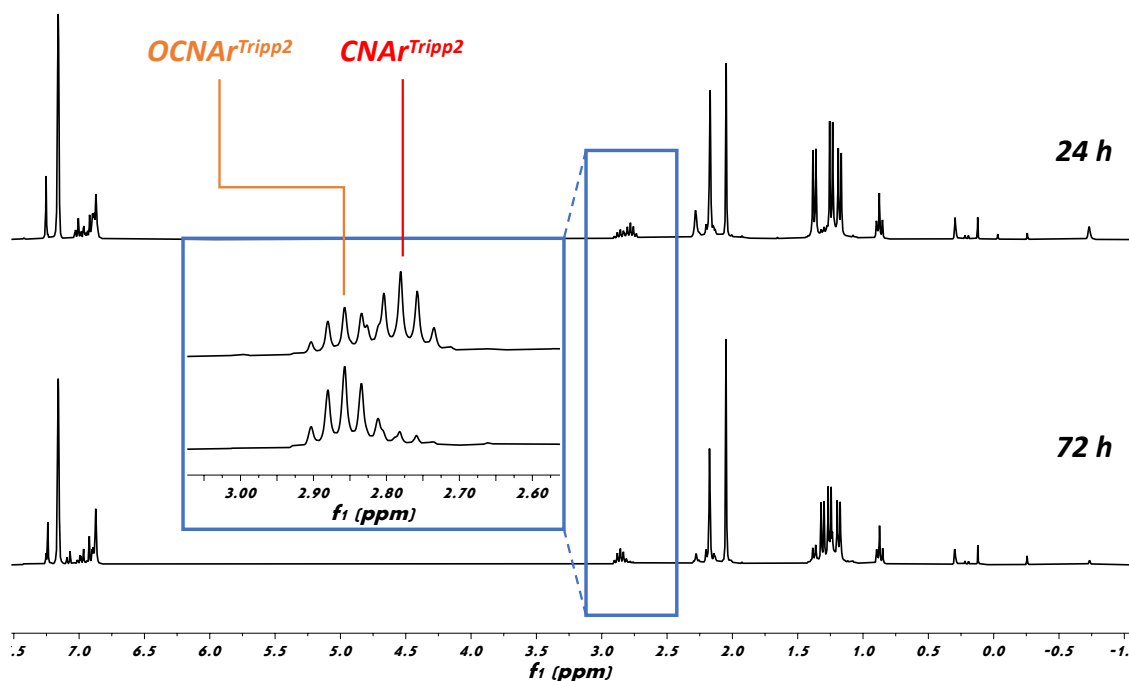
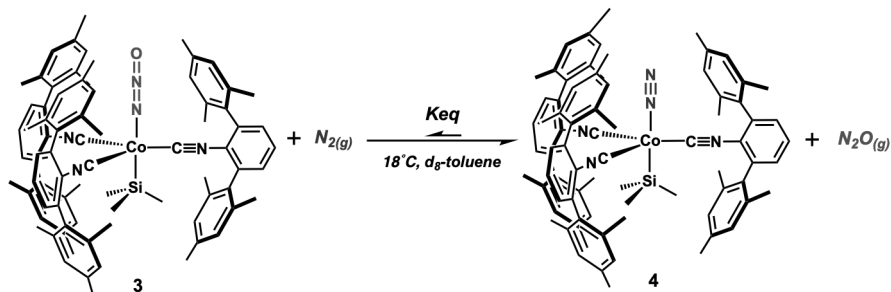


Figure 5.30. Stacked  $^1\text{H}$  NMR spectrum ( $\text{C}_6\text{D}_6$ ,  $25^\circ\text{C}$ ) showing the catalytic  $O$ -atom transfer reaction to  $\text{CNAr}^{\text{Tripp}2}$  using 20 mol% of **3** with 1ATM  $\text{N}_2\text{O}_{(\text{g})}$ .

## 5.8 Calculation of the $\text{N}_2/\text{N}_2\text{O}$ Equilibrium Binding Constant

**General Procedure:** The experiments were performed using crystalline materials of **3** with 1,3,5-tri-*tert*-butylbenzene as internal standard dissolved in 0.7 mL of  $d_8$ -toluene to ensure the purity and reliability of the results. The solution was then transferred into a J-young tube and brought to the Schlenk line. After 1 freeze-pump-thaw cycle, 1ATM of  $\text{N}_2\text{O}_{(\text{g})}$  was added at room-temperature. The tube was then transferred to the pre-cooled NMR instrument to equilibrate for 10 minutes before data collection.





Scheme 5.6. Reaction scheme of  $\text{N}_2\text{O}$  and  $\text{N}_2$  binding equilibrium on **2** under  $18^\circ\text{C}$  in a  $d_8$ -toluene solution.

**Calculate the  $\text{N}_2$  and  $\text{N}_2\text{O}$  equilibrium binding constant:** The equilibrium constant was calculated using the equation shown below. **[3]** and **[4]** were obtained from deconvoluting the  $^1\text{H}$  NMR spectrum using the program Mnova. (shown in Figure 5.31)  $[\text{N}_2\text{O}]$  was estimated as the solubility of  $\text{N}_2\text{O}_{(g)}$  in toluene under 1 ATM at  $18^\circ\text{C}$  ( $15\text{M}$ )<sup>50</sup> with the amount bound to cobalt (**[3]**) subtracted.  $[\text{N}_2]$  was calculated as the amount generated by displacement of  $\text{N}_2\text{O}$  which equals to **[3]**. The equation can be further simplified to the following:

$$K_{eq} = \frac{[4][\text{N}_2\text{O}]}{[\text{N}_2][3]} = \frac{[4][10.5 - [3]]}{[3][3]}, \Delta G = -RT \ln K_{eq}$$

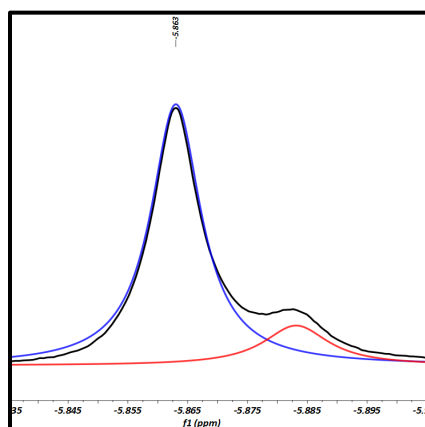
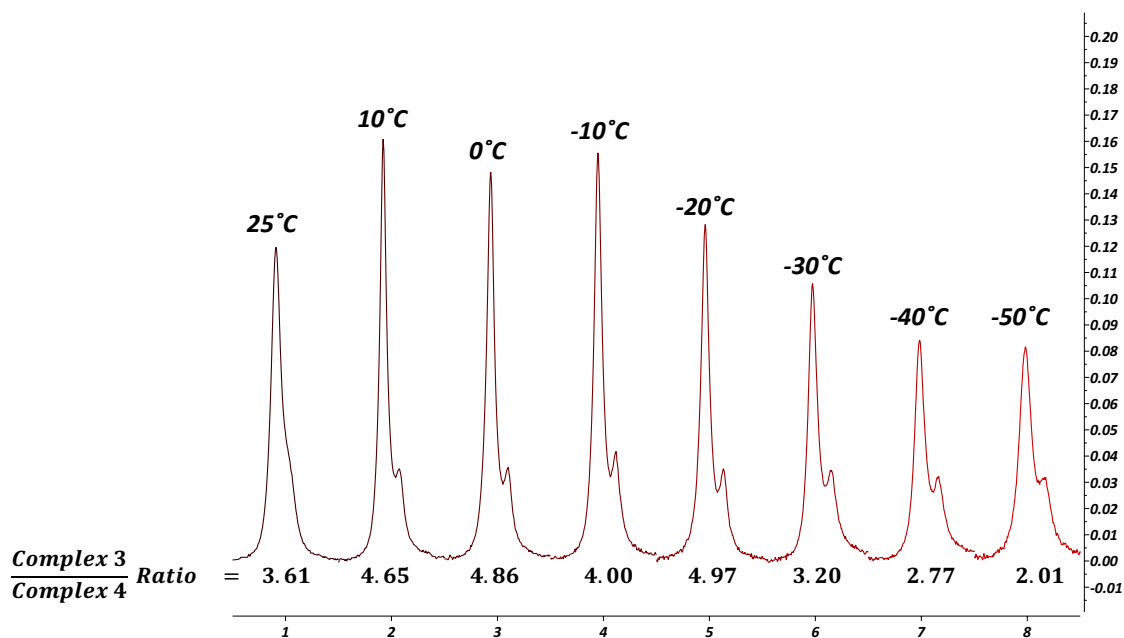


Figure 5.31.  $^1\text{H}$  NMR spectrum zoomed in at the  $\text{SiMe}_3$  peak region. Trace in black is the original spectra which was then deconvoluted into **3** (shown in blue) and **4** (shown in red) using the program Mnova.

**Table 5.7. Equilibrium constants and Gibbs free energies determination.**

Initial concentration of 4 (mM)	$K_{eq}$	$\Delta G$ (kcal/mol)
8.5 mM	466.67	-3.55
8.5 mM	336.00	-3.36
Average	401.34	-3.46



**Figure 5.32. Temperature-dependent <sup>1</sup>H NMR spectrum zoomed in at the SiMe<sub>3</sub> peak region. The ratio of complexes 3/4 showed a steady decrease upon lowering the temperature, indicates that complex 4 is more thermodynamically favored.**

## 5.9 Crystallographic Structure Determinations

**General.** Single crystal X-ray structure determinations were carried out at low temperature on a Bruker P4, Platform or Kappa Diffractometer equipped with a Mo or Cu radiation source and

a Bruker APEX detector. All structures were solved by direct methods with SIR 2004<sup>51</sup> or SHELXS<sup>52</sup> and refined by full-matrix least-squares procedures utilizing SHELXL within Olex 2 small-molecule solution, refinement, and analysis software package.<sup>53</sup> Crystallographic data collection and refinement information are listed in Table 5.8.

Complex  $\text{Co}(\text{SiMe}_3)(\text{CNAr}^{\text{Mes}_2})_3$  (**2**) has toluene solvent molecule co-crystallized which exhibited two-site positional disorder on a special positioned. One of the flanking mesityl rings exhibited two- site positional disorder. Both were fully modeled and refined anisotropically.

Complex  $(\kappa^1\text{-N-N}_2\text{O})\text{Co}(\text{SiMe}_3)(\text{CNAr}^{\text{Mes}_2})_3$  (**3**) has one *m*-terphenyl and one of the flanking mesityl rings exhibited two-site positional disorder which was fully modeled and refined anisotropically. The molecule also contained severely disordered solvent molecules of co-crystallization that could not be successfully modeled, the PLATON routine SQUEEZE<sup>54</sup> or the Olex2 implementation of BYPASS<sup>55</sup> was used to account for these disordered components as a diffuse contribution to the overall scattering without specific atom positions.

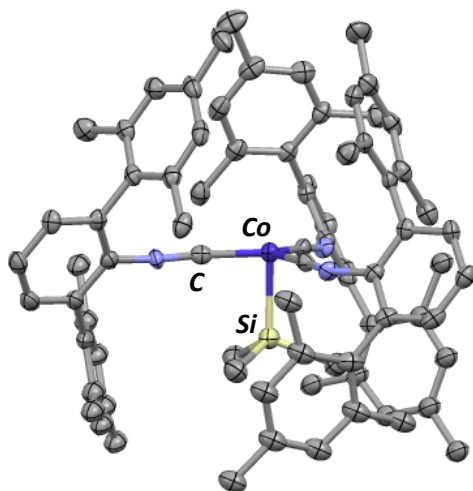


Figure 5.33. Molecular structure of  $\text{Co}(\text{SiMe}_3)(\text{CNAr}^{\text{Mes}_2})_3$  (2), with toluene solvent molecule and hydrogen atoms omitted for clarity. Selected distances (Å) and angles (°): Co-C = 1.792(3), Co-Si = 2.249(3), C-N = 1.178(3), C-Co-C = 119.9(2), C-Co-Si = 88.0(1).

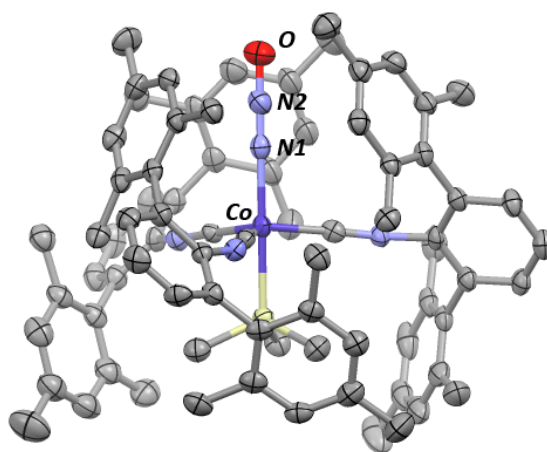
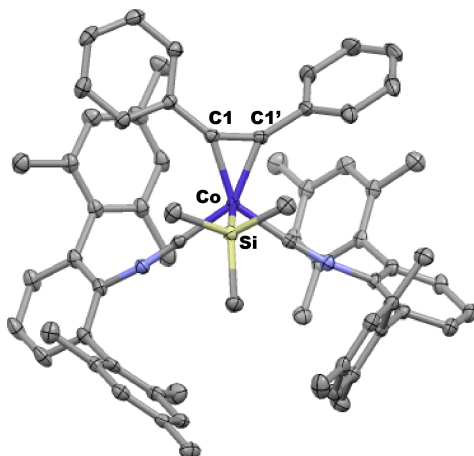


Figure 5.34. Molecular structure of  $(\kappa^1\text{-N-N}_2\text{O})\text{Co}(\text{SiMe}_3)(\text{CNAr}^{\text{Mes}_2})_3$  (3), with benzene, pentane solvent molecules and hydrogen atoms omitted for clarity. Selected distances (Å) and angles (°): Co-C = 1.806(4), Co-Si = 2.295(1), C-N = 1.190(5), N-N = 1.110(5), N-O = 1.210(5), C-Co-C = 114.9(2), C-Co-Si = 84.6(1), C-Co-N = 95.4(2).



**Figure 5.35.** Molecular structure of  $(\eta^2\text{-}C,C\text{-PhCCPh})\text{Co}(\text{SiMe}_3)(\text{CNAr}^{\text{Mes}_2})_2$  (**5**), with hydrogen atoms omitted for clarity. Selected distances (Å) and angles (°): Co-C1 = 1.869(2), Co-C1' = 1.884(2), C1-C1' = 1.292(3), Co-Si = 2.2506(6), C1-Co-Si = 106.69(6), C1'-Co-Si = 113.62(6).

**Table 5.8.** Crystallographic Data Collection and Refinement Information.

Name	Co(SiMe <sub>3</sub> ) (CNAr <sup>Mes<sub>2</sub></sup> ) <sub>3</sub> ( <b>2</b> )	(κ <sup>1</sup> -N-N <sub>2</sub> O)Co (SiMe <sub>3</sub> )(CNAr <sup>Mes<sub>2</sub></sup> ) <sub>3</sub> ( <b>3</b> )	(η <sup>2</sup> -C,C-PhCCPh)Co (SiMe <sub>3</sub> )(CNAr <sup>Mes<sub>2</sub></sup> ) <sub>2</sub> ( <b>5</b> )
Formula	C83.25 H90 Co N3 Si	C83.50 H93 Co N5 O Si	C67 H69 Co N2 Si
Crystal System	Cubic	Triclinic	Monoclinic
Space Group	I-43d	P-1	P 1 21/c 1
a, Å	30.635(3)	18.299(2)	17.4976(14)
b, Å	30.635(3)	19.688(2)	14.3661(12)
c, Å	30.635(3)	21.736(2)	22.9953(18)
α, deg	90	89.935(3)	90
β, deg	90	89.820(3)	105.747(2)
γ, deg	90	89.712(4)	90
V, Å <sup>3</sup>	28750(9)	7830.4(15)	5563.4(8)
Z	16	4	4
Radiation (λ, Å)	Mo-K <sub>α</sub> , 0.71073	Mo-K <sub>α</sub> , 0.71073	Mo-K <sub>α</sub> , 0.71073
ρ(calcd.), g/cm <sup>3</sup>	1.127	1.077	1.181
μ, mm <sup>-1</sup>	0.300	0.279	0.372
Temp, K	100	100	100
θ max, deg	25.347	25.821	25.440
data/parameters	4376/263	29514/1910	10269/655
R <sub>I</sub>	0.0477	0.0747	0.0366
wR <sub>2</sub>	0.1091	0.1385	0.0867
GOF	1.041	0.893	1.015

## 5.10 Acknowledgement

Chapter 5 is currently in preparation as a manuscript by C. Chan, A. E. Carpenter, R. P. Hughes, A. L. Rheingold, J. S. Figueroa. The dissertation author is the primary author of this manuscript. Prof. Stanley Opella, Prof. Charles L. Perrin, Dr. Anthony Mrse and Dr. XueMei Huang are thanked for assist of  $^{15}\text{N}$  NMR data collection and valuable discussions.

## 5.11 References

- (1) Prather, M. J. *Science* **1998**, *279* (5355), 1339–1341.
- (2) Ravishankara, A. R.; Daniel, J. S.; Portmann, R. W. *Science* **2009**, *326* (5949), 123–125.
- (3) Yang, G.; Peng, Y.; Marushchak, M.; Chen, Y.; Wang, G.; Li, F.; Zhang, D.; Wang, J.; Yu, J.; Liu, L.; Qin, S.; Kou, D.; Yang, Y. *Environmental Science & Technology* **2018**, acs.est.8b02271.
- (4) Brown, K.; Tegoni, M.; Prudencio, M.; Pereira, A. S.; Besson, S.; Moura, J. J.; Moura, I.; Cambillau, C. *Nature Structural Biology* **2000**, *7* (3), 191–195.
- (5) Prudêncio, M.; Pereira, A. S.; Tavares, P.; Besson, S.; Cabrito, I.; Brown, K.; Samyn, B.; Devreese, B.; Van Beeumen, J.; Rusnak, F.; Fauque, G.; Moura, J. J. G.; Tegoni, M.; Cambillau, C.; Moura, I. *Biochemistry* **2000**, *39* (14), 3899–3907.
- (6) Zumft, W. G.; Kroneck, P. M. H. *Advances in Microbial Physiology* **2006**, *52*, 107–227.
- (7) Pomowski, A.; Zumft, W. G.; Kroneck, P. M. H.; Einsle, O. *Nature Chemistry* **2011**, *477* (7363), 234–237.
- (8) Bar-Nahum, I.; Gupta, A. K.; Huber, S. M.; Ertem, M. Z.; Cramer, C. J.; Tolman, W. B. *J. Am. Chem. Soc.* **2009**, *131* (8), 2812–2814.
- (9) Arzoumanian, H.; Nuel, D.; Sanchez, J. *Journal of Molecular Catalysis* **1991**, *65* (3), L9–L11.
- (10) Harrold, N. D.; Waterman, R.; Hillhouse, G. L.; Cundari, T. R. *J. Am. Chem. Soc.* **2009**, *131* (36), 12872–12873.

- (11) Matsunaga, P. T.; Hillhouse, G. L.; Rheingold, A. L. *J. Am. Chem. Soc.* **1993**, *115* (5), 2075–2077.
- (12) Koo, K.; Hillhouse, G. L.; Rheingold, A. L. *Organometallics* **1995**, *14* (1), 456–460.
- (13) Vaughan, G. A.; Rupert, P. B.; Hillhouse, G. L. *J. Am. Chem. Soc.* **1987**, *109* (18), 5538–5539.
- (14) Lee, J.-H.; Pink, M.; Tomaszewski, J.; Fan, H.; Caulton, K. G. *J. Am. Chem. Soc.* **2007**, *129* (28), 8706–8707.
- (15) Laplaza, C. E.; Odom, A. L.; Davis, W. M.; Cummins, C. C.; Protasiewicz, J. D. *J. Am. Chem. Soc.* **1995**, *117* (17), 4999–5000.
- (16) Vaughan, G. A.; Sofield, C. D.; Hillhouse, G. L.; Rheingold, A. L. *J. Am. Chem. Soc.* **1989**, *111* (14), 5491–5493.
- (17) Demir, S.; Montalvo, E.; Ziller, J. W.; Meyer, G.; Evans, W. J. *Organometallics* **2010**, *29* (23), 6608–6611.
- (18) Leont'ev, A. V.; Fomicheva, O. A.; Proskurnina, M. V.; Zefirov, N. S. *Russian Chemical Reviews* **2007**, *70* (2), 91–104.
- (19) Tolman, W. B. *Angew. Chem. Int. Ed.* **2010**, *49* (6), 1018–1024.
- (20) Kapteijn, F. *Applied Catalysis B: Environmental* **1996**, *9* (1-4), 25–64.
- (21) Panov, G. I.; Dubkov, K. A.; Kharitonov, A. S. In *Modern Heterogeneous Oxidation Catalysis*; Wiley-VCH Verlag GmbH & Co. KGaA: Weinheim, Germany, 2009; pp 217–252.
- (22) Parmon, V. N.; Panov, G. I.; Uriarte, A.; Noskov, A. S. *Catalysis Today* **2005**, *100* (1-2), 115–131.
- (23) Severin, K. *Chemical Society Reviews* **2015**, *44* (17), 6375–6386.
- (24) Armor, J. N.; Taube, H. *J. Am. Chem. Soc.* **1969**, *91* (24), 6874–6876.
- (25) Pamplin, C. B.; Ma, E. S. F.; Safari, N.; Rettig, S. J.; James, B. R. *J. Am. Chem. Soc.* **2001**, *123* (35), 8596–8597.
- (26) Florian Paulat; Torben Kuschel; Christian Näther; V K K Praneeth; Ole Sander, A.; Lehnert, N. *Inorg. Chem.* **2004**, *43* (22), 6979–6994.
- (27) Piro, N. A.; Lichterman, M. F.; Harman, W. H.; Chang, C. J. *J. Am. Chem. Soc.* **2011**, *133* (7), 2108–2111.

- (28) Zhuravlev, V.; Malinowski, P. J. *Angew. Chem. Int. Ed.* **2018**.
- (29) Carpenter, A. E.; Margulieux, G. W.; Millard, M. D.; Moore, C. E.; Weidemann, N.; Rheingold, A. L.; Figueroa, J. S. *Angew. Chem. Int. Ed.* **2012**, *51* (37), 9412–9416.
- (30) Griggs, J. L., Jr.; Narahari Rao, K.; Jones, L. H.; Potter, R. M. *Journal of Molecular Spectroscopy* **1968**, *25* (1), 34–61.
- (31) Laskowski, C. A.; Bungum, D. J.; Baldwin, S. M.; Del Ciello, S. A.; Iluc, V. M.; Hillhouse, G. L. *J. Am. Chem. Soc.* **2013**, *135* (49), 18272–18275.
- (32) Pileio, G.; Carravetta, M.; Hughes, E.; Levitt, M. H. *J. Am. Chem. Soc.* **2008**, *130* (38), 12582–12583.
- (33) Pu, L. S.; Yamamoto, A.; Ikeda, S. *J. Chem. Soc. D* **1969**, *0* (5), 189b–190.
- (34) Yamamoto, A.; Kitazume, S.; Pu, L. S.; Ikeda, S. *J. Am. Chem. Soc.* **1971**, *93* (2), 371–380.
- (35) *Purification of Laboratory Chemicals*; Elsevier, 2003.
- (36) Pangborn, A. B.; Giardello, M. A.; Grubbs, R. H.; Rosen, R. K.; Timmers, F. J. *Organometallics* **1996**, *15* (5), 1518–1520.
- (37) Fox, B. J.; Sun, Q. Y.; DiPasquale, A. G.; Fox, A. R.; Rheingold, A. L.; Figueroa, J. S. *Inorg. Chem.* **2008**, *47* (19), 9010–9020.
- (38) Carpenter, A. E.; Mokhtarzadeh, C. C.; Ripatti, D. S.; Havrylyuk, I.; Kamezawa, R.; Moore, C. E.; Rheingold, A. L.; Figueroa, J. S. *Inorg. Chem.* **2015**, *54* (6), 2936–2944.
- (39) Gaussian 09, Revision D.01, M. J. Frisch, G. W. Trucks, H. B. Schlegel, G. E. Scuseria, M. A. Robb, J. R. Cheeseman, G. Scalmani, V. Barone, B. Mennucci, G. A. Petersson, H. Nakatsuji, M. Caricato, X. Li, H. P. Hratchian, A. F. Izmaylov, J. Bloino, G. Zheng, J. L. Sonnenberg, M. Hada, M. Ehara, K. Toyota, R. Fukuda, J. Hasegawa, M. Ishida, T. Nakajima, Y. Honda, O. Kitao, H. Nakai, T. Vreven, J. A. Montgomery, Jr., J. E. Peralta, F. Ogliaro, M. Bearpark, J. J. Heyd, E. Brothers, K. N. Kudin, V. N. Staroverov, T. Keith, R. Kobayashi, J. Normand, K. Raghavachari, A. Rendell, J. C. Burant, S. S. Iyengar, J. Tomasi, M. Cossi, N. Rega, J. M. Millam, M. Klene, J. E. Knox, J. B. Cross, V. Bakken, C. Adamo, J. Jaramillo, R. Gomperts, R. E. Stratmann, O. Yazyev, A. J. Austin, R. Cammi, C. Pomelli, J. W. Ochterski, R. L. Martin, K. Morokuma, V. G. Zakrzewski, G. A. Voth, P. Salvador, J. J. Dannenberg, S. Dapprich, A. D. Daniels, O. Farkas, J. B. Foresman, J. V. Ortiz, J. Cioslowski, D. J. Fox, Gaussian, Inc., Wallingford CT, (2013).
- (40) Becke, A. D. *The Journal of Chemical Physics* **1993**, *98* (7), 5648–5652.

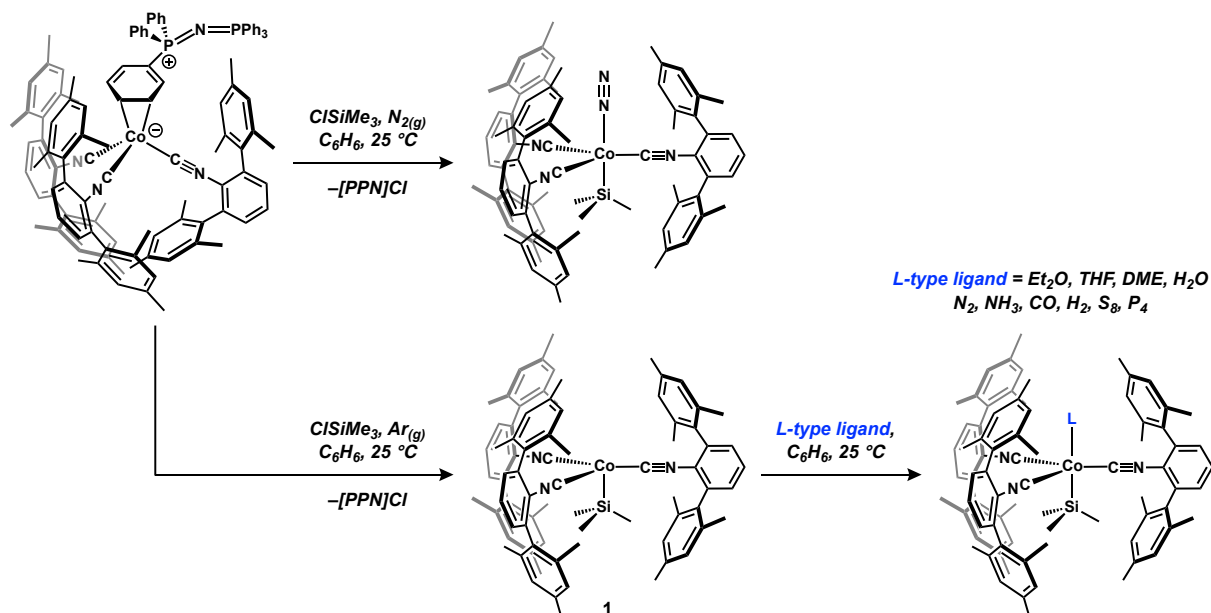


- (41) Stephens, P. J.; Devlin, F. J.; Chabalowski, C. F.; Frisch, M. J. *The Journal of Physical Chemistry* **1994**, *98* (45), 11623–11627.
- (42) Hariharan, P. C.; Pople, J. A. *Theoretica Chimica Acta* **1973**, *28* (3), 213–222.
- (43) Ehlers, A. W.; Böhme, M.; Dapprich, S.; Gobbi, A.; Höllwarth, A.; Jonas, V.; Köhler, K. F.; Stegmann, R.; Veldkamp, A.; Frenking, G. *Chemical Physics Letters* **1993**, *208* (1-2), 111–114.
- (44) Zhurko, G. A.; Zhurko, D. A. *Chemcraft ver. 1.5*; 2011.
- (45) Glendenning, E. D.; Landis, C. R.; Weinhold, F. *J Comput Chem* **2019**, *5*, 141.
- (46) Neese, F. *Wiley Interdisciplinary Reviews: Computational Molecular Science* **2012**, *2* (1), 73–78.
- (47) Guerra, C. F.; Snijders, J. G.; Velde, te, G.; Baerends, E. J. *Theor Chem Acc* **1998**, *99* (6), 391–403.
- (48) Velde, te, G.; Baerends, E. J.; Guerra, C. F.; van Gisbergen, S. J. A.; Snijders, J. G.; Ziegler, T. **2001**, *22* (9), 931–967.
- (49) Bickelhaupt, F. M.; computational, E. B. R. I.; 2000. *Wiley Online Library*.
- (50) Moshnyaga, A. V.; Khoroshilov, A. V.; Selivanova, D. I.; Aksenova, D. M. *Russ. J. Phys. Chem.* **2017**, *91* (11), 2117–2120.
- (51) Burla, M. C.; Caliandro, R.; Camalli, M.; Carrozzini, B.; Cascarano, G. L.; De Caro, L.; Giacovazzo, C.; Polidori, G.; Spagna, R. *Journal of Applied Crystallography* **2005**, *38* (2), 381–388.
- (52) Sheldrick, G. M. *Acta Crystallogr., A, Found. Crystallogr.* **2008**, *64* (Pt 1), 112–122.
- (53) Dolomanov, O. V.; Bourhis, L. J.; Gildea, R. J.; Howard, J. A. K.; Puschmann, H. *Journal of Applied Crystallography* **2009**, *42* (2), 339–341.
- (54) Spek, A. L. *Journal of Applied Crystallography* **2003**, *36* (1), 7–13.
- (55) van der Sluis, P.; Spek, A. L. *Acta Crystallogr., A, Found. Crystallogr.* **1990**, *46* (3), 194–201.

# Chapter 6 Solid State Host-Guest Interaction of *n*-Hexane with a Coordinatively Unsaturated Cobalt *m*-Terphenyl Isocyanide Complex

## 6.1 Organometallics Host-Guest Interaction with *n*-Hexane

Earlier in Chapter 5, we have shown that under an argon atmosphere with *rigorous exclusion* of adventitious Lewis bases, a C<sub>6</sub>H<sub>6</sub> solution of  $\eta^2$ -PPNCo(CNAr<sup>Mes2</sup>)<sub>3</sub> was combined with excess trimethylchlorosilane TMSCl to afford the coordinatively unsaturated Co(SiMe<sub>3</sub>)(CNAr<sup>Mes2</sup>)<sub>3</sub> (**1**). (Scheme 6.1) Single-crystal X-ray diffraction studies showed a trigonal monopyramidal geometry in the solid-state with DFT calculations supporting a low-lying cobalt *d*<sub>z<sup>2</sup> LUMO suitable for small molecule binding. Besides nitrous oxide, previous study in our group has shown that a variety of Lewis bases were able to bind as an L-type ligand to this cobalt center. For example, common organic solvents like Et<sub>2</sub>O, THF, H<sub>2</sub>O and DME; gases like N<sub>2</sub>, CO, NH<sub>3</sub> and H<sub>2</sub> particularly bind in a non-classical mode; elemental sulfur (S<sub>8</sub>) and white phosphorous (P<sub>4</sub>) interesting all coordinate as 2-electron L-type donor ligands.<sup>1,2</sup></sub>



**Scheme 6.1.** Synthesis of the coordinatively unsaturated  $\text{Co}(\text{SiMe}_3)(\text{CNAr}^{\text{Mes}2})_3$  (**1**) and its coordination chemistry towards L-type ligands.

To our surprise, when crystallizing  $\text{Co}(\text{SiMe}_3)(\text{CNAr}^{\text{Mes}2})_3$  (**1**) from concentrated *n*-hexane/benzene 80:20 v/v solutions at  $-35^\circ\text{C}$ , afforded two polymorphs of *n*-hexane containing  $\text{Co}(\text{SiMe}_3)(\text{CNAr}^{\text{Mes}2})_3$  (**1**) cavity-type inclusion complexes:  $(\mu^2-(\eta^2\text{-H,C},-(n\text{-C}_6\text{H}_{14}))[\text{Co}(\text{SiMe}_3)(\text{CNAr}^{\text{Mes}2})_3] \cdot (n\text{-C}_6\text{H}_{14}) \cdot 2(\text{C}_6\text{H}_6)$  (**1A-hexane**) and  $(\mu^2-(\eta^2\text{-H,C},-(n\text{-C}_6\text{H}_{14}))[\text{Co}(\text{SiMe}_3)(\text{CNAr}^{\text{Mes}2})_3] \cdot 1(\text{C}_6\text{H}_6)$  (**1B-hexane**). (Figure 6.1) The structure of polymorph **1A-hexane** was determined at 90 K and crystallizes in the space group *P*-1. The structure for polymorph **1B-hexane** was determined at 100 K and crystallized in the space group *P*21/*n*. In both polymorphs, an *n*-hexane molecule is encapsulated within the pocket created by the interlocked *m*-terphenyl mesityl rings from two  $\text{Co}(\text{SiMe}_3)(\text{CNAr}^{\text{Mes}2})_3$  (**1**) fragments. However, after a series of spectroscopy studies including variable-temperature IR and NMR techniques, we believed that this dimer forms upon *crystallization* from solution because of

significant van der Waals (vdW) host-guest interactions (also known as CH/ $\pi$  interactions) between the alkane molecule and the flanking mesityl rings of the *m*-terphenyl framework.<sup>3</sup>

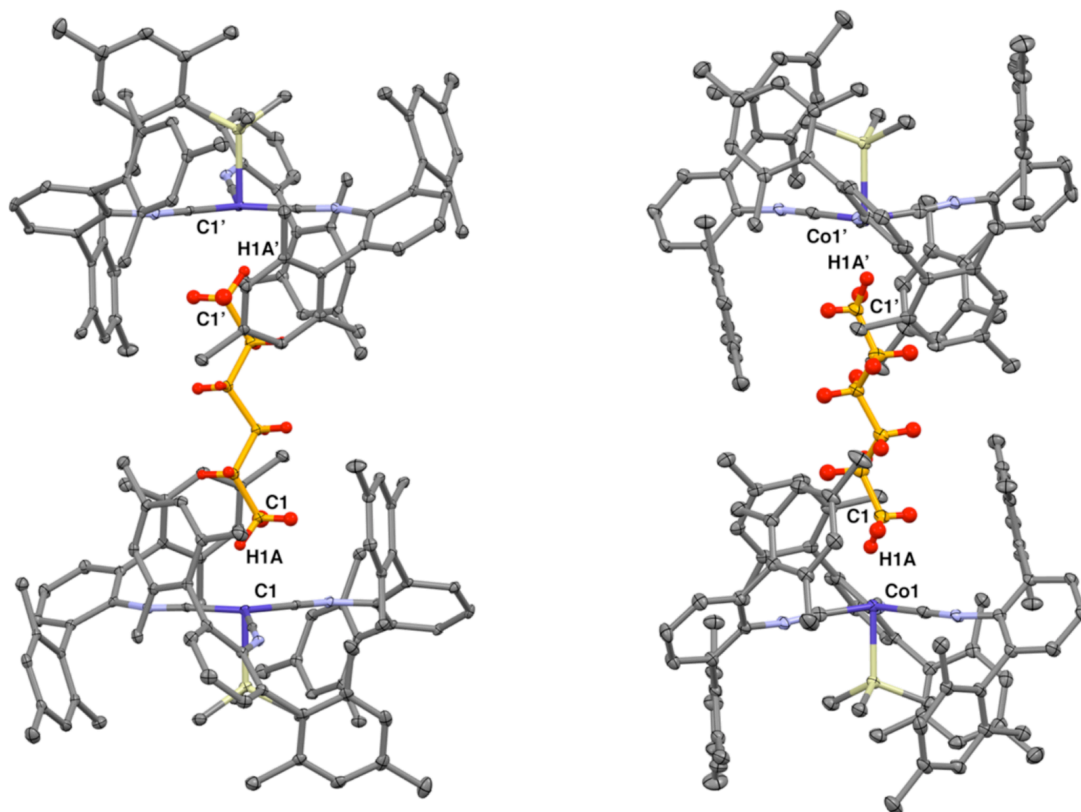


**Figure 6.1.** Molecular structures of *n*-hexane containing  $\text{Co}(\text{SiMe}_3)(\text{CNAr}^{\text{Mes}_2})_3$  (**1**) inclusion complexes. Left: Polymorph **1A-hexane** ( $\mu^2$ - $(\eta^2\text{-H,C},\text{-}(n\text{-C}_6\text{H}_{14}))[\text{Co}(\text{SiMe}_3)(\text{CNAr}^{\text{Mes}_2})_3] \cdot (n\text{-C}_6\text{H}_{14}) \cdot 2(\text{C}_6\text{H}_6)$ ). Right: Polymorph **1B-hexane** ( $\mu^2$ - $(\eta^2\text{-H,C},\text{-}(n\text{-C}_6\text{H}_{14}))[\text{Co}(\text{SiMe}_3)(\text{CNAr}^{\text{Mes}_2})_3] \cdot 1(\text{C}_6\text{H}_6)$ ). To aid in visual clarity, the enclosed *n*-hexane moiety is colored orange (carbons) and red (hydrogens). Solvent molecules of co-crystallization were omitted.<sup>1</sup>

Indeed, analysis of the metrical parameters for **1A-hexane** and **1B-hexane** suggest that a number of C-H/ $\pi$  interactions are present between the *n*-hexane moiety and the *m*-terphenyl mesityl framework. For example, **1B-hexane** contains five C-H $\cdots$ C contacts ranging from 2.877 Å to 3.027 Å between *n*-hexane and the flanking mesityl rings (Figure 6.2) with similar results obtained for **1A-hexane**. For comparison, an average of  $2.91 \pm 0.12$  Å CH/ $\pi$  interactions

is found in the recent study of CH/ $\pi$  interactions present in the Cambridge Structural Database (CSD), slightly less than the sum of the van der Waals radii of hydrogen ( $r_{\text{vdW}}(\text{H}) = 1.20 \text{ \AA}$ ) and the facial radii of a phenyl ring ( $r_{\text{vdW}}(\text{phenyl}) = 1.85 \text{ \AA}$ ).<sup>4,5</sup> Literature reports indicate that while C-H/ $\pi$  interactions are weak (1-3 kcal/mol),<sup>6-8</sup> they may play a significant role in the controlling host-guest interactions.<sup>3,9</sup> In this respect, it is important to note that similar host-guest interactions were observed in  $\sigma$ -alkane complexes recently reported by Meyer and Reed, suggesting that inclusion phenomena may help stabilize solid-state  $\sigma$ -alkane interactions.<sup>10,11</sup>

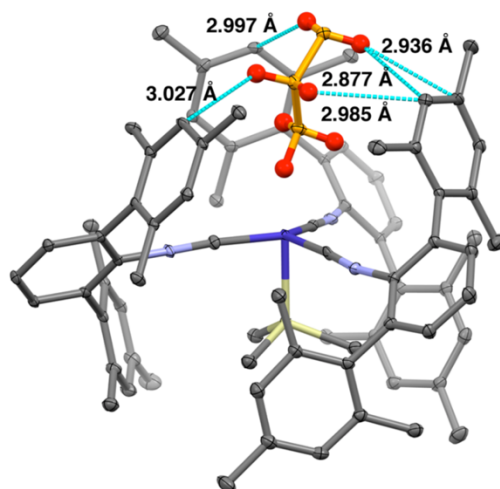


**Figure 6.2** Molecular structure of  $(\mu^2-(\eta^2-H,C)-(n-C_6H_{14})[Co(SiMe_3)(CNAr^{Mes}_2)_3] \cdot 1(C_6H_6)$  1B-hexane. Asymmetric unit shown with close contacts (light blue) between the encapsulated *n*-hexane in orange (carbon) and red (hydrogen) and the surrounding *m*-terphenyl framework.<sup>1</sup>

## 6.2 Energy Decomposition Analysis on 1-hexane

To further study this solid state “host-guest” interaction, we turned to Energy Decomposition Analysis (EDA) which allows partitioning of the overall attractive interaction ( $E_{\text{total}}$ ) between two fragments into its attractive and repulsive components. Shown in Figure

6.3 and 6.4 are the breakdown components on **1-hexane** molecule in different fragmentation. Model **1m-1** isolate the interaction between hexane molecule and the trimethylsilyl-cobalt (Co-TMS) fragment, shown in blue. The yellow dotted lines in model **1m-2** present the CH/ $\pi$  interactions between terphenyl cage and hexane. In model **1m-3**, the two fragments are the “host” (terphenyl-Co-TMS) and “guest” (hexane). All three models show net attractive interaction through the overall negative value of energy ( $E_{\text{total}}$ ) with the highest of -33.42 kcal/mol for **1m-3**. (Table 6.1) To our interest, the surprisingly large  $E_{\text{dispersion}}$  energy (-46.48 kcal/mol) in **1m-2** that quantifies the London dispersion forces, which is the main contributor in the attraction in van der Waals forces, support the stabilization of **1-hexane** with strong CH/ $\pi$  interactions. Recent studies from Powers<sup>12</sup> also showed the importance of strong dispersion interactions present in the m-terphenyl framework in stabilizing inorganic complexes.

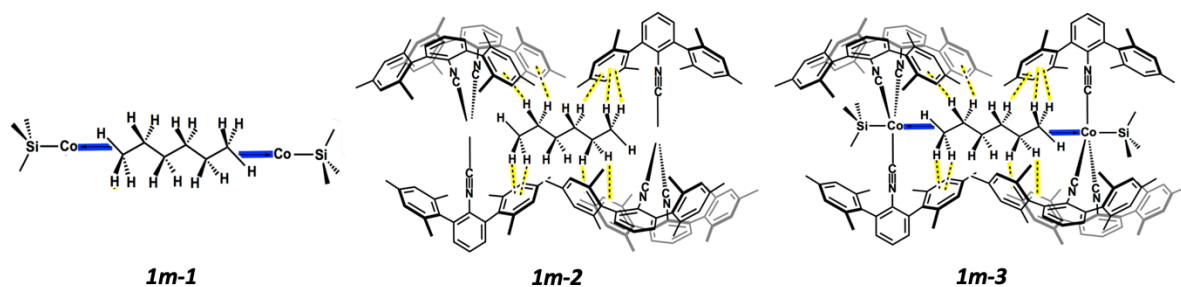


**Figure 6.3.** Energy decomposition analyses of 1-hexane using model with different fragmentation: **1m-1** (Co-TMS + hexane), **1m-2** (terphenyl cage + hexane) and **1m-3** (terphenyl-Co-TMS + hexane).

Table 6.1. Energy decomposition analyses of 1m-1, 1m-2 and 1m-3.

	<b>1m-1</b>	<b>1m-2</b>	<b>1m-3</b>
$E_{\text{electronic}}$	-29.9136	-41.4576	-54.924
$E_{\text{pauli}}$	57.636	68.2608	89.868
$E_{\text{dispersion}}$	-8.4648	-46.4808	-52.2672
$E_{\text{polarization}}$	-10.3392	-3.2208	-6.1128
$E_{\text{charge transfer}}$	-9.5688	-1.2984	-9.984
$E_{\text{total}}$	-0.6504	-24.1968	-33.42
			<b>Kcal/mol</b>

To understand the significance of this dispersion interaction, we conduct the EDA calculations on model **1m-1mono**, **1m-2mono** and **1m-3mono** that represents half of the cage. (Figure 6.4) As expected, the  $E_{\text{total}}$  decreased in half to only -16.39 kcal/mol for **1m-3mono**. We believe the stabilization energy required for the solid-state formation of these materials is between -16.39 (**1m-3mono**) and -33.42 (**1m-3**) kcal/mol. Note that these “monomers” were not observed experimentally.

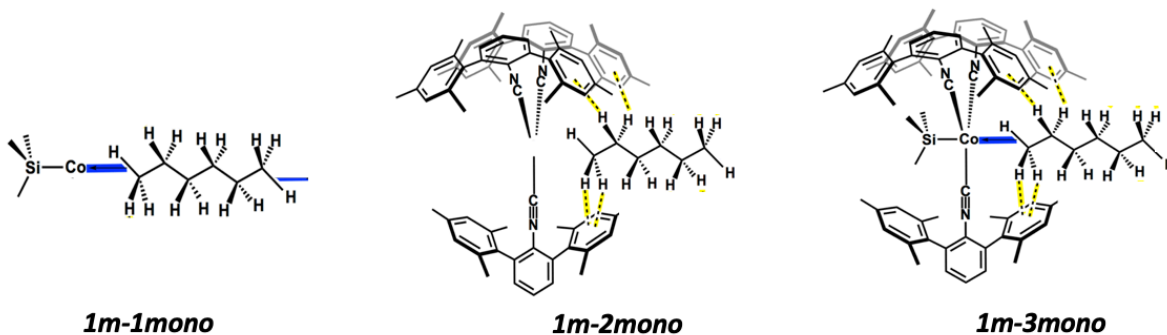


Figure 6.4. Energy decomposition analyses of 1-hexane using model with different fragmentation: 1m-1mono (monoCo-TMS + hexane), 1m-2mono (mono terphenyl cage + hexane) and 1m-3mono (mono terphenyl-Co-TMS + hexane).

Table 6.2. Energy decomposition analyses of 1m-1mono, 1m-2mono and 1m-3mono.

	<b>1m-1mono</b>	<b>1m-2mono</b>	<b>1m-3mono</b>
$E_{\text{electronic}}$	-7.26	-20.7696	-27.4392
$E_{\text{pauli}}$	16.368	34.0776	44.8008
$E_{\text{dispersion}}$	-3.0432	-22.9608	-25.8336
$E_{\text{polarization}}$	-3.2928	-1.644	-2.9352
$E_{\text{charge transfer}}$	-5.3496	-0.6432	-4.9824
$E_{\text{tot}}$	-2.5776	-11.94	-16.3896
			<b>Kcal/mol</b>

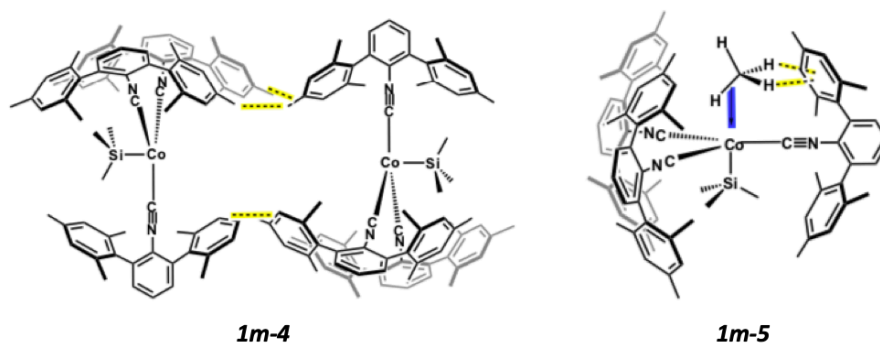


Figure 6.5. Energy decomposition analyses of 1-hexane using model with different fragmentation: **1m-4** (mono terphenyl cage + mono terphenyl cage) and **1m-5** (mono terphenyl-Co-TMS + methane).

The study on the interaction between two mono “cages” (**1m-4**) and mono “cage” with methane (**1m-5**) are also carried out. (Figure 6.5) Listed Table 6.3, the  $E_{\text{dispersion}}$  remains a big contributor in the attraction forces. However, even though the  $E_{\text{total}} = -7.29$  (**1m-4**) and  $-11.62$  (**1m-5**) kcal/mol show the overall attraction between fragments; they are not strong enough for the solid-state formation. This is consistent with the crystal structure of free  $\text{Co}(\text{SiMe}_3)(\text{CNAr}^{\text{Mes}2})_3$  (“cage”) where there is no short contact between two monomers.<sup>2</sup>



**Table 6.3. Energy decomposition analyses of 1m-4 and 1m-5.**

	<b>1m-4</b>	<b>1m-5</b>
$E_{\text{electronic}}$	-5.629	-17.641
$E_{\text{pauli}}$	9.308	29.686
$E_{\text{dispersion}}$	-10.722	-15.755
$E_{\text{polarization}}$	-0.166	-2.377
$E_{\text{charge transfer}}$	--0.082	-5.571
$E_{\text{tot}}$	-7.29	-11.62
		<i>Kcal/mol</i>

### 6.3 NMR Study on the Weakly Coordinated Alkylamine Model

While we were able to make the  $\text{NH}_3$  coordination complex,  $(\text{NH}_3)\text{Co}(\text{SiMe}_3)(\text{CNAr}^{\text{Mes}_2})_3$ ,<sup>2</sup> a weakly coordinated solution stable 1,6-diaminohexane dimer complex,  $(\mu^2\text{-}N\text{-}(\text{N}_2\text{C}_6\text{H}_{18}))[\text{Co}(\text{SiMe}_3)(\text{CNAr}^{\text{Mes}_2})_3]_2$  (**2**), was made for the approach to a solution persisted encapsulated complex. By treating  $\text{Co}(\text{SiMe}_3)(\text{CNAr}^{\text{Mes}_2})_3$  (**1**) with 0.5 equivalent of 1,6-diaminohexane, an immediate color change from hazel green to red was observed. Single red crystals were grown from a saturated benzene solution and characterized by x-ray crystallography (Figure 6.6 right). From the solid-state structure compared to **1A-hexane** (Figure 6.6 left), both structures remain similar geometry where two cobalt centers are facing each other with alkyl chains located inside the m-terphenyl pocket stabilized by the short contact with C-H/ $\pi$  interactions. Similar to **1A-hexane**, there is a crystallographic inversion center in the midpoint of the alkyl chain. Interestingly, the alkyl chain now remains in a “ladder-like” shape versus the traditional zigzag form in **1A-hexane**. We believe this is due to the maximization of C-H/ $\pi$  interactions that the complex now contains thirteen C-H $\cdots$ C contacts

ranging from 2.783 Å to 3.096 Å between 1,6-diaminohexane and the flanking mesityl rings. (Figure 6.7) To our benefit, this weakly coordinated alkylamine dimer can serve as a solution persisted model suitable for the CH/ $\pi$  interactions study using spectroscopy techniques.

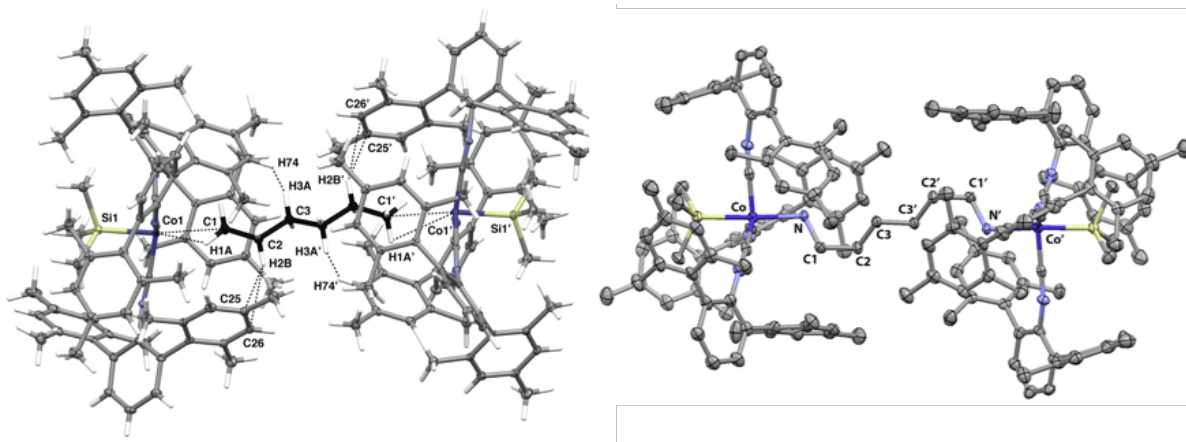


Figure 6.6. (Left) Crystal structure of a *n*-hexane containing  $\text{Co}(\text{SiMe}_3)(\text{CNAr}^{\text{Mes}_2})_3$  inclusion complex, 1A-hexane. (Right) Crystal structure of  $(\mu^2\text{-N}-(\text{N}_2\text{C}_6\text{H}_{18})[\text{Co}(\text{SiMe}_3)(\text{CNAr}^{\text{Mes}_2})_3]_2$  (2).

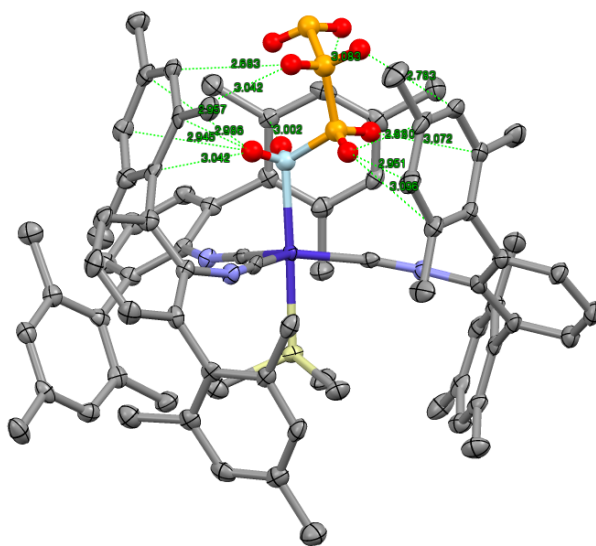


Figure 6.7. Molecular structure of  $(\mu^2\text{-N}-(\text{N}_2\text{C}_6\text{H}_{18})[\text{Co}(\text{SiMe}_3)(\text{CNAr}^{\text{Mes}_2})_3]_2$  (2). Asymmetric unit shown with close contacts (light green) between the encapsulated 1,6-diaminohexane in light blue (nitrogen), orange (carbon) and red (hydrogen) and the surrounding *m*-terphenyl framework.

By creating a solution persistent alkyl chain in the *m*-terphenyl framework cavities, we were able to monitor CH/ $\pi$  interactions using variable-temperature NMR (VT-NMR) techniques. The experiments are done between temperature of 20 °C and -60°C with 10°C intervals. Shown in Figure 6.8 is the full stacked spectrum of complex **2** in *d*<sub>8</sub>-THF. There was no significant peak number difference between variable temperatures, however; the NH<sub>2</sub> proton signals in the encapsulated 1,6-diaminohexane showed a *ca.* 0.15 ppm upfield shift when lowering the temperature. (Figure 6.9) The second, third and least protected CH<sub>2</sub> alkyl protons showed a *ca.* 0.12, 0.07 and 0.05 ppm upfield shift, respectively. Similar to the alkyl protons, the enclosed Si(CH<sub>3</sub>)<sub>3</sub> trimethylsilyl protons also shifted upfield. Interestingly, the aromatic protons located on the *m*-terphenyl “cage” shifted the opposite to the downfield region. To our excitement, there is no chemical shifts observed for the non-encapsulated alkyl solvent, pentane in this case.

To summarize, both the alkane CH<sub>2</sub> signals and the TMS signal that are in the *m*-terphenyl cavities shifted upfield, while the CH<sub>3</sub> signals of the flanking mesityl rings shift downfield when lowering the temperature. This observation is in consistent with the published CH/ $\pi$  interaction NMR results where the “guest” protons shifted upfield upon inclusion to the “host”.<sup>13</sup> We believe that during the temperature decline, the dynamic spinning of the *m*-terphenyl rings slow down and outstand the CH/ $\pi$  interaction significant enough to be determined by NMR.

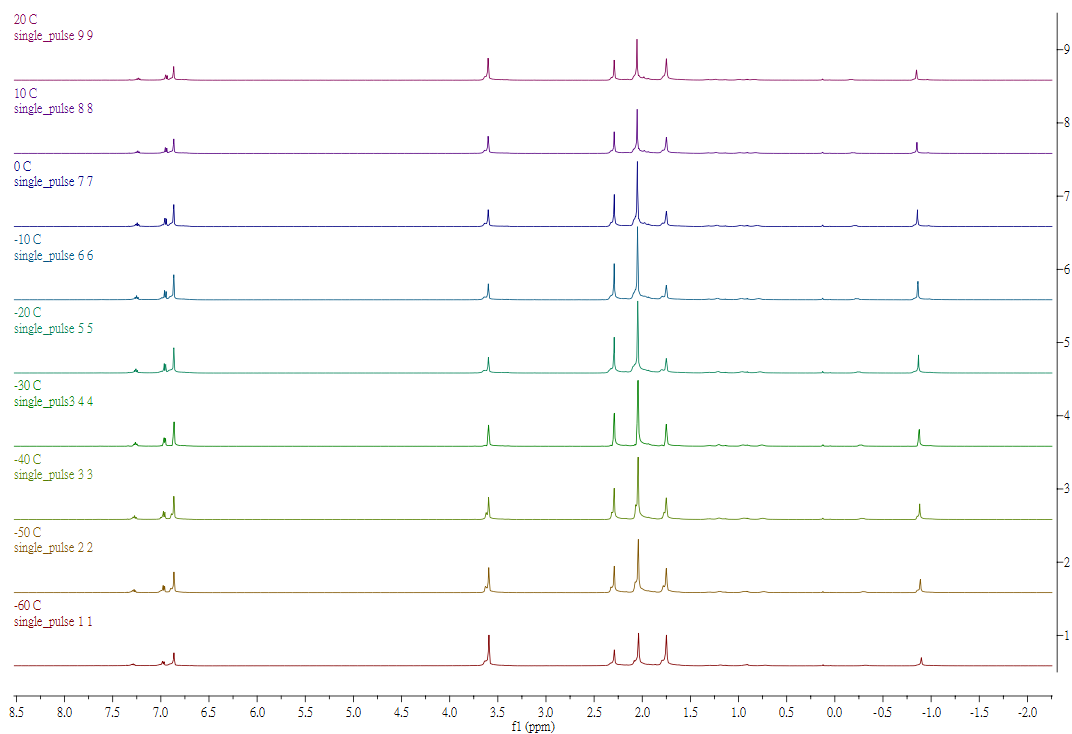


Figure 6.8. Stacked VT-NMR spectra of  $(\mu^2-N-(N_2C_6H_{18})[Co(SiMe_3)(CNAr^{Mes_2})_3]_2$  (**2**) in  $d_8$ -THF.

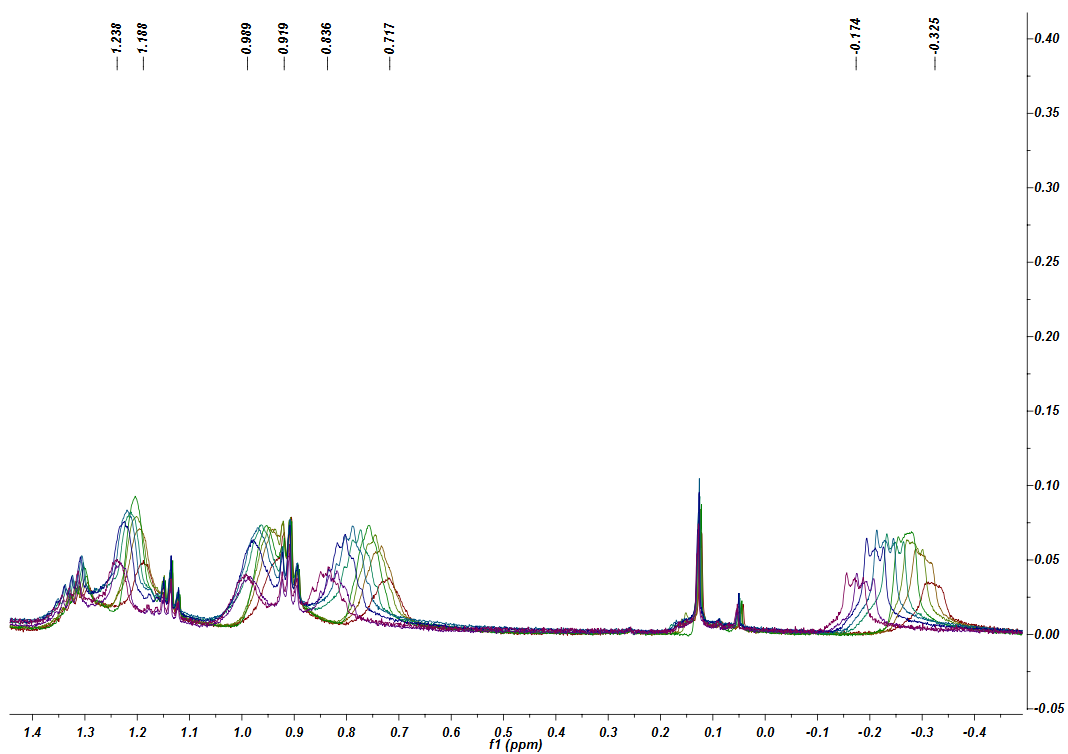
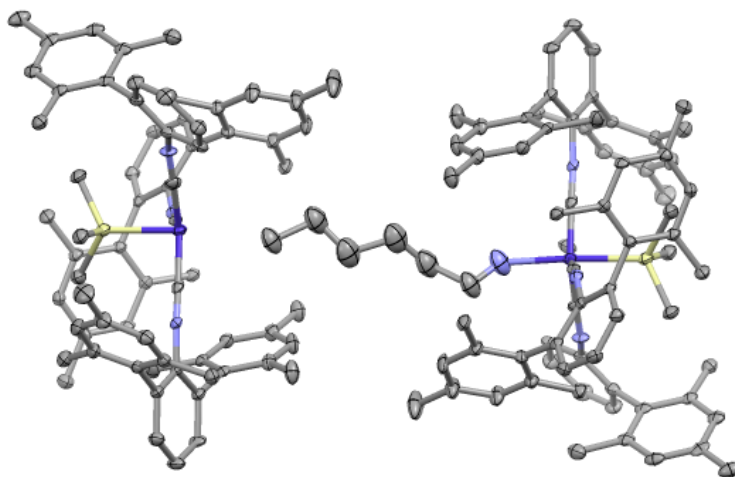


Figure 6.9. Overlapped VT-NMR spectra of  $(\mu^2-N-(N_2C_6H_{18})[Co(SiMe_3)(CNAr^{Mes_2})_3]_2$  (**2**) in  $d_8$ -THF zoomed in at the alkyl region.

More interestingly, an 1-hexylamine enclosed complex can be obtained upon recrystallization from a 1:1  $\text{Co}(\text{SiMe}_3)(\text{CNAr}^{\text{Mes}_2})_3$  (**1**) to  $(\text{C}_6\text{H}_{13}\text{NH}_2)\text{Co}(\text{SiMe}_3)(\text{CNAr}^{\text{Mes}_2})_3$  (**3**) solution. A mixture of single red and brown crystals was achieved. X-ray crystallography revealed  $(\text{C}_6\text{H}_{13}\text{NH}_2)\text{Co}(\text{SiMe}_3)(\text{CNAr}^{\text{Mes}_2})_3$  (**3**) as the red material and the brown crystals to be the 1-hexylamine encapsulated dimer,  $(\text{C}_6\text{H}_{13}\text{NH}_2)[\text{Co}(\text{SiMe}_3)(\text{CNAr}^{\text{Mes}_2})_3]_2$  (**4**). (Figure 2.5) However, detail solid state CH/ $\pi$  interaction information was not available due to a 180° positional disorder of the 1-hexylamine molecule. VT-NMR study of the (**1**) to (**3**) 1:1 mixture show both species at room-temperature and no significant new chemical shifts observed when lowering the temperature.



**Figure 6.10.** Molecular structure of  $(\text{C}_6\text{H}_{13}\text{NH}_2)[\text{Co}(\text{SiMe}_3)(\text{CNAr}^{\text{Mes}_2})_3]_2$  (**4**). Showing the encapsulated 1-hexylamine sitting in the *m*-terphenyl pocket.

## 6.4 Concluding Remarks

Despite the  $\text{N}_2\text{OCo}(\text{SiMe}_3)(\text{CNAr}^{\text{Mes}_2})_3$  and other  $\text{LCo}(\text{SiMe}_3)(\text{CNAr}^{\text{Mes}_2})_3$  ( $\text{L} = \text{L-type ligands}$ ) complexes mentioned in Chapter 5, a dimeric species,  $(\mu^2-(\eta^2\text{-}H,C\text{-}(\text{CH}_3(\text{CH}_2)_4\text{CH}_3))[\text{Co}(\text{SiMe}_3)(\text{CNAr}^{\text{Mes}_2})_3]_2$ , with the inclusion of a *n*-hexane molecule between

two cobalt centers was obtained. We believed that this dimer forms upon *crystallization* from solution due to the significant van der Waals (vdW) host-guest interactions (also known as CH/ $\pi$  interactions) between the alkane molecule and the flanking mesityl rings of the *m*-terphenyl framework. Spectroscopic investigations revealed these  $\sigma$ -alkane dimeric complexes only present in the solid state, supported solely by weak vdW interactions. To further study this vdW (CH/ $\pi$ ) interactions, a weakly coordinated solution stable 1,6-diaminohexane dimer complex,  $(\mu^2\text{-}N\text{-}(N_2C_6H_{18})[Co(SiMe_3)(CNAr^{Mes_2})_3]_2$ , were made and again characterized by x-ray crystallography. By creating a solution persistent alkyl chain in the *m*-terphenyl framework cavities, we were able to monitor CH/ $\pi$  interactions using variable-temperature NMR (VT-NMR) techniques. We believe that during the temperature decline, the dynamic spinning of the *m*-terphenyl rings slow down and outstand the CH/ $\pi$  interaction significant enough to be determined by NMR. Furthermore, EDA (Energy Decomposition Analysis) calculation was performed to support the significance of CH/ $\pi$  interaction through a high percentage contribution of dispersion energy.

## 6.5 Synthetic Procedures and Characterization Data

**General Considerations.** All manipulations were carried out under an atmosphere of Argon<sub>(g)</sub> using standard Schlenk and glovebox techniques. Unless otherwise stated, reagent-grade starting materials were purchased from commercial sources and either used as received or purified by standard procedures.<sup>14</sup> Solvents were dried and deoxygenated according to standard procedures.<sup>15</sup> Benzene, benzene-*d*<sub>6</sub> and toluene-*d*<sub>8</sub> (Cambridge Isotope Laboratories) were dried with Na/K and Benzophenone followed by distillation; thereafter, 7 freeze-pump-thaw cycles were executed and the solvents were stored on 4 Å molecular sieves for 3 days prior to use.

Celite 405 (Fisher Scientific) was dried under vacuum (24 h) at a temperature above 250 °C prior to use. ClSiMe<sub>3</sub> (Sigma-Aldrich) was treated with 7 freeze-pump-thaw cycles and dried over CaH<sub>2</sub> for 3 days prior to use. Hexylamine and 1,6-diaminohexane were purchased from Sigma-Aldrich, after 7 freeze-pump-thaw cycles the chemicals were stored in an Ar<sub>(g)</sub> filled glovebox prior to use. The compounds CNAr<sup>Mes2</sup>, (η<sup>2</sup>-PPN)Co(CNAr<sup>Mes2</sup>)<sub>3</sub> (**1**) were prepared by previously reported methods.<sup>16,17,18</sup>

Solution <sup>1</sup>H, <sup>13</sup>C{<sup>1</sup>H}, <sup>31</sup>P and <sup>15</sup>N NMR spectra were recorded on a Bruker Avance 300, a Bruker Avance 800, a Joel ECA 500, or a Varian X-Sens 500 spectrometer. <sup>1</sup>H and <sup>13</sup>C{<sup>1</sup>H} chemical shifts are reported in ppm relative to SiMe<sub>4</sub> (<sup>1</sup>H and <sup>13</sup>C δ = 0.0 ppm) with reference to residual solvent resonances of 7.16 ppm (<sup>1</sup>H) and 128.06 ppm (<sup>13</sup>C) for C<sub>6</sub>D<sub>6</sub>. FTIR spectra were recorded on a Thermo-Nicolet iS10 FTIR spectrometer. For solution FTIR spectra, solvent peaks were digitally subtracted from all spectra by comparison with an authentic spectrum obtained immediately prior to that of the sample. The following abbreviations were used for the intensities and characteristics of important IR absorption bands: vs = very strong, s = strong, m = medium, w = weak, vw = very weak; b = broad, vb = very broad, sh = shoulder.

Combustion analyses were performed by Midwest Microlab LLC of Indianapolis, IN (USA). Samples for combustion analysis were obtained from the first recrystallized batch of the reaction mixture. In a typical preparation, the crude, dry reaction mixture was dissolved in a minimum amount of solvent and stored at -35 °C for several days to produce crystalline material. This material was then collected, thoroughly dried under vacuum and then packaged under vacuum for shipment. In most cases, this material was also used for single-crystal X-ray structure determination.

**Synthesis of  $(\mu^2\text{-}N\text{-}(\text{N}_2\text{C}_6\text{H}_{18}))[\text{Co}(\text{SiMe}_3)(\text{CNAr}^{\text{Mes}2})_3]_2$  (**2**).**  $\text{Co}(\text{SiMe}_3)(\text{CNAr}^{\text{Mes}2})_3$  (**1**) (1 equiv., 0.040 g, 0.034 mmol) was stirred in a hexane/benzene solution (0.3/0.3mL) at room-temperature. 1,6-diaminohexane (0.5 equiv., 0.002 g, 0.017 mmol) was directly added as a solid and an instant color change from hazel green to red was observed. The solution was stirred for 30 seconds, filtered and sat at room temperature overnight. Single crystals are grown after 12 hours, washed with pentane/benzene and collected as a red material. Yield: 0.035 g, 0.014 mmol, 85 %.  $^1\text{H}$  NMR (499.9 MHz,  $d_8$ -THF, 20 °C): = 7.23 (t, 6H, *p*-Ph), 6.94 (d, 24H, *m*-Ph), 6.87 (s, 24H, *m*-Mes), 2.20 (s, 36H, *p*-CH<sub>3</sub> Mes), 2.05 (s, 72H, *o*-CH<sub>3</sub> Mes), 1.24 (m, 4H, CH<sub>2</sub>), 0.99 (m, 4H, CH<sub>2</sub>), 0.84 (m, 4H, CH<sub>2</sub>), -0.17 (m, 4H, NH<sub>2</sub>), -0.85 (s, 18H, SiMe<sub>3</sub>) ppm.  $^{13}\text{C}\{^1\text{H}\}$  NMR (125.7 MHz,  $d_8$ -THF, 20 °C):  $\delta$  = 186.7 (*broad*, CNR), 138.7, 138.6, 137.8, 137.5, 137.0, 133.8, 131.4, 131.2, 129.9, 129.8, 129.7, 126.2, 51.1, 37.9, 31.5, 30.8, 22.5, 22.4, 22.3, 21.2 ppm. (The CNR resonance extremely broadened, presumably due to coupling to  $^{59}\text{Co}$  ( $I = 7/2$ , 100 %)). FTIR (THF, KBr windows, 25 °C):  $\nu_{\text{CN}}$  = 1965 (sh), 1957 (sh) and 1907 (vs)  $\text{cm}^{-1}$ , also 2174 (m), 2673 (m), 2653 (m), 2531 (m), 1612 (m), 1354 (m), 1329 (m), 1285 (m)  $\text{cm}^{-1}$ .

**Synthesis of  $(\text{C}_6\text{H}_{13}\text{NH}_2)\text{Co}(\text{SiMe}_3)(\text{CNAr}^{\text{Mes}2})_3$  (**3**).**  $\text{Co}(\text{SiMe}_3)(\text{CNAr}^{\text{Mes}2})_3$  (**1**) (1 equiv., 0.020 g, 0.017 mmol) was stirred in a benzene solution (0.6mL) at room-temperature. Hexylamine (1.1 equiv., 0.0019 g, 0.019 mmol) was directly added and an instant color change from hazel green to red was observed. The solvent was removed by vacuum and a red solid was collected. Single crystals are grown from saturated ether solution with a drop of benzene, stored in the fridge (-35 °C) for 2 days. Yield: 0.015 g, 0.011 mmol, 71 %.  $^1\text{H}$  NMR (499.9 MHz, C<sub>6</sub>D<sub>6</sub>, 20 °C): = 6.94 (t, 3H, *p*-Ph), 6.89 (s, 12H, *m*-Mes), 6.84 (d, 6H, *m*-Ph), 2.22 (s, 18H, *p*-CH<sub>3</sub> Mes), 2.19 (s, 36H, *o*-CH<sub>3</sub> Mes), 1.57 (m, 2H, CH<sub>2</sub>), 1.49 (m, 2H, CH<sub>2</sub>), 1.37 (m, 2H, CH<sub>2</sub>),



1.24 (m, 2H,  $CH_2$ ), 1.15 (m, 3H,  $CH_3$ ), -0.06 (m, 2H,  $NH_2$ ), -0.51 (s, 9H,  $SiMe_3$ ) ppm.  $^{13}C\{^1H\}$  NMR (125.7 MHz,  $C_6D_6$ , 20 °C):  $\delta$  = 185.1 (*broad*, CNR), 139.9, 137.8, 137.4, 136.5, 136.3, 134.7, 132.5, 129.9, 129.4, 129.3, 128.8, 124.7, 49.8, 35.6, 34.5, 33.4, 30.3, 27.3, 23.4, 22.8, 21.4, 21.3, 20.3, 14.6, 14.3 ppm. (The CNR resonance extremely broadened, presumably due to coupling to  $^{59}Co$  ( $I = 7/2$ , 100 %)). FTIR ( $C_6H_6$ , KBr windows, 25 °C):  $\nu_{CN} = 2020$  (s), 1907 (vs)  $cm^{-1}$ , also 2961 (m), 2917 (m), 2878 (m), 2850 (m), 1576 (m), 1407 (m), 1038 (m), 852 (m)  $cm^{-1}$ . Anal. Calcd. for  $C_{84}H_{99}N_4CoSi$ : C, 80.60; H, 7.97; N, 4.48. Found C, 80.47; H, 8.02; N, 4.76.

**Synthesis of  $(C_6H_{13}NH_2)[Co(SiMe_3)(CNAr^{Mes2})_3]_2$  (**4**).**  $Co(SiMe_3)(CNAr^{Mes2})_3$  (**1**) (1 equiv., 0.020 g, 0.017 mmol) and  $(C_6H_{13}NH_2)Co(SiMe_3)(CNAr^{Mes2})_3$  (**3**) (1.1 equiv., 0.024 g, 0.019 mmol) was stirred in a benzene solution (0.6mL) at room-temperature for 20 minutes. The solvent was then removed by vacuum and a red-brown solid was collected. Single brown crystals are grown from saturated pentane solution with a drop of benzene, stored in the fridge (-35 °C) for 2 days. Yield: 0.008 g, 0.0003 mmol, 20 %. Note that this crystalline material only existed in the solid state,  $^1H$  NMR and IR spectroscopy show both starting materials.

## 6.6 VT-NMR study of the vdW Interaction

**General Procedures.** In the glovebox, 0.5 mL  $d_8$ -THF solution was added to single crystals of  $(\mu^2-N-(N_2C_6H_{18})[Co(SiMe_3)(CNAr^{Mes2})_3]_2$  (**2**) in an NMR tube. The reaction was then injected into a pre-cooled NMR instrument for variable-temperature measurement.

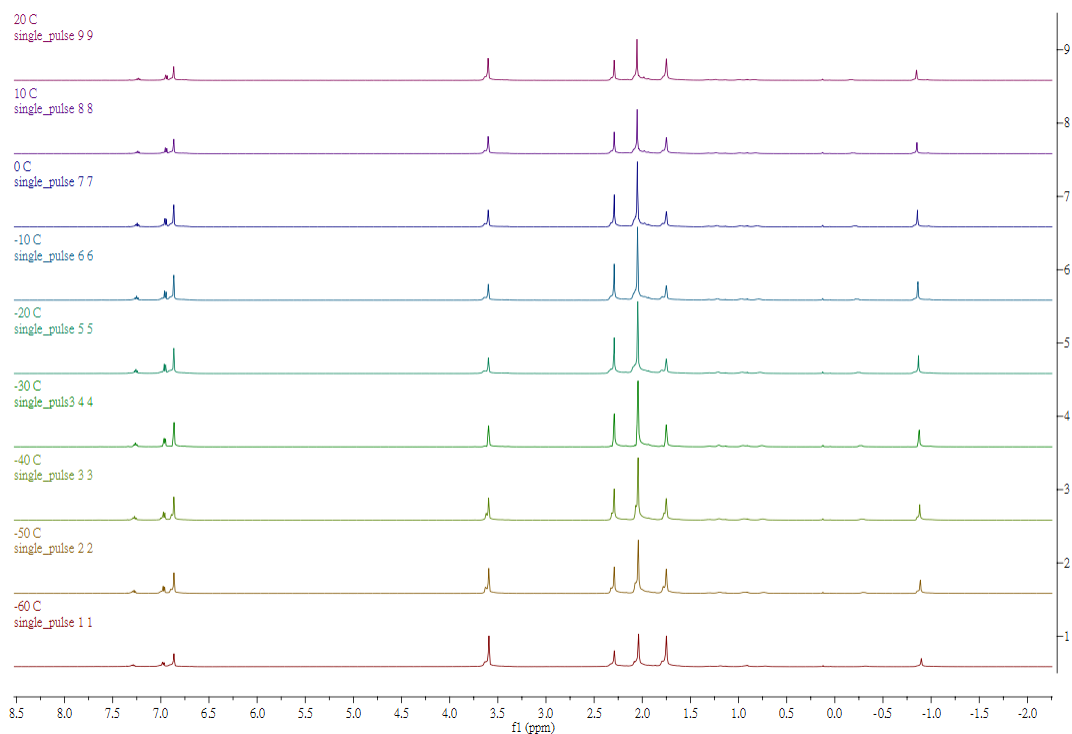


Figure 6.11. Stacked VT-NMR spectra of  $(\mu^2\text{-}N\text{-}(\text{N}_2\text{C}_6\text{H}_{18})[\text{Co}(\text{SiMe}_3)(\text{CNAr}^{\text{Mes}2})_3]_2$  (**2**) in  $d_8$ -THF.

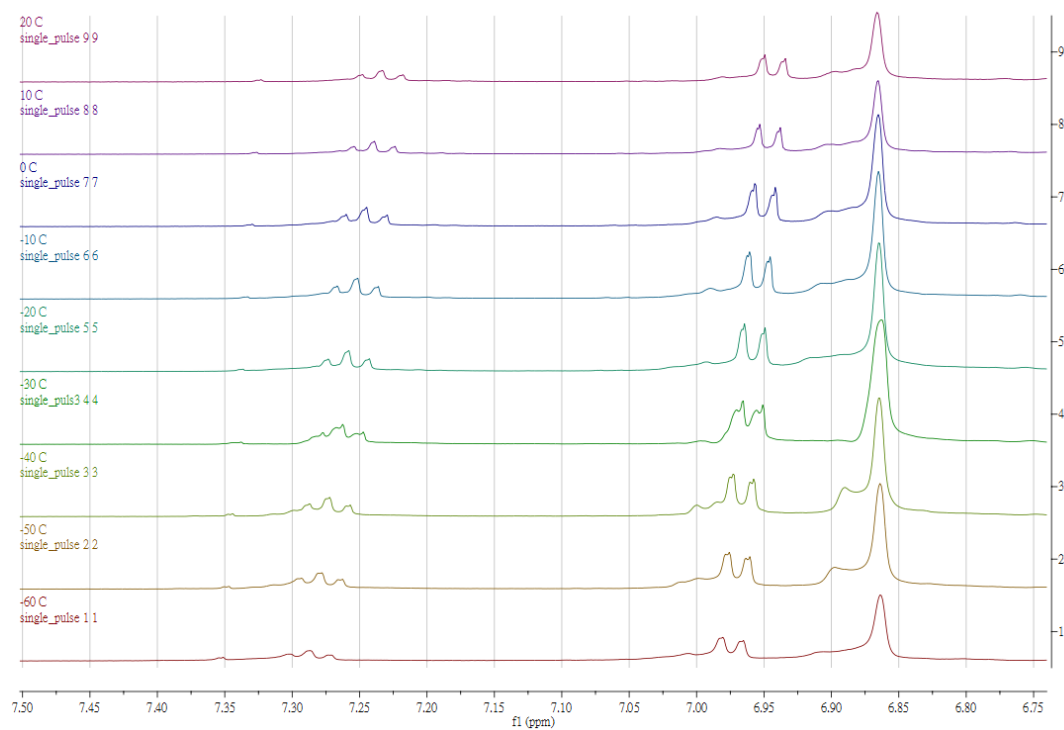


Figure 6.12. Stacked VT-NMR spectra of (**2**) in  $d_8$ -THF zoomed in at the aromatic proton region.

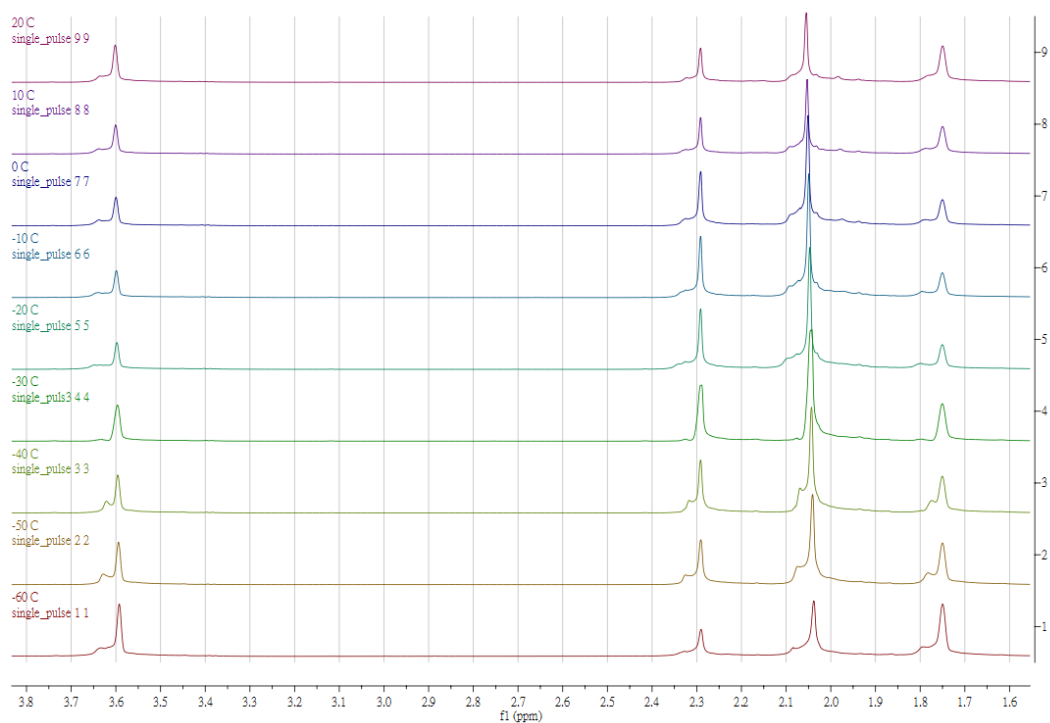


Figure 6.13. Stacked VT-NMR spectra of (2) in *ds*-THF zoomed in at the mesityl proton region.

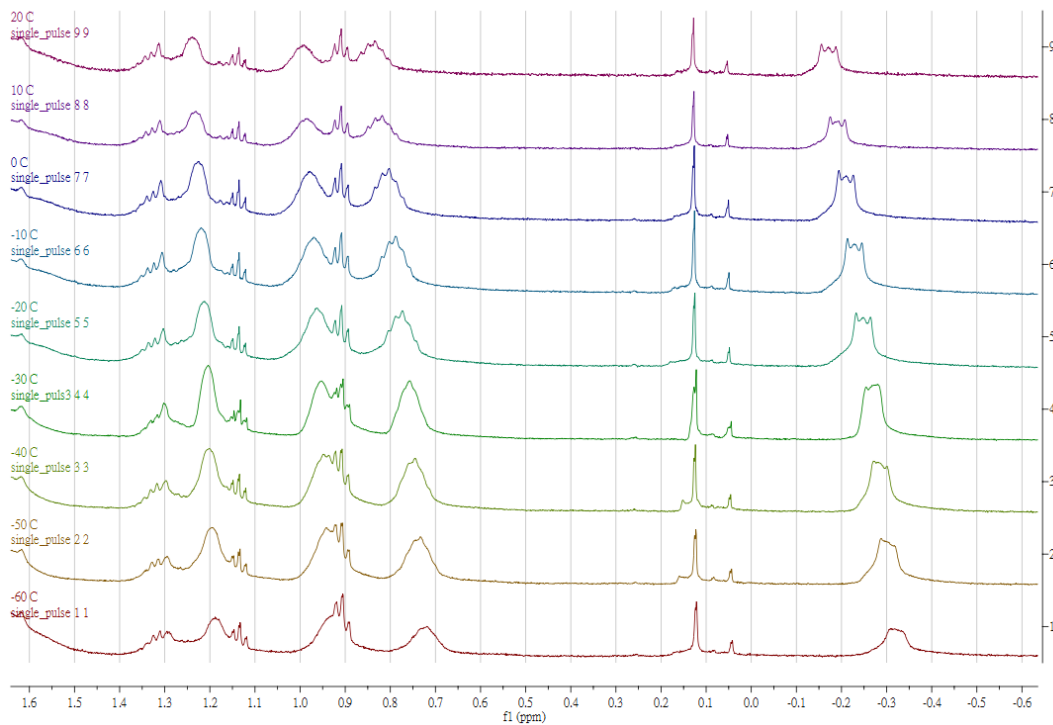
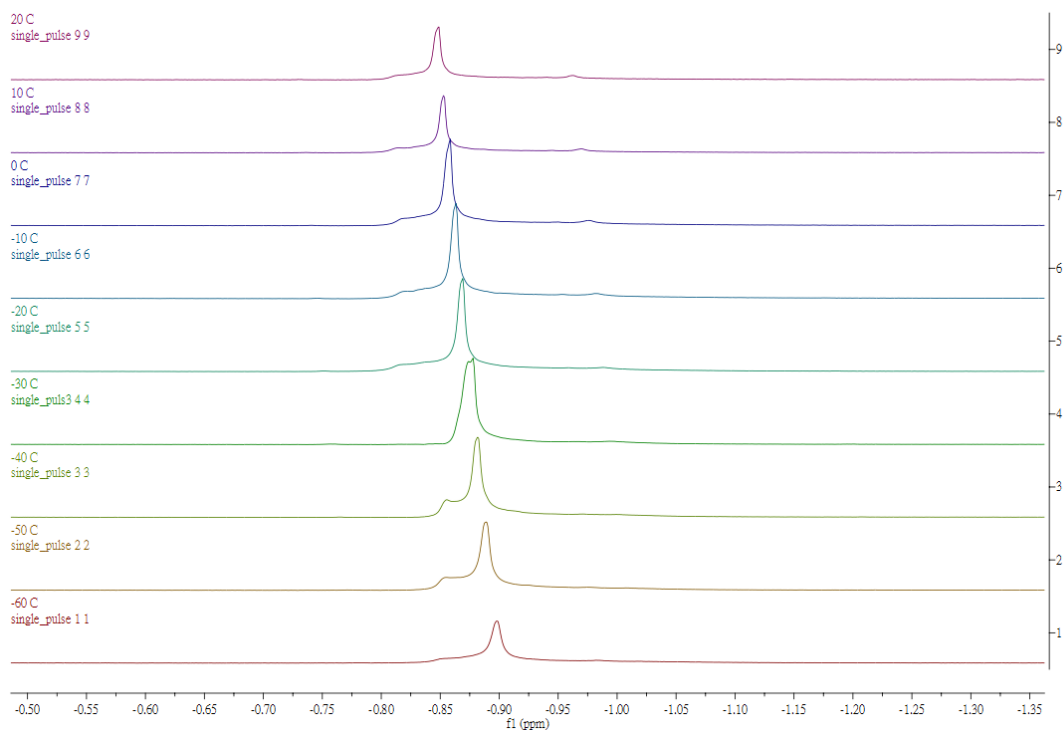


Figure 6.14. Stacked VT-NMR spectra of (2) in *ds*-THF zoomed in at the alkyl proton region.



**Figure 6.15.** Stacked VT-NMR spectra of (2) in *d*<sub>8</sub>-THF zoomed in at the trimethylsilyl proton region.

## 6.7 Crystallography Structure Determination

**General.** Single crystal X-ray structure determinations were carried out at low temperature on a Bruker P4, Platform or Kappa Diffractometer equipped with a Mo or Cu radiation source and a Bruker APEX detector. All structures were solved by direct methods with SIR 2004<sup>19</sup> or SHELXS<sup>20</sup> and refined by full-matrix least-squares procedures utilizing SHELXL within Olex 2 small-molecule solution, refinement, and analysis software package.<sup>21</sup> Crystallographic data collection and refinement information are listed in Table 6.4.

**Information on crystallographic disorder.** All disordered components were successfully modeled and refined anisotropically unless otherwise stated.

The solid-state structure of  $(\mu^2\text{-}N\text{-}(\text{N}_2\text{C}_6\text{H}_{18}))[\text{Co}(\text{SiMe}_3)(\text{CNAr}^{\text{Mes}_2})_3]_2 \cdot 2\text{C}_6\text{H}_6$  contains severely disordered solvent molecules of co-crystallization that could not be successfully modeled. The PLATON routine SQUEEZE<sup>4</sup> was used to account for these disordered components as a diffuse contribution to the overall scattering without specific atom positions.  $(\text{C}_6\text{H}_{13}\text{NH}_2)\text{Co}(\text{SiMe}_3)(\text{CNAr}^{\text{Mes}_2})_3 \cdot 2\text{Et}_2\text{O}$  exhibits positional disorder of the hexylamine group over two positions. Each hexylamine group is modeled at 51% and 49% occupancy for part 1 and part 2 respectively and refined anisotropically. One ether solvent molecule is shown on a crystallographic inversion center that has a two-site disorder. The PLATON routine SQUEEZE<sup>4</sup> was used to account for these disordered components as a diffuse contribution to the overall scattering without specific atom positions.

$(\text{C}_6\text{H}_{13}\text{NH}_2)[\text{Co}(\text{SiMe}_3)(\text{CNAr}^{\text{Mes}_2})_3]_2 \cdot \text{C}_6\text{H}_6$  exhibits positional disorder of the hexylamine group over two positions. The hexylamine group is set at part -1 due to locating on the crystallographic inversion center. The molecule is then and refined anisotropically.

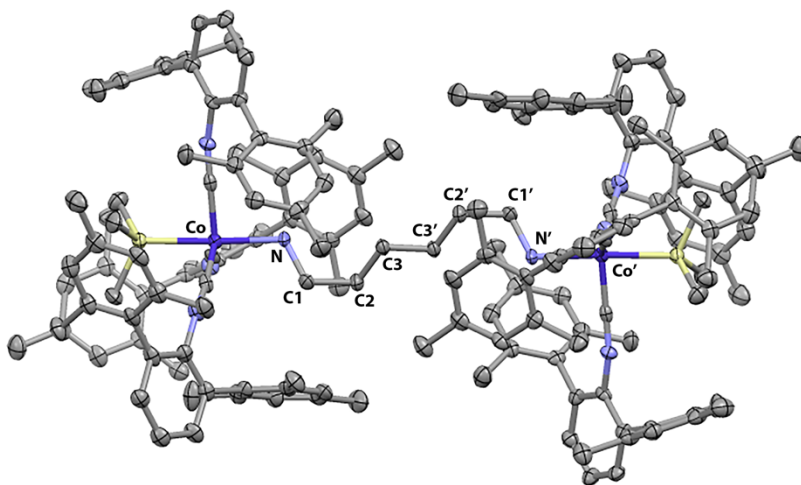


**Figure 6.16.** Molecular structure of  $(\mu^2\text{-}N\text{-}(\text{N}_2\text{C}_6\text{H}_{18}))[\text{Co}(\text{SiMe}_3)(\text{CNAr}^{\text{Mes}_2})_3]_2$  (2) with two benzene solvent molecule and hydrogen atoms omitted.

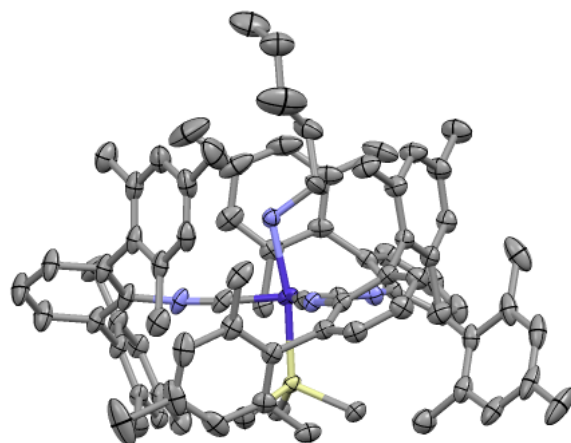


Figure 6.17. Molecular structure of  $(\text{C}_6\text{H}_{13}\text{NH}_2)\text{Co}(\text{SiMe}_3)(\text{CNAr}^{\text{Mes}_2})_3$  (3)  $\cdot 2\text{Et}_2\text{O}$  with two ether solvent molecule and hydrogen atoms omitted.

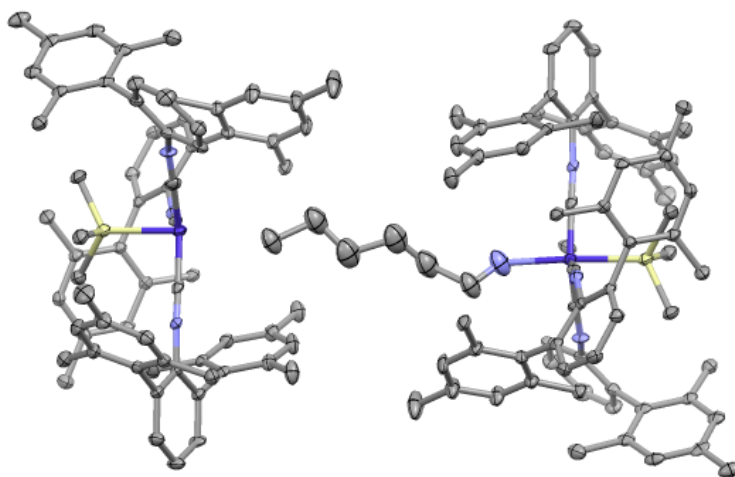


Figure 6.18. Molecular structure of  $(\text{C}_6\text{H}_{13}\text{NH}_2)[\text{Co}(\text{SiMe}_3)(\text{CNAr}^{\text{Mes}_2})_3]_2$  (4) with benzene solvent molecule and hydrogen atoms omitted.

**Table 6.4. Crystallographic Data Collection and Refinement Information.**

Name	( $\mu^2$ - <i>N</i> - (N <sub>2</sub> C <sub>6</sub> H <sub>18</sub> )[Co(SiMe <sub>3</sub> ) (CNAr <sup>Mes2</sup> ) <sub>3</sub> ] <sub>2</sub> (2) ·2C <sub>6</sub> H <sub>6</sub>	(C <sub>6</sub> H <sub>13</sub> NH <sub>2</sub> )Co(SiMe <sub>3</sub> ) (CNAr <sup>Mes2</sup> ) <sub>3</sub> (3) ·2Et <sub>2</sub> O	(C <sub>6</sub> H <sub>13</sub> NH <sub>2</sub> )[Co (SiMe <sub>3</sub> )(CNAr <sup>Mes2</sup> ) <sub>3</sub> ] <sub>2</sub> (4) ·C <sub>6</sub> H <sub>6</sub>
Formula	C198 H220 Co2 N8 Si2	C92H97 Co N4 O2 Si	C90 H102.50 Co N3.50 Si
Crystal System	Triclinic	Triclinic	Triclinic
Space Group	P-1	P-1	P-1
a, Å	14.095(3)	14.4325(8)	14.2279(11)
b, Å	14.345(3)	14.5619(8)	15.0872(12)
c, Å	21.832(4)	22.1242(12)	19.7544(16)
α, deg	92.280(6)	89.641(2)	102.130(2)
β, deg	94.892(5)	73.443(2)	109.917(2)
γ, deg	90.007(5)	66.184(2)	96.222(2)
V, Å <sup>3</sup>	4394.9(15)	4045.9(4)	3822.4(5)
Z	1	1	2
Radiation (λ, Å)	Mo-K <sub>α</sub> , 0.71073	Mo-K <sub>α</sub> , 0.71073	Mo-K <sub>α</sub> , 0.71073
ρ(calcd.), g/cm <sup>3</sup>	1.090	1.130	1.147
μ, mm <sup>-1</sup>	0.255	0.276	0.287
Temp, K	100	100	100
θ max, deg	25.456	25.349	25.350
data/parameters	16196 / 967	14810 / 977	13952 / 864
R <sub>1</sub>	0.1192	0.0637	0.1353
wR <sub>2</sub>	0.3112	0.1680	0.2055
GOF	1.124	1.021	1.190

## 6.8 Computational Details

The geometry of the full (dimer) complex with the trapped hexane molecule was obtained from crystallography. The monomer complex with methane was optimized with the B3LYP functional<sup>23</sup> using the cc-pVDZ basis set,<sup>24-27</sup> taking a single monomer complex and placing the methane molecule within the cavity as the initial structure for the optimization, since this structure did not crystallize. Energy decompositions were performed with the 2<sup>nd</sup> generation

ALMO-EDA method,<sup>28,29</sup> using the  $\Omega$ B97M-V functional.<sup>30</sup> The basis set used for the ALMO-EDA calculations included the 6-311G basis set centered on all Si, N, C, and H atoms,<sup>31,32</sup> and the 6-31G basis set centered on each Co atom.<sup>33</sup> All electronic structure calculations were carried out with Q-Chem 5.1.<sup>34</sup>

## 6.9 Acknowledgement

Chapter 6 is currently in preparation as a manuscript by C. Chan, A. E. Carpenter, C. K. Egan, M. Gembicky, C. E. Moore, A. L. Rheingold, F. Paesani, J. S. Figueroa. The dissertation author is the primary author of this manuscript.

## 6.10 References

- (1) Carpenter, A. E. *Low-Valent Cobalt Isocyanides : Analogues to Classical Carbonyls*; University of California San Diego, **2015**.
- (2) Millard, M. D. *Isolation of Four-Coordinate Iridium(I) Monohydrides and the X-ray Crystal Structure of a Cobalt Tris-Isocyanide Alkane sigma-Complex*; University of California San Diego, **2013**.
- (3) Nishio, M. *CrystEngComm* **2004**, *6* (27), 130–29.
- (4) Umezawa, Y.; Tsuboyama, S.; Takahashi, H.; Uzawa, J.; Nishio, M. *Tetrahedron* **1999**, *55* (33), 10047–10056.
- (5) Malone, J. F.; Murray, C. M.; Charlton, M. H.; Docherty, R.; Lavery, A. J. *Journal of the Chemical Society, Faraday Transactions* **1997**, *93* (19), 3429–3436.
- (6) Nishio, M.; Hirota, M. *Tetrahedron* **1989**, *45* (23), 7201–7245.
- (7) Morita, S.-I.; Fujii, A.; Mikami, N.; Tsuzuki, S. *J. Phys. Chem. A* **2006**, *110* (36), 10583–10590.
- (8) Tsuzuki, S. *Annual Reports Section "C" (Physical Chemistry)* **2012**, *108* (0), 69–95.
- (9) Steiner, T. *Angew. Chem. Int. Ed.* **2002**, *41* (1), 48–76.



- (10) Ingrid Castro-Rodriguez; Hidetaka Nakai; Peter Gantzel; Lev N Zakharov; Arnold L Rheingold, A.; Meyer, K. *Evidence for Alkane Coordination to an Electron-Rich Uranium Center*; American Chemical Society, 2003; Vol. 125, pp 15734–15735.
- (11) Daniel R Evans; Tatiana Drovetskaya; Robert Bau; Christopher A Reed, A.; Peter D W Boyd. *Heptane Coordination to an Iron(II) Porphyrin*; American Chemical Society, 1997; Vol. 119, pp 3633–3634.
- (12) Liptrot, D. J.; Power, P. P. *Nat Rev Chem* **2017**, *1* (1), 9574–12.
- (13) Trembleau, L.; Rebek, J. *Science* **2003**, *301* (5637), 1219–1220.
- (14) *Purification of Laboratory Chemicals*; Elsevier, 2003.
- (15) Pangborn, A. B.; Giardello, M. A.; Grubbs, R. H.; Rosen, R. K.; Timmers, F. J. *Organometallics* **1996**, *15* (5), 1518–1520.
- (16) Fox, B. J.; Sun, Q. Y.; DiPasquale, A. G.; Fox, A. R.; Rheingold, A. L.; Figueroa, J. S. *Inorg. Chem.* **2008**, *47* (19), 9010–9020.
- (17) Carpenter, A. E.; Mokhtarzadeh, C. C.; Ripatti, D. S.; Havrylyuk, I.; Kamezawa, R.; Moore, C. E.; Rheingold, A. L.; Figueroa, J. S. *Inorg. Chem.* **2015**, *54* (6), 2936–2944.
- (18) Carpenter, A. E.; Margulieux, G. W.; Millard, M. D.; Moore, C. E.; Weidemann, N.; Rheingold, A. L.; Figueroa, J. S. *Angew. Chem. Int. Ed.* **2012**, *51* (37), 9412–9416.
- (19) Burla, M. C.; Caliendo, R.; Camalli, M.; Carrozzini, B.; Cascarano, G. L.; De Caro, L.; Giacovazzo, C.; Polidori, G.; Spagna, R. *Journal of Applied Crystallography* **2005**, *38* (2), 381–388.
- (20) Sheldrick, G. M. *Acta Crystallogr., A, Found. Crystallogr.* **2008**, *64* (Pt 1), 112–122.
- (21) Dolomanov, O. V.; Bourhis, L. J.; Gildea, R. J.; Howard, J. A. K.; Puschmann, H. *Journal of Applied Crystallography* **2009**, *42* (2), 339–341.
- (22) Spek, A. L. *Journal of Applied Crystallography* **2003**, *36* (1), 7–13.
- (23) van der Sluis, P.; Spek, A. L. *Acta Crystallogr., A, Found. Crystallogr.* **1990**, *46* (3), 194–201.
- (24) Dunning, T. H., Jr. *J. Chem. Phys.* **1989**, *90* (2), 1007–1023.
- (25) Woon, D. E.; Dunning, T. H., Jr. *J. Chem. Phys.* **1993**, *98* (2), 1358–1371.
- (26) Balabanov, N. B.; Peterson, K. A. *J. Chem. Phys.* **2005**, *123* (6), 064107.

- (27) Balabanov, N. B.; Peterson, K. A. *J. Chem. Phys.* **2006**, *125* (7), 074110.
- (28) Horn, P. R.; Head-Gordon, M. *J. Chem. Phys.* **2015**, *143* (11), 114111.
- (29) Horn, P. R.; Mao, Y.; Head-Gordon, M. *Phys. Chem. Chem. Phys.* **2016**, *18* (33), 23067–23079.
- (30) Mardirossian, N.; Head-Gordon, M. *J. Chem. Phys.* **2016**, *144* (21), 214110.
- (31) Krishnan, R.; S, B. J.; Seeger, R.; Pople, J. A. *J. Chem. Phys.* **1980**, *72* (1), 650–654.
- (32) McLean, A. D.; Chandler, G. S. *J. Chem. Phys.* **1980**, *72* (10), 5639–5648.
- (33) Rassolov, V. A.; Pople, J. A.; Ratner, M. A.; Windus, T. L. *J. Chem. Phys.* **1998**, *109* (4), 1223–1229.
- (34) Shao, Y.; Gan, Z.; Epifanovsky, E.; Gilbert, A. T. B.; Wormit, M.; Kussmann, J.; Lange, A. W.; Behn, A.; Deng, J.; Feng, X.; Ghosh, D.; Goldey, M.; Horn, P. R.; Jacobson, L. D.; Kaliman, I.; Khaliullin, R. Z.; Kus, T. K.; Landau, A.; Liu, J.; Proynov, E. I.; Rhee, Y. M.; Richard, R. M.; Rohrdanz, M. A.; Steele, R. P.; Sundstrom, E. J.; Woodcock III, H. L.; Zimmerman, P. M.; Zuev, D.; Albrecht, B.; Alguire, E.; Austin, B.; Beran, G. J. O.; Bernard, Y. A.; Berquist, E.; Brandhorst, K.; Bravaya, K. B.; Brown, S. T.; Casanova, D.; Chang, C. M.; Chen, Y.; Chien, S. H.; Closser, K. D.; Crittenden, D. L.; Diedenhofen, M.; DiStasio Jr, R. A.; Dop, H.; Dutoi, A. D.; Edgar, R. G.; Fatehi, S.; Fusti-Molnar, L.; Ghysels, A.; Golubeva-Zadorozhnaya, A.; Gomes, J.; Hanson-Heine, M. W. D.; Harbach, P. H. P.; Hauser, A. W.; Hohenstein, E. G.; Holden, Z. C.; Jagau, T. C.; Ji, H.; Kaduk, B.; Khistyayev, K.; Kim, J.; Kim, J.; King, R. A.; Klunzinger, P.; Kosenkov, D.; Kowalczyk, T.; Krauter, C. M.; Lao, K. U.; Laurent, A.; Lawler, K. V.; Levchenko, S. V.; Lin, C. Y.; Liu, F.; Livshits, E.; Lochan, R. C.; Luenser, A.; Manohar, P.; Manzer, S. F.; Mao, S. P.; Mardirossian, N.; Marenich, A. V.; Maurer, S. A.; Mayhall, N. J.; Oana, C. M.; Olivares-Amaya, R.; O'Neill, D. P.; Parkhill, J. A.; Perrine, T. M.; Peverati, R.; Pieniazek, P. A.; Prociuk, A.; Rehn, D. R.; Rosta, E.; Russ, N. J.; Sergueev, N.; Sharada, S. M.; Sharma, S.; Small, D. W.; Sodt, A.; Stein, T.; Tschuck, D. S.; Su, Y. C.; Thom, A. J. W.; Tsuchimochi, T.; Vogt, L.; Vydrov, O.; Wang, T.; Watson, M. A.; Wenzel, J.; White, A.; Williams, C. F.; Vanovschi, V.; Yeganeh, S.; Yost, S. R.; You, Z. Q.; Zhang, I. Y.; Zhang, X.; Zhou, Y.; Brooks, B. R.; Chan, G. K. L.; Chipman, D. M.; Cramer, C. J.; Goddard III, W. A.; Gordon, M. S.; Hehre, W. J.; Klamt, A.; Schaefer III, H. F.; Schmidt, M. W.; Sherrill, C. D.; Truhlar, D. G.; Warshel, A.; Xue, X.; Aspuru-Guzik, A.; Baer, R.; Bell, A. T.; Besley, N. A.; Chai, J. D.; Dreuw, A.; Dunietz, B. D.; Furlani, T. R.; Gwaltney, S. R.; Hsu, C. P.; Jung, Y.; Kong, J.; Lambrecht, D. S.; Liang, W.; Ochsenfeld, C.; Rassolov, V. A.; Slipchenko, L. V.; Subotnik, J. E.; Van Voorhis, T.; Herbert, J. M.; Krylov, A. I.; Gill, P. M. W.; Head-Gordon, M. *Mol. Phys.* **2015**, *113*, 184–21.